

47th Textile Research Symposium 2019

June 17-19, 2019, Liberec, Czech Republic

Book of Abstracts



TECHNICAL UNIVERSITY OF LIBEREC
Faculty of Textile Engineering



The Textile Machinery Society of Japan

All rights reserved. No part of this publication may be reproduced, stored in a retrieval system, or transmitted in any form or by any means, electronic, mechanical, photocopying, recording, or otherwise without the prior permission of the copyright owner.

© Technical University of Liberec – 2019

ISBN 978-80-7494-473-4

Contents 3

A. P. Aneja, K. Kupka, J. Militky

TEXTILE INDUSTRY 4.0 – PREPARING FOR DIGITAL FUTURE 9

1. Fiber Science and Engineering

Zdzisław Czaplicki, Stanisław Strzelecki, and Henryk Wrzosek

INVESTIGATION INTO THE STRUCTURE AND PROPERTIES OF POLISH ALPACA WOOL 12

Małgorzata Giełdowska, Izabella Krucińska, Michał Puchalski

INVESTIGATION OF THE INFLUENCE OF PLA SUPRAMOLECULAR STRUCTURE ON THE THERMAL-SUPPORTED HYDROLITIC DEGRADATION OF WET SPINNING FIBRES 14

Jian HAN, Xiang Ji, Juanjuan SU, Yonghuan ZHAO

STUDY ON PROPERTIES OF POLYETHERAMINE FUNCTIONALIZED GRAPHENE OXIDE/ POLYAMIDE 6 COMPOSITE FIBERS 16

Gaku Kanazawa, Wataru Takarada, Takeshi Kikutani

STRUCTURE AND PROPERTIES OF POLYETHER-ESTER ELASTOMERIC FIBERS PREPARED BY HIGH-SPEED MELT SPINNING AND IN-LINE DRAWING PROCESSES 18

Michał Puchalski, Konrad Sulak, Grzegorz Szparaga, Izabella Krucińska

INVESTIGATION OF CRYSTALLISATION AND DISORDER-TO-ORDER PHASE TRANSITION OF PLA BY WAXD TECHNIQUE AS A METHOD IN THE OPTIMIZATION OF FIBROUS MATERIALS FORMING PROCESSES 20

Nanjanporn Rounpaissan, Wataru Takarada, Takeshi Kikutani

PREPARATION OF POLYLACTIDE FIBERS WITH HIGHLY-ORIENTED STEREO-COMPLEX CRYSTALS VIA HIGH-SPEED BICOMPONENT MELT SPINNING 22

Kotaku Saigusa, Wataru Takarada, Takeshi Kikutani

MECHANICAL PROPERTIES AND STRUCTURE OF POLY(GLYCOLIC ACID) FIBERS IMPROVED THROUGH CONTROL OF MOLECULAR ENTANGLEMENTS IN MELT SPINNING PROCESS 24

Ivan Ulman, Radek Jirkovec, Jiří Chvojka

COMBINATION OF KNOWN FIBROUS TECHNIQUES TO FORM A SUITABLE MATERIAL FOR SORBENT SUPPORT 26

Fumei Wang, Meiqin Wu

A NEW METHOD FOR MEASURING FIBER LENGTH 28

Takaichi Watanabe, Shohei Toyota, Tsutomu Ono

PREPARATION OF POLYMER FIBERS WITH CONTROLLED INTERNAL STRUCTURES USING MICROCHANNEL WET-SPINNING PROCESS AND PHASE SEPARATION 30

Wenqi Nie, Shu Zhang

GROUPING SUPERCAPACITOR FIBERS INTO ROPE: SCALING UP ENERGY WITH A SURGING VOLUME 32

2. Science and Technology of Textile Machinery

Bijoya Kumar Behera, Aman Katiyal, Adit Gupta

AUXETIC WOVEN STRUCTURES: DESIGN ENGINEERING, PRODUCTION PROCESS AND APPLICATIONS 36

Matsumoto Tatsumori

TWIST STRUCTURE OF THE VORTEX® YARN 38

3. Science and Technology of Textile Processing

Chong Heng, Fumei Wang

STUDY ON COTTON COLOR MEASUREMENT USING SCANNER 42

Aravin Prince Periyasamy, Kai Yang, Xiaoman Xiong, Mohanapriya Venkataraman, Jiri Militky, Rajesh Mishra, Dana Kremenakova

IMPACT OF SOL-GEL COATING ON THERMAL PROPERTIES OF CU- COATED NONWOVEN FABRIC	44
--	----

Sheikh Javed, Mukul Gupta, Indrajit Bramhecha, Nagender Singh

DEVELOPMENT OF MULTIFUNCTIONAL LINEN THROUGH IN-SITU SYNTHESIS OF SILVER NANOPARTICLES USING GROUNDNUT SHELL EXTRACT	46
---	----

Vildan Sölar, Filiz Ersoy

USEFUL LIFE OF TOWELS AFTER INDUSTRIAL LAUNDERING CYCLES	48
--	----

Shuichi TANOUE, Taiki YOSHIDA, Hideyuki UEMATSU

EFFECT OF ANNEALING AND ADDING MAGNESIUM OXIDE ON THE PROPERTIES OF POLYPROPYLENE/VAPOR-GROWN CARBON FIBER COMPOSITES	50
--	----

Martina Viková, Michal Vik, Jana Čandová

LCAM COTTON WHITE SCALE	52
-------------------------	----

Lina Wakako, Kai Kodama, Toshiyasu Kinari

FUNCTION OF COLOR IN AESTHETIC PROPERTIES OF PLAIN KNITTED FABRIC	54
---	----

Aleksandra Wyszowska, Zbigniew Draczyński

MICROENCAPSULATION OF PHENOLPHTHALEIN IN ALGINATE MICROSPHERES AS PH SENSOR SYSTEMS AND THEIR POSSIBLE DEPOSITION ON FIBERS OR OTHER TEXTILE MATERIALS	56
--	----

Yanfang Xu, Guangbiao Xu

STUDY ON OIL SORPTION AND RELEASE CHARACTERISTICS OF KAPOK FIBER POWDER	57
--	----

4. Dyeing and Finishing

MURAOKA Yumiko, YASUNAGA Hidekazu

ESTIMATION OF HAIR DAMAGE BY TENSILE MEASUREMENT AND EFFECT OF TREATMENT WITH BIOBASED MATERIALS FOR INVENTION OF DAMAGE SUPPRESSION TECHNIQUE	60
--	----

UCHIDA Akiko, YASUNAGA Hidekazu

RELATIONSHIPS BETWEEN COLOURING CONDITION AND RESULTING COLOUR IN HAIR COLOURING BY DYESTUFFS OBTAINED FROM (+)-CATECHIN PHOTO-OXIDISED WITH PHOTSENSITISERS UNDER VISIBLE LIGHT	61
--	----

YASUNAGA Hidekazu; OGIHARA Hiroki; VIKOVÁ Martina; VIK Michal

ESTIMATION OF HAIR DAMAGE BY USING BERBERINE III. FLUORESCENCE, ADSORPTION DEGREE AND DISTRIBUTION OF BERBERINE IN HAIR	63
--	----

5. Nano Fibers and Smart Textiles

Abdel-Fattah M. Seyam, Vamsi K. Jasti, William Oxenham, and Thomas Theyson

MECHANISM OF ELECTRIFICATION AND CHARGE DECAY ON WOVEN FABRIC STRUCTURES	66
---	----

YAMASHITA Yoshihiro, MIYAKE Hajime

WATER RESISTANT NANOFIBER FILTER CONSISTING OF EVOH / PU	68
--	----

Azam Ali, Vijay Baheti, Jiri Militky

COPPER AND SILVER COATED TEXTILES FOR SMART APPLICATIONS	69
--	----

Evren Boyraz, Fatma Yalcinkaya

OILY WASTE WATER SEPERATION BY USING NANOFIBROUS MEMBRANE	71
---	----

Sajid Faheem, Vijay Baheti, Maros Tunak, Jakub Wiener, Jiri Militky

COMPARATIVE INTUMESCENT FLAME RETARDANT FEATURES OF COTTON TEXTILES TREATED WITH ALKALINE AND ACIDIC CASEIN SUSPENSION	73
---	----

<i>Adit Gupta, Lakhan Vijayvargiya, Sayan Mukherjee, B.K. Behera</i>	
PREDICTION OF COMPRESSIONAL PROPERTIES OF FILAMENT WOUND COMPOSITES BY ANALYTICAL AND COMPUTATIONAL MODEL	75
<i>Hu Jiyong, Dong Xiaolong, Zhang Yong, Wang Tingting</i>	
EFFECT OF COVERING STRUCTURE ON THE PERFORMANCE OF WRAPPED CONDUCTIVE YARN AS STRAIN SENSOR	77
<i>Nazife KORKMAZ MEMİŞ, Sibel KAPLAN</i>	
DYNAMIC CREASE RECOVERY AND RETENTION OF WOOL FABRIC BY SHAPE MEMORY POLYURETHAN	79
<i>Muhammad Zaman Khan, Vijay Baheti, Jiri Militky</i>	
HYDROTHERMAL SYNTHESIS OF TiO ₂ NANOPARTICLES ON PET FABRIC AND THEIR FUNCTIONAL PROPERTIES	81
<i>Song Liu, Takuro Sumi, Yasuhito Mukai</i>	
DEVELOPMENT OF CIBACRON BLUE-ENHANCED AFFINITY NANOFIBER FABRIC FOR PROTEIN SEPARATION	83
<i>Yasuhito Mukai, Eiji Amano, Satoshi Hara</i>	
PREPARATION OF NANOCARBON-SUPPORTED NANOFIBER FABRIC FOR PURIFICATION OF CONTAMINATED WATER	85
<i>Shivangi Shukla, Renu Kumari, Mohanapriya Venkataraman, B K Behera</i>	
DEVELOPMENT OF FLEXIBLE FIBER REINFORCED SILICA AEROGEL BLANKETS/SHIELDS FOR THERMAL INSULATION IN AEROSPACE APPLICATIONS	87
<i>Yanfang Xu, Guangbiao Xu</i>	
POPLAR SEED FIBER AS A NATURAL ABSORBENT FOR OIL REMOVAL	89
<i>Kaori Yano, Yoko Okahisa</i>	
COMPARISON OF CELLULOSE NANOFIBER PROPERTIES OBTAINED FROM BAMBOOS OF DIFFERENT AGES	91
<i>Yini Fang, Yan Wang, Jiawei Chen, Liqiang Yi, Haonan Jin, Jiri Militky, Jaromir Marek, Juming Yao, Ming Zhang</i>	
PREPARATION OF PARAFFIN WAX/POLYACRYLONITRILE THERMO-REGULATING NANOFIBERS BY COAXIAL ELECTROSPINNING	93

6. Composite and Industrial Textiles

<i>A.K.Dash, Lekhani Tripathi, B.K.Behera</i>	
FORMABILITY OF 3D TEXTILE PREFORMS FOR COMPOSITE APPLICATIONS	96
<i>Mizue KAKEHI, Hiroto AKAGI, Hideyuki UEMATSU, Shuichi TANOUÉ</i>	
THE DEVELOPMENT OF THE FOAM CONTAINING PULP FIBER AND THERMOPLASTIC FOAMING AGENT FOR ACOUSTIC ABSORPTION MATERIALS	98
<i>Zunjarrao Kamble, B. K. Behera, Teruo Kimura, Ino Haruhiro</i>	
UPCYCLING TEXTILE WASTE INTO FIBRE REINFORCED COMPOSITES	100
<i>Vikas Khatkar, B K Behera</i>	
DESIGN, DEVELOPMENT AND CHARACTERIZATION OF 3D WOVEN STRUCTURE REINFORCED COMPOSITE LEAF SPRING	102
<i>Toshiyasu Kinari, Takuru Suehiro, Eiki Sakanishi, Lina Wakako</i>	
BENDING PROPERTIES OF BRIDED CFRP WITH SHELL - BULKHEAD PREFORM	104
<i>Brigita Kolčavová Sirková, Iva Mertová, Eva Moučková</i>	
PROPERTIES AND STRUCTURE OF SPUN YARNS IN RELATION TO THE SPINNING AND WEAVING TECHNOLOGIES	106
<i>Ashok Kumar, B. K. Behera</i>	
3D WOVEN STRUCTURES FOR AUTOMOTIVE SEAT COVERS	108

<i>Fenye Meng, Yuling Li</i>	
AUTOMATIC FORMATION TECHNIQUES AND UNIFORMITY EVALUATION OF CONICAL VASCULAR GRAFT	110
<i>Rajesh Mishra, Tao Yang, Xiaoman Xiong, Jiri Militky</i>	
ACOUSTIC PROPERTIES OF ADVANCED NONWOVENS	112
<i>Yasuhito Mukai, Eiji Amano, Satoshi Hara</i>	
PREPARATION OF NANOCARBON-SUPPORTED NANOFIBER FABRIC FOR PURIFICATION OF CONTAMINATED WATER	114
<i>Ghanshyam Neje, Bijoya Kumar Behera</i>	
EFFECT OF CELL GEOMETRICAL PARAMETERS ON THE MECHANICAL PROPERTIES OF 3D WOVEN SPACER SANDWICH COMPOSITES	116
<i>Jana Novotná, Hana Šourková, Miroslava Pechočiaková</i>	
DIELECTRIC ANALYSIS OF COMPOSITE MATERIALS WITH PLASMA TREATMENT RECYCLED CARBON FIBERS	118
<i>Sandeep Olhan, Vikas Khatkar, B. K. Behera</i>	
MECHANICAL BEHAVIOR OF NATURAL FIBER BASED 3D WOVEN STRUCTURAL COMPOSITES FOR AUTOMOTIVE APPLICATIONS	120
<i>Stanislaw Strzelecki, Zdzislaw Czaplicki</i>	
APPLICATION OF MULTILOBE JOURNAL BEARINGS IN THE DESIGN OF NEEDLE PUNCHING MACHINE	122
<i>Lekhani Tripathi, Ghanshyam Neje, B. K. Behera</i>	
MECHANICS OF 3D WOVEN HONEYCOMB STRUCTURE	124
<i>Veronika Tunakova, Zuzana Hrubosova, Jiri Prochazka</i>	
FASHION CLOTHING WITH ELECTROMAGNETIC RADIATION PROTECTION	126
<i>Vik M., Glombíková V., Víková M., Havelka A., Adamcová J., Pechová M.</i>	
PEDESTRIANS VISIBILITY AT NIGHT: EFFECTS OF PEDESTRIAN CLOTHING, BALANCING SAFETY AND CULTURE	128
<i>Pavčina Bílá, Monika Vyšanská</i>	
RECONSTRUCTION OF THE INDIVIDUAL FIBERS' TRAJECTORIES IN AIR-JET YARN	130
<i>Yuanfeng Wang, Daniel Karthik, Kai Yang, Tao Yang, Xiaoman Xiong, Vijay Baheti, Jiří Militký</i>	
ELECTRICAL HEATING PROPERTIES OF CARBON FABRIC/GREEN EPOXY COMPOSITES FILLED WITH FLY ASH	132
<i>Xiaoman Xiong, Mohanapriya Venkataraman, Tao Yang, Rajesh Mishra, Jiri Militky</i>	
THERMAL PROTECTION PROPERTIES OF AEROGEL-COATED KEVLAR WOVEN FABRICS	134
<i>Shivendra Yadav, Dipayan Das</i>	
EFFECT OF FIBER SIZE ON FILTRATION PERFORMANCE OF NONWOVEN SYNTHETIC FILTER MEDIA FOR ENGINE INTAKE AIR	136
<i>Kai Yang, Mohanapriya Venkataraman, Yuanfeng Wang, Jakub Weiner, Jiri Militky, Rajesh Mishra, Guocheng Zhu, Juming Yao</i>	
PREPARATION OF COATED POLYAMIDE NANOFIBROUS MEMBRANES WITH PHASE CHANGE MATERIAL	138
<i>Tao Yang, Xiaoman Xiong, Rajesh Mishra, Jean-Philippe Groby, Jiri Militky</i>	
OBTAINING NON-ACOUSTICAL PARAMETERS OF POLYESTER NONWOVEN MATERIALS BY USING ACOUSTIC METHOD	140
 7. Design, Comfort, Quality of Textiles and Sense Evaluation	
<i>Sachiko Sukigara, Tomoko Awazitani</i>	
OPTICAL PROPERTY OF TEXTILES RELATED TO HUMAN PERCEPTION AND PHYSICAL PROPERTIES	144

<i>Adine Gericke, Jiri Militky, Mohanapriya Venkataraman, Divan Coetzee</i>	
INVESTIGATING THERMAL COMFORT PROPERTIES IN MOHAIR FABRICS	146
<i>Meenakshi Ahirwar, Mesay Dubale, B. K. Behera</i>	
DEVELOPMENT OF HAND EVALUATION SYSTEM FOR BED LINEN	148
<i>Jeoun Gyonran, Takako Inoue, Morihiro Yoneda</i>	
THE OBJECTIVE EVALUATION OF TOTAL HAND OF TOWEL FABRICS AND ITS CONFIRMATION BY SENSORY TEST	150
<i>Takafumi Hata, Mari Inoue</i>	
OBJECTIVE HAND EVALUATION OF CAR INTERIOR MATERIAL	152
<i>Lubos Hes, Monika Boguslawska - Baczek</i>	
THERMAL COMFORT OF QUILTED BLANKETS	154
<i>Mari Inoue</i>	
HAND EVALUATION OF TOWEL AND WASHING DURABILITY	156
<i>Jinhua Jiang, Yi Geng, Qinghua Yu, Chenglong Zhang, Nanliang Chen</i>	
INVESTIGATION OF THE INFLUENCE OF COMPRESSION ON THE IN PLANE PERMEABILITY OF FABRIC PREFORMS IN VIMP	158
<i>Hiroyuki Kanai, Takuma Kobayashi, Hiroki Maru, Shuhei Hanashiro</i>	
COMFORT ASSESMENT OF BOTTOM MATTRESS FOR BEDDING APPARATUS	160
<i>Sibel KAPLAN, Betül AKGUNOGLU</i>	
PRESSURE COMFORT CHARACTERISTICS OF SPORTS SOCKS MADE OF MODIFIED SYNTHETIC MATERIALS WITH DIFFERENT WEAVES	162
<i>Yuki Karasawa, Mayumi Uemae, Hiroaki Yoshida, Masayoshi Kamijo</i>	
CLOTHING COMFORT EVALUATION OF UNDERWEAR THROUGH COMPARISON BETWEEN POLYPROPYLENE YARN AND POLYESTER YARN	164
<i>Kavita, Lalit jajpura, B. K. Behera</i>	
COMFORT BEHAVIOR OF UNCONVENTIONAL NATURAL FIBRE BASED UNION FABRICS	166
<i>KyoungOk Kim, Chen Lyu, Chunhong Zhu, Hiroaki Ishizawa, Masayuki Takatera</i>	
MEASUREMENT OF TEMPERATURE DISTRIBUTION ON LOWER LEG WEARING DIFFERENT SIZES OF TROUSERS	168
<i>Křemenáková Dana, Militký Jiří, Novosad Andriana, Venkataraman Mohanapriya, Večerník Josef</i>	
TEXTILE LAYERS ENABLING BACK REFLECTION OF HUMAN BODY THERMAL RADIATION	170
<i>Malgorzata Matusiak</i>	
THERMAL INSULATION PROPERTIES OF THE SEERSUCKER WOVEN FABRICS OF DIFFERENT STRUCTURE	172
<i>Sunny Pannu, B. K. Behera</i>	
ENGINEERING STRETCH FABRIC FOR IMPROVED MECHANICAL COMFORT	174
<i>Raphael Santos, Yuta Yamaguchi, Sachiko Sukigara</i>	
TRAJECTORY SIMILARITY OF THE THUMB AND INDEX FINGER DURING NATURAL FABRIC ASSESSMENT BY A NON-EXPERT	176
<i>Lexi Tu, Haoxuan Shi, Xinrong Luo, Hua Shen</i>	
DEPENDENCE OF TEXTILE STRUCTURE ON HEAT TRANSMISSION	178
<i>Liu Su, Sun Kexia, Long Hairu</i>	
THE INVESTIGATION ON THERMAL PROPERTIES OF CONDUCTIVE KNITTED FABRICS UNDER DIFFERENT VOLTAGES	180
<i>Run Qiu, Na Li, Run Wen</i>	
VISUAL PERCEPTION AND EVALUATION OF WOMEN'S SHIRT FABRICS BASED ON FAST FASHION E-COMMERCE PLATFORM	182

Morihiro Yoneda, Chie Nakajima

- MEASUREMENT OF EFFECTIVE THERMAL CONDUCTIVITY OF FIBER ASSEMBLY AND 3D
HEAT CONDUCTION ANALYSIS 186

KyoungHou KIM, Kohei OYA, Kouta MOCHIZUKI, Toshifumi IKAGA, Yutaka OHKOSHI

- ANALYSIS FOR STRUCTURAL DISTRIBUTION OF MELTBLOWN NONWOVEN FABRIC TO
THICKNESS DIRECTION USING X-RAY CT 215

8. Apparel Science and Production Technology

Frederick Tungshing Fung, Lubos Hes, Vladimir Bajzik

- REVIEW OF MEN'S DRESS SHIRT PATTERN DEVELOPMENT FOR THE LAST 100 YEARS 190

Qing Li, Jin Peng

- CIRCULATING PRE-OWNED FASHION ---- O2O TRADE OF SECONDHAND TEXTILES IN
CHINA 192

9. Environment and Sustainability

Arun Aneja, Karel Kupka, Jiri Militky

- MULTICOMPONENT FIBER RECYCLING – ANALYSIS OF HETEROGENOUS HYDROLYTIC
KINETICS 196

Helena Březinová, Milena Bravermanová

- RESEARCH OF ARCHAEOLOGICAL TEXTILES IN THE CZECH REPUBLIC 198

Hafsa Jamshaid, Ali Raza, Sikander Abbas Basra, Rajesh Mishra

- DEVELOPMENT OF THERMALLY INSULATED CONSTRUCTION STRUCTURE BY
SUSTAINABLE NATURAL FIBERS 200

Hana Křížová, Jakub Wiener

- ECOLOGICAL TREATMENT OF WOOL USING NATURAL POLYPHENOL SUBSTANCES 202

Rui-Hua Yang

- A SMART AND SUSTAINABLE SPINNING FOR COLORFUL TEXTILES 204

Dhirendra Sharma, Priyal Sawla, Meenakshi Ahirwar, B. K. Behera

- INDUSTRIAL HEMP AS A SUSTAINABLE TEXTILE FIBRE TO PRODUCE HIGH QUALITY
APPAREL FABRIC 206

10. Biomedicals

Z. Oulehlová, M. Klíčová, J. Horáková, A. Klápšťová, V. Liška, J. Rosendorf, R. Pálek, L. Červenková

- PLANAR POLYMERIC NANOFIBROUS PATCHES FOR SEALING THE GASTROINTESTINAL
ANASTOMOSES 210

Pavla Těšínová

- INTERNATIONAL COOPERATION OF FACULTY OF TEXTILE ENGINEERING FROM LIBEREC
WITH JAPAN PARTNERS 213

TEXTILE INDUSTRY 4.0 – PREPARING FOR DIGITAL FUTURE

A P Aneja¹, K Kupka² J Militky³

¹East Carolina University, Dept. of Eng., 110 Slay Hall, Greenville, NC 27858, USA, e-mail: anejaap@gmail.com

²TriloByte Statistical Software Ltd., CZ 53352 Pardubice, Czech Republic

³Faculty of Textile Engineering, Technical University of Liberec, Czech Republic

Abstract: *The classical textile industry in the US, Europe and Japan has been in a state of flux for the past few decades. This has been characterized by massive reduction in work force, production outsourcing to SE Asia (mainly China and India), virtually no new infrastructure/asset investment, reduced R&D spending with no novel polymers developed which forms the basis of man-made fibers, etc. Companies like DuPont, Celanese, and Toray which were once synonymous with fibers are now a shadow of their former prowess. The rise of the fourth industrial revolution, or Industry 4.0, is likely to hold the growth panacea, drive changes for a better future and set a trajectory to attain its former glory.*

Keywords: Industry 4.0, Digital Transformation, Cyber Physical Production Systems, Textile Industry

1 INTRODUCTION

The textile sector, as we know it, in the US, Europe and Japan must give way to the emerging new paradigm of an industry driven by innovation, agility, technology, growth and profits. Some promising areas are technical and smart textiles, composites, biomimetic, nonwovens, Cyber Physical Systems (textile touchpads, health care monitoring) to name a few. These are indeed heady times for textile and fiber science poised for growth in a fascinating high-tech field with enormous potential. This can only be realized if the industry has a robust and up-scalable intelligent manufacturing systems. With emergence of industry of the fourth industrial revolution, or Industry 4.0 this sector can aspire to again be the model of growth it once was for the other “classic” industries to emulate.

2 WHAT IS INDUSTRY 4.0

So, what is Industry 4.0? It is transformation of “classic,” industries by the Internet of things (IoT), data and services with real time integration of products, processes, and infrastructure which marks the start of the fourth cycle. This is possible through increasing interconnectedness via internet of supply production, maintenance, delivery, and customer service. Hence, seemingly rigid value chains turn into highly flexible value networks. The goal is an intelligent factory, “smart factory,” which is characterized by adaptability, resource efficiency, and ergonomics as well as the integration of customers and human partners for joint value creation. The technological bases are the cyber-physical systems and IoT.

Hence, it is the next-generation manufacturing system that is obtained by adopting new models, new forms, and new methodologies to transform the traditional manufacturing system into a smart system. This gives rise to a smart and connected factory with Internet of Things and Cyber Physical Systems for the classical five level automation architecture as technology basis consisting of machine level, station level, cell level, process control level, and factory operation management level. In the Industry 4.0 era, an intelligent manufacturing system (IMS) uses service-oriented architecture via the Internet to provide collaborative, customizable, flexible,

and reconfigurable services to end-users, thus enabling a highly integrated human-machine manufacturing system. This high integration of human-machine cooperation aims to establish an ecosystem of the various manufacturing elements involved in IMS so that organizational, managerial, and technical levels can be seamlessly combined [1].

As we explore the ways in which information is used to create value, it is important to understand this from the perspective of the manufacturing value chain, where organizations create value from information via the movement from physical to digital, and back to physical. Industry 4.0 combines the connected technologies inherent in the Internet of Things (IoT) with relevant IT and operations technology (OT), including cyber security, horizontal and vertical system integration, analytics, additive manufacturing, robotics, high-performance cloud computing, artificial intelligence, cognitive technologies, advanced materials, and augmented reality, to drive the physical act of manufacturing. Industry 4.0 incorporates and extends these connected technologies to complete the physical-digital-physical cycle. The physical-to-digital and digital-to-physical leaps are unique to manufacturing processes; it is the leap from digital back to physical—from connected, digital technologies to the creation of a physical object or an improved process—that constitutes the essence of Industry 4.0 [2]. Hence the key principles are (i) the factory becomes digital and flexible, (ii) The use of advanced simulation tools and powerful big-data processing and analysis, and (iii) an efficient factory for energy and resource use. This leads to flexibility, efficiency, productivity, quality, mass customization, and competitiveness. It thus enables companies to cope with the challenges of producing increasingly individualized products with a short lead-time to market, improved decision making and higher quality. Typical resources are converted into intelligent objects so that they are able to sense, act, and behave within a smart environment to perhaps reverse the fortunes of the textile sector and lead us to nirvana. How much of this “star gazing” will come to pass may be estimated by the Gartner Hype Cycle for Emerging Technologies.

3 KEY COMPONENTS OF INDUSTRY 4.0

Cyber-Physical Systems

An important component of Industry 4.0 is the fusion of the physical and the virtual world. This fusion is made possible by Cyber-Physical Systems (CPS) as seen in Table 2. CPS are integrations of computation and physical processes. Embedded computers and networks monitor and control the physical processes, usually with feedback loops where physical processes affect computations and vice versa.

Internet of Things

The integration of the Internet of Things (IoT) and the Internet of Services (IoS) in the manufacturing process has initiated the fourth industrial revolution. The IoT allows “things” and “objects,” such as RFID, sensors, actuators, mobile phones, which, through unique addressing schemes, interact with each other and cooperate with their neighboring ‘smart’ components to reach common goals. Therefore, the IoT can be defined as a network in which CPS cooperate with each other through unique addressing schemes. An application example of IoT are smart factories.

Smart Factory/Smart Manufacturing

Smart factories constitute a key part of Industry 4.0. The smart factory can be defined as a factory where CPS communicate over the IoT and assist people and machines in the execution of their tasks. Hence, smart manufacturing is a highly connected knowledge enabled industrial enterprise where all business operation actions are optimized to achieve substantially enhanced productivity, energy/sustainability, an economic performance. The technical enablers consist of the convergence and application of nine stand alone digital technologies.

4 CASE FOR TEXTILE

The textile value chain presents its own unique set of challenges with several implementation barriers. These include risk and uncertainty about financial gains, no clear leader to educate the value of concept and demonstrate benefits of transformation, lack of skills and talent, and reluctance of participating in cyber space due to intrinsic conservative historical beliefs. Fiber production is capital intensive with large multinational entities in control while as we move downstream to fabric and garments the market becomes more fragmented. Furthermore, the circumstance varies from country to country. Thus, adoption of Industry 4.0 in textile will most likely occur in the early stages of product transformation i.e. fiber and fabrics. A prototype Textile Learning Factory 4.0 exists in Aachen, Germany [3]. Their case studies have shown smart personal devices can be used to make production more transparent by providing relevant production key parameters in a sophisticated way [4, 5]. Aspects of tele-maintenance, such as repair of machine supported by the machine produces are possible with self-optimization of the warp tension in a weaving process by using digital technologies.

5 CONCLUSIONS

The challenges of Industry 4.0 confronting the textile sector are daunting. These include communication reliability and quality of service, cyber security, maturity of

machine intelligence and ability to handle big data. Further exacerbating the issue, from a societal perspective, are general reluctance to change by shareholders, availability of adequate skill sets, and concern of unemployment. However, Textile Industry 4.0 offer numerous benefits:

- Increased productivity thru a higher level of automation that reduces production time, enable better asset utilization and inventory management.
- Increased manufacturing flexibility thru machines and robots that can execute the production steps for a wide variety of products.
- Increased speed from the first product or factory idea to the finished product thru consistent data and new simulation opportunities
- And finally, increased quality of products via sensors and actuators that monitor the current production in real time and intervene to correct an error, if necessary.

How will the textile sector participate in this moment? Time is of essence. Will we be the leader of tomorrow or part of the “heap dust” of missed opportunities. Only time will tell!

6 REFERENCES

- [1] Roblek V, Messo M, Krapez A 2016 SAGE Open April-June2016
- [2] Zhong R, Xu X, Klotz E, Newman S 2017 Engineering 3 Elsevier 616
- [3] Kuster D, Prab N, Gloy Y 2017 Procedia Manufacturing 9 214
- [4] Prisecaru, P 2016 Knowledge Horizons-Economics 18 1 57-62
- [5] Greenfield, R 2016 Japan Economic Foundation 35 4 1-7

1. Fiber Science and Engineering

INVESTIGATION INTO THE STRUCTURE AND PROPERTIES OF POLISH ALPACA WOOL

Zdzisław Czaplicki¹, Stanisław Strzelecki², and Henryk Wrzosek³

¹ Polish Textile Association, Lodz, Poland: zczaplicki@wp.pl

² Polish Textile Association, Lodz, Poland: Poland: stanislaw.strzelecki@p.lodz.pl
Technical University of Łódź, Łódź, Poland: henryk.wrzosek@p.lodz.pl

Abstract: The paper reports the structure and most significant parameters of wool from alpaca bred in Poland. The fiber external and internal structures are based on microscopic observations of the fiber surface and cross sections. It was determined that both the surfaces as well as the cross sections of the alpaca fibers show differences when compared to wool fibers. The diameter, which is the most important fiber parameter, was measured using a Laser – Scan method. The investigations were made on 15 samples taken from various alpacas from a herd of 100 animals. Depending on various investigation methods there were certain differences in the fiber diameter. Large variations of the fiber thickness in various samples prove the non-uniformity of wools in the whole alpaca herd. It indicates that the alpacas are bred in an uncontrolled (random) way.

Keywords: alpaca wool, diameter, surface fibres, cross – sections, strength, elongation at break

1 INTRODUCTION

Alpacas, animals from the family of camelids have been introduced to Poland 15 years ago. From year to year their population is growing and thus a new textile raw material has become available at home – the alpaca wool. At the moment no rational concept exists how to use this raw material. The Institute of Natural Fibers and Medicinal Plants (INF&MP) is presently trying to solve the problem of scouring alpaca wool [6]. The knowledge of the fiber structure and its physical and mechanical properties is necessary in the elaboration of the concept of how to apply alpaca wool in textile products. There are two alpaca breeds, the huacaya and suri [1]. They have a different appearance and the type of fleece. The huacaya has wool similar to sheep, with small crimps and a yearly fiber growth of 9 – 12 cm.

The suri alpaca wool is more delicate than that of huacaya wool, has more luster and the yearly fiber growth of 10 – 12 cm. Alpacas are kept mainly for their wool which has particularly high quality and end use properties. The alpaca wool is light, cool and at the same time well protects against cold.

The world population of alpacas is approximately 5 millions. In Peru there are about 3,6 millions, in Bolivia and Chile about 500 and 150 thousand, respectively. From begin of 80th last century the breeding of alpacas started on the other continents. The largest number of alpacas, without South America is in Australia (over 200 thousand), USA, Canada, New Zealand and Europe. Among the European countries, the breeding of alpacas is in Great Britain (50 thousand), Switzerland, Germany (30 thousand), Austria, France, Spain and Poland (6 thousand).

The problems of breeding alpacas, its wool and properties, the wool structure and its processing is quite new in Poland. Initial studies of the process of scouring alpaca wool are the second polish publication [3]. The first carried out in Poland investigation into the structure and properties of alpaca fibers [5] were published in 2012.

2 TEST MATERIALS AND METHODS

Wool fibers from polish alpacas were the studied material. The studies were made for 15 fiber samples taken from various animals from a herd of 100 alpacas. The fiber length, strength, elongation at breakpoint, diameter as well as the external and internal fiber structure was investigated. The alpaca fiber diameter was tested with the use of a laser method – Laser-Scan.

All the tests were made according to ISO standards. To assess the internal and external structure microscope tests were made using the FEI NOVA NANOSEM 230 and JSM-5200 LV scanning microscope.

3 TEST AND ANALYSIS OF RESULTS

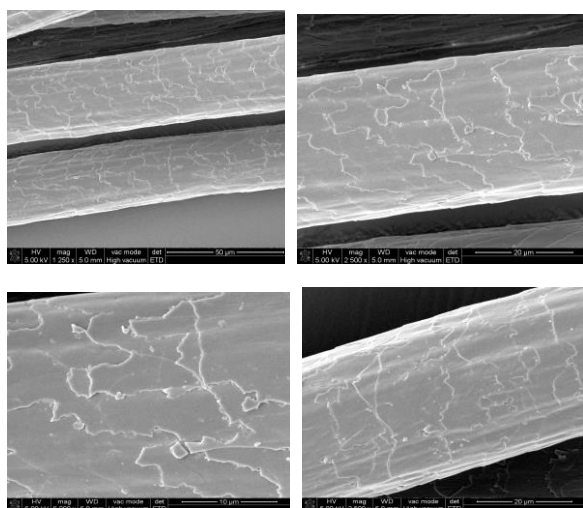
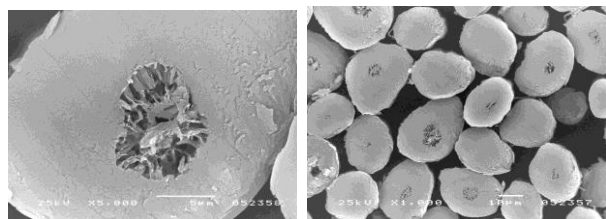
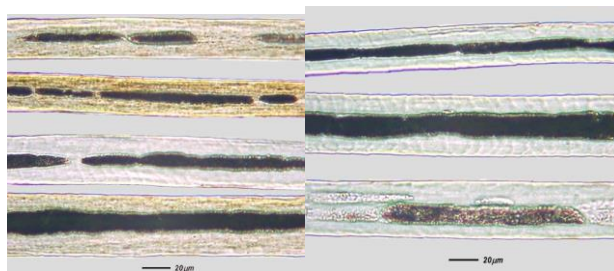
The results of physical, mechanical tests and fiber diameter are shown in table 1. The results of measurements of fiber surfaces, cross – sections and longitudinal views are shown in Fig. 1 through Fig. – 3.

From the results of physical and mechanical fiber properties tests (table 1) one can see that in various samples (taken from various animals), the alpaca fibers differ in length, strength and elongation at break point. The results of diameter tests also show a big difference of fiber diameters (20 – 35 µm) in samples from one herd.

The results of studies of the fiber surface cross sections and longitudinal views, shown in figures 1 – 3 indicate that alpaca fibers differ a lot from wool fibers. The alpaca fiber surface has also scales but their shape character is different. The scales are smaller and more delicate. The cross section of alpaca fibers is not as round as for sheep wool fibers. Channels with a core type structure are observed in the fiber center. These channels make the alpaca fiber lighter than the sheep wool fiber. The fiber longitudinal views clearly show the internal structure of these fibers. They show a large core character with air filled channels. This specific internal alpaca fiber structure is quite different than the internal structure of the sheep wool fiber.

Table 1 Parameters of alpaca wool

Item	Color of the specimen	Laser-Scan		Length lock [mm]	Length fibre (L)		Breaking strength (F)		Elongation at break, %
		μm	V_d , %		mm	V_L , %	cN	V_F , %	
1	dark beige	20.2	25.0	120	110	8.5	7.3	53.5	42
2	dark bronze	20.8	22.5	85	75	23.0	7.6	40.6	45
3	dark bronze	24.0	28.6	90	80	10.2	8.0	40.2	46
4	white	24.8	21.3	200	180	17.0	7.7	38.5	48
5	grey	25.0	23.4	100	70	38.0	13.2	45.2	38
6	light bronze	25.5	26.0	150	100	12.0	10.4	42.0	51
7	dark bronze	26.2	24.6	115	110	8.0	12.3	49.1	47
8	dark bronze	26.8	25.1	85	80	17.8	11.8	35.7	48
9	grey bronze	28.1	20.6	90	86	11.0	13.2	50.1	52
10	beige / white	29.0	26.6	92	85	13.5	14.2	37.6	51
11	black	29.4	25.8	75	65	12.4	12.5	34.8	50
12	black	31.0	23.8	75	70	12.6	10.8	42.3	38
13	black	32.8	19.5	80	75	10.5	13.7	45.1	37
14	light bronze	34.8	22.8	110	95	10.2	13.5	52.0	46
15	white	35.2	24.6	115	110	10.8	11.3	43.1	42

**Figure 1** Fibres surfaces of alpaca wool (dia. 29.1 μm)**Figure 2** SEM cross sections of alpaca wool fibres (dia. 29.1 μm)**Figure 3** SEM longitudinal views of alpaca wool fibres (29.1 μm)

4 CONCLUSIONS

The results of these studies of the alpaca fibre external and internal structure allow stating that the structure of alpaca fibre differs a lot from the structure of sheep wool fibres. The external surface of alpaca fibres is more delicate with smaller and less pronounced scales. The cross sections are mostly oval in shape with a clearly defined channel with a core structure.

The physical and mechanical alpaca fibre properties, strength, elongation, length and diameter are varied in particular samples. The reason for that is the uncontrolled herd breeding.

It is interesting, that the information from the world literature [1-4] concern mainly the history of alpacas, the conditions of their life and profits effecting from the use of wool in the textile products.

5 REFERENCES

- [1] Villarreal J., Future of the textile uses of alpaca fibre. Proceedings of World Wool Conference – Bradford UK, 2003, pp.164-169.
- [2] Rainsford F.E.B. The Alpaca Ladies Aregnipa's Colea Valley. Textiles No.3, 2004.
- [3] Rainsford F.E.B. Concern over Peru's Coarsening Alpaca Fibre. Textile No. 2, 2005.
- [4] Greaves P., Rainsford F.E.B. Camelid Fibres – Compared and Contrasted. Textiles No.3/4. 2005, pp.46-48.
- [5] Czaplicki Z.: Properties and structure of Polish alpaca wool. Fibres and Textiles in Eastern Europe, 2012, 20, 1, pp. 8 – 12.
- [6] Czaplicki Z., Ruszkowski K.: Optimization of scouring alpaca wool by ultrasonic techniques. Journal of Natural Fibres, 2014, 2, pp. 169 – 183.

INVESTIGATION OF THE INFLUENCE OF PLA SUPRAMOLECULAR STRUCTURE ON THE THERMAL-SUPPORTED HYDROLITIC DEGRADATION OF WET SPINNING FIBRES

Małgorzata Giełdowska¹, Izabella Krucińska¹ and Michał Puchalski¹

¹Lodz University of Technology, Department of Material and Commodity Sciences and Textile Metrology, Żeromskiego 116, 90-924 Lodz Poland, e-mail: malgorzata.gieldowska@edu.p.lodz.pl

Abstract: The influence of PLA supramolecular structure on the hydrolytic degradation of wet spinning fibers will be presented. Hydrolysis is the basic phenomenon of PLA degradation in natural conditions, but it is a process that requires a long time. In order to accelerate the hydrolytic degradation this process in laboratory condition was thermal-supporting which shortened the experiment and enabled it to show the supramolecular structure's impact on the degradation rate just after a few weeks.

Keywords: PLA, wet-spinning fibers, hydrolytic degradation, D-lactide content, crystallisation, α' – α form transition

1 INTRODUCTION

Poly(lactide) (PLA) is the most popular biodegradable and produced from renewable sources polymer to substitute for petroleum-based polymers in many areas of life include a textile applications [1]. Though the possible applications of PLA are well known, PLA has still not been fully characterized and understood scientifically. According to applied and scientific point of view the investigations of supramolecular structure creation of PLA during the fibrous forming processing and its influence on the mechanical properties of fabrics was precisely analyzed. The melt-spinning [2] and wet-spinning [3] fiber forming processes, and spun-bonded nonwoven [4] forming process are the main well investigated textile technologies of PLA processing.

From the other hand the analysis of the degradation of PLA is also interesting subject realized by many research groups on the world [5-7] but this subject is still the open question what was a motivation for performing of presented experiment.

In this presentation the results of the investigation of influence of PLA supramolecular structure on the hydrolytic degradation of wet spinning fibers will be presented. The hydrolysis is a process that requires a long time. In order to accelerate this process authors decided for the thermal-supporting of hydrolytic degradation which shortened the experiment and enabled it to show the supramolecular structure's impact on the degradation rate after just a few weeks.

2 MATERIAL AND METHODS

2.1 Material

The experiment was performed for the four different types of polylactide fibers differing in molecular and supramolecular structure. The fibers were prepared by using the wet spinning method [3] and commercially available poly(L-lactide) with low content of D-lactide isomer purchase from Nature Works (USA) :

- PLA12.S1 – Polymer: Ingeo 4060D; Content of D-lactid isomer: 12%; Total draw ratio: 400%; Linear mass: 158 tex; Degree of crystallinity: 2.6%; Crystal form: α' ;
- PLA12.S1 – Polymer: Ingeo 4060D; Content of D-lactid isomer: 12%; Total draw ratio: 600%; Linear mass: 80 tex; Degree of crystallinity: 12.3%; Crystal form: α' ;
- PLA1.4.S1 – Polymer: Ingeo 6201D; Content of D-lactid isomer: 1.4%; Total draw ratio: 500%; Linear mass: 96.0 tex; Degree of crystallinity: 33.0%; Crystal form: α' ;
- PLA1.4.S1 – Polymer: Ingeo 6201D; Content of D-lactid isomer: 1.4%; Total draw ratio: 700%; Linear mass: 60.3 tex; Degree of crystallinity: 36.5%; Crystal form: α ;

2.2 Hydrolytic degradation

Hydrolytic degradation process was performed under laboratory conditions. The fibers samples were incubated in three types of water solution with different pH (pH=3, pH=7, pH=10). In order to accelerate the process of hydrolytic degradation, experiment was carried out at elevated temperature 90 °C. The samples of fibers were carefully measured before the degradation process and their mass was about 0,5 g. After being placed in the solution, the samples were removed after specified period (1, 3, 5, 7, 10 and 14 days), rinsed with water and dried under normal conditions. Then the samples were weighed to evaluate the degree of mass loss.

2.3 Mass loss

The mass loss after each period of hydrolytic degradation was determined by the following equation:

$$\text{Mass loss} = \frac{m_i - m_d}{m_i} \quad (1)$$

where: m_i is the initial mass of sample and m_d is the mass of degraded sample measured by the using Radwag WTB 200.

2.4 WAXD method

The analysis of supramolecular structure of fibers was carried out using the wide-angle X-ray diffraction X'Pert PRO (PANalytical B. V., Almelo, The Netherlands). The diffractometer uses CuK α radiation ($\lambda=0,154$ nm) with the following parameters: accelerating voltage kV and anode current 30 mA. The powdered samples were analysed in the angle range 2θ 5-45° at a speed of 0.5°/min. The obtained diffractograms were numerically analyzed in WAXSFIT program [8] to the determination of degree of crystallinity and d-spacing.

3 RESULTS

In the Figure 1 and Figure 2 the influence of hydrolytic degradation time on crystallinity degree, d-spacing and mass loss are presented. As is clearly presented, during the process of degradation the degree of crystallinity of the fibers increases for all samples. Based on the analysis of the graph in Figure 2, the strong influence of the content of D-lactide isomer on the rate of mass loss is visible.

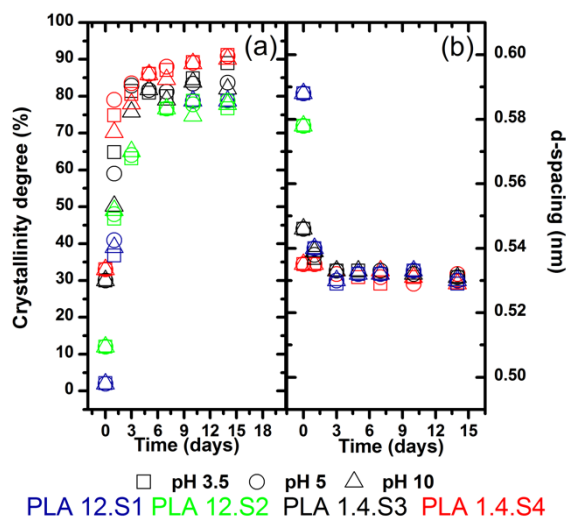


Figure 1 Influence of time of hydrolytic degradation on crystallinity degree (a) and d-spacing (b) of fibers

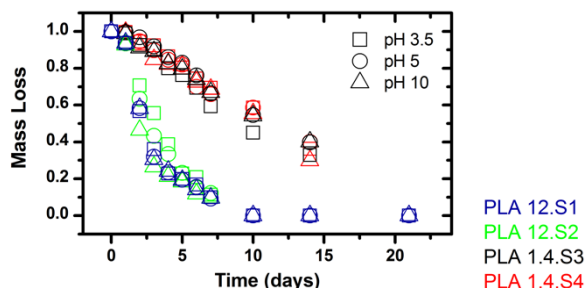


Figure 2 Influence of time of hydrolytic degradation on mass loss of fibers.

4 CONCLUSIONS

The investigations of the influence of D-lactide content and supramolecular structure on the process of hydrolytic degradation of PLA fibers at elevated temperature showed allows formulating following conclusions:

- During the time of hydrolytic degradation the crystallization of the PLA is induced up to range 80-90 %, also in the case amorphous poly(L-lactide) contained 12% of D-lactide isomer;
- The hydrolytic degradation results in the α' – α form transition what is visible as the increase the d-spacing calculated for the most visible crystalline peak corresponding to (200)/(110) lattice plane;
- The performed investigation clearly shown the stronger influences of molecular structure of commercially available PLA (D-lactide content) then supramolecular structure of fibers (crystallinity degree and crystal form) on the rate of hydrolytic degradation.

ACKNOWLEDGEMENT: This research was partially funded by the European Regional Development Fund in the frame of a key project entitled "Biodegradable fibrous products" (acronym: Biogratex) No. POIG.01.03.01-00-007/08-09 and part of the work was funded by statutory activity by Lodz University of Technology, Department of Material and Commodity Sciences and Textile Metrology, Poland, No. 14-148-1-2117.

5 REFERENCES

- [1] Krucińska I, Biodegradowalne wyroby włókniste, Wydawnictwo PŁ.: Łódź, 2014.
- [2] Manich AM, Miguel R, Lucas J, Franco F, Baena B, Carilla J, Montero L, Cayuela D, Textile Research. Journal 2011, 81, 1788.
- [3] Puchalski M, Kwolek S, Szparaga G, Chrzanowski M, Krucińska I, Polymers 2017, 9, 18.
- [4] Puchalski M, Sulak K, Chrzanowski M, Sztajnowski S, Krucińska I, Textile Research. Journal 2015, 85, 535.
- [5] Chen H, Shen Y, Yang J, Huang T, Zhang N, Wang Y, Zhou Z, Polymer 2013, 54, 6644.
- [6] Saha SK, Tsuji H, Polymer Degradation and Stability 2006, 91 1665.
- [7] Zhang N, Ju X, Duan J, Yang J, Huang T, Qi X, Wang Y, Polymer Degradation and Stability 2018, 148 1.
- [8] Rabiej M Journal of Applied Crystallography. 2013, 46, 1136–1144.

STUDY ON PROPERTIES OF POLYETHERAMINE FUNCTIONALIZED GRAPHENE OXIDE/ POLYAMIDE 6 COMPOSITE FIBERS

Jian HAN^{1,2}, Xiang JI¹, Juanjuan SU^{1,2}, Yonghuan ZHAO¹

¹Collage of Materials and Textiles; ²Zhejiang Provincial Key Lab. of Industrial Textile Materials and Manufacturing Tech., Zhejiang Sci-Tech University, Hangzhou 310018, China, e-mail:

hanjian8@zstu.edu.cn

Abstract: The polyetheramine functionalized graphene oxide/ polyamide 6 (PEA-GO/PA6) composite fibers were obtained by melt spinning. The characterization of PEA-GO and the properties of PEA-GO/PA6 fibers were investigated by Fourier transform infrared spectroscopy (FTIR), scanning electron microscope (SEM), X-ray diffraction (XRD), differential scanning calorimetry (DSC) and universal material testing machine. The results showed that PEA-GO can be well dispersed in PA6 fibers. PEA-GO played a role of heterogeneous nucleation in the crystallization of PA6 fibers, which promoted the crystallization of PA 6 fibers and induced the transformation of PA6 from α crystal to γ crystal. When the content of PEA-GO was only 0.1%, the mechanical property of the PEA-GO/PA6 composite fiber increased clearly.

Keywords: graphene oxide, polyamide 6, melt-spinning, mechanical property

1 Introduction

Polyamide 6 (PA6) fiber is one of the widely used synthetic fibers. It has many advantages such as high strength, light weight and good elasticity [1]. However, the lower modulus of polyamide fiber causes it to be easily deformed in using, which seriously affects its service life. In addition, with the development of high-speed spinning technology, higher requirements are placed on the properties of PA6 fiber. In recent years, various nanomaterials have been used as fillers to improve the property of PA6 fiber.

As a 2-dimensional nanomaterial, the graphene has attracted extensive attention among researchers. Due to its excellent thermal conductivity, electrical conductivity and mechanical properties, graphene has been successfully applied to produce high performance polymer composites [2,3]. The dispersion of graphene in polymers has always been a problem present because of the strong interaction between the graphene sheets (van der Waals force and π - π conjugate force). Graphene oxide (GO) as an important derivative of graphene possesses a large number of oxygen-containing functional groups [4]. It is the key to achieve its effective dispersion of GO in the polymer matrix by surface modification [5].

In this paper, polyetheramine functionalized graphene oxide (PEA-GO) was synthesized. PA6 fiber and PEA-GO/PA6 composite fibers by melt spinning with different PEA-GO contents were prepared, and their properties were studied. It is expected to provide a useful idea for the theoretical research and application of GO/PA6 composite fibers.

2 Experimental

2.1 Materials

Graphite powder (300 mesh), concentrated H₂SO₄, HCl, NaNO₃, K₂MnO₄, H₂O₂, ethanol, deionized water, polyetheramine (PEA, D2000), PA6 (spinning grade).

2.2 Synthesis of PEA-GO

Graphene oxide was firstly synthesized according to modified Hummers' method [6]. Next, the dispersed GO in

deionized water/ethanol (3:1) sonicated for 0.5h. The mixture of GO dispersion and a certain amount of PEA were added to a 250ml three-necked round bottomed flask. After stirring for 24h at 80°C, the black pieces were repeatedly washed using ethanol. The PEA-GO powders were obtained by drying at 80°C for 48h in vacuum.

2.3 Preparation of PEA-GO/PA6 composite fibers

Firstly, the PA6 pellets were placed in a vacuum oven at 100°C for 24h. Then, PA6 and PEA-GO/PA6 composite fibers (mass ratio of 100/0, 100/0.1, 100/0.3, 100/0.5, 100/1) were prepared by melt-spinning using a micromixer (HAAKE Mini Lab II). All fibers were melt-spun by heating to 250°C and under N₂ atmosphere to prevent degradation of PA6. At last, the melt-spun fibers were drawn at 4 times by heating to 120°C.

2.4 Characterization

PEA-GO was characterized by Fourier transform infrared spectroscopy analyzer from Nicolet, USA. The morphology of PA6 fiber and the PEA-GO/PA6 composite fibers were observed by field emission scanning electron microscope with a scanning voltage of 3KV, and the tensile strength and elongation at break of composite fibers are also characterized.

3 Result and discussion

3.1 FTIR of GO and PEA-GO

Fig. 1 shows the FTIR spectra of GO and A-GO. It can be seen that the broad peak at 1600 cm⁻¹ of GO are assigned to the C=C double bonds. The one at 1740 cm⁻¹ of GO are assigned to the C=O stretch of the carboxylic acid groups. The stretching vibration peaks of the carboxyl group and the epoxy group of GO at 1726 cm⁻¹ and 1227 cm⁻¹ disappeared, and new peaks were generated. The C-N stretching vibration and the N-H bending vibration occurred at 1103 cm⁻¹ and 1451 cm⁻¹, indicating that PEA and GO reacted. Since the epoxy group on GO undergoes a nucleophilic substitution reaction with the amino group of PEA and the amidation reaction of the carboxyl group with

the amino group, it was confirmed that PEA was successfully grafted onto GO.

3.2 SEM of PEA-GO/PA6 composite fibers

The surface and cross-section morphologies of PA6 and PEA-GO/PA6 are shown in Fig. 2. It is found that the surface morphology of PEA-GO/PA6 containing 0.1% PEA-GO is smooth with no obvious defects. Owing to the effect of successful surface modification by PEA, PEA-GO shows better dispersibility in the PA6 matrix.

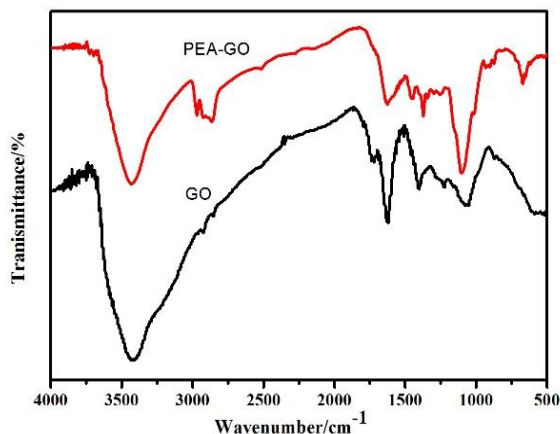


Fig.1 FTIR spectra of GO and PEA-GO

Moreover, there are many wrinkles in the cross section of 0.1%PEA-GO/PA6 composite fiber. The roughness of the cross section of the 0.1%PEA-GO/PA6 composite fiber is significantly higher than that of the pure PA6 fiber. The functionalized GO uniformly dispersed in the PA6 matrix greatly improves the interfacial adhesion between the filler and the matrix. The composite fiber exhibits a ductile fracture process that results in a rough cross-section. [7].

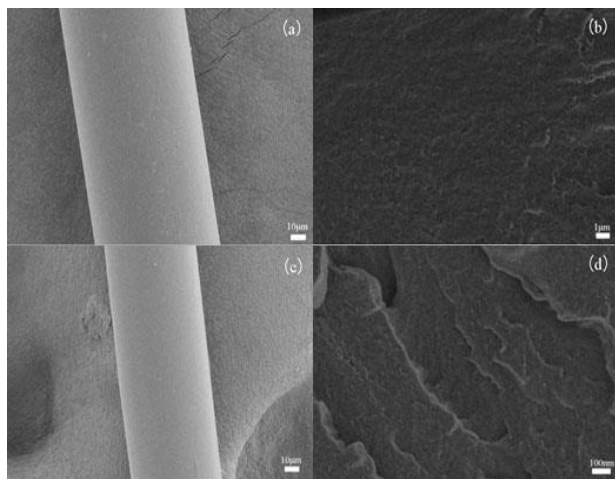


Fig.2 SEM images of surface structure and cross-sectional structure of pure PA6 fibers(a)(b) and 0.1wt%PEA-GO/PA6 composite fiber (c)(d)

3.3 Mechanical properties of PEA-GO/PA6 composite fibers

As shown in Fig. 3, the strength of the composite fiber with 0.1%PEA-GO content reaches to 3.5cN/dtex. Well-dispersed PEA-GO in the PA6 exhibits strong interfacial interactions between PEA-GO and PA6 substrate. The strong interfacial interactions allow the stress to be transferred to the functionalized graphene, thereby

effectively improving the mechanical property of composite fibers[8]. Increased crystallinity also increases the mechanical properties of the fiber. It is a promising method for preparing high strength GO/PA6 composite fibers.

4 Conclusion

The surface modification of GO was carried out by PEA, and the dispersion of PEA-GO in PA6 can be achieved

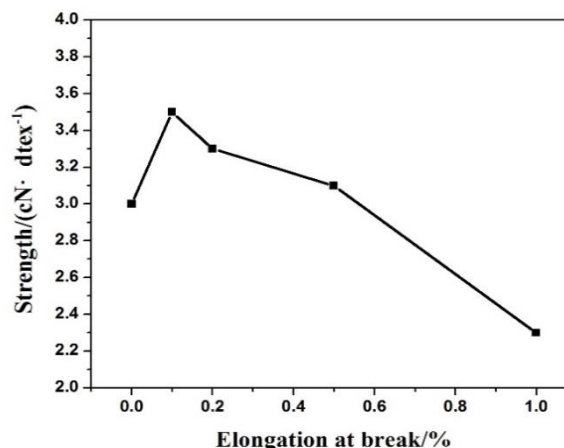


Fig.3 Tensile strength of PEA-GO/PA6 composite fibers with different loadings of graphene.

effectively. PA6 and PEA-GO/PA6 composite fibers were prepared by melt spinning. When the content of PEA-GO was only 0.1wt%, the tensile strength of the PEA-GO/PA6 composite fiber reached to 3.5cN/dtex.

References

- [1] Lim J G, Gupta B S, George W. The potential for high performance fiber from nylon 6[J]. Progress in Polymer Science, 1989, 14(6):763-809.
- [2] Geim A K, Novoselov K S. The rise of graphene[J]. Nature Materials, 2007, 6(3):183-91.
- [3] Geim A K. Graphene: Status and Prospects[J]. Science, 2009, 324(5934):1530-1534.
- [4] Dreyer D R, Park S, Bielawski C W, et al. The chemistry of graphene oxide[J]. Chemical Society Reviews, 2009, 39(1):228-240.
- [5] Young R J, Kinloch I A, Gong L, et al. The mechanics of graphene nanocomposites: A review[J]. Composites Science & Technology, 2012, 72(12):1459-1476.
- [6] Jiang Y L, Tian M, Yu Y H, et al. Preparation and Property of Reduced Graphene for Hummers[J]. Key Engineering Materials, 2014, 591:301-304.
- [7] Ramanathan T, Abdala A A, Stankovich S, et al. Functionalized graphene sheets for polymer nanocomposites[J]. Nature Nanotechnology, 2008, 3(6):327-331.
- [8] Xu Z, Gao C. In situ Polymerization Approach to Graphene-Reinforced Nylon-6 Composites[J]. Macromolecules, 2010, 43(16):6716-6723.

STRUCTURE AND PROPERTIES OF POLYETHER-ESTER ELASTOMERIC FIBERS PREPARED BY HIGH-SPEED MELT SPINNING AND IN-LINE DRAWING PROCESSES

Gaku Kanazawa, Wataru Takarada and Takeshi Kikutani

Department of Materials Science and Engineering, Tokyo Institute of Technology,
O-okayama, Meguro-ku, Tokyo, Japan, e-mail: kikutani.t.aa@m.titech.ac.jp

Abstract: Three types of polyether-ester elastomeric polymer with different hard-segment (HS) composition and different chain length of soft-segment (SS) were subjected to the high-speed melt spinning process and the in-line drawing process. In the high-speed melt spinning process, orientation-induced crystallization started to occur in the spinning-line from the take-up velocity of around 2 km/min. The polymer with lower HS composition showed lower crystallizability in the spinning process, and lower crystallinity of the as-spun fibers. The as-spun fibers exhibited lower tenacity and higher elongation at break. On the other hand, if the polymers with similar composition of the HS but different chain length of the SS are compared, the as-spun fibers from the polymer with lower molecular weight of SS showed significantly higher tensile modulus and slightly higher tenacity. Lower molecular weight of SS corresponds to the lower molar fraction of HS, however, crystallizability was not much affected. In-line drawing of the elastomeric polymer was performed setting the first godet roll speed to 1 or 2 km/min, and the in-line draw ratio up to 3 or 1.9 respectively. Simple elastomeric stretching was expected to occur in the drawing process, however, for the first godet roll speed of 2 km/min, elastic contraction of fibers after processing was higher than the expected value, indicating that structure formation at the first godet roll was incomplete. In comparison with the high-speed spun fibers with similar elongation at break, in-line drawn fibers showed higher tenacity and better elastic recoverability after applying high strain.

Keywords: orientation, crystallization, elastomeric recovery, tensile strength

1 INTRODUCTION

Elastomeric polymers are normally composed of soft segment (SS) and hard segment (HS). The SS with its glass transition temperature lower than room temperature is the origin of elastomeric properties, whereas the HS acts as the physical cross-linking point. Lower composition of the HS leads to the better elastomeric properties, however crystallizability of the polymer would be deteriorated. In this research, high-speed melt spinning was applied for the elastomeric polymers with the aim of utilizing the stress-induced crystallization to overcome the drawback of low crystallizability. In-line drawing was also applied for the further improvement of fiber properties.

2 EXPERIMENTAL

2.1 Materials

Three types of polyether-ester thermoplastic elastomers, TPE-A, B and C, were used in this research. The HS was composed of poly(butylene terephthalate) (PBT) while the SS was composed of poly(tetramethylene ether)glycol (PTMG). Weight fraction of the HS was similar for TPE-B and TPE-C, while that of TPE-A was lower. Molecular weight of the SS was similar for TPE-A and TPE-B, while that of TPE-C was about a half of the other two polymers.

2.2 Melt Spinning and In-line Drawing

High-speed melt spinning of the three types of polymer was performed with the extrusion temperature of 210 °C

and through-put rate of 3.0 g/min. Attainable maximum take-up velocities for TPE-A, B and C were 9, 6 and 8 km/min, respectively. During the spinning process, variation of fiber diameter along the spin-line was measured. In-line drawing was performed with the first roll speeds of 1 and 2 km/min, and in-line draw ratios of 1.5 – 3 and 1.3 – 1.9, respectively. After the melt spinning and in-line drawing, fibers wound up on the bobbin were cut to evaluate the elastic contraction.

2.3 Characterization

Structure of the prepared fibers was characterized through the wide-angle X-ray diffraction (WAXD) and small-angle X-ray scattering (SAXS) measurements. Mechanical properties of the as-spun fibers were evaluated through the tensile test, and recovery test.

3 RESULTS AND DISCUSSION

3.1 High-Speed Melt Spinning

Results of WAXD and SAXS measurements for selected as-spun fibers are shown in Fig.1. Crystalline reflections of oriented PBT started to appear in the WAXD patterns from around 2 km/min. The polymer with lower HS content (TPE-A) obviously showed lower crystallizability. Two-spot patterns were observed in the SAXS patterns for low-speed spun fibers, while meridional reflections gradually

widened along the azimuthal angle with the increase of take-up velocity. Widening of the reflection was more significant for TPE-A, and even the splitting of meridional reflection was observed. On the other hand, the polymer with shorter SS (TPE-C) obviously showed lower long period.

Variations of tensile modulus and tenacity of as-spun fibers with the increase of take-up velocity are shown in Fig. 2. Tensile modulus was strongly dependent on the type of polymer, and did not affected much by the take-up velocity. The polymer with short SS (TPE-C) showed the highest value while the polymer with the lowest HS content (TPE-A) showed the lowest value. Tenacity of the as-spun fibers gradually increased with the increase of take-up velocity. The higher HS content obviously lead to higher tenacity while shortening of the SS also resulted in the slight improvement of the tenacity.

3.2 In-line Drawing

Elastic contraction after the in-line drawing process of TPE-A with the first roll speeds of 1 and 2 km/min were plotted against the final take-up velocity in Fig. 3. The estimated elastic contraction assuming the pure elastic stretching in the drawing process are also shown for comparison. For the first roll speed of 1 km/min, estimated values matched well with the experimental results. On the other hand, for the first roll speed of 2 km/min, experimental results were significantly higher than the estimated values. This result may indicate that the fiber structure formation was not completed when the fiber passed through the first roll.

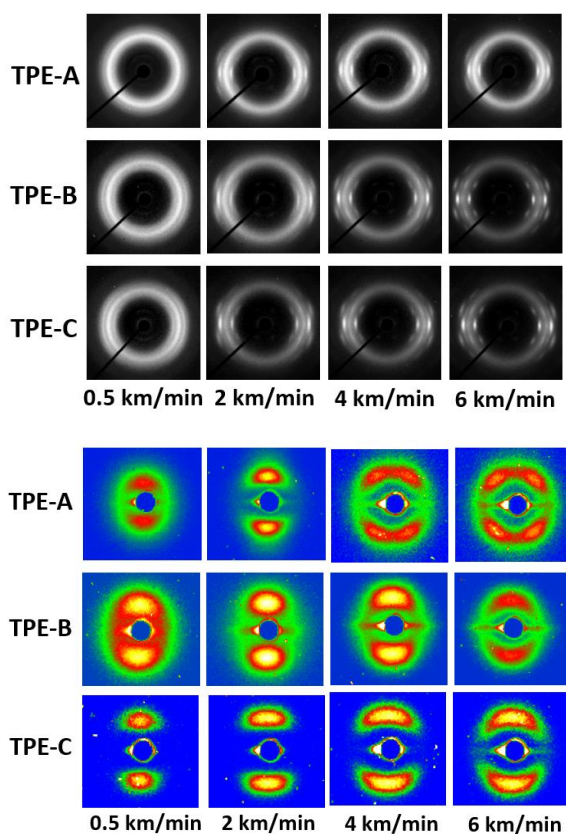


Figure 1 WAXD (Top) and SAXS (Bottom) patterns of high-speed spun polyether-ester elastomeric fibers of three types of polymer prepared at various take-up velocities.

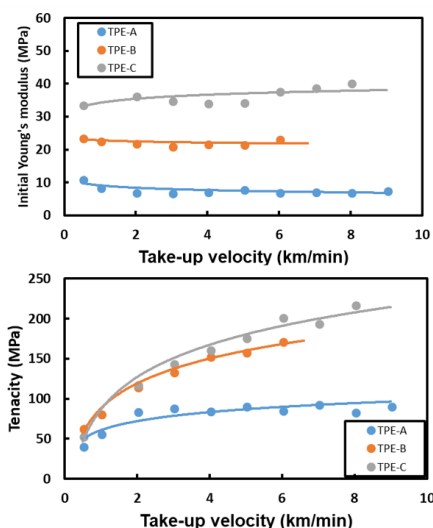


Figure 2 Tensile modulus and tenacity of high-speed spun polyether-ester elastomeric fibers of three types of polymer prepared at various take-up velocities.

Tenacity of the high-speed spun fibers and the in-line drawn fibers were plotted against elongation at break as shown in Fig. 4. Comparing the fibers with similar elongation, the in-line drawn fibers exhibited higher tenacity than the high-speed spun fibers. From the view point of structural difference, it was found that the meridional reflections in the SAXS pattern showed further splitting for the in-line drawn fibers.

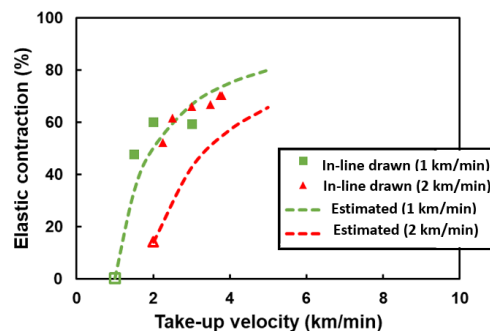


Figure 3 Elastic contraction of polyether-ester elastomeric fibers after in-line drawing at various draw ratios. Speeds of first godet roll are indicated. Dotted lines correspond to the estimated values with the assumption of pure elastic stretching in drawing process.

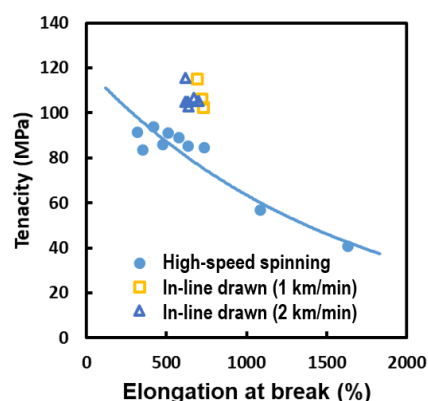


Figure 4 Tenacity versus elongation relationship for the polyether-ester elastomeric fibers prepared through high-speed melt spinning process and in-line drawing process.

INVESTIGATION OF CRYSTALLISATION AND DISORDER-TO-ORDER PHASE TRANSITION OF PLA BY WAXD TECHNIQUE AS A METHOD IN THE OPTIMIZATION OF FIBROUS MATERIALS FORMING PROCESSES

Michał Puchalski¹, Konrad Sulak², Grzegorz Szparaga¹, Izabella Krucińska¹

¹ Lodz University of Technology, Department of Material and Commodity Sciences and Textile Metrology, Żeromskiego 116, 90-924 Lodz Poland, e-mail: michal.puchalski@p.lodz.pl

² Institute of Biopolymers and Chemical Fibres, Marii Skłodowskiej-Curie 19/27 90-570, Lodz Poland,

Abstract: The influence of the molecular ordering and $\alpha' - \alpha$ form transition of PLA on the fibrous fabrics mechanical properties on the example of wet-spinning fibers, and spun-bonderd nonwovens is presented. Fibrous samples were investigated by wide-angle X-ray diffraction (WAXD) and tensile machine. The results are discussed in terms of the structural changes of the polylactide and the meso-phase content during the fibrous fabric forming process. The structural changes of the PLA explain the observed changes in the mechanical properties of the fibers and nonwovens obtained under different technological conditions.

Keywords: crystallization, WAXD, wet-spinning fibers, spun-bonderd nonwovens, mechanical propeties

1 INTRODUCTION

Poly(lactide) (PLA) is aliphatic polyester which can be synthesized from renewable source such as biomass. PLA, in comparison with conventional petroleum-based polymers, is environmental friendly biodegradable polymer and it has attracted increased attention in recent years. In the 90-ties in the United States a commercial production of polylactide was put on stream under the trade mark of NatureWorks™ [1]. The improved availability of polylactide opened new ways toward a wider application of the biodegradable polymer. The preparation, structure and properties of products made of polylactide are subject of intensive scientific and technological investigations.[2].

The properties of PLA fabrics depend strongly on stereochemical form of polylactide and its crystallization. Four crystal structures, α , α' , β , γ , exist in PLA depending on the crystallization conditions. From the fibrous materials forming processing view point, the most often observed is the α -form, which can be formed under conventional melt and solution crystallization conditions (crystallization temperature (T_c) > 120 °C)], what was reported for many years. The novel look at PLA crystallizations presented Pan et al. [3] and Zhang et al. [4] who reported that a disordered α' -form, of PLA could be crystalized below 120 °C, which showed similar helical chain conformation compared to α -form, but less compact packed and different mechanical properties. Additionally, the complex information about possibility of ordering PLA under tensile drawing and creation of mesophase and α' -crystals were presented by Stoclet et al. [5].

In this presentation, the influence of the molecular ordering and $\alpha' - \alpha$ form transition of PLA on the fibrous fabrics mechanical properties on the example of wet-spinning fibers [6], and spun-bonderd nonwovens [7] is presented. Fibrous samples were studied by wide-angle

X-ray diffraction (WAXD). Additionally, the physical and mechanical properties of the fibrous fabrics were determined. The structural changes of the PLA explain the observed changes in the physical and mechanical properties of the fibers and nonwovens obtained under different technological conditions.

2 MATERIALS AND METHODS

2.1 Polymer

Fibers and nonwovens were obtained from commercially available poly(L-lactide)s from Nature Works LLC (USA) Ingeo 6201D (1.2% of D-lactide, $M_w = 59100$ g/mol and $\bar{D} = 1.29$) and Ingeo 6251D (1.4% of D-lactide, $M_w = 75300$ g/mol and $\bar{D} = 1.55$) respectively.

2.2 Wet-spinning technology

The PLA fibers were prepared using a laboratory technological stand. The coagulation process was carried out in a bath containing a solution of ethanol and dichloromethane (90:10) at 10°C. The drawing process was performed in a water bath at 45°C using a godet system and carried out to obtain the maximum draw ratio.

2.3 Spun-bonderd method

The spun-bonderd nonwovens were prepared using a laboratory technological stand. The calender temperature was varied from 70°C to 110°C.

2.4 WAXD method

The supramolecular structures of the PLA materials were analysed by means of wide-angle X-ray diffractions method (WAXD) (PANalytical X'Pert Pro with Cu K α $\lambda=0.154$ nm X-ray source).

2.5 Physical properties measurements

The physical parameters of studied materials such as stress at break, mass per unit area and linear mass were analysed by according EU standards [8-11].

3 RESULTS

In the Figure 1 the example of X-ray diffraction profile of PLA deconvoluted on the crystalline peaks and amorphous halo by the WAXSFIT software [9] are presented. The results of numerical analysis of supramolecular structure such as values of crystallinity degree (X_c) and d-spacing (d_{hkl}) are presented for the fibers and nonwovens in Table 1 and Table 2 are presented respectively. In the Tables 1 and 2 the physical parameter of studied materials such as mass per unit area (M_P), linear mass (T_L) and stress at break (σ) are also presented.

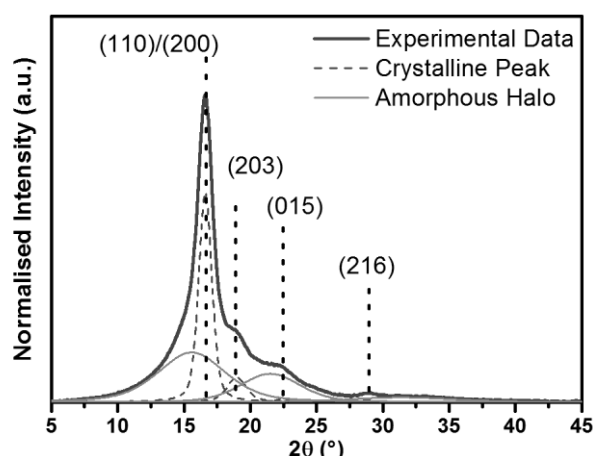


Figure 1 Example of X-ray diffraction profile of PLA after numerical analysis.

Table 1 Supramolecular structure and physical factors of PLA fibres formed at various total draw ratio.

Total draw ratio	X_c	$d_{(200)/(110)}$	Crystal-line form	T_L	σ
(%)	(%)	(nm)	-	(tex)	(cN/tex)
500	33.0	0.535	α'	96.0	18.2
550	33.6	0.536	α'	91.3	21.4
600	35.7	0.536	α'	85.3	26.0
650	35.6	0.531	α	68.3	24.8
700	36.5	0.529	α	60.3	23.2

Table 2 Supramolecular structure and physical factors of PLA nonwovens formed at various calendar temperature.

Calendar Temp.	X_c	$d_{(200)/(110)}$	Crystal-line form	M_P	σ
(°C)	(%)	(nm)	-	(g/m ²)	(N/g/m ²)
70	7.2	0.538	α'	49.4	1.07
80	32.3	0.538	α'	48.2	1.26
90	48.4	0.537	α'	50.1	1.52
100	51.1	0.533	α	51.1	1.11
110	51.3	0.532	α	51.3	0.69

4 CONCLUSIONS

A performed investigation of the structural changes of PLA fibrous materials under various technological parameters showed the major importance of disorder-to-order phase transition of PLA in the optimization of forming processes. The most important conclusions include the following:

- In the process of fiber wet spinning from the solution of semi-crystalline PLA, occur the total draw ratios disadvantageously affecting the fiber strength. Under these conditions, significant changes occur in the supramolecular structure, including the polymer crystallization to crystallographic form α .
- The structural changes proceeding in the polymer of nonwovens calendarized at temperatures over 90°C, and the disorder-to-order phase transition (α' to α form), observed by the WAXD technique, cause a considerable decrease in the tenacity of the nonwovens made.

ACKNOWLEDGEMENT: This research was partially funded by the European Regional Development Fund in the frame of a key project entitled "Biodegradable fibrous products" (acronym: Biogratex) No. POIG.01.03.01-00-007/08-09 and part of the work was funded by statutory activity by Lodz University of Technology, Department of Material and Commodity Sciences and Textile Metrology, Poland, No. 14-148-1-2117.

5 REFERENCES

- [1] Bilal MB, Viallier-Raynard P, Haidar B, Colombe G, Lallam A, Textile Research Journal 2011, 81, 838.
- [2] Krucińska I, Biodegradowalne wyroby włókniste, Wydawnictwo PŁ.: Łódź, 2014.
- [3] Pan P, Kai W, Zhu B, Dong T, Inoue Y, Macromolecules 2007, 40, 6898.
- [4] Zhang J, Tashiro K, Tsuji H, Domb AJ, Macromolecules 2008, 41, 1352.
- [5] Stoclet G, Seguela R, Vanmansart C, Rochas C, Lefebvre JM, Polymer 2012, 53, 519-5288.
- [6] Puchalski M, Sulak K, Chrzanowski M, Sztajnowski S, Krucińska I, Textile Research Journal 2015, 85, 535.
- [7] Puchalski M, Kwolek S, Szparaga G, Chrzanowski M, Krucińska I, Polymers 2017, 9, 18.
- [8] PN EN ISO 1973:1997: Textile fibres - Determination of linear density - Gravimetric method and vibroscope method.
- [9] PN EN ISO 2062:2010: Textiles - Yarns from packages - Determination of single-end breaking force and elongation at break using constant rate of extension (CRE) tester.
- [10] PN-EN ISO 9073-1:1989: Textiles - Test methods for nonwovens - Part 1: Determination of mass per unit area.
- [11] PN-EN ISO 9073 -3:1989: Textiles - Test methods for nonwovens - Part 3: Determination of tensile strength and elongation.
- [12] Rabiej M Journal of Applied Crystallography. 2013, 46, 1136–1144.

PREPARATION OF POLYLACTIDE FIBERS WITH HIGHLY-ORIENTED STEREO-COMPLEX CRYSTALS VIA HIGH-SPEED BICOMPONENT MELT SPINNING

Nanjanporn ROUNGPANISAN¹, Wataru TAKARADA¹ and Takeshi KIKUTANI¹

¹Department of Materials Science and Engineering, Tokyo Institute of Technology, O-okayama, Meguro-ku, Tokyo, Japan, e-mail: kikutani.t.aa@m.titech.ac.jp

Abstract: The aim of this research was to develop polylactide fibers consisting of highly oriented stereo-complex (SC) crystals of high melting temperature. The poly-L-lactide (PLLA) and poly-D-lactide (PDLA) with the optical purity higher than 99.5% and the MFR of 16 and 25, respectively, were used. Melt spinning of the blend of PLLA and PDLA was not possible because of its low viscosity. Melt-mixing of the high optical purity PLLA and PDLA requires high temperature because of the formation of SC crystals, and high mixing temperature causes thermal degradation of the polymer. Instead of this, bicomponent fibers of PLLA and PDLA with the cross-sectional configurations of the core-sheath (C-S) and the islands-in-the-sea (I-S) were prepared through the bicomponent melt spinning process. Spinnability of these fibers was good, and the maximum take-up velocities of 10 km/min for the C-S and 7 or 9 km/min for the I-S fibers could be attained at the extrusion temperatures of 230 and 250 °C, respectively. When the take-up velocity was higher than 5 km/min, development of highly oriented α -form crystals was observed in the WAXD patterns of both C-S and I-S fibers. Birefringence measurement of the C-S fibers of high take-up velocities revealed that the orientation of the PLLA in the sheath was high while that of the PDLA in the core was low. When the C-S and the I-S fibers of high take-up velocities were annealed at 120 °C for 1 hour, only highly oriented α -form crystal was formed in the C-S fibers, while a small amount of the SC crystals was found to be formed for the I-S fibers. In the cross-section of the C-S fibers, distinct increase of birefringence took place for the core part. When the annealing temperature was raised to 190 °C, i.e. higher than the melting temperature of the α -form crystal, the high-speed spun C-S fibers could not maintain their shapes, while the I-S fibers exhibited either slight shrinkage or elongation depending on the take-up velocity but maintained their shapes. For the I-S fibers of high take-up velocities, surprisingly, the WAXD pattern changed from the highly oriented α -form crystals to highly oriented SC crystals with the increase of annealing period. These results suggested that the mutual diffusion of the PLLA and PDLA molecules proceeded to form the SC crystals in the cross-section of the I-S fibers.

Keywords: polylactides, high-speed melt spinning, islands-in-the-sea fibers, Stereocomplex crystals

1 INTRODUCTION

Bicomponent high-speed melt spinning is a choice for producing fibers of particular properties, which depends on various factors such as intrinsic properties of polymers, and controlled processing conditions [1], [2]. Core-sheath (C-S) and islands-in-the-sea (I-S) cross-sectional configurations can be adopted for expanding applications. It has been reported that fiber formation behavior for the I-S fiber shows the die-swelling higher than that of the C-S fiber because of higher interfacial area [3].

It is known that mixing of two enantiomeric polymers of poly-L-lactide (PLLA) and poly-D-lactide (PDLA) leads to the generation of stereo-complex (SC) crystals with improved thermal properties. Nevertheless, crystal form in the blend changes between α -form to SC crystals, and the amount of SC crystals can be controlled through the processing techniques and operation conditions [4]–[6]. For the formation of the SC crystals, generally pre-melt-mixing of PDLA and PLLA needs to be carried out. In this study, preparation of the PLLA+PDLA as-spun fibers was conducted through the high speed melt spinning of the 50:50 blend as well as through the bicomponent spinning with the C-S and I-S configurations. The obtained fibers were subjected to the subsequent annealing process in order to investigate the effect of heat treatment conditions on the formation of crystalline structure.

2 EXPERIMENTAL

Three types of polylactide, i.e. PLLA, PDLA and the PLLA+PDLA (50:50) blend were used in this study. The PLLA and PDLA have the high optical purity of >99.5% and the melt-flow rate of 16 and 25 g/10 min, respectively. In the melt spinning process, extrusion temperatures of 230 and 250 °C was adopted. For the blend mass flow rate was set to 5.0 g/min, whereas that for the C-S (PDLA-PLLA) and I-S (PDLA-PLLA) bicomponent spinning was 2.5:2.5 g/min. The attained highest take-up velocities are summarized in Table 1. Melt spinning of the blend was not possible because of its low viscosity. After the spinning, C-S and I-S fibers were annealed at 120 or 190°C. Investigation of fiber structure was carried out by optical microscope (OM) and wide-angle X-ray diffraction (WAXD) measurements.

Table 1 Attained highest take-up velocity

Samples condition	blend T230	blend T250	I-S T230	I-S T250	C-S T230	C-S T250
Take-up velocity (Km/min)	-	-	7	9	10	10

3 RESULTS AND DISCUSSION

Observation of all free-fall bicomponent fibers under an optical microscope revealed that only in the case of I-S fibers, boundary separating the two components could be observed, whereas the boundary between the core and sheath could not be distinguished in the C-S fibers as shown in Fig.1. Normally, if there was no application of elongational stress, both polymer phases were probably in an amorphous state. In this case, it would be rather hard to see the difference between the two components as was seen for the C-S fiber. For the I-S fiber, because total interfacial area in the I-S fiber was higher than that of the C-S fiber, mutual interaction of the two components may become more influential either for the crystallization behavior or molecular orientation development [2], [3]. Development of crystalline structure was investigated through the WAXD measurement as shown in Fig.2. Result for the as-spun fibers (No-annealing) showed that both C-S and I-S fibers obtained at the take-up velocity of 1 km/min were in an amorphous state while the 6 km/min fibers showed highly oriented crystalline diffractions only from α -form crystals. The diffraction patterns were still covered with relatively strong amorphous halo.

After the annealing of the fibers at 120 °C for 1 hour, crystallization of all fibers was promoted as can be seen from the lower intensity of amorphous halo and higher intensity of ordered crystalline reflections. It was notable that a small amount of the SC crystals was formed in the I-S fibers obtained at 6 km/min.

Annealing at 190 °C was successful only for the I-S fiber while the C-S fiber was melted. This result suggested that mutual diffusion of the PLLA and PDLA molecules at the boundary was limited for the C-S configuration and most of crystalline structure consisted of α -form crystal which has melting temperature of about 170–180 °C. This is the reason for the melting of the fiber at 190 °C. On the other hand, for the I-S fibers, both 1 and 6 km/min fibers maintained their shape after the annealing at 190 °C, and crystalline structure with low oriented or highly oriented SC crystals were developed, respectively, most probably because of the enhanced mutual diffusion of the PLLA and PDLA molecules through the interface of large area. For the 1 km/min fiber, the annealing process proceeded starting from the amorphous state, which may cause orientation relaxation as well as a slight shrinkage and mutual adhesion of fibers during the melting-recrystallization processes.

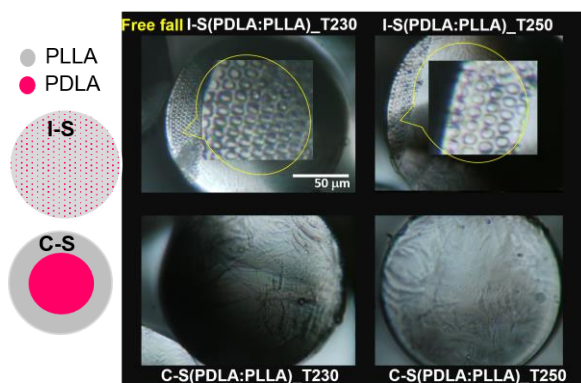


Figure 1 Cross-sectional view of PDLA/PLLA bicomponent fibers captured under optical microscope. Top and bottom pictures are I-S and C-S free fall fibers prepared at the spinning temperatures of 230 and 250 °C.

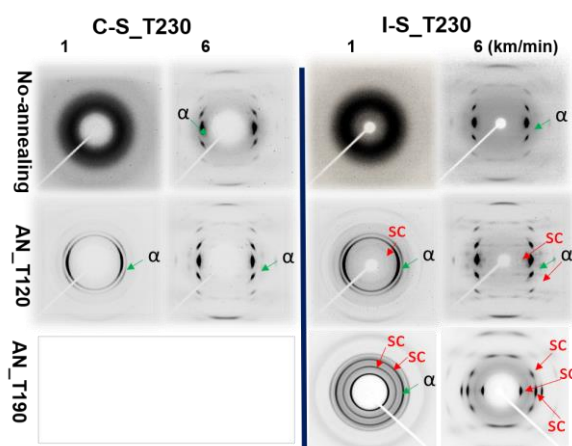


Figure 2 WAXD patterns of C-S and I-S fibers prepared at 230 °C and take-up velocities at 1 and 6 km/min. Results for as-spun fibers and fibers annealed at 120 and 190 °C for 1 h are compared.

For the fibers prepared at 6 km/min, as can be seen in Fig.2, significant amount of highly oriented SC crystals was formed. It can be said that increase of interfacial area was necessary for the enhancement of inter-diffusion of PLLA and PDLA molecules, which caused the stability of fiber shape during the annealing process with phase transformation from the α -form to the SC crystals of high melting temperature.

Acknowledgement: We would like to express our sincere gratitude to Corbion for supporting our research.

4 REFERENCES

- [1] Dasdemir M., Maze B., et al.: Influence of polymer type, composition, and interface on the structural and mechanical properties of core/sheath type bicomponent nonwoven fibers. *J. Mater. Sci* 2013, pp. 5955–596
- [2] Radhakrishnan J., Kikutani T., Okui N., et al.: High-speed melt spinning of sheath-core bicomponent polyester fibers: high and low molecular weight poly(ethylene terephthalate) system. *Text. Res. J* 1997, pp. 684–693.
- [3] Chen Y., Takarada W., Kikutani T., et al. Effect of cross-sectional configuration on fiber formation behavior in the vicinity of spinning nozzle in bicomponent melt spinning process. *J. Fiber Sci. Technol* 2016, pp. 154–159.
- [4] Takasaki M., Ito H., Kikutani T., et al. Development of stereocomplex crystal of polylactide in high-speed melt spinning and subsequent drawing and annealing processes. *J. Macromol. Sci. Part B* 2003, pp. 403–420.
- [5] Masaki D., Fukui Y., Toyohara K., Ikegame M., Nagasaka B., Yamane H. Stereocomplex formation in the poly(L-lactic acid)/poly(D-lactic acid) melt blends and the melt spun fibers. *Fiber* 2008, pp. 212–219.
- [6] Tsuji T., Fukui I., et al. Enhanced thermal stability of poly(lactide)s in the melt by enantiomeric polymer blending. *Polymer* 2003, pp. 2891–2896.

MECHANICAL PROPERTIES AND STRUCTURE OF POLY(GLYCOLIC ACID) FIBERS IMPROVED THROUGH CONTROL OF MOLECULAR ENTANGLEMENTS IN MELT SPINNING PROCESS

Kotaku Saigusa¹, Wataru Takarada¹ and Takeshi Kikutani¹

¹ Department of Materials Science and Engineering, School of Materials and Chemical Technology, Tokyo Institute of Technology, S8-32, 2-12-1, Ookayama, Meguro-ku, Tokyo 152-8550, Japan, e-mail: k-saigusa@kureha.co.jp

Abstract: We installed a heating chamber in the vicinity of the spinning head to reduce the Deborah number in the spin-line to improve the mechanical properties of poly(glycolic acid) (PGA) fibers based on the concept of "melt structure control". As a result, we accomplished the improvement of the toughness of the as-spun fibers, and we could obtain the drawn fibers of high-strength and high toughness. Through the analysis on the state of molecular entanglement of as-spun fibers based on the concept of network draw ratio and entanglement density, the entanglement density in the as-spun fibers was found to increase by installing a heating chamber. However, when the as-spun PGA fiber with different take-up velocities were drawn to various draw ratios, mechanical properties of the drawn fibers showed different characteristics depending on the take-up velocity of the as-spun fibers. Accordingly, when we analyzed the network draw ratio of the drawn fibers, the master curves of drawn fibers prepared from the as-spun fibers of different take-up velocities could not be superposed each other. This result suggested that the as-spun fibers of different take-up velocities had different intrinsic network structure. The fibers prepared from the as-spun fibers of lower take-up velocities showed higher mechanical properties. Consequently, it was concluded that the reduction of Deborah number by producing as-spun fibers at lower take-up velocities also resulted in the improvement of mechanical characteristics of PGA fibers.

Keywords: Biodegradable polymer, Poly(glycolic acid) fiber, molecular entanglement

1 INTRODUCTION

Poly(glycolic acid), PGA, is a biodegradable aliphatic polyester with the simplest chemical structure. Because of its excellent biodegradability, PGA has been applied for biomedical applications such as surgical suture. Additionally, PGA shows good mechanical properties in comparison with poly(lactic acid), which has similar chemical structure with PGA. One of the disadvantages of the PGA, however, is a narrow window of processing conditions. This problem makes it difficult to produce high-strength fibers. Generally, fibers of good mechanical properties are produced through the drawing of as-spun fibers of low molecular orientation. For PGA fibers, even though the take-up velocity was kept at a low level, maximum draw ratio of the as-spun fibers was limited and achievable mechanical properties was also limited. In a previous study of developing high-strength poly(ethylene terephthalate) (PET) fibers, we introduced the concept of "melt structure control" [1]. Control of the state of molecular entanglement is the more concrete description for the melt structure control, which might be accomplished through the change of the flow behavior of polymer melt in the melt spinning process. By drawing the obtained as-spun fibers, we could produce high-strength PET fibers. We speculated that the reduction of Deborah number lead to the formation of fibers of high mechanical properties because formation of the highly homogeneous state of molecular entanglement could be achieved. In this study, we tried to improve the mechanical properties of PGA fibers based on the concept of "melt structure control". To accomplish this objective, we installed a heating chamber in the vicinity of a spinning head to reduce the Deborah number in the spin-line. Moreover, we analyzed the network draw ratio and entanglement density of the as-spun fibers to verify the concept of controlling the state of molecular entanglement.

2 EXPERIMENTAL

2.1 Sample Preparation

We prepared PGA fibers through the spin-draw method. The PGA pellets were melted using an extruder and extruded at 245 °C using a gear pump. The spinneret had 24 holes of 0.25 mm diameter. The through-put rate per hole was set to 0.29 g/min. A heating chamber was installed in the vicinity of the spinning head. Temperature of the chamber was kept at 120 °C. Take-up velocity was changed from 100 to 1,500 m/min. In the in-line drawing process, temperature of the rollers was kept at 65 °C, speed of the first roller was set at 150 or 300 m/min, and the draw ratio was varied from 2.5 to 6.0 times.

2.2 Tensile testing

Tensile strength and elongation at break of PGA fibers were evaluated with a tensile testing machine (Orientec Tensilon RTC-1210A) at the strain-rate of 100 %/min. The gage length for PGA fibers was 100 mm.

2.3 Measurement of the Network Draw Ratio and entanglement density

To obtain information regarding the state of molecular entanglement, network draw ratio and entanglement density were analyzed according to the method proposed by Ward [2]. For the estimation of the network draw ratio (eq.1-3), the true-stress vs true-strain curves of the fibers were shifted along the true-strain axis to match the curves each other. The amount of shift (γ_s) with respect to the fiber of no orientation corresponds to the network

draw ratio. In this theory, the reference fiber needs to be an amorphous fiber of no orientation. Instead of this, the as-spun fiber of the lowest take-up velocity was selected as the reference fiber. Network draw ratio of the reference fiber was estimated from the thermal shrinkage.

$$\lambda_s = 1 / (1-S) \quad (1)$$

$$\lambda_{rel} = \exp(\gamma_s) \quad (2)$$

$$\lambda_{net} = \lambda_{rel} \lambda_s \quad (3)$$

λ_{net} : Network draw ratio, λ_{rel} : Relative network draw ratio,

λ_s : Network draw ratio of reference fiber,

S : Thermal shrinkage, γ_s : True strain shift for matching

Once the network draw ratio is known, the network density can be estimated by measuring the shrinkage stress. The classical rubber elasticity theory was applied for the estimation of the entanglement density (eq.4).

$$\sigma = NKT (\lambda_{net}^2 - \lambda_{net}^{-1}) \quad (4)$$

σ : Peak shrinkage stress, N : Entanglement density, K : Boltzmann constant, T : Absolute temperature

3 RESULTS AND DISCUSSION

Figure 1 shows the relation between elongation at break and tensile strength. In general, tensile strength of fibers increases with increasing take-up velocity whereas elongation at break decreases. With the use of the heating chamber, this relation shifted to the upper right direction. This result means that the toughness of the as-spun fiber was improved through the installation of the heating chamber.

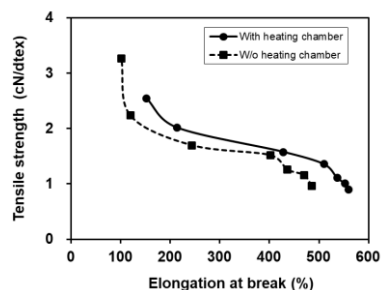


Figure 1 Relationship between elongation at break and tensile strength

Figure 2 shows the correlation between network draw ratio and heat shrinkage stress. From the linear relation, the entanglement density was estimated based on the rubber elasticity theory. The entanglement density in the as-spun fibers was found to increase by installing a heating chamber.

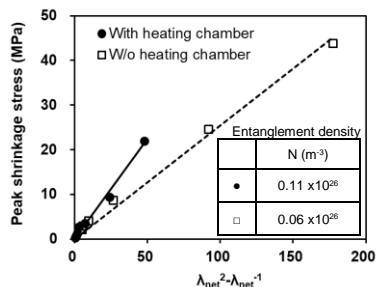


Figure 2 Correlation between network draw ratio and heat shrinkage stress. Estimated entanglement densities are shown. Figure 3 shows the mechanical properties of drawn fibers. Tensile strength of the drawn fibers prepared with the heating chamber was improved. This result may suggest that the formation of highly homogeneous state of

molecular entanglement of the as-spun fiber resulted in the improvement of the essential mechanical characteristics of the PGA fibers.

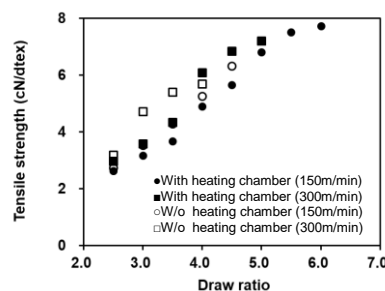


Figure 3 Mechanical properties of PGA drawn fibers produced from as-spun fibers of two different take-up velocities prepared with or without installing the heating chamber

In the analysis of the network draw ratio, polymers were assumed to have the same intrinsic network structure, and the affine deformation of the network was assumed to occur with the stretching. However, when the as-spun PGA fiber with different take-up velocities were drawn to various draw ratios, mechanical properties of the drawn fibers showed different characteristics depending on the take-up velocity of the as-spun fibers (Figure 3). Accordingly, when we analyzed the network draw ratio of the drawn fibers, the master curves of drawn fibers prepared from the as-spun fibers of different take-up velocities could not be superposed each other (Figure 4). This result suggested that the as-spun fibers of different take-up velocities had different intrinsic network structure. Comparing those master curves, it was found that the starting point of the strain hardening shifted to lower strain for the drawn fibers prepared from the as-spun fibers of lower take-up velocities. Those fibers showed higher mechanical properties, suggesting that the change in the entanglement structure also occurred by preparing the as-spun fibers at different take-up velocities. Consequently, it was concluded that the reduction of Deborah number by producing as-spun fibers at lower take-up velocities also resulted in the improvement of mechanical characteristics of PGA fibers.

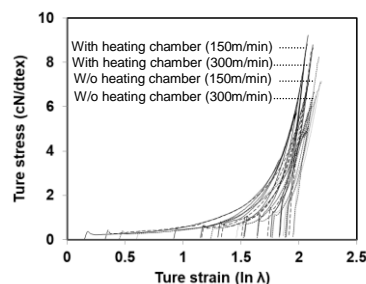


Figure 4 Comparison of master curves of drawn fibers produced from the as-spun fibers of two different take-up velocities prepared with or without installing the heating chamber

4 REFERENCES

- [1] M. Masuda, W. Takarada, and T. Kikutani, *Int. Polym. Process.*, Vol. 25, No. 2, pp. 159-169(2010).
- [2] S. D. Long and I. M. Ward, *J. Appl. Polym. Sci.*, 42, 1921 (1991).

COMBINATION OF KNOWN FIBROUS TECHNIQUES TO FORM A SUITABLE MATERIAL FOR SORBENT SUPPORT

Ivan Ulman¹, Radek Jirkovec², Jiří Chvojka³

¹ Department of Nonwovens and Nanofibrous Materials, Technical university of Liberec, e-mail: ivan.ulman@tul.cz

² Department of Nonwovens and Nanofibrous Materials, Technical university of Liberec, e-mail: radek.jirkovec@tul.cz

³ Department of Nonwovens and Nanofibrous Materials, Technical university of Liberec, e-mail: jiri.chvojka@tul.cz

Abstract: Article deals with design and production of composite material with the incorporation of sorbent-activated carbon, which is sputtered on nonwoven material. The final product is then composed of several layers - spunbond, nonwoven textile with activated carbon and nanofibers produced by AC spinning technology. It mainly deals with the design of layers, the method how to incorporate activated carbon and the bonding of finished composites. The finished material is finally subjected to several tests, such as breathability, vapor permeability, decrease of activated carbon particles and penetration of chemical warfare agents. The resulting material is compared with FOP-96 military clothing. The final product should serve as a protective layer for military purposes.

Keywords: army clothing, AC spinning, activated carbon, CBRN – Chemical, biological, radiological and nuclear defense

1 INTRODUCTION

The aim was to produce suitable composite layers for incorporation of sorbent for filtration purposes. The final layers are made of needle-punched carded fabric with incorporated particles of activated carbon as a sorbent. The functional layer is provided with nanofibers against the release of activated carbon particles and protected with carded and spunbond textiles. The composite material was primarily designed to replace current military clothing used in combat situations where chemical warfare agents are used.

2 MATERIALS AND BONDING METHODS

2.1 Combination of available fibrous materials

With the effort to create a suitable layer for sorbents, prepared fabrics were logically layered, used materials are described in Table 1. For composed materials was necessary to find a compromise between its size, possible application of sorbent and preservation of its functionality after application of the sorbent. Other requirements for the resulting composite are: preservation of textile properties as a vapor permeability, windproof properties and achieving suitable properties for wearing comfort.

Table 1 Used materials

Technology	Basic weight	Material
Spunbond -SB	16 g/m ²	Polyetylen/Polypropylen
Needle punched carded textile - NP	80 g/m ²	Polyester
Meltblown - MB	150 g/m ²	Polypropylen
Struto - SNP	220 g/m ²	Polypropylen
Nanofibers	50 g/m ²	Polyvinyl butyral

Materials were not only layered but after composition was samples also bonded by laminating into one composite material. As a best composite material showed up a sample composed in this sequence: SB, NP, MB, NP, MB, NP, SB. Later meltblown layers were replaced with

nanofibers which were made by alternating current spinning (AC spinning).

2.2 Bonding

Lamination served good until meltblown was replaced with nanofibers. During lamination were nanofibers melted into nonproof layer. In attempts to bond composite layers by ultrasound, it was found that the cover spunbond layer (PE / PP) did not bond with the carded fibers (PES), which was also true for bonding by lamination.

Hot-melt bonding is a fast type of joining textiles by adding of polymer glue. Thus, a partial step was to apply the polymer to the textile layer on which another layer was manually added. By laminating and applying the polymer adhesive on each layer, the entire sample was formed. Sewing was next but not last type of bonding of samples. After penetration of the needle through the material, holes larger than the thread itself are formed and reduce the functionality of the layer, thus increasing the possibility of passage of chemical warfare agents. Here is the solution by ultrasound bonding. By sewing with a suitable yarn, it is possible to continue bonding the material with ultrasound, when the yarn melts and the holes are sealed, Figure 1.

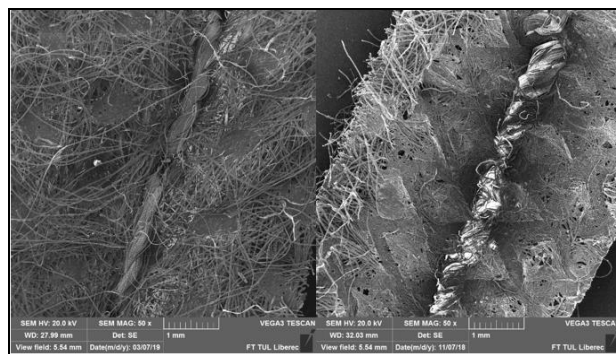


Figure 1 The structure of the sewn joint before and after bonding by ultrasound

3 TESTING OF PREPARED SAMPLES

Samples were tested for wearing comfort such as vapor permeability, wind proof and loss of particles, and were also tested for resistance to chemical warfare agents. For testing were used three samples named by type of their bonding – Ultrasound, Laminated and Hot-melt. Samples also were compared with military clothing (type FOP-96) normally used for combat situations where chemical warfare agents are used.

3.1 Vapor permeability

Vapor permeability is important property of textile material for wearing comfort. The vapor-permeable material is able to remove sweat from the body surface and prolong comfort wearing time. Results are shown in Figure 2. Blind samples were testing without activated carbon particles.

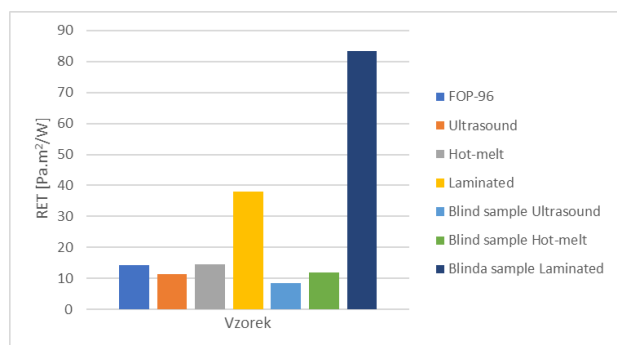


Figure 2 The measured vapor permeability values of the samples

Higher is not better. As can be seen, the Laminated is vapor nonpermeable, and therefore would be very unsuitable for use in the garment industry. Better results are achieved by the Hot-melt sample, which with its RET value, approaches the FOP-96 sample, but it is still higher. The Ultrasound sample, which is even a few units lower by RET, is best used to measure vapor permeability, providing better comfort properties. When comparing results With Table 2, it can be seen that the ultrasound sample even falls into a better class than the FOP-96.

Table 2 Evaluation of vapor permeability in terms of both RET and MVTR

Ret [Pa.m ² /W]	Verbal evaluation	MVTR [g/m ² x 24 hours]
6 and less	Very good	more than 20 000
6 - 13	Good	9 000 - 15 000
13 - 20	Satisfying	5 000 – 9 000
20 and more	Unsatisfying	under 5 000

3.2 Resistance of samples against chemical warfare agents

The evaluation of the resistance of samples is based on the standard ČSN EN 16523-1 and 16523-2. The evaluation criterion is the permeation rate $F = 1 \mu\text{g}/\text{cm}^2/\text{min}$. In the case of chemical warfare agents, the lower permeation rate $F = 0.1 \mu\text{g}/\text{cm}^2/\text{min}$ may also be used as a criterion. The current standards EN 16523-1/2 report the primary permeation rate $F = 1 \mu\text{g}/\text{cm}^2/\text{min}$ [1,2]. Some other standards, such as ASTM F739, operate at $0.1 \mu\text{g}/\text{cm}^2/\text{min}$ [3].

- Yperit permeation - The graph of Figure 3 describes the process of testing the resistance of samples to penetration mustard gas. The mustard gas penetration for the Hot-melt sample was measured in 398 minutes, for ultrasound sample at 480 minutes

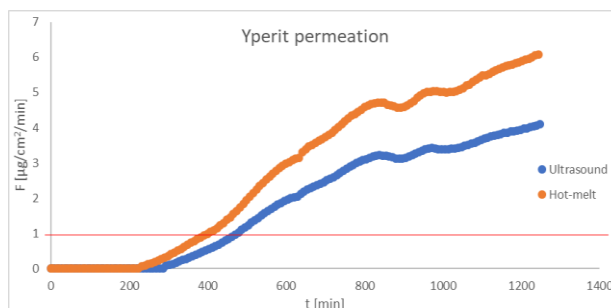


Figure 3 Yperit permeation

- Dimethylmethylphosphonate (DMMP) permeation - because of their similar form of volatility and water solubility, they are used as non-toxic substitutes for soman or sarin, which are highly toxic substances, for testing materials. The process of testing the resistance of samples is described of Figure 4. The DMMP penetration for the Hot-melt sample was measured in 198 minutes, for Ultrasound sample at 281 minutes

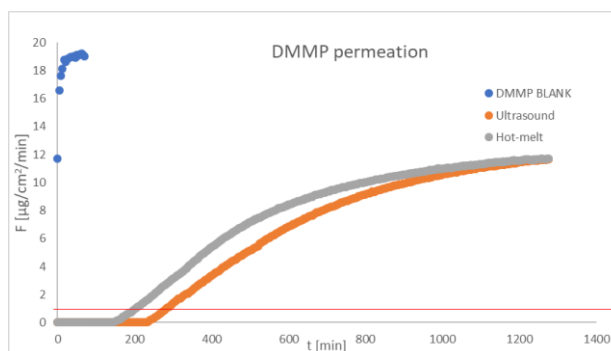


Figure 4 DMMP permeation

As it shown in the graphs, the Ultrasound and Hot-melt samples are able to withstand chemical warfare agents for a long time. During testing for real Soman it was over 15 hours for sample Hot-melt and over 25 hours for sample Ultrasound.

4 REFERENCES

- ČSN EN 16523-1. Determination of resistance to chemical permeation of material - Part 1: Permeation of gaseous chemicals under permanent contact conditions Czech Standards Institute, 2015.
- ČSN EN 16523-2. Determination of resistance to chemical permeation of material - Part 2: Permeation of liquid chemical under permanent contact conditions. Czech Standards Institute, 2015.
- ASTM F739. Standard Test Method for Permeation of Liquids and Gases through Protective Clothing Materials under Conditions of Continuous Contact. American National Standards Institute, 2012.

A NEW METHOD FOR MEASURING FIBER LENGTH

Fumei Wang^{1,2} and Meiqin Wu^{1,2}

¹College of Textiles, Donghua University, Shanghai, China 201620, e-mail: wfumei@dhu.edu.cn

²Key Laboratory of Textile Science & Technology, Ministry of Education, China, e-mail: feiyang082@126.com

Abstract: Three current instruments for measuring cotton and wool fiber length are briefly analyzed, and their advantages and disadvantages are pointed out. Then, the new image instrument for fiber length measurement was introduced, and its testing principle was presented. Finally, the advantages and challenges of this new instrument were summarized.

Keywords: fiber length, image method, dual-beard, cotton, wool

1 INTRODUCTION

1.1 Existing instruments for measuring cotton length

HVI system is High Volume Instrument, whose length module was originated from the traditional fibrograph, in which fibers in the outside of the holes are held by a row of needles, and floating fibers were combed, the random-beard was scanned by a light slit to generate fibrograms. HVI mainly provides average length, the "Short Fiber Index" (SFI) and of HVI is a predicted parameters. AFIS is Advanced Fiber Information System, which can quickly measure the lengths of individual fiber, fibers were opening and fly through the photoelectric sensor by a high-speed air flow.

1.2 Existing instruments for wool

In case of Almeter100, the fiber beard with one end in a line must be made by a Special machine. Then this beard passes through the capacitive sensor at a certain speed, the sensor transfer the fiber mass on every cross-section along the fiber beard into electric signals. Finally, the fiber length distribution curve (Fibrogram) and related parameters can be calculated.

In case of OFDA 4000, the number of fibers in the cross-section along the fiber beard can be counted every 5 mm, based on the CCD and microscopic and image analysis technique. And several beards have to be measured in order to have 4000 total fiber numbers.

2 OUR NEW METHOD FOR FIBER LENGTH MEASUREMENT

2.1 Sample preparation for cotton

Our new method is called Random-beard Image Method. The first step is making sample which is a random-beard. For cotton, the sample was drawing three times by this device to make a sliver in which fibers are arranged parallel and randomly.

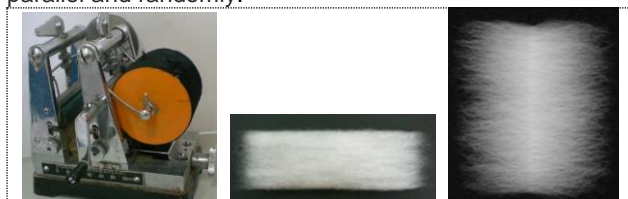


Figure 1 cotton sample making

Then, the sliver was randomly clamped, and the floating fibers on both sides of the clamping line were combed away, a dual-beard specimen was completed.

2.2 Sample preparation for wool

It is similar to that in cotton, the only difference is the length of random-beard.



Figure 2 wool sample making

2.3 random-beard image method

Our instrument mainly consists of two parts, the one is Photoelectric detecting device, another is a computer which do signal processing.

The grayscale image was obtained (256 shades in a resolution of 1000ppi) by our Photoelectric detecting device, in which the light is transmitted through the specimen.

Then, the linear density curve of random-beard was calculated according to the image, and the fiber length distribution was analyzed according to the linear density

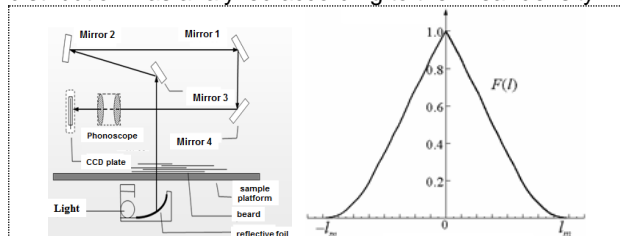


Figure 3 (a) Photoelectric detecting device (b) linear density curve of random-beard

2.4 Calculation equation for mass distribution of random-beard

We have derived the calculation equation for the mass distribution of random-beard.

$$W_r = \frac{W}{W_{\max}} = \frac{f_w X}{f_w X_{\max}} = \frac{\ln\left(\frac{1-R_{\infty}^2 + \sqrt{(1-R_{\infty}^2)^2 + 4T^2 R_{\infty}^2}}{2T}\right)}{\ln\left(\frac{1-R_{\infty}^2 + \sqrt{(1-R_{\infty}^2)^2 + 4T_{\max}^2 R_{\infty}^2}}{2T_{\max}}\right)} \quad (1)$$

Here $W_r(y, z)$ is the relative density for any point (y, z) of random-beard. $T(y, z)$ is the image gray level. R_{∞} is an optical parameters of fibers, the reflection rate of the infinite layers.

2.5 Analysis of fiber length distribution

The relationship between the fiber length distribution & linear density curve of random-beard.

$$p_w(l) = lF''(l). \quad (2)$$

3 COMPARING WITH EXISTING METHODS

3.1 Comparing with single fiber measuring method

Single fiber measurement is a basic method, in China there is a standard GB/T 16257-2008. Figures show very good agreement between our new method and the standard.

3.2 Comparing with HVI and AFIS system in case of cotton

The mean lengths of three methods are very close to each other. The difference of three methods may be due to random error and different measuring specimens. The square of correlation coefficient was between our new method and AFIS, and between our new method and HVI. The modal lengths of our new method are so close to AFIS's, the new method is agreed well with AFIS's of the two methods was 0.8316.

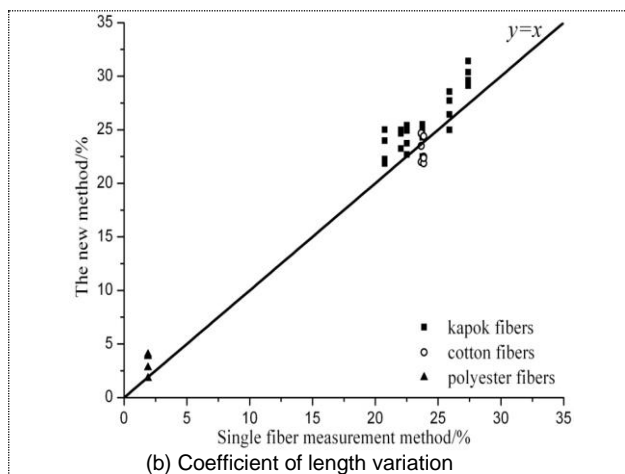
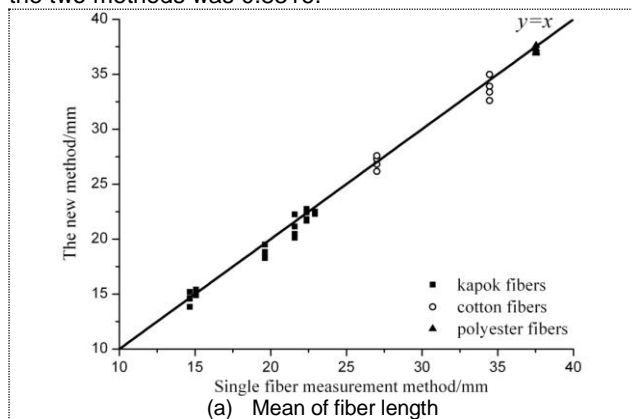


Figure 4 Photoelectric detecting device linear density curve of random-beard

3.3 Compared with Almeter 100 in case of wool

Barbe Length is weight mean length. Hauteur Length is numerical mean length. Parameter of our new method is close to that in Almeters. Variation coefficient of our new method is agreed with that in Almeter.

4 ADVANTAGES OF OUR NEW METHOD

a) Best representative sample.

Dual-beard includes all fiber length information.

b) Sufficient fiber length distribution information.

Enough parameters for characterizing fiber length distribution, include Mean length, Modal length, Quality length, Coefficient of variation and short fiber contents, while the HVI can not do this.

c) High precision

Based on fiber assemblies' optical quality distribution algorithm and the advanced photo-electronic and digital imaging hardware, the precision of our new instrument is higher than the existing equipments.

5 REFERENCES

- [1] KUBELKA P. New contributions to the optics of intensely light-scattering materials. Part I [J]. Josa, 1948, 38(5): 448-457.
- [2] DZIMBEG-MALCIC V, BARBARIC-MIKOCEVIC Z, ITRIC K. Kubelka-Munk theory in describing optical properties of paper (I)[J]. Tehnicki Vjesnik, 2011, 18(1): 117-124.
- [3] DZIMBEG-MALCIC V, BARBARIC-MIKOCEVIC Z, ITRIC K. Kubelka-Munk theory in describing optical properties of paper (II)[J]. Tehnicki Vjesnik, 2012, 19(1): 191-196.
- [4] VAHEY D, ZHU J, HOUTMAN C. On measurements of effective residual ink concentration (ERIC) of deinked papers using Kubelka-Munk theory[J]. Progress in Paper Recycling, 2006, 16(1): 3-12.
- [5] YANG L, KRUSE B. Revised Kubelka-Munk theory. I. Theory and application[J]. Josa A, 2004, 21(10): 1933-1941.

PREPARATION OF POLYMER FIBERS WITH CONTROLLED INTERNAL STRUCTURES USING MICROCHANNEL WET-SPINNING PROCESS AND PHASE SEPARATION

Takaichi Watanabe¹, Shohei Toyota¹ and Tsutomu Ono^{1*}

¹ Department of Applied Chemistry, Graduate School of Natural Science and Technology, Okayama University, Japan, 3-1-1, Tsushima-naka, Kita-ku, Okayama, Japan 700-8530, *e-mail: tono@okayama-u.ac.jp

Abstract: We report a facile approach to preparing polymer micro/nanofibers with controlled internal structures by microchannel wet-spinning process using a microfluidic device. This method is based on the preparation of oil-in-water (O/W) jetting stream, followed by solvent diffusion and phase separation. An organic solution containing polystyrene (PS), tetrahydrofuran (THF) and perfluorooctylbromide (PFOB) was used as an inner phase. The PFOB was used as a non-solvent to induce phase separation. An aqueous solution containing Tween80 was used as an outer phase. These solutions were fed into the microfluidic device to prepare O/W jetting stream. After the jetting stream formation, the THF that was miscible with water diffused from the inner to the outer phase, inducing phase separation between PS-rich phase and PFOB and the precipitation of PS. The coarsening of the phase separation in the jetting stream finally gave PS nanofibers with porous internal structures. We investigated the effects of the initial viscosity of inner phase and flow rate ratios of outer to inner phase on the resultant structures of the fibers. We found that the internal structure of the PS fibers changed from hollow to porous with increasing the initial viscosity of the inner phase. We also found that the diameter of the hollow fibers decreased with increasing the flow rate ratio and that the hollow fibers with a diameter of 400 nm were obtained under the optimum condition.

Keywords: microfluidics, porous, hollow, phase separation, non-solvent

1 INTRODUCTION

In recent years, there is an increasing interest in the fabrication of functional polymer fibers that can be applied to the fields of engineering, clothes, and pharmaceuticals. The functionalization of fibers can be generally achieved by controlling their structures. For example, fibers with a large hollow space in the core have high internal surface area as well as high heat and moisture retaining properties, which can be used as dialysis membrane and functional fabrics. Such hollow polymer fibers are produced using extrusion or spinning technologies including melt-extrusion, wet-spinning, or electrospinning [1]. However, regardless of the production method, it is required to use complex nozzles or multiple nozzles to control the internal structure of fibers. This drawback may lead to the increase in the cost of investment for industrial production.

On the other hand, we have reported the structural control of polymer microparticles by internal phase separation [2,3]. We succeeded in the preparation of polymer microcapsules with a large hollow space by microfluidic formation of polymer droplets containing non-solvent and subsequent rapid solvent removal that induced phase separation in the droplets. This process does not need complex microfluidic devices and fluid operations.

In this study, we develop a facile approach to preparing polymer micro/nanofibers with controlled internal structures by microchannel wet-spinning process [4]. This process is an analogue of the aforementioned microcapsule formation and consists of the preparation of oil-in-water (O/W) jetting stream, solvent diffusion of jet to the continuous phase, and phase separation in the jetting stream. We investigate the effects of the initial viscosity of inner phase and flow rate ratios of outer to inner phase on the resultant structures of the fibers. Then, we make a phase diagram to describe the

relationship between flow conditions and the resultant structures of polymer fibers.

2 EXPERIMENTAL

2.1 Materials

Polystyrene (PS) (M_w = 35,000 and 280,000) and perfluorooctyl bromide (PFOB) were purchased from Sigma-Aldrich (USA). Tetrahydrofuran (THF) was purchased from Wako Pure Chemical Industries, Ltd. (Japan). Tween 80 was purchased from Tokyo Chemical Industry Co., Ltd. (Japan). Ultrapure water was produced by a Millipore Milli-Q purification system (EMD Millipore Corporation, USA).

2.2 Preparation of PS fibers

A schematic illustration of the preparation of PS fibers is shown in **Fig. 1**. Inner phase (5–15 wt% PS in THF solutions and PFOB (20/1, v/v)) and outer phase (2 wt% Tween80 aqueous solution) were injected into the microfluidic device using a syringe pump (Model 33, Harvard Apparatus, MA, USA) at various flow conditions to form jetting stream. After jetting stream formation, THF in the inner phase, which is water-miscible, subsequently diffused from the jetting stream into the outer aqueous phase. The diffusion of THF into the outer aqueous phase induced polymer solidification and phase separation between PS-rich phase and PFOB, leading to the formation of PS microfibers. The fibers were washed with ultrapure water three times to remove surfactant, followed by freeze drying to remove PFOB in the PS fibers. It is noted that when preparing nano-sized PS fibers, a microfluidic device with an orifice was used.

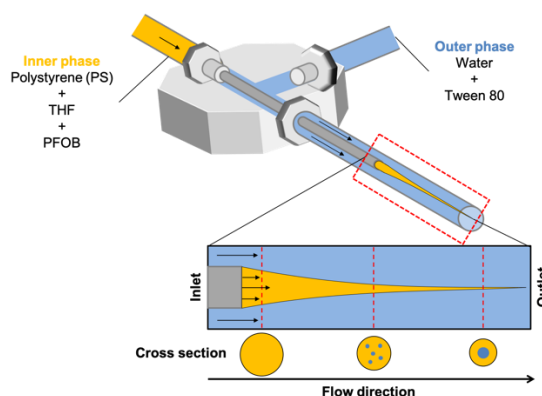


Figure 1. Schematic image of the preparation process of hollow polymer microfibers by microfluidic wet-spinning process.

3 RESULTS AND DISCUSSION

We first evaluated the effect of flow rate and molecular weight (M_w) on the structure of the resultant structures of PS fibers (Table 1). In the case of M_w at 35,000, we obtained PS microparticles when the outer flow rate (Q_{out}) was less than 6,000 $\mu\text{L}/\text{min}$ (Fig. 2 Entry 1), while hollow fibers were successfully obtained at Q_{out} over 6,000 $\mu\text{L}/\text{min}$ (Fig. 2, Entry 3). On the other hand, in the case of M_w at 280,000, PS fibers with porous internal structures were only obtained, regardless of Q_{out} (Fig. 2 Entry 4 and 5). These results indicate that M_w and flow rate ratios of Q_{out} to Q_{in} affect the resultant structures of the products.

Next, we made a phase diagram showing the relationship among flow rates, initial viscosity of the inner phase and the resultant structure of the products (Fig. 3). We found that when the initial viscosity of the inner phase was higher than 40 $\text{mPa}\cdot\text{s}$, PS fibers with hollow structures were obtained, while when that was in the range between 10 and 30 $\text{mPa}\cdot\text{s}$, porous PS fibers were obtained. These results indicate that the initial viscosity of the inner phase plays an important role in determining the structures of the products. We consider that when the initial viscosity of the inner phase is relatively high, the migration of non-solvent during phase separation in jet is retarded and polymer solidifies before the non-solvent forms a single core in the fibers, which leads to porous structures. On the other hand, the initial viscosity of the inner phase is between 10 and 30 $\text{mPa}\cdot\text{s}$, the migration of non-solvent during phase separation rapidly proceeds and the non-solvent forms a single core in the fibers before the solidification of polymer, which results in the formation of hollow fibers.

Table 1. Preparation conditions of PS fibers using microchannel wet-spinning process.

Entry	M_w [g/mol]	Q_{in} [$\mu\text{L}/\text{min}$]	Q_{out} [$\mu\text{L}/\text{min}$]
1	35,000	10	3,000
2	35,000	10	6,000
3	35,000	10	10,000
4	280,000	10	3,000
5	280,000	10	6,000
6	280,000	10	10,000

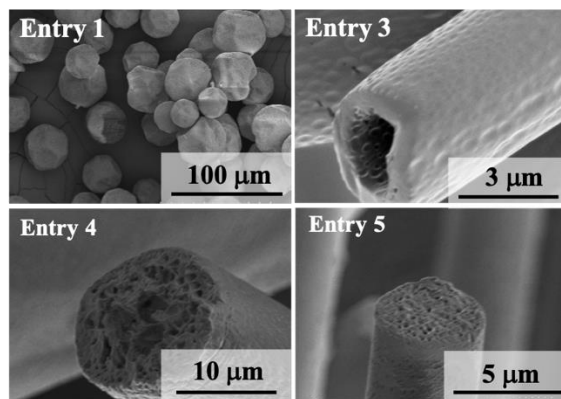


Figure 2. Representative SEM images of the products. (Entry 1: Particles, Entry 3: Hollow fibers, Entry 4 and 5: Porous fibers).

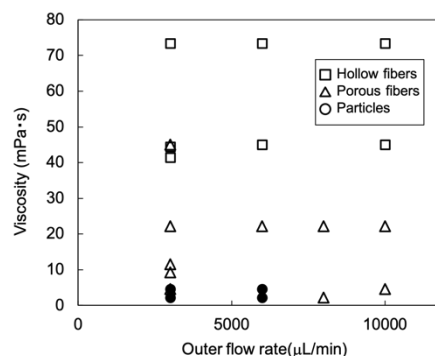


Figure 3. Phase diagram showing the relationship among outer flow rate, viscosity of inner phase and the product structures.

4 REFERENCES

- [1] Niu C., Meng J., Wang X., et al.: General synthesis of complex nanotubes by gradient electrospinning and controlled pyrolysis. *Nat. Commun.*, 2015, 6, pp. 37402.
- [2] Watanabe T., Kimura Y., Ono T.: Microfluidic Fabrication of Monodisperse Polylactide Microcapsules with Tunable Structures through Rapid Precipitation. *Langmuir*, 2013, 29, pp. 14082–14088.
- [3] Watanabe T., Kimura Y., Ono T.: Watanabe T., Kimura Y., Ono T.: Microfluidic Fabrication of Monodisperse Polylactide Microcapsules with Tunable Structures through Rapid Precipitation. *RSC Adv.*, 2014, 4, pp. 4872–4877.
- [4] Ono T., Kimura Y.: Nanofiber exerting excellent biodegradability and biocompatibility, and method for producing said nanofiber (WO2012029710).

ACKNOWLEDGEMENT: This work was supported by Program for Creating Start-ups Advanced Research and Technology, START Program, JST (ST293011NS).

GROUPING SUPERCAPACITOR FIBERS INTO ROPE: SCALING UP ENERGY WITH A SURGING VOLUME

Wenqi Nie¹, Shu Zhang²

¹ Key Laboratory of Textile Science&Technology, Ministry of Education, Donghua University, Shanghai, China e-mail: wengnie@163.com

² Key Laboratory of Textile Science&Technology, Ministry of Education, Donghua University, Shanghai, China e-mail: shuzhangjy@163.com

Abstract: Scaling up the energy with the volume is an everlasting and challenging issue for flexible energy storage devices. Opposite to the steady advance in film-shaped devices, a stagnant situation is confronted by fiber-shaped devices. Here for the first time we take advantage of the processing flexibility of fibers to group thousands of fibers into a rope. As a result, a rope supercapacitor is achieved with a tremendous 12000-fold volume increase compared to the fiber supercapacitor. Moreover, a volume-independent energy density is verified due to the programmed arrangements of fibers. And the rope supercapacitor possesses a record high device energy that is 5 times and 35 times higher than that of the state-of-the-art film and fiber supercapacitors, respectively. The method here can be extended to other tiny fiber-shaped devices to achieve a highly integrated bulky one.

Keywords: supercapacitor, flexibility, energy density, fiber

1 INTRODUCTION

As an integral part of flexible electronics, flexible energy storage devices (FESDs) gain much attention over the last decade, which are constituted by two electrodes immersed in electrolyte and sandwiched with a separator.[1] However, a lethal drawback stemming from nanostructured electrodes and dimension-reduction devices is the ultra-small device energy of FESDs. For instance, a fiber supercapacitor composed of carbon nanotubes exhibited a device energy of 0.058 μWh . [2] And film supercapacitors consisting of MnOx/Au multilayers and graphene sheets derived device energies of 0.0021 μWh [3] and 0.00375 μWh [4], respectively. The above issue can be addressed from two aspects, i.e., electrodes and devices. However, one big challenge to be faced is augmenting the energy whilst maintaining the energy density, i.e., scaling up the energy with the volume. Recently Gogotsi and co-workers reported a supercapacitor film electrode with thickness-independent energy density from 40 μm to 200 μm , giving a 5-fold increase both in volume and energy. [5] However, thickening film electrodes normally requires elaborate processes and sacrifices the flexibility to some extent. As for fiber FESDs, the stagnant situation of fiber FESDs has become a pressing issue.

Herein, the volume surge of the fiber supercapacitor is achieved by grouping thousands of fibers into a rope via scalable twisting and braiding. A tremendous magnification of 12000 times in volume is realized by 1500-fold increase upon thickening the electrode and 8-fold increase upon lengthening the device. More importantly, both electrodes and devices exhibit volume-independent energy density. Considering the volume of 0.3 cm^3 , the resulting rope supercapacitor reaches a record high device energy of 62.6 μWh , which is 5 times and 35 times higher than that of the state-of-the-art film and fiber FESDs, respectively.

2 METHODS AND RESULTS

2.1 Experiment

Fig.1 shows the fabrication and application of rope supercapacitors. Simply says, Polylactic acid (PLA) filament as substrate, then PPy/rGO@PLA is made by a simple methods which contains graphene oxide (GO) coated and polypyrrole (PPy) polymerized. After that, 12 PPy/rGO@PLA filaments were braided into a PPy/rGO@PLA rope using a braiding machine. This rope set as the inner electrode, on which the separator was wound and 12 PPy/rGO@PLA filaments are braided in sequence, getting a coaxial rope supercapacitor. This supercapacitor can be inserted into textile as an energy device.

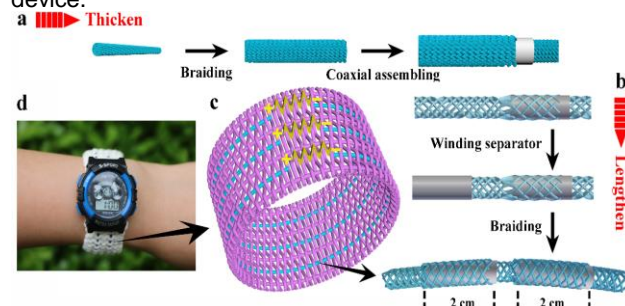


Figure.1 The fabrication and application of rope supercapacitors.

2.2 Result

Prior to the electrochemical properties test, the resistance of PPy/rGO@PLA yarn was measured to be 260 Ω/cm , which renders PPy/rGO@PLA a promising supercapacitor electrode material. PPy/rGO@PLA fiber, yarn and rope served as the electrodes all with a workable length of 2 cm, whose volumes are $5.09 \times 10^{-6} \text{ cm}^3$, $5.09 \times 10^{-4} \text{ cm}^3$

and $7.69 \times 10^{-3} \text{ cm}^3$, respectively. The redox peaks of PPy are manifest for PPy/rGO@PLA fiber, yarn and rope in cyclic voltammetry (CV) spectra at low scan rates (Fig. 2a). Actually, the discrepancies of specific capacitances between fiber and yarn and between fiber and rope are both less than 10% in a scan rate range of 5 to 100 mV s^{-1} (Fig. 2b), which verifies the volume-independent specific capacitance and also energy density within the 1500-fold volume increase.

Figure 2c shows a plot of the peak-current density against the scan rate for PPy/rGO@PLA fiber, yarn and rope. The relation of the peak current and the scan rate abides by the power law:

$$I_p = a \cdot S^b,$$

I_p is the peak current, S is the scan rate, and a , b are adjustable parameters. When b is close to 1, it indicates a high-rate capacitive storage mechanism. And when b is close to 0.5, slow semi-infinite diffusion is dominant.[5] Here, b values are near to 1 for PPy/rGO@PLA fiber, yarn and rope at scan rates less than 20 mV/s , which demonstrates the charge-storage kinetics are controlled by surface reaction. After that, the diffusion-limited mechanism is gradually evident with increasing the scan rate. Furthermore, the disparities of b values among three kinds of electrodes become obvious when the scan rate is larger than 100 mV/s (Fig. 2c).

From Fig. 2d, volumetric specific capacitances for PPy/rGO@PLA fiber are 92.1, 74.0 and 49.8 F/cm^3 at 5, 10 and 20 mV/s , respectively. And correspondingly 95.9, 76.5 and 54.7 F/cm^3 are for PPy/rGO@PLA yarn and 87.8, 67.6 and 46.6 F/cm^3 for PPy/rGO@PLA rope. The volumetric energy densities for PPy/rGO@PLA fiber, yarn and rope are 12.8, 13.3 and 12.2 mWh/cm^3 at 5 mV/s , respectively.

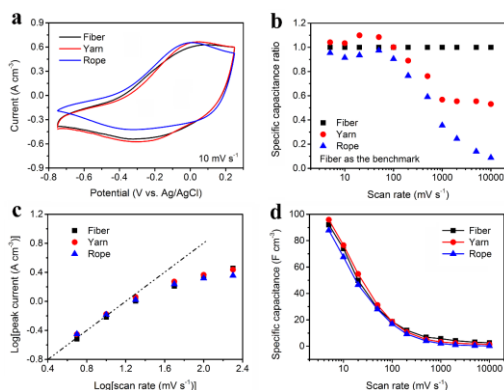


Figure.2 Electrochemical properties of PPy/rGO@PLA fiber, yarn and rope

Galvanostatic charge/discharge curves for 1-unit, 2-unit, 4-unit and 8-unit rope supercapacitors at a current of 0.1 mA are shown in Fig. 3a. Seen from Fig. 3a, tandem rope supercapacitors with up to 8 units are demonstrated with the similar discharge time and proportional voltages to the number of units. 1-unit, 2-unit, 4-unit and 8-unit rope supercapacitors produce capacitances of 83.0, 41.8, 22.1 and 11.0 mF at 0.1 mA, respectively, scaling down with the number of units. As for the device energy, 1-unit, 2-unit, 4-unit and 8-unit rope supercapacitors generate 7.4, 14.9, 31.4 and 62.6 μWh at 0.1 mA, respectively (Fig. 3b), scaling up with the number of units.

Considering the volumes, energy densities of 189, 195, 208 and 209 $\mu\text{Wh/cm}^3$ are attained for 1-unit, 2-unit, 4-unit

and 8-unit rope supercapacitors at 0.1 mA, respectively. Since the differences are less than 10%, a volume-independent character is demonstrated when lengthening the device within the 8-fold volume increase. Moreover, this volume-independent virtue is remained in a large current range from 0.1 to 1.0 mA (Fig. 3c). Additionally, the rope supercapacitors exhibit an excellent long-life performance, which can endure up to 10000 cycles (Fig. 3d).

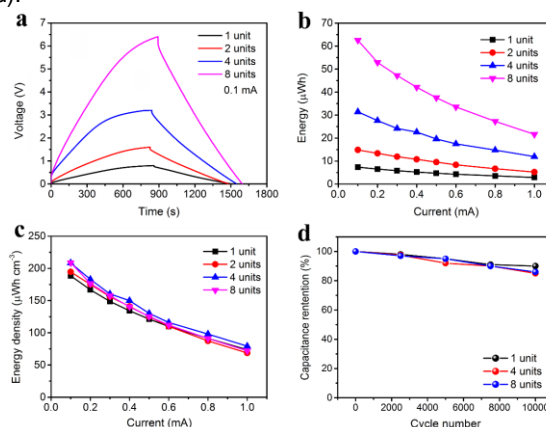


Figure.3 electrochemical properties of 1-unit, 2-unit, 4-unit and 8-unit rope supercapacitors

3 CONCLUDE

This work exhibits a novel way to grouping tiny fiber devices into an integrated bulky one meantime with undeteriorated performance. A rope supercapacitor is achieved with a tremendous 12000-fold volume increase compared to the fiber supercapacitor. Moreover, a volume-independent energy density is verified due to the programmed arrangements of fibers. A high energy of 62.6 μWh is achieved.

4 REFERENCES

- [1] Liu, W., M.S. Song, B. Kong, Y. Cui, Flexible and Stretchable Energy Storage: Recent Advances and Future Perspectives[J]. *Advanced Materials*, 2017. 29,1 p: 34.
- [2] Chen, X., L. Qiu, J. Ren, G. Guan, H. Lin, Z. Zhang, et al., Novel electric double-layer capacitor with a coaxial fiber structure[J]. *Adv Mater*, 2013. 25,44 p: 6436-6441.
- [3] Si, W., C. Yan, Y. Chen, S. Oswald, L. Han, O.G. Schmidt, On chip, all solid-state and flexible micro-supercapacitors with high performance based on MnOx/Au multilayers[J]. *Energy & Environmental Science*, 2013. 6,11 p: 3218-3223.
- [4] Wu, Z.S., K. Parvez, X. Feng, K. Mullen, Graphene-based in-plane micro-supercapacitors with high power and energy densities[J]. *Nat Commun*, 2013. 4 p: 2487.
- [5] Xia, Y., T.S. Mathis, M.Q. Zhao, B. Anasori, A. Dang, Z. Zhou, et al., Thickness-independent capacitance of vertically aligned liquid-crystalline MXenes[J]. *Nature*, 2018. 557,7705 p: 409-412.

2. Science and Technology of Textile Machinery

AUXETIC WOVEN STRUCTURES: DESIGN ENGINEERING, PRODUCTION PROCESS AND APPLICATIONS

Bijoya Kumar Behera¹, Aman Katiyal¹ and Adit Gupta¹

¹Focus incubation center for 3D weaving and structural composites

Department of Textile Technology, Indian Institute of Technology Delhi

Abstract : Focus incubation center for 3D weaving in Indian Institute of Technology Delhi has been working to design and develop novel auxetic woven structures for various applications. It is realized that woven auxetic fabrics produced from auxetic fibre and yarn have cost and mass production limitations; knitted auxetic fabrics have stability issues; whereas 3-D-woven auxetic fabrics are not wearable. However, each of these categories has its own merit. Exploratory work has been carried out to develop innovative weave designs which can offer perceptible auxeticity in resulting fabric for several end uses such as protection and smart applications. It is observed that fabric with random geometry produces highest auxeticity; fabrics with oblique folded stripes and rotating quadrilateral geometry produce moderate auxeticity; whereas fabric with re-entrant hexagonal geometry produces lowest auxeticity. It is unambiguous that the auxeticity of the woven constructions is predominantly dependent on the weave designs. However, conceptualising novel geometry is key to develop auxetic woven structures.

Keywords : auxetic material, negative poisson's ratio, foldable geometry, rotating pattern

1 INTRODUCTION

Auxetic material falls under the category wherein it becomes fatter when stretched or narrower when compressed and hence results in negative Poisson's ratio (NPR). The Auxeticity (NPR value) is associated with specific geometrical features and deformation mechanisms of a system. In textile it is possible to produce auxetic fibre or polymer, auxetic yarn and auxetic fabric. In this research, efforts are being made to design a proto type yarn development system by combining elastic and stiff components at appropriate proportion to produce predetermined auxeticity in the resulting yarn which can ultimately be used to produce auxetic fabric. Both analytical and computational models are developed to engineer auxetic woven structures. Mathematical models are developed to analyse and predict how much auxeticity could be achieved by various manufacturing techniques [1].

2 MATERIALS AND METHODS

Auxetic woven structures based on foldable geometries, rotating quadrilaterals, re-entrant hexagonal geometry and random patterns were produced using combination of stiff and soft stretchable spun yarns. Theoretical models were developed for all these structures to determine poisson's ratio values from the geometry of each of these structures. Computational models were developed for few patterns to predict the poisons ratio values. Suitable weave designs were introduced to weave the fabrics from these structures. Finally fabrics were characterized for actual auxeticity and the experimental values were compared with model results.

3 RESULTS AND DISCUSSION

3.1 Approach to develop auxetic structure

The basic philosophy to engineer woven auxetic structure consists of conceptualizing Auxetic Geometry, Engineering Auxetic Design, Modeling and simulation of auxetic structure, Production and characterization of auxetic fabric, and Exploring innovative applications of 2D and 3D Woven Textile structures primarily in the Technical Textiles domain.

3.2 Theoretical calculations of poisson's ratio of rotating pattern

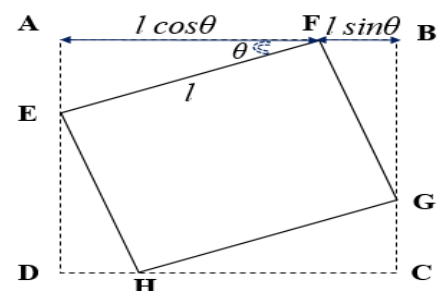


Figure 1 Geometry of a rotating structure

The Figure 1 shows the geometry of a rotating structure. From the geometry, we can have :

The horizontal length of the unit is x :

$$x = l (\cos\theta + \sin\theta) \text{ and}$$

The vertical length of the unit is y :

$$y = l (\cos\theta + \sin\theta)$$

Now if we change the angle of bend from θ to Φ that means if we rotate the square by stretching across y-axis, then we have

$$\Delta y = l(\cos\theta + \sin\theta) - l(\cos\Phi + \sin\Phi)$$

$$\Delta x = l(\cos\theta + \sin\theta) - l(\cos\Phi + \sin\Phi)$$

Then Poisson's ratio will be :

$$\begin{aligned} \nu &= - (d\epsilon_y / d\epsilon_x) \\ &= - \Delta y / \Delta x \\ &= -1 \end{aligned}$$

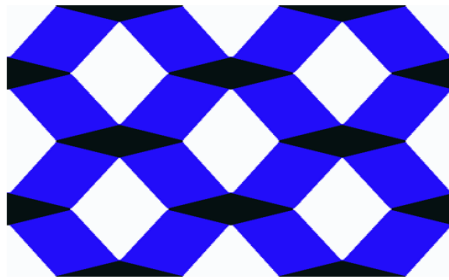


Figure 2 The unit cell of interlacement pattern of single layered fabric based on rotating geometry

The unit cell of interlacement pattern of single layered fabric based on rotating geometry is given in Fig. 2.

3.3 Rotating quadrilateral geometry

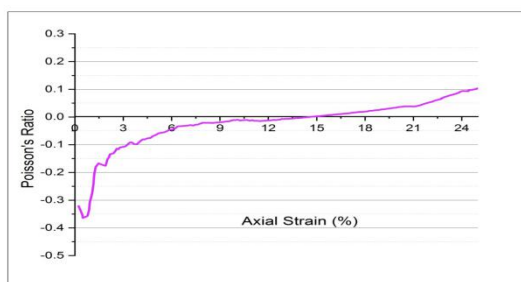


Figure 3 Poisson's ratio as a function of longitudinal strain when stretched along weft direction

The Fig. 3 shows the poisson's ratio as a function of longitudinal strain when stretched along weft direction in case of a rotating quadrilateral geometry. On analysing, it is observed that fabric with quadrilateral geometry produced NPR upto 14.5% of axial strain and maximum poisson's ratio of (- 0.37) is produced at a axial strain of around 0.50% .

3.4 Re-entrant hexagonal geometry

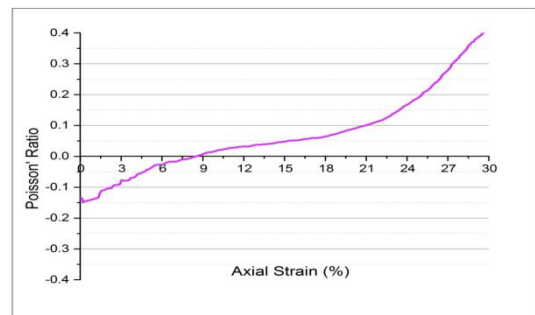


Figure 4 Poisson's ratio vs axial strain

Figure 4 demonstrates that the fabric with re-entrant hexagonal geometry produced NPR upto 8.15% of axial strain and a maximum poisson's ratio of (0.15%) produced at a axial strain of around 0.2% .

Several other geometries are developed and analysed in this research.

4 CONCLUSION

It is observed that auxeticity in woven construction can be brought by several means such as by inserting zig zag weave in both warp way and weft way, inserting rotating and foldable geometry, choosing elastic and non-elastic yarn, changing weave effect in warp and weft direction, varying float length and introducing many other specific effects in weave design.

5 REFERENCE

- [1] Wang, Z. and Hu, H., 2014. Auxetic materials and their potential applications in textiles. Textile Research Journal, 84(15), pp.1600-1611.

Matsumoto, Tatsumori

Murata Machinery Ltd., 136 Takeda Mukaishiro-cho, Fushimi-ku, Kyoto, Japan

e-mail: tamatsumoto@p-att.muratec.co.jp

Abstract: Yarns properties of spun yarn and its fabric hand or appearance depend deeply on the twist structure. They are defined by yarn forming principles. As already known, Vortex spinning system provides superior productivity and unique yarn and fabric characteristics, which are distinguished from prominent Ring or OE-Rotor yarns. In this paper, twist structures of the Vortex yarn is discussed with comparing to Ring yarns. The twist number is a fundamental property to characterize spun yarns, and is controlled by machine parameters on Ring or OE-Rotor spinning systems. On the other hand Vortex spinning can't define twist number nor control it precisely. For yarn and garment handlers, it is not easy to purchase a quantity of Vortex yarn from different spinners. Because the yarn characteristics are not appointed except yarn count. Therefor common indicator suggesting twist structure of Vortex yarn is expected.

Keywords: Vortex spinning, MVS, Twist structure of yarn

According to the spinning machinery shipping statistics latest 10 years, Ring system dominates at 79% of world capacity. The second is OE Rotor system at 17%. Vortex system occupies only 4% [1]. As the rapid increase of Vortex yarn inquiry, yarn and fabric handlers have to purchase them from plural yarn sourcings. Then handling of Vortex yarns is not simple because there is no absolute value to specify the yarn structure. Yarn count and twist number are commonly used in Ring and OE Rotor yarns. Murata provides the Rolling test, which could indicate the resistance against abrasion or pilling. But it does not define the yarn structure itself. In this paper, a Vortex twist number is proposed by using image processing technology, and fiber behavior during yarn forming is unveiled.

The twist structure of Vortex yarn consists of core fiber strand with very low twist (it has been assumed zero twist) and lapping fibers with multi twist angles. Leading fiber ends must be core strand and their tailing ends are lapping up on the core strand. The percentage of lapping fibers and core strand varies with depending on fiber length, yarn count and of course machine parameters. The degree of encapsuturation of core strand is not constant and differs from place to place along yarn axis. More over, Yarn twist number is not measurable except 100% cotton yarn. Fig.1 is a model of twist structure from representative yarns [2]. In Vortex cotton yarns coarser than Ne10, the twist structure is not always like Fig.1. It is rather a double layered twist structure as illustrated in Fig.2. The twist number provided by twist tester is the twist of core strand and not lapping strand on yarn surface. Nevertheless, we may believe that majority of Vortex yarns in markets are as showed in Fig.1. Then we can evaluate the twist structure by observing just yarn surface. At first, 100% cotton Vortex yarns (showed in Fig.3) are investigated, because the twist number is measurable by the twist tester. The estimated twist number from twist angle on the SEM photograph showed close similarity to that of twist tester as in Table 1. But it is quite laborious work to evaluate the twist angle from SEM pictures by human eyes.

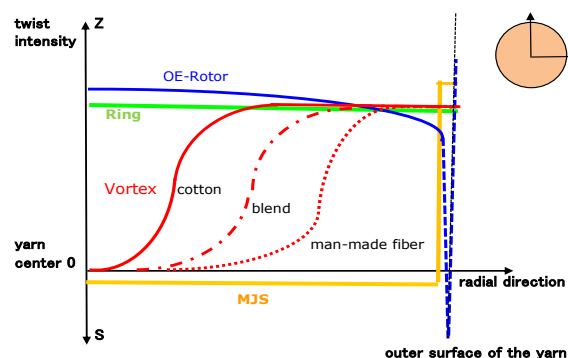


Figure 1 Twist structure of spun yarn

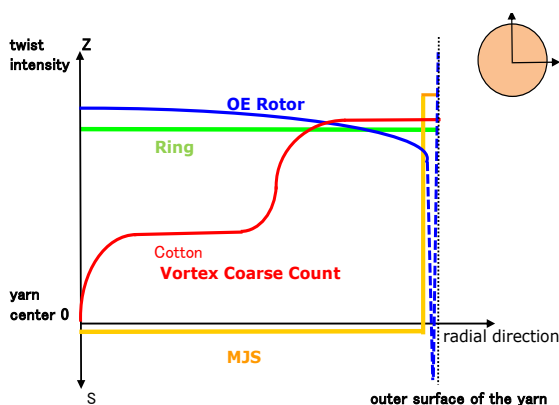


Figure 2 Twist structure of coarse count Vortex cotton yarn

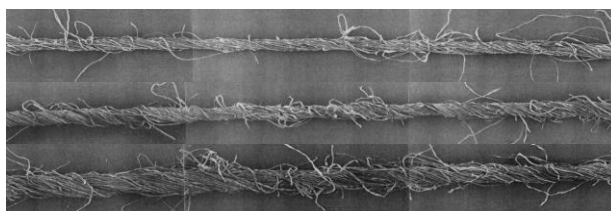


Figure 3 Vortex Cotton 100% Yarn (SEM), Ne40, Ne28, Ne18

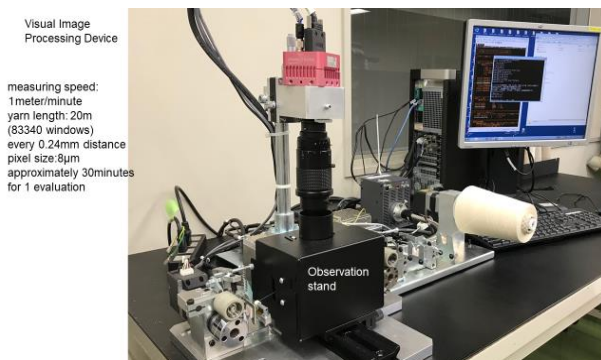
So that the investigation was very limited yarn length. For example, 100 fibers are selected from 10mm yarn length.

Table 1 Zweigle M2 twist number and yarn twist angle by SEM

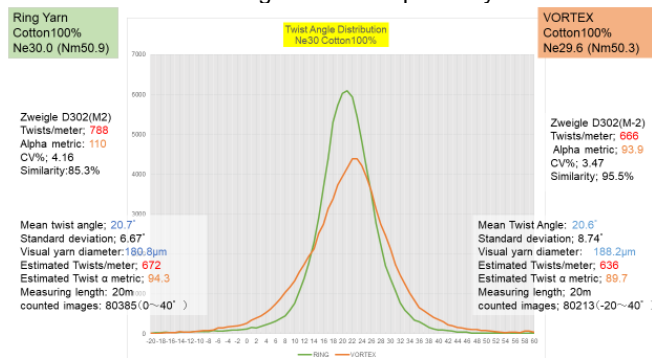
Yarn Count	Zweigle Twists Method2	Zweigle Twist Factor	Estimate Twist angle	SEM Yarn Diameter	SEM Twist angle	Estimate Twists	Twist Similarity SEM/Zweigle
Ne	1/meter	α m	degree	mm	degree	1/meter	%
40.0	812	99	19.4	0.138	18.5	772	95.1
27.7	652	96	20.0	0.178	19.3	626	96.0
18.6	474	84	22.3	0.275	21.4	454	95.8

Naturally it is suspicious that the results represent the yarn structure or not. To get statistically satisfied results, an image processing system was developed as in Fig.4.

It consists of video camera, observation stand with yarn feeder at a constant speed, yarn tension control system, CPU for image processing, and monitor screen. The system takes approximately 30 minutes for evaluating 20 meters of yarn. At every 0.24mm distance, a window is taken in and processed to assess fiber angle and yarn diameter. Over 83 Kilo windows are classified by fiber angle. The results are provided as the frequency of twist angle distribution, mean and median angle, averaged yarn diameter, their standard deviations and visual images at windows.

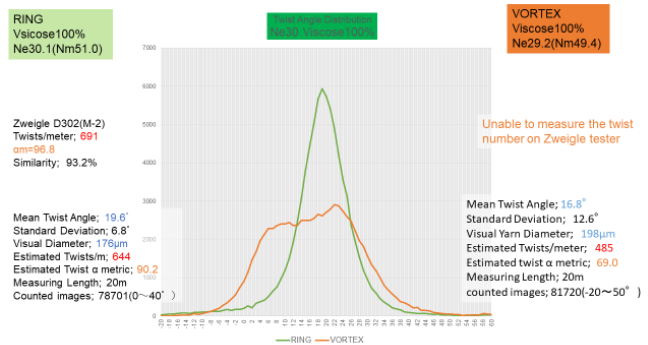
**Figure 4** Image processing system

At first, to confirm the reliability of the system, twist number by Zweigle D302 (method-2) is compared with that from fiber angle observation on the system. For example, 100% cotton and Viscose yarn of Ring and of Vortex are showed in Fig. 5 and 6 respectively.

**Figure 5** Twist angle distribution of cotton yarn (Ring, Vortex)

Twist numbers did not coincide with that of the twist tester. Presumably the image processing system takes in every images without bias. In Fig.3, I observed twist angle from SEM picture by human eye. Human eye would not chose suspicious fibers and avoids hairiness intentionally. This operation made closer twist number from the twist tester to that of mean twist angle from SEM observation.

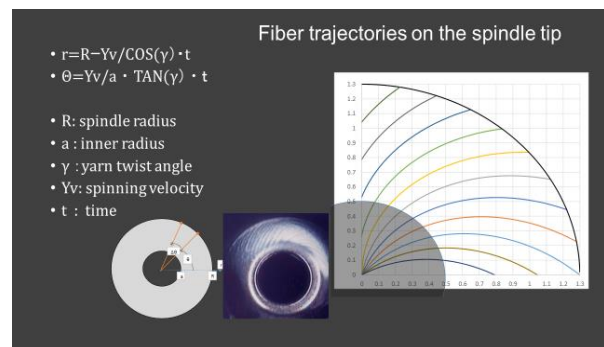
Relatively lower twist number in visual processor may be caused by existence of faulty, hairy protruding fibers. In the beginning, I thought these fibers were oriented randomly and cancel out each other's statistically. But it is

**Figure 6** Twist angle distribution of Viscose yarn (Ring, Vortex)

too optimistic. Finally I restricted the object window, which fiber angle is 0 to +40 degree for Ring yarns. On the other hand, Vortex yarn has a wider range of fiber angle. So that the windows having between -20 to +40 degree are taken in consideration. Anyway, yarn twist number or twist factor is obtainable from yarn surface observation.

2.2 Yarn Formation

The process of Vortex yarn forming is not disclosed completely. Direct observation of fiber movements in the spinning nozzle had been fulfilled by using high speed video camera [3]. The results confirmed us the images already anticipated. By chance, in polyester spinning trials, we found fiber trajectories on the spindle. There were streaks created by discarded finishing oil from polyester fibers. These deposits normally lead to weak yarn. Fortunately this discover brought us a concrete idea of yarn forming as shown in Fig.7.

**Figure 7** Fiber trajectories on the spindle tip

It is obvious that higher spinning speed is expected in near future, because the angular velocity of swirling fibers is proportional to the spinning speed, which can be set mechanically. However fiber rotation is constrained from tail-end-contacts with inner wall of the nozzle. But they look swirl with injection flow. If air velocity at spindle tip is at sound speed, approximately 2 million rpm could be achieved. Actual fiber rotation was 0.3 to 0.35 million rpm at 400 m/min. of spinning speed [3]. This means that there are wide spaces to improve the productivity.

- [1] ITMF, Textile Machinery Shipment Statistics 2017, 2018
- [2] <http://www.muratec-vortex.com/vortex02.html>
- [3] not published, 2004

3. Science and Technology of Textile Processing

STUDY ON COTTON COLOR MEASUREMENT USING SCANNER

Chong Heng¹, Fumei Wang^{1,2*}

¹College of Textiles, Donghua University, Renmin North Road, Shanghai, 201620, China, Email: 1185062@mail.dhu.edu.cn

²Key Laboratory of Textile Science & Technology of Ministry of Education, College of Textiles, Donghua University, Shanghai, 201620, China, Email: wfumei@dhu.edu.cn

Abstract: Color is an important property for the cotton and it plays a key role in the grading of cotton. In this paper, we present a method of image analysis to study the color of cotton. The Rd (reflectance) and +b (yellowness) obtained by the scanner and HVI (High Volume Instrument) were analyzed. It was found that the Rd and +b values of the two machines have strong relationship. The a value (redness or greenness) of different cottons varies greatly, so it is more reasonable to grade the color of cotton in the three-dimensional Hunter color space.

Keywords: Scanner; HVI; Hunter color space; Color grading; image analysis

1 INTRODUCTION

Color is an important part of cotton quality inspection, which represents the quality and affects directly the processing, application and price [1-3]. The paper presents a study on the color measurement of cotton using color scanner.

2 MATERIALS AND METHODS

2.1 Samples and instruments

The color measurement was performed for 12 cotton samples. They were placed in a laboratory (20 ± 2°C, 65 ± 4% RH) for 24 hours before the test. The color reflection image of cotton was obtained using the MRS-3500 scanner (MICROTEK Co., Ltd, China), and a Uster's HVI-1000 was used to measure the Rd and +b values.

2.2 Image acquisition

The image of the cotton fiber is obtained using the scanner. During the measurement, the cotton sample (10 ± 0.5g) was placed evenly into 10 × 10cm, 5cm high in size, then move the biscuit into the reflection platform of scanner. 20 pounds weight was applied on the sample to remove shadows. The resolution of scanner is 1000 and images were stored in sRGB (standard RGB) format.

2.3 The conversion of color space

The RGB value of every pixel is obtained by Matlab, The conversion from the RGB color space to the Hunter color space Rd, +b requires the transformation matrix. The calculation process is as follows

$$\begin{pmatrix} x \\ y \\ z \end{pmatrix} = \begin{pmatrix} 0.4125 & 0.3576 & 0.1804 \\ 0.2127 & 0.7152 & 0.07218 \\ 0.0193 & 0.7152 & 0.9503 \end{pmatrix} \begin{pmatrix} r \\ g \\ b \end{pmatrix} \quad (1)$$

$$Rd = Y$$

$$+b = 70f_y (Y - 0.847Z)$$

$$a = 175f_y (1.02X - Y) \quad (2)$$

$$f_y = 0.51 \left(\frac{21 + 20Y}{1 + 20Y} \right)$$

3 RESULTS AND DISCUSSION

The color parameters of cotton are simplified three-dimensional Hunter color space (Rd and +b). This paper analyzes the relationship of Rd and +b measured by scanner and HVI.

3.1 The relationship of Rd

Figure 1, 2 give the result of Rd obtained by the scanner and HVI. It is found that the Rd of the two tests is relatively close and Rd obtained by scanner correlated well with Rd obtained by HVI.

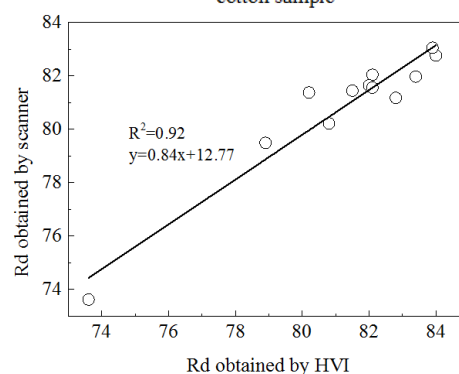
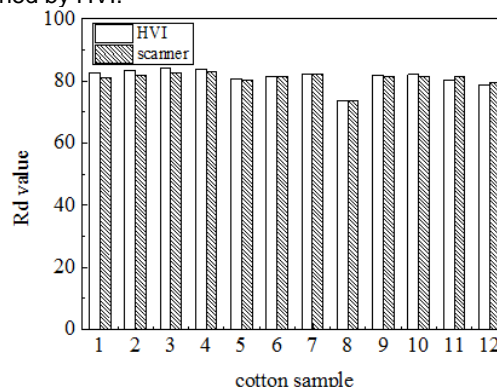
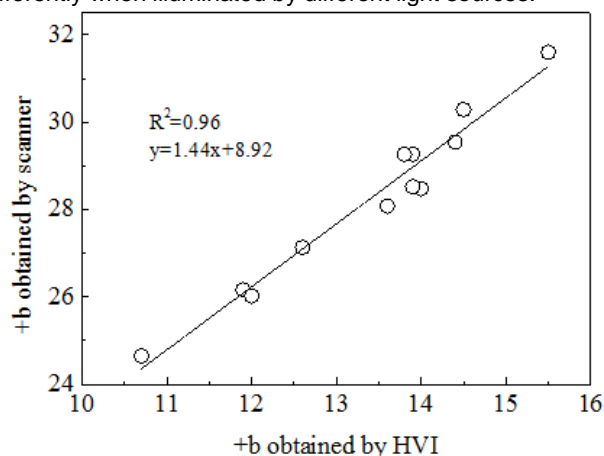


Figure 1 Comparison of Rd obtained by HVI and scanner

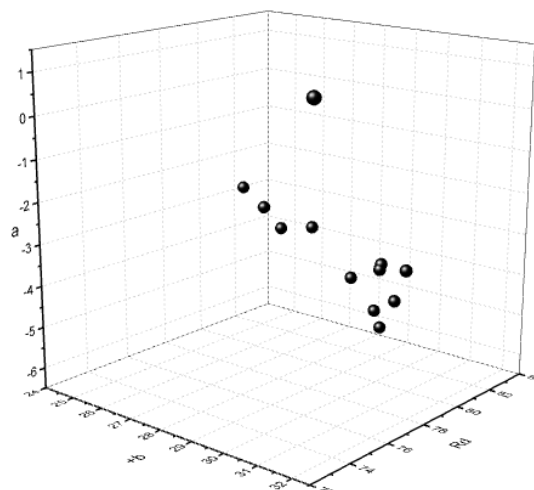
3.2 The relationship of +b

As shown in figure2, +b values obtained from scanner provide a strong linear relationship with HVI results. However, there are some differences between the values measured by the two instruments. The difference may be related to the light source. The light source of HVI is xenon and scanner is LED [4]. The spectral components and color temperature are different, so the same color will appear differently when illuminated by different light sources.

**Figure 2** Comparison of +b obtained by HVI and scanner

3.3 Distribution of cotton in the three-dimensional Hunter color space

At present, almost all cotton colorimeters use Rd and +b to grade cotton color. It is pointed that the a value is not negligible, as shown in figure 3. In the three-dimensional Hunter color space, different types of cotton are distributed in different horizontal planes. When grading cotton color, it may be more reasonable to consider a parameter.

**Figure 3** Distribution of cotton in the three-dimensional Hunter color space

4 CONCLUSION

The primary object of this study is to survey the color of cotton using the method of image analysis obtained from scanner. The results of the experiment indicate that there is a high correlation between Rd and +b measured by the two instruments. At the same time, the a value of different cottons varies greatly, and it may be necessary to classify cotton in the three-dimensional color space.

5 REFERENCES

- [1] Nickerson, D. Journal of the Optical Society of America. [J]. 1931(21):640-642.
- [2] Małgorzata Matusiak, Anetta Walawska. Important Aspects of Cotton Colour Measurement [J]. Fibres & Textiles in Eastern Europe, 2010, 18(3):17-23.
- [3] Nickerson, D, R Hunter, and M. Powell. Journal of the Optical Society of America. [J]. 1950(40):446-449.
- [4] VIK M, KHAN N, VIKOVA M. LED utilization in cotton color measurement [J]. Journal of Natural Fibers, 2017, 14(4):1-12.

IMPACT OF SOL-GEL COATING ON THERMAL PROPERTIES OF CU- COATED NONWOVEN FABRIC

Aravin Prince Periyasamy¹, Kai Yang¹, Xiaoman Xiong¹, Mohanapriya Venkataraman¹, Jiri Militky¹, Rajesh Mishra¹, Dana Kremenakova¹

¹Department of Material Engineering, Technical University of Liberec, Studentska 2, 46117, Liberec, Czech Republic, e-mail: aravinprince@gmail.com

Abstract: Current situation, the electromagnetic radiation (EMR) become the fourth most source of public pollution after water, air and noise. Therefore, the reduction or protection of EMR is very important for the people who frequently use the electrical and electronic equipment's. Unwanted EMR may cause electromagnetic interference (EMI). Textile based structure with electromagnetic shielding ability has a promising replacement of conventional materials due to its flexibility, air permeability and comfort properties. In this paper, thermal properties of Cu-coated nonwoven fabrics have been investigated with respect to before and after sol-gel coating, for coating, three different silanes were used to stabilize the Cu deposition on the nonwoven fabric. Primarily this fabric has developed for the electromagnetic shielding, however, thermal properties alone discussed here.

Keywords: copper coated, non-woven, silanization, EMI, thermal properties

1 INTRODUCTION

Since last two decades, there is a major growth of electronics and their utilization. It severely emits the electromagnetic radiation which is harm to the human health. Therefore, interest in the development of electromagnetic interference (EMI) shielded textiles have been increased since it has huge potential and scope. Previous decades, the metal wires were used for the EMI shielding, however, it is not comfortable due to its weight. Recently the metal coated textile has been an alternative for such conventional metal wires. Nevertheless, the durability of metal is serious issues. Also, metal like copper easily affected by the atmospheric oxygen, resulting in cuprous oxide formation, which drastically reduces its EMI properties. In this work, we tried to stabilize the copper coating on the nonwoven fabric by simple sol-gel coating. In this paper we focused on the thermal properties of copper coated fabrics and their effect on the sol-gel coating.

2 EXPERIMENTS

2.1 Materials

100 % polyester filament cross laminated composite nonwovens (Milife) have been used for this study. It is denoted as MIC (copper coated), MIWC as without copper coating. Milife has a unique structure which allows surface metallization and lamination with other materials (paper, film, other nonwovens, etc.) easily.

2.2 Sol-gel synthesis

In this work three different silanes were used, namely Octyltriethoxy silane (OTES), Phenyltriethoxy silane (PhTES), and Tetraethoxy silane (TEOS), initially silane, solvent and catalyst were added and stirred until to get a clear solution. Later, deionized water was added to the above solution by using a syringe pump at the speed of 1 mL.h⁻¹. The solution was continuously stirred for 24 h at room temperature to allow the complete hydrolysis of precursors.

2.3 Testing

Thermal measurement:

Alambeta was used to measure the various thermal properties which including thermal conductivity, thermal resistance, thermal diffusivity and absorptivity of control and coated fabrics, according to EN 31092 standard.

Infrared thermography:

Infrared thermography measurement was conducted by using Infrared thermo camera (FLIR E5 with the spectral range of 7.5 to 13 μm, IR resolution of 120*90 pixels were used for this study) to find the thermal insulation values (Equation. 1. A thermal image reveals the amount of radiation emitted by the heat plate through the fabric. The insulation value can be calculated by;

$$I = \left(\frac{B - F}{B - R} \right) \quad (1)$$

3 RESULTS AND DISCUSSION

Generally, thermal properties depend on various physical properties, the thickness is one among. The thickness of control samples and sol-gel coated fabrics shown in Table 1. After sol-gel coating it showed considerable improvement in fabric thickness. Especially for the PhTES coating. The various thermal properties of MIC and MIWC are shown in Fig. 1-4. The total thermal conduction of a fabric is mainly contributed by the conduction through air and fibers. Thermal resistance expresses the ability of material to prevent heat flow through the thickness over unit surface area, which is strongly dependent on fabric thickness. It is clearly shown that the fabrics (MIWC and MIC) coated by OTES and TEOS had relatively lower thermal conductivity (Fig. 1).

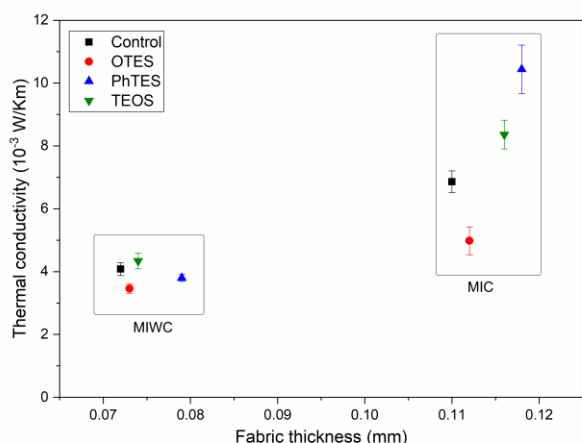


Figure 1 Thermal conductivity of MIC and MIWC fabrics.

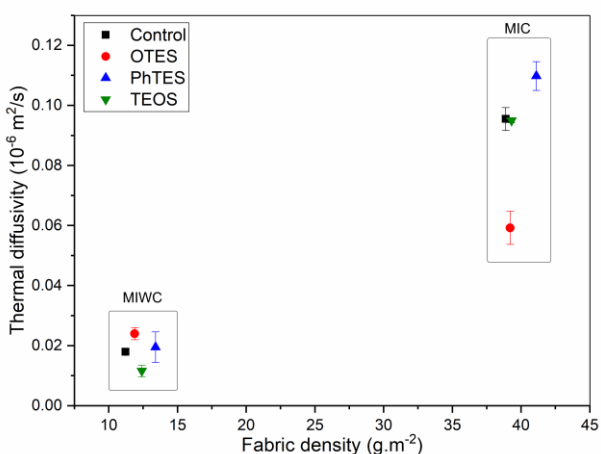


Figure 2 Thermal diffusivity of MIC and MIWC fabrics.

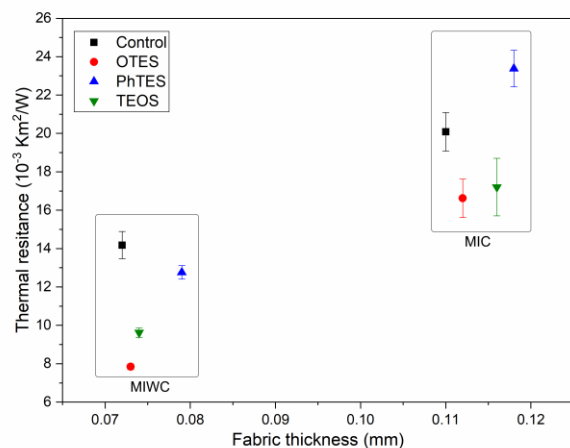


Figure 3 Thermal resistance of MIC and MIWC fabrics.

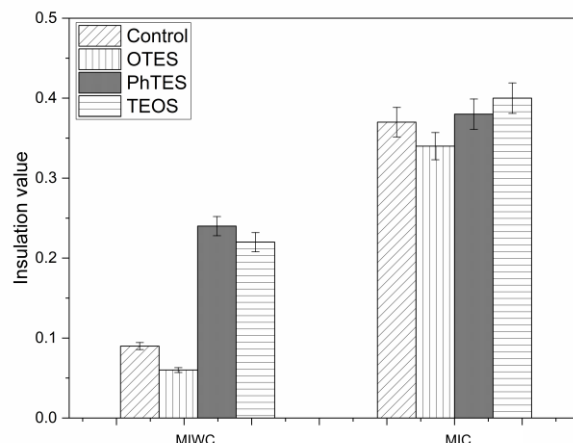


Figure 4 Thermal insulation value of MIC and MIWC fabrics.

PhTES coating gave obvious decrease to thermal conductivity. Thermal resistance also the similar trend as like thermal conductivity (Fig. 3). The results of thermal diffusivity for MIC and MIWC are shown in Fig. 2. The thermal diffusivity values are depending on the fabric density, perhaps the fabric density has been increased by the sol-gel coating. Therefore, thermal diffusivity values are increased significantly with respect to the sol-gel coating, among the three silanes, PhTES provides the highest thermal diffusivity values. The comparison of calculated thermal insulation values is presented in Fig. 4. It is confirmed that the MIWC had the lowest thermal insulation value. After sol-gel coating, a remarkable increase in insulation ability was found for samples using PhTES and TEOS. MIC exhibited better insulation, however, there was insignificant change after silane coating.

Table 1 Thickness of MIC and MIWC after sol-gel coating.

Silanization	Sample	Thickness (mm)
Control	MIWC	0.072
	MIC	0.110
OTES	MIWC	0.073
	MIC	0.112
PhTES	MIWC	0.079
	MIC	0.118
TEOS	MIWC	0.074
	MIC	0.116

Acknowledgement: This work was supported by the Ministry of Education, Youth and Sports of the Czech Republic and the European Union - European Structural and Investment Funds in the frames of Operational Programme Research, Development and Education - project Hybrid Materials for Hierarchical Structures (HyHi, Reg. No. CZ.02.1.01/0.0/0.0/16_019/0000843).

DEVELOPMENT OF MULTIFUNCTIONAL LINEN THROUGH IN-SITU SYNTHESIS OF SILVER NANOPARTICLES USING GROUNDNUT SHELL EXTRACT

Sheikh Javed, Mukul Gupta, Indrajit Bramhecha, Nagender Singh

Dept. of Textile Technology, Indian Institute of Technology (I.I.T.), Delhi, India, e-mail: jnsheikh@iitd.ac.in

Abstract: Functional textiles are widely demanded in the globalized textile market. The growth of technical textiles is also adding to the demand of such materials. Silver nanoparticles are widely utilized for this purpose; however, durability of the functional effect is a severe limitation. Chitosan is a film forming functional biopolymer which can be utilized as a template for in-situ generated silver nanoparticles. The polyphenolic compounds can be effectively utilized for generation and stabilization of nanoparticles on the chitosan-treated substrate. In the present work, the linen fabric was finished with chitosan-based formulations in order to react chitosan to linen through ester linkage. The modified linen is further imparted with multifunctional properties through in-situ synthesis of silver nanoparticles using groundnut shell extract. The functionalized linen was analyzed for change of appearance through computer colour matching. The functional properties like antibacterial activity, UV protection, antioxidant activity, wrinkle resistance were also evaluated. The formation of nanoparticles was confirmed through various characterization methods. The modified linen displayed excellent functional properties along with satisfactory durability towards repeated laundering treatments.

Keywords: linen, functional properties, silver nanoparticles, groundnut shell extract.

1 INTRODUCTION

Textile materials are becoming functional need of human beings and the functional properties in textiles are widely demanded by the consumers. Nanoparticles are widely reported for imparting functional properties to textile materials. Silver nanoparticles are one of the widely researched nanoparticles for preparing functional textile materials. The functional properties can be imparted using much lower dosages of nanoparticles; however, the efficient immobilization of such nanoparticles on textiles is necessary to achieve durability of functional effects. Chitosan is a highly basic polysaccharide and is one of the most bountiful polysaccharides available on earth. The presence of amino group, which can get protonated in acidic conditions and hold variety of anionic chemicals, made it a highly attractive polymer across the research community. Apart from this, it is a film forming polymer and its solution in polycarboxylic acids can be attached to cellulosic substrates. The reports regarding functional finishing of cellulosic fibres using chitosan are available in literature [1-3]. The combination of functional finishing of linen with chitosan-based formulations and the further *in-situ* synthesis of nanoparticles on modified substrate can result in generation of wash-fast functional effects. Groundnut/peanut shell extract (GSE) is known for the presence of flavonoids, polyphenols [4-6] and lignin which can act as reducing and stabilizing agents for silver nanoparticles. Hence utilization of such extracts can also act in the synergistic way to achieve the variety of functional properties.

In the present work, linen fabric was imparted with multifunctional properties using the combination of chitosan-based formulation, silver nanoparticles and GSE. The efficacy of functional properties viz. antibacterial activity, UV protection, antioxidant activity along with their durabilities towards repeated launderings were explored.

2 MATERIALS AND METHODS

2.1 Materials

Chitosan was purchased from the market. Linen fabric was supplied by Jayashree Textile, India. Citric acid, sodium hypophosphite, sodium hydroxide were supplied by Sigma chemicals.

2.2 Methods

Linen fabric (sample 1) was finished using chitosan-based formulation (Chitosan-1%, Citric acid- 8%, SHP-3%). The fabric was padded with the expression of 75%, dried at 80 °C for 4mins and cured at 180°C for 1 min. The finished fabric was treated with AgNO₃ solution (0.25%, on weight of fabric) at room temperature for 20 mins. The fabric was further treated with GSE (5%, pH-9) for 60 mins under sonication. The fabric was further washed with cold water for 5mins and dried (sample 2). The modified fabric was characterized using FTIR and SEM techniques. The change in appearance of fabric was measured using Gretag Macbeth Color-Eye 7000A spectrophotometer. The functional properties like crease recovery angle, antibacterial activity [7], UPF values [8] and antioxidant activity [2] were evaluated using standard methods. The modified fabric was subjected to repeated launderings as per AATCC-61 test method [7] followed by the evaluation of functional properties.

3 RESULTS AND DISCUSSION

3.1 Functional properties of the modified linen

The treatment of linen with chitosan-based formulation resulted in attachment of chitosan film to cellulose through ester linkage. Further treatment with silver nitrate resulted in introduction of silver ions on the finished linen. When

such linen was treated with GSE, the silver ions were reduced to silver nanoparticles and distributed throughout the chitosan film via attachment with various functional groups available on chitosan film. This resulted in stabilization of AgNPs on the modified linen.

Table 1 Functional Properties of modified linen

Sample No.	CRA	Bacterial Reduction ^{\$} (%)		UPF ^{\$}	Antioxidant activity ^{\$} (%)
		SA	EC		
1	98	N	N	5.6	N
2	162	100	100	65.9	98.2
2 (20wash)	148	95.5	96.3	49.1	82.5

1-Control, 2-Lin-CTS-AgNPs, \$-Average value of three determinations, S.A-S. Aureus, E.C.-E. Coli

The functional properties of the modified linen are presented in Table 1. The modified linen showed higher crease recovery angle which might be because of crosslinking of hydroxyl group by citric acid and the deposition of chitosan film thereby preventing the hydrogen bonding responsible for wrinkle formation. The efficient antibacterial activity against *S. aureus* and *E. coli* bacteria was also displayed by modified linen. The presence of antibacterial agents like chitosan, AgNPs, polyphenolic compounds resulted in synergistic antibacterial activity. The mechanisms of antibacterial activity of each of these antibacterial agents are available in literature. The use of GSE as reducing and capping agent was found to be a promising method of functionalization of linen. The polyphenolic compounds of GSE might also get attached to linen, as also indicated by colour change of fabric, resulting in enhanced functional properties.

The modified linen displayed UPF rating of 50⁺ indicating the excellent level of protection against UV light. This may be attributed to the presence of crosslinked chitosan film, silver nanoparticles and polyphenolic compounds on the modified linen. The modified linen also displayed efficient radical scavenging activity. The polyphenolic compounds and AgNPs are known for their radical scavenging activities. The polyphenolic compounds have ability to stabilize the DPPH radical resulting in discolouration of radical. This results in enhanced antioxidant activity. The colour of the sample turned brown after modification which might be attributed to the formation of AgNPs along with retention of polyphenolic biomolecules from GSE.

3.2 Characterization of Modified linen

The modified linen was characterized using FTIR technique. FTIR spectra (Fig.1A) confirms the attachment of chitosan through ester linkage along with the presence of silver nanoparticles. The SEM (Fig. 1B) images of modified linen showed surface deposition which might be because of chitosan film formation on the surface. The immobilized AgNPs were also evident from the images.

The method reported in the present work thus enable the modification of cellulosic textiles for performance enhancement with respect to functional properties.

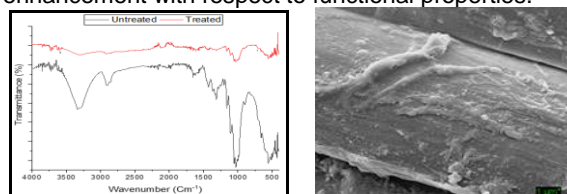


Figure 1: A) FTIR spectra of sample 1 and sample 2 B) SEM image of sample 2

3.3 Durability of Multifunctional properties

The modified linen was subjected to repeated launderings and the functional properties of the washed fabric are presented in Table 1. All the functional properties were retained to the significant extent till 20 washes. Further study regarding durability is under progress.

4 CONCLUSIONS

Successful preparation of multifunctional linen was carried out using a combination of chitosan-based finish, AgNPs and GSE. The efficient multifunctional properties were achieved which were found durable till 20 washes.

ACKNOWLEDGEMENT: Authors gratefully acknowledge Science and Engineering Research Board (SERB, India) for ECRA funding (project File no. ECR/2017/001041)..

5 REFERENCES

- [1] Hebeish A., Sharaf S., Farouk A.: Utilization of chitosan nanoparticles as a green finish in multifunctionalization of cotton textile. *International Journal of Biological Macromolecules* 2013, 60, pp.10–17.
- [2] Sheikh J., Bramhecha I.: Multifunctional modification of linen fabric using chitosan-based formulations. *International Journal of Biological Macromolecules* 2018, 118, pp. 896–902.
- [3] Teli M. D., Sheikh J., Bhavsar P.: Multifunctional finishing of cotton using chitosan extracted from bio-waste. *International Journal of Biological Macromolecules* 2013, 54, pp.125–130. A. E.
- [4] Nepote V., Grosso N. R., Guzman C. A.: Extraction of antioxidant components from peanut skins. *Grasas y aceites* 2002, 53(4), pp. 391-395.
- [5] Qiu J., Chen L., Zhu Q., Wang D., et al: Screening natural antioxidants in peanut shell using DPPH–HPLC–DAD–TOF/MS methods. *Food chemistry* 2012, 135(4), pp. 2366-2371.
- [6] Wee J. H., Moon J. H., Eun J. B., Chung J. H. et al: Isolation and identification of antioxidants from peanut shells and the relationship between structure and antioxidant activity. *Food Science and Biotechnology* 2007, 16(1), pp.116-122.
- [7] AATCC Technical Manual (2007), Research Triangle Park, NC, USA.
- [8] AS/NZS 4399. Sun protective clothing evaluation and classification; 1996.

USEFUL LIFE OF TOWELS

AFTER INDUSTRIAL LAUNDERING CYCLES

Vildan Sülar¹, Filiz Ersoy²

¹ Dokuz Eylul University Textile Engineering Department e-mail: vildan.sular@deu.edu.tr

² Dokuz Eylul University Graduate School of Natural and Applied Science, İzmir, Turkey

Abstract: While people use towels in hotels/holiday villages, the expectations are different because of being service sector. In hotels, the expectations of customers are high and towels are laundered at least once a day and the same performance such as softness, strength, hydrophilicity are expected after many washing cycles. In this research, six bath towels used in hotels were chosen to examine their usage and laundering performance. To understand the useful life of hotel towels and to examine the performance after washing, 1, 5, 25, 50 industrial laundering cycles were used. For that reason, seven white bath towels were collected from textile companies that produces home textiles only for hotels/holiday villages. Dimensional change, hydrophilicity, tear strength, whiteness index and softness were tested and statistically evaluated. Pulling out through a nozzle test was used for objective softness assessments. Consequently, the test results were compared with the values given in the related standard to make a better evaluation.

Keywords: Terry towel, industrial laundering, washing cycle, performance

1 INTRODUCTION

Terry towel is one of the commonly used home textile product. This type of fabric is made with loop pile on one or both sides that is generally covering the entire surface. Terry is a warp pile fabric with loops of warp threads alternating with ground threads. Such fabrics are produced by three systems namely ground warp, weft, and pile warps [1]. Towels produced in different sizes are textile products that have important properties such as water absorption and softness. They may be classified according to their dimensions as hand-, face-, bath-towels and etc.[2]. The main consumer property of terry towels is the high water sorption. Their better sorption capacity in comparison to the other fabrics is as a result of the pile layer, which forms greater sorption surface [3].

The towels have almost similar physical properties according to their end use such as hydrophilicity, softness and dimensional stability. The degree of softness should be as high as possible, because of contact with skin during daily use; the dimensional variation of towels after washing should also be as low as possible. These characteristic parameters define the performance of towels and determine their quality [2]. Besides, mechanical performance is also very essential for terry towels. These kinds of products are exposed to wet rubbing, washing and drying processes. The structural parameters such as fabric type, fabric weight, and yarn characteristics play determinative role on mechanical strength of the terry towels.

In related literature, many studies about effects of fabric structural properties have been performed [1-6]. In general, the effects of 1, 5 and 10 “domestic washing” cycles and drying processes are examined.

In this current research, different from the previous studies, effects of “industrial washing” cycles on

mechanical performance of the towels. For this purpose, seven different types of towels suitable for hotels were supplied for the experiments.

2 MATERIALS AND METHODS

In the experimental study, seven towels were used and conditioned in a textile testing laboratory under standard atmospheric conditions of 65 ± 2 % RH and 20 ± 2 °C temperature at least for 24 hours. Basic structural parameters of towels were tested before and after industrial laundering cycles. Industrial laundering processes contains four washing cycles such as 1, 5, 25 and 50 washing. Dimensional change, fabric unit weight, thickness, water absorption, tear strength, whiteness index and softness were tested and statistically evaluated. Pulling out through a nozzle test was also used for objective softness assessments.

Table 1. The basic structural parameters of the towels

Fabric code	Yarn count (Ne)			Yarn setting (threads/cm)			Mass per unit area (g/m ²)	Thickness (mm)
	Warp/	Weft/	Pile	Warp/	Weft/	Pile		
H1	20/2	16	16	14	18	14	443.7	3.65
H2	20/2	16	16	14	18	12	464.8	3.68
H3	20/2	16	16	14	18	12	505.4	4.66
H4	20/2	16	16	14	18	14	548.1	3.70
H5	20/2	16	20/2	14	18	12	551.7	4.58
H6	20/2	16	20/2	14	18	12	581.0	4.88
H7	20/2	16	20/2	14	18	14	836.8	6.16

*under 5g/cm²

Washing processes were conducted in a professional laundry company, which is well known in hometextiles laundering. Professional machines and washing programmes were used during laundering cycles.

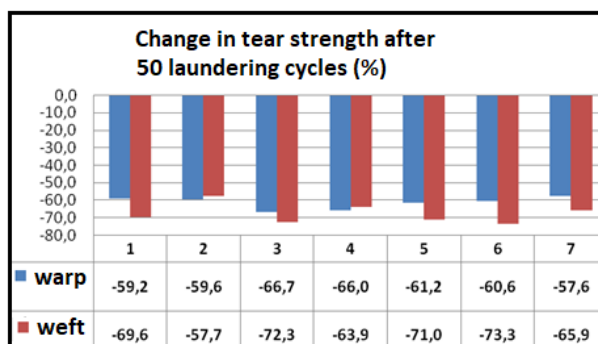
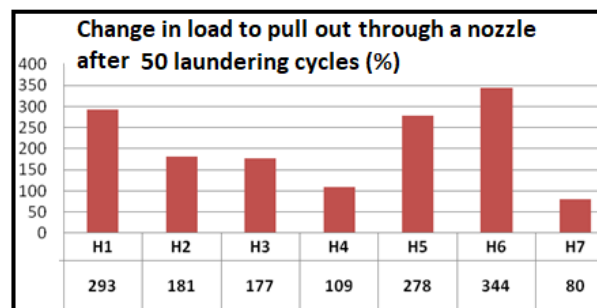
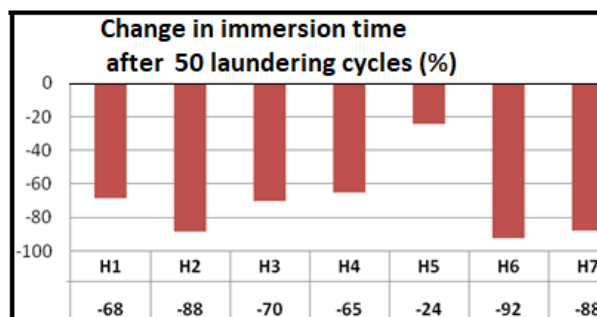
Table 2. The industrial washing process details and workflow chart for the towels

Washing machine: Tolon, 20kg			
Process	Time (min.)	Temperature and speed	Water+chemical
Main washing	15	60 °C	Cold+Hot+ Washing chemical
Wringing out	3	M (Middle speed)	
Rinsing	3		Cold
Rinsing	3		Cold
Rinsing	3		Cold+ Softening agent
Last wringing out	7	H (high speed)	
Tumble drying	45		

**Figure 1 a)** Test samples after tear strength **b)** Test sample during pulling through a nozzle test

3 RESULTS AND DISCUSSION

When all the results are evaluated, first laundering cycle was found critical for mass per unit area and dimensional shrinkage. The critical laundering cycle was found as 1-25. Five laundering cycle is determined to be critical for tear strength values. After five washing cycles, slight differences were noticed due to the stable fabric structural parameters. In Figure 2, the change in tear strength values can be seen after 50 laundering cycles. When load to pull out through a nozzle values were examined, it can be said that the necessary load to pull out the towels through a nozzle increased with the increasing laundry cycles meaning that the handle and the softness properties getting worse. In Figure 3, change in load values were given to make a good comparison after 50 laundering cycles. The hydrophilicity values of the towels depend on different factors, such as raw material type, fabric density, twist level of pile yarn and pile yarn fold. In the current research, the immersion time values decreased after every laundering cycle meaning that the hydrophilicity of towels increased by the increasing number of laundering cycles. The results of the whiteness measurements showed that all the towels used were bleached with the optical whitener; here was a decrease in the whiteness values after five cycles. This decrease became more pronounced after the 25 washings.

**Figure 2.** Change in tear strength values after 50 laundering cycles**Figure 3.** Change in load values to pull out towels through a nozzle after 50 laundering cycles**Figure 4.** Change in immersion time values after 50 laundering cycles

ACKNOWLEDGEMENT: The authors gratefully acknowledge to EKE Tekstil and ARIKAYA Laundry for their support for test materials and for the laundering processes. Special thanks to DEU Graduate School of Natural and Applied Sciences, DEU Textile Engineering Department, which support us to perform our work. **REFERENCES**

- [1] El-Badry, Kh., Saleh Salah M. & Bahlool Shereen O., (2013). Effect of Mercerization Techniques on Cotton Towels Properties, Journal of Applied Sciences Research, 9(3), 2386-2393.
- [2] Koç, E. & Zervent, B. (2006). An Experimental Approach on the Performance of Towels – Part I. Bending Resistance or Softness Analysis, Fibres & Textiles in Eastern Europe, 14, 1(55), 39-46.
- [3] Germanova-Krasteva, D.S., Kandzhikova, G.D. & Bochev, A.G. (2013). Influence of terry fabrics structure on dynamic sorption, International Journal of Clothing Science and Technology, 25(4), 243-256.
- [4] Karahan, M. (2007). Experimental investigation of the effect of fabric construction on dynamic water absorption in terry fabrics, Fibres & Textiles in Eastern Europe, 15, 3(62), 74-80.
- [5] Karahan, M. & Eren, R. (2006). Experimental Investigation of the Effect of Fabric Parameters on Static Water Absorption in Terry Fabrics, Fibres & Textiles in Eastern Europe, 14, 2(56), 59-63.
- [6] Petrulyte S. & Nasleniene J. (2010). Investigation of the liquid retention capacity of terry fabrics, Fibres & Textiles in Eastern Europe, 18, 5(82), 93-97.

EFFECT OF ANNEALING AND ADDING MAGNESIUM OXIDE ON THE PROPERTIES OF POLYPROPYLENE/VAPOR-GROWN CARBON FIBER COMPOSITES

Shuichi TANOUE¹, Taiki YOSHIDA¹ and Hideyuki UEMATSU¹

¹University of Fukui, 3-9-1 Bunkyo, Fukui 910-8507, JAPAN, e-mail: tanoue@matse.u-fukui.ac.jp

Abstract: In this study, we discussed the effect of annealing process and the localization of Vapor-Grown Carbon Fiber (VGCF) in Polypropylene (PP)/VGCF composites by adding Magnesium Oxide (MgO) with thermal conductivity and insulation properties. The surface resistivity of PP/VGCF composites decreased by annealing and adding MgO. In case of the composite without MgO, the surface resistance increased with the annealing time. However, in case of the composite with 30vol% MgO, there is no effect of the annealing time on the surface resistance of the composite. The thermal conductivity of the composites increased with the volume fraction of MgO because of the increase of the volume fraction of MgO and the localization of VGCF by adding MgO. However, the effect of annealing process on the thermal conductivity of PP/VGCF composites was quite smaller than the effect of annealing process on the surface resistance.

Keywords: Vapor-Grown Carbon Fiber, Composite, Thermal Conductivity, Surface Resistivity

1 INTRODUCTION

One of the methods for giving the high performance to fiber and polymer materials is the melt compounding which the material and functionalized fillers are mixed in the melting state of the material. Multiwall carbon-nanotube (MWCNT) is one of the functionalized fillers used for giving the high thermal and electrical conductivities to fiber and polymer material. Especially, MWCNT has the high thermal and electrical conductivities to the axial direction of the fibers. Then, the dispersion state of MWCNT in a polymer composite would significantly affect the properties of the composite. The annealing is one of the methods for improving the dispersion state of MWCNT in the composite. Chen et al. [1] reported the effect of annealing on the conductivity of the composites. In addition, the concentration of MWNT in the part of polymer with localized MWCNT increased when MWCNT is localized in a specific polymer because the number of contacts between MWCNT in the composite increased.

As the mentioned above, the concentration of MWCNT in a polymer is increased by adding MWCNT and other filler with high thermal conductivity and typical large size in the polymer. In addition, the improvement of thermal conductivity of the composites with a small amount of MWCNT can be expected by the annealing. In this study, we discussed the effect of annealing and the localization of fillers on the thermal and electrical conductivities of a polymer composites adding two kinds of filler with high thermal conductivity and different size each other.

2 EXPERIMENTAL

Polypropylene (PP) (MFR = 26–29g/10min, Thermal conductivity of 0.2 W/(m · K), Volume resistivity of 10^{16} – 10^{18} Ω ·cm, Supplier of Sumitomo Chemical, co. Ltd, Japan) was used as the polymer material. Vapor-Grown Carbon Fiber (VGCF) (Thermal conductivity of 1200 W/(m · K), Volume resistivity of 10^{-4} Ω ·cm, Supplier of Showa Denko, K.K, Japan) was used as MWCNT. Magnesium Oxide (MgO) (Thermal conductivity of 42–60 W/(m · K),

Volume resistivity of 10^{17} Ω ·cm, Supplier of Ube Material Industries, Ltd., Japan) was used as the other thermal conducting filler.

The composite samples were prepared by melt compounding using a co-rotating twin-screw extruder after dry mixing of raw materials. Obtained composite samples were molded by the compression molding using the heat press machine. After compression molding, the annealing was done under the constant temperature and time.

The surface resistance of the sample sheet after molding and annealing was measured by the resistivity meters produced by Mitsubishi Chemical Analytech Co., Ltd., Japan. The thermal conductivity of the sample was measured by the quick thermal conductivity meter QTM-500 produced by Kyoto Electronics Manufacturing Co. Ltd., Japan.

3 RESULTS AND DISCUSSIONS

In this abstract, we discussed the surface resistance of the composites. Figure 1 shows the comparison of surface resistance as a function of VGCF contents between PP/VGCF and PP/MgO/VGCF. The MgO is MgO-10 and the contents of MgO was 30 vol%. The thermal conductivity of the composites decreased by adding MgO in the composites at VGCF contents of 1 vol% or less. The contents of VGCF in PP matrix increased by adding MgO. Then, the surface resistance of the composite became decreased by increasing the contacting number of VGCF in this composite.

Next, we compared the surface resistance of PP/MgO/VGCF between the heat-treated (Annealing) sample at 200 deg C and 30 min and no heat-treated one (No Annealing). Figure 2 shows the experimental results for these comparisons. Used MgO was MgO-10 and the contents of MgO was 30 vol%. In case of VGCF content of 1 vol%, the surface resistance of PP/MgO/VGCF significantly decreased by the annealing. The connecting points between VGCF in the composite would be created by the annealing. On the other hand, in case of VGCF

content of 1.5 vol%, the surface resistances of PP/MgO/VGCF were independent of the annealing. This result implies that the creation of the connecting points between VGCF in the composites would reach the steady-state in case of VGCF content of 1.5 vol% and the renewed connecting points between VGCF would not be created by annealing.

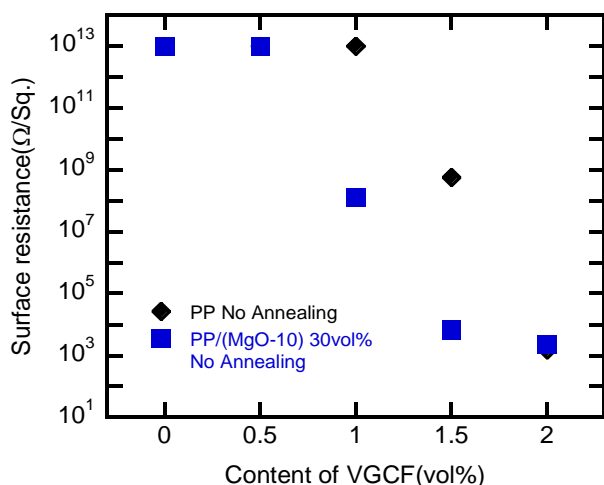


Figure 1 Surface resistance of PP/VGCF and PP/(MgO-10) 30vol%/VGCF composites versus VGCF content.

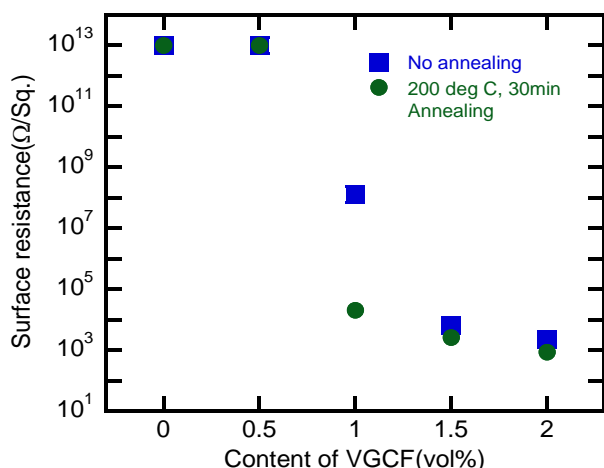


Figure 2 Surface resistance of PP/(MgO-10) 30vol%/VGCF annealing composites versus VGCF content.

Next, we discussed effect of annealing time on the surface resistance of PP/MgO/VGCF. In case of the annealing time of 0 min, i.e. no-annealing, the surface resistance decreased with an increase of MgO content for the composite because the content of MgO for PP decreased by adding MgO in the composite. In case of the annealing time of 30 min, the surface resistance is smaller than that in case of no-annealing on the whole. In addition, the surface resistance also decreased with an increase of MgO content for the composite. This result implies that the electrical conductivity of PP/MgO/VGCF by adding MgO and the annealing are simultaneously progressive. On the other hand, in case of the annealing time of 120 min, the surface resistance was almost independent of MgO content because the connecting point between VGCF may reach to the equilibrium state without adding MgO in the composite. This implies that the electrical conductivity of this PP/MgO/VGCF does not improve even if MgO add in this composite.

In addition, we discussed the thermal conductivity of PP/MgO/VGCF at various annealing time. VGCF content was 1 vol% and the annealing temperature was 200 deg C. The thermal conductivity of PP/MgO/VGCF increased with MgO content, and the thermal conductivity of the composite at same MgO content increased a little by the annealing. However, the increasing rate of the thermal conductivity by the annealing was smaller than the increasing rate of the surface resistance. The reason may be the difference of the conveyance medium, a phonon for the heat conduction and an electron for the electrical conduction.

4 CONCLUSIONS

The surface resistance of PP/MgO/VGCF decrease by the annealing and adding MgO. The synergy effects of the annealing and adding MgO for improvement of electrical conduction of PP/MgO/VGCF was carried out by selecting the annealing condition. In addition, the effect of annealing on the heat conduction of PP/MgO/VGCF is smaller than that on the electrical conduction of this composite.

5 REFERENCES

- [1] Chen Y., Yang Q., Huang Y., Liao X., Niu Y.: Influence of phase coarsening and filler agglomeration on electrical and rheological properties of MWNTs-filled PP/PMMA composites under annealing. *Polymer* 2015, 79, pp. 159-170

LCAM COTTON WHITE SCALE

Martina Viková¹, Michal Vik¹ and Jana Čandová¹

¹Technical University of Liberec, Studentská 2, Liberec, Czech Republic, e-mail: martina.vikova@tul.cz

Abstract: At present, a quantitative measurement of degree of whiteness is focused on simulation of outdoor lighting D65, based on that direct comparison of whiteness values obtained is confusing in case of light source, which is far in point of view of spectral power distribution to filtered xenon flash lamp that is installed in measuring device. In this presentation is discussed preparation of simple cheap cotton white scale capable of differentiation between violet and greenish whites together with tint scale allowing assessment of nearly white products under artificial light sources as LEDs and fluorescent tubes.

Keywords: whiteness, whiteness index, cotton, fluorescent whitening agent, colorimetry

1 INTRODUCTION

The color appearance of nearly white materials is dependent on many factors such as reflectance of used substrate, used fluorescent whitening agent (FWA), and spectral power distribution of light source [1]. Well known CIE linear whiteness formula is optimized for D65, which is a model of outdoor light, nevertheless many of nearly white materials are used indoor and there are assessed under artificial light sources with different correlated color temperature (CCT) and wide range of spectral power distribution far from CIE illuminant D [2]. Based on these differences measured whiteness of products as lingerie, shirts, tablecloth, etc. is frequently mismatched and customers unsatisfied. New light sources such as solid state (LED) produce less amount of UV radiation that allows increase of observed white of product. Until now isn't available acceptable whiteness formula allowing solution of above-mentioned problem.

One of possible solution is development of simple white scale, which allows visual assessment under different light sources and transfer visual scale into CIE whiteness units. Generally, for visual arbitrary estimation of differences in the degree of whiteness are used some of custom scales. The differences may be in the hue, the range of visual whiteness over which the such scale is used and of course in the size of individual steps [3]. Besides knowing the quality of the visual assessment of whiteness, we should be able to express the effect of whiteness quantitatively. We need thus require a unit of measurement relating to whiteness, which should be based on visually perceptible threshold value and equal step [4]. The magnitude of this just noticeable threshold difference (JND) as the smallest visual unit for whiteness must correlate with common scales as CIE whiteness. For example, well known Hohenstein white scale that is used for calibration of UV content in daylight simulator used in measuring device is based on only 4 steps starting at CIE whiteness almost 90 units till CIE whiteness about 155 - 160. That means whiteness difference step between individual samples is almost 17.5 unit [5].

Other disadvantages relating to these scales are that scales manufactured from textiles or paper aren't sufficiently lightfast and rapidly become soiled. Alternative durable whiteness scale can be prepared from set of white plastic samples produced by Avian company. Unfortunately, such samples are shifted around 1 unit in positive (green) tint direction from neutral axis and doesn't

cover high whiteness, which is obvious for some of application in textile industry.

Due to this alternative whiteness formulae such as Whiteness Index based on CIECAM02 [6].

2 MATERIALS AND METHODS

2.1 Materials

In order to prepare different white samples, the scoured and chemically-bleached plain woven cotton fabrics were treated with selected commercial fluorescent whitening agent (FWA) RYLUX DK, at 18 different concentrations, from which 9 concentrations were chosen as suitable for final scale. These concentrations of applied FWAs, are shown in Table 1 together with colorimetric data.

Table 1 Table of LCAM CWS sample set, colorimetric data are measured for illuminant D65 and 10° observer

	Conc. (mg/L)	X (-)	Y (-)	Z (-)	x (-)	y (-)
1	0.21	87.1	91.9	95.7	0.3171	0.3344
2	0.51	88.2	92.7	99.8	0.3143	0.3301
3	0.98	88.7	93.0	102.4	0.3123	0.3272
4	1.65	89.3	93.3	105.5	0.3100	0.3238
5	2.67	89.8	93.6	108.1	0.3080	0.3210
6	4.31	90.7	94.2	113.0	0.3046	0.3161
7	6.90	91.3	94.5	116.2	0.3023	0.3128
8	11.00	92.2	95.1	120.0	0.3000	0.3094
9	17.50	92.6	95.4	123.3	0.2974	0.3064

2.2 Methods

Total radiance factor and computed luminescence factor of each sample was derived from CIBA Plastic White Scale, Avian white plastic set, which was used during calibration of Datacolor SF600+ spectrophotometer in de:8° mode. The measurement was carried out in the range 360 to 700 nm at 5 nm intervals.

Visual test was made in SPL III lighting cabinet with panel of 6 color normal observer with use of D65 filtered tungsten simulator with UV tube enhancing the content of UV radiation to level adequate to CIE D65 illuminant. As comparative test was used the fluorescent tube kind of daylight simulator without additional UV radiation. Both daylight simulators were in category C based on ISO 23603:2005(E)/CIE S 012/E:2004 standard.

3 RESULTS AND DISCUSSION

Produced set of white cotton samples show that 18 samples starting on 70 units of CIE whiteness till 160 with equal step around 5 unit is on the border of JND, nevertheless for number of naïve observers was difficult to recognize individual sample whiteness. Due to this problem we have reduced number of samples and final whiteness grading was near to 10 CIE whiteness unit. On picture in Fig. 1 is visible that under daylight simulator with suitable amount of UV radiation is simple to recognize individual steps of scale.

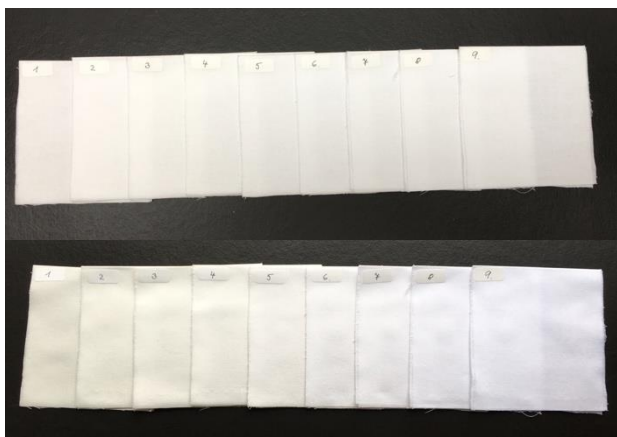


Figure 1 LCAM CWS under daylight without UV (top) and with UV radiation (bottom)

Also, reflectance, respectively total radiance factor measurement shows equal steps between individual members of CWS as shown on graph in Fig. 2.

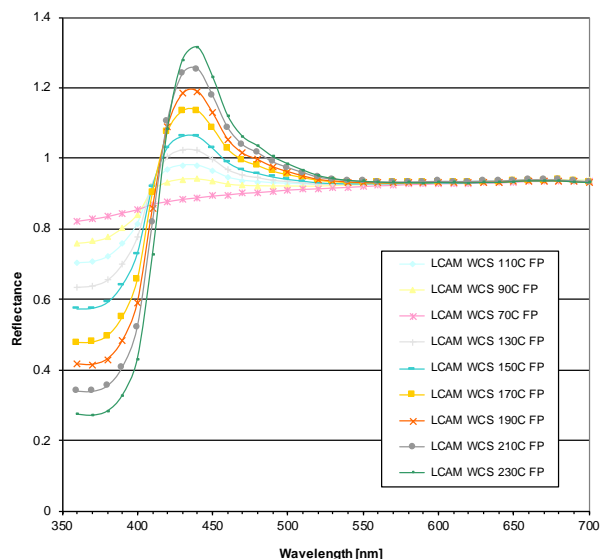


Figure 2 Reflectance of LCAM CWS sample set

Main importance of whiteness scale for visual assessment lying in its linearity on CIE xy diagram because based on that it is possible to use such scale for computing of tint difference and also such set of samples is suitable for UV/Whiteness calibration of measuring devices. On graph in Fig. 3 is visible acceptable linearity of LCAM CWS and relating tint steps according to Ganz-Griesser [7]. Angle between reference wavelength (RWL) and neutral line of

LCAM CWS computed via linear regression is 16.4° , which is near to expected CIE whiteness value of 16° .

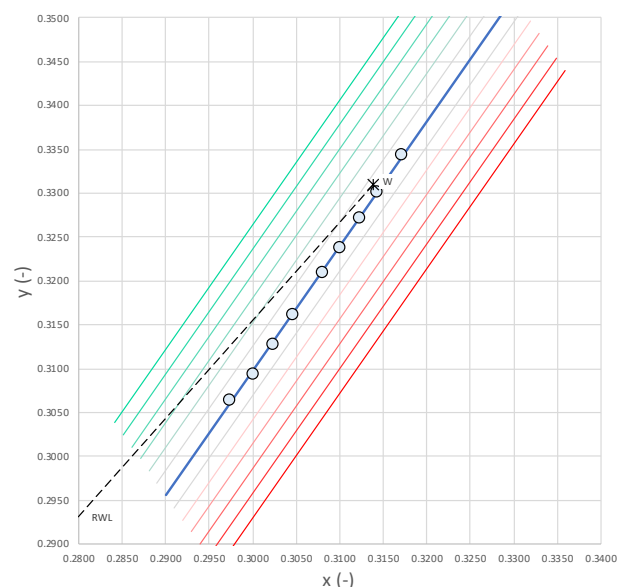


Figure 3 LCAM CWS on CIE xy diagram with calculated tint differences according Ganz-Griesser

4 CONCLUSION

It was shown that LCAM Cotton White Scale isn't only visual scale but it is also usable as set of samples allowing UV/Whiteness calibration of suitable measuring devices. Our experience with production of LCAM CWS show that reproducibility of this scale is almost ± 3 CIE whiteness units.

5 REFERENCES

- [1] Vik, M. & VIKOVÁ, M., **2018**. Color Rendition of Artificial Light Sources: Past and Future. In 7th Lighting Conference of the Visegrad Countries, LUMEN V4 2018 - Proceedings. IEEE, pp. 1–4. doi: 10.1109/LUMENV.2018.8520968
- [2] Vik, M., Khan, N. & VIKOVÁ, M., **2017**. LED Utilization in Cotton Color Measurement. *Journal of Natural Fibers*, 14(4), pp.574–585.
- [3] Anders, G., **1968**. Control of Whites: The Cibanoid White Scale. *Journal of the Society of Dyers and Colourists*, 84(2), pp.125–132.
- [4] Abbasi, A., Vik, M. & VIKOVÁ, M., **2014**. Color difference formulae evaluation by method of adjustment. *World Journal of Engineering*, 11(1), pp.89–94.
- [5] Hirschler, R. & Zwinkels, J., **2007**. *Appendix 3: Use of CIE Colorimetry in the Pulp, Paper, and Textile Industries*, Hoboken, NJ, USA: John Wiley & Sons, Ltd.
- [6] Vik, M. & VIKOVÁ, M., **2017**. Development of Whiteness Formula Based on CIECAM02, PROCEEDINGS of the Conference on "Smarter Lighting for Better Life" at the CIE Midterm Meeting 2017 October 23–25, 2017 Jeju, South Korea
- [7] Ganz, E.; Griesser, R. Whiteness: Assessment of Tint. *Applied Optics* **1981**, 20 (8), 1395–1396.

FUNCTION OF COLOR IN AESTHETIC PROPERTIES OF PLAIN KNITTED FABRIC

Lina Wakako¹, Kai Kodama² and Toshiyasu Kinari¹

¹ Institute of Science and Engineering, Kanazawa University, Ishikawa, Japan, e-mail: linawakako@se.kanazawa-u.ac.jp

² Graduate School of Natural Science and Technology, Kanazawa University, Ishikawa, Japan

Abstract: A required aesthetic property of pantyhose (PS) is the desirable surface roughness of the PS on a bare leg. This study aims to clarify the effect of PS color on the visually perceived surface roughness of the leg with PS, which was examined through visual sensory evaluation using a plate-like leg model and commercially available PS. The results indicated that the PS color, particularly the L^* value, affects the visually perceived surface roughness of the leg with PS. That is, when the color of the leg with PS or the PS fabric is bright, the visually perceived surface roughness of the leg with PS will be “fine (grain).”

Keywords: knitted fabric, aesthetic property, color, surface roughness, pantyhose

1 INTRODUCTION

Aesthetic performance is important in textile products. Pantyhose (hereinafter, PS) is composed of thin circular plain knitted fabrics; its aesthetic properties are regarded as important. An aesthetic property is the visually perceived surface roughness of the leg with PS [1]. From sensory evaluation by visual sense using a leg model and PS in beige, it was found that the visually perceived surface roughness of the leg with PS changed by the PS color despite a constant stitch density of the PS fabric on a bare leg [2]. Meanwhile, visual features of the leg with PS include the color gradation by the apparent stitch density of the PS fabric on a bare leg as well as shading by illumination light. These visual features are cues for judging the surface roughness of an object. The effect of the PS color on the visually perceived surface roughness of the leg with PS is unclear. Through sensory evaluation by visual sense using a plate-like leg model and commercially available PS, the effect of PS color on the visually perceived surface roughness of the leg with PS was investigated.

2 MATERIALS AND METHODS

2.1 Samples

The sample fabrics were commercially available PS. The sample fabrics were circular plain knitted fabric with a single covered yarn whose apparent yarn count was 3.2 tex. The apparent yarn count was calculated from the mean mass. This was determined when a 1 m test length of a yarn sample, which was collected by loosening a PS sample, was placed under a tension of 0.5 cN. The mass was measured using an electronic force balance (Mettler-Toledo International Inc. MT5) and the mean mass was calculated as the average of 10 measurements. The colors were eight types of beige, and the color values are shown in Table 1. The color values were measured using a colorimeter (NIPPON DENSHOKU IND. CO., LTD. NF333). The measurement was repeated 15 times per sample and the average color value was obtained. During the measurement of the color values of the sample fabrics, the sample fabrics were layered into a thick sample of more than 20 sheets to prevent incident light from being transmitted through the sample. The stitch density of the

extended sample fabric was three conditions, the wale density was 25.3 wales/cm, the course densities were 21.9, 27.9, and 57.5 courses/cm. The extended state represents the apparent stitch density around the knee of the leg with PS. The leg size was based on that of a Japanese female in her 20–30s [3]. The plate instead of a bare leg was completely covered with a thick and lusterless beige paper. The color of the paper was $L^* = 76.1$, with $a^* = 6.7$ and $b^* = 26.7$. The plate sample is a plate-like leg model covered with the extended sample fabric, and 24 types are available. The color ranges of the plate samples are shown in Figures 1 (a)–(c).

2.2 Sensory Evaluation by Visual Sense

Sensory evaluation by visual sense was performed in a darkroom. The plate samples were illuminated by artificial sunlight illuminants (Duro-Test Lighting, Inc. TRUE-LITE, color temperature at 5500 K). The intensity of illumination near the front of the plate samples was 400 ± 10 lx. This value was adjusted using an illuminance meter (TOKYO PHOTOELECTRIC CO., LTD. ANA-F11). In the sensory evaluation, we used the ranking method with the best–worst scaling. Because the results are given according to an ordinal scale, they were transformed into scores that were the interval scale, i.e., the expected values of normal order statistics or rankit. Subsequently, the scores were analyzed statistically. “fine (grain) - coarse (grain)” were used as the evaluation word. This word represents the visually perceived surface roughness of the leg with PS, and was based on the results of a factor analysis subsequent to a preliminary survey of evaluation words most frequently used in reference to the aesthetic properties of PS [1]. Sixteen individuals participated in the sensory evaluation and all of the evaluators were Japanese females in their twenties. The observation distance between the observer and the plate samples was 1.5 m.

3 RESULTS AND DISCUSSIONS

3.1 Visually Perceived Surface Roughness

To investigate how much the judged rank of each evaluator agrees overall, Kendall's coefficient of concordance (W) was calculated. W was moderately high at 0.64, and was significant at the 1% level. This implies a difference in the visually perceived surface roughness of the plate sample depending on the color of the plate sample. Additionally, differences among scores on plate samples with different colors were analyzed by multiple comparison using Scheffé's method. Statistical significance ($p < 0.01$) was observed in an analysis of variance test for one source of the plate sample color. No significant difference was found between the plate samples with different stitch densities in the same color of the sample fabric. However, a significant difference was indicated in some color pairs of the sample fabrics. It was confirmed that the visually perceived surface roughness of the plate sample was affected by the color of the plate sample regardless of physical roughness in the surface of the plate sample.

3.2 Correspondence of Color to Visual Impression

The relation between color value and the visually perceived surface roughness of the plate sample was investigated. Figure 1 shows the correspondence relations. In Figures 1 (a) and (b), the markers of the plate samples were scattered, there no tendency was observed. It appears that the visually perceived surface roughness of the plate sample does not correspondence clearly with the chromaticities of a^* and b^* . Contrary to this, Figure 1 (c) shows a linear distribution of the markers of the plate samples. From the correlation analysis, an extremely strong correlation, i.e., a coefficient of 0.9 and significance at a 1% level was demonstrated.

4 CONCLUSIONS

The color of PS fabric, particularly the L^* value, affected the visually perceived surface roughness of the leg with PS. Namely, when the color of the leg with PS or the PS fabric was bright, the visually perceived surface roughness of the leg with PS was "fine (grain)."

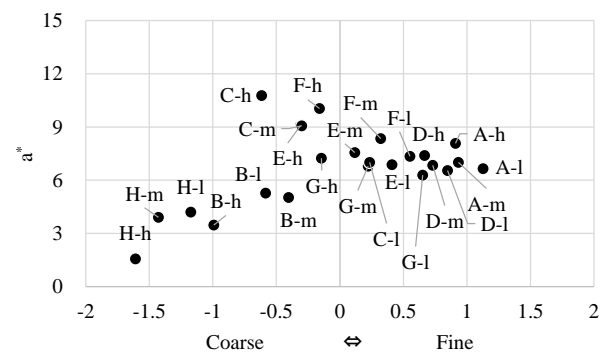
5 REFERENCES

- [1] Wakako L., Shimokawa T. and Kinari T.: Analysis of the evaluation factors and indexes for the aesthetic properties of pantyhose. Journal of fiber science and technology 2016, 72, 5, pp. 112-119.
- [2] Wakako L. and Kinari T.: Visual surface roughness of legs with pantyhose and color effect of pantyhose fabric. Book of abstracts - the 45th textile research symposium 2017, p. 79.
- [3] Research institute of human engineering for quality life: Japanese body size data book 2004 – 2006. Research institute of human engineering for quality life, Japan, p. 151, 307, 309, 311, 313.

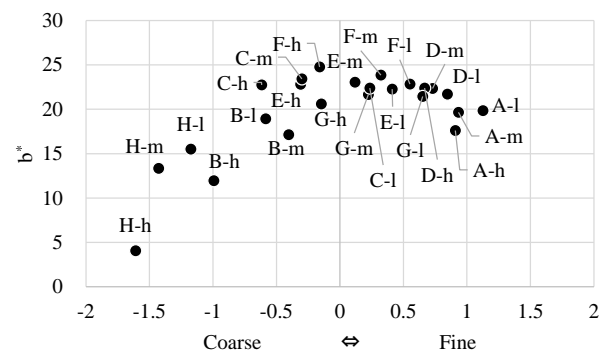
ACKNOWLEDGEMENT: In carrying out this research, we would like to express our sincere appreciation to Mr. Shin Murase and other students at Kanazawa University for their assistance. This work was supported by JSPS KAKENHI Grant Numbers 15K16179 and 18K02253.

Table 1 Color values of sample PS fabrics.

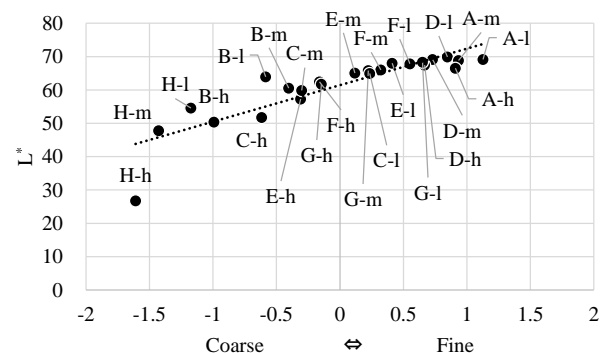
Samples	L^*	a^*	b^*
A	62.1	8.9	11.2
B	34.5	0.4	2.7
C	40.8	8.3	15.6
D	62.9	7.5	19.4
E	52.2	7.7	17.7
F	53.4	10.2	20.6
G	53.7	5.9	14.8
H	14.3	-0.3	-1.9



(a) a^*



(b) b^*



(c) L^*

Figure 1 Relationship between color values and visually perceived surface roughness of the plate sample. -l, -m and -h are 21.9, 27.9 and 57.5 courses/cm, respectively.

MICROENCAPSULATION OF PHENOLPHTHALEIN IN ALGINATE MICROSPHERES AS PH SENSOR SYSTEMS AND THEIR POSSIBLE DEPOSITION ON FIBERS OR OTHER TEXTILE MATERIALS

Aleksandra Wyszowska¹, Zbigniew Draczyński¹

¹Department of Material and Commodity Sciences and Textile Metrology, Lodz University of Technology, 90-924 Lodz, Poland, email: aleksandra.wyszowska@edu.p.lodz.pl

Abstract: Microencapsulation is a versatile approach because it can be used to encapsulate an unlimited number of materials, in both solid and liquid phase. It is possible to incorporate microcapsules into composites, fibers or coatings. The preparation of particles with core/shell structures is most effective by combining hydrophilic core materials with hydrophobic polymers as shell forming components or reverse. Alginate is a water-soluble polysaccharide. Alginates make an ideal candidates for producing particles with different applications thanks to its easy availability, versatility and sol-gel transition properties.

It was assumed that it is possible to obtain microcapsules from alginate as a polymeric coating with core active component in form of indicator phenolphthalein; and it is possible to create such system in which, under certain conditions, the layer separating the active component is destroyed/permeable, which will result in the possibility of using such systems as simple pH sensors, in addition, it will be possible to deposit such microcapsules on e.g. fibers. Main goal of work was to obtain functional microcapsules which can easily monitor changes taking place by color change; introduction of functional microcapsules / microspheres into polymer films, nonwovens, or polymer fiber matrix.

Sodium alginate is a water-soluble polysaccharide. Sodium salt of alginates make an ideal candidates for producing particles with different applications thanks to its easy availability, versatility and sol-gel transition properties. The development of pH indicator microcapsules for a pH change sensing involves: encapsulation method development and indication function testing. A good example would be phenolphthalein, because of its color change, when exposed to basic pH conditions, it is more pronounced and easier to detect with the naked eye than that of other possible indicators. This makes the color change for phenolphthalein easier to detect visually (change from colorless to purple instead of from one color to another color). Alginate monomers linkages can be cleaved by pH degradation mechanism, it is more stable near neutral pH and with extreme pH its degradation increases. The degree of swelling can be controlled by adjusting for example the acidity of the medium. Such pH changes will indicate color change of encapsulated phenolphthalein.

Keywords: alginate, microspheres, pH sensor

STUDY ON OIL SORPTION AND RELEASE CHARACTERISTICS OF KAPOK FIBER POWDER

Yanfang Xu¹, and Guangbiao Xu²

¹ College of textile, Donghua University, Shanghai, China, e-mail: 1169124@mail.dhu.edu.cn

² College of textile, Donghua University, Shanghai, China, e-mail: guangbiao_xu@dhu.edu.cn

Abstract: In this study, kapok fiber powder was evaluated as a wicking material which related to both the oil sorption and release properties for the application of mechanical lubricating field. The kapok fiber powder was obtained by mechanical pulverization method. The length distribution of kapok fiber powder was among several micrometers to 2 mm. Preliminary experiments showed that, compared with raw kapok fiber, the oil sorption capacity of kapok fiber powder decreased significantly. However, compare with wood pulp fiber powder whose oil sorption capacity to mineral oil, PAO synthetic oil and synthetic lubricant was 7.7 g/g, 7.6 g/g and 7.4 g/g, respectively, kapok fiber powder depicted nearly three times higher oil sorption capacity. The oil release property of oil-containing wicking material was test by a home-made device which simulated the usage of lubricant in the bearing of a typical fractional horsepower motor end shield. Results showed that oil release ratio increased with the increasing oil sorption ratio and temperature.

Keywords: : kapok fiber powder, oil sorption, oil release, lubricating

1 INTRODUCTION

Kapok fiber is a natural lignocellulosic fiber obtained from the seedpod of kapok tree. Single kapok fiber has a big cylindrical lumen and very thin cell wall which mainly consists of cellulose (64%), lignin (13%) and polysaccharide (23%). Currently, the research on the oil sorption of kapok fiber mostly focuses on how to increase the oil sorption capacity¹⁰. Few researches on the oil release of oil-containing kapok fibers. In the field of mechanical lubrication, fiber materials can be used as a wicking material, which would deliver sufficient lubricating oil to the rotating bear. When the bearing is not running, the oil-containing wicking material could store the oil well. When the bearing is running, the wicking material in contact with the bearing surface releases oil under the action of heat and capillary. The fiber materials used in the field of lubrication are mainly short fibers or fiber powders, which facilitates the delivery of oil-containing wicking material to the storage location, such as in bearing end caps or bearing recesses, by manual or mechanical indentation. As a sorption carrier, the oil sorption capacity of kapok fiber is significantly higher than that of cotton fiber and wood pulp fiber. From this point of view, a higher oil sorption amount means the material has great potential to release more oil. Therefore, it is necessary to study the oil sorption of kapok fiber powder and the oil release performance under specific conditions to expand the application fields of kapok fiber. And the wetting property between wicking material and liquid would be further studied to explore the oil sorption/release mechanism of oil-containing wicking material.

2 MATERIALS AND METHODS

2.1 Materials

The kapok fiber used in this study was java kapok got from Pate County, Java Tengah, Indonesia. The wood pulp paperboard was got from a local company, Wuxi, China. Three test oils, two of them are lubricating base oil (mineral oil, PAO synthetic oil). One is synthetic lubricant. They were purchased from local workshop.

2.2 Oil sorption test of wicking material

0.2g material was placed in the test oil for 15 min to make sure that it reached the equilibrium stage. Then it's taken out and drained for 15 min and weighted. After drained for 24 h, it was weighed again to obtain its static oil retention ratio. Raw kapok fiber, kapok fiber powder and wood pulp fiber were test, respectively. Every test was repeated three times to obtain an average value.

2.3 Oil release test of wicking material

A device to test the dynamic oil release performance of oil-containing wicking material was built. The test device consists of three parts: heating unit, rotating unit and oil collecting unit. Oil release versus time was determined by periodically weighing sample.

3 RESULTS AND DISCUSSION

3.1 Characterization of wicking materials

Kapok fiber has a smooth surface and a distinct hollow structure without any ripple. The fiber has an average external diameter of 16.29 μm , internal diameter of 14.29 μm and length of 22 cm¹⁷. Compared with raw kapok fiber, the kapok fiber powder is mechanically sheared due to the pulverization process, part of the middle cavity is crushed, part of the length direction is mechanically twisted due to shearing. Wood pulp powder depicted flat structure, along with a small number of grooves along the length direction. The kapok fiber powder had a wider length distribution than that of wood pulp powder, with all the length of fibrous powder below 2 mm. For wood pulp powder, 84.18% below 0.3 mm, however, that of kapok fiber powder was 38.6%. The structure and length distribution of fibrous materials would result in different oil sorption property and further had an impact on the oil release property which will be discussed below.

3.2 Characterization of oil sorption capacity

The oil sorption capacity and oil retention capacity of raw kapok fiber, kapok fiber powder and wood pulp powder

were test, respectively. As shown in Fig. 1a, compared with raw kapok fiber, the oil sorption capacity of the kapok fiber powder dropped by almost half. It's mainly contributed to two aspects reasons. Firstly, after cutting into a fibrous powder, its natural bulk density is larger than that of the original kapok fiber, and the void in the aggregate is reduced, which means that the oil storage space is reduced. Secondly, the mechanical shearing action causes the lumen of a part of the fiber to be crushed, resulting in a reduced oil absorption capacity. However, compared to the wood pulp powder which is also present in powder form, the kapok powder has a significantly higher sorption capacity for test oils than that of wood pulp powder. The reason may be that, on the one hand, there is a surface wax on the surface of the oil kapok fiber, which makes it hydrophobic and oleophilic. On the other hand, some kapok fiber powder still retains its hollow structure, which provides more space for oil storage. Fig.1b showed the oil retention ratios of test materials at room temperature were all above 85% and below 90%, which provide a basis for the selection of oil sorption ratio for fibrous powder used in the field of lubrication. Because the oil-containing wicking material must retain all the when the bearing was not working, which meant that the oil retention ratio of oil-containing materials must be 100%.

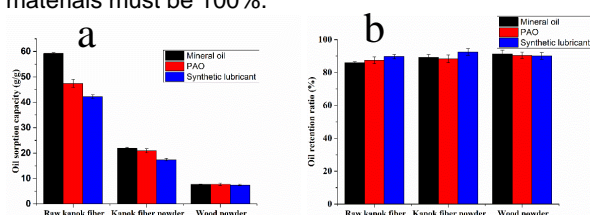


Figure 1 (a) oil sorption capacity (b) oil retention ratio of raw kapok fiber, kapok fiber powder and wood pulp fiber

3.3 Characterization of oil release of oil-containing wicking material

It can be seen from Fig. 2 that the release of the oil-containing wicking material can be divided into two stages. At the beginning of the test was the rapid release phase of the oil, and with the extension of time, the release rate of the oil gradually decreased, which can be called the slow release phase. The overall release rate is exponentially reduced. For kapok fiber powder at 70 °C, the oil release ratio of synthetic lubricant after 40 h was 37.4%, 44.5% and 57.1% at the oil sorption ratio of 10 g/g, 12 g/g and 14 g/g, respectively, indicating the oil release ratio increased by the increasing of the oil sorption ratio of wicking material. For wood pulp powder, the oil release ratio after 40 h was 31.8% and 38.9% at the oil sorption ratio of 5 g/g and 6 g/g, respectively. To compare the release properties of kapok fiber powder with wood pulp powder, the oil sorption ratio of 14 g/g and 6g/g for kapok fiber powder and wood pulp powder was chosen, respectively, both of which accounts for about 80% of the respective saturated oil sorption. Results showed that the oil release ratio of kapok fiber powder was 57.1% and that of wood pulp powder was 38.9%, indicating the better oil release property of kapok fiber

powder. Since the oil absorption capacity of the kapok fiber itself was much larger than that of the wood pulp fiber powder, and its ability to release the oil liquid was also superior to the wood pulp fiber powder. It can be speculated that the kapok fiber powder has great potential to be used as an excellent wicking material in the field of mechanical lubrication.

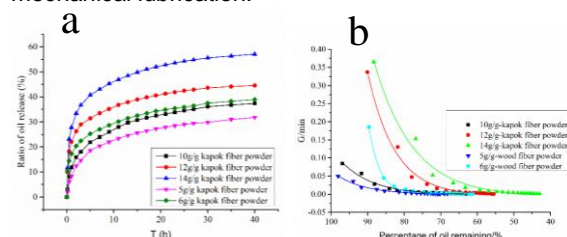


Figure 2 (a) oil release ratio versus time, and (b) oil release rate versus percentage of oil remaining of oil-containing wicking materials to synthetic lubricating oil at the temperature of 70 °C.

It is necessary to study the oil release properties of the oil-containing fibers under different temperature conditions, since the heat generated during the rotation of the bearing, and the properties of the oil vary greatly with temperature. As the temperature increases, the oil release ratio and oil release rate of the oil-containing fibers increase. The oil release ratio increased from 25.2% at 30 °C to 40.1% at 90 °C, and further to 49.2% at 130 °C. The main reason for this phenomenon is that the viscosity of the oil is sensitive to temperature, and as the temperature increases, the viscosity of the oil drops significantly, which leads to an increase in the fluidity of the oil.

4 CONCLUSION

Compare with wood pulp fiber powder whose oil sorption capacity to mineral oil, PAO synthetic oil and synthetic lubricant was 7.7 g/g, 7.6 g/g and 7.4 g/g, respectively, kapok fiber powder depicted nearly three times higher oil sorption capacity. The oil release ratio increased with the increasing oil sorption ratio and temperature. For oil-containing kapok fiber powder at 70 °C, the oil release ratio of synthetic lubricant after 40 h was 37.4 %, 44.5 % and 57.1 % at the oil sorption ratio of 10 g/g, 12 g/g and 14 g/g, respectively. When the oil sorption ratio was 10g/g, the oil release ratio increased from 25.2 % at 30 °C to 40.1 % at 90 °C, and further to 49.2 % at 130 °C.

5 REFERENCES

- [1] Abdullah, M.A., Rahmah, A.U., Man, Z. 2010. Physicochemical and sorption characteristics of Malaysian Ceiba pentandra (L.) Gaertn. as a natural oil sorbent. *Journal of Hazardous Materials*, 177(1-3), 683-691.
- [2] Dong, T., Wang, F., Xu, G. 2015. Sorption kinetics and mechanism of various oils into kapok assembly. *Marine Pollution Bulletin*, 91(1), 230-237.
- [3] Hori, K., Flavie, M.E., Kuga, S., Lam, T.B.T., Iiyama, K. 2000. Excellent oil absorbent kapok Ceiba pentandra (L.) Gaertn. fiber: fiber structure, chemical characteristics, and application. *Journal of Wood Science*, 46(5), 401-404.

4. Dyeing and Finishing

ESTIMATION OF HAIR DAMAGE BY TENSILE MEASUREMENT AND EFFECT OF TREATMENT WITH BIOBASED MATERIALS FOR INVENTION OF DAMAGE SUPPRESSION TECHNIQUE

MURAOKA Yumiko and YASUNAGA Hidekazu

Kyoto Institute of Technology, Kyoto Sakyo-ku, 606-8585, JAPAN, e-mail: m9661012@edu.kit.ac.jp, yasunaga@kit.ac.jp

Abstract: The change in mechanical properties and elasticity of hair samples were measured by a tensile test to estimate the hair damage in the study. The stress-strain curves were measured for hair samples, of which degree of water content w_w was controlled. The stress at rupture point σ^* and Young's modulus E were obtained. The results show that σ^* and E for black human hair decrease with an increase in the degree of water content. The change in the σ^* and E is reversible with respect to the w_w . An equation of the relationship between w_w and σ^* for black human hair was obtained from the experimental data plots. The σ^* at any degree of water content for such hair can be estimated by the equation.

Keywords: Hair Damage, Damage Suppression, Mechanical Properties of Hair, Degree of Water Content, Biobased Material

1 INTRODUCTION

Human hair is damaged by heat, sunbeam, ultraviolet light, inadequate brushing, permanent waving, decolourising, dyeing and etc. The chemical and physical higher ordered structures in hair are changed with the progress of its damage. Protecting human hair against such damage and inventing a novel hair care technique are desired.

The authors have been studying the estimation technique of hair damage [1] and the suppression of hair photodamage by using bio-reductants [2]. It was found that the damage of hair caused by light irradiation including ultraviolet is suppressed by the treatment of hair using bio-reductants.

Hair is damaged also by heating, for example, the drying process for wet hair, curling iron, straightening iron and so on. A lot of people heat their hair routinely. Therefore, it is important to suppress the damage caused by heating and to protect hair from heat.

Under such situation, the authors have started to study the technique to suppress the heat-damage of hair. The change in mechanical strength (stress at rupture point σ^*) and Young's modulus E of hair samples were first measured by a tensile test to estimate the hair damage in the study. Such mechanical properties of hair are changed with the degree of water content. Therefore, the degree of water content of hair should be controlled and fixed when they are measured. The stress-strain curves were measured for hair samples, of which degree of water content w_w was controlled.

2 EXPERIMENTAL

Black human hair samples (Beaulax, Healthy hair obtained from Asians) were washed with distilled water three times and air-dried. They were allowed to stand for 24 h under constant humidity at constant temperature in a closed box equipped with a solution tray. The moisture vapor from water and each metallic salt solution in the tray controls the humidity in the box. The degree of water content of hair samples w_w was measured by a moisture analyser (METTLER TOLEDO HG53).

The tensile tests were made by a creep meter (YAMADEN RE2-3305S). The humidity during the measurements was controlled by a closed box equipped with a nebuliser. In the study, the σ^* was calculated by the force at the rupture of hair sample F and the cross-section area of each of the hair samples A as $\sigma^* = F / A$. The E was calculated by the stress and strain values at the Hookean region.

3 RESULTS AND DISCUSSION

The representative σ^* values are 222 MPa for hair with $w_w = 7.92\%$ and 194 MPa for $w_w = 17.68\%$. The same representative E values are 3.46 GPa for $w_w = 7.92\%$ and 1.62 GPa for $w_w = 17.68\%$. The results show that σ^* and E for black human hair decrease with an increase in w_w . The change in the σ^* and E is reversible with respect to the w_w . Hair is swollen chiefly at the CMC regions under higher humidity and the density of keratin and other protein network as a whole decreases.

Furthermore, an equation of the relationship between w_w and σ^* for black human hair was obtained from the experimental data plots. The σ^* at any degree of water content for such hair can be estimated by the equation.

The change in σ^* and E of hair by heat treatment is reported and discussed in the presentation.

4 REFERENCES

- [1] Ogihara H.; Viková M.; Vik M.; et al.: Estimation of Hair Damage by Fluorescence from Berberine. *46th Textile Research Symposium* 2018.
- [2] Yasunaga H.; Shomura A.; Viková M.; et al.: Suppression of Hair Photo-damage by Using Bio-Reductants. *46th Textile Research Symposium* 2018.

RELATIONSHIPS BETWEEN COLOURING CONDITION AND RESULTING COLOUR IN HAIR COLOURING BY DYESTUFFS OBTAINED FROM (+)-CATECHIN PHOTO-OXIDISED WITH PHOTSENSITISERS UNDER VISIBLE LIGHT

UCHIDA Akiko and YASUNAGA Hidekazu

Kyoto Institute of Technology, Kyoto Sakyo-ku, 606-8585, JAPAN, e-mail: m8661003@edu.kit.ac.jp, yasunaga@kit.ac.jp

Abstract: We tried to dye hair by dyestuffs obtained from (+)-Catechin (Cat.) combined with photosensitisers under visible light in this study. Photosensitisers absorb visible light and shift to excited states. Their high energy promotes the generation of oxidising species to give hair colourants. Rose bengal (RB) and Methylene Blue (MB) were used as photosensitisers. The relationships between the treatment / colouring conditions and the colouration results were investigated in order to find an optimum condition for the effective colouration of hair. The results show that Cat. is photo-oxidised and coloured in the presence of RB and/or MB under visible light. The hair is coloured, when it is pretreated with Cat. and irradiated in wet system.

Keywords: Hair Colouring, (+)-Catechin, Catechinone, Photosensitiser, Visible Light, Photo-Oxidisation

1 INTRODUCTION

The oxidation dyes are most frequently employed in hair dye products to colour human hair throughout the world today and the number of the people dyeing their hair with such dye products is increasing. Some constituents of the oxidation hair dye products and the side products formed during the dyeing process cause occasionally sensitisation dermatitis and other symptoms after the dyeing. Therefore, the hair dyeing technique which is safer for human body is desired and the invention of such dyeing technique is important. The author group has been studying the hair dyeing technique that colours hair by using biobased materials in order to invent a novel milder and safer one [1]-[5].

In the study, the oxidation of (+)-catechin (Cat.) by visible light irradiation under mild conditions was tried to obtain colourants for dyeing hair. The oxidation system was combined with photosensitisers which absorb visible light and generate oxidising species. People receive visible light on a daily basis and if such light is applied for the hair dyeing, it can contribute to the efficient use of daily light energy. It is expected that a slow hair dyeing by the use of visible light may reduce deleterious effects on human body and may be able to contribute to improve the safety of dyeing. Therefore, such a hair dyeing technique should be advantageous. Rose bengal (RB) and Methylene Blue (MB) were used as the visible light photosensitiser in the study. RB and MB are used as a food dye and for intravital staining, respectively. Here, the relationships between the treatment conditions and the colouration results were investigated in order to find an optimum condition for the effective colouration of hair.

2 EXPERIMENTAL

We tried two kinds of methods, which were dry system and wet system. The hair was irradiated with light in dried condition (dry system) or in wetted condition (wet system). First of all, hair samples were washed with distilled water for 10 min in 5 times. The hair samples were air-dried.

2.1 Light irradiation treatment in dry system

Each of the (1) Cat. (4.0 mM), (2) RB (0.20 mM), (3) Cat. (4.0 mM) / RB (0.20 mM), (4) MB (0.010 mM), (5) Cat. (4.0 mM) / MB (0.010 mM), (6) RB (0.10 mM) / MB (0.010 mM) and (7) Cat. (4.0 mM) / RB (0.10 mM) / MB (0.010 mM) aqueous solutions was prepared with distilled water as treatment solutions. A bundled white hair sample was immersed into each of the treatment solutions and shaken in the dark 40 °C for 40 min. The liquor ratio was 125:1. The treated hair sample was air-dried in the dark. The dried hair samples was irradiated with artificial sunbeam by using Atlas Material Testing Technology GmbH SUNTEST XLS+ (light total intensity: 765 Wm⁻², illuminance: 1.2×10^5 lx) for until 18 h.

The colour and spectrophotometry of treated hair samples were measured by spectrophotometer (Konica Minolta CM-2600d) and their λ - K/S spectra were obtained. The optical colour density, K/S , value is defined from Kubelka-Munk theory and calculated as $K/S_\lambda = (1 - R_\lambda)^2 / 2R_\lambda$, where K is the absorption coefficient, S the scattering coefficient and R_λ the reflectance of the light at a wavelength λ . Higher K/S value indicates higher intensity of a colour, i.e., deeper colour. The K/S value at 430 nm (K/S_{430}) is chosen to evaluate the dyeability of hair in the study.

2.2 Light irradiation treatment in wet system

Each of the (9) RB (0.10 mM), (10) MB (0.010 mM) and (11) RB (0.10 mM) / MB (0.010 mM) aqueous solutions were prepared with distilled water as treatment solutions. A bundled hair sample was immersed into each of the treatment solutions and shaken in the dark 40 °C for 40 min. The liquor ratio was 125:1. The treated hair sample was immersed into 4.0 mM Cat. aqueous solution in a transparent cell culture flask. The flask was irradiated with artificial sunbeam for until 4 h. The treated hair sample was air-dried in the dark, and measured by the spectrophotometer.

3 RESULTS AND DISCUSSION

The colour of the hair samples treated with RB, MB or RB / MB turns from white to pink, blue or reddish purple, respectively before light irradiation, because RB and MB show pink and blue colour, respectively and work as colourants. After light irradiation of treated hair samples, their colours due to RB and MB fade away. However, it was not observed with the naked eye that the colour of samples treated in dry system turns to target colour (brown) with light irradiation even for 18 h.

The colours of the hair samples were evaluated by K/S_{430} value in order to judge specifically the colouring behaviour. All of the K/S_{430} values for each of the hair samples scarcely change with light irradiation. It is concluded that the colourants are not produced effectively and hair samples are not coloured in dry system.

On the other hand, the colours of the hair samples due to RB and MB fade away with the light irradiation in wet system in a similar manner as the dry system. The colour of hair samples untreated or treated with, RB, MB or RB / MB turns from white, pink, blue or reddish purple into light brown, reddish brown, pale gray or deep reddish brown, respectively with light irradiation for 4 h. All of the K/S_{430} values for the samples increase with irradiation time. The K/S_{430} values of the hair samples pretreated with the photosensitiser solutions are higher at 4 h of irradiation time than that of the untreated one. The results show that the treatment of hair with RB and/or MB solution promotes the colouration of the hair under light irradiation in wet system. This indicates that such photosensitisers contribute to the effective oxidation of Cat. to give colourants. It can be said that the wet condition throughout the light irradiation works favourably for the colouration of hair. Hair is coloured in the process that the

active oxidants generated from RB and MB by the light irradiation react with Cat. to give colourants and they penetrate into hair matrixes and are adsorbed onto hair. It is thought that the Cat. solution gives favourable condition for the process and the colouration proceeds effectively.

4 REFERENCES

- [1] Yasunaga H.; Takahashi A.; Ito K.; et al.: Hair Dyeing by Using Catechinone Obtained from (+)-Catechin. *J. Cosmet., Dermatological Sci. Appl.* 2012, 2, pp. 158-163. DOI: 10.4236/jcdsa.2012.23031.
- [2] Matsubara T.; Wataoka I.; Urakawa H.; et al.: Effect of reaction pH and CuSO_4 addition on the formation of catechinone due to oxidation of (+)-catechin. *Int. J. Cosmet. Sci.* 2013, 35, pp. 362-367. DOI: 10.1111/ics.12051.
- [3] Matsubara T.; Taniguchi S.; Morimoto S.; et al.: Relationship between Dyeing Condition and Dyeability in Hair Colouring by Using Catechinone Prepared Enzymatically or Chemically from (+)-Catechin. *J. Cosmet., Dermatological Sci. Appl.* 2015, 5, pp. 94-106. DOI: 10.4236/jcdsa.2015.52012.
- [4] Matsubara T.; Seki C.; Yasunaga H.: The Relationships between Dyeing Methods and Dyeability in Hair Colouring by Utilising Enzymatic Oxidation of (+)-Catechin. *Am. J. Plant Sci.* 2016, 7, pp. 1058-1066. DOI: 10.4236/ajps.2016.77101.
- [5] Matsubara T.; Seki C.; Yasunaga H.: Relationships between Species of Dyestuff Precursor and Dyeability in Hair Colouring Made by Enzymatic Oxidation Technique Using Bio-Catechols. *Am. J. Plant Sci.* 2017, 8, pp. 1471-1483. DOI: 10.4236/ajps.2017.86101.

ESTIMATION OF HAIR DAMAGE BY USING BERBERINE

III. FLUORESCENCE, ADSORPTION DEGREE AND DISTRIBUTION OF BERBERINE IN HAIR

YASUNAGA Hidekazu¹; OGIHARA Hiroki¹; VIKOVÁ Martina²; VIK Michal²

¹ Kyoto Institute of Technology, Kyoto Sakyo-ku, 606-8585, JAPAN, e-mail: yasunaga@kit.ac.jp

² Technická univerzita v Liberci, 461 17 Liberec 1, CZECH REPUBLIC, e-mail: michal.vik@tul.cz

Abstract: The relationships between the hair damage and the fluorescence behaviours from hair adsorbing berberine were investigated in order to invent a novel practical technique estimating hair damage. A series of human hair samples having systematic degree of damages was prepared by oxidation treatment of black hair using aqueous solution of H_2O_2 and NH_3 . The damaged hair samples were treated with berberine aqueous solution. The results show that the higher damaged hair shows more intense fluorescence and the fluorescence emission light colour changes from green to yellowish green according to the damage. It was found that the amount of berberine adsorbed on hair as a whole (n_{ad} , against unit mass of dry hair) increases with increasing the concentration of H_2O_2 (CH_2O_2) used in the treatment and the damage. It was also found that the emission signal shifts to longer wavelength with the increase in CH_2O_2 and an increase in the amount of S=O groups of hair. The distribution of berberine in hair was also investigated.

Keywords: Hair Damage, Oxidation, Estimation, Berberine, Fluorescence

1 INTRODUCTION

It is important to protect human hair against damage and to invent a novel hair care technique. The estimation of the hair damage is indispensable for the protection and care, because the information on the hair damage is the base of the countermeasure to stop the damage progressing. The hair damage is complicated. The chemical and physical higher ordered structures in hair are changed by the damage. Therefore, there is no single convenient evaluating value to estimate the damage. The tensile testing, observing by SEM, estimation of amino acid composition and so on that are the techniques for the evaluation are made by special apparatuses and the accurate evaluation requires technical knowledge. Then a practical and convenient technique estimating the hair damage, for example, at professional beauty parlors and home is desired.

The disulphide and main chain chemical bonds of hair keratin are cleaved, when hair is damaged. The cut sulphide groups are usually oxidised to give sulphonic acid groups. The amount of negative charge in hair networks increases consequently.

On the other hand, the berberine obtained from plants, such as *Phellodendron amurense*, is a cationic alkaloid shows fluorescence with ultraviolet (UV) light, which is used as e. g. antidiarrhoeal and antifatulent.

The estimation of the hair damage by using berberine combined with UV light was studied to invent a novel practical technique, which can be performed by nonprofessionals. If the berberine is used as the indicator, the damage estimation for hair may be possible without cutting out hair sample from a head, because its toxicity is lower than artificial dyestuffs and it is applicable to a human head. The relationships between the fluorescence behaviours from hair adsorbing berberine and the hair damage were investigated.

2 EXPERIMENTAL

A series of human hair samples having systematic degree of damages was prepared by oxidation treatment of black hair (Beaulax Japan) using aqueous solution of H_2O_2 (0.50 – 29 wt%) and NH_3 (1.0 wt%). Each of the hair samples was immersed into the solution and shaken at 30 °C for 25 min. After washing and drying, the bleached hair samples obtained and untreated black hair sample were treated with 4.9 mM berberine aqueous solution at 40 °C for 40 min, rinsed with distilled water and air-dried.

The images of the hair samples fixed in a home-made equipment were taken by a 3CCD camera. The samples were irradiated with UV light (centre wavelength: 365 nm). Maximum luminance values (I_{max}) were obtained from the colour and greyscaled images.

The FT-IR spectra of hair samples were measured by Perkin Elmer Spectrum One FT-IR spectrometer using ATR method and analysed to obtain information on the change in chemical groups in hair. The number of measurements was 64 and the spectra were measured at 10 points of a sample.

Absorption spectra of berberine solution before and after treatment were measured by a HITACHI U-3900H UV-visible spectrophotometer and the amount of berberine adsorbed onto hair was evaluated.

The fluorescence spectra of hair samples were measured by a HITACHI F-7100 fluorescence spectrophotometer. The hair samples were cut into small pieces. The signal intensities of obtained spectra were normalised for comparison of the peak wavelength and shape.

3 RESULTS AND DISCUSSION

The colour of hair samples turns from black to brown by the oxidation treatment (bleaching) and their lightness

increases with an increase in the concentration of H_2O_2 ($C_{H_2O_2}$) used in the treatment.

The hair samples treated with berberine were irradiated with the UV light and their images were obtained. The I_{max} for hair treated with berberine increases with increasing $C_{H_2O_2}$ up to 14 wt% and it does not change so much over 14 wt% of $C_{H_2O_2}$. The results show that the higher damaged hair shows more intense fluorescence in the initial hair damage region ($C_{H_2O_2} \leq 14$ wt%). They suggest that the degree of hair damage at the initial damage stages can be estimated by this method using berberine and UV light for hair.

It was clarified that the amount of berberine adsorbed onto hair as a whole (n_{ad} , against unit mass of hair) increases with increasing $C_{H_2O_2}$. The results show that hair adsorbs more berberine with the progress of damage and this causes the higher luminance for hair. It indicates that the negative charges in hair may increase with the progress of damage.

On the other hand, the FT-IR spectra of hair samples were obtained. The IR signal at 1040 cm^{-1} corresponds S=O group and that at 1635 cm^{-1} corresponds to C=O groups of hair protein. The absorption intensity ratio (A'_{1040} / A'_{1635}) increases with increasing $C_{H_2O_2}$. The results show that the amount of S=O group in hair increases with an increase in $C_{H_2O_2}$. It was also found that I_{max} increases with increasing the amount of S=O groups of hair. The similarity for the increase in I_{max} and A'_{1040} / A'_{1635} with $C_{H_2O_2}$ was revealed. The disulphide bonds in hair are cut and oxidised by the bleaching and then negative charges such as SO_3^- groups increase. This and the breakage of S-S bonds promote the absorption of berberine onto hair. Therefore, it can be concluded that the hair damage is estimated by the technique using berberine.

It was also found that the colour of the fluorescence emission light changes from green to yellowish green according to the amount of S=O group. The fluorescence emission signal shifts to longer wavelength with the increase in $C_{H_2O_2}$ and an increase in the amount of S=O groups of hair.

The distribution of berberine in hair is also reported and discussed in the presentation.

5. Nano Fibers and Smart Textiles

MECHANISM OF ELECTRIFICATION AND CHARGE DECAY ON WOVEN FABRIC STRUCTURES

Abdel-Fattah M. Seyam, Vamsi K. Jasti, William Oxenham, and Thomas Theyson

Wilson College of Textiles, NC State University, Raleigh, NC, USA, aseyam@ncsu.edu

Abstract: We developed equipment to understand and assess the mechanism of charge decay after cyclic frictional electrification using two probes; one placed on the top of the rubbed area and the other placed some distance from the rubbed area. To demonstrate the capability of the equipment, range of woven fabrics from ring spun cotton yarns, ring spun polyester yarns, and flat continuous filament polyester yarns treated with topical finishes are reported. The topical finishes include commercially available ionic anti-static finishes, one commercially available hydrophilic finish, and a new experimental moisture management finish. The fabrics were rubbed against surface of steel and PTFE (Teflon®) and their frictional electrification and charge dissipation were monitored. It was found that the generated charge migrated from the rubbed areas to other parts of the sample. This behavior is more pronounced for fabrics treated with hydrophilic and moisture management finishes, which cause the charge to decay exponentially.

Keywords: friction electrification, charge decay, ionic anti-static finishes, hydrophilic finish

1 INTRODUCTION

Static charges are generated on two surfaces when they are contacted and separated or rubbed against each other. The charges dissipate in case of electrically conductive materials [1]. However, if the materials are insulator (such as polymers and textile fabrics), the charge remains and dissipates with time depending on the materials' type, surface finish, and environment. The static electrification of insulator is still not clearly understood. The research on static charging in textiles is important due to the negative impact that it creates such as fabric clinging and spark discharges that may cause fire at gas station and shortage of electrical equipment. If the charge decay is fast enough, issues associated with electrification charge would be resolved. For these reasons, significant studies on charge decay have been conducted on yarns, polymer films and fabrics [2,3]. Researchers proposed different mechanisms of charge dissipation: decay through air [4], penetration through the bulk [5], grounded to the nearest metal parts [6], or flow along the surface and discharge to another material and ultimately to ground [7]. There is no generally accepted mechanism of charge decay that has been experimentally verified. This prompted us to undertake a research program with target to develop innovative electrostatic charge measuring system based on proven equipment that was developed by Seyam, Cai, and Oxenham [8] in order to investigate the mechanism of charge dissipation on textiles' surfaces.

2 EXPERIMENTAL

2.1 Materials

Standard fabrics' specifications, which were acquired from Testfabrics Inc., used in this work are shown in table 1. Table 2 shows surface finishes employed to control charge generation/decay.

Table 1 Fabric specifications

Style no	Fiber type	Warp Yarn (tex)	Weft Yarn (tex)	Yarn Type	Fabric Thick (mm)	Cover Factor (%)
418	cotton	14.4	13.6	Ring spun	0.174	81.9
441	cotton	14.0	15.8	Ring spun	0.180	56.4
700-3	polyester	9.5	9.6	Filament	0.120	72.1
777	polyester	2x39.5	21.1	Ring spun	0.231	73.6

Table 2 Surface finishes

Finish Type	Levels
Ionic antistatic agents	0.1% Leomin® PN (C12 Phosphate, K+ Neutralized finish, produced by Hoechst AG) 0.1% Larostat® 264 A (Dimethyl Oleyl Amine Diethyl Sulfate Quaternary Finish, produced by BASF)
Hydrophilic finishes	0.5% Hydroperm® T (produced by Clariant Inc.) 0.5% Hydrophilic Finish (Experimental Moisture Management produced by Tenstech Inc)

2.2 Equipment and procedures

The procedure for applying the finishes is described in [9] and a complete description of measuring static generation/decay using equipment designed and built at NC State Wilson College of Textiles is provided in [8,9]. Modifications to the equipment to measure cyclic friction static generation/decay were done to monitor the static build up on the rubbed fabric area and a distance away from the rubbed area using two voltmeter probes as shown in figure 1. A fabric specimen was mounted on top of PTFE plate. A rubbing head, which moves forward and backward and rubs against the fabric to create charge on the fabric is driven by a stepper motor.

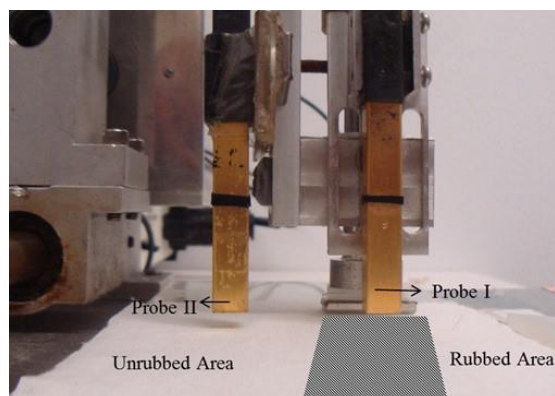


Figure 1 Surface potential measurement equipment during rubbing with two voltmeter probes

In this set up, in forward movement, probe I trails the rubbing head and measures the generated surface charge on the fabric. In case of the backward motion probe I leads the rubbing head and measures the charge retained on the surface. Probe II measures the surface charge on the unrubbed area 23 mm away from the rubbed area. After fifty cycles of rubbing maximum charge is attained and the motion stops to allow the two probes to monitor the charge decay with time.

3 RESULTS

Figure 2 shows the surface potential accumulation and decay on finish-free cotton-I fabric when rubbed with steel. After the 1st and 50th cycle of rubbing, the surface potential measured on cotton I were approximately 80 and 300 Volts, respectively. The surface potential decayed quickly and reduced to almost zero within 30 seconds. Cotton II fabric exhibited less charge: 39 Volts after 1st cycle and 68 Volts after the 50th cycle. The surface potential decay observed for both fabrics follows a single exponential behavior with time. However, for the finish-free filament polyester fabric, the surface charges after 1st and 50th cycle were 100 and 490 Volts, respectively. The decay was very slow compared to cotton samples and retains more than 80% of its charge after 60 seconds. Surface potential measured using two probes on filament polyester treated with 0.5% Hydroperm® T is shown in Figure 3. The charge increased with number of cycles on rubbed and unrubbed areas. It can be seen that the charge is rapidly migrating over the surface of the fabric at the start of each cycle.

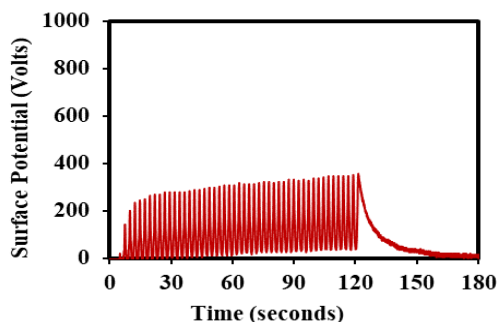


Figure 2 Charge accumulation/decay after 50 cycles on cotton-I

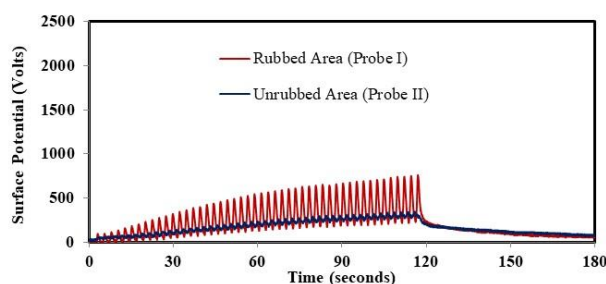


Figure 3 Charge in 50 cycles and decay of rubbed and unrubbed areas of filament PET treated with 0.5% Hydroperm® T

4 CONCLUSION

Ionic antistatic agents and hydrophilic finishes were applied to fabric surface. With the ionic antistatic agents applied to the fabric sample, little or no charge was observed during the rubbing tests. Fabrics treated with hydrophilic finish are able to decay the charge through migration from the rubbed area to unrubbed area. The application of hydrophilic surface treatments to the polyester fabric samples produced fabrics with complex patterns of both exponential and linear decay.

Different modes of charge decay were observed: (1) A slow linear decay exhibiting no spreading of charge on the test sample, (2) An exponential decay associated as a result of spreading of charge on the test sample, and (3) A combination of linear and exponential decay mechanism indicating the existence of two types of charges on the fabric surface.

5 REFERENCES

- [1] Cross J. A., *Electrostatics: Principles, Problems and Applications*, IOP Publishing Limited, Bristol, 1987.
- [2] Tsai P. P., Huang H-Y., Wadsworth L.C., *Electrostatic decay of corona-charged melt blown electret at ambient and elevated temperatures. TAPPI Proceedings*, 63-77, 1999
- [3] Lu L., Ph.D. Dissertation, North Carolina State University, Raleigh, USA, 2010.
- [4] Jonassen N., *Electrostatics*, Chapman & Hall, New York, 1998.
- [5] Harper W.R., *Contact and static electrification*, Oxford at the Clarendon Press, 1967.
- [6] Hearle J. W. S & Morton W. E., *Physical Properties of Textile Fibers*, The Textile Institute, 1997.
- [7] Whitesides G.M. & McCarty L.S., *Electrostatic charging due to separation of ions at interfaces: Contact electrification of ionic electrets. Angew. Chem. Int. Ed.*, 47, 2188-2207, 2008.
- [8] Seyam A. M., Cai Y. & Oxenham W., *Devices for measuring electrostatic generation and dissipation on the surface of polymeric materials. The Jour. of Tex. Inst.*, 100, 338-349, 2009.
- [9] Lu L., Ph.D. Dissertation, North Carolina State University, Raleigh, USA, 2010.

Water resistant nanofiber filter consisting of EVOH / PU

YAMASHITA Yoshihiro¹ and MIYAKE Hajime²

¹Osaka Seikei College, 3-10-62 Aikawa, Osaka, 533-0007 Japan, e-mail: yoshihiro_yamashita1958@goo.jp

²Northeastern Industrial Research Center of Shiga Prefecture

27-39 Mituya motomachi, Nagahama, 526-0024 Japan e-mail: miyake.hajime@shiga-irc.go.jp

Abstract: PM0.3 particle capture filter was obtained by laminating EVOH / PU nanofibers excellent in water resistance on urethane foam. The basis weight of the nanofibers is 0.1 g / m² or less.

Keywords: electrospinning, nanofiber, EVOH, PU, filter, PM0.3

【Introduction】

A mask made of polyurethane form elastomer has a good fit and it is very popular. On the other hand, due to the coarseness of the urethane foam, it is possible to remove 99% of PM 2.5 level such as pollen, but particles and viruses below (PM0.3) that are difficult to remove. Therefore, we investigated to increase the removal performance while maintaining the pressure loss by coating this urethane foam with nanofibers.

【Experiment】

The urethane foam used commercially available PITTA (Arax Co., Ltd.). Kato Tech's NEU was used for electrospinning. The nanofibers were adjusted to have a basis weight of 0.05 g / m². The nanofibers were prepared in a 30% solid concentration aqueous solution consisting of an EVOH emulsion and a polyurethane emulsion. The voltage between the nozzle and the target is 40 kV and the distance is 15 cm (Fig.1).

【Results and discussion】

The air permeability at a basis weight of 0.05 g / m² was 4.33 m/s, and for the urethane mask alone, the difference was hardly observed at 4.4 m/s. Moreover, in order to apply | coat uniformly on the urethane mask surface, the spot which was seen in the case of non-processing was eliminated by carrying out surfactant treatment on the urethane surface (Fig2). The air permeability of the urethane / nanofiber / urethane laminate was 4.13 m / s. practically, it was confirmed that the durability can be improved by sandwiching the nanofiber layer with urethane. The thickness of a commercially available urethane sheet is 2 mm, and when two sheets are stacked, it is too thick. In this method, it is desirable to devise a technique such as applying nanofibers on a thinner urethane sheet and adhesively laminating the urethane sheet.

【Acknowledgments】 We thank Mr. Umehara of Aired Co., Ltd. for supporting this research.

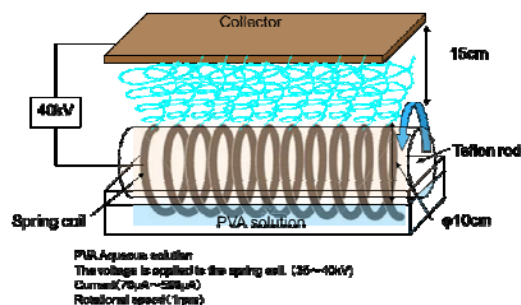
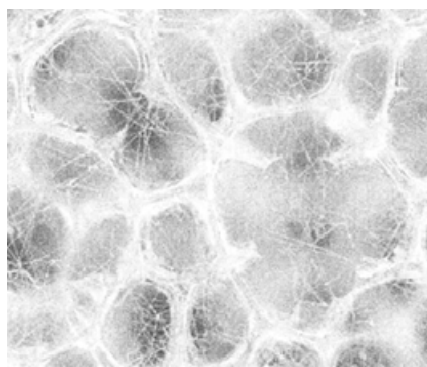
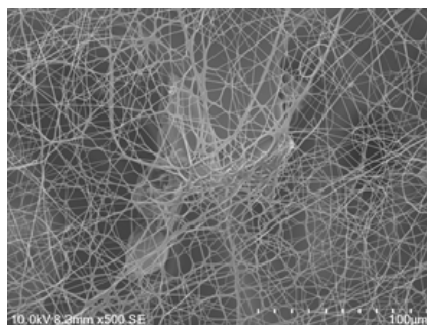


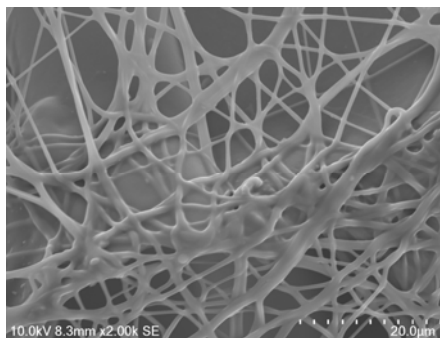
Fig.1 Coil electrospinning device.



(a) X100



(b) X500



(c) x2000

Fig.2 EVOH/PU nanofiber mat on the urethane form

【references】

- [1] "Water Resistant PU / EVOH Nanofiber Filter Made from Aqueous Solution", Yoshihiro YAMASHITA; Hajime MIYAKE, Journal of Textile Engineering. 2018, 64, No.6, pp179-183

COPPER AND SILVER COATED TEXTILES FOR SMART APPLICATIONS

Azam Ali¹, Vijay Baheti¹, Jiri Militky¹

¹Department of Material Engineering, Faculty of Textile Engineering, Technical University of Liberec, Czech Republic
mehr_azam91@yahoo.com

Abstract: In this study, we make the electrically conductive multifunctional and durable fabrics by silver and copper nanoparticles. The fabric structure was pretreated and then nanoparticles were directly grown on fabric structure. The dynamic light scattering, SEM and XRD techniques were employed to study the morphology of deposited silver and copper particles. The utility of conductive fabrics was analyzed for electromagnetic shielding ability. Furthermore, the role of deposited particles on antibacterial properties was examined against pathogenic bacteria such as *Staphylococcus aureus* and *Escherichia coli*.

Keywords: Electrically conductive, EMI Shielding, antibacteria, copper and silver particles

1 INTRODUCTION

The demand for metallized fabrics is continuously increasing day by day and gaining attention in technical, high-tech and commercial applications. The most in applications are electromagnetic shielding, energy harvesting, anti-static, anti-bacterial properties, radar reflectivity, UV radiation screen and some important medical applications like the development of electrodes for TENS, ECG and EMG machine etc[1][2]. In this case selection of natural fibre based textile is more suitable. Because now a days, a major challenge is concern with the production and post-disposal processes of synthetic fibres regarding environmental pollution. So to overcome this issue researchers are fully conscious to develop the technical and smart textiles with natural fibre sources [3][4]. Cotton fabric is well known for its environmental friendly properties like biodegradable and sustainability. It is well known that virgin cotton fabric is not intrinsically conductive. Generally, different types of conductive material imparts to insulator to make it conductive [5]. Textile surface metallization is done by various methods. However, metallic fabric produced in such traditional manners consists of defects, such as stiffness, poor air permeability and heavy in weight. The present work deals with the development of electrically conductive and multifunctional cotton fabrics by in-situ deposition of copper and silver particles.

2 METHOD

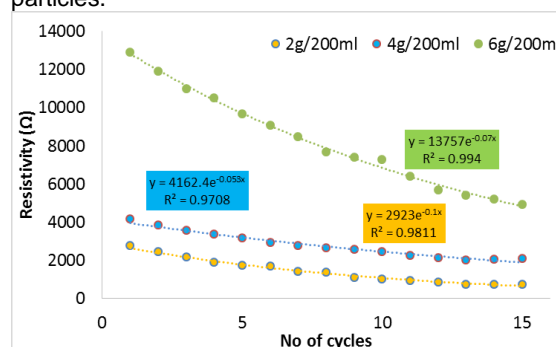
At first, different concentration of copper sulphate from 6g/200ml, 4g/200ml and 2g/200ml was dissolved in distilled water. Then, the cotton fabric was dipped in the solution and dried at 100 °C for 3 minutes. This procedure of dipping and drying was continuously carried out for 15 cycles. Subsequently, the treated fabrics were transferred to the 6g/200ml sodium hydrosulphite solution. Likewise, for the deposition of silver particles, silver nitrate 0.30 M, 0.20 M and 0.10 M was dissolved in distilled water. The aqua ammonia (28wt %) was added drop wise into aqueous solution of AgNO₃, and stirred continuously until a transparent solution of [Ag(NH₃)₂]⁺ was obtained. Alkali treated cotton fabric was dipped in this solution for 3 minutes and dried at 100°C for 3 minutes. The dip and dry process was repeated a number of times to deposit the maximum concentration of

[Ag(NH₃)₂]⁺ on the fabric. This procedure of dipping and drying was continuously carried out for 15 cycles. Subsequently, the treated fabrics were transferred to 0.1M glucose stock solution. The reaction was allowed to proceed for 15 min. Finally, the fabrics were rinsed with water and dried in air. The microstructure of silver coated fabrics was observed on scanning electron microscope at accelerated voltage of 15 kV. Electrical resistivity was observed according to ASTM D257-07. Electromagnetic shielding ability was tested according to ASTM D4935-10 over frequency range of 30 MHz to 1.5 GHz. Antibacterial properties were tested by zone of inhibition (ZOI). The durability of fabrics were checked by using ISO 105-C01 washing test.

3 RESULTS

3.1 Electrical Resistivity Measurements

The effect of Silver nitrate and copper sulfate concentration and number of dipping cycles for increase in the conductivity of the fabrics was investigated. The resistivity of the samples were the mean values of three measurements as shown in Figure 1. The results showed the clear decrease in resistivity (increase in electrical conductivity). This behavior can be attributed to the formation of big sized copper particles at higher concentration of copper and silver salts solution. The lower concentration salts produced more conductive fabrics due to formation of percolated network by creation of continuous connectivity between the small metal particles.



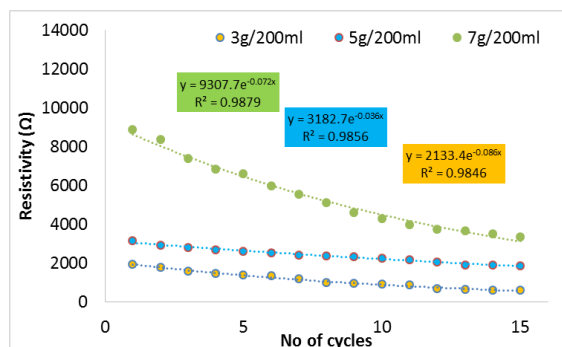


Figure 1 Electrical resistivity behavior of copper and silver coated fabric

3.2 SEM Analysis

The scanning electron microscopy was employed to observe the deposition of particles on fabric surface. The SEM images shown in Figure 2 revealed the nanometer scale of copper and silver particles deposited on fabric surface. With increase in number of dips, the deposition of particles was found more uniform and dense. This further indicated the higher tendency of formation of percolated network of particles when number of dipping cycles increased. It clearly showed the increase in contents of silver and copper metals with higher number of dips.

3.3 XRD Analysis

Figure 3 shows the XRD patterns of samples for the 2θ range of 20 to 80 degrees with a step of 0.02 degree. The phase purity of the prepared silver particles can be clearly seen from perfect indexing of all the diffraction peaks to the silver structure. Compared to the untreated cotton fabric, four new peaks at 2θ values of 38.1° , 44.3° , 64.5° and 77.5° were detected for silver coated fabrics, which were respectively attributed to the diffraction peaks of the (1 1 1), (2 0 0), (2 2 0) and (3 1 1) planes of silver. Figure 3 also shows the XRD patterns of samples for copper particles. The diffraction peaks appeared at 2θ of 43.3° , 50.5° , and 74.2° represented (1 1 1), (2 0 0) and (2 2 0) planes of copper, respectively [3]. The crystalline nature of copper particles was confirmed from the sharp peak. As such no characteristic peaks of impurities were detected, except the peak of copper oxide Cu_2O phase at 2θ of 38.0° [4].

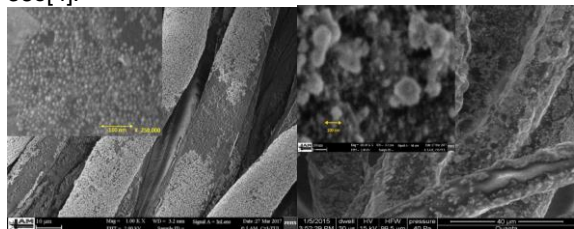


Figure 2 SEM Images of silver and copper coated fabrics

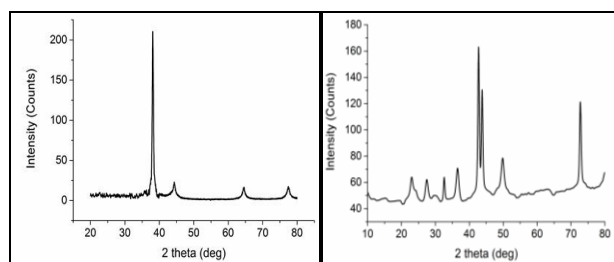


Figure 3 XRD pattern of silver and copper coated fabrics

3.4 Electromagnetic Shielding

The high EMI SE was investigated coupled with good electrical properties. The maximum EMI SH values at 5, 10 and 15 cycles for silver coated fabric were 9.55, 15.04 and 18.54, while for copper coated fabric were recorded as 5.8, 9.5, 14.96 and 12.65 dB respectively. It is also clear from the figure that sudden increase in EMI SE of fabric samples occurred up to the frequency range between 300 to 400 MG Hz and then it is stable. It means that fabric samples are able to achieve high EMI at low frequency range, additionally EMI values are so stable till 1500 MG Hz. Furthermore the samples developed at 15 number of cycles has the highest value of EMI shielding because of highest electrical conductivity (low resistivity) among all samples

3.5 Antibacterial Properties

The antibacterial activity of silver and copper coated fabrics was tested against Gram-negative E.coli and Gram-positive S. aureus. Samples shows the zones of inhibition around fabric samples after 24 h of incubation in dark at 37°C . The zone of inhibitions for Staphylococcus aureus increased from 8.5 to 13.43 mm (for silver coated) and 9.5 to 15.5 mm (for copper coated), while for Escherichia coli it increased from 7 to 11.78 mm (for silver coated) and (7.5 to 12 mm for copper coated) with increasing number of dipping cycles.

4 CONCLUSION

It was concluded that nanoparticle take up can be improved by increasing the number of dips for better covering of the fabric surface. The sample produced from 15 cycles exhibited the shielding ability of 18.54 dB for silver and 12.65 dB for copper coated fabric for respective frequency 1.5 GHz. For multifunctional behavior, the conductive fabrics were further examined for antibacterial properties against pathogenic bacteria such as Staphylococcus aureus and Escherichia coli. The zone of inhibitions for Staphylococcus aureus and Escherichia coli significantly increased with increasing number of dips. Therefore, the outcome of this work could provide alternative inexpensive and easier ways to obtain

ACKNOWLEDGEMENT: Authors acknowledge the student grant competition 21304.

5 REFERENCES

- [1] Chung, C., Lee, M., Choe, M.K. Characterization of cotton fabric scouring by FT-IR ATR spectroscopy. *Carbohydr Polym*, 2004, 58, pp 417–420.
- [2] Shateri K. Fabricating multifunctional silver nanoparticles-coated cotton fabric. *Arab J Chem*, 2017, 10, pp 1016.
- [3] Gan, X., Wu, Y., Liu, L., et al. Electroless plating of Cu-Ni-P alloy on PET fabrics and effect of plating parameters on the properties of conductive fabrics. *J Alloys Compd*, 2008, 455, pp 313.
- [4] Zhao, Y., Cai, Z., Fu, X., et al. Electrochemical deposition and characterization of copper crystals on polyaniline/poly(ethylene terephthalate) conductive textiles. *Synth Met*, 2013, 175, pp 1–8.
- [5] Studer, A. Nanoparticle cytotoxicity depends on intracellular solubility: Comparison of stabilized copper metal and degradable copper oxide nanoparticles. *Toxicol Lett*. 2010, 197, pp 169–174.

OILY WASTE WATER SEPERATION BY USING NANOFIBROUS MEMBRANE

Evren Boyraz¹, and Fatma Yalcinkaya²

¹ Department of Material Engineering, Faculty of Textile, Technical University of Liberec, Studentska 1402/2, 46117, Czech Republic, e-mail: evrenboyraz@gmail.com

² Department of Nanomaterials and Informatics, Centre for nanomaterials, Advanced Technology and Innovation, Technical University of Liberec, Studentska 1402/2, 46117, Czech Republic, e-mail: fatma.yalcinkaya@tul.cz

Abstract: In this work, we have demonstrated a facile method to separate oily wastewater using polyvinylidene fluoride (PVDF) nanofibrous membranes. Various density of PVDF nanofibers were produced using needle-free electrospinning system. A nonwoven supporting layer has been adhered to the nanofibers using a heat press lamination process without any damages. An emulsion with oil droplets size in between 200-1000 nm has been prepared. The structure, permeability and the fouling/anti-fouling of PVDF membranes were studied systematically. Results indicated that, the PVDF membranes selectively separated oil from oily water and showed oleophilic/hydrophobic characteristics. On the contrary, the non-ionic surfactant used in emulsion has changed the membrane wettability and created oleophobic/hydrophilic membrane due to surfactant-membrane interaction. The prepared PVDF membranes in this work promise a potential uses in the separation of oily water due to excellent physical/chemical resistance, permeability and mechanical properties.

Keywords: nanofiber, PVDF, wastewater, emulsion, oil separation

1 INTRODUCTION

Industrial or domestic use water contains oil, water, energy, organics, phosphates, nitrogen, cellulose, rare earth, and other resources. Recovering the water, energy, nutrients and other valuable materials which are in the wastewater is a crucial opportunity and new opportunities [1]. The untreated wastewater discharging to the seas and oceans affect roughly 45,000 km² marine ecosystem, fishing, livelihoods and food chains. By 2030, global energy is expected to increase by 40% and water demand by 50% [2]. Generally, the following problems arise due to oily wastewater pollution: [3] (a) Affecting water sources, drinking water etc., (b) putting human health endanger, (c) pollution of the atmosphere, (d) affecting crop production, (e) harming nature. Oily wastewater occurs after many industrial processes such as food, ship, oil refinery, petrochemical, leather, and metal finishing. The oils, and greases (FOGs) in the wastewater must be cleaned and removed before reusing the water in a closed circuit operation or discharged into sewer systems and to the surface waters. To produce clean water, the estimation of the current global market value is about 59\$ billion, and it is expected that it will increase over the next 8 years [4]. Therefore, the oily wastewater separation is essential and valuable. Fibers with a diameter range around 100-1000 nm are generally classified as nanofibers. Compared to conventional fibers, nanofibers are with higher porosity, lower density, higher surface area to volume ratios and smaller pore size, offer an opportunity for use in a wide variety of applications including composite, filtration, protective clothing, composite materials, biomedical application (tissue engineering, scaffolds, bandages, and drug release systems), electronic applications, sensors, design of solar sails and flexible photocells [5]. To treat oily wastewaters, membranes are developed based on

nano-porous structures. Electrospun nanofibers as filter have high flux due to their extremely porous structure. Therefore, electrospun nanofibers as a filter which have high hydrophilicity are an excellent alternative for the oil/water separation [6]. The properties of PVDF membranes are better than other organic membranes. For instance; good mechanical property, thermostability, chemical stability, and impact resistance properties allow using PVDF membranes in many fields such as microfiltration, ultrafiltration, membrane bioreactor, membrane distillation, gas separation and stripping [7]. Against a wide range of harsh chemicals such as halogens and oxidants, inorganic acids (apart from fuming sulphuric acid), as well as aromatic, aliphatic and chlorinated solvents, PVDF has excellent chemical resistance.

2 MATERIALS & METHODS

Different density of PVDF nanolayers were obtained from the Institute of Advanced Technology and Innovation at the Institute of Nanomaterials, Liberec Technical University (TUL). Nanofibers were prepared using NS-1S500U Nanospider (Elmarco, Czech Republic) under the controlled conditions. To prepare oily wastewater emulsion, 100 mL of Vita D'or (Czech Republic) sunflower oil was mixed with 100 mL of distilled water in ratio 1:1 v/v. The red water soluble/oil insoluble food coloring was dropped into the emulsion to see separation performance and behavior of the membrane. 2 gr of Triton X-100 (Sigma-Aldrich Corporation) was also dropped into the emulsion to get better stability of oil droplets diameter and it is shown in Figure 1. The average of oil droplet diameter was 1058.02 nm \pm 345.39 nm and it is shown in Figure 1. It was checked after a few weeks and observed that the

average drop size was the same. The water contact angle of the samples is measured using a Krüss Drop Shape Analyzer DS4 (Krüss GmbH, Hamburg, Germany), at five different points, using distilled water (surface tension 72.0 mN.m⁻¹) on the clean and dry samples at room temperature. Bursting strength test was done using a custom-made equipment.



Figure 1 Oil/water emulsion - oil droplets in the emulsion

Separation of oily wastewater emulsion was done using Amicon® Stirred Cell 50mL (EMD Millipore Corporation, USA). Selectivity was determined by observing the color of permeate and it was checked under the microscope which was purchased from Levenhuk Company (USA).

3 RESULTS & CONCLUSION

The pore size and operating conditions (pH, temperature, etc.) of the membranes play a huge role on the selectivity, filtration flux, membrane fouling, and solute rejection. The pore size of PVDF_1 which had 1 gsm was $2.52 \mu\text{m} \pm 0.31$, PVDF_2 which had 2 gsm was $1.15 \mu\text{m} \pm 0.07$, and PVDF_3 which had 3 gsm was $0.72 \mu\text{m} \pm 0.04$. From the obtained results, it was observed that in lower gsm, membranes had bigger pore sizes. It was assumed that once the membrane contact with oil/water emulsion, the contact angle characteristics changed due to surfactant and the oil contaminations in the emulsion and it is shown in Table 1.

Table 1 Contact angle of samples

Sample	CA before separation	CA after separation	Image
PVDF_1	71.23 ± 1.31	62.4 ± 2.17	
PVDF_2	80.83 ± 1.53	47.76 ± 1.94	
PVDF_3	89.41 ± 4.69	35.32 ± 8.72	

The surface hydrophobicity is related with the surface roughness. Under heat and pressure, the surface of the web can be changed. Moreover, the adhesive web has hydrophilic characteristics which might affect the surface of the nanofiber web too. The CA of the membranes changed after separation due to the surfactant effect and the hydrophilicity increased. Normally PVDF is hydrophobic and oleophilic. But after circulating with emulsion, the selectivity of PVDF changed. PVDF changed to hydrophilic/oleophobic characteristic. It is shown in Figure 2 that PVDF_1 and PVDF_2 had fouling problem while circulation. PVDF_3 had better performance than PVDF_1, and PVDF_2.

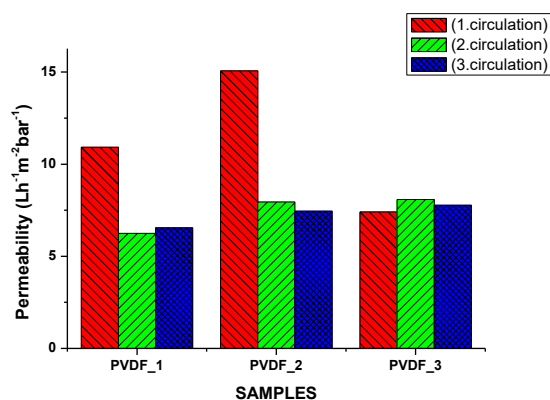


Figure 2 Permeability performance of samples

4 REFERENCES

- [1] CHEN, Yang, Dabo GUAN, Heike SCHROEDER, Jianghua LIU, Zhifu MI, Jingru LIU, Shuai SHAO, Qiang ZHANG, Zhu LIU a Yuli SHAN. CO₂ emissions inventory of Chinese cities. *Atmospheric Chemistry and Physics Discussions* [online]. 2016, 1–26 [vid. 2019-03-30]. ISSN 1680-7375. Dostupné z: doi:10.5194/acp-2016-176
- [2] KONCAGÜL, Engin ., Michael. TRAN, Richard. CONNOR, Stefan. UHLENBROOK, Angela. RENATA a Cordeiro. ORTIGARA. Wastewater the untapped resource. Facts and figures. The United Nations World Water Development Report 2017 [online]. 2017, 12. ISSN 1941-6016. Dostupné z: doi:10.4249/scholarpedia.2433
- [3] YU, Li, Mei HAN a Fang HE. A review of treating oily wastewater. *Arabian Journal of Chemistry* [online]. 2017, 10, S1913–S1922. ISSN 18785352. Dostupné z: doi:10.1016/j.arabjc.2013.07.020
- [4] JING, Benxin, Haitao WANG, Kun Yi LIN, Paul J. MCGINN, Chongzheng NA a Yingxi ZHU. A facile method to functionalize engineering solid membrane supports for rapid and efficient oil-water separation. *Polymer* [online]. 2013, 54(21), 5771–5778. ISSN 00323861. Dostupné z: doi:10.1016/j.polymer.2013.08.030
- [5] BOYRAZ, Evren a Fatma YALCINKAYA. Polymeric Nanofibers Produced By Needleless. In: *22nd international conference Structure and Structural Mechanics of Textile Fabrics (22.nd STRUTEX,2018)*. 2018, s. 363–366. ISBN 9788074941399.
- [6] OBAID, M., Nasser A.M. BARAKAT, O. A. FADALI, Moaaed MOTLAK, Abdulhakim A. ALMAJID a Khalil Abdelrazek KHALIL. Effective and reusable oil/water separation membranes based on modified polysulfone electrospun nanofiber mats. *Chemical Engineering Journal* [online]. 2015, 259, 449–456 [vid. 2019-03-30]. ISSN 13858947. Dostupné z: doi:10.1016/j.cej.2014.07.095
- [7] LIU, Cong, Lili WU, Chaocan ZHANG, Wanyu CHEN a Shuo LUO. Surface hydrophilic modification of PVDF membranes by trace amounts of tannin and polyethyleneimine. *Applied Surface Science* [online]. 2018, 457, 695–704. ISSN 01694332. Dostupné z: doi:10.1016/j.apsusc.2018.06.131

COMPARATIVE INTUMESCENT FLAME RETARDANT FEATURES OF COTTON TEXTILES TREATED WITH ALKALINE AND ACIDIC CASEIN SUSPENSION

Sajid Faheem¹, Vijay Baheti², Maros Tunak³, Jakub Wiener² and Jiri Militky²

¹Department of Material Engineering, Technical university of Liberec, Liberec, Czech Republic: msajidfaheem@gmail.com

²Department of Material Engineering, Technical University of Liberec, Liberec, Czech Republic: vijaykumar.baheti@tul.cz

³Department of Textile Evaluation, Technical University of Liberec, Liberec, Czech Republic: maros.tunak@tul.cz

Abstract: The objective of present study was to investigate the effect of coating of different concentrations and pH of aqueous casein suspension on thermo-oxidative properties and intumescent flame retardant behavior of cotton fabrics. The flame retardant behavior was found to increase with increase in concentration of casein suspension in both alkaline and acidic pH conditions. The casein suspension of acidic pH was found to produce more char residue than the alkaline casein suspension, which indicated their better thermo-oxidative properties. Furthermore, the phenomenon of intumescence was largely observed in case of samples coated with acidic casein suspension due to easier release of ammonia from protonated casein.

Keywords: Casein, Cotton, Intumescent, Flame retardant, Thermo-oxidative stability

1 INTRODUCTION

Cellulosic fiber is one of the most important biopolymers in the world due to its availability in large quantities, good mechanical properties, biodegradability, and hydrophilicity [1]. However, for further applications in transportation, automobiles, protective garments, military, furniture upholstery, bed linen and nightwear, it is necessary to improve the thermal degradation, ignition and burning behavior of cellulosic materials [2]. In recent years, intumescent systems are considered as the most performing solution available to withstand the fire threat [3]. The term intumescence refers to the substances which are able to grow and increase in volume against the heat. To overcome the limitations of intumescent systems, search for alternative environmentally-friendly intumescent materials containing all three components altogether (i.e. acid source, carbon source and blowing agent) became important. In this context, the effectiveness of different biomacromolecules (whey proteins, caseins, hydrophobins, and deoxyribonucleic acid) has been assessed for textiles recently [4].

The present work deals with the effect of coating different concentration and pH of aqueous casein suspensions on thermo-oxidative properties and intumescent flame retardant behavior of cotton fabrics. In this way, the present research could be very useful for valorization of dairy industry by utilization of casein wastes in applications of semi-durable but comfortable textile flame retardants.

2 EXPERIMENTAL METHODS

2.1 Materials

The plain woven 100 % cotton bleached fabric having 145 g/m² aerial density was selected for the study. Bovine milk casein (technical grade) was received from Sigma-Aldrich, Czech Republic.

2.2 Method

The aqueous suspensions of casein under alkaline and acidic pH conditions were prepared at three different

concentrations (i.e. 50 g/L, 100 g/L and 150 g/L). The prepared casein suspensions were applied by spreading on the surface of cotton fabrics with a spatula, while the excess of the suspensions were removed gently by pressing with rotary drum. Then, the samples were dried at 100°C in lab scale hot air dryer (Mathis AG, Switzerland). The uptake (add on percentage) of casein was calculated using the Equation (1).

$$\text{Add on (\%)} = \frac{W_f - W_i}{W_i} \times 100 \quad (1)$$

Where W_i is weight of bleached cotton fabric before padding and W_f is weight after padding and drying.

3 CHARACTERIZATION AND TESTING

Casein treated cotton fabrics were characterized for surface structure (FTIR) and (SEM) analysis, thermo-oxidative stability (TGA) and flame retardancy according to standard test methods.

4 RESULTS AND DISCUSSION

Data collected from characterization and testing of developed samples were analyzed and discussed to study and investigate reasons for the behavior of different functional properties.

4.1 Flame retardancy of casein treated cotton fabrics

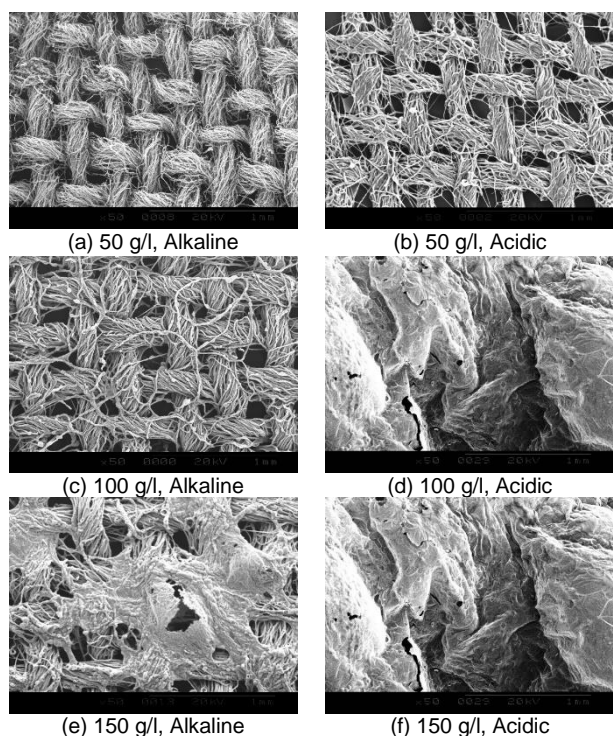
The effect of concentration and pH of casein suspension was studied for improvement in flame retardancy of casein treated cotton fabrics. From Table 1, the total burning time (s) and residue (%) were used to estimate the resistance for flame propagation. When a methane flame was applied for 3 sec, the untreated cotton fabric completely burnt without leaving any residue. The casein treatment was found to promote increase in total burning time, and thus exhibited their ability for the partial flame protection. The burning time was found to increase in linear trend with increase in casein concentration.

Table 1 Burn characteristics of casein treated cotton fabrics

Sample	Alkaline casein suspension		Acidic casein suspension	
	Total burning time (s)	Residue (%)	Total burning time (s)	Residue (%)
Untreated	36	-	36	-
50 g/L casein	38	23	44	29
100 g/L casein	44	37	52	45
150 g/L casein	52	48	58	51

Furthermore, the fabrics treated with acidic casein suspension burnt at slower rate and resulted into stronger char residue as compared to those treated with alkaline casein suspension. The 44% increase of total burning time as well as 48% final residue was found for 150 g/L alkaline casein suspension, whereas it was 61% and 51%, respectively for acidic casein suspension.

Moreover, the samples of acidic casein suspension preserved their original texture even after burning. The produced char exerted a protective effect on the underlying cotton fabric, limiting the oxygen diffusion, avoiding formation of combustible volatile products and absorbing the heat evolved during the combustion. This flame retardant effectiveness of casein macromolecules was attributed to phosphate groups located on the shell of casein micelles, which, upon heating, released phosphoric acid that favored the degradation of cellulose towards the formation of a stable char [5].

**Figure 1** SEM images of burnt treated cotton fabrics with casein suspensions of alkaline and acidic pH

The morphology of burnt residue 50, 100 and 150 g/L casein treated fabrics for both pH conditions can be observed from SEM images in Figure 1. The residue for

alkaline casein suspension showed the formation of globular micrometric structures at localized spaces (Figure 1a, 1c and 1e). On the other hand, the residue for acidic casein suspension showed the formation of more expanded globular micrometric structures (i.e. global intumescence) at enlarged spaces (Figure 1b, 1d and 1f). The globular micrometric structures are phosphorus-rich bubbles that blow up during the combustion [5].

5 CONCLUSIONS

The study presented the application of casein protein for environment friendly flame retardant finish of cotton fabrics. The effect of coating of different concentration and pH of aqueous casein suspension on intumescent flame retardant properties were investigated. From thermogravimetric analysis, the shift of Tonset10% values to lower temperature indicated stronger sensitization of the cellulose decomposition by treatment of casein macromolecules under acidic pH. The samples coated with acidic casein suspension produced higher amount of residue than alkaline casein suspension and it increased with increase in casein concentration. From SEM microstructures, the residue of alkaline casein suspension showed the formation of globular micrometric structures at localized spaces only. On the other hand, the uniform formation of more expanded globular micrometric structures (i.e. global intumescence) with release of oily substances was observed for residue of acidic casein suspension. These observations of coating the acidic casein suspension have never been reported in previous studies. Therefore, the casein treatments on cotton textiles can be employed to prevent second-degree burn injuries from low intensity heat flux accidents.

ACKNOWLEDGEMENT: The financial support for conducting the present research work was provided from the Student Grant Competition Technical University of Liberec no. 21315 granted by Ministry of Education, Youth and Sports of Czech Republic.

6 REFERENCES

- [1] Baheti, V., Maqsood, H. S., Wiener, J., & Miličky, J. (2016). Reinforcement of ozone pre-treated and enzyme hydrolyzed longer jute micro crystals in poly lactic acid composite films. *Composites Part B: Engineering*, 95, 9–17.
- [2] Horrocks, A. R. (1996). Developments in flame retardants for heat and fire resistant textiles—the role of char formation and intumescence. *Polymer Degradation and Stability*, 54(2–3), 143–154.
- [3] Fang, F., Zhang, X., Meng, Y., Gu, Z., Bao, C., Ding, X., ... Tian, X. (2015). Intumescent flame retardant coatings on cotton fabric of chitosan and ammonium polyphosphate via layer-by-layer assembly. *Surface and Coatings Technology*, 262, 9–14.
- [4] Malucelli, G., Bosco, F., Alongi, J., Carosio, F., & Di, A. (2014). RSC Advances Biomacromolecules as novel green flame retardant systems for textiles: an overview †. *RSC Advances*, 4, 46024–46039.
- [5] Alongi, J., Carosio, F., & Malucelli, G. (2014). Current emerging techniques to impart flame retardancy to fabrics: An overview. *Polymer Degradation and Stability*, 106, 138–149.

Prediction of Compressional Properties of Filament Wound Composites by Analytical and Computational Model

Adit Gupta*, Lakhan Vijayvargiya, Sayan Mukherjee and B.K. Behera

Department of Textile Technology, Indian Institute of Technology Delhi

*corresponding author e-mail: Adit.Gupta.tt115@textile.iitd.ac.in

Abstract: The focus of this research is to investigate the response of carbon/ epoxy filament wound cylindrical tubes under axial and radial compression. For that, analytical, computational and experimental approaches have been followed. The variation of process parameter, particularly winding angle, on the compressive mechanical property was observed in the filament winding process. The elastic properties of the composites were calculated for each angle using the rule of mixtures and classical laminate theory. The values obtained from the test were convergent with the analytical and computational model. It is found that nature of pattern obtained for winding angle is different for radial compression and axial compression.

Keywords: Filament Winding, Axial Compression, Radial Compression, Winding angle

1. INTRODUCTION

Textile composites are being used widely in various applications and has replaced materials like iron, steel, wood etc. The reason for this includes high strength, light weight, long life, flexibility and minimum maintenance requirements. They are used for the heavily loaded parts where a stress concentration may often occur and for structural parts where strongest structural elements are needed. Textile composites can be produced through numerous methods depending on the applications. One such technique used for production is Filament Winding. Filament winding is a fabrication technique mainly used for manufacturing open or closed cylinders or axisymmetric hollow structures. In this process, continuous strand of resin impregnated fibres/filaments/tow is wound onto a specific designed mandrel with a predetermined orientation and the mandrel is removed after curing it to make a hollow composite[1]. The mechanical properties of the composites produced in this method depend on many parameters such as number of layers, angle of wind, thickness, arrangement of winding layers, percentage of resin take up, winding speed, winding pitch, geometry of the mandrel, choice of the material system (the reinforcing fibres and the matrix), cross-section of the fibre's bundle (bandwidth, thickness), initial fibre's tension, initial fibre's degree of impregnation, processing temperature, path of the fibres onto the mandrel, lay-up sequence and curing time after winding[4]. Since a large number of processing variables are directly involved, the simultaneous interaction of a great number of complex physical phenomena is a difficult challenge in processing of filament winding. In order to develop an accurate methodology for these layered composites, an improved understanding and significant computational modelling of these complex composite systems, simulation of the operation of a real-world process or system is carried out to review the properties before manufacturing. The simulation of filament wound composites using Finite Element Method (numerical method for solving problems of engineering and mathematical physics) provide solution regarding the mechanical properties through ANSYS. The model of the desired composite is designed on Creo parametric. The model results obtained both from analytical and computational techniques are validated with experimental values by producing a predesigned cylindrical product.

2. MATERIALS AND METHODS

In this project, for the production of filament wound composites we used these industrial grade fibers for reinforcement ie. Carbon Fibre Torayca Grade T300B-6k-50B. This is a high performance carbon fibre made of PAN. This untwisted yarn has 6000 filaments with the following physical property.

Table 1 Fibre Property

Physical Properties of Carbon Fibre				
Tensile strength (MPa)	Modulus of elongation (GPa)	Elongation (%)	Finenes s tex (g/ 1000m)	Density (g/cm ³)
3530	230	1.5	396	1.76

These fibres are impregnated into Epoxy resin Araldite LY556 along with Anhydride Hardener HY 917 and Accelerator DY 070 for adjusting the reactivity.

Table 2 Resin Property

Physical Properties of Resin				
Tensile strength (MPa)	Modulus of elongation (GPa)	Elongation (%)	Viscosity (mPa s)	Density (g/cm ³)
345-375	25.5-26	1-2	10000 - 12000	1.15-1.20

The samples were fabricated on 4-axes CNC Filament Winding Machine. This includes simultaneous Axes of movement of Mandrel Rotation, Carriage, Cross Carriage and Payout eye Rotation.



Figure 1 4-axes CNC Filament winding machine

2.1. Specimens

The specimens were fabricated with three different winding angle of the following stacking sequence[3],
Table 2 Stacking Sequence

Stacking Sequence	Thickness	Fibre Volume Fraction(v_{fr})
$[\pm 30/0/\pm 30/0/\pm 30]_{FW}$	41.92	0.511
$[\pm 45/0/\pm 45/0/\pm 45]_{FW}$	46.3	0.485
$[\pm 55/0/\pm 55/0/\pm 55]_{FW}$	34.1	0.508

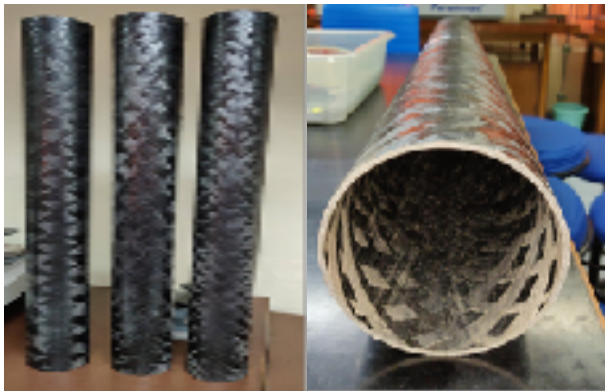


Figure 2 Filament Wound Composite

2.2. Test Methods

ASTM D2412-10: This test method covers the determination of radial compressive strength of cylindrical composites. The radial compressive loading of the tubes was performed in an Instron Universal machine model 3382 at a crosshead speed of 10 mm/min. Four samples (free of burrs and jagged edges) of each family were tested. Gauge length of specimen was 90mm. Maximum load capacity of machine is 5KN.

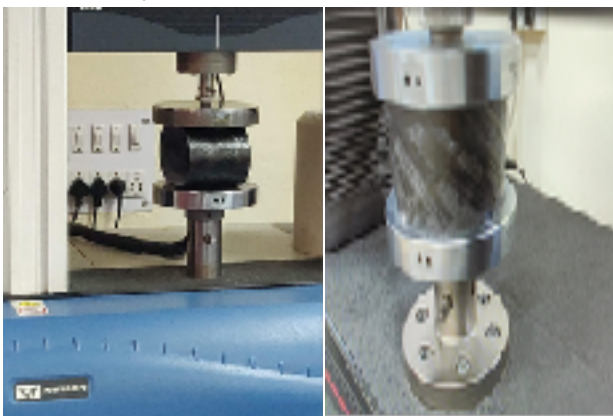
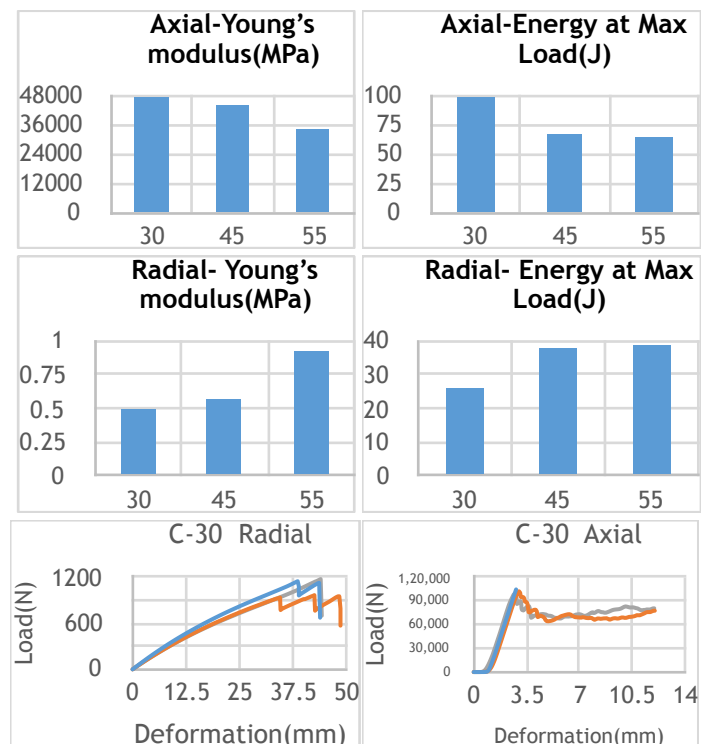


Figure 3 Axial and Radial Compression Test

ASTM D2412-11: This test method covers the determination of axial compressive strength of cylindrical composites. The axial compressive loading of the tubes was performed in an Instron Universal machine model 3382 at a crosshead speed of 10 mm/min. Four samples (free of burrs and jagged edges) of each family were tested. Gauge length of specimen was 80mm. Maximum load capacity of machine is 100KN.

3. RESULTS AND DISCUSSIONS



4. CONCLUSION

The variation of process parameter, particularly winding angle, on the compressive mechanical property was observed in the filament winding process. The samples with higher winding angle showed lower Maximum load under axial compression analysis and in case radial compression it indicated higher Maximum Load at higher winding angle. Essentially, Young's modulus, Energy at Maximum load shifted in a similar way. As the Computational results are very similar with the experimental, so we could foresee the mechanical property of bigger measurements with a similar exactness. This aides in lessening wastage of material and time.

5. REFERENCES

1. T. Martinec, J. Mlýnek, M. Petrů, et al.: Calculation of the robot trajectory for the optimum directional orientation of fibre placement in the manufacture of composite profile frames, *Rob. Comput. Integr. Manuf.*, 35 (2015), pp. 42-54
2. Hugo Faria, et al.: Analytical and numerical modelling of the filament winding process, Universidade do Porto 2013
3. A. Ortenzi, J. Carvalho, A. Corvi, et al.: Comparison between elastic properties of theoretical, computational method and experimental results for filament wound composite pipes, *J Braz. Soc. Mech. Sci. Eng.* (2017)
4. Ha, S. K. and Jeong, J. Y., et al.: Effects of winding angles on through- thickness properties and residual strains of thick filament wound composite rings, *Composites Science and Technology*, Vol. 65, Issue 1, 2005, pp. 27–35.

EFFECT OF COVERING STRUCTURE ON THE PERFORMANCE OF WRAPPED CONDUCTIVE YARN AS STRAIN SENSOR

Hu Jiyong¹, Dong Xiaolong², Zhang Yong², Wang Tingting²

¹ Key Laboratory of Textile Science & Technology, Ministry of Education, Donghua University, Shanghai 201620, China; hujiy@dhru.edu.cn

² College of Textiles, Donghua University, Shanghai 201620, China;

Abstract: Elastic wrapped yarn has a spiral wrap structure, which is favored in the design of flexible strain sensors. However, the relationship between the structural parameters of the wrapped yarns and their sensing properties has not been deeply studied so far. In terms of the structural parameters of the wrapped yarns - the spirally wrapping density and the number of wrapped layers, the wrapped yarns with a wrapping density of 20~40 twists/cm as well as single- and double-layer wrapper were respectively fabricated. And then, these wrapped elastic yarns were finished to form a conductive yarn by in-situ PPy polymerization, and their electrical resistance changes under different stretching strain were tested. On the basis of strain-resistance relationship, it is evaluated on the response sensitivity and the repeatability of these conductive wrapped yarns as strain sensor. The results show that the resistance response of the strain sensor varies with the wrapping density, the sensitivity is best at 40 twists/cm, and the motion with elongation as low as 0.5% can be detected. Moreover, the double-layer wrapper sensor with high wrapping density has high sensitivity and low hysteresis as well as low drift. It concludes that wrapped yarn as strain sensor should choose the double-layer structure and maximize the wrapping density in the limitation of good formation structure and wrapping technology.

Keywords: component, formatting, style, styling, insert (keywords)

1 INTRODUCTION (HEADING 1)

Yarns as strain sensors are generally studied. Most of yarn sensors are based on the core-spun yarn and the wrapped yarn. To being used as strain sensor, both the core-spun and wrapped yarn are usually dipped or deposited a conductive layer, and the stretching properties and stability of the sensors are related to both the yarn structure and the coated materials[8]. Cheng et al made a sensor by graphite-based composite yarn[1], of which is a 'compression spring' structure by dipping PU/PE wrapped yarn into rGO (reduced oxidation graphite) solution, and the sensor can detect tensile, bending and torsion strain. Their results demonstrated the good sensing performance of strain sensor made of wrapped yarn. And also, Cheng et al established a simplified geometrical structure model of wrapped yarn, and speculated that the relative change of resistances is majorly determined by the wrapping density of the wrapper fibers[9].

The strain sensor made of wrapped yarn can also be prepared by helically wrapping the conductive materials on the non-conducting filament/yarn [2]. Huang et al [3] used polyester and Lycra as the core, the carbon-coated fiber as the wrapper, and prepared the single- and double-layer wrapped yarn, and they didn't observe a significant influence of the wrapping density (i.e. twists per meter, TPM, 1.50 twists/cm, 2.50 twists/cm and 2.75 twists/cm) on the relative resistance change during yarn stretching. And meanwhile, they observed that the sensor with double-layer conductive wires has higher linearity than that with single-layer wires. Similarly, Wang et al [4] prepared the wrapped yarn made up of the single-wall carbon nanotube film tape wrapping polyester multifilament with 1.00~2.50 twists/cm, and double-layer yarn with 0.80~2.00 twists/cm. Under stretching strain, the wrapped yarn with 1.20 twists/cm has the maximum

strain-resistance change. Obviously, it is unknown how the sensing performance of strain sensor made of wrapped yarn depends on the wrapping density.

Above all, the strain-resistance relationship probably depends on the wrapped materials and the wrapped structures, and previous studies mainly focused on the conductive coating or depositing process of wrapped yarn, and verified their potential as strain sensor. However, few work discussed about the relationship between the structural parameters of wrapped yarn and its sensing properties. This study will study the effect of wrapped structure, especially the wrapping density, on sensing performance.

2 EXPERIMENT AND CHARACTERIZATION

2.1 Preparation of Wrapped Yarn Sensor

The single-layer and double-layer wrapped yarns with different wrapping density are spun and then processed by in-situ PPy polymerization[5]. The core layer is 140D/2f spandex multifilament, the wrapper fibers are 70D/48f polyamide multifilament. In the preliminary experiment, it is observed that the wrapped yarn with no more than 40 twists/cm has stable structure, and therefore the wrapping density is set as 20 twists/cm, 25 twists/cm, 30 twists/cm, 35 twists/cm, and 40 twists/cm, respectively..

2.2 Characterization of Sensing Performance

According to AATC76-2011, the customized tester was used to [5] record the real-time resistance during stretching yarn. The initial length of the yarn is 5.0 cm, and the stretching rate is 0.5 cm/s. In order to analyze the sensitivity of the sensor, the changes of resistance at 100% and 80% of the tensile strain were recorded,

respectively. The sensitivity was expressed by the gauge factor, i.e. the ratio of the relative resistance change to the relative length change, which is defined as $G = (\Delta R/R_0)/(\Delta L/L_0)$. In the meantime, the method of gradually reducing strain[1] was used to study the detection threshold of the yarn sensor at a stretching speed of 0.5 cm/s, respectively.

3 RESULTS AND DISCUSSIONS

3.1 Sensitivity

Figure 3 gives the strain-sensitivity relationship of wrapped yarn as strain sensor, and initially the gauge factor sharply rises and then rapidly declines. These wrapped yarns have the highest sensitivity at 10% strain or so. These phenomena are consistent with the previous studies. Cheng dipped wrapped yarn into rGo solution, and a similar strain-resistance curve was observed[1]. This phenomenon is mainly attributed to the increasing pitch of the helically wrapping fibers when stretched.

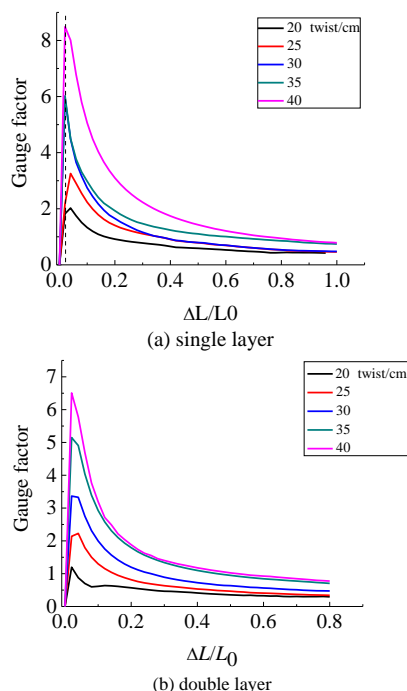


Figure 1 Strain-resistance response of sensor based on different wrapped yarn

The sensitivity change of double-layer wrapped yarns with different wrapping density is similar to that of single-layer wrapped yarns. Furthermore, the gauge factor increases when the wrapping density increases from 20 twists/cm to 40 twists/cm. Generally, the maximum sensitivity of the single-layer wrapped yarns with the same wrapping density is higher than that of the double-layer wrapped yarns, but the latter reaches stable earlier as the strain increases. Obviously, the wrapping structure significantly affects the strain-resistance relationship of wrapped yarns.

3.2 Dynamic Responses

For single- and double-layer wrapped yarns with 30, 35 and 40 twists/cm, Figure 7 shows the strain-resistance curve under 20 stretch/release cycles at 5%, 2%, 1% and 0.5% strain, respectively. Observably, at 0.5% strain the resistance still has a distinct change. Intrinsically, a small

strain just straightens the helical wrapper fibers, and causes a negligible slippage between the core yarn and the wrapper fibers. And also, the yarn sensor can make a more stable response at a strain of 0.5%. Therefore, the wrapped yarn sensor can detect limb movements under a small strain. Furthermore, the peak resistance increases with an increase of wrapping density, and it represents a major role of inter-wrapper-fibers contact resistance in the strain-resistance relationship.

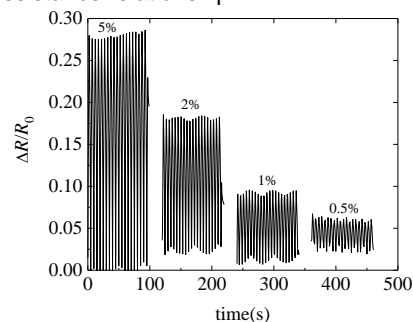


Figure 2 Dynamic resistance responses of single-layer wrapped yarn under different maximum strain

From the above results, it can be summarized that strain sensors made of wrapped yarn with large wrapping density offer higher sensitivity and lower hysteresis. Meanwhile, the sensors made of double-layer wrapped yarn show low drift. Therefore, the application of the strain sensors of double-layer wrapped yarn into monitoring human finger movements was investigated to analyze their performance as strain sensors

4 CONCLUSIONS

the sensitivity of the wrapped yarn as strain sensor increases with the wrapping density, and relatively the double-layer wrapped yarn has a higher sensitivity than that of single-layer yarn. The repeatability of the single-layer wrapped yarn sensor decreases with the increasing wrapping density, while that of the double-layer wrapped yarn sensor increases with an increase of the wrapping density. For the wrapped yarn with the wrapping density in the range of 20–40 twists/cm, the double-layer wrapped yarn with 40 twists/cm has better sensitivity, detection threshold and repeatability.

REFERENCES

- [1] Cheng Y., Wang R., Sun J. et al. A stretchable and highly sensitive graphene-based fiber for sensing tensile strain bending, and torsion *Adv. Mater.* 2015, 27, pp.7365–7371.
- [2] Mi Q., Wang Q., Zang S., et al. RGO-coated elastic fibres as wearable strain sensors for full-scale detection of human motions *Smart Mater Struct* 2018, 27, pp.015014.
- [3] Huang C. T., Shen C. L., Tang C. F. et al. A wearable yarn-based piezo-resistive sensor *Sensors and Actuators A: Physical* 2008, 141, pp.396–403.
- [4] Wang J., Pang S., Liu W., et al. Preparation and property of carbon nanotube / polyester wrapping Yarn *Journal of Donghua University* 2016, 42, pp.350–355.
- [5] Zhang X., Li G., Hu J., et al. Mechanic-electrical property characterization of PPy-coated conductive woven fabric for human upper limb motion monitoring *Chinese J Biomedical Eng.* 2016, 34, pp.670–676.

DYNAMIC CREASE RECOVERY AND RETENTION OF WOOL FABRIC BY SHAPE MEMORY POLYURETHANE

Nazife KORKMAZ MEMİŞ¹ and Sibel KAPLAN¹

¹Süleyman Demirel University, Engineering Faculty, Textile Engineering Department, Isparta, Turkey
e-mail: nazifekorkmaz@sdu.edu.tr

Abstract: In this study, crease recovery and retention performances of wool fabric, whose performance is poor especially in wet condition, were enhanced by shape memory polyurethane (SMPU) finishing. Crease recovery of a flat garment and crease retention of a pleated skirt during washing and drying cycles by shape memory effect of SMPU were compared with a commercial polyurethane based agent. The recovery and retention performances of wool fabric were investigated by a comprehensive test procedure including air and water at different temperatures simulating laundry and drying processes. Chemical and morphological analyses (FT-IR and SEM), bending rigidity and tear resistances were tested to determine the applied smart finishing on mechanical and hand properties of the fabric. The results show that SMPU finishing treatment may be a solution for smart crease recovery or retention during standard cleaning processes without the need of iron.

Keywords Shape memory polyurethane, shape memory effect, crease retention, crease recovery, hot water, hot air

1 INTRODUCTION

Wool, the most used animal fiber for garments, is a crucial and high-quality textile material for industry due to its comfort, warm effect, moisture absorption and good dry crease resistance attributes [1]. Crease recovery of the garment is a desired property especially after laundry cycles but for some end used such as pleating of a garment part, crease retention is required [2]. An alternative method to the commercial ones including shape memory polymers (SMPs) may be used to obtain novel shape memory effect creating environmental adoptable crease recovery and retention behavior as well as dimensional stability, pattern keeping and bagging recovery upon application of external heat stimuli during home laundry, steaming and hot wind tumble drying process [3, 4]. Among these polymers, SMPU has gained much popularity in textile industry with their shape memory effect developing smart garments which have adaptability to dynamic environmental and body physiological changes, recently [5]. Results in literature revealed that SMPU application on wool and cellulosic fabrics may be a tool for producing smart garments that have functions such as wrinkle recovery, crease retention and bagging recovery on account of shape memory effect [6].

2 MATERIALS AND METHODS

2.1 Materials

In this study; 100% wool plain weave fabric supplied from Yünsa Woollen Co., was used. The wool fabrics were treated with thermally responsive SMPU (pellet-type MM-3520, SMP Technologies Inc., Japan) which has a T_{trans} temperature ($T_{trans}=T_g$) of 35°C suitable for body temperature. Also, a commercial polyurethane (Pulcra HPU®) having no shape memory effect was used as a control finishing agent. N, N-dimethylformamide (DMF) purchased from Sigma-Aldrich and deionized water were used as solvents.

2.2 Methods

SMPU emulsions were prepared by completely dissolving granules with concentration of 10 wt% in DMF at 60°C for 6 hours. Also, solution of Pulcra HPU was prepared according to manufacturer's recommendation with concentration of 8 wt%. Functional finishing of wool fabric samples was carried out by using pad-dry-cure process. Surface morphologies and chemical structure of the raw and treated wool fabric samples were identified by SEM and FT-IR analyses. The weight (TS 251:2008), bending rigidity (ASTM D 1388-92:2002) and tear strength (TS EN ISO 13937-2) of treated fabrics were determined. In order to determine crease retention and recovery performances according to the shape memory effect of SMPU, treated fabrics were ironed to form crease line (crease retention) and flat appearance (crease recovery) at 120°C under 100 g/cm² pressure for 30 s before final curing. Smart crease recovery and retention behaviors of treated fabrics were tested under different media such as water and air at different temperatures. Test procedure consists of 4 stages listed below;

(i) Evaluation of the original shape: The original angles of the flat and creased fabrics on both warp and weft were measured. **(ii) Shape deformation:** The samples were then pressed by 1 kg/m² pressure for 24 h for creased forms of flat samples and flat forms of creased samples (temporary shapes). **(iii) Recovery process:** Shape recovery process was carried out at 20, 40 and 65°C water and 20, 40 and 65°C air to simulate washing and drying conditions. Then, samples were conditioned within a drying frame for 24 h at 65% RH, 20°C. **(iv) Evaluation of shape recovery:** The crease recovery and retention performances of fabrics were determined by angle measurements in the final state and shape recovery and retention ratios were calculated according to Equation 1.

$$C_r = \frac{\theta_{p,load} - \theta_f}{\theta_{p,load} - \theta_o} \times 100 \quad (1)$$

The effects of finishing agent type, media and also temperature were determined by multivariate analysis of variance (MANOVA) at the 95% confidence level.

3 RESULTS AND DISCUSSIONS

According to SEM results, scales of wool fibres were partially coated with a thin Pulcra HPU film and very few inter-fibre connections were formed. A relatively uniform and thicker coating effect was obtained for SMPU treated fabrics with polymer fillings among fibres. Pulcra HPU and SMPU polymer were successfully introduced on the surface of wool fabrics according to FT-IR spectrum. The mechanical results showed that SMPU treatment increased weight, bending rigidity and tear strength of the fabrics significantly as expected. The film layer created by SMPU polymer was thicker compared to Pulcra HPU and also this film could cover completely cuticle scales of fibre surface and the gaps between the fibres, thereby preventing their relative movement during bending. Strictly speaking, preventing relative movement of the cuticle scales would, in turn, significantly increase the bending rigidity of an individual fibre, and thus of the overall fabric [7]. Also, a significant tear strength increase especially in weft direction with SMPU treatment which can be explained by thicker SMPU film accumulating the gaps among fibres and decreasing inter-fibre and yarn friction. It is thought that, the mentioned structure not only increased individual yarn strength but also inter-yarn movement, leading an increase in tear strength.

The crease recovery and retention ratios of the wool fabrics with different polymers according to different water and air temperatures are compiled in Table 1.

Table 1 Crease recovery and retention ratios of the wool fabrics at different temperatures of water and air

	Samples	Temperature		
		20°C	40°C	65°C
Crease Recovery (%) (Air/Water)	Raw wool fabric	50.55±0.73 62.41±3.57	53.80±0.42 65.37±1.12	54.81±6.85 68.43±1.25
	WO-Pulcra HPU	53.47±1.67 68.15±1.76	53.24±0.64 68.70±1.78	53.7±4.97 68.89±2.47
	WO-SMPU-10	66.76±1.97 74.54±7.86	68.52±1.53 78.15±2.08	73.8±2.13 78.80±1.53
	Raw wool fabric	0±0 23.89±1.47	3.9±0 39.44±2.65	1.76±0 41.48±3.49
	WO-Pulcra HPU	7.87±2.89 31.76±0.32	11.20±2.23 42.22±6.13	11.94±4.87 45±7.14
Crease Retention (%) (Air/Water)	WO-SMPU-10	22.03±1.37 53.89±1.55	31.67±0.73 68.43±0.89	47.5±1.00 70±1.27

According to MANOVA analysis results, besides polymer type, both media and temperature had statistically significant effects on crease recovery and retention, meaning a smart shape memory function for enabling dynamic formability of fabric. Except for sample-media, all other double and triple interactions of the parameters have significant effects on crease retention. According to polymer type, raw and WO-Pulcra HPU treated fabrics had statistically identical and lower crease recovery values. On the other hand, these fabric samples had statistically different crease retention values from each other. Among all samples, the significantly highest crease recovery and retention values belong to WO-SMPU-10. Increased fabric elasticity with SMPU treatment may also a reason of this function [7]. Also, the significant differences between both crease recovery and retention of the SMPU and Pulcra-HPU treated fabrics may be caused from thicker polymer film formation on wool fibres for SMPU treated fabrics. As crease recovery and retention values were evaluated according to

temperature, statistical analyses show that crease recovery of all fabric increased abruptly for 65°C which reached up to 73.80% in dry air and 78.80% in water for SMPU treated fabric, respectively. According to crease recovery results, it can be concluded that wool fabric can recover from accidental crease of wear conditions during home drying but especially laundry process with help of temperature. Also, fabrics treated with SMPU had the maximum crease retention values like as 47.5% in dry air and 70.1% in water media at 65°C for SMPU treated fabric which are significantly higher than the other treatment. SMPU treated samples showed their environmental adoptable memory effect more on crease retention that may be a solution for setting pleated skirts.

4 CONCLUSIONS

According to the results, SMPU polymer deposited on wool fabric effectively with a thicker film formation confirming higher weight, bending rigidity and tear strength results. SMPU treated wool fabrics had apparently higher recovery and especially retention ability as a result of shape memory effect increasing with temperature of air and especially water. Summing up, garments can recover to their original flat appearance and designed creased states with help of SMPU treatment during standard home washing, drying or wearing conditions. These kind of SMPU treatments have advantages to produce smart garments that change form dynamically according to the environmental conditions with less disadvantages about hand and mechanical properties. Moreover, these smart fabrics developed with SMPU treatment can meet the consumer's add-valued requirements about easy care performance of garments without need of iron.

ACKNOWLEDGEMENT: We thank the Scientific and Technological Council of Turkey (Project No. 112M228) and Suleyman Demirel University (Project No. 05424-DR-14). Furthermore, we would like to express our gratitude to Yünsa Woollen Co. to Er-sa Group for fabric and chemical supply, respectively.

5 REFERENCES

- [1] Shen J.: Wool finishing and the development of novel finishes. In *Advances in wool technology* Woodhead Publishing 2009, pp. 147-182.
- [2] Hu J. Shape memory polymers: fundamentals, advances and applications. *Smithers Rapra* 2014.
- [3] Lu J., Hu J.L., Zhu Y., Liu Y.J. Shape memory finishing of wool fabrics and garments. *Advanced Materials Research* 2012, 441, pp. 235-238.
- [4] Li Y.K.S. Ph.D, The Hong Kong Polytechnic University, Hong Kong, 2007.
- [5] Jahid M., Hu J., Wong K., Wu Y., Zhu Y., Sheng Luo H., Zhongmin D.: Fabric coated with shape memory polyurethane and its properties. *Polymers* 2018, 10(6), pp. 681.
- [6] Liu X., Hu J., Murugesh Babu K., Wang S.: Elasticity and shape memory effect of shape memory fabrics. *Textile Research Journal* 2008, 78(12), pp. 1048-1056.
- [7] McNeil S.J., Standard O.C.: Increased bending rigidity of wool fabric imparted by hybrid organic-inorganic sol-gel coatings. *Textile Research Journal* 2017, 87(5), pp. 607-616.
- [8] Korkmaz Memiş N., Kaplan S.: Enhancing wool fabric bagging recovery by shape memory polyurethane finishing. *International Congress on Wool and Luxury Fibres – ICONWOOLF* 2019, 2019.

HYDROTHERMAL SYNTHESIS OF TiO₂ NANOPARTICLES ON PET FABRIC AND THEIR FUNCTIONAL PROPERTIES

Muhammad Zaman Khan¹, Vijay Baheti², and Jiri Militky³

^{1, 2, 3}Department of Material Engineering, Faculty of Textile Engineering, Technical University of Liberec, Czech Republic

e-mail: zamankhan017@yahoo.com

Abstract: The present study is aimed at *in situ* deposition of TiO₂ nanoparticles on polyester fabric through hydrothermal method by changing the process conditions. The morphology of as-deposited particles has been studied by using SEM. The chemical composition of nanoparticles was determined using energy dispersive spectroscopy. The functional properties were examined like photocatalytic activity, UV protection and moisture management. The study of UV protection and photocatalytic activity of the coated fabric showed that it had excellent UV protection factor and self cleaning properties. Also, the coated samples exhibited good moisture management properties.

Keywords: Hydrothermal, Nanoparticles, UV protection, Functional properties

1 INTRODUCTION

Due to growing market demand, the researchers have recently focused their research on development of multifunctional textiles using non-conventional techniques. TiO₂ happens to be an excellent functionalizing agent due to its multifunctional properties and possibility to be deposited in the form of nanoparticles at low temperature. It is a very well-known photocatalyst and has been extensively used to degrade the coloring substances in effluent as well as in the development of self-cleaning surfaces like glasses and textiles [1–3]. Due to its photocatalytic nature, it absorbs the light in UV region, thus providing protection against harmful rays of UV. The present work is aimed at *in situ* deposition of nanoparticles of TiO₂ on polyester fabric using seeding method and studying the multifunctional properties.

2 MATERIALS AND METHODS

2.1 Materials

Tetrabutyl orthotitanate (97%) and titanium isopropoxide (98%) were purchased from TCI Japan. HCl (37%), granulated caustic soda, ethanol (99.9%) and petroleum ether were purchased from Sigma Aldrich and were used without any further purification. A plain woven polyester fabric (areal density 110 g/m²) was supplied by a local industry.

2.2 Growth of nanoparticles

The fabric was cleaned with petroleum ether using Soxhlet apparatus. The cleaned fabric was treated with 30 g/L caustic soda solution at 90 °C for 30 minutes. The growth of nanoparticles was carried out using two a steps process. In the first, TiO₂ nanoseeds were deposited on caustic soda treated polyester fabric, and then nanoparticles were grown on these seeds in the subsequent step. The nano seeds were prepared using sol-gel method. Ethanol (50 mL) and acetic acid (1.5 mL) were taken in a round bottom flask. The tetrabutyl orthotitanate (5 mL) was added drop wise into flask with continuous stirring of solution at 60°C. The solution became nearly transparent after 5 hours. The as-prepared seed solution was applied to caustic soda treated polyester fabric by padding and dried at 120 °C.

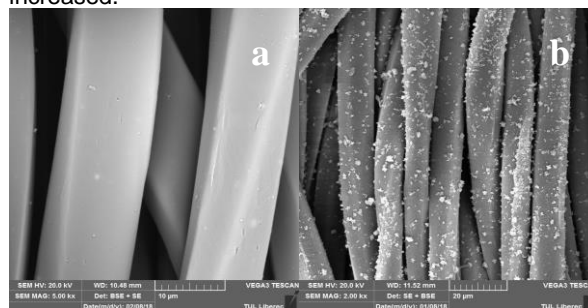
This process was repeated 5 times and finally the fabric was cured at 150 °C.

In the second step, hydrothermal method was used for the development of nanoparticles on the seeded fabric. 60 mL of distilled water was mixed with 60 ml of HCl (37 wt%) in a conical flask and then different amounts of titanium isopropoxide were added in it and stirred for 10 minutes. The resulting solution with seeded polyester fabric was transferred into 150-mL Teflon-lined stainless-steel autoclave and heated at 120 °C for 1 h.

3 RESULTS AND DISCUSSIONS

As, TiO₂ nanoparticles were grown by seeding method, therefore, the polar groups were generated on polyester fabric by treating with caustic soda before the seeding step. The caustic soda hydrolyzed the polymer chain by generating hydroxyl and carboxyl acid groups. These polar groups attached the nano seeds which are pre-requisite for the growth of nanoparticles.

When seeded samples were placed in solutions having different concentrations of titanium isopropoxide and were heated to 120 °C at pressure, the nanoparticles grew on them but their coverings were different at different concentrations as show in Figure 1. The covering of fibers with nanoparticles increased with increase in precursor concentration. With the increase in titanium isopropoxide concentration, more and more growth species were generated in the solution which led to increased deposition of TiO₂ on fibers and hence their covering was increased.



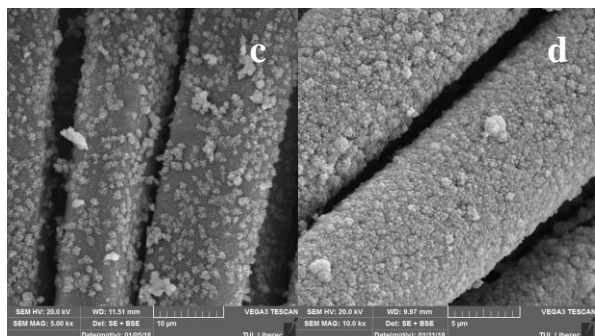


Figure 1. SEM micrographs of sample; (a) Untreated sample, (b) sample treated with 5 ml titanium isopropoxide, (c) 10 ml titanium isopropoxide, and (d) 15 ml titanium isopropoxide.

UV-protection properties of samples

UV-protection property of samples was tested by using standard test method AATCC 183-2000. Table 1 shows the results of UV protection factor (UPF), percentage blocking of UVA and UVB of untreated sample (S1), caustic soda treated (S2) and nanoparticles treated samples (S3). Untreated sample showed lowest UPF as compared to all other two samples. It also provided lowest UVA and UVB blocking %. Caustic treated sample exhibited almost same UPF and UV blocking ability as cleaned sample. TiO₂ nanoparticles treated sample showed very high UVA and UVB blocking ability.

Table 1. UV-protection results for different samples.

Sr.No	Sample Name	Mean UPF	UVA Blocking %	UVB Blocking %
1	Untreated sample (S1)	46.95	86.3	99.2
2	Caustic Treated sample (S2)	49.1	86.9	99.3
3	15 mL TTIP treated sample (S3)	338	97.7	99.8

Moisture management of fabrics

Fig. 2 represents the moisture management test results of cleaned (S1), caustic soda treated (S2) and nanoparticles treated (S3) samples. The sample S2 has high OMMC value than S1. The sample S3 has highest OMMC value (0.63) as compared to S2 and S1. It is due to two possible reasons. First important reason is the covering of TiO₂ nanoparticles with –OH groups. The second reason is the generation of capillaries due to deposition of nanoparticles on fibers. These capillaries enhance the absorption and spreading speeds of moisture on treated samples.

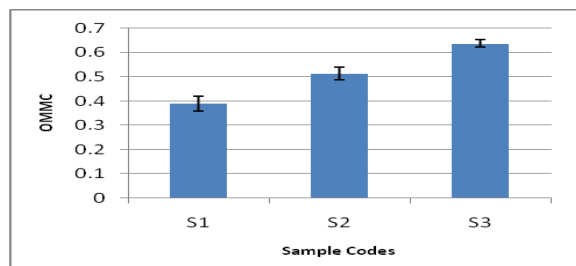


Figure 2. Moisture management results, S-1= untreated sample, S-2=caustic treated sample, S-3= 15 mL TTIP treated sample.

Solution Discoloration

Fig. 3 represents the absorbance of solution during course of UV irradiation. The absorbance decreases with the passage of time which indicates that the concentration of dye in solution decreases due to photocatalytic degradation. To check the UV fastness of dye, an untreated sample was placed in dye solution and exposed to UV light. It was observed that the dye had good fastness properties as there was no significant decrease in absorbance (Fig. 3).

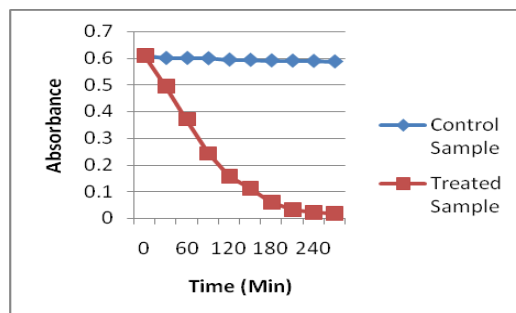


Figure 3. Absorbance values of dye solution during UV irradiation.

4 CONCLUSION

The study was focused on development of multifunctional polyester fabrics. The nanoparticles of TiO₂ were successfully deposited on polyester fabric using hydrothermal method. The treated fabrics showed excellent UV protection and photocatalytic self-cleaning. The deposition of TiO₂ nanoparticles significantly enhanced the moisture management properties of polyester fabric. On the basis of these findings, it can be said that the treated fabric has multifunctional as well as excellent comfort properties.

ACKNOWLEDGEMENT

This work was supported by the research project of Student grant competition (2019) of Technical University of Liberec no. 21312 granted by Ministry of Education Youth and Sports of Czech Republic.

REFERENCES

- [1] S. Ge, B. Wang, D. Li, W. Fa, Z. Yang, Z. Yang, G. Jia, and Z. Zheng, "Surface controlled photocatalytic degradation of RhB over flower-like rutile TiO₂superstructures," *Appl. Surf. Sci.*, vol. 295, pp. 123–129, 2014.
- [2] J. Yuenyongsuwan, N. Nithiyakorn, P. Sabkird, E. A. O'Rear, and T. Pongprayoon, "Surfactant effect on phase-controlled synthesis and photocatalyst property of TiO₂ nanoparticles," *Mater. Chem. Phys.*, vol. 214, pp. 330–336, 2018.
- [3] Y. Li, J. Liu, and Z. Jia, "Morphological control and photodegradation behavior of rutile TiO₂ prepared by a low-temperature process," *Mater. Lett.*, vol. 60, no. 13–14, pp. 1753–1757, 2006.

DEVELOPMENT OF CIBACRON BLUE-ENHANCED AFFINITY NANOFIBER FABRIC FOR PROTEIN SEPARATION

Song Liu, Takuro Sumi, Yasuhito Mukai

Department of Chemical Systems Engineering, Nagoya University, Furo-cho, Chikusa-ku, Nagoya 464-8603, Japan, e-mail: liu.song@g.mbox.nagoya-u.ac.jp

Abstract: The separation of protein, which influences on the purity and the production cost of downstream processing, plays a critical role in the protein production process. The affinity separation method using a ligand is often used for separation of protein. In this study, a functionalized fabric was prepared by immobilizing cibacron blue (CB), a dye with an affinity for specific proteins, on a polyvinyl alcohol (PVA) nanofiber nonwoven fabric produced by an electrospinning method. To evaluate its separation performance, the adsorption test of bovine serum albumin (BSA), a kind of proteins, was conducted using it. The CB molecules were immobilized by covalent bonding of hydroxyl group of PVA and chlorinated triazine ring of CB under alkaline condition. The adsorption test of CB-enhanced affinity PVA nanofiber fabric was conducted by soaking it into the BSA solution as an adsorbate. After immersing the PVA nanofiber fabric in 15 ml of the BSA solution and shaking for 4 hours, the adsorption amount of BSA was obtained from the reduction in the concentration. Furthermore, the dependence of pH was also examined by testing the BSA adsorption amount under various pH conditions. As a result, after enhancing affinity by CB, the BSA adsorption amount of the PVA nanofiber fabric indicates a significant increase due to functionalization. The adsorption amount of BSA became a maximum at pH 5.0, which is the isoelectric point of BSA. In conclusion, the BSA adsorption performance of the PVA nanofiber fabric could be greatly improved by the modification with CB. Moreover, the adsorption characteristics were heavily dependent on the solution environment.

Keywords: nanofiber fabric, protein, adsorption, affinity separation, functionalization

1 INTRODUCTION

Separation and purification of protein, which is one of the important components of creatures, are vitally important in such widely diversified fields as bio-technology, biomedicine, and dairy and food industry. The affinity separation method using a ligand is often used for separating and purifying protein. Recently, nanofiber fabrics have been attracted attention as a scaffold for immobilizing affinity materials with highly efficient functional groups attributing to their nano-size effect and high specific surface area [1-3].

In this study, a functionalized nanofiber fabric was prepared by immobilizing cibacron blue (CB), a dye with an affinity for specific proteins, on a polyvinyl alcohol (PVA) nanofiber fabric produced by an electrospinning method. To evaluate its separation performance, the adsorption and desorption tests were conducted using bovine serum albumin (BSA), a kind of proteins. The influence of protein concentration and pH on protein capture was examined.

2 PREPARATION OF AFFINITY FABRIC

2.1 Preparation of Nanofiber Fabric

The PVA nanofiber fabric was used as a base material for immobilizing CB. A schematic layout of the electrospinning apparatus for preparing the nanofiber fabric is illustrated in Fig. 1. Nanofibers were electrospun using the solution of partially saponified PVA. Since partially saponified PVA is easily dissolved in water, insolubilization is required to use it in water. Hence, maleic acid was added to the PVA solution before electrospinning and the prepared electrospun PVA fabric was heated. Then, the PVA fabric had water resistance as a result of cross-linkage by maleic acid. In Fig. 2, the SEM image of prepared PVA fabric is

shown. The mean fiber diameter was estimated at 149 nm from SEM observation, and the dissolution rate in water of this nanofiber fabric was 9.9%.

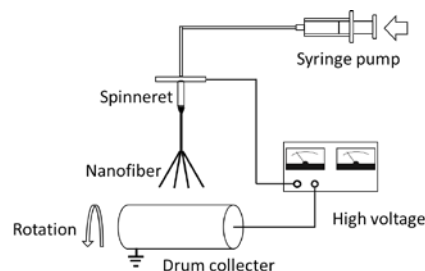


Figure 1 Electrospinning apparatus

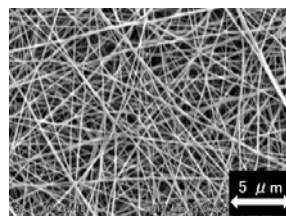


Figure 2 SEM image of PVA nanofibers

2.2 Functionalization of Nanofiber Fabric

The prepared PVA fabrics were immersed in a solution containing CB and NaCl and heated at 60 °C for 1 hour, and then Na₂CO₃ was added to the solution and heated at 80 °C for 2 hours. After taking the fabrics out of the solution and washing them with pure water, the CB-supported nanofiber fabrics were completed as shown in Fig. 3.

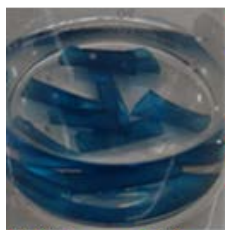
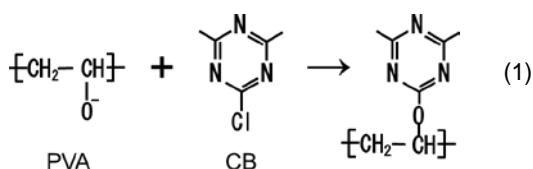


Figure 3 CB-supported PVA fabrics

The white PVA fabrics were dyed with vivid blue CB. The CB molecules were immobilized onto the PVA nanofibers by covalent bonding between hydroxyl group of PVA and chlorinated triazine ring of CB under alkaline condition as the following chemical equation.



The amount of CB immobilized on PVA fabric was 91 mg/g.

3 RESULTS AND DISCUSSION

3.1 Results of BSA Adsorption Test

The PVA fabrics were immersed in 15 ml of the BSA solution and shaken for 4 hours. The adsorption amount q of BSA per unit fabric mass was obtained from the difference between the BSA concentrations before and after adsorption test. Fig. 4 depicts the result of adsorption amount q against the equilibrium BSA concentration C^* . All plots can be expressed by the Langmuir adsorption isotherm, and the saturated adsorption amount q_s can be estimated by applying the Langmuir equation. At pH 6.0, the q_s -values are estimated at 179 mg/g and 714 mg/g before and after immobilizing CB, which means 4 times increase by means of functionalization. Furthermore, the q_s -value of functionalized nanofiber fabric at pH 5.0 is 769 mg/g slightly larger than at pH 6.0. These q_s -values of CB-supported PVA nanofiber fabrics are remarkably larger than that of CB-supported cellulose nanofiber fabric [4] and CB-supported chitosan particles [5]. Moreover, the BSA adsorption amount on CB itself at C^* of 10 g/L at pH 6.0 is estimated at 2.50 g/g, which indicates an extremely high BSA adsorption ability of CB.

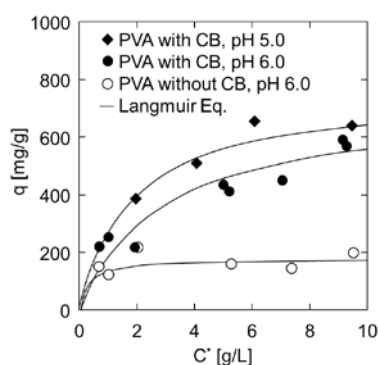


Figure 4 Adsorption isotherms

3.2 Effect of pH on BSA Adsorption

The dependence on pH of BSA adsorption amount was examined, and the experimental results were plotted in Fig. 5. The adsorption amount q became a maximum at pH 5.0, the isoelectric point of BSA, where the net charge of a BSA molecule becomes zero. This is because a BSA molecule becomes most compact due to no intramolecular repulsion.

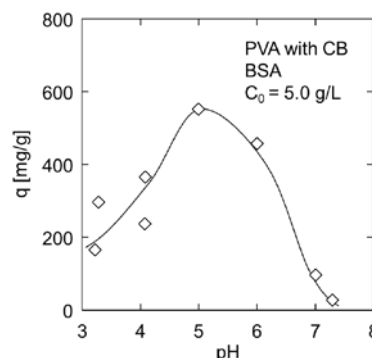


Figure 5 Effect of pH on adsorption amount

3.3 Results of Desorption Test

To recover BSA molecules from the BSA-adsorbed nanofiber fabric, the desorption test was conducted by immersing the nanofiber fabric in the electrolyte solution after the BSA adsorption test. As a result, 90.2% BSA molecules were desorbed into 0.5 M NaCl solution from the surface of the nanofiber fabric.

4 CONCLUSIONS

The BSA adsorption performance of the PVA nanofiber fabric could be greatly improved by the modification with CB. The experimental data clearly demonstrated that the BSA adsorption and desorption characteristics were heavily dependent on the solution environment. The experimental data clearly demonstrated that the BSA adsorption and desorption characteristics were heavily dependent on the solution environment.

5 REFERENCES

- [1] Duan C., Fu Q., Si Y., et al.: Electrospun regenerated cellulose nanofiber based metal-chelating affinity membranes for protein adsorption. *Composites Communications* 2018, 10, pp. 168-174.
- [2] Wang W., Zhang H., Zhang Z., et al.: Amine-functionalized PVA-co-PE nanofibrous membrane as affinity membrane with high adsorption capacity for bilirubin. *Colloids and Surfaces B: Biointerfaces* 2017, 150, pp. 271-278.
- [3] Zhang H., Nie H., Yu D., et al.: Surface modification of electrospun polyacrylonitrile nanofiber towards developing an affinity membrane for bromelain adsorption. *Desalination* 2010, 256, pp. 141-147.
- [4] Ma Z., Kotaki M., Ramakrishna S.: Electrospun cellulose nanofiber as affinity membrane. *Journal of Membrane Science* 2005, 265, pp. 115-123.
- [5] Zhang J., Zhang Z., Song Y., et al.: Bovine serum albumin (BSA) adsorption with Cibacron Blue F3GA attached chitosan microspheres. *Reactive and Functional Polymers* 2006, 66, pp. 916-923.

PREPARATION OF NANOCARBON-SUPPORTED NANOFIBER FABRIC FOR PURIFICATION OF CONTAMINATED WATER

Yasuhito Mukai, Eiji Amano and Satoshi Hara

Department of Chemical Systems Engineering, Nagoya University, Furo-cho, Chikusa-ku, Nagoya 464-8603, Japan,
e-mail: mukai.yasuhito@material.nagoya-u.ac.jp

Abstract: In this study, the composite fabric was prepared by combining nanofiber having an extremely high specific surface area with nanosized carbon black (CB) having a solute adsorption capacity to purify contaminated water. The nanofiber fabric made of polyacrylonitrile with mean fiber diameter of 400 nm was used as a base material. The CB particles with an original size of 20 nm were used as adsorbent and dispersed in pure water at the concentration of 10 g/L. Before preparation, the CB particles were oxidized by mixing CB with 70% nitric acid at a rate of 1 g to 1 ml and heating for 2 hours with agitation. The surface of CB particles became hydrophilic by oxidization and as a result the size of CB particles became original one in the dispersion. The nanofiber fabric was immersed in the CB dispersion and shaken for 2 hours. After taking out and rinsing it lightly, CB was immobilized on the surface of nanofibers by heating for 1 hour at 150°C. The adsorption test of prepared CB-supported nanofiber fabric was conducted by soaking them into the aqueous solutions of methylene blue (MB) used as a contaminant, and the adsorbed amount of MB was measured under various MB concentrations. As a result, whereas the saturated adsorbed amount to the original nanofiber fabric was 1.9 mg/g and that to untreated CB-supported nanofiber fabric was 5.0 mg/g, that to oxidized CB-supported nanofiber fabric was remarkably large 96.2 mg/g. In conclusion, the oxidization of CB is an essential pretreatment to attain high solute adsorption performance.

Keywords: nanofiber fabric, carbon black, composite, adsorption, water purification

1 INTRODUCTION

Recently, the nanofiber is attracting attention in widely diversified fields and being developed for various applications [1]. One of the typical applications of the nanofiber material is a nanofiber filter medium, and it is considered to be promising as an alternative to conventional membrane filter. The nanofiber fabric with a nanosized effect and a high porosity is expected to serve as a new filter medium for water treatment since both performances of water permeation and particle retention are very high [2, 3]. Furthermore, if such functions as adsorption or ion exchange are added to the surface of nanofibers, the functionalized fabric developed from extremely high specific surface area can be produced for application to the water purification process [4, 5].

In this study, the composite fabric with great adsorption capacity for contaminant was prepared by combining a nanofiber fabric with functionalized nanocarbon to purify contaminated water. And then, the adsorption capacity of the prepared composite fabric was evaluated through the static adsorption test with a test solution.

2 PREPARATION OF CB-SUPPORTED NANOFIBER FABRIC

2.1 Pretreatment of CB Particles

Carbon black (CB) with original particle size of 20 nm was used as an adsorbent. With the aim of improving the adsorption capacity, the CB particles were subjected to any of the following pretreatments (1) – (3).

(1) pH control of CB dispersion

In the preparation of the CB dispersion, pH was adjusted to a given value by the addition of HCl or NaOH.

(2) Activation by KOH of CB particles

The CB particles were activated by mixing KOH and CB and heating for 1 hour at 800°C under an atmosphere of N₂ gas flow of 0.5 L/min. Finally, activated CB particles were rinsed well in water after neutralization with HCl for the removal of residual KOH.

(3) Oxidization of CB particles

The CB particles were oxidized by mixing CB with 70% nitric acid at a rate of 1 g to 1 ml and heating for 2 hours with agitation. Finally, oxidized CB particles were rinsed well in water for the removal of residual nitric acid.

The size distributions of the CB particles pretreated by the methods (1) – (3) were measured. As a result, (1) The pH condition has little effect on particle size; (2) The activation of CB led to an increase in specific surface area of CB, but also caused the flocculation of CB particles; (3) The oxidization of CB shrank the particles down to original size of 20 nm because of the formation of some hydrophilic groups to the surface of CB particles.

2.2 Immobilization of CB onto Nanofibers

The nanofiber fabric supplied by Japan Vilene Co. was used as a base material. This fabric is made of polyacrylonitrile and has mean fiber diameter of 400 nm and areal weight of 17.2 g/m². The CB particles were dispersed in pure water at the concentration of 10 g/L. The nanofiber fabric was immersed in the CB dispersion and shaken for 2 hours. After taking out and rinsing it lightly, CB particles were immobilized on the surface of nanofibers by heating for 1 hour at 150°C.

Figure 1 shows appearances and SEM photographs of the nanofiber fabrics before and after treatment. The oxidized CB-supported nanofiber fabric does not turn so

black because the CB particles are dispersed to nanosize.

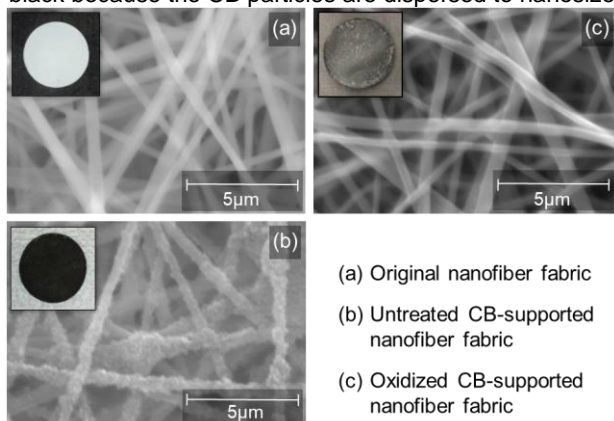


Figure 1 Images of CB-supported nanofiber fabric

And also, the oxidized CB particles are too small to be observed in a SEM photograph.

3 EVALUATION OF CB-SUPPORTED NANOFIBER FABRIC

Methylene blue, a type of colored component, was used as an adsorbate. The static adsorption test of prepared CB-supported nanofiber fabrics was conducted by soaking them into the aqueous solutions of methylene blue prepared at various concentrations with shaking until a state of adsorption equilibrium was reached. The equilibrium concentration C^* and the equilibrium adsorption amount Γ of methylene blue were measured, and the relations between Γ and C^* for different fabrics were depicted in Fig. 2. All the adsorption behaviors in the figure can be expressed by the following equation of Langmuir-typed adsorption isotherm.

$$\Gamma = \frac{\Gamma_s K C^*}{1 + K C^*} \quad (1)$$

The saturated amount Γ_s of adsorption was estimated based on Eq. (1). As a result, the value of Γ_s was 1.9 mg/g for original nanofiber fabric, 5.0 mg/g for untreated CB-supported nanofiber fabric, 6.1 mg/g for CB-supported nanofiber fabric prepared under the acid environment, 18.3 mg/g for activated CB-supported nanofiber fabric, and 96.2 mg/g for oxidized CB-supported nanofiber fabric. The effects of pretreatment of the CB particles on the adsorption capacity of the composite fabric are discussed below.

(1) Preparation in acidic environment

When CB-supported nanofiber fabric was prepared under the acid environment, the amount of supported CB was slightly increased due to the reduction of electrostatic repulsion between CB particles and polyacrylonitrile fibers.

(2) Activated CB-supported nanofiber fabric

The adsorption amount was increased by the activation of CB because of the increase in specific surface area of CB from 105 m²/g to 774 m²/g. However, the activation induced the flocculation of CB particles as mentioned above and consequently reduced the rate of increase in the amount of supported CB, resulting in not so much adsorption amount as expected.

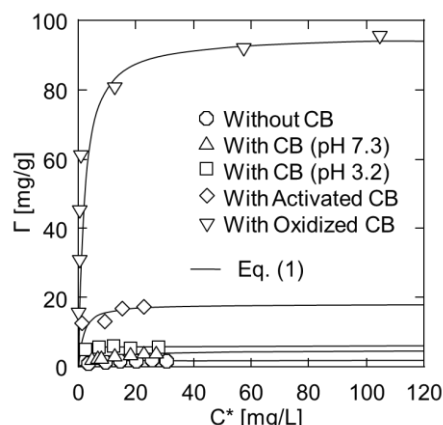


Figure 2 Adsorption isotherms of CB-supported nanofiber fabrics

(3) Oxidized CB-supported nanofiber fabric

The adsorption amount was significantly increased by the oxidation of CB because the surface of CB particles became hydrophilic and as a result the size of CB particles became original one as mentioned above. Thus, a significantly increased surface area of nanosized CB particles enhanced adsorption performance.

In conclusion, the oxidation of CB is an essential pretreatment to attain high adsorption performance.

4 CONCLUSIONS

The CB-supported nanofiber fabric developed in this study is effective in adsorption of contaminants in effluent. Especially, the composite fabric supported by oxidized CB has markedly high adsorption performance. In addition, the process of solute adsorption onto the CB-supported nanofiber fabric can be described by Langmuir adsorption model.

ACKNOWLEDGEMENT: This work was supported in part by JSPS KAKENHI Grant No. 25420801 and No. 16K06824. The authors would like to express the sincere gratitude for the financial support.

5 REFERENCES

- [1] Hongu T.: *Nanofiber Technology*. Nikkan Kogyo Shinbun, Tokyo, 2006, pp. 42-45.
- [2] Mukai Y.: Preliminary study to apply nanofiber nonwoven cloth as filter media for water treatment. *Nanofiber*, 2011, 2, pp. 20-25.
- [3] Yoon K., Hsiao B. S., Chu B.: Functional nanofibers for environmental applications. *J. Mater. Chem.*, 2008, 18, pp. 5326-5334.
- [4] Teng M., Li F., Zhang B., Taha A. A.: Electrospun cyclodextrin-functionalized mesoporous polyvinyl alcohol/SiO₂ nanofiber membranes as a highly efficient adsorbent for indigo carmine dye. *Colloids Surf A: Physicochem. Eng. Asp.*, 2011, 385, pp. 229-234.
- [5] Neghlani P. K., Rafizadeh M., Taromi F. A.: Preparation of aminated-polyacrylonitrile nanofiber membranes for the adsorption of metal ions: Comparison with microfibers. *J. Hazard. Mater.*, 2011, 186, pp. 182-189.

DEVELOPMENT OF FLEXIBLE FIBER REINFORCED SILICA AEROGEL BLANKETS/SHIELDS FOR THERMAL INSULATION IN AEROSPACE APPLICATIONS

Shivangi Shukla¹, Renu Kumari¹, Mohanapriya Venkataraman² and B K Behera¹

¹Focus incubation center for 3D weaving and structural composites

Department of Textile Technology, Indian Institute of Technology Delhi, email:

shiwangishukla112@gmail.com

²Department of Material Engineering, Technical University of Liberec, Czech republic, email:

mohanapriya.venkantaraman@tul.cz

Abstract: Aerogels are highly porous structures commonly synthesized by the Sol-gel process (formation of wet gel) followed by supercritical drying (drying of wet gel to form aerogel). With the reinforcement using polymers, the mechanical properties of silica aerogels can be tailored to meet the specifications as fire proof blankets subject to aero engine operating conditions. Aircraft components such as pipes, wires, and electronic accessories within the fire zones can be protected using thin blankets of aerogel whilst simultaneously enabling weight saving compared to conventional thick insulation sheets & metal sheets. This material application can be easily extended to various parts of the aircraft for thermal insulation, fire protection, and acoustics purposes as lighter material. Composition can further be tweaked to enhance inherent damping which when bonded with structural components like tubes in aircraft engine can sustain vibratory loads. This will make the support structures of such components lighter & less in number & hence significant weight & cost saving. This research is carried out to explore different potential Aramid fibers (heat-resistant and strong synthetic fibers) to improve the mechanical properties of silica aerogel for the above said applications & establish the synthesis process for the same & introduce for aerospace application. To improve the mechanical strength of aerogels, silica fiber is incorporated into the aerogels. Similarly carbon nanofibers are introduced to improve compressive modulus and tensile strength of aerogels.

Keywords: silica aerogel, kevlar non woven web, aerogel composite, acoustic insulation

1 INTRODUCTION

In aviation world light weight thermal insulation materials are required particularly as fire proof material. Silica aerogel as a fiber-reinforced blanket can meet necessary criteria of the Federal Aviation Regulations for fire retardation in aeroengine. For the required application in aeroengine, currently aerogel in its virgin state has major drawbacks such as- they absorb moisture, they are fragile, cannot be easily handled, and cannot be used to insulate complex shaped bodies. Therefore, fiber reinforced aerogel fabric is required to meet aero engine operating conditions such as elevated temperatures longevity, chemical (aviation fuels and lubricants) and erosion resistance, withstand high vibration and engine operation loads, and maintenance requirement along with FAR 33 & FAR 25 fire proof requirements. Silica aerogel exhibits the most remarkable physical properties, possessing low bulk density (~ 0.1 g/cm³), very low thermal conductivity (~ 0.015 W/mK), kinetic energy absorption, & acoustical insulation property (low sound velocity of 100m/s). Being ultra-light & excellent fire retardant, it makes a very promising choice as fire retardant insulation material for aero engines which will give significant fuel savings due to lower take-off weight.

2 EXPERIMENT AND METHODS

2.1 Materials for the sol

The chemicals used for the preparation of silica aerogel blankets were and the subsequent silylation of silica alcogel blankets were tetraethoxysilane (TEOS, 98%, (Sigma Aldrich)), deionized H₂O (Organo Biotech Laboratories, India)), ammonium hydroxide (NH₄OH (Fisher Scientific)) ammonium fluoride (NH₄F, (Fisher Scientific)), ethanol (EeOH, (Merck, India)), and . Double distilled water was used for the preparation of all the solutions.

2.2 Preparation of the non-woven web

The non-woven felt was made from Kevlar (p-aramid) fibre of 50mm staple length with the punch density of 110 punches/cm² and penetration depth of 10mm on a laboratory model needle punching machine (Dilo, Germany).

2.3 Preparation of the aerogel composite

Silica aerogel composite was prepared by impregnating the Kevlar fibrous non-woven fabric with the silica gel and further drying it to transform it into aerogel.

The aerogel was prepared by a two-step base catalysed sol gel process followed by supercritical drying. The sol was prepared by using TEOS precursor diluted in ethanol. This is the alkoxide solution. The stock solution was prepared by adding NH_4F and NH_4OH into deionized water. Further this solution was added dropwise into the a beaker containing water and ethanol. This is the catalyst solution. Further this catalyst solution was added into the alkoxide solution and continuously stirred and poured over the Kevlar non-woven web kept in a petri plate and allowed to gel at room temperature. The gelation took place in 10 minutes. Then the petri dish containing the samples was aged in ethanol and was wrapped with aluminum foil. The sample was aged for 36 hours in ethanol. Further the samples were dried by super critical method using super critical fluid CO_2

2.4 Characterization of aerogel composite

The prepared samples were tested for their bending rigidity, compression and flame retardancy.

3 RESULTS AND DISCUSSION

The Kevlar fibres were processed in laboratory model needle punching nonwoven machine. The nonwoven webs were needle punched to impart desired mechanical strength. The gelation process is successfully carried out in the non-woven web and aerogel composite was prepared. These composites were evaluated for their mechanical performance and fire retardancy. The flexural rigidity of the composite increases substantially. The formability of silica aerogel composite material is reduced

because of the increase in web stiffness. However, it is realized that uniform impregnation of aerogel might help to improve the formability and other essential functionality.

4 CONCLUSION

Preparation of needle punched nonwoven web from carbon and Kevlar staple fibre is critical and requires careful material handling. Proper impregnation of silica aerogel in single layer nonwoven web plays important role to achieve desired functionality in terms of flexural rigidity and formability of the silica aerogel composite. Further studies to examine acoustic insulation and thermal properties will help to optimize both nonwoven web preparation and silica aerogel impregnation.

5 REFERENCES

- [1] N. Bheekhun et al., "Aerogels in Aerospace: An Overview", *Advances in Materials Science and Engineering*, Volume 2013 2) S. Chakraborty et al., "Synthesis and Characterization of Fiber Reinforced Silica Aerogel Blanket for Thermal Protection", *Advances in Materials Science and Engineering*, Volume 2016
- [2] 3) A. Venkateswara Rao et al., "Modifying the surface energy and hydrophobicity of the lowdensity silica aerogels through the use of combinations of surface-modification agents" *J. Mater. Sci.* 2010, 45, 51–63.
- [3] 4) A. Slosarczyk, "Recent Advances in Research on the Synthetic Fiber Based Silica Aerogel Nanocomposites", *Poznan University of Technology* 2017
- [4] Kyosev Y., Nicolau A., Schacher L., et al.: Investigation about the influence of the yarn tension over the mechanical properties of tubular braided fabrics. *Vlákna a Textil* 2015, 1, pp. 31-33. (references)

POPLAR SEED FIBER AS A NATURAL ABSORBENT FOR OIL REMOVAL

Yanfang Xu¹ and Guangbiao Xu¹

¹ College of textile, Donghua University, Shanghai, China, e-mail: 1169124@mail.dhu.edu.cn

¹ College of textile, Donghua University, Shanghai, China, e-mail: guangbiao_xu@dhu.edu.cn

Abstract: Poplar seed fiber is a kind of natural water-repellent and lipophilic fiber with a large lumen, which has potential applications in the field of oil sorption. For loose fibers, compared with cotton fibers and kapok fibers, poplar seed fibers showed highest oil sorption capacity. In this study, fractal-like sorption kinetic model was employed to study the oil sorption characteristics of poplar seed fibers under different bulk densities. Results showed that poplar seed fiber absorbing different oils exhibited large differences in terms of maximum oil sorption capacity per unit mass of absorbent and observed mass transfer coefficient. The oil sorption capacity is directly related to the bulk density of the fiber assembly, and the higher bulk density means lower oil sorption capacity. Compared with diesel oil and motor oil, under the same packing density, poplar seed fiber has the greatest sorption capacity for vegetable oils due to its highest density. Sorption rate of fiber and oil is mainly related to the viscosity of the oil. The higher the viscosity, the lower the adsorption rate. Results showed that poplar seed fiber has great potential application in oil spill clean-up.

Keywords: poplar seed fiber, absorbent, surface energy, kinetic

1 INTRODUCTION (HEADING 1)

With the rapid development of a wide range of oil production and transportation, oil spill accidents have caused not only environmental problems but also great loss of energy resources [1]. For oil spill management, apart from the oil sorption capacity, high sorption rate is another critical factor for effective oil removal. A quick collect of a major part of the spilled oil is important after an oil spill, especially in coastal areas [2]. In our previous work, the oil sorption theory of hollow kapok fiber which showed great oil adsorption characteristic was reported. In this work, an attempt has been made to develop poplar seed fibers with three different bulk densities by wicking tests to study the oil sorption kinetic behavior.

2 MATERIALS AND EXPERIMENT

2.1 Materials

First, confirm that you have the correct template for your paper size. This template has been tailored for output on the A4 paper size. The poplar seed fibers studied in the work were from Henan Province, China and hand harvested during the blooming period in May. The oil types studied in this work were diesel oil, vegetable oil and motor oil, which differed significantly in their viscosities. Viscosity measurement of the tested oils were performed using a SNB2 Digital Rotary at room temperature. Density and surface tension measurements of the test oils were carried out using a dynamic contact angle measuring instruments and tensiometer (DCAT11, Dataphysics, Germany).

2.2 Oil sorption experiments

The dried sample (1g) was put into 200 ml of oil for 15 min at room temperature. Then the sample was taken out and drained for 1 min, and quickly weighted.

2.3 Evaluation of oil sorption kinetics

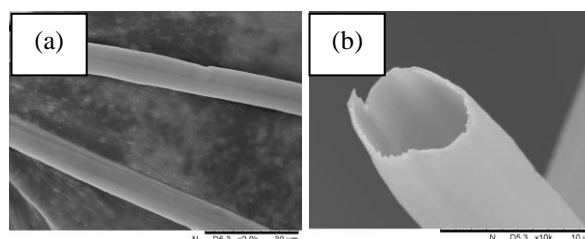
The sorption capacity and sorption rate of poplar seed fibers were measured using a wicking method carried out

on Tensiometer DCAT11. A cylindrical sample tube with internal diameter of 12 mm and length of 40 mm was used. The different bulk densities of the fiber assemblies were controlled by packing different weight fibers evenly in the tube and compressed by screwing the piston of the tube to a filled length of 20 mm. After the experiment started, the test oil level was then increased until the liquids touched the fibers. The data of the weight change vs. time was detected by the electro-balance and recorded on a computer. Every test was characterized three times and plotted as an average of three trials with error bars depicting the standard deviation. The test temperature was maintained at 22-24 °C.

3 RESULTS AND DISCUSSION

3.1 Characterization of fibers

As shown in Fig.1(a) and Fig.1(b), poplar seed fiber has a smooth surface and hollow lumen with an average external diameter of $12.7 \pm 4.8 \mu\text{m}$, tube wall of $600 \pm 100 \text{ nm}$ and length of $4 \pm 1 \text{ mm}$. This demonstrated that 90.77 % of the fiber total volume is empty lumen which is larger than that of kapok fiber (77 %) [41]. As a comparison, kapok fiber has a smooth surface, and the surface of cotton fiber has a natural twist as depicted in Fig.1 (c) and Fig.1(d), respectively.



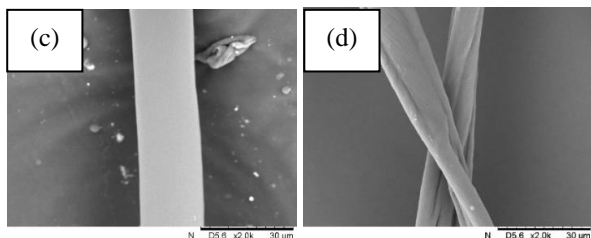


Figure 1 (a) surface of poplar seed fiber, (b) cross-section of poplar seed fiber, (c) surface of kapok fiber, (d) surface of cotton fiber.

3.2 Oil sorption capacity of loose fibers

The oil sorption capacity of loose poplar seed fibers to three test oils was demonstrated in Fig. 4, taking kapok fiber and cotton fiber as reference samples. Here the loose fibers refer to the assembly of fibers in a natural state without external force. The packing density of loose poplar seed fibers, loose kapok fibers and loose cotton fibers was 0.0036 g/cm³, 0.0053 g/cm³ and 0.073 g/cm³, respectively. The oil sorption capacity of poplar seed fiber to diesel oil, vegetable oil and motor oil was 53.74 g/g, 67.96 g/g, 65.73 g/g, respectively, which was about 1.7 times higher than that of cotton fiber, and about 1.3 time higher than that of kapok fiber. The excellent oil sorption of poplar seed fiber was mainly attributed to the small packing density of the loose fibers, besides its large lumen and oil-loving surface characteristic.

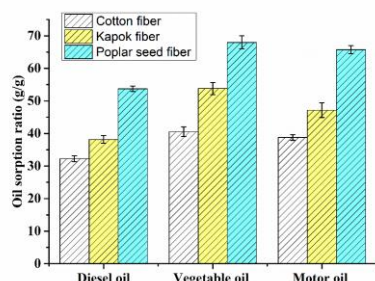


Figure 2 Oil sorption capacity of loose fibers

3.3 Sorption kinetics of poplar seed fiber

The oil mass square (m^2) vs. sorption time (t) of poplar seed fibers at three packing densities to diesel oil, vegetable oil and motor oil were presented in Fig. 3a-c, respectively. The recorded points indicated that the sorption process of oil mainly consists of two phases, including an initial rapid phase with relatively high sorption speed and then a slow phase which gradually reduced to reach sorption equilibrium. The high rate of oil sorption at the first stage may be attributed to the filling up of fiber lumens and capillaries formed between fibers. However, less sorption sites were available hence a small amount of oil uptake occurred after the initial quick sorption period. The calculated oil sorption capacity per unit mass (M) of poplar seed fibers at various packing densities to test oils were listed in Table 3. For each test oil, M decreases with the increasing of packing density, which was ascribed to the reduction of the available voids inside the poplar fiber assembly, especially among the inter-fiber pores.

Besides, under the same packing density of fibers, they were under the same pore volume, the differences in sorption capacities among the three oils were mainly a result of their different densities. Therefore, the sorption capacity of poplar seed fibers to vegetable oil depicted the highest value, resulting from the highest density of vegetable oil. It's worth mentioning that, the oil sorption capacity of poplar seed fibers at the packing density of 0.07 g/cm³ to diesel oil, vegetable oil and motor oil was 13.20 g/g, 15.14 g/g, and 13.96 g/g, respectively. The value was slightly higher than that of kapok fiber reported by our previous paper²², which largely resulted from shorter fiber length, better fineness and smaller microtubes of poplar seed fibers.

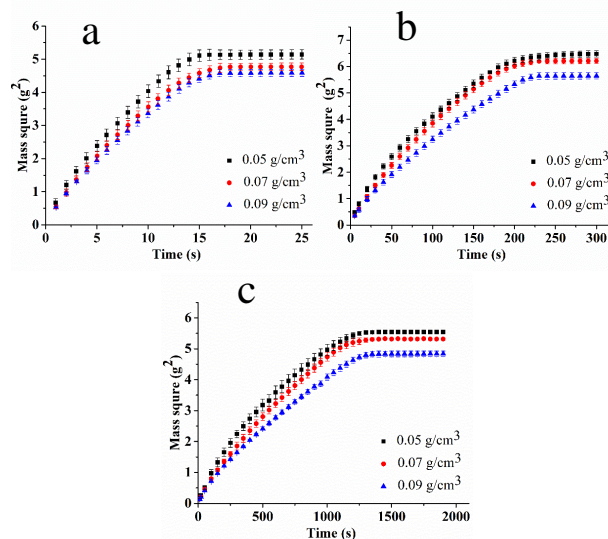


Figure 3 Plots of oil mass square with time (a) diesel oil (b) vegetable oil (c) motor oil into poplar seed fibers at different packing densities

4 CONCLUSION

The physicochemical and sorption characteristics of poplar seed fiber as an oil sorbent were presented. According to the experimental results and analysis, the following conclusions can be drawn. Oil sorption tests exhibited that loose poplar seed fibers could absorb 53.74 g/g of diesel oil, 65.85 g/g of motor oil and 67.97 g/g of vegetable oil, which showed great oil sorption capacity. Kinetics results showed that the oil sorption capacity of poplar seed fiber was closely related to the packing density of fiber assembly, with an apparent decrease when the packing density increased.

5 REFERENCES

- [1] Laffon B, Pasaro E and Valdiglesias V. Effects of exposure to oil spills on human health: Updated review. *J Toxicol Env Health-Pt b-Crit Rev* 2016; 19: 105-128. Review.
- [2] Agarwal S, Arnim VV and Stegmaier T, P, Role of surface wettability and roughness in emulsion separation. *Separation & Purification Technology*, 2013, 107:19-25.

COMPARISON OF CELLULOSE NANOFIBER PROPERTIES OBTAINED FROM BAMBOOS OF DIFFERENT AGES

Kaori Yano¹ and Yoko Okahisa²

¹ Department of Biobased Materials Science, Kyoto Institute of Technology, Matsugasaki, Sakyo-ku, Kyoto 606-8585, Japan, e-mail: yanokaori@icloud.com

² Faculty of Fiber Science and Engineering, Kyoto Institute of Technology, Matsugasaki, Sakyo-ku, Kyoto 606-8585, Japan, e-mail: okahisa@kit.ac.jp

Abstract: The cellulose nanofibers (CNF) samples were obtained from bamboos of different ages and CNF sheets were prepared. Their morphological, thermal and mechanical properties were compared. The relationships between the bamboo age and the characteristics of CNF obtained from the bamboo samples were studied.

Keywords: Cellulose nanofiber sheet, Bamboo, Age-dependent differences

1 INTRODUCTION (HEADING 1)

Bamboo is one of the most economically important raw materials in Asian countries. It grows faster than every woody plant and has been used as basic tools, furniture and building materials for centuries. However, the utilization of bamboo culms has decreased recently in Japan due to the changes in peoples' lifestyles and abandoned bamboo forests are increasing drastically [1]. One of the approaches to solving this problem is the invention of new applications of bamboo.

Cellulose is the major constituent of plant cell walls. Recently, the studies on cellulose nanofibers (CNF) and their composite materials have been attracted a lot of attention because of their high Young's modulus, high strength, low thermal expansion, low weight, biodegradability and renewability [2].

The expected applications of CNF include structural materials for automobiles, flexible electronic substrates, packaging for foods and medical supplies with high oxygen-barrier properties and gas separation membranes [3]. The production of CNF from bamboos and CNF-based of materials should be an effective new utilization of them to solve the problem of the abandoned bamboo.

The degree of polymerization of cellulose and the structure, morphology, and surface properties of the resulting CNF depend on the origin [4]. Bamboo craftsmen use three- to five-year bamboo culms more than any others because they are easy to bend and show high strength. These mechanical characteristics may be due to the density of the entire culm, the radial distributions of fibers and parenchyma cells, and/or the thickness of the cell walls. It was thought that the performances of the CNF and its composite could also depend on the bamboo age.

The relationships between the bamboo age and the morphological, thermal and mechanical properties of CNF obtained from the bamboo samples were investigated in the study.

2 EXPERIMENTAL

2.1 Material

Moso bamboo stems (*Phyllostachys pubescens* Mazel) were taken from a bamboo plantation located in Kyoto, Japan. The selected stems were 1, 2, 3, 4, 7, 10, 13 and 16 years old. All samples were ground and dried under reduced pressure at ambient temperature.

2.2 Preparation Methods

Sample extracts were prepared with a 1:2 (v/v) methanol/toluene solution using a Soxhlet apparatus over 12 h. Samples were cyclically treated in an acidified sodium chlorite (NaClO₂) solution at 70 °C for 1 h to leach lignin. To leach hemicelluloses, samples were treated in a 5 wt% potassium hydroxide (KOH) solution overnight at ambient temperature, and then at 80 °C for 4 h.

After the chemical treatments, the samples were filtered and rinsed with distilled water until the residues were neutral.

A slurry of 1 wt.% of purified cellulose was passed once through a grinder (MKCA6-3, Masuko Sangyo Co., Saitama, Japan) at 1500 rpm with the grinding stones (NKG6-120, Masuko) pressed closely together. The material was filtrated of the fibers under reduced pressure with a membrane filter and put between sheets of iron and then, vacuumed drying at 40 °C for 1 day. Then we were able to make CNF sheets.

2.3 Measurements

Thermogravimetric analysis (TGA) of the CNF sheets was conducted using a thermogravimetric analyzer (STA7200 RV, Hitachi High-Tech Science Co., Tokyo, Japan) with a rate of 10 °C min⁻¹ from ambient temperature to 600 °C after heating at 110 °C for 20 min to dehydrate the samples. The analyses were performed in a nitrogen atmosphere with a 60 ml min⁻¹ flow rate.

The CNF sheets were tested using tension testing machines and the mechanical properties of tensile strength, tensile strain to failure, and Young's modulus was calculated for the results.

The surface images of the CNF sheets were investigated with an atomic force microscope (AFM). Nanostructure was observed on the fibers.

3 RESULT AND DISCUSSION

The 10% weight reduction temperature of CNF sheet obtained from one year is 307.5, two years 309.9, three years 308.6, four years 307.3, seven years 310.6, ten years 307.0, thirteen years 311.1 and sixteen years 307.4. The results show that thermal decomposition temperatures of the CNF are constant for all of the samples irrespective of their age. These suggest that the chemical and physical structures of CNF obtained from bamboos of different ages are same and the difference in the mechanical characteristics of bamboo culm may be based on their higher ordered structures.

The results on the morphological and mechanical properties are also reported and discussed in the presentation.

4 REFERENCES

- [1] Suzuki, S., Nakagoshi N.: Expansion of bamboo forests caused by reduced bamboo-shoot harvest under different natural and artificial conditions. *Ecol. Res.*, 2008, 23, 641–647.
- [2] Siró, I., Plackett, D.: Microfibrillated cellulose and new nanocomposite materials: A review. *Cellulose*, 2010, 17, 459–494.
- [3] Isogai, A.: Wood nanocelluloses: Fundamentals and applications as new bio-based nanomaterials. *Journal of Wood Science*, 2013, 59, 449–459.
- [4] Su, Y., Burger, C., Ma, H., et al.: Morphological and property investigations of carboxylated cellulose nanofibers extracted from different biological species. *Cellulose*, 2015, 22, 3127–3135.

PREPARATION OF PARAFFIN WAX/POLYACRYLONITRILE THERMO-REGULATING NANOFIBERS BY COAXIAL ELECTROSPINNING

Yini Fang¹, Yan Wang¹, Jiawei Chen¹, Liqiang Yi¹, Haonan Jin¹, Jiri Militky², Jaromir Marek³, Juming Yao¹, Ming Zhang^{1*}

¹ College of Materials and Textiles, Zhejiang Sci-Tech University, Hangzhou 310018, PR China, e-mail: zhangming@zstu.edu.cn

² Department of Material Engineering, Faculty of Textile Engineering, Technical University of Liberec, Czech Republic, e-mail: jiri.militky@tul.cz

³ Institute for Nanomaterials, Advanced Technologies and Innovations, Technical University of Liberec, Czech Republic, e-mail: jaromir.marek@tul.cz

Abstract: With the diversified development of functional fibers, intelligent thermo-regulating fibers have attracted a great attention in the development of new materials. In this work, paraffin wax eicosane (C₂₀) and tetradecane (C₁₄) as phase change materials (PCM) were coaxial electrospun as core with polyacrylonitrile (PAN) as shell into core-shell structured paraffin wax/polyacrylonitrile nanofibers (PAN@C₂₀:C₁₄-NFs). Solution concentration of shell material and ratio of C₂₀ and C₁₄ were adjusted to realize controllable PCM encapsulation efficiency and thermal properties. Morphology thermal mechanical properties were characterized by scanning electron microscope (SEM), transmission electron microscope (TEM), differential scanning calorimetry (DSC) and thermo gravimetric analysis (TGA). PAN@C₂₀:C₁₄-NFs performs good spinnability and thermo-regulating property which indicates a wide application prospect. The result reveals the melting and crystallization enthalpy reached 38.07 and 34.06 J/g respectively with fiber diameter 600±100 nm while the concentration of PAN solution was at 15%. Cs₁₂W₃₄O₁₀₈ nanoparticles enhanced the solar utilization efficiency of PAN@C₂₀:C₁₄-NFs.

Keywords: Thermo-regulating nanofibers; phase change material; polyacrylonitrile; coaxial electrospinning; core-shell structure

1 INTRODUCTION

Generally, paraffin wax is used as the most common phase change material for low to medium temperature storage applications because it has a large latent heat and low cost besides being stable, non-toxic and non-corrosive. [1,2] Electrospun form stable PCMs exhibit remarkable advantages and the method of coaxial electrospinning, namely simultaneous electrospinning of two or more different materials into core-shell structured nanofibers, has attracted more and more attention.[3]

In this work, C₂₀ and C₁₄ as PCM were coaxial electrospun as core with PAN as shell into core-shell structured paraffin wax/polyacrylonitrile nanofibers and their thermal properties were studied. Cs₁₂W₃₄O₁₀₈ nanoparticles were incorporated into the nanofibers in order to enhance its solar utilization efficiency.

2 EXPERIMENTAL

2.1 Materials

Polyacrylonitrile (PAN) with molecular weight 1.4×10⁵ used as shell of nanofibers was manufactured by Sinopec Shanghai Petrochemical Co., Ltd., China. paraffin wax eicosane (C₂₀) and tetradecane (C₁₄) used as core of nanofibers with purity of 98% and 99% and phase change temperatures of 5.86°C and 36.8°C respectively were purchased from Aladdin Biochemical Technology Co., Ltd., China.

2.2 Methodology

PAN was washed and dissolved in DMF/ethanol with 12 h stirring by a magnetic stirrer to form homogeneous solutions with concentration 10, 12, and 15%wt. C₂₀ and liquid C₁₄ under room temperature were mixed in ration 1:3, 1:5, and 1:7 as PCM.

The spinneret of the device consists of two stainless steel coaxial needles with outer diameters of 1.49 and 1.01 mm and inner diameters of 0.72 and 0.41 mm, respectively, connected to medical syringes as reservoirs. The aluminum foil wrapped cylinder was placed 15 cm from the coaxial nozzles to effectively collect the nanofibers. Coaxial needles and aluminum foil wrapped cylinder were connected to voltage 13 kV and 1.5 kV and the feeding speed for core and shell materials were 0.1 mL/h and 0.5 mL/h.

Nanofibers were air dried, immersed in petroleum ether for 24 h to dissolve the core materials and their surface morphology and inner structure were observed by JSM-6700F field emission scanning electron microscope (FE-SEM, JEOL, Japan) and JSM-2100 transmission electron microscope (TEM, JEOL, Japan). The phase change temperature and enthalpies of thermo-regulating nanofibers were obtained using differential scanning calorimetry (DSC, TA, USA) at a temperature range of -10 to 40°C with heating and cooling rate of 10°C/min while a nitrogen flux was used as the purge gas for the furnace. Thermogravimetric (TG, PE, USA) analysis of the samples was performed from 40 to 700°C at a heating rate of 10°C/min. The thermographic images of the samples (about 1cm×1cm) were photographed by the infrared imager (FLIR E60) after irradiating by IR lamp

(Philips, Infrared-R95E, wavelength of 780-1400 nm) for 20 s. The distance between the samples and IR lamp kept at 10 cm.

3 RESULT AND DISCUSSION

3.1 Effect of PAN solution concentration

The ratio of C₂₀ to C₁₄ was fixed to 1:5 to observe the effect of concentration of PAN solution. Morphologies of three samples were figured in Fig. 1.

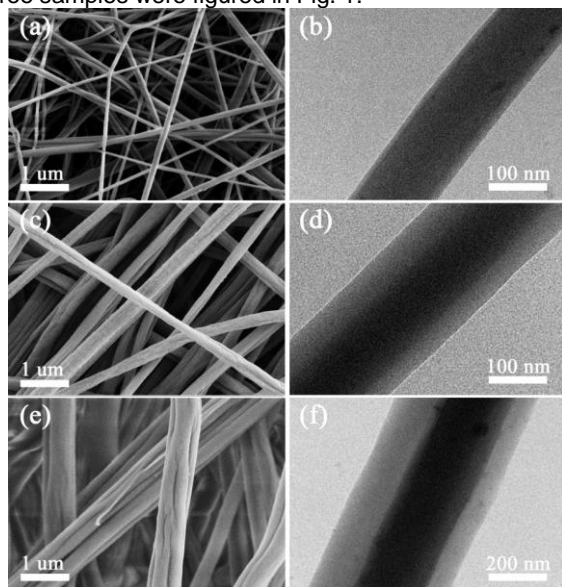


Figure 1 Morphologies of three samples obtained from SEM (a, c, e) and TEM (b, d, f): a, b) PAN10@C₂₀:C₁₄-1:5; c, d) PAN12@C₂₀:C₁₄-1:5; e, f) PAN15@C₂₀:C₁₄-1:5.

SEM pictures in Fig. 1 shows an increase in fiber diameter as the shell solution concentration increased may due to the increasing surface tension which needed to be broken during the fiber formation. Grooves grew with the growing of shell solution concentration may since the core PCM remaining and the thickening of the shell solution. What ought to be noticed is that these three concentrations of PAN solution were all able to form nano scale fibers with good processability.

3.2 Effect of PCM ratio

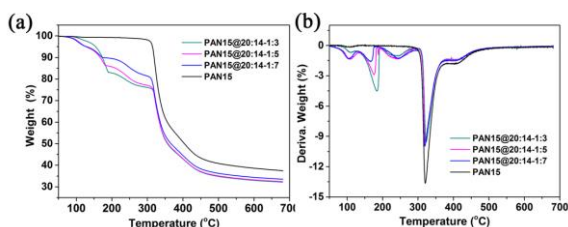


Figure 2 TG (a) and DTG(b) curves of samples with 15% concentration PAN solution.

Fig. 2 shows the thermal behavior of a series samples of PAN15@C₂₀:C₁₄ under high temperature. TG curves show first dropping around 100°C due to evaporation of water and the main decreasing at over 300°C by the decomposition of PAN. The decomposition points of C₁₄ and C₂₀ caused two peaks in DTG graphs at around 170°C and 250°C. Samples were thermally stable at common room temperature which indicates their broad developing prospect in intelligent apparel products.

3.3 Effect of CsWOx

To investigating the effect of Cs₁₂W₃₄O₁₀₈, the infrared imager is applied to detect the temperature change of four Samples based on PAN15@C₂₀:C₁₄-1:5 after irradiating by IR lamp. Fig. 3 shows the thermographic images of the samples with 0, 5, 10 and 15% of Cs₁₂W₃₄O₁₀₈ nanofibers placing on the watch glass. After irradiated by IR lamp for 20s, the PAN15@C₂₀:C₁₄-1:5 sample keeps the same temperature as the environmental temperature. But the temperature of the other three nanofibers are much higher than the ambient temperature. The temperature changes are labeled on the figures, which reveal the outstanding heat absorbing property and photo-thermal conversion effect of the adding of Cs₁₂W₃₄O₁₀₈. Importantly, after 10, 15 and 50 s, the temperature of all the samples declined, but samples with higher Cs₁₂W₃₄O₁₀₈ concentration possess higher temperature.

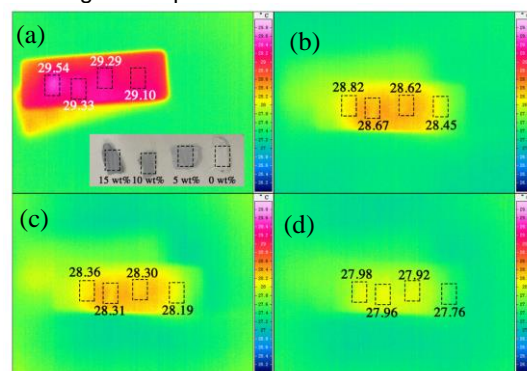


Figure 3 Thermographic images and temperature variations of the four samples with durable radiation time of (a) 1s (b) 10s (c) 15s and (d) 50s. The samples were irradiated by IR lamp for 20 s.

4 CONCLUSION

PAN was chosen as shell material which covered two-component PCM core material to be coaxial electrospun into thermo-regulating nanofibers. Concentration of PAN solution of 15% was found as the optimized concentration. The analysis of C₂₀ / C₁₄ ratio shows higher concentrate of C₂₀ results in higher melting and crystallization enthalpy. Incorporating the Cs₁₂W₃₄O₁₀₈ nanoparticles into the shell of PCM can enhance its thermo-regulating effect.

ACKNOWLEDGEMENT: This work was supported by the project of The Key Program for International S&T Innovation Cooperation Projects of China (Project No.: 2016YFE0131400), the International Industry Joint R&D Program (Project No.: 2019C54003), and the National Natural Science Foundation of China (Project No.: 51803182).

5 REFERENCES

- [1] Bose, P. and V.A. Amirtham, A review on thermal conductivity enhancement of paraffinwax as latent heat energy storage material. Renewable & Sustainable Energy Reviews, 65 (2016): 81-100.
- [2] S. Mondal, Phase change materials for smart textiles – An overview. Applied Thermal Engineering, 28 (2008): 1536–1550.
- [3] Y. Lu, X. Xiao, J. Fu, C. Huan, et al., Novel smart textile with phase change materials encapsulated core-sheath structure fabricated by coaxial electrospinning. Chemical Engineering Journal, 355 (2019): 532-539.

6. Composite and Industrial Textiles

Formability of 3D textile preforms for composite applications

A.K.Dash, Lekhani Tripathi and B.K.Behera

Focus incubation centre for 3D weaving and structural composites

Department of Textile Technology, Indian Institute of Technology Delhi

¹ lekhanitri@gmail.com

Abstract: Formability refers to the adoptability and ability of a preform to attain a desired shape or geometry in the context of composite applications. Forming energy which is obtained from the area of the load deformation curve refers to the ease or difficulty of forming into a shape. Definitely, good formability means as the ability of a preform to reach a shape without any defects such as wrinkles or gaps and to attain a desired fibre orientation. But still, energy required for the forming process by the preforms may be taken as a measuring index to ascertain formability of a specimen to attain near net shape for the composite applications. Hence in this work, eighteen different types of 3D fabrics prepared with E-glass tows (six of different weave designs, six of different stuffer layers, and six of different fibre volume fractions (FVFs) of orthogonal and interlock designs) were developed for the determination of forming energy for attaining a hemispherical shape from a flat specimen. Further, bending rigidity was observed to have very good correlation with forming energy. Also, fabric crossover points were correlated with bending rigidity as well as forming energy. Reasonably, good correlations were obtained in both the cases.

Keywords: Orthogonal , Bending rigidity , Weave Design , Formability .

1 INTRODUCTION

Textile preforms possess superior shaping characteristics as compared with laminates for composite applications . It is the interlacement patterns among warp and weft yarns which primarily bear the responsibility of forming complex shapes without defects. An important step of composite production is the forming of textile preforms in a three dimensional shape and size. Once the desired shape is achieved, it is easier to inject resin for further consolidation. A double-curved shape formation is a critical phase due to in-plane deformations particularly in-plane shear [3]. Most of the literatures are available which are based on the studies with 2D textile reinforcements forming processes . However, 3D fabrics find themselves in huge application due to their superior performance particularly in the application of textile structural composites. Formability refers to the adoptability of a material to attain a shape or geometry. Forming energy refers to ease of formation of a shape. Definitely good formability indicates as the ability of a preform to reach a shape without any defects such as wrinkles or gaps and to attain a desired fibre orientation. But still, energy required for the forming process by the reinforcements may also a decisive factor to attain near net shape for the composite applications. So it can be ascertained that forming energy is one of the criteria to test the ability of a reinforcement to attain a desired shape. Tight or jammed fabric construction may not require same energy to that of loosely woven fabrics to form a shape. Less requirement of forming energy will definitely have an extra edge, as chances of constituent yarn breakage are minimum towards a shape formation. Frank Ko et al defined forming energy as one of the measuring index to determine the ability of a reinforcement to attain a desired shape. Further, they tried to find out one or more dominant

experiments which show the closest relation to the forming energy by considering some different weave designs of 2D textile preforms. In this research, forming behavior of different 3D woven structures are investigated. The correlation between forming energy and bending rigidity of various 3D structures are examined.

2 OBJECTIVES

- (i) To study the load deformation behavior during forming.
- (ii) To compare the energy required to form a shape of different 3D fabrics.
- (iii) To correlate forming energy with bending rigidity.

3 FABRIC PRODUCTION, FABRICATION OF EXPERIMENTAL SET UP AND EVALUATION OF FORMING BEHAVIOR

Hence in this work, eighteen different types of 3D fabrics prepared with E-glass tows (six of different weave designs, six of different stuffer layers, and six of different fibre volume fractions (FVFs) of orthogonal and interlock designs) were developed for the determination of forming energy for attaining a hemispherical shape from a flat specimen. A special attachment was fabricated and mounted on INSTRON 3365 tensile testing machine and the preforms were tested in compression mode upto a fixed deformation level.

4 RESULTS AND DISCUSSION

4.1 Effect of yarn orientation on load displacement characteristics during forming operation

Yarn orientation within the plane of the fabric influences the deformation process during forming. Hence two different yarn orientation was presented for one particular weave (W1), for the comparison purpose as shown in Figure 1 (a) and (b).

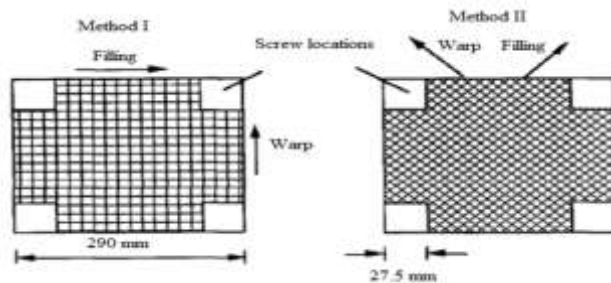


Figure .1 (a)

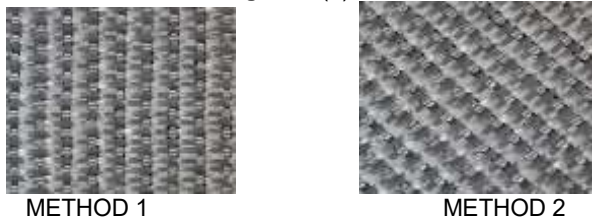


Figure.1 (b)

Figure1 (a) Schematic representation of Method-I and II showing yarn orientation in the sample (b) Actual view of the sample showing yarn orientation in the sample in both the direction

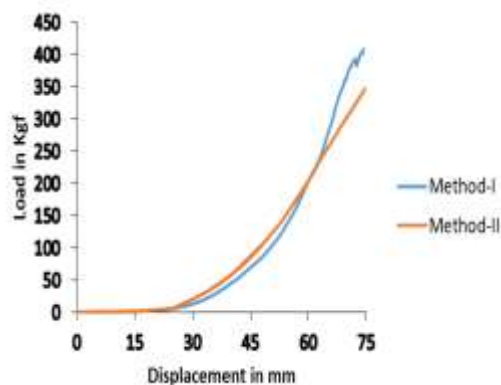


Figure 2 Typical load displacement curve in both the methods for sample W1.

Here the load displacement curve of one sample nearing to averaged test results is presented in Figure 2 for comparison purpose.

4.2 Comparison of load-displacement characteristics during forming operation

1 DIFFERENT WEAVE DESIGN

The load-deformation curves of six different weave designs of samples are plotted in Figure 3.

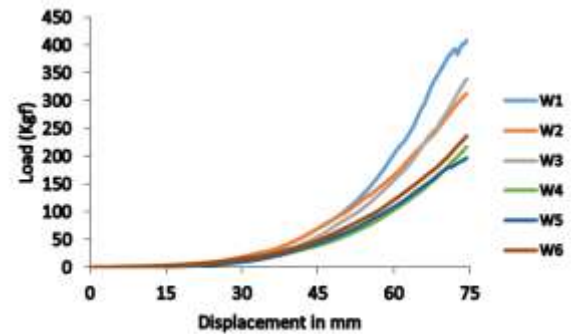


Figure 3 typical load displacement characteristic curves of 3D fabrics of different weave designs up to a defined extension (75mm).

2 DIFFERENT STUFFER LAYERS

The load-deformation curves of three different stuffer layers (2, 4, and 6) of orthogonal, Interlock

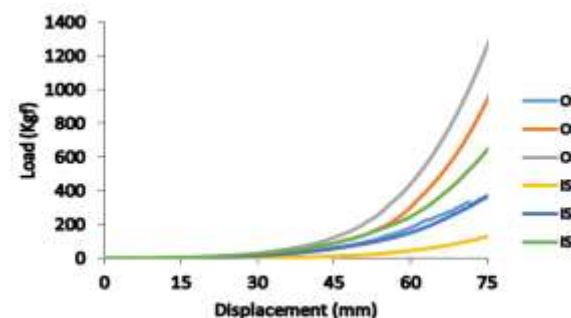


Figure 4 typical load displacement characteristic curves of 3D fabrics of different stuffer layers

In this way experiment is also done for different volume fractions.

Forming energy is associated with the difficulty of a forming process. Normalised forming is also calculated for different weave design, stuffer layers and different volume fractions.

5 CONCLUSION

The forming energy can be used as a measuring index to assess formability characteristics of preforms. In all cases i.e. different weave designs, stuffer layers, and VFVs, the orthogonal structures require more energy than corresponding interlock structures. Regular weave patterns of binder tows, more number of cross over points over a unit area facilitate orthogonal weave designs to consume more forming energy leading to restriction of relative fibre movement and the rearrangement of fibres due to more frictional contact among the tows. Fabric cross over points have a good correlation with fabric bending rigidity but the correlation is not so significant with forming energy.

6 REFERENCES

- [1] A.K. DASH, Ph. D. Thesis, 2019, INDIAN INSTITUTE OF TECHNOLOGY, DELHI.
- [2] SAKTHI VIJAYALAKSHMI A G, M.TECH Thesis, 2018, INDIAN INSTITUTE OF TECHNOLOGY , DELHI.

THE DEVELOPMENT OF THE FOAM CONTAINING PULP FIBER AND THERMOPLASTIC FOAMING AGENT FOR ACOUSTIC ABSORPTION MATERIALS

Mizue KAKEHI¹, Hiroto AKAGI², Hideyuki UEMATSU³ and Shuichi TANOUE⁴

¹ Industrial Technology Center of Fukui Prefecture, Kawaiwashizuka 61, Fukui-City, Fukui 910-0102, Japan, e-mail: m-kakehi@fklab.fukui.fukui.jp

²⁻⁴ Graduate school of Engineering, University of Fukui, Bunkyo, Fukui-City, Fukui 910-8507, Japan, e-mail: hiro.a0302@gmail.com, ³e-mail: uematsu@matse.u-fukui.ac.jp, ⁴e-mail: tanoue@matse.u-fukui.ac.jp

Abstract: Flexible acoustic absorption materials that can be absorbed some noises with extensive frequencies in various usage environments are required in the recent industry. Previously, a laminated glass fiber (glass wool) and the urethane foam based on the polyurethane resin have been used as sound absorption materials. However, the recyclability of glass wool and urethane foam are poor because of mineral and thermosetting resin, respectively. Additionally, it is necessary to combine an another acoustic absorption materials for the glass wool in order to absorb noises with extensive frequencies bands. Therefore, the purpose of our study is to development a novel eco-friendly absorption material which has wider range on acoustic absorption band without including an another sound adsorption materials. We suggest the new porous sound absorption material consist of the pulp fiber and the thermally expandable foaming agent which is composed of the acrylic polymer and liquid hydrocarbon. It is reported that the manufacturing process for pulp foaming based on the papermaking and the relationship between the internal structure and absorption behavior depending on the foaming time.

Keywords: Pulp fiber, foam, rheology, acoustic absorption material, sound absorption coefficient.

1 INTRODUCTION

The Glass wools which are laminated glass fibers and the urethane foam which foamed by polyurethane resin are normally used as porous sound absorption materials. However, it is difficult to control the sound absorption property in broad frequency region with same material system. These samples are also poor recycling efficiency. Therefore, the main purpose of our study is to development a novel eco-friendly absorption material which has wider range on acoustic absorption band without including another sound absorption material. We have investigated the process of creating of a new porous materials consist the pulp fibers and the thermally expandable foaming agent which is composed of the acrylic polymer and liquid hydrocarbons. It is reported that the porous structure in laminated pulp fibers could be created by foaming agent[1][2]. The internal structure strongly depended on the foaming time. Especially, we found that our method of preparing for eco-friendly foam based pulp fibers is useful as absorption materials because of having wider range on acoustic absorption band. However, the effect of the concentration of pulp fibers in sample preparation on the foaming behavior and absorption properties are not clear yet. Therefore, in this study, to clarify the relationship between the dispersion state of pulp fiber in aqueous solution and foaming behavior, rheological properties of pulp aqueous solution and internal structure of foam were investigated. Furthermore, we considered that the effective dispersion state of pulp fibers for the sound absorption performance.

2 EXPERIMENTAL

2.1 Samples

We used Needle Bleached Kraft Pulp (NBKP) as a pulp, a foaming agent designed to core-shell structure was selected. The core and shell components are respectively consisted of a hydrocarbon with low boiling temperature and acrylic polymer with glass transition temperature of about 90 °C. Average diameter of foaming agent was 10~16 µm. After the pulp/water suspensions with pulp content ranged from 0.18 vol% to 0.53 vol%, the foaming agent of 40wt % was added as against pulp fiber. After mixing for pulp fiber and foaming agent in aqueous solution, the pulp/foaming agent was filtrated from aqueous solution by aspirator. The substrates of pulp/foaming agent were foamed at temperature 110 °C on various foaming times in the range from 0 to 35 min.

2.2 Measurements

The dispersion state of pulp fibers in the aqueous solution was examined by measurement of the rheological properties. The samples were blended at pulp concentrations in the range from 0.18vol% to 0.53vol% without the foaming agent, and made into five types of stirred solutions. The viscosity measurement was carried out in the various shear rates ranged from 0.1 s⁻¹ to 100 s⁻¹ with parallel plate of diameter of 50 mm at temperature of 25 °C.

The internal structures of the foams various foaming times were observed by SEM. The normal incident sound absorption coefficient of the foam was measured by an acoustic impedance tube.

3 RESULTS AND DISCUSSION

3.1 Rheological properties of pulp fiber aqueous solutions

The flow curves of pulp fiber aqueous solutions were shown the non-Newtonian behavior independent of the content of pulp fiber. The magnitude of viscosity for pulp fiber aqueous solution rapidly increased above 0.35 vol% of pulp fiber content in the overall range of shear rates. Fig.1 shows the relationship between shear stress (viscosity) at 10 s^{-1} of shear rate and the content of pulp fiber. The slope of shear stress (viscosity) against the content of pulp fiber was 0.74 below 0.35 vol% of pulp fiber content. On the other hand, the shear stress was proportional to the fiber concentration to 3.95 above 0.35 vol% of pulp fiber content. In the past reports [3], the slope of the shear stress (viscosity) against the content of pulp fiber was about 4 above a critical concentration which is related to the size of pulp fiber. The phenomenon was also related to a interaction of pulp fibers in aqueous solution. In other words, it is implied that the agglomerations of pulp fiber develops above 0.35 vol% of pulp fiber content in the aqueous solution.

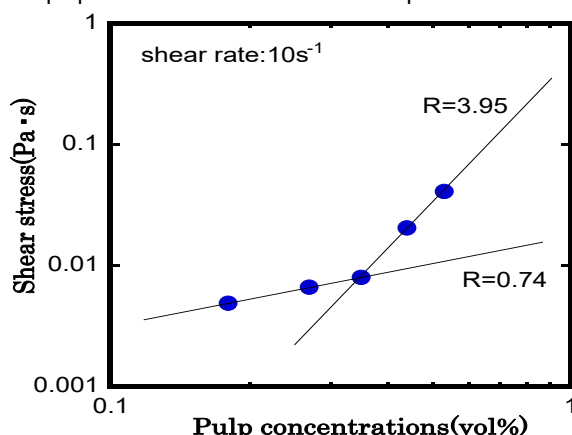


Figure 1 Dependence of shear stress on the pulp concentrations, at shear rate 10 s^{-1} .

3.2 Relationship between fiber concentration and internal structure of foam

Fig.2 shows the SEM photographs of foams (pulp fiber/foaming agent) at two kinds of fiber concentrations, Fig.2(a) and Fig.2(b) are respectively 0.18vol% and 0.53vol%, at 15 minutes of foaming time. The swelled spherical shape of foaming agent and non-spherical shape of foaming agent, which is attributed to shrink after swelling were shown in the two kind of foams. However, in Fig.2(a), the pulp fiber was individually located in the Fig.2 (a) as compared with the state of pulp fiber in the Fig.2 (b). In other words, the agglomeration of pulp fibers was shown in the Fig.2 (b).

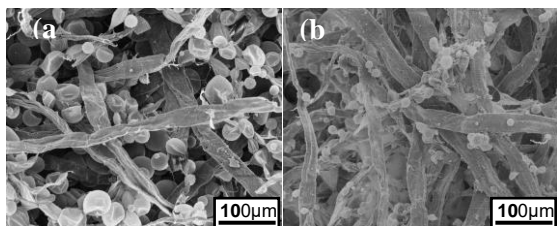


Figure 2 SEM photos of pulp fiber foam at pulp concentrations of (a)0.18vol% and (b)0.53vol%, foaming time 15min.

3.3 Acoustic absorption characteristics

Fig.3 shows the sound absorption characteristics of three kinds of foams with different fiber concentrations (0.18vol%, 0.35vol%, 0.53vol%) with foaming time of 10 minutes. The sample of non-foaming isn't included the foaming agent as a reference sample. In each sample, the sound absorption coefficient was high above 2000 Hz. Especially, the sound absorption coefficient improved in the pulp fiber containing the foaming agent. It is interesting to note that the frequency band of sound absorption coefficient shifted to the lower frequency band with increase of the content of pulp fiber. We consider an agglomerate of fibers in the foam to be effective to the acoustic absorption in the low frequency region. Therefore, it is concluded that fiber concentration is an important factor for control the acoustic absorption property.

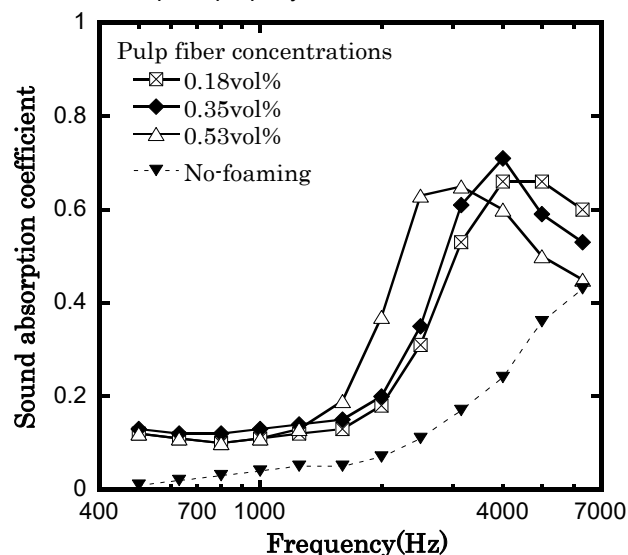


Figure 3 Sound absorption coefficient for different internal structures of pulp fiber foam, foaming time 15min.

4 CONCLUSIONS

- The sound absorption band would be controlled with pulp fiber concentrations in aqueous solution.

5 REFERENCES

- [1] Mizue Kakehi, et al.:Acousitc properties and internal structure of foam containing pulp and foaming agent composed of acrylic polymer/liquid hydrocarbon, *Extended Abstract of 45th Textile Research Symposium*,pp.53(2017)(Jpn).
- [2] Mizue Kakehi, et al.:The development of the foam containing pulp and foaming agent composed of acrylic polymer/liquid hydrocarbon for acoustic absorption materials, *Journal of Textile Eng.,Japan*,Vol.64,5,pp.111-116(2018) (Jpn).
- [3] Daisuke Tatsumi, et al.:Rheology of Cellulose Fiber Disperse Systems and Cellulose Solutions, *Journal of the Society of Rheology,Japan*, Vol.35,5,pp.251-256(2007) (Jpn).

UPCYCLING TEXTILE WASTE INTO FIBRE REINFORCED COMPOSITES

Zunjarrao Kamble¹, B K Behera¹, Teruo Kimura², Ino Haruhiro²

¹ Department of Textile Technology, Indian Institute of Technology Delhi, Hauz Khas, New Delhi-110016, India.
e-mail: ttz178482@textile.iitd.ac.in.

² Department of Advanced Fibro Science, Kyoto Institute of Technology, Matsugasaki Hashikamicho, Sakyo Ward, Kyoto, Kyoto Prefecture 606-8585, Japan.
e-mail: tkimura426@gmail.com.

Abstract: The linear way of operating textile system has laid world to face the serious issue of sustainable textile waste management. Textile waste is challenging today's world in terms its sustainable disposal and recycling of waste textiles became very important. It has been anticipated that total fashion waste in 2030 will be 148 million tons which would be equivalent to annual waste of 17.5 kg per capita across the planet. Also, more than 150 million tonnes of clothing would be landfilled or burned in 2050. The present research is an approach to recycle the textile waste generated in the textile industry for thermoset composites manufacturing. The textile waste fabrics obtained from the textile industry were converted into the shoddy fibre form using the rag-tearing machine. The fibrous web was produced using a carding machine. The thermoset composites reinforced with fibres recovered from textile waste were produced varying fibre volume fraction using compression moulding. The composite specimens were characterized for static and dynamic mechanical properties. It has been observed that mechanical properties of the composites changes with fibre volume fraction. The effect of water absorption on mechanical properties of the composites was also studied.

Keywords: Upcycling, Textile waste, Mechanical properties, thermoset composites

1 INTRODUCTION

Textiles are the second most important thing for a human being to live and be protected from different weather conditions. However with increasing population, the need of textiles is also increased and correspondingly textile waste. Textile wastes are broadly classified as pre-consumer waste, post-industrial waste and post-consumer waste. The pre-consumer wastes are generated during textile manufacturing, post-industrial wastes are generated during garment manufacturing. The post-consumer wastes are those who have served their useful life.

The studies have already reported recycling of textile waste for thermoset and thermoplastic composites. The composites developed from textile wastes can be used for as replacement of wood, insulation materials etc. The present research is aimed at development of composites reinforced with fibres recovered from pre-consumer textile waste for applications such as furniture, low load bearing automotive components etc.

2 MATERIALS AND METHODS

2.1 Materials

The reinforcement materials were obtained by garneting the pre-consumer textile waste made of 100% cotton fibres. The Z1 epoxy resin was used as thermoset matrix material along with its curing agent 20.

2.2 Methods

The pre-consumer textile waste was garneted to recover the fibres and then the fibres were carded to produce web. The carded web was used as reinforcement material and composite specimens were developed varying fibres

volume fraction (0.1 to 0.4) using compression moulding technique. The composite specimens were characterized for tensile, flexural and notched izod impact strength according to ASTM standards. The composite specimens were also characterized for thermogravimetric and dynamic mechanical properties. The water absorption tests on composites were performed using ASTM D7264. The fractured surfaces of tensile and impact tested specimens were analyzed using scanning electron microscope.

3 RESULTS AND DISCUSSION

3.1 Effect of carding speed on tensile strength of composite

The composite specimens with 0.2 fibre volume fraction were developed by reinforcing it with carded web produced with four different cylinder speeds namely 100, 150, 200 and 250 rpm. It has been observed that with increase in cylinder speed from 100 to 250rpm there is no significant change in maximum tensile stress of the composites in the machine direction.

3.2 Effect of fibre volume fraction on mechanical properties of green composites

It has been observed that the maximum tensile stress increases as fibre volume fraction increases from 0.1 to 0.3 and it was observed to decrease at 0.4 fibre volume fraction. The Young's modulus of the composite increases with observed to increase with increase in fibre volume fraction. The load elongation curves of the composite specimens are shown in figure 1. The maximum flexural

stress and izod impact strength of the composite specimen was also increased with increase in fibre volume fraction from 0.1 to 0.4.

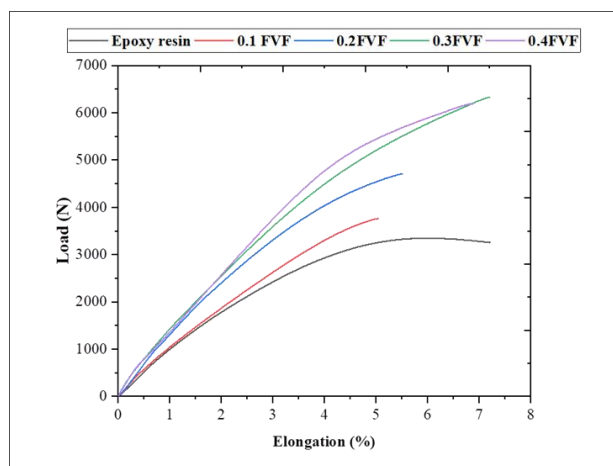


Figure 1 Load-elongation curves of composites with different fibre volume fraction.

3.3 Thermogravimetric analysis

The thermogravimetric analysis of the composite specimens is shown in figure 2.

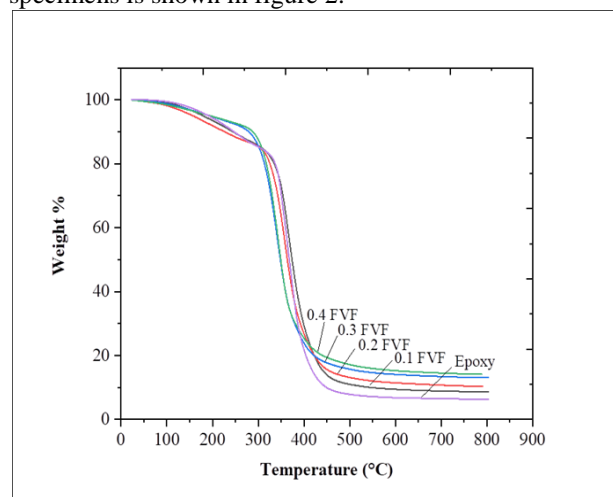


Figure 2 Thermogravimetric curves of the composite specimens.

3.4 Dynamic mechanical analysis

It has been observed that the storage modulus increases with increase in fibre volume fraction of the composite. The composites developed in the present research can be safely used between room temperature to 50°C.

3.5 Water absorption test

It has been observed that amount of water absorbed by the composite decreases with time. It has been observed that with increase in fibre volume fraction the moisture absorbed was also increased. The maximum amount of water absorbed was 8.34% for composite with 0.4 fibre volume fraction.

It has been observed that the wet flexural and notched - izod impact strength increases with fibre volume fraction. However, the wet flexural strength was lower than corresponding dry strength and wet notched izod impact strength was higher than corresponding dry strength.

4 CONCLUSIONS

The present research shows that fibres recovered from textile waste can be successfully employed to produce composite materials. The composites developed in the present research shows good thermal and mechanical properties. The tensile, flexural and izod impact strength of the composites increases with increase in fibre volume fraction. The composites with 0.4 fibre volume fraction shows higher storage modulus also it has been found that these composites can be safely used between room temperature and 50°C. The maximum water absorption of the water immersed composite with 0.4 FVF was 8.34% on seventh day.

Acknowledgement: The author would like to acknowledge Prof. Teruo Kimura, Prof. Ino Haruhiru and Kyoto Institute of Technology, Japan for helping and providing facilities for conducting the experiments.

5 REFERENCES

- [1] H. Alamri, I.M. Low, Mechanical properties and water absorption behaviour of recycled cellulose fibre reinforced epoxy composites, *Polym. Test.* 31 (2012) 620–628.
- [2] W.F. Zonatti, B. Maria, G. Guimarães, W. Duleba, J.B. Ramos, Thermoset composites reinforced with recycled cotton textile residues, *Textiles and Clothing Sustainability* (2015) 1–12.
- [3] T.G. Sadikoglu, C. Shikim, C.G. Guleryuz, B. Eryurek, Usage of polyester textile wastes in composites, *J. Sci. Ind. Res. (India)*. 62 (2003) 462–467.
- [4] Umar, Muhammad, et al. "Investigating the mechanical behavior of composites made from textile industry waste." *The Journal of The Textile Institute* 108.5 (2017): 835-839.
- [5] Kotliar, Abraham M. "Woodlike properties from carpet and textile fibrous waste: mitigating the coming landfill crisis." *Polymer-Plastics Technology and Engineering* 38.3 (1999): 513-531.

DESIGN, DEVELOPMENT AND CHARACTERIZATION OF 3D WOVEN STRUCTURE REINFORCED COMPOSITE LEAF SPRING

Vikas Khatkar, B K Behera

Focus incubation center for 3D weaving and structural composites,

Department of Textile Technology, Indian Institute of Technology Delhi

e-mail: vikas.khatkar@textile.iitd.ac.in e-mail: behera@textile.iitd.ac.in

Abstract: This research presents development of composite leaf springs and their primary performance investigation. Influence of various reinforcement architecture on the leaf spring performance were analyzed. E - Glass based three dimensional (3D) orthogonal woven fabric reinforced epoxy were considered for development of composite leaf spring and compared with Chopped fiber, unidirectional tows (UD), bidirectional (2D) counterparts. Developed composite leaf springs performance were analyzed for its tensile strength, load deflection behavior, energy absorption, and relaxation behavior. Overall the performance 3D woven based composite leaf spring were found better compared to chopped, UD and 2D counterparts.

Keywords: 3D woven structure, Composite leaf spring, Mechanical Performance

1 INTRODUCTION

Automotive emission is the major contributor to the environmental pollution, considering the severity of the issue govt. bodies came up with strict regulations in transportation sectors. Automotive industries are now searching for alternative materials that could be a potential replacement for conventional materials used in automobile, metallic alloys. Apart from lightweight metallic alloys and multi materials design option, fiber reinforced hybrid composite structures provides a feasible solution for lightweight vehicle due to high strength to weight ratio [1]. However, anisotropy of fiber reinforced polymer (FRP) is always a challenge because many complications associated with design and manufacturing of composite. Decrease in vehicle weight helps in improving fuel efficiency of vehicle, reduction of 10 % vehicle weight can improve fuel efficiency up to 6 to 7% [2]. Fiber reinforced composite is being used in automobile sector for various semi structural (Non load bearing) component since last two decades. However there is no significant changeover noticed from semi structural component to structural component (load bearing) in automotive industry. Leaf spring is one of the structural element of automobile and consist of 10 -15% of the unsprung weight (weight of chassis, suspension system etc.) of the vehicle. It is evident from several basic research that fiber architecture can contribute as high as up to 90% of the total load bearing capacity, if its geometry is properly designed and preserved. In order to analyses this fact, in this work attempt was made to fabricate composites leaf spring by reinforcing various basic textile structures starting with simple cut staple E-glass fiber dispersed epoxy resin system to complex 3D woven structure reinforced composite. Leaf spring are examined for their mechanical behavior under various loading conditions to check its suitability for leaf spring application.

multi-beam sample weaving machine. The same tow was cut into staples of 10 mm for chopped fiber. Epoxy LY556 were used as matrix material as leaf spring is a load bearing element in automobile, so it becomes necessary to choose a strong matrix material. For complex structure like leaf spring epoxy can be suitable due to presence of creep stresses in leaf spring.

2.2 Methods

All the composite leaf spring were prepared using Vacuum assisted resin infusion molding (VARIM). Fig. 1 shows the VARIM setup and developed composite leaf spring. Leaf spring is available in various profiles and sizes, but the most common profile is semi elliptic, in this study a semielliptical composite leaf spring of constant width and thickness were developed. Leaf spring dimension 500 mm x 65 mm x 6.5 mm were chosen. Length and thickness of composite leaf spring were restrained due to space constraint between the columns of the existing universal testing and weaving constraints for production of 3D woven fabric.

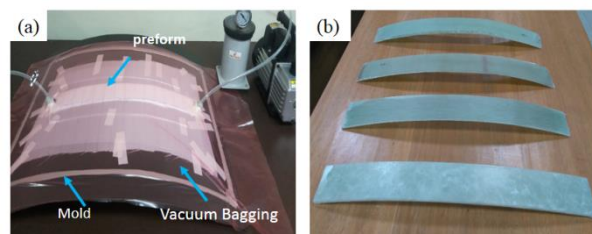


Figure. 1 Development of composite leaf spring (a) VARIM setup (b) composite leaf spring

2 MATERIAL AND METHODS

2.1 Materials

E- Glass tows (supplied by Owens Corning, India) were used to prepare the textile fiber architecture. UD, 2D and 3D woven structures were produced using a rigid rapier

3 CHARACTERISATION

3.1 Tensile properties

Tensile test were conducted in accordance with ASTM D 3039 on universal testing machine (INSTRON 5982). Strain rate were kept 1 mm/min. Average of five test were

recorded. Load deflection behavior, Hysteresis damping and relaxation behavior were investigated in accordance with standard SAE J 1528

3.2 Load deflection behaviour

Load deflection behavior of composite leaf springs were determined in accordance with standard SAE J 1528 using in house fabricated test fixture (as shown in Figure. 2) integrated with INSTRON 5982 universal tensile tester of capacity 100 KN.



Figure. 2 Leaf spring test fixture

3.3 Relaxation Behaviour

Relaxation characteristics of composite leaf springs were determined in accordance with standard SAE J 1528. Leaf spring were strained at a rate of 2.4 mm/s up to a constant deflection of 12 mm and kept at same deflection for 14400 s to record the relaxation behavior. Load drop for a constant period of 14400 sec were recorded to measure the relaxation properties of various composite leaf spring.

4 RESULTS AND DISCUSSION

4.1 Tensile properties

Table 1 summarizes the results obtained from tensile test. The UD composite gives highest tensile strength and chopped composite is the weakest one. Strength of 2D and 3D reinforced materials remains between these two in the order of disposition of volume fraction in their respective direction. Typical stress strain curve obtained from tensile test is shown in figure 3.

4.2 Energy absorption behaviour

From the test results spring stiffness of 3D reinforced composite leaf spring were found highest with a value of 17.25 N/mm and approximately 63%, 6% and 14% higher compared to chopped, UD, and 2D respectively. Spring stiffness of 3D were about 2.5 times of chopped leaf spring and comparable to UD and 2D with a difference of 10 – 15%. The high spring stiffness of 3D were attributed due to presence of through thickness reinforcement.

Table 1 Tensile properties of composites

Material	Tensile strength (MPa)	Young's Modulus (GPa)
Chopped	56.11 ± .85	5.49 ± 0.2
UD	455.90 ± 1.6	6.85 ± 0.15
2D WP (Warp)	321.1 ± 1.25	4.47 ± 0.31
2D WF (Weft)	313.79 ± 2.2	3.84 ± 0.24
3D WP (Warp)	236.04 ± 3.1	3.36 ± 0.27
3D WF (Weft)	358.20 ± 1.3	4.84 ± .30

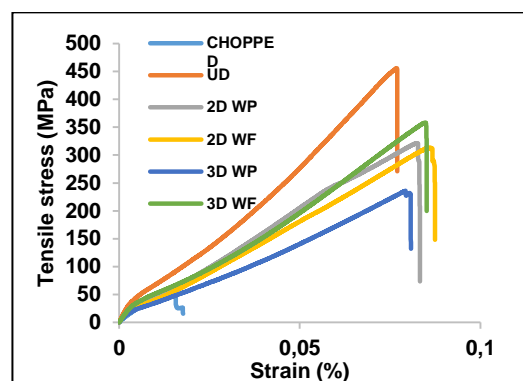


Figure 3 Typical stress strain curve

4.3 Load relaxation characteristics

Load at total relaxation were found 55.81, 17.62, 24.70 and 28.64 N for chopped, UD, 2D and 3D respectively. From the results it was observed that reinforcement fiber architecture has a direct impact on relaxation behavior. Chopped fiber leaf spring depicted highest load at total relaxation this could be due to presence of more number of fiber ends. UD found with lowest load at total relaxation as all the fibers are present in one direction. Similarly in 2D and 3D it was higher than UD due to fiber present in two and three direction respectively. From the results it was observation that load at total relaxation was reduced with the reduction of fibers from multidirectional to unidirectional.

5 CONCLUSION

From experimental investigation it was clear that performance of 3D woven based composite leaf spring were found better in terms of energy absorption and relaxation behavior compared to all other reinforced leaf spring of comparable volume fraction. However further investigation of properties like damping, fatigue, friction and wear behavior and fabrication potential of 3D woven reinforced composite leaf spring material needs to be carried out to check its suitability for automotive leaf spring.

6 REFERENCES

1. Pervaiz M, Panthapulakkal S, Birat K. C, Sain M, & Tjong J.: Emerging trends in automotive lightweighting through novel composite materials. Mater. Sci. Appl. 7(01), 26 (2016)
2. Cheah L. W.: Cars on a diet: the material and energy impacts of passenger vehicle weight reduction in the US. Doctoral dissertation, Massachusetts Institute of Technology (2010)

BENDING PROPERTIES OF BRIDED CFRP WITH SHELL - BULKHEAD PREFORM

Toshiyasu Kinari¹, Takuru Suehiro², Eiki Sakanishi² and Lina Wakako¹

¹ Institute of Science and Engineering, Kanazawa University, Kanazawa, Japan: kinari@se.kanazawa-u.ac.jp

² Graduate School of Natural Science and Technology, Kanazawa University: sakanishieiki828@stu.kanazawa-u.ac.jp

Abstract: Carbon fiber reinforced plastics (CFRP) is drawing attention as high strength, high modulus and lightweight materials. Determination of the mechanical properties of a composite structure is essential to be applied in accordance with its requirements. One feature of braided structure is the continuity of the fiber with diagonal orientation. Another feature is the ability to tailor the braiding angles and the neutral yarn those are not controlled by isotropic materials those have the same strength and stiffness in all directions. With these advantages, the braided structure has a flexibility to design so that various complex structures can be designed to fulfill certain requirements. In this report, we tried to braid several kinds of shell-bulkhead preforms as monolithic structures by using a multi-braider that could freely design yarn paths. After CFRP is formed by Vacuum Assisted Resin Transfer Molding (VaRTM) technique, these samples were tested with three-point bending tests. Experimental results are discussed related to yarn paths employed on the multi-braider.

Keywords: carbon fiber reinforced plastics, bending properties, shell-bulkhead braided preform

1 INTRODUCTION

Braiding technology is suitable in order to produce many kinds of three-dimensional carbon fiber preform on a mandrel [1, 2]. At the same time, braiding technology is a method suitable for agile development. Compared with a conventional hand layup technology such as textile, unidirectional prepreg or woven fabric, in braiding preparation you simply re-wind the yarn on bobbins. The structure is braided directly on the mandrel. After producing the preform, it is molded by resin transfer molding process to make machine parts CFRP. The preform is formed into the same shape of the mandrel as a monolithic structure. Therefore, curved or cross-sectional complex formed preforms, based on biological forms, can be easily made [3]. The modulus and strength of CFRP can be controlled by the braiding angle or the insertion of core threads. So the mechanical properties of CFRP can be variously designed according to the requirements [4]. In this report, we tried to braid several kinds of shell-bulkhead preforms as monolithic structures by using a multi-braider that could freely design yarn paths. After CFRP is formed by Vacuum Assisted Resin Transfer Molding (VaRTM) technique, these samples were tested with three-point bending tests. Experimental results are discussed related to yarn paths employed on the multi-braider.

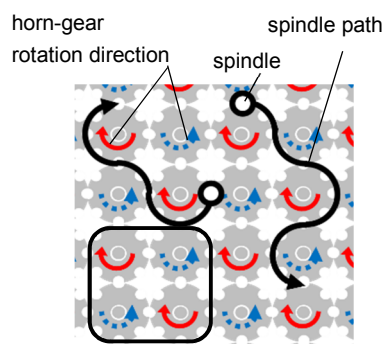


Figure 1 Multi-braider

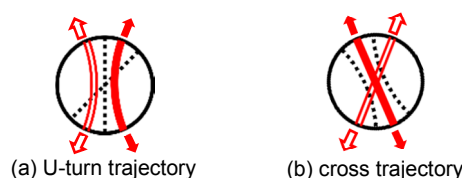


Figure 2 Switching device

2 MULTI-BRAIDER

Multi-braider enables the braiding of various preforms those have complex cross sections [5]. We use the 10×8 horn gear multi-braider (Kokubun LTD: 10×8 HMLT), whose 80 horn gears are disposed on a plane as shown in Figure 1. Driving power of each horn gear is transmitted by cutout blades. All spindle tracks created by horn gears can be setup variously by their switching devices those generate an U-turn trajectory or a cross trajectory as shown in Figure 2. Spindles can move tracks flexibly by switching devices of spindle tracks as shown in Figure 3. A 7- axes robot arm (NACHI: MR20L) is used for mandrel drawing.

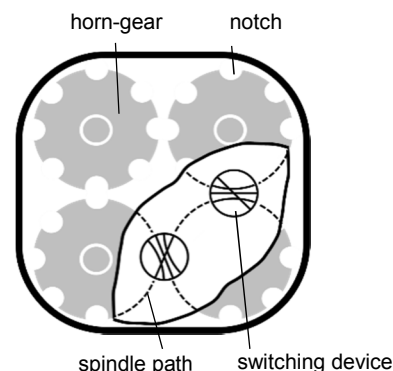
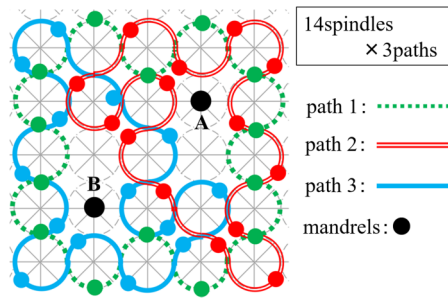


Figure 3 Details of multi-braider



(a) Locus chart of spindles



(b) Sectional view of preform

Figure 4 Shell + I shaped bulkhead preform

3 PREPARING THE SPECIMEN

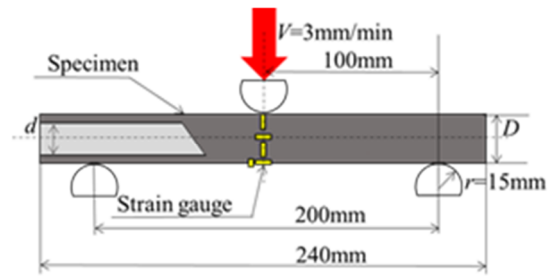
Using a multi braider, the first trial manufacture of “shell + I-shaped bulkhead” structure by continuous PAN carbon fiber yarn (Toray Torayca T700SC 12K) preform was carried out. Spindle tracks are shown in Figure 4 (a). Using switching devices, the clock wise revolution of spindles on a path 1 and the counter clock wise revolution of spindles on a path 2 make a braided structure on the mandrel A.

Table 1 Details of specimen

Braiding structure			N_f	D [mm]	d [mm]	mass [g]	V_f [%]	Z [mm ³]	S
①	Shell and bulk-head	I	7	27.4	24.6	39.0	37.2	565 747	⊖ ⊖
②			22	27.6	25.3	37.4	41.8	570 796	⊖ ⊖
③			18	28.4	25.7	52.0	32.6	550 897	⊖ ⊖
④			22	27.2	25.1	39.0	43.8	517 810	⊖ ⊖
⑤		X	24	28.9	26.3	56.3	30.2	908	⊕
⑥			40	29.0	26.8	64.7	35.4	836	
⑦		I	32	28.1	26.0	52.3	41.7	648 745	⊖ ⊖
				28.5	26.2	52.7	33.2	836	⊕
⑧		X	28	28.8	26.2	55.9	31.5	919	
⑨		I	32	28.4	26.6	48.0	46.0	548 708	⊖ ⊖
	X	28.5		26.1	56.4	31.9	846	⊕	
⑩	Simple stacking			27.1	24.8	28.9	52.5	529	○

N_f : number of yarn bobbins in bulkhead section

S: cross sectional shape

**Figure 5** Schematic of 3 point bending test

On the other hand, the clock wise revolution of spindles on a path 1 and the counter clock wise revolution of spindles on a path 3 make a braided structure on the mandrel B. Spindles on path 2 and 3 cross each other at the midsection, which makes the braided structure that is corresponding to a bulkhead. These processes make it enable to braid a shell + I-shaped bulkhead preform as a monolithic structure by PAN carbon fiber yarn. Each path carries 14 spindles which revolve at regular intervals. The cross sectional shape of preform depends on that of mandrel, so a couple of mandrels with a semicircular section can make a circular cylindrical shell as shown Figure 4 (b).

4 BENDING TEST

After braiding process, CFRP is formed by Vacuum Assisted Resin Transfer Molding (VaRTM) technique. Epoxy resin (Axson Epolam 230 resin/Axson Epolam 230 hardener = 100/26 wt.%) was used as matrix. Then, the specimens listed in Table 1 were tested with three-point bending tests. Using Universal/Tensile Testing Machine (Shimadzu AGX), bending tests were performed as shown in Figure 5. The distance between the fulcrums was 200mm and its center was pushed down at a constant rate 3mm/min. Semi-round bar lacking its top is used for both fulcrums and an indenter.

ACKNOWLEDGEMENT: Several aspects of this work were financially supported by Innovative Design/Manufacturing Technologies, Strategic Innovation Promotion Program (SIP) in Japan. Now, this work is supported by JSPS KAKENHI Grant Number JP18K03869.

5 REFERENCES

- [1] Hamada H., Nakai A., “Fabrication and Mechanical Properties of Braided Composites”, SEN’I GAKKAISHI, 52, 1996, pp. 469 – 474 (in Japanese).
- [2] Tada M., Uozumi T., Nakai A., Hamada H., “Structure and machine braiding procedure of coupled square braids with various cross sections”, Applied Science and Manufacturing, 32, 2001, pp. 1485-1489.
- [3] Kinari T., Sakamoto J., Kitayama S., et al.: Bio-innovative Design Technology and Manufacturing System for CFRP Preform by Braiding Structure, Proceedings of International Symposium on Flexible Automation, 2018, Paper No. L88.
- [4] Endriatno N., Kawai K., Kinari T., et al.: Experimental Study on Hoop Stress Affecting Braided Carbon Fiber Reinforced Plastics Subjected to Internal Pressure. *Journal of Textile*, 2019, pp. 11-17.
- [5] Kinari T., Endriatno N., Suehiro T.: Bending properties of CFRP with braided structure. Abstracts of 46th Textile Research Symposium, 2018, pp. 15.

PROPERTIES AND STRUCTURE OF SPUN YARNS IN RELATION TO THE SPINNING AND WEAVING TECHNOLOGIES

Brigita Kolčavová Sirková¹, Iva Mertová¹ and Eva Moučková¹

¹ Technical University of Liberec. Faculty of Textile Engineering. Department of Technologies and Structures. Liberec. The Czech Republic. Studentská 2. 461 17. e-mail: brigita.kolcavova@tul.cz

Abstract: This paper is focused on description of the structure and selected yarn spun properties for possible evaluation of the yarn process-ability during weaving. Parameters of construction of woven fabric and setting of individual parts of the weaving machine are given by definition of structure and properties input yarns. Today, three spinning methods are widely used for manufacturing staple spun yarn of medium to fine count from man-made fibres: the ring spinning, the rotor spinning and air-jet spinning. Research work is focused on the analyses of the structure and properties of 100% Tencel ring, rotor and Rieter Air-jet spun yarns in term of their utilization in the woven fabric.

Keywords: woven fabric. air-jet spun yarn. rotor spun yarn. ring spun yarn. properties

1 INTRODUCTION

Woven fabric structure, balance of variable forces during weaving, deformation of binding cells in woven fabric, fabric densities, stability of the weaving etc. can be deduced from description of input yarns and mutual relations between tension and geometrical changes of the binding cell [1]. The structure of input yarns as well as yarn properties are given by the technology of yarn production. Spun yarns are possible to produce using three main spinning methods [2]. The first, the ring spinning system, the drawn fibrous strand is twisted due to rotation of spindle thanks to traveller circling around spindle [3]. The second, the rotor spinning method is characterized by the combing-out individual fibres from the input sliver, their collection into fine strand in the rotor groove and twisting-in fibres to the rotating open end of yarn made before. The third, the air-jet spinning uses the sliver, which is drawn in a drafting device. Attenuated thin fibres strand is transformed into the yarn by means of vortex air in the nozzle housing. Swirling air current separates trailing ends of surface fibres and twist them to the yarn body [4], [5].

2 FORCES IN WOVEN FABRIC

The whole process of weaving is the process of creation of binding points. Their dimensions and the tensions gradually change from the cloth fell in the forming zone as far as some place of the steady state inside of fabric Figure 1. The structure of the formed fabric is determined by the quantity of weft, tension which is formed in weft during insertion, and the tension of warp [1].

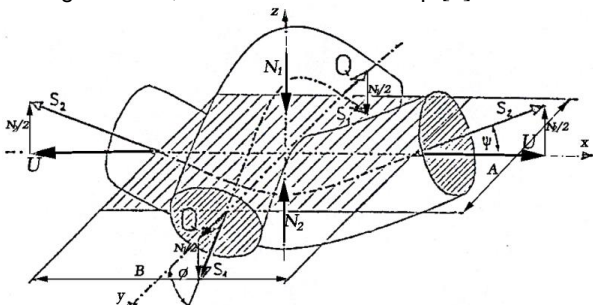


Figure 1 Geometrical and forces ratio in interlacing of threads

3 EXPERIMENTAL ANALYSES OF YARNS

For the experimental part of work was used 100% Tencel yarns of nominal count 23 tex spun by three different spinning technologies (air-jet, ring, and rotor). All yarns were spun from the same sliver of count 4.6 ktex, which were 3 times drawn (condition for air-jet spinning). The roving of count 670 tex were produced before spinning of the ring yarn. Main characteristics of tencel fibers was: fineness 1.3dtex, cut length 38 mm, tenacity 39.25 ± 1.17 cN/tex, breaking elongation: 10.53 ± 0.46 %. Twist of ring spinning yarn Yarn twist: 768 m^{-1} , nominal yarn twist: 870 m^{-1} of rotor spinning machine. Main technological conditions of yarns spinning are mentioned in full text. Longitudinal views on the yarns as well as yarn cross-sections are presented in Figure 2.

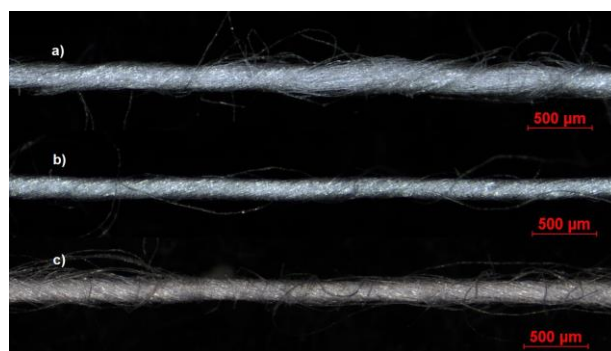


Figure 2 Longitudinal view on yarn and cross-section of yarn - a) Air-jet spun yarn, b) Ring spun yarn, c) Rotor spun yarn

Mechanical properties and basic parameters of yarns were selected for evaluation of the yarn process-ability during weaving. Measurement conditions (tenacity, breaking elongation): 0.5 m clamping length, cross-beam speed 500 mm/min, pre-tension 0.5 cN/tex. The results you can see in Figure 3-4. Yarn mass irregularity CV_m , yarn diameter $2D$, variation of yarn diameter CV_{2D} 0.3 mm, and yarn hairiness H was tested using Uster-Tester IV-SX at speed $400 \text{ m} \cdot \text{min}^{-1}$ for 1 min. Because number of

usually evaluated yarn faults (thin places (-50 %), thick places (+50 %), and neps (+200 %, or +280 %) was very low, we observed thin places (-40 %), thick places (+35 %), and neps (+140 %).

For completion yarn characteristics, the yarn hairiness S12 and S3 was tested using Zweigle hairiness tester.

The summary criterion S12 expresses number of hairs in length category 1mm and 2 mm. The category S3 indicates the total number of protruding fiber ends which are as long as 3 mm. In both cases relative to yarn length of 100 m. The results (average values and 95% confidence limits of mean value) are presented in Table 1.

Table 1 Selected yarn properties

Yarn	T [tex]	CVm [%]	Thin places -40% [1/km]	Thick places +35% [1/km]	Neps +140% [1/km]	2D [mm]	CV2D 0.3mm [%]	H	S12 [1/100m]	S3 [1/100m]
Air-jet spun	23.19 (23 - 23.38)	10.51 (10.45 - 10.57)	8 (6 - 10)	37 (33 - 41)	66 (50 - 83)	0.231 (0.231 - 0.232)	10.67 (10.63 - 10.71)	4.15 (4.11 - 4.18)	1095.00 (1066 - 1124)	2.55 (1.85 - 3.25)
Ring spun	22.93 (22.77 - 23.08)	11.17 (10.18 - 12.16)	5 (3 - 7)	92 (61 - 123)	70.00 (57 - 83)	0.215 (0.213 - 0.217)	11.88 (11.03 - 12.73)	6.22 (5.74 - 6.69)	14004.00 (13383 - 14625)	1415.00 (1319 - 1512)
Rotor spun	22.36 (22.05 - 22.67)	13.51 (13.30 - 13.72)	139 (118 - 160)	304 (277 - 331)	638.00 (537 - 738)	0.248 (0.247 - 0.249)	12.95 (12.70 - 13.19)	5.12 (5.08 - 5.16)	1257.00 (1191 - 1324)	411.00 (318 - 504)

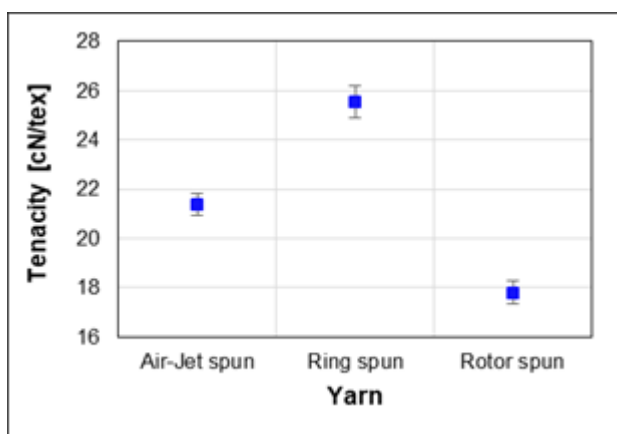


Figure 3 Presentation of yarn tenacity (presentation of breaking elongation in full text).

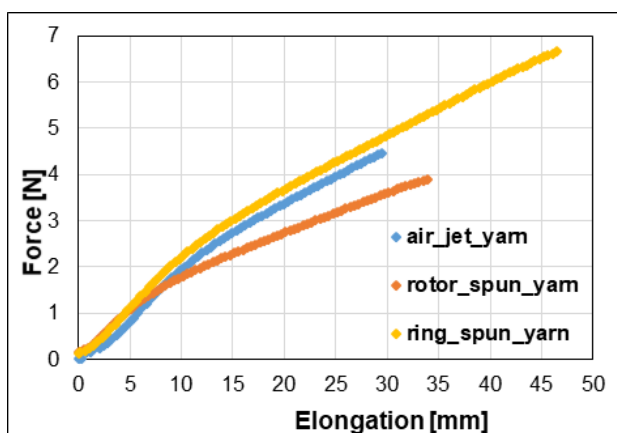


Figure 5 Presentation of stress-strain curve of spun yarns

4 RESULTS

The results confirmed the known fact that the ring spun yarn has the highest tenacity and breaking elongation due

to fibers arranged in parallel before twisting, whereas these characteristics are the lowest in the case of the rotor spun yarn. Mass irregularity of air-jet spun yarn as well as thin places (-40%), thick places (+35%) and neps (+140%) was, in term of statistics, the same as in the case of ring spun yarn. Wider 95% confidence limit of mean values of CVm and observed faults of ring spun yarn is given by setting of drafting device of the flyer frame and the ring spinning machine. Mass irregularity of rotor spun yarn was higher compare to ring and air-jet spun yarns. The same trend was observed in the case of optical unevenness CV2D 0.3mm. The spinning technology and arrangement of fibers in the yarn caused that ring spun yarn showed the lowest yarn diameter, and highest hairiness indexes H, S12 and S3, whereas the highest diameter was recorded in the case of rotor spun yarn, and lowest hairiness had the air-jet spun yarn.

ACKNOWLEDGEMENT: Authors would like to thanks for support to student grant competition (SGS-21303) by TUL, Liberec, Czech Republic.

5 REFERENCES

- [1] Nosek, S.: Theory of weaving process I-III part, Dům techniky ČSVTS, 1988 Pardubice
- [2] Lawrence C. A.: *Fundamentals of spun yarn technology*. Boca Raton: CRC Press. 2003.
- [3] Ernst H.: *The Rieter Manual of Spinning*. Volume 5 – Rotor Spinning. Wintherthur: Rieter Machine Works Ltd., 2014.
- [4] Stalder H. *The Rieter Manual of Spinning*. Volume 6 – Alternative Spinning Systems. Wintherthur: Rieter Machine Works Ltd., 2014.
- [5] Erdumlu N., Ozipek B., Oxenham, W.: Vortex spinning technology. *Textile progress*, 44:3-4, pp. 141-174.
- [6] Ahmad Z., Eldeeb M., Iqbal S. and Mazari A. A.: Effect of yarn structure on cover factor in woven fabrics. *Industria Textila*, 69 (3), pp 197-201.

3D WOVEN STRUCTURES FOR AUTOMOTIVE SEAT COVERS

Ashok Kumar & B. K. Behera

Focus incubation center for 3D weaving and structural composites

Department of Textile Technology, Indian Institute of Technology Delhi

Abstract: Among others, automotive textile is considered to be fastest growing sector of technical textiles. Many researchers are working on physiological comfort and utility performance of automotive seat covers. Automotive seat covers exhibit four important functions namely durability, physiological comfort, hygienic properties, and hand behavior. This paper presents comparative advantages of 3D woven solid structures over conventional 2D fabrics in various aspects related to utility performance and physiological comfort properties. Utility performance and physiological comfort behavior have been studied by measuring abrasion weight loss, tensile strength, pilling resistance, tear strength, air permeability, water vapor transmission, and thermal behavior. Air texturized polyester yarn is used as raw material for manufacturing 3D structures and 2D fabrics using plain, matt, twill & satin weaves. It has been found that 3D structures is more suitable structure than conventional 2D fabric for automotive seat cover use in terms of durability and comfort. Because of textile structure plays a vital role to decide above characteristics. In 3D structure, three-axis yarns are held together bestow structural stability and improve durability of automotive seat cover.

Keywords: 3D structures, automotive textiles, utility performance, Physiological comfort

1 INTRODUCTION

The automobile industry is the largest user of technical textiles, with about 20 kg in each of the 45 million or so cars made every year worldwide. Every middle-size vehicle uses between 12 and 14 Kg of textile products, without including tire cords for pneumatic and fibres which are used in composite materials. The 65% of this quantity is used, approximately, in the interior (40 to 45 m² of textile material per car) with a weight between 200 and 450 g/m² for the seats upholstery [1].

On behalf of car seat cover related issues, it is found that customers want more comfortable seat cover with better serviceability. Hence, project thrust is to design and develop innovative 3D woven structures for car seat cover and investigate their mechanical property and physiological comfort by using various weaves in these structures. These structures must be fulfilled the essential requirement of automotive seat covers; such as abrasion resistance, tensile strength, tear resistance, pilling resistance, thermal behavior, air permeability, water vapour permeability and hand value etc. In this research, 3D woven structures are introduced in place of conventional 2D woven structures to bestow better utility performance & comfort.

2 EXPERIMENTAL

2.1 Materials

Air texturized (ATY) polyester yarn of 400dtex is used to weave all 2D conventional & 3D orthogonal samples with same areal density under controlled weaving conditions, to obtain exact constructional properties. Because of good durability and stability [2]. Eight (four 2D & four 3D orthogonal) samples are produced using plain, matt 3/3, twill 3/1, and satin 5 end on customized CCI loom in industry. After weaving, all samples were stitched together and washed with water at room temperature and stentered without tension at 180°C for 60 sec. to heat set.

2.2 Methods

2.2.1 Abrasion Resistance

Martindale abrasion tester is used to determine abrasion resistance of samples (ASTM D4966). Weight loss after abrasion is calculated as percentage by the formula – $\{(A - B) / A\} \times 100$

Where A – Weight of sample before abrasion

B – Weight of sample after abrasion

2.2.2 Tensile Strength

To determine tensile strength, strip test is used on Instron Tensile tester (ASTM D5035).

2.2.3 Tear Strength

To determine tear strength, CRE principle based Instron tester is used (ASTM D5587).

2.2.4 Air Permeability

Air permeability of samples is measured by using TEXTTEST FX 3300 air permeability tester (ASTM D737).

2.2.5 Water Vapour Transmission Rate

W3/060 water vapour transmission tester is used for water vapour transmission rate (ASTM D1653).

2.2.6 Thermal behaviour

Thermal resistance or insulation was measured with the KES-FB5 (Thermolabo II). When a preheated hot plate (as a simulator of human skin) is placed on the fabric sample, a heat flux versus time curve is generated. Maximum (pick) heat flow (Q_{max}) is measured in a fraction of second after the hot plate contacts the fabric.

Evaluation value: $Cool/warm = q_{max}$

Thermal conductivity = (Heat flow rate x thickness) / (area x temperature difference)

$$K = Q \times h / (A \times \Delta T)$$

Thermal resistance = Thickness / thermal conductivity

$$R = h / K$$

$$TIV = [(1 - h_c) / h_b] \times 100$$

Where h_c is the heat loss from covered hot body and h_b the heat loss from the uncovered body.

3 RESULTS & DISCUSSION

3.1 Abrasion resistance

The 3D fabrics are defined as “a single-fabric system, the constituent yarns of which are supposedly disposed in a three mutually perpendicular plane relationship” [3]. According to fabric structure, it was revealed that 3D textile structure exhibited better abrasion resistance than 2D samples. Because of multilayer structure, third axis of yarn provided more structural stability and binder yarn which directly contact with abrader was placed at alternate position of stuffer yarn. However, in 2D structure stuffer yarn was absent so contact area with abrader was higher than 3D textile structure. Consequently, 2D samples attributed low abrasion resistance.

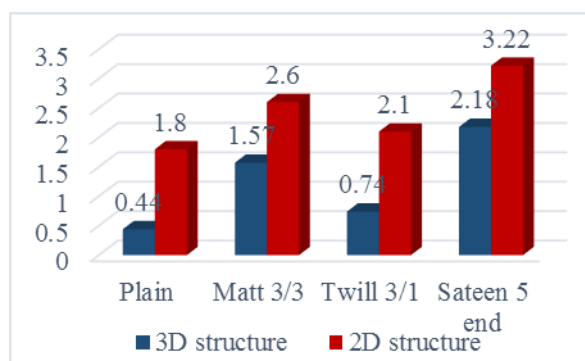


Figure 1. Weight loss after 10000 cycles

3.2 Tensile strength

It can be seen that tensile strength is totally depends on thread density irrespective of weaves & more floats on the fabric structure facilitate more thread densities and lessen the extension [4].

3.3 Tear strength

It can be shown that tear strength of 3D sample is much higher than 2D sample in both warp and weft direction. Though greater extensibility or reduced frictional constraints allow the yarns to bunch at the tear and therefore increase the tearing strength, it is clear that higher yarn strength may not necessarily lead to higher tear strength [5].

3.4 Air permeability

Air permeability is the rate of air flow passing vertically through a known area under a prearranged air pressure differential between the two surfaces of a material. Air and water vapour permeability are also the most significant properties of textile materials that ensure their comfort. It is found that air permeability of 3D woven structure is higher than 2D conventional fabric due to 3D woven structure has more volume for same areal density.

3.5 Water vapour transmission rate

Water vapour permeability is one of the most important properties that determine the velocity of water vapour

transmission through a textile material. This is a vital parameter in appraising comfort characteristics of a fabric, as it stands for the capability of transporting perspiration. It is found that water vapour transmission rate of 3D woven structure is higher.

3.6 Thermal behaviour

Thermal properties are explained as the amount of heat transmitted through the thickness of the fabric in a measured surface area. Thermal conductivity and resistance are immensely influenced by the fabric structure and thickness. The long float open loop structure with higher fabric thickness produces lowest thermal conductivity. The thermal resistance shows high response for thermal conductivity and thickness of fabric. Comfort property is depending on the fabric thickness, and thermal conductivity was established as a significant aspect leading to the thermal insulation of textiles.

4 CONCLUSION

It was found out that utility performance is complex property of fabric. Abrasion will differ by changing weave, structure, float length, thickness, cumulative no of interlacing point per unit area, type of yarn, structure tightness, areal density and continuous contact area of fabric with abrader etc. It can be seen that long float length and low no. of interlacing point show more abrasion because of continuous contact area of yarn expanded and it facilitate yarn to lose easily as result of abrasion. Tensile strength is depends on thread density. Tear strength of 3D woven structure is far better than 2D conventional fabric. Comfort property is depended on air permeability, water vapour transmission rate & thermal conductivity. Comfort property is depending on the fabric thickness, and thermal conductivity is established as a significant aspect leading to the thermal insulation of textiles. It is revealed that comfort property of 3D woven structure is better than 2D conventional fabrics.

It has been found that 3D structures is more suitable structure than conventional 2D fabric for automotive seat cover use in terms of durability and comfort. Because of textile structure plays a vital role to decide above characteristics. In 3D structure, three-axis yarns are held together bestow structural stability and improve durability of automotive seat cover.

5 REFERENCES

- [1] Jerkovic I, Pallares J.M. & Capdevila X. *Study of the abrasion resistance in the upholstery of automobile seat*. Autex Research Journal (2010)
- [2] Williams, J. *Texturing Today. Presented at Shirley Inst. Conf.* Shirley Inst. Special Publication (1982).
- [3] Behera, B. K. 3-Dimensional weaving. *Indian Journal of Fibre & Textile Research*, 274-287 (Sep 2008).
- [4] Peter Reeves Lord, Mansour H. Mohamed. *Weaving: Conversion of Yarn to Fabric*. Woodhead Publishing (1982).
- [5] Mukhopadhyay A., Ghosh S. and Bhaumik S.. Tearing and tensile strength behaviour of military khaki fabrics from grey to finished process. *International Journal of Clothing Science and Technology*, Vol. 18, 247-264, (2006).

AUTOMATIC FORMATION TECHNIQUES AND UNIFORMITY EVALUATION OF CONICAL VASCULAR GRAFT

Fenye Meng¹, Yuling Li²

^{1,2}Key Laboratory of Textile Science and Technology of Ministry of Education, College of Textiles, Donghua University, Shanghai, e-mail¹: karenmfy@163.com e-mail²: lylu@dhu.edu.cn

Abstract: Conical vascular tubes are of strong demand owing to their formed shape and excellent characters to mimic human blood vessels. In this study, the automatic shuttle loom and Computer Aided Design (CAD) system were customized to prepare a conical vascular graft with the equal-cover-factor principle, which was built through identifying the terms of the lift-drop front rest, and the geometrical relations established between the cloth fell, front rest and back rest. While, the uniformity of its wall structure was investigated after loom-off. The experiment results showed that the conical vascular prosthesis designed with the equal-cover-factor principle has statistically uniform structure along the conical prosthesis wall in terms of the gram weight per unit area, the wall thickness, porosity and pore size. These results suggest the advantage and potential of the equal-cover-factor principle in automatic fabrication technique of the woven conical vascular prosthesis.

Keywords: vascular graft, conical tube, weaving, uniformity

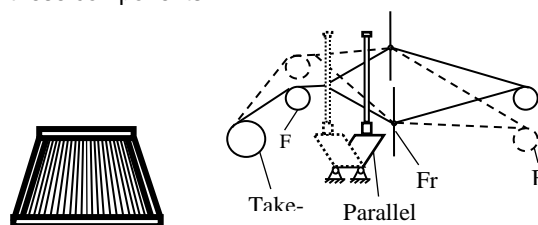
1 INTRODUCTION

The automatic manufacture technique for cylindrical vascular grafts has been set up successfully, especially in the commercial production of medium and large diameter arteries. However, the blood vessels are not a tube with constant diameter, but with a variable diameter along their longitude direction and a taper angle of about 1° or more. Further, the hemodynamic study on blood vessels showed that such a small angle has a considerable influence on the vascular wall and organic reaction, and the blood flow distributions along axial of conical vascular are different compared with cylindrical tube[1-3]. Therefore, the automatic weaving technique is required to obtain stable conical vascular graft which can't be satisfied through current weave technique [4]. The aim of this study is to establish the automatic weave technique with equal-cover-factor principle to produce a conical vascular graft with smooth surface and continuous varied cross-section.

2 FORMATION THEORY FOR THE CONICAL VASCULAR GRAFT

The front rest in a loom is commonly considered as the basic reference line for the adjustment of cloth fell, and the heddle and the back rest were used to guarantee a constant and steady followed-up weaving process. Hence, the front rest is not moved in terms of the classic weaving principle. However, this principle would be challenged when a conical vascular graft is prepared by a trapezoidal reed in combination with the lift-drop motion of the front rest to realize the change of fabric width and warp density, as illustrated in Fig. 1. The lift-drop motion of the front rest would result in an unexpected conical tube construction according to previous study. Therefore, it should theoretically analyze the influence of the lift-drop front rest on: (1) location change of cloth fell, shuttle box, rapier and the back rest and (2) change of warp tension and weft density. After that, a weaving parameter can be

configured to realize the overall coordinate movement of these components.



a) Trapezoid reed b) Lift-drop motion of the front rest
Fig.1 Illustration for the lift and drop motion of the front rest

3 MOVABLE ASSEMBLY UNIT AND CAD SOFTWARE DESIGN

The automatically lift-drop movements of front rest, cloth fell, back rest, rapier and shuttle box were controlled by the electric cylinder employed in the shuttle loom, and their synchronous movements were realized through a new CAD software according to the geometrical relations established. The working flow chart of the loom during weaving is illustrated in figure 2.

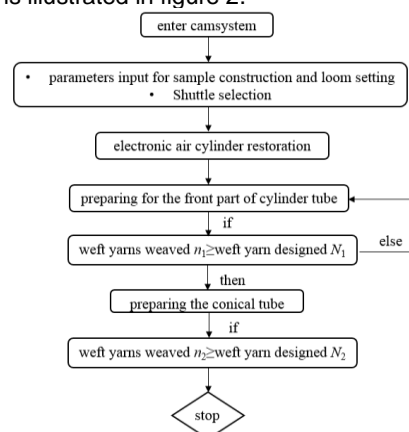


Fig. 2 Working flow of the loom

4 SAMPLE PREPARATION

In this experiment, 3 level conical degree of 1°, 1.5° and 2° were designed according to the structure and application requirements of woven vascular prosthesis, then fabric weave patterns of 1/3 broken twill, 2/2 twill and 3/1 twill, together with a weave tightness of 70% were determined to prepare the ultra-high-density CVC woven tubular samples based on the preliminary experiments. 9 kinds of prototype samples with 3 level conical degree (1°, 1.5° and 2°) and 3 weave patterns (1/3 broken twill, 2/2 and 3/1 twill) were designed and prepared on the shuttle loom. Then heated for 10min at 190°C in a air-dry oven to converted samples into resilient circular structures to meet clinical requirements.

4.1 Structural Characteristic

Properties of 9 kinds conical woven tubular samples were tested according to ISO 7198-1998. Wall thickness and gram weight per unit area were measured with reference to GB 3820-83. For sample's wall thickness, YG141N tester with a pressing foot area of 100mm² and a pressure of 25cN were selected. Results were averaged from 5 replicates of the large, medium and small end of each sample. For gram weight per unit area, 5 specimens with an area of 1cm² were taken from the large, medium and small ends of each sample, then measured and averaged. A stereomicroscope (PXS8-T, Cewei Photoelectric Technology Co., Ltd, Shanghai, China) was used to observe the surface morphology of each CVC woven tubular samples' large, medium and small ends, respectively. And the microphotographs were analyzed through Image processing method to calculate the porosity of each specimen. The test results were shown in table 1

Table 1 Structure property test results

Sample No.	Thickness/mm	Gram weight/g · m ²	Porosity/%
1 [#]	0.110±0.046	67.289±4.590	23.440±2.974
2 [#]	0.109±0.048	62.200±4.018	24.080±2.914
3 [#]	0.107±0.032	65.250±3.810	21.740±2.179
4 [#]	0.112±0.002	61.799±2.356	23.000±2.647
5 [#]	0.109±0.001	64.708±3.257	23.867±1.933
6 [#]	0.117±0.001	64.769±3.108	20.920±2.495
7 [#]	0.118±0.002	73.433±3.604	19.000±1.787
8 [#]	0.118±0.001	71.288±1.531	18.171±2.745
9 [#]	0.122±0.001	69.435±2.990	19.475±1.656

4.2 Results and Discussion

The data is recorded as mean ± standard deviation for each sample. A Student's t-test was performed to determine any statistically significant differences between specimens. All statistical tests were performed at a 99% confidence interval ($p < 0.01$).

Results showed that the thickness of the 9 kinds conical woven tubular samples was about 0.12mm, and the gram weight per unit area was different within the range of 61-71 g/m² based on 3 weave patterns designed. The standard deviations of thickness and gram weight per unit area between the large, medium and small end of each sample were less than 0.2% and 4%, respectively. And 3/1 twill samples were thicker and heavier than others.

The porosity test results showed that the discrepancy rates of each sample's large, medium and small end part was less than 3%.

One-way analysis of variance was applied to analyze the porosity of 9 kinds conical woven tubular samples varied in weave pattern and conical degree, and there was no significant difference between samples in different conical degree ($p < 0.05$). However, fabric weave pattern has significant impact on porosity ($p = 0.00914$). The fabric weave pattern of 3/1 has the smallest porosity compared with others, and samples with a conical degree of 2° has the minimum porosity compared with samples with degrees of 1° and 1.5°.

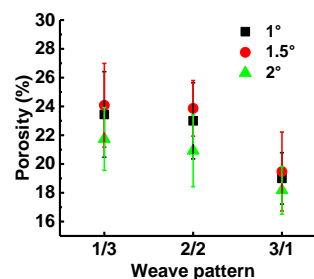


Fig.3 Porosity comparison

5 CONCLUSION

This study evaluated the structural and physical properties of conical woven conical tubular prostheses on the bases of the equal-cover-factor principle, and focused on the uniform distribution of structural properties like thickness, gram weight per unit area, porosity along the tubular axis for different conical degree and fabric weave pattern. Generally, the results confirmed the advantage of conical tubular prostheses fabricated by the equal-cove-factor weaving technique.

ACKNOWLEDGEMENT

The author(s) would like to acknowledge the following financial support for the research: The Fundamental Research Funds for the Central Universities and Graduate Student Innovation Fund of Donghua University (No. CUSF-DH-D-2019033), and the Fundamental Research Funds of Central Universities.

6 REFERENCES

- [1] Black A R, How T V. Attenuation of Flow Disturbances in Tapered Arterial Grafts, *Trans of The ASME[J]*, Biomechanical Engineering, 1989, 111:303.
- [2] Marsden A L. Optimization in Cardiovascular Modeling. *Annual Review of Fluid Mechanics*, 2014, 46: 519-546.
- [3] Singh C, Wong C, Wang X, Medical Textiles as Vascular Implants and Their Success to Mimic Natural Arteries[J]. *Journal of Functional Biomaterials*, 2015, 6(3): 500-525.
- [4] Dong X Q, Li Y L, Ding X. Research on The Manufacture of Tapered Artificial Vascular[C]. *Advanced Material Research*, 2011:512-515(in Chinese).

ACOUSTIC PROPERTIES OF ADVANCED NONWOVENS

Rajesh Mishra¹, Tao Yang¹, Xiaoman Xiong¹ and Jiri Militky¹

¹ Department of Material Engineering, Faculty of Textile Engineering, Technical University of Liberec, Liberec 46117, Czech Republic, e-mail: rajesh.mishra@tul.cz

Abstract: Sound absorption property of perpendicularly-laid nonwovens were tested by Brüel and Kjær measuring instrument. The effect of manufacturing techniques on sound absorption performance was investigated. The effect of porosity and airflow resistivity on sound absorption ability was studied. It is found that there is no significant influence of two manufacturing techniques on sound absorption performance. The increase of areal density results in improvement of sound absorption ability. The increase of thickness can improve sound absorption coefficient at low-frequency range, but decrease of the coefficient occurred at high-frequency range. A quadratic relationship between porosity and sound absorption ability has been found. The airflow resistivity is a key parameter to predict accurately the acoustical properties of fibrous media. There is a large number of theoretical and empirical models which can be used to predict the airflow resistivity of this type of porous media. However, there is a lack of experimental data on the accuracy of these models in the case of multi-component fibrous media. This study presents a detailed analysis of the accuracy of several existing models to predict airflow resistivity which make use of the porosity, bulk density and mean fiber diameter information. The AFD300 AcoustiFlow device was employed to measure airflow resistivity. It is shown that some existing models largely under- or overestimate the airflow resistivity when compared with the measured values. A novel feature of this work is that it studies the relative performance of airflow resistivity prediction models that are based on the capillary channel theory and drag force theory. These two groups of models are then compared to some purely empirical models. It is found that the mean absolute values of relative error (MAVRE) by some models is unacceptably high (e.g. >20-30%). The results suggest that there are existing models which can predict the airflow resistivity of multi-component fibrous media with 12.8% accuracy. A simple empirical model based on fiber diameter and fabric bulk density has been obtained through power-type model. This model exhibits very small error which is 5.1%.

Keywords: sound absorption coefficient, air permeability, nonwoven, porosity

1 INTRODUCTION

Perpendicularly-laid nonwoven samples were made by two different manufacturing techniques: vibration and rotating perpendicular lapper. Heat-pressing method was employed to form samples with varying thickness. This study determines the influence of some structural characteristics and laying techniques on the sound absorption properties of perpendicularly-laid nonwovens [1,2].

Normally incident sound absorption coefficient and surface impedance were measured by Brüel and Kjær type 4206 impedance tube. Several airflow resistivity models grouped in theoretical and empirical categories were used to study the suitable model for perpendicularly-laid nonwoven fabrics. The commonly used impedance models such as Delany-Bazley, Miki, Garai-Pompoli and Komatsu models were applied to predict the acoustic properties. The measured and predicted values were compared to figure out the accuracy of the existing models. One simple model was developed to rapidly obtain the airflow resistivity of perpendicularly-laid nonwovens [3,4]. The compression energy and compression load of perpendicularly-laid nonwovens were carried out by using a universal testing machine (TIRATEST 2300). The potential compression mechanism of the nonwoven fabric was identified with support of the compression stress-strain curve, work done and efficiency at different compression stages.

Perpendicularly-laid nonwoven fabrics have special thermal and air permeability behavior compared with traditional cross-laid nonwovens due to their through-plane fiber orientation. Hence this research work also investigates the influence of different structural parameters

of perpendicularly-laid nonwoven fabrics, such as areal density, porosity, thickness, on thermal properties and air permeability. The potential relationships between thermal resistivity, air permeability and acoustic properties were also investigated.

2 EXPERIMENT

2.1 Materials

Polyester nonwoven samples made by vibrating and rotating perpendicular technology were selected for this study. All of the samples in current study have the same fiber content: 45% staple polyethylene terephthalate (PET), 30% hollow PET and 25% bi-component PET.

2.2 Impedance tube measurement

One four-microphone impedance tube was applied to carry out the measurements to recover the reflection R and transmission coefficients T . Then the dynamic density $\tilde{\rho}_{eq}$ and dynamic bulk modulus \tilde{K}_{eq} can be calculated straightforwardly [1].

3 RESULTS

The Brüel and Kjær impedance tube contains a large tube (100 mm in diameter) and a small tube (29 mm in diameter) which used to obtain the sound absorption coefficient in low-frequency range from 50-1600Hz and high-frequency range 500-6400Hz respectively. Later the measurement data from large and small tube were

combined to form the curves for the frequency range between 50-6400 Hz. The normal incidence sound absorption coefficient of original perpendicularly-laid nonwovens is shown in Figure 1.

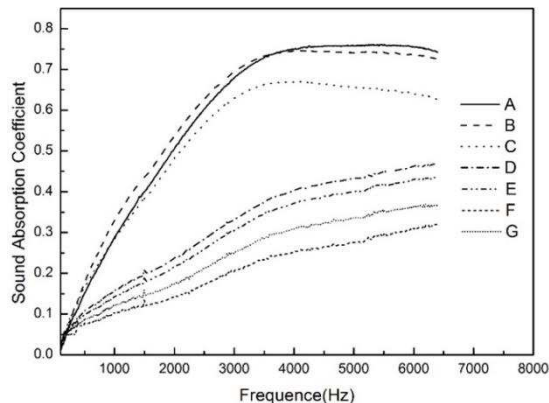


Figure 1 Sound absorption coefficient of original perpendicularly-laid nonwovens

It is observed that sound absorption coefficient of the test samples lies in the range of 0.017-0.76. Apparently, the value of absorption coefficient for samples A, B and C sharply increases at frequency bands 50 Hz-3500 Hz and the maximum value of absorption coefficient occurs at frequency bands 4000 Hz-5400 Hz. However, samples D, E, F and G show lower absorption coefficient value in comparison to samples A, B and C, and the value of absorption coefficient increases with the increasing of frequency at the whole measurable frequency bands (50Hz-6400 Hz). Results indicate that perpendicularly-laid nonwoven exhibits much better sound absorption ability at frequency bands 3000 Hz-6400 Hz.

The coefficient of determination is the proportion of the variance in the dependent variable that is predictable from the independent variable(s). The use of an adjusted R² is an attempt to take account of the phenomenon of the R² automatically and spuriously increasing when extra explanatory variables are added to the model. It is a modification that adjusts for the number of explanatory terms in a model relative to the number of data points.

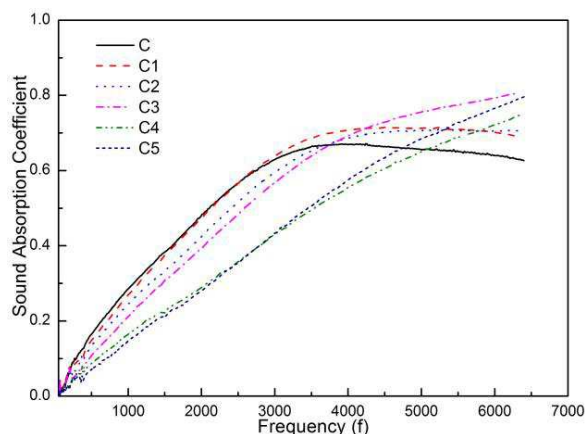


Figure 2 SAC of samples with a different thickness

Samples C1, C2, C3, C4 and C5 were made from sample C through heat-pressing method. As the material gets

thicker, the sound absorption at low-frequency range increases as well.^{92, 104-105} Sound absorption performance of samples with same areal density but different thicknesses are shown in Figure 4.5. It can be seen that samples sound absorption ability at low-frequency bands decreased with the decrease of samples thickness. Meanwhile, the SAC increases at high-frequency bands with the decrease of thickness. This can be explained by the resonance, the resonance phenomena occur towards the low-frequency band for thicker samples.⁹⁷ It is also found that the peak values of SAC increase and shift towards the higher frequencies side with decrease of sample thickness. But the effect of decreasing thickness on SAC peak values is limited, since the peak values no longer increase after the thickness reaches a critical value. In addition, samples (C4, C5) with thickness less than 16.85 mm show a significant decrease of SAC at 50-4500 Hz range.

4 CONCLUSION

Sound absorption property of perpendicularly-laid nonwovens were tested by Brüel and Kjær measuring instrument. The effect of manufacturing techniques on sound absorption performance was investigated. The effect of porosity and airflow resistivity on sound absorption ability was studied. It is found that there is no significant influence of two manufacturing techniques on sound absorption performance. The increase of areal density results in improvement of sound absorption ability. The increase of thickness can improve sound absorption coefficient at low-frequency range, but decrease of the coefficient occurred at high-frequency range. A quadratic relationship between porosity and sound absorption ability has been found.

ACKNOWLEDGEMENT: This work was supported by the Ministry of Education, Youth and Sports of the Czech Republic and the European Union – European Structural and Investment Funds in the frames of Operational Programme Research, Development and Education – project Hybrid Materials for Hierarchical Structures (HyHi, Reg. No. CZ.02.1.01/0.0/0.0/16_019/0000843), project “Modular platform for autonomous chassis of specialized electric vehicles for freight and equipment transportation”, Reg. No. CZ.02.1.01/0.0/0.0/16_025/0007293.

5 REFERENCES

- [1] Niskanen M., Groby J., Duclos A., et al.: Deterministic and statistical characterization of rigid frame porous materials from impedance tube measurements. *Journal of the Acoustical Society of America* 2017, 142, pp. 2407-2418.
- [2] Johnson D. L., Koplik J., Dashen R.: Theory of dynamic permeability and tortuosity in fluid-saturated porous media. *Journal of Fluid Mechanics* 1987, 176, pp. 379-402.
- [3] Champoux Y., Allard J.-F.: Dynamic tortuosity and bulk modulus in air-saturated porous media. *Journal of Applied Physics* 1991, 70, pp. 1975-1979.
- [4] Lafarge D., Lemarinier P., Allard J.-F., et al.: Dynamic compressibility of air in porous structures at audible frequencies, *Journal of the Acoustical Society of America* 1997, 102, pp. 1995-2006.

PREPARATION OF NANOCARBON-SUPPORTED NANOFIBER FABRIC FOR PURIFICATION OF CONTAMINATED WATER

Yasuhito Mukai, Eiji Amano and Satoshi Hara

Department of Chemical Systems Engineering, Nagoya University, Furo-cho, Chikusa-ku, Nagoya 464-8603, Japan,
e-mail: mukai.yasuhito@material.nagoya-u.ac.jp

Abstract: In this study, the composite fabric was prepared by combining nanofiber having an extremely high specific surface area with nanosized carbon black (CB) having a solute adsorption capacity to purify contaminated water. The nanofiber fabric made of polyacrylonitrile with mean fiber diameter of 400 nm was used as a base material. The CB particles with an original size of 20 nm were used as adsorbent and dispersed in pure water at the concentration of 10 g/L. Before preparation, the CB particles were oxidized by mixing CB with 70% nitric acid at a rate of 1 g to 1 ml and heating for 2 hours with agitation. The surface of CB particles became hydrophilic by oxidization and as a result the size of CB particles became original one in the dispersion. The nanofiber fabric was immersed in the CB dispersion and shaken for 2 hours. After taking out and rinsing it lightly, CB was immobilized on the surface of nanofibers by heating for 1 hour at 150°C. The adsorption test of prepared CB-supported nanofiber fabric was conducted by soaking them into the aqueous solutions of methylene blue (MB) used as a contaminant, and the adsorbed amount of MB was measured under various MB concentrations. As a result, whereas the saturated adsorbed amount to the original nanofiber fabric was 1.9 mg/g and that to untreated CB-supported nanofiber fabric was 5.0 mg/g, that to oxidized CB-supported nanofiber fabric was remarkably large 96.2 mg/g. In conclusion, the oxidization of CB is an essential pretreatment to attain high solute adsorption performance.

Keywords: nanofiber fabric, carbon black, composite, adsorption, water purification

1 INTRODUCTION

Recently, the nanofiber is attracting attention in widely diversified fields and being developed for various applications [1]. One of the typical applications of the nanofiber material is a nanofiber filter medium, and it is considered to be promising as an alternative to conventional membrane filter. The nanofiber fabric with a nanosized effect and a high porosity is expected to serve as a new filter medium for water treatment since both performances of water permeation and particle retention are very high [2, 3]. Furthermore, if such functions as adsorption or ion exchange are added to the surface of nanofibers, the functionalized fabric developed from extremely high specific surface area can be produced for application to the water purification process [4, 5].

In this study, the composite fabric with great adsorption capacity for contaminant was prepared by combining a nanofiber fabric with functionalized nanocarbon to purify contaminated water. And then, the adsorption capacity of the prepared composite fabric was evaluated through the static adsorption test with a test solution.

2 PREPARATION OF CB-SUPPORTED NANOFIBER FABRIC

2.1 Pretreatment of CB Particles

Carbon black (CB) with original particle size of 20 nm was used as an adsorbent. With the aim of improving the adsorption capacity, the CB particles were subjected to any of the following pretreatments (1) – (3).

(1) pH control of CB dispersion

In the preparation of the CB dispersion, pH was adjusted to a given value by the addition of HCl or NaOH.

(2) Activation by KOH of CB particles

The CB particles were activated by mixing KOH and CB and heating for 1 hour at 800°C under an atmosphere of N₂ gas flow of 0.5 L/min. Finally, activated CB particles were rinsed well in water after neutralization with HCl for the removal of residual KOH.

(3) Oxidization of CB particles

The CB particles were oxidized by mixing CB with 70% nitric acid at a rate of 1 g to 1 ml and heating for 2 hours with agitation. Finally, oxidized CB particles were rinsed well in water for the removal of residual nitric acid.

The size distributions of the CB particles pretreated by the methods (1) – (3) were measured. As a result, (1) The pH condition has little effect on particle size; (2) The activation of CB led to an increase in specific surface area of CB, but also caused the flocculation of CB particles; (3) The oxidization of CB shrank the particles down to original size of 20 nm because of the formation of some hydrophilic groups to the surface of CB particles.

2.2 Immobilization of CB onto Nanofibers

The nanofiber fabric supplied by Japan Vilene Co. was used as a base material. This fabric is made of polyacrylonitrile and has mean fiber diameter of 400 nm and areal weight of 17.2 g/m². The CB particles were dispersed in pure water at the concentration of 10 g/L. The nanofiber fabric was immersed in the CB dispersion and shaken for 2 hours. After taking out and rinsing it lightly, CB particles were immobilized on the surface of nanofibers by heating for 1 hour at 150°C.

Figure 1 shows appearances and SEM photographs of the nanofiber fabrics before and after treatment. The oxidized CB-supported nanofiber fabric does not turn so

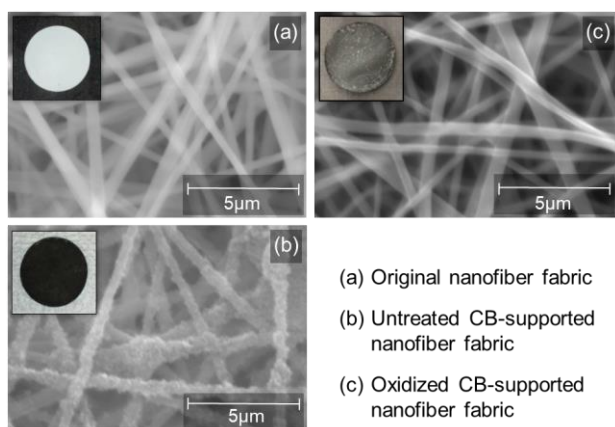


Figure 1 Images of CB-supported nanofiber fabric

black because the CB particles are dispersed to nanosize. And also, the oxidized CB particles are too small to be observed in a SEM photograph.

3 EVALUATION OF CB-SUPPORTED NANOFIBER FABRIC

Methylene blue, a type of colored component, was used as an adsorbate. The static adsorption test of prepared CB-supported nanofiber fabrics was conducted by soaking them into the aqueous solutions of methylene blue prepared at various concentrations with shaking until a state of adsorption equilibrium was reached. The equilibrium concentration C^* and the equilibrium adsorption amount Γ of methylene blue were measured, and the relations between Γ and C^* for different fabrics were depicted in Fig. 2. All the adsorption behaviors in the figure can be expressed by the following equation of Langmuir-typed adsorption isotherm.

$$\Gamma = \frac{\Gamma_s K C^*}{1 + K C^*} \quad (1)$$

The saturated amount Γ_s of adsorption was estimated based on Eq. (1). As a result, the value of Γ_s was 1.9 mg/g for original nanofiber fabric, 5.0 mg/g for untreated CB-supported nanofiber fabric, 6.1 mg/g for CB-supported nanofiber fabric prepared under the acid environment, 18.3 mg/g for activated CB-supported nanofiber fabric, and 96.2 mg/g for oxidized CB-supported nanofiber fabric. The effects of pretreatment of the CB particles on the adsorption capacity of the composite fabric are discussed below.

(1) Preparation in acidic environment

When CB-supported nanofiber fabric was prepared under the acid environment, the amount of supported CB was slightly increased due to the reduction of electrostatic repulsion between CB particles and polyacrylonitrile fibers.

(2) Activated CB-supported nanofiber fabric

The adsorption amount was increased by the activation of CB because of the increase in specific surface area of CB from 105 m²/g to 774 m²/g. However, the activation induced the flocculation of CB particles as mentioned above and consequently reduced the rate of increase in the amount of supported CB, resulting in not so much adsorption amount as expected.

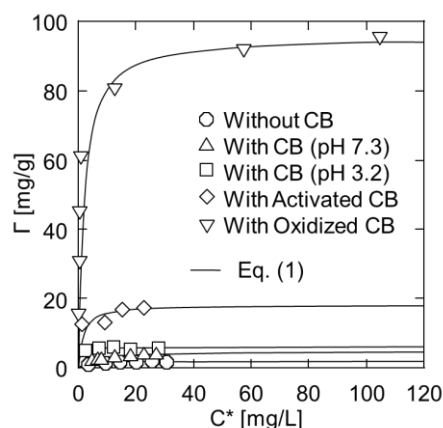


Figure 2 Adsorption isotherms of CB-supported nanofiber fabrics

(3) Oxidized CB-supported nanofiber fabric

The adsorption amount was significantly increased by the oxidation of CB because the surface of CB particles became hydrophilic and as a result the size of CB particles became original one as mentioned above. Thus, a significantly increased surface area of nanosized CB particles enhanced adsorption performance.

In conclusion, the oxidation of CB is an essential pretreatment to attain high adsorption performance.

4 CONCLUSIONS

The CB-supported nanofiber fabric developed in this study is effective in adsorption of contaminants in effluent. Especially, the composite fabric supported by oxidized CB has markedly high adsorption performance. In addition, the process of solute adsorption onto the CB-supported nanofiber fabric can be described by Langmuir adsorption model.

ACKNOWLEDGEMENT: This work was supported in part by JSPS KAKENHI Grant No. 25420801 and No. 16K06824. The authors would like to express the sincere gratitude for the financial support.

5 REFERENCES

- [1] Hongu T.: *Nanofiber Technology*. Nikkan Kogyo Shinbun, Tokyo, 2006, pp. 42-45.
- [2] Mukai Y.: Preliminary study to apply nanofiber nonwoven cloth as filter media for water treatment. *Nanofiber*, 2011, 2, pp. 20-25.
- [3] Yoon K., Hsiao B. S., Chu B.: Functional nanofibers for environmental applications. *J. Mater. Chem.*, 2008, 18, pp. 5326-5334.
- [4] Teng M., Li F., Zhang B., Taha A. A.: Electrospun cyclodextrin-functionalized mesoporous polyvinyl alcohol/SiO₂ nanofiber membranes as a highly efficient adsorbent for indigo carmine dye. *Colloids Surf A: Physicochem. Eng. Asp.*, 2011, 385, pp. 229-234.
- [5] Neghlani P. K., Rafizadeh M., Taromi F. A.: Preparation of aminated-polyacrylonitrile nanofiber membranes for the adsorption of metal ions: Comparison with microfibers. *J. Hazard. Mater.*, 2011, 186, pp. 182-189.

EFFECT OF CELL GEOMETRICAL PARAMETERS ON THE MECHANICAL PROPERTIES OF 3D WOVEN SPACER SANDWICH COMPOSITES

Ghanshyam Neje¹ and Bijoya Kumar Behera²

^{1,2}Department of Textile Technology, Indian Institute of Technology Delhi, Hauz Khas, New Delhi 110016

¹e-mail: ghanshyamneje9@gmail.com, ²e-mail: behera@textile.iitd.ac.in

Abstract: Woven spacer fabrics connected with woven cross-links and having cells of rectangular, trapezoidal and triangular shape were used as reinforcement to produce sandwich composites. Number of spacer composites with different cell geometrical parameters were produced to study their effect on the mechanical performance. These produced composites were then characterized for their lateral compressive and flexural performance to analyze their failure load and energy absorbing capacity. In rectangular structures, the specific compressive load and absorbed energy/volume of the structures decreased with increase in the cell widths (at constant cell height) and cell height (at constant cell width). In trapezoidal structures, specific compressive load and absorbed energy/volume increased with increase in the cell wall opening angle, while in case of triangular structures, increase in cell wall opening angle increased the specific compressive load, but energy/volume was observed to be higher for 42.5° cell wall opening angle structure. The specific bending load and flexural stress followed the same trend as that of the specific compressive load for these structures.

Keywords: woven spacer, sandwich composites, hollow structures, energy absorbency

1 INTRODUCTION

Sandwich structures are characterized by properties like superior bending stiffness, light weight, thermal insulation, and acoustic damping behavior, due to which these are used in aerospace, marine. Locomotive, automobiles and civil engineering applications. Conventional sandwich structures utilize different core materials like honeycomb core, expanded polymeric foams and balsa wood along with metallic or polymer composite face sheets [1]. Despite the advantages of these core materials like light weight and good damage tolerance, core-to-face sheet delamination under various loading conditions acts as the main mode of failure due to material dissimilarity and/or weak interface between the face sheets and the core.

Textile manufacturing processes like knitting and weaving enable production of integral preforms for the reinforcement of sandwich structures that have very high delamination resistances. Sandwich composite structures manufactured by reinforcing woven spacers connected with core piles have demonstrated ductile failure and very good energy absorbency [2]. But increase in the height of core piles reduced their compressive load and impact damage threshold [3,4]. Though these spacer composites connected with core piles are better than traditional sandwich composites in some respect, these structures are not strong enough for flexural loading conditions.

The manufacturing possibility of woven spacers with woven cross-links have been reported in the literature. The mechanical properties of spacer composites with different cell geometries have been compared in [5]. But the effect of cell geometrical parameters on the mechanical performance of such composites has not been reported yet. An attempt has been made in this paper by studying 14 different spacer structures for their compressive and flexural performance.

2 MATERIALS AND METHODS

2.1 Materials

Woven spacer fabrics with different cell geometries and cell geometrical parameters have been manufactured using 600 tex multifilament E-glass tows supplied by Owens Corning. A customized weaving machine equipped with modified take-up system and multi-beam negative let-off system was used to produce all the structures in this study. The mixture of epoxy LY556 and curing agent Aradur HY951 was used as matrix system for producing composites.

2.2 Weaving of spacer architectures

The cross-sectional representation of the spacer architectures have been demonstrated in Fig. 1. The curved lines represent warp threads while the dots represent weft threads. A generalized weave design was developed for each of the structures. As each section of the structure is a 2D woven fabrics, its length can be varied by changing number of picks in it. The number of picks required in each section of the fabric, based on the final cell geometry required in the composites, were calculated, and the weave design was modified accordingly. In rectangular structures, the cell height of the structure was varied keeping the width of the cells almost constant, similarly cell width variation samples were produced with almost constant cell height. Seven structures were produced for rectangular geometry which constituted four height and four width variations. In trapezoidal spacer structures, four different structures were produced by varying the cell wall opening angle, while in triangular structures three samples were produced with different cell wall opening angles at almost constant cell height.

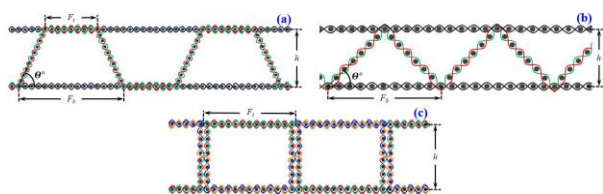


Figure 1 Cross-sectional representation of (a) trapezoidal, (b) triangular and (c) rectangular spacer fabrics

2.3 Composite manufacturing

Wooden blocks of appropriate size and shape were used to keep the fabric in its 3D shape during resin impregnation and curing stages. Vacuum assisted resin infusion molding (VARIM) technique was used to impregnate the fabrics with the resin, and the composites were left for curing at room temperature inside vacuum bagging for 24 hours. The produced composite samples have been shown in Fig. 2.

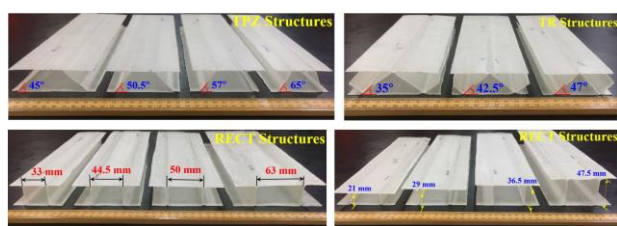


Figure 2 Produced spacer composite samples

2.4 Characterization of composites

2.4.1 Lateral compressive testing

The composite samples produced were evaluated for their lateral compressive performance according to ASTM C365 at a loading rate of 2 mm/min. Square shaped samples were compressed between the parallel loading platens of Instron 5982 universal testing machine. The sample size chosen for each structure was different due to different cell size and shape.

2.4.2 Bending test

Three-point-test was carried out for all the composite samples according to ASTM C393. The span length of 240 mm was kept constant for all the tested specimen but the width was chosen based on the cell size and shape. The testing speed used was 1 mm/min, and the testing set up comprised three rollers of 40 mm diameter.

3 RESULTS AND DISCUSSIONS

Lateral compressive performance

Compressive load increased with increase in the cell width of rectangular spacer, due to increased specimen size which increased the length of load bearing walls. On the other hand, in case of different height variation samples the compressive load decreased with increase in the height of the rectangular cell, as the increased height of the wall made them easier to buckle under lower loads. In case of trapezoidal and triangular spacer structures the compressive load increased with increase in the cell wall opening angle. As the specimen sizes were different for different composite structures, their masses also differed. Therefore, to compare these structures, mass specific compressive strength was calculated. The specific compressive strength was found to have decreasing order with increasing cell width and height of the rectangular

cells. Whereas, the specific compressive strength increased with increase in the cell wall opening angles for trapezoidal and triangular structures. The absorbed energy/volume was calculated for all the structures from their load-deformation curves and it was found to decrease with increase in the cell width and height of the rectangular cell. In trapezoidal structures, it increased with increase in cell wall opening angle. But in triangular structures, it was observed to be highest for structure with 42.5° cell wall opening angle.

Flexural performance of spacer composites

The specific bending load was found to have decreasing order with increase in the rectangular cell width and cell height. In trapezoidal and triangular structures, the specific bending load increased with increase in the cell wall opening angle. To assimilate the effect of change in the cell geometrical parameters on the flexural performance of these sandwich composites, maximum flexural stress was calculated. The maximum flexural stress decreased with increase in the rectangular cell width and cell height, and in trapezoidal and triangular spacer structures, it increased with increase in the cell wall opening angle.

3. CONCLUSIONS

Woven spacer sandwich structures with different cell geometrical shapes and cell geometrical parameters have been successfully manufactured. These structures have been analyzed for their out-of-plane compressive and bending properties. Rectangular structures with minimum cell width and minimum cell height were found to have higher specific compressive loads and specific bending loads. While for trapezoidal and triangular structures, the specific compressive load and specific bending load increased with increase in the cell wall opening angle of the structure. The outcomes of this study can be used in designing of the woven spacer sandwich structure with desired load bearing capabilities as per the end use requirements.

4 REFERENCES

- [1] Karlsson K., Åström B.: Manufacturing and applications of structural sandwich components. *Compos Part A Appl Sci Manuf* 1997, 28, pp.97–111.
- [2] Fan H., Zhao L., Chen H., Kuang N., et al.: Ductile deformation mechanisms and designing instructions for integrated woven textile sandwich composites. *Compos Sci Technol* 2012, 72, pp. 1338–1343.
- [3] Van Vuure A., Ivens J., Verpoest L.: Mechanical properties of composite panels based on woven sandwich-fabric preforms. *Compos Part A Appl Sci Manuf* 2000, 31, pp. 671–680.
- [4] Vaidya U., Hosur M., Earl D., Jeelani S.: Impact response of integrated hollow core sandwich composite panels. *Compos Part A Appl Sci Manuf* 2000, 31, pp. 761–772.
- [5] Neje G., Behera B.: Investigation of mechanical performance of 3D woven spacer sandwich composites with different cell geometries. *Compos Part B Eng* 2019, 160, pp. 306–314.

DIELECTRIC ANALYSIS OF COMPOSITE MATERIALS WITH PLASMA TREATMENT RECYCLED CARBON FIBERS

Jana Novotná¹, Hana Šourková² and Miroslava Pechočiaková¹

¹Department of Material Engineering, Technical University of Liberec, Textile faculty, Czech Republic, e-mail: jana.novotna3@tul.cz

²Faculty of Mechatronics, Informatics and Interdisciplinary Studies, Technical University of Liberec, Czech Republic, e-mail: hana.sourkova@tul.cz

Abstract: In present work are analyzed the changes dielectric properties of epoxy composites filled with 2,5wt% recycled short carbon fibers. Main objective was to study the influence of plasma treatment of fibers to permittivity of composites.

Keywords: recycled carbon fibers, epoxy composites, plasma treatment, permittivity

1 INTRODUCTION

The electric permittivity (the dielectric constant) can be estimated by means of additive quantities and is a basal material property that affect electrical applications of composites [1]. Once is the surface of the fibers modified by plasma, the adhesion between the filler and the matrix will improve, and thus improve the mechanical properties of the composite. In our study, we want to find out whether and how the dielectric properties are changes.

2 EXPERIMENT

2.1 Materials

With the technology pouring recommended in [2], a range of thin epoxy composites filled with recycled carbon fiber in the 2,5wt% concentrations was prepared. The used fillers were Carbiso Milled Carbon Fiber with average diameter about 7 µm, and average length 100 µm [3]. It was prepared 8 different plasma intensities of samples. Specific functionalization of fibers was prepared by microwave plasma treatment, a gas mixture of oxygen and hydrogen was used for this purpose.

As matrix was used low viscosity epoxy resin LR 285, and cyclic-alifatic polyamine curing agent H 508 (mixing ratio 100:40 by weight) [4].

2.2 Plasma treatment

The fibers were processed in the low-pressure laboratory plasma system (LA 400 SurfaceTreat) [5]. Plasma is generated by microwave source with a power of 1 kW. Working pressure 100 Pa was secured by rotary vacuum pump with pump speed 40 m³/h and Roots pump with pump speed 240 m³/h. Pressure measurement was done using Pirani gauge, regulation of pressure was secured by butterfly valve. The treatment chamber was filled with working gasses – oxygen 200 sccm and helium 50 sccm during the plasma treatment. This mixture was chosen due to oxygen functionalization of the material surface, which is observed after hydrophilisation of the surface. Fibers were placed in the mixing unit designed for processing of powder materials. The batch size of 5 g was treated for 10-80 min.

Contact angle measurement with water (WCA) was done on Drop Shape Analyzer – DSA30 (Krüss) using water volume of 3 µl. The Carbiso was spread on the adhesive tape in order to measure the contact angle. 12 sessile drops were placed on every prepared sample and then approximate WCA was calculated.

Table 1 List of testing composites samples

Sample	Plasma treatment time [min]
P	0
P0	0
P10	10
P20	20
P30	30
P40	40
P50	50
P60	60
P70	70
P80	80

Notice: Sample **P** its sample without carbon fibres, just matrix.

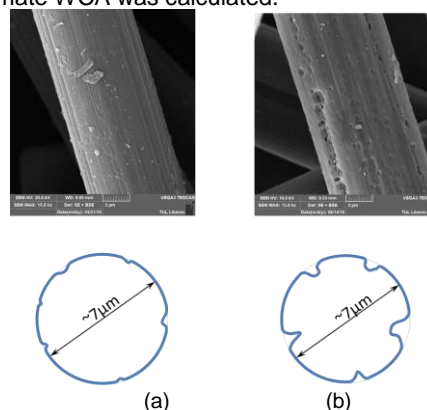


Figure 1 Influence of plasma treatment on surface changes and fiber diameter: (a) carbon fiber, (b) carbon fiber with plasma treatment 80min.

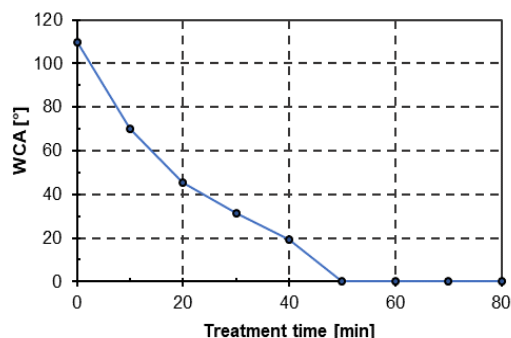


Figure 2 Dependence of WCA on plasma treatment time

The apparent contact angle value is measured only due to surface roughness and it shows only trend of plasma treatment effect. It can be observed from the measured values, that Carbiso plasma treatment has significant influence on change of hydrophobic character. Non-treated fibres show hydrophobic behaviour, plasma treated fibres then show hydrophilic behaviour. Increased hydrophilicity of the fibres is probably caused by binding of oxygen groups on the fibres surface together with surface roughness caused also by plasma treatment.

2.3 Permittivity

The common polymers are dielectrics. The relative dielectric constant of insulating materials is the ratio of the capacities of a parallel plate condenser measured with and without the dielectric material placed between the plates [1]. The permittivity ϵ was calculated using the relationship (1) where capacitance C was measured with the RCL meter INSTRON LCR821 [6]. The measured frequency was 1 kHz.

$$\epsilon = \frac{Cd}{\epsilon_0 S} \quad (1)$$

where $\epsilon_0 = 8.85 \times 10^{-12} \text{ F/m}$ is called *permittivity of free space*. It is universal constant. Further d is the sample thickness and S is the area of the sample.

3 CONCLUSION

The aim of this work was to verify the effect of plasma treatment of carbon recycled fibres on the resulting dielectric properties of composite materials made from them. The permittivity value from literature for the epoxy matrix is 5 [1] while for the carbon fibres value is about 4500 [7]. Our results range are from 4.42-9.66.

At the minimal used plasma treatment, almost is no change in the permittivity values compare to composites filled carbon fibers without plasma treatment (samples P0 and P10). But there are already extensive defect in the

surface of the fibers with longer treatment time (samples 20-80), see Figure 1. The permittivity values approaching to matrix values, see Table 2.

Table 2 List of measurement permittivity

Sample	Permittivity ϵ [-]	Variation coefficient [%]	Confidence interval lower	Confidence interval upper
P	4,42	0,03	4,41	4,42
P0	9,66	0,30	9,46	9,86
P10	9,08	0,10	9,06	9,09
P20	6,07	0,12	6,06	6,08
P30	5,84	0,15	5,82	5,85
P40	5,42	0,07	5,42	5,43
P50	5,69	0,06	5,68	5,70
P60	5,71	0,10	5,70	5,72
P70	5,84	0,06	5,83	5,85
P80	6,00	0,02	6,00	6,00

Finally was find out that composite materials will have changes dielectric constant through plasma treatment on the fibers surface. The used plasma treatment results of permittivity decrease, resulting values fall into the dielectric category.

ACKNOWLEDGEMENT: Authors are grateful for the financial support from the Student research project 2019 No. 21308 supported by Czech Ministry of Education, and by Faculty of Textile, Technical University of Liberec.

4 REFERENCES

- [1] D. W. Van Krevelen and K. Te Nijenhuis, *Properties of Polymers*. 2009.
- [2] A. Balzano, I. M. De Rosa, F. Sarasini, and M. S. Sarto, "Effective properties of carbon fiber composites: EM modeling versus experimental testing," in *IEEE International Symposium on Electromagnetic Compatibility*, 2007.
- [3] "Technical Information for Carbiso Mil 10 μ Milled Carbon Fibre," 2018. [Online]. Available: <http://www.easycomposites.co.uk>.
- [4] "Technical Information for EPIKOTE Resin MGS LR285." [Online]. Available: 2010 www.swiss-composite.ch/pdf/t-Epoxyd-Harz-L-285-LF-e.pdf.
- [5] Surfacetreat a.s., "Laboratorní zařízení pro plazmové povrchové úpravy," 2019. .
- [6] "INSTEK LCR 821," *Technical Informacion*, 2018. [Online]. Available: <http://www.testequipmentdepot.com/instek/meters/lcr821.htm>.
- [7] D. D. L. Chung, "Electric permittivity of carbon fiber," *Carbon N. Y.*, 2018.

Mechanical Behavior of Natural Fiber Based 3D woven Structural Composites for Automotive applications

Sandeep Olhan, Vikas Khatkar and B K Behera

Focus incubation centre for 3D weaving and structural composites

Department of Textile Technology, Indian Institute of Technology Delhi

sandeepolhan@gmail.com

Abstract: Natural fiber reinforced bio polymers are getting attention due to their biodegradable nature and can be easily recycled. Moreover composites offer incredible advantages over metals in terms of design flexibility, damping and more importantly, high strength-to-weight ratio. Therefore, this work is focused on comparing the mechanical performance of sisal based bio composites for automotive applications. The composites were prepared by reinforcing sisal in form of unidirectional yarns, bidirectional (2D) woven fabric and three dimensional (3D) woven orthogonal fabric in biopolymer. Mechanical behavior was investigated in form of tensile, flexural and Izod/Charpy Impact test. Influence of reinforcement architecture was investigated for a comparable volume fraction for all composites. It was observed that the sisal based bio composite depicts excellent mechanical properties in addition to superior strength-to-weight ratio and can potentially replace the metal counterparts in the today's automobile body panels.

Keywords: Sisal, Bidirectional (2D) woven fabric, 3D woven orthogonal.

1 INTRODUCTION

Concerning the environmental and ecological issues natural fibres have the point of attention for the polymer composite due to their advantage over the glass and carbon fibre composite. The importance of the natural fibre polymer composite is increasing the industrial and human application. Natural fibres have a lot of advantages compare to synthetic fibre such as renewable, cheap, bio-degradable and partially or fully recyclable [1]. Sisal fibre has several advantages in terms of product design flexibility, insulation, noise-absorption and impact resistance. Due to these properties sisal reinforced composite used in building material (like roofing sheets etc.), locomotive (like gear case, main doors etc.), automobile (like German automotive industry, Door panel of E-class Mercedes etc.), aerospace and military (like transportation vehicle, safety equipment etc.) applications [2]. Sisal fibre has the characteristics of ideal substitute of asbestos for brake composites [3].

2 MATERIALS AND METHODS

2.1 Materials

The sisal and epoxy AY-105 were used as reinforcement and matrix respectively. The hardener HY-951 was used as curing agent. In this work the sisal fibre, epoxy and hardener were purchased from local supplier. Epoxy has the viscosity and lap shear at 25 °C, 11345 mPa-s and 12.63 MPa respectively. The density of the neat epoxy was calculated 1.109 g/cm³ at room temperature. The mechanical, physical and chemical properties of sisal fibres are given in table 1.

Table 1 Mechanical, physical and chemical properties of Sisal fibre [4]

Properties	Sisal fibre
Diameter (mm)	1.16
Density (g/cm ³)	1.45
Cellulose (%)	65-78
Hemi-cellulose (%)	10-14
Pectin (%)	10
Lignin (%)	9.9
Wax (%)	2
Elongation at break (%)	4-9
Tensile strength (MPa)	365
Young's Modulus (GPa)	12.25

2.2 Methods

The VARTM process is used for making sisal-epoxy composite. The curing is done under vacuum in room temperature. The final orthogonal fabric which produced with higher fabric FVF is converted into composite by Vacuum Assisted Resin Transfer Molding (VARTM) process. VARTM process is used for this fabric for two major reasons. Firstly, the FVF in composite can be improved by VARTM process, which will again enhance the mechanical performance of composites. Secondly, this process helps for the proper impregnation of the resin throughout the fabric with higher areal density and fabric FVF. LY556 Epoxy resin along with Aradur 22962 hardener with comparatively lesser viscosity is used for the proper flow and the impregnation. The resin to hardener ratio is maintained at 10:1. Proper mixing of resin and hardener is ensured for the proper curing during the process. The curing time is 24 hrs.

3 TESTING OF COMPOSITE

3.1 Tensile Testing of Composites

Tensile testing of composites is performed with Instron Tensile Testing Machine (UTM) using 100 KN load-cell according to ASTM D3039. The sample size is 150mm X 25mm. Gauge length is set at 75 mm. Cross head speed is 2mm/min. Five readings are taken for each sample. Tensile testing is carried out in warp direction for UD, 2D and 3D fabric reinforced composites

3.2 Flexural Testing of Composites

Three-point bending is performed with Instron 3365 using 5 KN load-cell according to the ASTM D 7264. The sample size is 150 mm. The support span is set at 80mm. Cross head speed is 1mm/min. Three readings are taken for each sample. For UD, 2D and 3D fabric reinforced composites, the flexural testing is done warp wise. The span to depth ratio is chosen to be around 32:1.

3.3 Low Velocity Impact Testing of Composites

Impact test of all composites is to be carried out to estimate the amount of impact energy absorbed by each composite. The tests are performed as per the ASTM D 7136. The sample size is 12cm X 12cm and impactor speed is 4.5m/s.



Figure 1. Development of 3D woven sisal fabric.



Figure 2. Development of 3D woven sisal fabric.

4 RESULTS AND DISCUSSION

This research explored the potential of natural fiber waste 3D structural reinforced composite to replace conventional metals in the body panels of an automobile. The results were also compared with the performance of similar 3D structures based composites made from glass tows of identical areal density. The comparison of tensile properties of composites with above reinforcements so that both glass fiber and natural fiber reinforced 3D composite can replace their metallic counterpart. The composites with 3D fabric reinforcement, does not undergo any delamination during loading. The low velocity impact test results of composites show better energy absorption by the composites with 3D fabric reinforcement due to the yarn in the through thickness direction.

5. CONCLUSION

It is encountered from the results that the composites show better results than metals in the weft direction of 3D structures. However there is significant reduction in specific modulus compare to metals.

6. REFERENCES

1. Badrinath R, Senthivelan T. Comparative investigation on mechanical properties of banana and sisal reinforced polymer based composites. *Procedia Materials Science*2014;5:2263-2272.
2. Kalia S, Kaith BS, Kaur I. *Cellulose fibres: bio- and nano-polymer composites*. New Yark: Springer; 2011.
3. Xin X, Xu CG, Qing LF. Friction properties of sisal fibre reinforced resin brake composites. *Wear*2007;262:736–741
4. Sreekumar PA, Joseph K, Unnikrishnan G, Thomas S. A comparative study on mechanical properties of sisal-leaf fibre-reinforced polyester composites prepared by resin transfer and compression moulding techniques. *Composites science and technology*2007;67:453–461.

APPLICATION OF MULTILOBE JOURNAL BEARINGS IN THE DESIGN OF NEEDLE PUNCHING MACHINE

Stanislaw Strzelecki¹, Zdzislaw Czaplicki²

¹ Polish Textile Association, Lodz, Poland: stanislaw.strzelecki@p.lodz.pl

² Polish Textile Association, Lodz, Poland: zczaplicki@wp.pl

Abstract This paper presents the design of high-speed needle punching machine and its journal bearings system, which is dynamically loaded. There is the possibility to use the cylindrical or multilobe journal bearings with pressurized oil supply. Developed code of the numerical computation of journal bearings gives the results in form of bearing characteristics and its journal centre trajectory, which is important in the development of design and monitoring of very reliable journal bearings system.

Keywords: needle punching machine, journal bearings, non-woven textiles

1 INTRODUCTION

Needle punching machines (needle looms) are applied in manufacturing of the wide range of nonwoven materials [1-4]. These machines are "critical" in the textile industry because they are the last machines in the production line processing the raw material. The damage of machine generates great economic losses and high costs of the repair. Main malfunctions during the exploitation of needle punching machines concern the journal bearings of crankshaft and crank-slide node [4].

The reliable design of machine bearings can be reached by the knowledge of dynamic loads [2] that allow the determination of journal centre trajectory, which gives the information on the values of: minimum oil film thickness, maximum oil film pressure and temperature [5, 6]. The dynamic models of the tribological system "journal - oil film - sleeve" mostly concern the rotating machinery such as turbogenerators or compressors but the conditions of operation of needle looms are different than in case of rotating machinery.

This paper considers the application of the journal bearings of needle punching machines that can run at high speeds in the conditions of dynamic loads [6]. An effect of the type of bearing on the journal trajectory was investigated, too. The procedure that allows calculation, analysis of obtained results and design the journal bearings of high performances needle-punching machines was applied. The solution of geometry, Reynolds, energy and viscosity equations allows obtaining the oil film pressure and temperature distributions that are the required for the calculations of journal centre trajectory. Author's programs of bearing calculation allow applying its results to the other commercial programs for obtaining the deformation of bearings [5, 6].

2 GENERAL INFORMATION ON THE MODERN NEEDLE PUNCHING MACHINES

Modern needle punching machines are characterized by the module design. The mechanisms of the driving module of needling bench are placed in one closed housing. The technical data of some machines gives Table 1 and Fig. 1 shows exemplary design solution. There are design solutions of needle punching machines that differ by the layout of the needling zones, number of needling benches, width of machines.



Figure 1 Needle punching machine IN-2 designed and manufactured in Research and Development Centre of Textile Machinery, Lodz, Poland

3 FORCES GENERATING THE LOAD OF NEEDLE PUNCHING MACHINE ELEMENTS

The needle punching machine elements are loaded by the following external forces: inertia of links, technological, friction, gravity and aerodynamic; the inertia forces are the most important [1 -4].

For the reasons of the durability of design, the links masses, i.e. inertia forces are significant. These masses perform rotary or reciprocating motion. The masses in reciprocating motion include the mass of the needle bench, sliders, elements fixing the bench to the sliders, the connecting rod pin and the reduced part of the connecting rod mass.

On the main bearings acts the resultant inertia force of masses being in rotational movement and masses in the plane-back motion. Equation (1) determines the value of this resultant according to [5].

Table 1 Producers of needle punching machines

Producer	Working width m	Way of needle plate mm	Needling frequency Hz
Dilo-RFN	0,6-16	15-60	13,33-58,33
Fehrer-Austria	0,7-16,5	25-90	10-50,83
IN 2, Poland	2,5	60	13,33

$$W = F_p \sqrt{\beta^2 + (1-2\beta)\cos^2 \varphi_s + 2(1-\beta)\lambda c_s + \lambda^2 \cos^2 2\varphi_s} \quad (1)$$

where: m_p - mass in reciprocating motion, r - crank radius, ω - angular velocity of shaft, $F_p = m_p r \omega^2$ force in reciprocating motion, β - balance coefficient of masses in the reciprocating motion, $c_s = \cos \varphi_s \cos 2\varphi_s$, φ_s - angle of shaft rotation, $\lambda = r/l$, l - length of connecting rod.

Equation (1) gives the total inertia force of the first and second order. The direction of non-balanced inertia force is determined from the relation,

$$\tan \psi = \frac{-\beta \sin \varphi_s}{(1-\beta)\cos \varphi_s + \lambda \cos 2\varphi_s} \quad (2)$$

4 JOURNAL CENTRE TRAJECTORY

The journal centre trajectory can be computed from the solution of: geometry, Reynolds, energy, viscosity equations [5, 6].

Equation (3) presents the general equation of the geometry of lubrication gap (Fig. 4) for cylindrical or multilobe journal bearing:

$$\bar{H}(\varphi) = \psi_s + (\psi_s - 1) \cdot \cos(\varphi - \gamma) - \varepsilon \cdot \cos(\varphi - \alpha) \quad (3)$$

where: \bar{H} - dimensionless oil film thickness, ε - relative eccentricity, α - attitude angle, φ - peripheral co-ordinate, ψ_s - pad relative clearance (if $\psi_s=1$ then geometry of cylindrical bearing).

The Reynolds equation applied in calculation of journal centre trajectory has the form [5]:

$$\frac{\partial}{\partial \varphi} \left[\frac{\bar{H}^3}{\bar{\eta}} \frac{\partial \bar{p}}{\partial \varphi} \right] + \left(\frac{D}{L} \right)^2 \frac{\partial}{\partial \bar{z}} \left[\frac{\bar{H}^3}{\bar{\eta}} \frac{\partial \bar{p}}{\partial \bar{z}} \right] = 12S_h \cdot \varepsilon \cdot \cos(\varphi - \alpha) - 6 \cdot \varepsilon (1 - 2S_h \alpha) \sin(\varphi - \alpha) \quad (4)$$

where: D - bearing diameter and length, \bar{H} - dimensionless oil film thickness, \bar{p} - dimensionless oil film pressure, S_h - Strouhal number, \bar{z} - dimensionless axial coordinate, $\bar{\eta}$ - dimensionless viscosity of lubricant.

Equation (4) allows receiving the resultant force \bar{F} of bearing from the computed pressure fields. Equating the oil film force \bar{F} and applied load \bar{W} yields at any instant,

$$\bar{W} = \bar{F} \left(\frac{L}{D}, \varepsilon, \alpha, \dot{\varepsilon}, \dot{\alpha} \right) \quad (5)$$

where: $\dot{\varepsilon}, \dot{\alpha}$ - derivatives of journal eccentricity and attitude angle with respect to time.

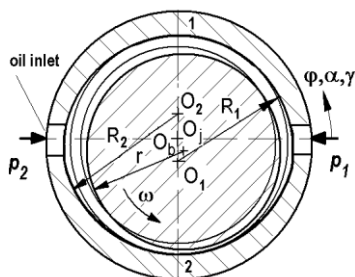


Figure 2 Geometry of 2-lobe journal bearings; a)- 2-lobe bearing; r - journal radius (m), R_b - bush radius (m), R_1, R_2 - radius of upper and bottom lobe, O_b, O_j, O_1, O_2 - centre of bearing, journal, bottom and upper bearing halves, p_1, p_2 - oil supply pressure, α - attitude angle ($^\circ$), γ - angle of lobe centre ($^\circ$), φ - circumferential coordinate ($^\circ$), ω - angular velocity (s^{-1})

5 EXEMPLARY RESULTS OF CALCULATIONS

The calculations were carried out for the cylindrical and 2-pockets cylindrical ($\psi_s=1$) journal bearings with horizontal pressurized oil supply (Fig. 2). Different aspect ratios, bearing relative clearances e.g. $L/D = 0.6$, $\psi = 1.0$ ‰ were used at the journal rotational speed $n = 4000$ rpm. The values of dynamic load were obtained from experimental investigation [1-3] and they were the input data for the calculation of the journal centre trajectory [5].

The run of dynamic load and oil film thickness versus the crank angle that were obtained for the cylindrical journal bearing of needle punching machine presents Fig. 3.

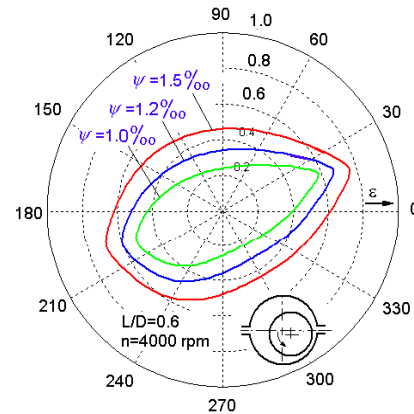


Figure 3 Journal centre trajectory of dynamically loaded 2-lobe journal bearing of needle punching machine for different values of bearing clearance

6 FINAL REMARKS

The application of multilobe journal bearings in the design of the bearing system of needle punching machine should be supported by the calculation of the journal centre trajectories. It gives the basis for the design of reliable dynamically loaded journal bearings. Continuous and durable operation of IN-2 needle punching machine bearings certifies its computed parameters.

7 REFERENCES

- [1] Kapusta H., Strzelecki S., Tribological System of Dynamically Loaded Journal bearings of Needle Punching Machine. *Proc. First Mediterranean Tribology Conference*, 8-9 November 2000. Jerusalem, Israel.
- [2] Kapusta H., Analysis of the Dynamics of a Double-Crank Driving Unit for a Needle Bench. *Fibres and Textiles in Eastern Europe*. No.4. 2002. pp. 83-88.
- [3] Kapusta H., Dynamics of punching and punching elements mechanisms. *Scientific Journal of the Technical University of Lodz*. No. 917, 2002.
- [4] Kapusta H., Diagnostic Simulation Model of Needle Assembly of Needle Punching Machine. *Fibres and Textiles in Eastern Europe*, 2004, No.3. pp. 75-78.
- [5] Strzelecki S., Swiatek J., Dynamically Loaded 2-Lobe Journal Bearing. *TRIBOLOGIA. Finnish Journal of Tribology*, 2004. Vol. 23, pp. 13-22.
- [6] Strzelecki S., Kapusta H., Czaplicki Z., Ruszkowski K., High-speed needle punching machine with cylindrical journal bearings. *FIBERS & TEXTILES in Eastern Europe*. 2009, Vol. 17, No. 4 (75), pp.72-76.

MECHANICS OF 3D WOVEN HONEYCOMB STRUCTURE

LEKHANI TRIPATHI, GHASHYAM NEJE and B . K. BEHERA

Focus incubation centre for 3D weaving and structural composites

Department of Textile Technology, Indian Institute of Technology Delhi

lekhanitri@gmail.com

Abstract: Lightweight engineering is trying to find new solutions to make product lighter but not weaker, at its best even stronger. One solution for lighter products is the usage of cellular structures and materials, which include honeycombs. The hollow spaces reduce weight but also ensure required strength, provided that they were designed correctly. In this study, two honeycomb fabrics are produced with different cell structures by changing the number of picks using 600 tex E-glass tows. All the sections of the structures were plain 2D fabrics with all constituent layers having the same construction. These fabric structures were then converted to composites, with epoxy resin as matrix, using vacuum assisted resin infusion molding (VARIM) technique. The produced composite samples were characterized for their Flatwise compressive properties. This study provides an insight into the production of honeycomb structures connected with woven cross-links, and their load bearing capabilities.

Keywords: 3D Honeycomb, Flatwise Compression, Energy Absorption.

1 INTRODUCTION

Cellular solids such as sandwich panels have been used as advanced materials in aerospace, automobile and marine industries for decades due to their unique combination of properties derived from their cellular structures [1, 2]. Textile reinforced honeycomb composite can be regarded as a kind of cellular solid due to its hollow core structure and as an innovative product, much interests have been drawn on it to find out its mechanical performance under various loading conditions [3,4].

The compressive deformation behavior of honeycomb composite was progressed by an elastic and plastic buckling of cell walls, deboning fracture at the interfaces of cell walls, and followed by a fracture of resin layer on cell walls. The shear deformation of honeycomb composite was progressed by an elastic shear deformation, plastic shear deformation, fracture of resin layer on cell walls, and followed by deboning fracture at core/face sheet interfaces. The shear strength of honeycomb composite showed strong anisotropy dependent on the loading direction. The shear strength in longitudinal direction was about 1.4 times higher compared to that in transversal direction due to the different thickness of cell walls mainly loaded during the shear deformation.

In this study, two honeycomb fabric with different cell structures were manufactured by changing number of picks using same material. All fabric samples were converted to composites and characterized for their Flatwise compressive properties in order to understand their applicability along with their manufacturing possibility.

2 MATERIALS AND METHODS

The 3D woven honeycomb structure were produced using 600 Tex E-glass roving on a customized weaving machine (Fig. 1) specially designed to handle multiple beams and take-up mechanism. The machine is capable of releasing the required length of fabric in the backward direction in synchronization with the pull back of floated

warp beams. The machine is also equipped with 16-shaft electronic dobby, to produce a variety of weave architectures. Epoxy LY556 was used as resin along with Aradur HY951 as hardener to produce composites.



Figure 1 Customized weaving machine equipped with two beams and modified take-up system

3 HONEYCOMB FABRICS AND COMPOSITES

3.1 Weaving of Honeycomb Fabric Preforms

The detailed weaving procedure for each of the Honeycomb structures produced in this study is given in the following sections:

The cross-sectional representation of the Honeycomb fabric is shown in Fig. (2,3); the curved lines represent the warp yarns while dots represent weft yarns. From this cross-sectional representation, a generalized weave design was created. There are number of picks given in bonded (L_b) and free wall length (L_f) and angle is kept same as 60° .

Fabric construction of 10×10 (ends per inch \times picks per inch i.e. EPI \times PPI) and glass tow linear density (600 Tex) in warp and weft were kept same for all the individual fabric layers in the structures. The part of the structure where two or more layers were required to be combined, EPI of that part increased correspondingly but PPI was

kept the same. Arrangement is made for mounting extra beams to supply four warp sheets in existing 2D weaving system. Extra care has been taken during weaving process to control warp tension.

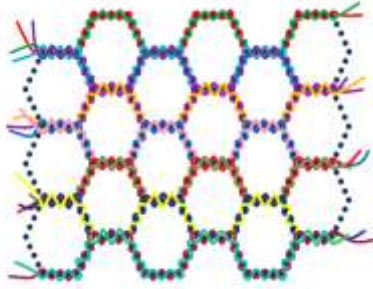


Figure 2. Lb , Lf = 5 picks

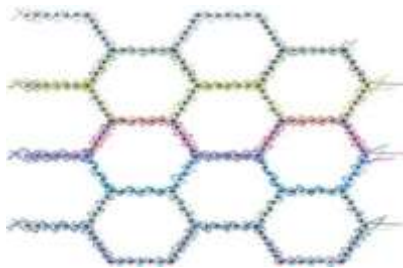


Figure 3. Lb , Lf = 7 picks

3.2 Production of 3D Honeycomb Composites

Wooden blocks of appropriate size and shape were used to keep the fabrics in their 3D shape, and vacuum assisted resin infusion molding technique (VARIM) was used to impregnate the structures with epoxy resin. All the composites were cured at room temperature for 24 h. Figure 4 shows the cured composite samples. Fibre volume fraction is kept 50%. Since all the individual fabric layers in the structures were having same fabric construction, the resulting fibre volume fraction (FVF) was same in warp and weft direction.



Figure.4 (a) 7 PICK and (b) 5 PICK Honeycomb composite

3.3 Characterization for Flatwise Compressive Properties

The composite specimen of required size were cut for compression test depending on the cell size and shape, and were then characterized for their Flatwise compressive properties according to ASTM C365 on

Instron 5982 universal testing machine at loading rate of 2 mm/min (shown in Fig. 5).



Figure.5 Flatwise compression test of Honeycomb composite

4 RESULTS AND DISCUSSION

4.1 Specific Compressive Energy

The size of the specimen was chosen according to the cell size of each structure, so the mass of the specimen was different for different structures. Hence, to compare these structures, the energy absorbed by each structure was normalized using their respective mass and volume.

$$E_w = E/M, \quad E_v = E/V$$

Where E_w and E_v denotes the mass and volume specific energy. M , V are mass and volume of the composite specimen. The results for specific energy are given in the table 1.

Table 1 Specific energy of specimen with different core height

7 pick composite specimen core height	E_w (joule/gm)	E_v (joule/cm ³)
20 MM	4104.59	634.73
30MM	5359.9085	729.195

5 CONCLUSION

3D honeycomb woven structures are produced on a 2D weaving machine by incorporating multi beam arrangement. The values of compressional energy are higher for 30 mm core height as it absorbs more energy as compared to the 20 mm core height sample.

6 REFERENCES

- [1] Torre, L. and Kenny, J.M., Impact testing and simulation of composite sandwich structures for civil transportation, *Composite Structure*, 2000, 50, 257-267
- [2] UK Shin, K.B., Lee, J.Y. and Cho, S.H., An experimental study of low-velocity impact responses of sandwich panels for Korean low floor bus, *Composite Structure*, 2008, 84, 228-240
- [3] Sun, Y. Engineering of 3D textile honeycomb composites for energy absorption, M.Phil thesis, University of Manchester, 2005.
- [4] Tan, X. and Chen, X., Parameters affecting energy absorption and deformation in textile composite cellular structures, *Material & Design*, 2005, 126(5), 424-438.

FASHION CLOTHING WITH ELECTROMAGNETIC RADIATION PROTECTION

Veronika Tunakova¹, Zuzana Hrubosova¹ and Jiri Prochazka²

¹ Technical University of Liberec, Faculty of Textile Engineering, Studentska 2, 46117 LIBEREC,
e-mail: veronika.tunakova@tul.cz

² Sintex, a.s., Moravská 1078, 56002 ČESKÁ TŘEBOVÁ, e-mail: prochazka@sintex.cz

Abstract: Development of lightweight flexible materials for electromagnetic interference shielding has obtained increased attention in recent years particularly for clothing, textiles in-house use and technical applications especially in areas of aircraft, aerospace, automobiles and flexible electronics such as portable electronics and wearable devices. There are many references in the literature concerning development and investigation of electromagnetic shielding lightweight flexible materials especially textile based with different electrically conductive additives. However, only little attention is paid to designing and enhancing the properties of these special fabrics by textile finishing processes. Moreover, offer of fashion for daily use having in addition electromagnetic radiation protection is very limited. The main purpose of this study is firstly to analyze the possibilities of transferring design onto the surface of electrically conductive fabrics by digital printing and to study the effect of surface modification on performance of conductive fabric. Beside this, its durability, more precisely wet processing was studied. Woven fabric made of yarns containing 10 % of extremely thin stainless steel fiber was used as a conductive substrate and garment prototypes made of printed conductive fabric were introduced.

Keywords: electromagnetic shielding, digital printing, garment prototypes

1 INTRODUCTION

Over the last few years, there has been mounting concern about the possibility of adverse health effects resulting from exposure to radiofrequency electromagnetic (EM) fields, such as those emitted by wireless communication devices.

Protective clothing is a major type of personal protective equipment (PPE), defined in European Directive 89/686/EEC [1] as “any device or appliance designed to be worn or held by an individual for protection against one or more health and safety hazards”. Those hazards include mechanical hazards, thermal hazards, water, chemical hazards, biochemical and biological hazards, electrical hazards, electromagnetic wave hazards, acoustic hazards, radioactive hazards and industrial hazards [1]. There are five requirements related to the application of any clothing system: 1) aesthetic properties, 2) functional performance, 3) clothing comfort, 4) mobility, 5) durability, whereas the emphasis for protective clothing is laid on functional performance (protection), thermal comfort and human mobility. As stated in [2], aesthetic properties including fashion, color, and style should be also considered when designing protective clothing for daily use. Price is another important parameter to get clothing with electromagnetic radiation protection to market.

In this study, electrically conductive and electromagnetically shielding woven fabric was modified by digital printing. The work considers the aesthetic possibilities, production opportunities and also effect of surface modification on performance of patterned conductive fabric. Durability of printed conductive fabric represented by washing and drying was also inspected. Woven fabric with twill 2/1 weave made of conductive yarn containing 10 wt% stainless steel staple fibers was used as a substrate. Fashion garment prototypes made of printed conductive fabric were introduced in the end.

2 METHODS

2.1 Hybrid fabric

Metal fiber containing fabric for patterning was created using following hybrid yarns. Hybrid yarns were composed of conventional polyester (PET) fiber (59 wt%) and cotton (CO) fiber (31 wt%). Both nonconductive fibers had white color. As a conductive component staple BEKINOX stainless steel (SS) metal fibers (10 wt%) was used. Hybrid fabric has twill 2/1 weave made of 100 % of conductive yarn (warp sett 39 1/cm, weft sett 22 1/cm). Raw fabric has light grey color due to presence of metal fiber.

2.2 Digital printing

Digital textile printing was chosen because it's low price (approximately 7 €/m) and flexibility (easy to print various colors and detailed designs, small runs of each design). Fabric was printed using following steps: 1) design preparation in RGB color model, 2) substrate pretreatment to increase washing durability and rich colors, 3) during the printing process, the conductive fabric was fed through the printer using rollers and ink was applied to the surface in the form of thousands of tiny droplets. Industrial printer having 8x Ricoh Gen5 typehead with following colors (2x black, light black, cyan, magenta, violet, red, yellow) was used together with pigment ink Elvjet PR 540 supplied by Sensient Switzerland. 4) fabric was finished using heat using infrared oven ($T = 160\text{ }^{\circ}\text{C}$, $t = 3\text{ min.}$) to cure the ink.

2.3 Washing and drying process

Samples were subjected to repeat wet processing (washing and drying). The conventional washing was performed according to EN ISO 6330 standard using Miele Professional W6071. Residual moisture dryer Miele Professional PT 5137 was used for drying. Samples were washed at 40 °C washing temperature, using 3 rinsing steps; 900 RPM spin speed and phosphate-free ECE 98 standard detergent without optical brighteners.

2.4 Electromagnetic shielding effectiveness evaluation

Electromagnetic shielding effectiveness (SE) of irradiated fabrics was measured according to ASTM D 4935-18 for planar materials using a plane-wave, far-field EM wave. SE of samples was measured over frequency range of 30 MHz to 1.5 GHz. results and discussion

2.5 Effect of digital printing on electromagnetic shielding effectiveness

It is visible that both samples embody relatively high ability to shield electromagnetic field. The SE exceeds 30 dB for frequency higher than 1.2 GHz and therefore fabric meets requirements for “excellent” grade according to [3]. It seems that the untreated sample reaches lower values of electromagnetic shielding efficiency throughout the whole frequency band ($SE \sim 31$ dB for $f = 1.5$ GHz), see Fig. 1. It is assumed that this behavior is connected with decrease of porosity of printed sample accompanied by lower penetration of electromagnetic wave through the sample.

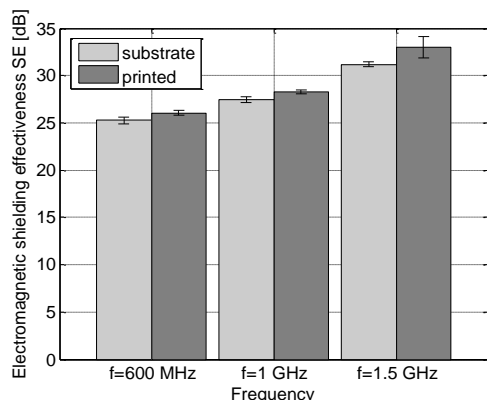


Figure 1 Electromag. shielding of substrate and printed sample

2.6 Effect of washing and drying on electromagnetic shielding effectiveness

It can be observed from the figures that the shielding effectiveness drops after 3 washing and drying cycles of about 2 dB compared to the original SE value of unwashed printed sample. This phenomenon is probably caused by removal of printing ink and unblocking of pore. Dependence of electromagnetic shielding effectiveness on the number of wash cycles can be described using a linear function.

2.7 Fashion clothing with electromagnetic shielding protection

While the performance of traditional protective clothing depends on the structural design of the clothing and the properties of fabric, the latter is essential. On the other hand, clothing for daily use with protective function should

also satisfied current fashion requirements including color, shape, design and style. It is impossible to design electromagnetic radiation clothing with complete protection of human body from electromagnetic radiation, because each aperture (placket, button holes, etc.), openings (collar, lack bottom, hem, etc.) and free spaces (uncovered head) in clothing will cause electromagnetic wave penetration to human body. Nevertheless, recent findings about electromagnetic radiation and human health aim to protect at least body torso where sensitive organs (reproduction system, fetus of pregnant women, etc.) are placed. Prototypes of clothing can be seen in Fig. 2. Skirts were made of printed conductive fabric.



Figure 2 Fashion clothing with electromagnetic radiation protection intended for pregnant women.

3 CONCLUSION

It was found that electrically conductive fabric satisfies requirements on functionality. Its electromagnetic shielding on higher frequencies (working frequencies of cell phones, radars, wireless networks, etc.) is higher than 30 dB which classifies the fabric as “excellent” according to grading published in [3]. Slight increase of electromagnetic shielding ability of printed samples is dedicated to decrease of sample porosity after printing. It has been shown, that washing and drying has not statistically significant effect on electromagnetic shielding effectiveness. Last, but not least, design and preparation of radiofrequency protective clothing for daily use was discussed and prototypes of protective clothes made of printed electrically conductive fabric were sewn and documented.

ACKNOWLEDGEMENT: This work was supported by the research project CZ.01.1.02/0.0/0.0/15_019/0004465 entitled *Extreme shielding textile materials for special applications* granted by the Ministry of Industry and Trade of the Czech Republic.

4 REFERENCES

- [1] MAO, Ningtao. High performance textiles for protective clothing. In: *High performance textiles and their applications*. Sawston: Woodhead Publishing, 2014, p. 91-143, doi: 10.1016/C2013-0-17069-9.
- [2] SHI, Hui, WANG, Jianping, CHEN, Xiaona. Research on electromagnetic shielding clothing. In: *Proceedings of Cross strait quad-regional radio science and wireless technology conference*. Harbin, 2011, doi: 10.1109/CSQRWC.2011.6036923.
- [3] FTTS-FA-003 Specified Requirements of Electromagnetic Shielding Textiles, Tucheng City: Committee for Conformity Assessment of Accreditation and Certification on Functional and Technical Textiles, 2005.

PEDESTRIANS VISIBILITY AT NIGHT: EFFECTS OF PEDESTRIAN CLOTHING, BALANCING SAFETY AND CULTURE

Vik, M.¹, Glombíková, V.², Víková, M.¹, Havelka, A.², Adamcová, J.², Pechová, M.¹

¹ Laboratory Color and Appearance Measurement, Technical University of Liberec, Czech Republic

² Department of Clothing Technology, Technical University of Liberec, Czech Republic
michal.vik@tul.cz

Abstract: This field of study was designed to investigate effects of retroreflector size, shape and production technology on conspicuity of nighttime pedestrians. The subject's task was to compare two different almost inverse design of retroreflector with focus on effectiveness two reflective transfer films and screen-printed version of retroreflector made from glass spheres glued on textile substrate. The subject didn't know location of retroreflective targets on human body. It is shown that simple screen printing of suitable glass spheres gives only 27% of retroreflective factor of retroreflective transfer film system. Effectiveness of retroreflector made from retroreflective transfer film covering only 25% of tested area is comparable with inverse design made by screen printing method covering 86% of whole retroreflector.

Keywords: high-visibility, photometry, colorimetry, retro-reflectance, phosphorescence

1 INTRODUCTION

Pedestrian fatalities are a major road safety issue. In the Czech Republic, 1,133 pedestrians were injured and 21 pedestrians were killed in the year 2016; pedestrian fatalities accounting for 85% of all non-occupant fatalities in that year. One of the basic driver errors responsible for such collisions is believed to be the late detection of other road users. The visibility distance of dark-clad pedestrians is typically less than one-third the stopping distance at normal speed of car [1]. Driving is often described as a visual task and driver licensing regulation appear universally to require screening tests of visual acuity and color vision. We are not aware of any that require a test of night vision. If driving is really mentioned visual task and vision is seriously degraded at night, then one would expect drivers to avoid the task or at least slow down to compensate for their visual impairment [2].

A less expensive approach to enhance the conspicuity of pedestrians involves using retroreflective material that has been engineered to reflect light back in the direction of its source. Some of sportswear use the reflective cloth to cut and splice; some use thin film to transfer and burn, by machine laser cutting graphics, designed and made into different shapes of reflective patterns; some also add light zipper, reflective ribbon, reflective strip, or use reflective wire in local line. Some of the clothes, too, seem to have regular small prints in the daytime, but in fact, it is a simple decoration that turns the whole dress into a shiny silver grey when it is illuminated at night [3].

The pressure sensitive transfer film is bonded to durable fabric. The wide angle and the exposed reflexive glass bead are made up, and the pressure sensitive adhesive is coated on the back of the cloth bottom and can be directly attached to the fabric. Due to this technology is resulting retroreflective pattern relatively rigid. Important property of sportswear beside design and visibility is also comfort of sportsmen. Due to less water vapor permeability retroreflectors are preferred net design of retroreflective sign or its alternatives allowing increasing of permeability via sufficient free space area.

Screen printing technology it is a kind of small reflective glass bead printed ink with the effect of reflection. Due to less amount of adhesive are such retroreflectors more water vapor permeable than reflective sign made with use of retroreflective transfer film.

2 MATERIALS AND METHODS

2.1 Materials

Retroreflective pattern with two almost inverse patterns were made with use of retroreflective transfer film C750 company 3M and retroreflective transfer film WL-RF-1001 company Weallight. Third retroreflector was prepared by screen printing method with use of printing paste TEXTILAC CAT-EYE containing glass beads with diameter less than 50 μm . As supporting textile fabric was used Coolmax Athletic containing 50% of PET and 50% of Coolmax fibres.

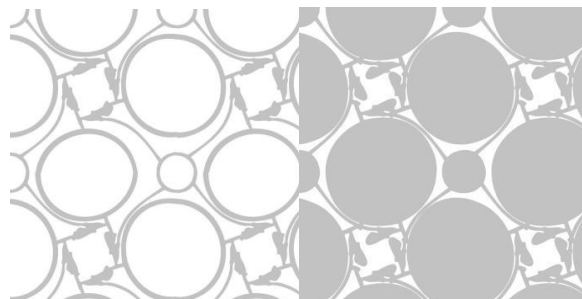


Figure 1 Design of tested retroreflector covering 25% (left) and covering 86% of whole area.

2.2 Methods

The coefficient of retroreflection (RA, in cd/lux/m^2) of tested reflective materials was measured by methods

based on either of the following retroreflective intensity testing procedures:

- ASTM E809-02 and E810-03 (RA)
- CIE 54.2:2001 (R')

with use of head lamp equipped halogen lamp Osram H4, illuminance meter T10 made by Konica-Minolta and spectroradiometer PhotoResearch PR 740.

3 RESULTS AND DISCUSSION

Was found that screen printing was less effective for both design of retroreflector as it is shown on graph in Fig. 2. There is also visible that retroreflective transfer film C750 is slightly more effective than film WL-RF-1001.

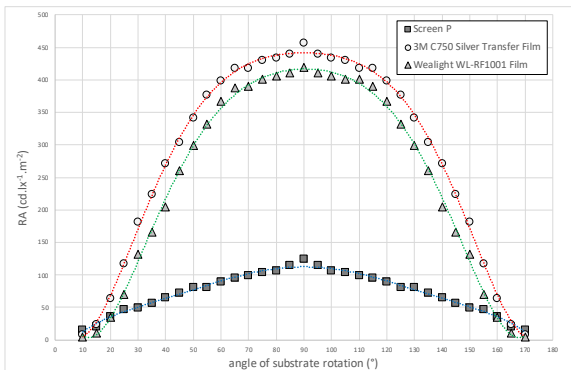


Figure 2 Distribution of coefficient of retroreflection RA of tested samples with 86% pattern coverage

Explanation of this result is present on microscopic images in Fig. 3, where random distribution of glass beads is visible. Beads are partially nested in fabric structure and effective area of retroreflection is reduced by overlapping of these beads.

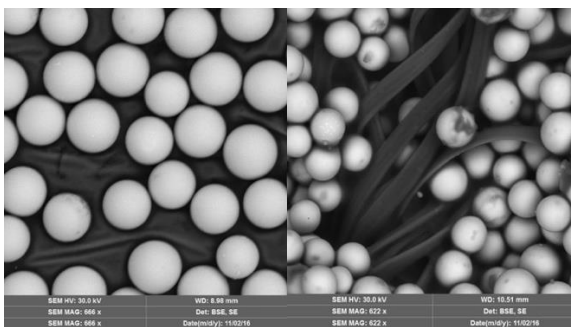


Figure 3 SEM of reflective film 3M C750(left) and screen-printed sample(right).

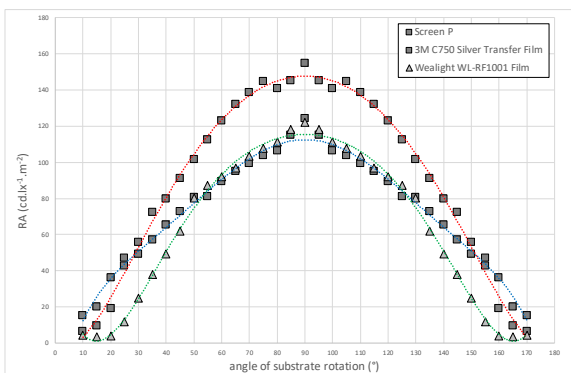


Figure 4 Distribution of coefficient of retroreflection RA of tested samples with 25% pattern coverage

Coefficient of retroreflection, which is shown on graph in Fig. 4 documents that transfer film RA of open design covering 25% of retroreflector area is near to RA of screen-print covering 86% of retroreflector.

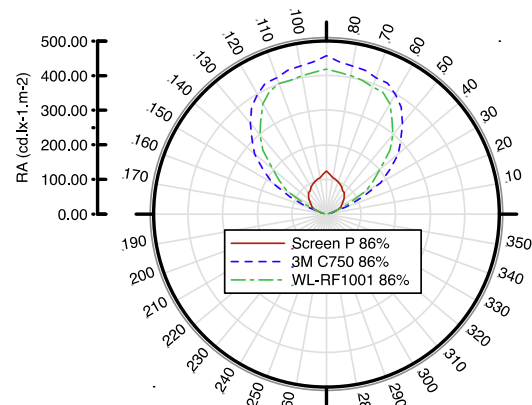


Figure 5 Indicatrix of coefficient of retroreflection of tested samples with 86% pattern coverage

From graph in Fig. 5 it is possible to conclude that the indicatrix of retro-reflected light from tested retroreflectors made from transfer film cover almost 60° angle of sample rotation with sufficient coefficient of retroreflection RA around 400 $\text{cd} \cdot \text{lx}^{-1} \cdot \text{m}^{-2}$. That confirms the expected category of retroreflective transfer film as retroreflectors of high visibility.

4 CONCLUSION

In summary, the outcome of both tested retroreflective transfer film gives a super high visibility category of retroreflectors with 86% covering of whole area. Each such retroreflector yielded significantly longer recognition distance due to super high RA. It was shown that covering 25% with use of transfer film or 86% covering with use of screen-print fulfils high visibility category and screen-printed retroreflector with 25% covering is less usable as a system of enhancement of pedestrian visibility. While it is encouraging to consider the benefits of existing marking - retroreflector systems, the problem of poor visibility in night driving remains serious.

REFERENCES

- [1] Blomberg, R.D., Hale, A., and Preusser, D.F., 1986. Experimental evaluation of alternative conspicuity-enhancement techniques for pedestrians and bicyclist. *Journal of Safety Research*, 17, pp. 1-12.
- [2] Vik, M. et al., 2014. Decay of Phosphorescent Warning Design on Textile Substrates, *Applied Mechanics and Materials* Vol. 440 (2014) pp. 112-117, ISSN: 1662-7482
- [3] Vik, M. et al., 2016. Measuring Techniques for Retroreflectivity Levels of Small Signs. *Defect and Diffusion Forum*, 368, pp. 193-197.

RECONSTRUCTION OF THE INDIVIDUAL FIBERS' TRAJECTORIES IN AIR-JET YARN

Pavlaína Bílá¹, Monika Vyšanská¹

¹Technical University of Liberec, Department of Textile Technology, Liberec, Czech. Republic,
e-mail: pavlina.bila@tul.cz, monika.vysanska@tul.cz

Abstract:

Detailed knowledge of the individual fiber position in yarn is important for the mechanical properties studying. Presented study introduces a methodology for fiber extracting from sequence of planar sections. Small amount of the dyed fibers was added to the raw material during the technological process of the yarn production. Consequently the new yarn was cut to get the sections, which were analysed by optical microscope in order to get the centers of the dyed fibers. The set of identified fiber centers was used for reconstruction of individual fibers' trajectories. The principle of the reconstruction will be presented.

Keywords: reconstruction, fiber trajectory, sequence, air-jet yarn, core, wrapper fibers, migration

1 INTRODUCTION

The mechanical properties of yarns are very important aspect for their use in the final products. These properties are mainly influenced by the internal arrangement of the fibers in the structure of yarns [1]. Air-jet yarn is a beam-type structure that consists of two parts. The first part is a **core**, where the fibers are almost parallel. The second part is created by the **wrapper fibers**, into which the twist is inserted. The position and orientation of these fibers in yarn structure depends on type of the yarn production technology and on the specific settings parameters of the spinning machine [2]. These settings of parameters are followed by the type of materials (e.g. cotton, polyester, wool etc.) and basic characteristic of fibers, which was used [3].

As was mentioned above, the arrangement of the fibers in the structure, their position and orientation are important for the final yarn properties. Changes in these characters can be described by the character which we call the **migration**. This term was first defined by W.E. Morton in 1956 and he used it as a description of the differences of the real fiber curve from the ideal helix model [1].

1.1 Migration of fibers in yarns

The ideal helix model doesn't correspond to reality at all. The yarn that would have been modeled in this way would have to break apart itself, because the inter-fiber forces would be almost zero here. From the real yarn we know that the fibers are intertwined and thanks to this effect a so-called "self-locking" shape is created. This shape thus causes yarn stability and contributes to the generated force effects within the yarn.

We can distinguish two components of migration:

- Radial migration - the fiber has a variable distance r from the yarn axis.
- Twist migration - the fiber has a variable Z-twist at each location.

Because of the importance of migration parameters, this work should be able to create a real model of individual fibers trajectories, on which we could be able measured important characteristics [4].

1.2 Materials and methods

For the experiment in this study was used 100% viscose air-jet yarn (spinning machine J 20 from Rieter CZ s.r.o. Ústí nad Orlicí, 340mm/min and 6bar). The basic yarn and fiber parameters were verified. The measured

value was verified on normality and homogeneity. The verification values are in the table 1.

Table 1 Parameters of yarn and fibers (CV= coefficient of variation)

Property	Value	Verification	
		average	CV [%]
Count of yarn	20 tex	19,72 tex	2,74
Fineness of fibers	1,3 dtex	1,44 dtex	12,15
Length of fibers	40 mm	38,67 mm	6,93

1.3 Preparation of yarn

Therefore, in order to trace individual fibers from the cuts, it is necessary to mark them. For this reason, some of the fibers have been dyed (by dye *Saturn Black A (B5528)*), these fibers should make up about 1.5% of the total number of fibers in the yarn. The dyed fibers were then added to the sliver preparation stage.

1.4 Preparation and Sampling

Samples were taken according to ČSN EN 12751 Textiles. A total of 10 samples were prepared according to internal norm IN 46-108-01 / 01 (cut thickness was 10μm). For the purpose of the experimental method, it was necessary at this stage to add a so-called "guide fiber" (PAD 6.6. monofilament). This guide fiber gives us information about the specific position of cuts.

2 THE METHOD OF RECONSTRUCTION

The first experiments on the spatial shapes of fibers in the yarn were done by Pavlov N.T., Pejsachov V.K. [5], and Pejsachov V.K. [6].

This method consists in creating sequential cuts. In each section, it is necessary to mark the centers of the dyed fibres that symbolize the intersections of the fibrous axes with the cutting plane. Thanks to the sequence of cuts and the position of fiber centers, the trajectory of individual fibers in the yarn can be reconstructed.

The first important step is the orientation of the cuts by the image analysis in the sampling phase. One important point of orientation is the guide fiber that was added to the sample at the sample preparation stage. The guide fiber has to be placed in the **definition frame** by image analysis as it is shown in figure 1. This definition frame, which we used, was located on the first image and his position has to be unchanged for all images of sequence.

Second important point of orientation is location of yarn matter (=mass). The mass of yarn has to be in the centre of image. Therefore, to place the guide fiber in a defined

frame, we need to rotate with camera on microscope. However, we also move the mass of yarn because the guide fiber and the yarn are firmly connected. For this reason, a second orientation point is required. For this location, we chose an image **phase-ring** that gives us the proper position of the cut. The position of the full yarn mass in a single annulus is indicated as the correct position. This position is shown on *figure 2*. The rule for phase-ring is the same as for the definition frame. The phase-ring was located on the first image and it's position has to be unchanged for all images of sequence.

The next phase is the actual measurement on the created sequential images with the correct orientation. In whole sequence of images, we were traced the dyed fibers by accurately tracing their shape. Thus, with the NIS elements software, a file with calculated center positions of the individual fibers is created. The information about centers of guide fiber and dyed fibers are entry to the MATLAB software reconstruction 3D graphs. In the figures 3, we are able to see green line for guide fiber, blue dot-and-dash line for yarn axis and red trajectories of individual reconstructed fibers.

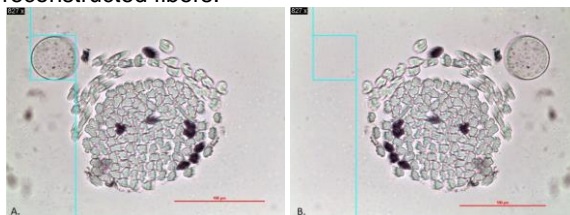


Figure 1 – Example of orientation to definition frame
A. – correct orientation B. – wrong orientation

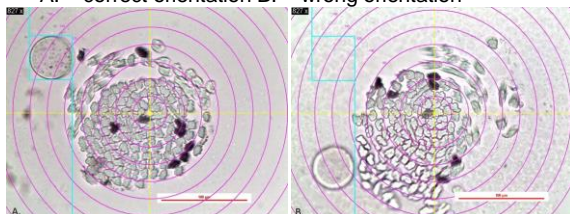


Figure 2 – Example of orientation to phase-ring
A. – correct orientation B. – wrong orientation

With these 3D reconstructions, we can notice the different trajectory of individual fibers in the air-jet yarn. Visually, these fibers can be divided into 4 categories (or groups).

- 1) Full core fibers – fiber 03 in figure 3
- 2) Partly core fibers- this means around 25% length of fiber in wrap and 75% in core (fiber 06 in figure 3)
- 3) Half core/half wrapper fibers – this means 50% length of fiber is in core and 50% in wrap
- 4) Wrapper fibers – this means more than 75% length of fiber is in wrap (fiber 09 in figure 3)

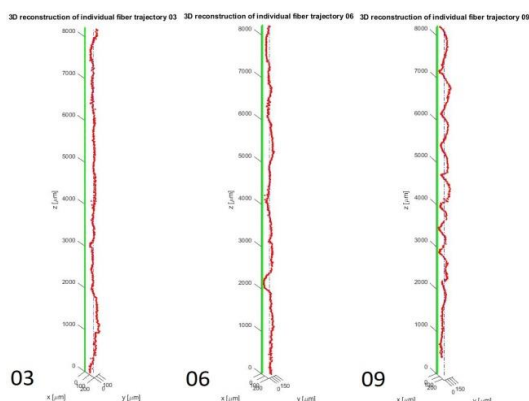
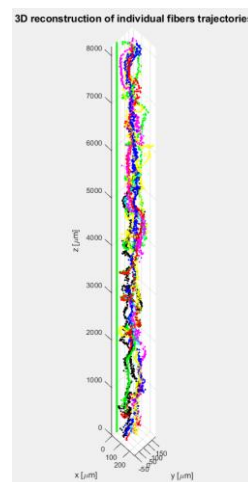


Figure 3- Reconstruction models for fibers 03, 06 and 09

In the figure 4 we can observe the course of the reconstructed fourteen fibers trajectories, which can be divided for individual analysis. By this way was reconstructed 8,21mm of air-jet yarn as can be seen on figures 3 and 4.

Figure 4 (right side) - Reconstruction model of 14 fibers in MATLAB software ->



Acknowledgement: Thanks for the support belongs to the Rieter s.r.o. Ústí nad Orlicí for the provided material for the experiment and Department of Textile Technology (FT TUL) for providing test instruments. And finally thanks belong to the Student Grant Competition Technical University of Liberec no. 4240-21305 granted by Ministry of Education, Youth and Sports of Czech Republic.

3 CONCLUSION

In this study, a method for the reconstruction of the trajectory of individual fibers in the air-jet yarn (by RIETER s.r.o.) was presented. Thanks to this method of reconstruction, we get some (better) information of the internal arrangement of individual fibers in the air-jet yarn, whose complete structure analysis is normally very problematic [1],[5].

In the future we would like to create better m-files for reconstruction in Matlab software with some correction factors to create an even more accurate reconstruction models.

The mentioned categories of fibers trajectories in air-jet yarn were defined just on the visual base of reconstructed fibers. Next step in future will be precisely measuring of percentile count of points (centres of fibers) in 2 sets. s With this method of reconstruction individual fibers trajectories, we will be able measure the internal structural parameters such as fiber directional angles to the yarn axis, but also the parameters of the fiber migration properties in air-jet yarns, which will be point of interest to further studies [2],[4].

4 REFERENCES

- [1] MORTON W.E.: The arrangements of fibers in single yarns. *Textile research journal* 1956, vol.26 (5), pp. 325-331.
- [2] ZHUANYONG Z., LONGDI CH., et al.: Investigation of fiber trajectory affected by some parameter variables in vortex spun yarn. *Textile research journal* 2015, vol. 85 (2), pp. 180-187.
- [3] BASAL B., OXENHAM W., Effects of some process parameters on the structure and properties of Vortex spun yarn. *Textile research journal* 2006, vol. 76(6), pp. 492-499.
- [4] NECKÁŘ B., DAS. D., Theory of structure and mechanics of yarns. *Woodhead publishing India Pvt. Ltd. New Delhi* 2018, ISBN: 978-93-85059-40-7
- [5] PAVLOV N.T., PEJSACHOV V.K., Těkst. Prom. 1976, no 9-10, pp. 17
- [6] PEJSACHOV V.K., Struktura chlopčatobumažnoj prjaži. [candidate dissertation], Mosk. Text. Inst., Moskva 1947

ELECTRICAL HEATING PROPERTIES OF CARBON FABRIC/GREEN EPOXY COMPOSITES FILLED WITH FLY ASH

Yuanfeng Wang, Daniel Karthik, Kai Yang, Tao Yang, Xiaoman Xiong, Vijay Baheti and Jiří Militký

Department of Material Engineering, Technical University of Liberec, Studentská 1402/2, Liberec 1, 461 17 Czech Republic, email: yuanfeng.wang@tul.cz

Abstract: The joule heating behavior and electrical property of the carbon fabric/green epoxy composite laminates filled with various concentrations of unmilled fly ash and milled fly ash were investigated in present work. The infrared camera was used to record the change in surface temperature of composites over a period of time (i.e. from 0 to 240 sec) by varying the voltage from 0 to 10 V. The results show that composite containing 0.5% fly ash exhibited the maximum temperature under different applied voltages. The maximum temperatures of epoxy/carbon composites could be finely tuned by controlling the concentrations fly ash fillers as well as the applied voltage. When a certain voltage was applied to the composite, the surface temperature of composite reached the maximum and became stable at time shorter than 120 s. In addition, the milled fly ash filled epoxy/carbon composites were found to reveal improvement in electrical heating performance and structural stability over unmilled fly ash filled composites.

Keywords: Ohmic heating, Fly ash, Green epoxy, Carbon fabric, Composite laminates

1 INTRODUCTION

Epoxy/ carbon composite is one of the typical examples of such Ohmic heating composites [1,2]. Epoxy resins as organic have high strength, good stiffness, good thermal stability, excellent heat, moisture and chemical resistance. However, epoxy resin shows poor performance in structural stability under heating conditions due to its limited mechanical properties, shrinkage ratio and acclimatization [3]. To overcome these problems, various fillers are introduced into the resins during processing in previous studies [4,5]. Fly ash is the residue from combustion of pulverized coal in thermal power stations. It has been shown, that fly ash filler provides enhancement of the mechanical properties of composites, especially for highly packed systems [6]. Thermal conductivity can also be improved through the addition of greater amounts of the filler into composites based on epoxy resin [7]. In present study, carbon fabric/ green epoxy composites containing various concentrations of milled and unmilled fly ash filler were fabricated by hand layup and cure technique. Ohmic heating and property of the composite films were characterized using multi-ohmmeter and infrared camera.

2 EXPERIMENTAL

2.1 Materials

Fly ash was obtained from the city of Plzeň located in the Czech Republic with the help of SILO Transport organization. TELALIT 0600 were supplied by Spolchemie, Czech Republic.

2.2 Preparation of composites

The composite samples were prepared by hand layup technique taking fabric to epoxy weight ratio of 50:50. However, when 0.5, 1, and 3 wt% fly ash fillers were added, weight fraction of epoxy resin was reduced but fabric weight fraction was fixed at 50 %.

2.3 Ohmic heating

The heating behavior of composite samples was characterized using an electrical power supply and infrared camera (FLIR-E6390, FLIR SWEDEN).

3 RESULT AND DISCUSS

The temperature– voltage (T–V) curves of the composite samples FA and UFA are represented in Fig. 1 (a) and (b), respectively. From the (T–V) curves, it is the temperature for the 0.5% FA and 0.5% UFA composites is obviously higher than those of other two composites when the same voltage is supplied.

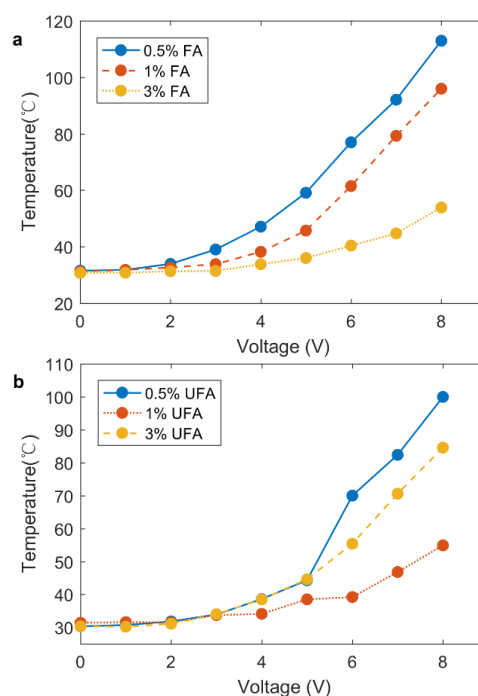


Figure 1 Example of a figure caption

The time-dependent temperature changes under constant voltage were shown in Fig.2. It is clear that the magnitude of maximum temperature for the 0.5% FA and UFA composites are higher than the other two composites, the 1% and 3% composites, under the same applied voltage.

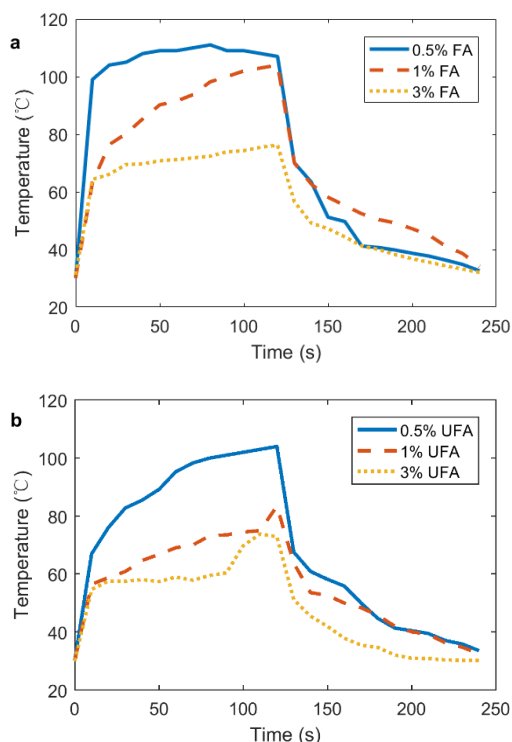


Figure 2 Time-dependent temperature changes of composite FA (a) and UFA(b).

To pursue more detailed analysis for the characteristic thermal properties we introduce three parameters, characteristic growth time constant τ_g , efficiency of heat transfer $hr+c$ and characteristic decay time constant τ_d [8]. At the first section, the temperature growth with time can be empirically expressed as:

$$\frac{T_t - T_0}{T_m - T_0} = 1 - e^{(-t/\tau_g)} \quad (1)$$

At the second region in equilibrium, the heat transferred by radiation and convection, $hr+c$, is thus expressed as:

$$h_{r+c} = \frac{I_c V_0}{T_m - T_0} \quad (2)$$

At the third region, the temperature decreases with time can be described by the following empirical formula:

$$\frac{T_t - T_0}{T_m - T_0} = e^{(-t/\tau_d)} \quad (3)$$

Table 3 Characteristic parameters (τ_g , h_{r+c} , and τ_d) for electric heating performance of composites with different concentrations of FA and UFA under applied voltages.

Samples	τ_g [S]	$hr+c$ [mW/°C]	τ_d [S]
0.5% FA	8.31±3.15	18.79	103.67±34.177
1% FA	21.21±4.88	22.73	139.90±32.25
3% FA	12.22±4.24	8.89	115.12±44.56
0.5% UFA	19.70±4.84	14.09	121.79±34.99
1% UFA	25.15±10.12	19.55	144.25±53.76
3% UFA	20.83±9.17	21.91	73.67±32.81

4 CONCLUSION

Various concentrations of milled nanoparticles were incorporated into epoxy matrix and the mixture was applied in between each layer of carbon fabric to prepare three layered laminated composite. The maximum temperatures of epoxy/carbon composites could be finely tuned by controlling the concentrations fly ash fillers as well as the applied electric power. When a certain voltage was applied to the composite, the surface temperature of composite reached the maximum and became stable at time shorter than 120 s. Overall, it is highly conjectured that epoxy/ carbon/ fly ash composites, which were quick heating and wide adjustability of temperature with the thermally stable up to 110 °C, can be widely used in various fields.

ACKNOWLEDGEMENT: This work was supported by the student grant competition 21310 at Technical University of Liberec.

5 REFERENCES

- [1] Alian A R, Kundalwal S I, Meguid S A. Multiscale modeling of carbon nanotube epoxy composites. *Polymer*: 2015; 70: 149-160.
- [2] Ray B C. Temperature effect during humid ageing on interfaces of glass and carbon fibers reinforced epoxy composites. *Journal of colloid and interface science*: 2006; 298(1): 111-117.
- [3] Huang F, Liu Y, Zhang X, et al. Effect of elastomeric nanoparticles on toughness and heat resistance of epoxy resins. *Macromolecular rapid communications*: 2002; 23(13): 786-790.
- [4] Ramakrishna H V, Priya S P, Rai S K. Utilization of flyash as filler for polybutyleneterephthalate - toughened epoxy resin. *Polymer Engineering & Science*: 2006; 46(7): 946-953.
- [5] Chaowasakoo T, Sombatsompop N. Mechanical and morphological properties of fly ash/epoxy composites using conventional thermal and microwave curing methods. *Composites Science and Technology*: 2007; 67(11-12): 2282-2291.
- [6] Sroka J, Rybak A, Sekula R, et al. Two-Step procedure of fly ash modification as an alternative method for creation of functional composite. *Journal of Polymers and the Environment*: 2017; 25(4): 1342-1347.
- [7] Dorigato A, Sebastiani M, Pegoretti A, et al. Effect of silica nanoparticles on the mechanical performances of poly (lactic acid). *Journal of Polymers and the Environment*: 2012; 20(3): 713-725.
- [8] El-Tantawy F, Kamada K, Ohnabe H. In situ network structure, electrical and thermal properties of conductive epoxy resin–carbon black composites for electrical heater applications. *Materials Letters*: 2002; 56(1-2): 112-126.

THERMAL PROTECTION PROPERTIES OF AEROGEL-COATED KEVLAR WOVEN FABRICS

Xiaoman Xiong, Mohanapriya Venkataraman, Tao Yang, Rajesh Mishra, and Jiri Militky

Department of Material Engineering, Faculty of Textile Engineering, Technical University of Liberec, Liberec 46117, Czech Republic, e-mail: xiaoman.xiong@tul.cz

Abstract: This paper investigated the thermal properties of aerogel-coated Kevlar fabrics under both the ambient temperature and high temperature with laser radiation. It is found that the aerogels combined with a Kevlar fabric contribute to a higher thermal insulation value. Under laser radiation with high temperature, the aerogel content plays a vital role on the surface temperature of the fabrics. At laser radiations with pixel time 330 μ s, the surface temperatures of the aerogel coated Kevlar fabrics are 400-440°C lower than that of the uncoated fabric. Results also show that the fabric temperature is directly proportional to pixel time. It can be concluded that the Kevlar fabrics coated with silica aerogel provides better thermal protection under high temperature.

Keywords: Kevlar, aerogel, thermal, laser

1 INTRODUCTION

Aramid fiber has the advantage of lower density, lower thermal conductivity and higher mechanical strength with flexibility, which makes it the first choice for an ever-growing number of applications where a reduction of weight, increase in strength and resistance to corrosion provide significant improvements in safety and efficiency [1]. The decomposition temperature of aramid fibers in air reaches up to 450 °C which is much higher than that of other organic fibers [2]. High-performance fabrics and composites made of aramid fibers are used in Military body armor, firemen's uniforms, protective clothing and motorcyclist's suits. Thermal behavior analysis of these materials under a severe environment, is important.

As highly porous open cell solid materials that features extremely low thermal conductivities, silica aerogels have well been acknowledged as one of the most attracting thermal insulating materials [3]. Aerogels are commonly used to incorporate with fibers or textile structure to achieve improved thermal performance of the overall structure [4]. It can be inferred that the silica aerogel embedded aramid fabrics would be suitable for some higher temperature insulation rather than the ambient temperature only.

In this paper, Kevlar woven fabric coated with aerogel particles were fabricated. Thermal properties of the prepared fabrics under ambient temperature were evaluated by a thermal camera. Thermal protection under high temperature up to several hundred degree were determined with a laser system and thermometer.

2 EXPERIMENT

2.1 Materials

Plain woven fabric of Kevlar 29 with 5.7 ends/cm and 10 picks/cm was selected. The fabric has an areal density of 265.80 g/m² and a thickness of 0.562 mm. Silica aerogel granules of particle size 0.1 to 0.7mm (average pore diameter of 20nm) was sourced from Cabot Corporation and used as received. Thermosetting resin ZA 13 Mould 45 purchased from Zhermack SpA was used as coating paste. The ZA 13 MOULD WT 45 is a bi-component addition type room temperature curing silicone rubber, comprising a putty component and a catalyst component.

2.2 Fabrication of aerogel-coated Kevlar fabrics

The two components of the resin were mixed with a ratio of 1:1 and stirred at 23°C to form a homogeneous mixture. The aerogel particles were added into the as-prepared resin with continuous stirring. The mixture was stirred with a high-speed stirrer to prevent the aggregation of aerogel particles. The Kevlar fabric was coated with the prepared aerogel/resin mixture on one side and then placed at 23°C for 8 hours to allow thermal setting. After that, it was cured at 120°C. Kevlar fabrics coated with different content of aerogel particles were prepared in order to investigate the effect of aerogel content on thermal performance. In addition, one piece of Kevlar fabric coated with fly ash nanoparticles and another one coated with both the fly-ash and aerogel particles were prepared, dried and finally cured.

2.3 Infrared thermography

Infrared thermography measurement was conducted by using a thermal camera. A vertical hot plate maintained at constant temperature was used as heat source, the specimen was flatly attached onto the hot plate with the help of a frame tool, thermal images were taken by thermal camera at a selected distance from the hot plate. The room temperature was kept at 23± 2°C. A thermal image reveals the amount of radiation emitted by the heat plate through the fabric. The thermal insulation value, I , can be calculated via the following equation

$$I = \frac{T_{hot\ plate} - T_{fabric}}{T_{hot\ plate} - T_{air}} \quad (1)$$

where $T_{hot\ plate}$ is the hot plate temperature (°C), T_{fabric} is the fabric surface temperature (°C), T_{air} is the room temperature (°C).

2.4 Laser radiation

A commercial pulsed CO₂ laser (MARCATEX 150 FLEXI, EasyLaser) was used to perform the measurement with laser radiation. The laser system provides a laser beam which interacts with fibers by thermal processing including solid heating, melting, evaporation, and high temperature

combustion [5]. The sample to be tested was placed in the testing cabinet with the coated surface facing to the laser beam. A 5cm by 5cm square opening located in the bottom body of the testing cabinet gives access to the measurements of surface temperature from the backside of the fabric. An IR thermometer connected to the Optris software was fixed under the cabinet to record the fabric temperature through the opening.

3 RESULTS

According to the thermography, thermal insulation values of different fabrics are compared in Figure 1. Results further confirmed that the aerogel plays a role in improving thermal insulation at low temperature.

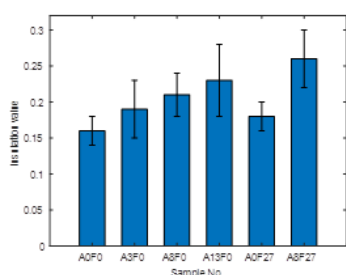


Figure 1 Comparison of thermal insulation values from different fabrics

Figure 2 shows the maximum temperatures of the Kevlar fabric and aerogel coated fabrics on the back surface under thermal radiation. The coated Kevlar fabrics show much lower temperature in comparison with the uncoated Kevlar fabric. Especially at laser radiations with pixel time 330 μ s, the surface temperatures of the coated fabrics are 400-440°C lower than that of the uncoated fabric. The fly ash nanoparticles demonstrate insignificant effect on thermal protection under high temperature. Meanwhile, all the Kevlar fabric and coated fabrics exhibit increased back-surface temperature as the pixel time increases. The linear fittings for the samples found that the correlation coefficients are all above 0.90, meaning that the temperature from back side of the fabrics are directly proportional to the pixel time.

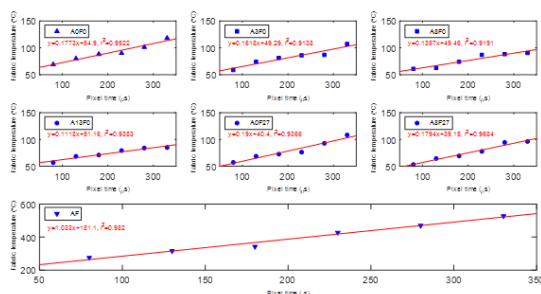


Figure 2 Effect of pixel time on fabric temperature

Figure 3 shows clearly the effect of aerogel content on surface temperature of different fabrics under laser radiation. The temperature of the coated Kevlar fabric decreases with the increase in aerogel content, and this trend becomes more obvious when the pixel time for laser radiation is increased. The analysis of linear fit model found that the temperature of the coated Kevlar fabric decreases linearly with the increase in aerogel content. It can be concluded that the Kevlar fabrics coated with silica aerogel provides better thermal protection under high temperature.

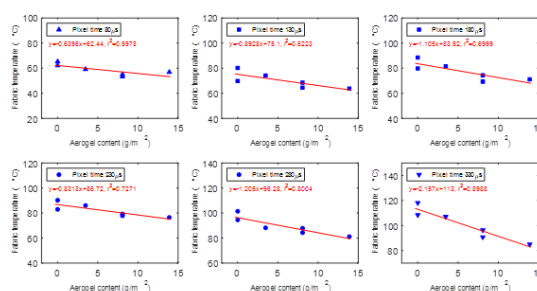


Figure 3 Dependence of fabric temperature on aerogel content

4 CONCLUSION

Kevlar woven fabric coated with aerogel particles were fabricated to evaluate thermal protection properties under both ambient temperature and high temperature up to several hundred degrees. The content of aerogel plays a vital role on the surface temperature of the fabrics under laser radiation with high temperature. A better protection from the laser radiations is achieved by increasing the aerogel content. At laser radiations with pixel time 330 μ s, the surface temperatures of the aerogel coated Kevlar fabrics are 400-440°C lower than that of the uncoated fabric. Moreover, the temperature from back side of the fabrics are directly proportional to pixel time. It can be concluded that the Kevlar fabrics coated with silica aerogel provides better thermal protection under high temperature.

Acknowledgement: This work was supported by the Ministry of Education, Youth and Sports of the Czech Republic and the European Union – European Structural and Investment Funds in the frames of Operational Program Research, Development and Education – project Hybrid Materials for Hierarchical Structures (HyHi, Reg. No. CZ.02.1.01/0.0/0.0/16_019/0000843), project “Modular platform for autonomous chassis of specialized electric vehicles for freight and equipment transportation”, Reg. No. CZ.02.1.01/0.0/0.0/16_025/0007293.

5 REFERENCES

- [1] Kabir R.B., Ferdous N.: Kevlar-the super tough fiber. *International Journal of Textile Science* 2012,1(6), pp. 78-83.
- [2] Li Z., Gong L., Cheng X.: Flexible silica aerogel composites strengthened with aramid fibers and their thermal behaviour. *Materials & Design* 2016, 99, pp. 349-355.
- [3] Hoseini A., McCague C., Andisheh T. M., Bahrami M.: Aerogel blankets: From mathematical modeling to material characterization and experimental analysis. *International Journal of Heat and Mass Transfer* 2016, 93, pp.1124-1131.
- [4] Sanz P.D., Sanz A.D., Bedoya F.C., Flatt R.J. and López A.S.: Anhydrite/aerogel composites for thermal insulation. *Materials and Structures* 2016, 49(9), pp. 3647-3661.
- [5] Sulaiman F.A., Yilbas B.S., Karakas F.C., Ahsan M., Mokheimer E.M.A.: Laser hole cutting in Kevlar: modeling and quality assessment. *The International Journal of Advanced Manufacturing Technology* 2008, 38, pp. 1125.

EFFECT OF FIBER SIZE ON FILTRATION PERFORMANCE OF NONWOVEN SYNTHETIC FILTER MEDIA FOR ENGINE INTAKE AIR

Shivendra Yadav¹, Dipayan Das²

¹Shivendra Yadav, Indian Institute of Technology Delhi, Hauz Khas, New Delhi, e-mail: shivender.iitd@gmail.com

²Dipayan Das, Indian Institute of Technology Delhi, Hauz Khas New Delhi, e-mail: dipayan@textile.iitd.ac.in

Abstract: In this work, a series of needle-punched nonwoven filter media was prepared by using polypropylene fibres of three different size (2.5 denier, 6 denier, 15 denier) in accordance with a three-component augmented simplex lattice design. The experimental data of initial filtration efficiency, final filtration efficiency, pressure drop and dust holding capacity were analysed by means of response surface methodology. Statistical model equations were developed for initial filtration efficiency, final filtration efficiency, pressure drop and dust holding capacity by using Design-Expert® software. The filtration efficiency, pressure drop and dust holding capacity were expressed as linear functions of proportion of fibres of different size. Statistical checks (ANOVA, R² and p-value) indicated that these models were adequate for representing the Experimental data. By means of contour plots, the effect of filter constituents on filtration performance was analysed. In case of different fibre size, the filter media consisting of the 2.5 denier exhibited highest filtration efficiency but at the cost of highest pressure drop and lowest dust holding capacity. On the other hand, the filter media consisting of 15 denier exhibited lower pressure drop and highest dust holding capacity but at the cost of lowest filtration efficiency

Keywords: Needle-punched Nonwovens, Filtration efficiency, Pressure Drop, Dust Holding Capacity

1 Introduction

The modern automotive engine intake air filter media are expected to comply with the filtration performance as laid down in the following relevant specifications under all operating conditions. 1) Filtration efficiency should be greater than or equal to the minimum specified efficiency. 2) The pressure drop should be less than or equal to the terminal or maximum acceptable pressure drop. 3) The dust holding capacity should be very high for greater service life. In keeping view with this, three types of filter media are mostly used nowadays - foam filter media, paper filter media, and nonwoven filter media. Each of these media has its own limitations with respect to the manufacturing processes, structure-property relationship, and operating conditions, which are known to affect their filtration performance. While the foam filter media offer low filtration efficiency, low pressure drop, and high dust holding capacity, the paper filter media offer moderate filtration efficiency, high pressure drop, and low dust holding capacity. On the other hand, the nonwoven filter media offer high filtration efficiency, moderate pressure drop, and moderate dust holding capacity. Of the three filter media, the nonwoven filter media are comparatively "young" in engine intake air filtration. As forecasted by Mueller et al. (2016), the nonwoven air filter media would evolve significantly in engine intake air filtration within the next decade.

2 Material and Method

2.1 Materials

In this work, we used polypropylene fibers of three different cross-sectional sizes. All the fibers have the same length (51 mm). The three polypropylene fibers have the same cross-sectional shape (round), but they

vary in terms of diameter (19.7 μm , 30.5 μm , and 48.3 μm).

2.2 Methods

The three polypropylene fibers of different size were mixed homogeneously in different weight proportions to prepare a set of nonwoven filter media by employing needle punching nonwoven technology. A three-component augmented simplex lattice design was followed for preparation of this set of nonwoven filter media. While needle punching, the punch density was kept constant at 250 punches/cm² and the depth of needle penetration was maintained constant at 10 mm. The nominal basis weight and thickness of the nonwoven filter media was kept at 300 g/m² and 3 mm, respectively.

The nonwoven air filter media were tested for their basis weight, thickness, pore size, and filtration properties. The basis weight was determined in accordance with ASTM D 6242-98 standard and the thickness was determined in accordance with ASTM D 5729-97 standard. The pore size was measured in accordance with ASTM F316 standard. Further, the nonwoven filter media were tested for filtration efficiency, pressure drop, and dust holding capacity, following internationally accepted standards: ISO 5011

3 Results and Discussion

In order to investigate the effect of fiber size on filtration efficiency, pressure drop, and dust holding capacity, a set of ten needle-punched nonwoven air filter media was prepared by mixing circular polypropylene fibers of three different levels of fineness (2.5 denier, 6 denier, and 15 denier) in different weight proportions. Thus prepared

nonwoven air filter media were tested for their basis weight, thickness, and filtration properties. Table 3.1 displays the experimental results of ten needle-punched nonwoven air filter media. It can be seen that the basis weight and thickness of all the ten media were practically constants. It can be observed that the nonwoven air filter media prepared with 100% smallest fiber (2.5-denier fineness) registered the highest filtration efficiency, highest pressure drop, and lowest dust holding capacity. On the other hand, the nonwoven air filter media prepared with 100% largest fiber (15-denier fineness) registered the lowest filtration efficiency, lowest pressure drop, and highest dust holding capacity. As the fiber size increased, the filtration efficiency reduced, but the pressure drop also

reduced and the dust holding capacity increased. The experimental data were compared to those desired by the OEMs. As known, the OEMs desire higher initial and final filtration efficiency lower the pressure drop and higher dust holding capacity for better field performance of nonwoven filter media. It was observed that none of the ten needle-punched nonwoven filter media could meet the filtration efficiency, pressure drop and dust holding capacity simultaneously as desired by the OEMs. We were tried to design and develop the optimal filter media with the help of Design-Expert® software. The predicted response was found in close agreement with the experimental data.

Table 3.1 Experimental results of needle-punched nonwoven filter media prepared with fibers of different sizes

Weight proportions of fibers in nonwoven air filter media			Average fiber diameter (μm)	Basis weight (g/m ²)	Thickness (mm)	Initial filtration efficiency (%)	Final filtration efficiency (%)	Pressure drop (mm aqua)	Dust holding capacity (g)
2.5 denier	6 denier	15 denier							
1	0	0	19.7	294.29	3.43	98.84	99.62	10.73	7.10
0	1	0	30.5	298.33	3.47	96.76	98.32	4.33	12.30
0	0	1	48.3	305.27	3.64	93.55	96.12	1.63	25.00
½	½	0	23.4	294.34	3.44	98.04	98.92	6.95	7.70
½	0	1/2	25.8	296.04	3.45	97.64	98.91	6.52	8.80
0	½	1/2	36.5	303.00	3.57	95.54	97.58	3.12	16.40
2/3	1/6	1/6	22.6	294.17	3.44	98.09	98.98	7.45	7.60
1/6	2/3	1/6	28.7	297.67	3.47	97.02	98.38	5.04	11.30
1/6	1/6	2/3	33.3	301.47	3.55	95.62	97.66	3.25	13.70
1/3	1/3	1/3	27.0	296.86	3.45	97.22	98.48	5.19	10.40

4 Conclusions

The nonwoven filter media consisting of 2.5 denier fibres exhibited highest filtration efficiency but highest pressure drop and lowest dust holding capacity too. On the other hand, the filter media consisting of 15 denier fibres showed lowest pressure drop and highest dust holding capacity but lowest filtration efficiency. As a compromise for simultaneously achieving maximum filtration efficiency of 97.78%, minimum pressure drop of 3.59 Pa and maximum dust holding capacity of 14.4 g, the optimum fiber mixture was predicted to consist of 79% 6-denier fibres and 21% 15-denier fibres. The predicted filtration performance was found in close agreement with the experimental data.

5 References

- [1] Das, D., Pradhan, A. K., Chattopadhyay, R. and Singh, S., N. (2012a), Mixed fibrous filter media for separation of most penetrating particles, *Journal of Environmental Research and Development*, 7, 146-152.
- [2] Mueller, T., Batt, T., Heim, M., Pelz, G.-M., Klein, G. (2016), Technology change towards fully synthetic air filter elements in engine air filtration, *Proceedings of 16th Internationales Stuttgarter Symposium*, Germany.

PREPARATION OF COATED POLYAMIDE NANOFIBROUS MEMBRANES WITH PHASE CHANGE MATERIAL

Kai Yang¹, Mohanapriya Venkataraman¹, Yuanfeng Wang¹, Jakub Weiner¹, Jiri Militky¹, Rajesh Mishra¹, Guocheng Zhu², Juming Yao²

¹ Faculty of Textile Engineering, Department of Material Engineering, Technical University of Liberec, Liberec 46117, Czech Republic, e-mail: kai.yang@tul.cz

² College of materials and textiles, Zhejiang Sci-tech University, Xiasha Education Park, P.R. China, e-mail: zgc100100@hotmail.com

Abstract: In this study, phase change materials were prepared and coated on the nanofibrous membranes. A PCM is a substance which can store and release large amounts of energy, typically in the form of heat. Polyethylene glycol 1500 (PEG) was used as phase change material and polyamide (PA) nanofibrous membranes were used as supporting materials. PEG powders were dissolved in water and the solution was evenly applied to the surface of PA nanofibrous membranes with different ratios of the weight of the weight of applied PEG to PA6 nanofibrous membrane. DSC was used to test thermal properties of PA nanofibrous membrane coated with PEG. The results revealed the enthalpy increased with higher ratio of the weight of applied PEG to PA nanofibrous membrane with no difference between the melting temperatures of all the coated PA nanofibrous membranes.

Keywords: polyethylene glycol, polyamide nanofibrous membrane, thermal properties, coating

1 INTRODUCTION

Phase change materials (PCMs) as a group of substances which can intrinsically absorb or release latent heat energy at a certain temperature during melting or solidification process respectively, have attracted more and more attention from researchers to be used various application[1]. To enhance their thermal storage and thermal conductivity, nano-size materials are used to modify PCMs[2]. However, the effect of nanofiber on thermal behavior of PCMs is not clear now. Polyethylene glycol, as one kind of PCMs has stable thermal properties, high latent heat of fusion and non-corrosiveness to other materials, has been applied in various application as well including textile, building, solar energy storage and so on[3-4]. Besides, polyamide nano fibers with controlled diameter have been proved to be prepared via electrospinning[5]. Better to know the effect of nanofibers as fillers on thermal behavior of PCM, polyamide fibrous membranes coated with PEG are aimed to be prepared and thermal behavior is to be shown.

2 EXPERIMENTAL

2.1 Materials

Polyethylene glycol 1500 powders (PEG 1500) were purchased from Aldrich and were used without further purification during the experiments. Besides, polyamide 6 nanofibrous membrane was provided by Institute for Nanomaterials, Advanced Technologies and Innovation and characterized with 7.48 g/m² and 0.11 mm thickness.

2.2 PEG-Coated PA6 Nanofibrous Membranes

10wt% PEG aqueous solution was obtained via mixing PEG 1500 powders with distilled water. Then the prepared 10wt% PEG aqueous solution was applied on the surface of PA6 nanofibrous membrane at room temperature and then the PEG-coated fibrous membrane was placed under 60 to evaporate the water inside. Finally, the PEG-coated fibrous membrane was obtained. The ratio of dry PEG weight in the coated fibrous membrane to the weight of the

applied PA6 nanofibrous membrane was set as 50:50, 60:40, 70:30, 80:20 and 90:10, and 5 PEG-coated fibrous membranes were obtained named as C1, C2, C3, C4 and C5 with different ratios as shown in table 1.

Table 1 Details of PEG-coated PA6 Nanofibrous Membrane

Sample Code	Components in Composite	
	Weight Percentage of Dry PEG in Composite (wt%)	Weight Percentage of PA6 Nanofibrous Membrane in Composite (wt%)
C1	50	50
C2	60	40
C3	70	30
C4	80	20
C5	90	10

2.3 Methods and Tests

Differential scanning calorimetry was used to test the thermal properties of multi-layer composites containing PCM at a temperature from 15°C to 60°C with a heating rate of 10°C/min under N₂ gas purge with a rate of 20mL/min.

3 RESULTS AND DISCUSSION

The thermal behavior of PEG-coated PA6 nanofibrous membrane tested by DSC was shown in Figure 2. The melting temperature, solidification temperature and enthalpy of PEG-coated PA6 nanofibrous membranes were listed in Table 2.

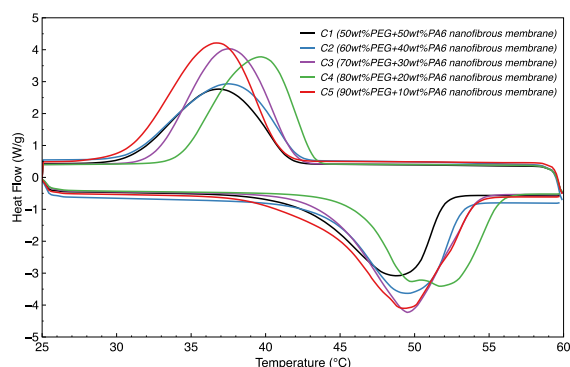


Figure 2 DSC Curves of different PEG-coated PA6 Nanofibrous Membrane

The DSC curves suggested that the melting temperature and solidification temperature were not affected

obviously by the different weight percentage of PEG coated in the PA6 nanofibrous membranes. The coated PA6 nanofibrous membranes had the latent heat of fusion and the enthalpy increased significantly when the weight percentage of PEG in the coated PA6 nanofibrous membrane reached 70wt% and then changed not much with the continuous weight percentage of PEG in the coated PA6 nanofibrous membrane.

The results shown that PEG-coated PA6 nanofibrous membrane obtained the thermal behavior. The weight percentage of PA6 nanofibrous membrane in the coated fibrous membrane made little effect on phase transition process but affected enthalpy when the content reached 70wt% in the PEG-coated nanofibrous membranes.

Table 2 Thermal Performance of PEG-coated PA6 Nanofibrous Membranes Calculated from DSC Curves

Sample	T _{om} (°C)	T _{pm} (°C)	T _{em} (°C)	ΔH _m (J/g)	T _{oc} (°C)	T _{pc} (°C)	T _{ec} (°C)	ΔH _c (J/g)	ΔT (°C)
C1	42.42	48.71	52.09	98.08	41.60	37.21	31.00	93.05	7.11
C2	44.17	49.55	53.25	105.27	42.18	37.50	30.92	100.24	12.05
C3	44.06	49.50	54.19	133.41	41.96	37.59	32.54	127.07	11.91
C4	46.12	51.80	55.80	120.18	39.58	33.84	28.69	113.11	17.96
C5	43.18	49.28	54.10	150.36	41.01	36.69	30.77	143.11	12.59

T_{om}: onset melting temperature; T_{pm}: peak melting temperature; T_{em}: endset melting temperature; T_{oc}: onset cooling temperature; T_{pc}: peak cooling temperature; T_{ec}: endset cooling temperature; ΔH_m: melting enthalpy change; ΔH_c: solidification enthalpy change; ΔT: super cooling degree (ΔT= T_{pm}- T_{pc})

4 CONCLUSIONS

PEG-coated PA6 nanofibrous membranes have been prepared and latent heat of fusion of all samples was approximately larger than 100J/g. The all PEG-coated PA6 nanofibrous membranes had similar phase transition process but the latent heat of fusion was affected by the content of PEG in the coated samples. The latent heat of fusion increased obviously when the content of PEG was larger than 70wt%.

ACKNOWLEDGEMENT: This work was supported by the research project of Student Grant Competition of Technical University of Liberec no. 21307/2019 granted by Ministry of Education, Youth and Sports of the Czech Republic and the European Union – European Structural and Investment Funds in the research project of Student Grant Competition of Technical University of Liberec no. 21307/2019 granted by Ministry of Education Youth and Sports of Czech Republic and the Ministry of Education, Youth and Sports of the Czech Republic and the European Union – European Structural and Investment Funds in the Frames of Operational Programme Research, Development and Education – project Hybrid Materials for Hierarchical Structures (HyHi, Reg. No. CZ.02.1.01/0.0/0.0/16_019/0000843), project 'Design optimization and application of smart heat-insulating nano-layers' [LTACH – 17014, 18301] and project 'Intelligent thermoregulatory fibers and functional textile coatings

based on temperature resistant encapsulated PCM' SMARTTHERM (Project No. TF06000048).

5 REFERENCES

- [1] Madad, A., Mouhib, T., and Mouhsen, A. 2018. Phase Change Materials for Building Applications: A Thorough Review and New Perspectives. Buildings 8, 5, 63.
- [2] Sarı, A. and Karaipekli, A. 2007. Thermal conductivity and latent heat thermal energy storage characteristics of paraffin/expanded graphite composite as phase change material. Applied Thermal Engineering 27, 8-9, 1271–1277.
- [3] Sharma, A., Tyagi, V. V., Chen, C. R., and Buddhi, D. 2009. Review on thermal energy storage with phase change materials and applications. Renewable and Sustainable Energy Reviews 13, 2, 318–345.2
- [4] Kou, Y., Wang, S., Luo, J., Sun, K., Zhang, J., Tan, Z., and Shi, Q. 2019. Thermal analysis and heat capacity study of polyethylene glycol (PEG) phase change materials for thermal energy storage applications. The Journal of Chemical Thermodynamics 128, 259–274.
- [5] AFSHARI, M., KOTEK, R., TONELLI, A. E., and JUNG, D.-W. 2007. Producing polyamide nanofibers by electrospinning. In *Nanofibers and Nanotechnology in Textiles*. Elsevier, 71–89.

OBTAINING NON-ACOUSTICAL PARAMETERS OF POLYESTER NONWOVEN MATERIALS BY USING ACOUSTIC METHOD

Tao Yang¹, Xiaoman Xiong¹, Rajesh Mishra¹, Jean-Philippe Groby², and Jiri Militky¹

¹ Department of Material Engineering, Faculty of Textile Engineering, Technical University of Liberec, Liberec 46117, Czech Republic, e-mail: tao.yang@tul.cz

² Laboratoire d'Acoustique de l'Université du Maine, UMR6613 CNRS/Univ. du Maine, F-72085 Le Mans Cedex 9, France, e-mail: Jean-Philippe.Groby@univ-lemans.fr

Abstract: This paper investigated the acoustic performance and non-acoustical parameters of perpendicular-laid polyester nonwovens, such as tortuosity, static flow and thermal characteristic lengths, static viscous and thermal permeabilities. The acoustic properties of polyester nonwovens were measured by 4 microphone impedance tube. The non-acoustical parameters were obtained using inverse method based on the results of impedance tube measurement. The inversed non-acoustical parameters were compared from both front and back sides. It was found that that inverse method is useful for estimate tortuosity, airflow resistivity, thermal permeability and viscous characteristic length of polyester nonwoven materials.

Keywords: polyester, nonwoven, acoustic, inversion

1 INTRODUCTION

Some non-acoustical parameters are very important for acoustic properties analysis, such as thickness, fiber diameter, porosity, tortuosity, airflow resistivity (static viscous permeability), static thermal permeability, etc. Although the existing ways can measure many non-acoustical parameters, some methods require specific device and complicated to carry out. Inverse characterization methods are becoming more interesting since they are able to simultaneously reckon several parameters [1].

The semi-phenomenological models consider the frame of porous material as rigid. These models use four to eight non-acoustical parameters (i.e. porosity, tortuosity, airflow resistivity, viscous and thermal characteristic length) to calculate the dynamic density and dynamic bulk modulus. Consequently, the surface impedance and sound absorption coefficient can be rapidly calculated. One of the most popular semi-phenomenological model are collectively called Johnson-Champoux-Allard-Lafarge model (JCAL) [2-4].

This paper presented the application of inverse method based on the JCAL model on anisotropic polyester material.

2 EXPERIMENT

2.1 Materials

Polyester nonwoven samples made by vibrating and rotating perpendicular technology were selected for this study. All of the samples in current study have the same fiber content: 45% staple polyethylene terephthalate (PET), 30% hollow PET and 25% bi-component PET.

2.2 Impedance tube measurement

One four-microphone impedance tube was applied to carry out the measurements to recover the reflection R and transmission coefficients T . Then the dynamic density $\tilde{\rho}_{eq}$

and dynamic bulk modulus \tilde{K}_{eq} can be calculated straightforwardly [1].

3 JCAL MODEL AND INVERSE METHOD

3.1 JCAL model

If saturating fluid is air, the JCAL model assumes the porous media are rigid and motionless at the frequency higher than the phase decoupling frequency. In the model, the equivalent dynamic density describes as:

$$\tilde{\rho}_{eq} = \frac{\rho_0}{\phi} \tilde{\alpha}(\omega), \quad (1)$$

where $\tilde{\alpha}(\omega)$ is the dynamic tortuosity,

$$\tilde{\alpha}(\omega) = \alpha_\infty + \frac{jv\phi}{\omega k_0} \sqrt{1 - \frac{j\omega}{v} \left(\frac{2\alpha_\infty k_0}{\phi\Lambda} \right)^2}, \quad (2)$$

where ρ_0 is the density of the saturating fluid, ϕ is the open porosity, α_∞ is the dynamic tortuosity, j is the complex number, $v = \eta/\rho_0$ is the kinematic viscosity, where η is the dynamic viscosity, $\omega = 2\pi f$ is the angular frequency, $k_0 = \eta/\sigma$ is the static viscous permeability, where σ is the airflow resistivity, and Λ is the viscous characteristic length [2].

The dynamic bulk modulus describes as:

$$\tilde{K}_{eq} = \frac{\gamma P_0}{\phi} \left(\gamma - \frac{\gamma-1}{\tilde{\alpha}'(\omega)} \right)^{-1}, \quad (3)$$

where $\tilde{\alpha}'(\omega)$ is the thermal tortuosity,

$$\tilde{\alpha}'(\omega) = 1 + \frac{jv'\phi}{\omega k'_0} \sqrt{1 - \frac{j\omega}{v'} \left(\frac{2k'_0}{\phi\Lambda'} \right)^2}, \quad (4)$$

where $v' = \frac{v}{Pr}$, where Pr is the Prandtl number, k'_0 is the static thermal permeability, k'_0 is the static thermal permeability, Λ' is the thermal characteristic length [3-4].

3.2 Inverse method

The statistical inversion method used for recover non-acoustical parameters of polyester materials was adopted from the research that proposed by Niskanen *et al* [1]. The statistical inversion was not only applied for parameter estimates, but also for evaluating probability density,

standard deviations and the correlation between the parameters. The Bayes' formula, Metropolis-Hastings algorithm (MCMC) and maximum a posteriori (MAP) were implemented in the second method.

4 RESULTS

The inversed tortuosity for all of the samples are 1 with low standard deviation. However, the estimations on porosity are inaccurate compare to measured values.

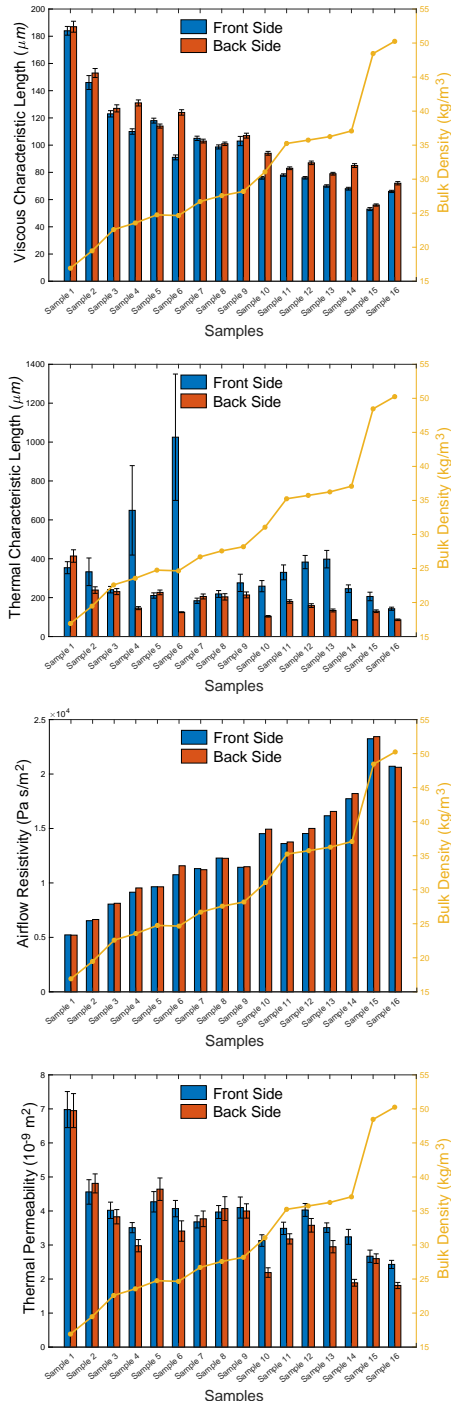


Figure 1 Inversed characteristic lengths Λ and Λ , airflow resistivity σ , and thermal permeability k'_0 of two sides

Figure 1 presents the comparison of some inversed non-acoustical parameters between two sides. It can be seen that as increase on density the viscous characteristic length

decreases, while the airflow resistivity increases. It is obviously found that the inversed thermal characteristic length yields significant difference on the two sides. Also, the standard deviation are extremely high. This phenomenon can be attributed to the following reasons: interface difference on the two sides, and small frequency range or large measurement uncertainty [1].

The inversed airflow resistivity from back side was chosen to compare measured value in Figure 2. The correlation between measured and inversed was presented. It can be seen that the regression lines have slope values close to 1 and the coefficients of determination is over 0.94.

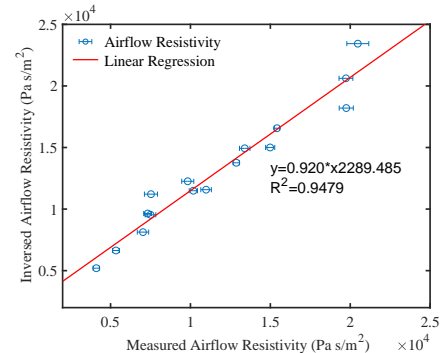


Figure 2 Comparison between measured and inversed airflow resistivity

5 CONCLUSION

This work applied the inverse method on anisotropic polyester materials to get some non-acoustical parameters. The results indicated that the inverse method is inaccurate on porosity estimation. The inversed tortuosity is reasonable. The values of thermal characteristic length exhibits significant difference and standard deviation based on two sides measurements. In contrast, other parameters have relative low difference and standard deviation. Moreover, the increase of density resulted in decrease on viscous characteristic length and increase on airflow resistivity was found. Whereas, there is no clear relationship between density and thermal characteristic length, thermal permeability.

ACKNOWLEDGEMENT: This work was supported by the research projects of Student Grant Competition of Technical University of Liberec no. 21239 granted by the Ministry of Education Youth and Sports of the Czech Republic, and Short Term Scientific Mission funding scheme COST Action DENORMS CA-15125.

6 REFERENCES

- [1] Niskanen M., Groby J., Duclos A., et al.: Deterministic and statistical characterization of rigid frame porous materials from impedance tube measurements. *Journal of the Acoustical Society of America* 2017, 142, pp. 2407-2418.
- [2] Johnson D. L., Koplik J., Dashen R.: Theory of dynamic permeability and tortuosity in fluid-saturated porous media. *Journal of Fluid Mechanics* 1987, 176, pp. 379-402.
- [3] Champoux Y., Allard J.-F.: Dynamic tortuosity and bulk modulus in air-saturated porous media. *Journal of Applied Physics* 1991, 70, pp. 1975-1979.
- [4] Lafarge D., Lemarinié P., Allard J.-F., et al.: Dynamic compressibility of air in porous structures at audible frequencies, *Journal of the Acoustical Society of America* 1997, 102, pp. 1995-2006

7. Design, Comfort, Quality of Textiles and Sense Evaluation

OPTICAL PROPERTY OF TEXTILES RELATED TO HUMAN PERCEPTION AND PHYSICAL PROPERTIES

Sachiko Sukigara¹ and Tomoko Awazitani¹

¹ Kyoto Institute of Technology, Matsugasaki, Sakyo-ku, Kyoto city, Kyoto, JAPAN, sukigara@kit.ac.jp

Abstract: Woven fabric is made from the arrangement of interlaced yarns. This weave structure consists of repeated unit and generates the concave-convex surface. We have developed a method whereby a goniospectrophotometer measurements for the overall specular and diffuse reflection of a rotating fabric. This method was applied to characterize unique feature of Japanese traditional weave made from silk and carbon yarns. When the light incidents into the fabric, we sometimes feel the stereoscopic shape and aesthetic even the fabric is placed as flattened. This phenomenon was obviously observed traditional silk woven fabric, carbon fiber woven fabrics and confirmed by the subjective evaluation.

Keywords: lightness, goniospectrophotometric measurement, carbon fiber, silk fiber

1 INTRODUCTION

When the light incidents into the woven fabric, light reflected from a fabric surface. The various reflection patterns are observed. We have developed a method whereby a goniospectrophotometer measurements for the overall specular and diffuse reflection of a rotating fabric[1]. This method was applied to differentiate between fine cashmere hairs alignment on fabrics. It is proved the capable of distinguishing between fuzz-surface and clear-finish wool fabrics at different finishing[2]. We have investigated the reflection patterns of fabrics to extract the features of fabric surface using this method. Woven fabric is made from the arrangement of interlaced yarns. This weave structure consists of repeated unit and generates the concave-convex surface. This concave-convex surface made from weave design pattern might be characterized by the light reflection pattern. When the light incidents into the fabric, we sometimes feel the stereoscopic shape and aesthetic even the fabric is placed as flattened. This paper introduces the characterization method of light reflection pattern and further application of aesthetic using carbon fiber products.

2 MEASUREMENT OF FABRIC LIGHT REFLECTION

The reflectance of the fabric samples was measured with a goniospectrophotometric color measurement system, GCMS-4 (Murakami Color Research Laboratory Co., Ltd, Japan).

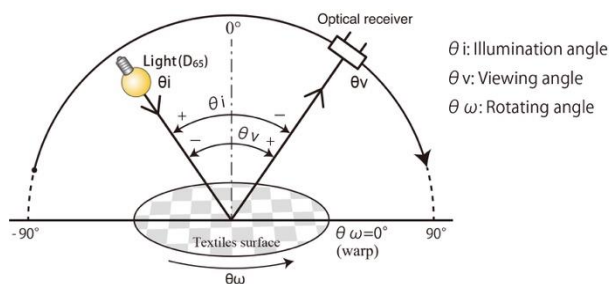


Figure 1 Illumination and viewing geometry used in the measurement

Figure1 shows the illumination and viewing geometry used in the measurement. CIEL*a*b* values are obtained.

3 TRADITIONAL JAPANESE SILK FABRICS (NISHIJIN WEAVE, KYOTO)

The Nishijin textiles of Kyoto, which are a traditional type of Japanese textile, have their unique weave pattern based on a traditional design as well as their use of gold, silver yarns. We characterized the optical properties of seven Nishijin textiles using the system as shown in Figure1[3].

In Figure 2, L* values are plotted for θ_ω in the range from -15° to 180° . Samples N4 and N5, which have the same weave structure and were woven from three different colors yarns; N4: silver thread(84dtex), Silk(91dtex) for warp, Silk (109dtex) for weft, N5: gold thread(87dtex), Silk(99dtex) for warp, Silk (111dtex) for weft.

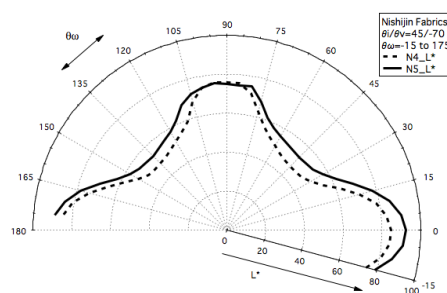


Figure 2 L* profiles as functions of the fabric rotation angle θ_ω at $\theta_i / \theta_v = 45^\circ / -70^\circ$.

The maximum L* value were observed at $\theta_\omega = 0^\circ$ and minimum in the vicinity of $\theta_\omega = 45^\circ$ and 135° . These lightness change were confirmed by the subjective evaluation.

In Figure3, subjectively observed lightness values are plotted against θ_ω . The results indicate that the subjectively observed lightness clearly changes with θ_ω ,

and that this change in lightness tends to correspond to the change in L^* with respect to θ_ω as shown in Figure 2. Grittering of metallic fibers were also confirmed by this method.

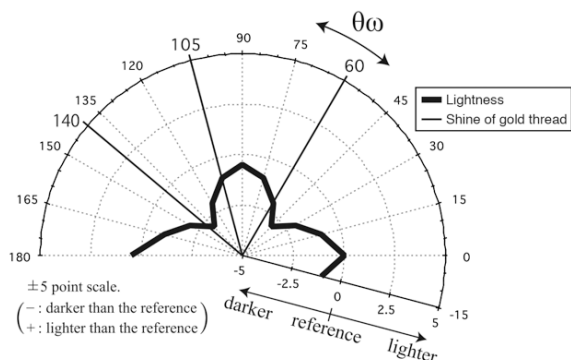


Figure 3. Changes in lightness obtained through visual assessment for sample N5[3].

4 LIGHTNESS OF CARBON FIBER FABRICS OF NISHIJIN WEAVE STRUCTURE

Carbon fibers were well known as industrial used fibers. Seven fabrics woven from carbon fiber yarns (PAN type, Tow = 3K, by FUKUOKA-kigyou, Kyoto, Japan) were used as samples. These weave structures were the same as Japanese traditional NISHIJIN, Kyoto obi (belt). Figure 4 shows how the appearance was changed by the direction of illumination and viewing angles for the same carbon fiber fabric (Arranged Shamon weave). Specially, we saw the stereoscopic image in photo (b).

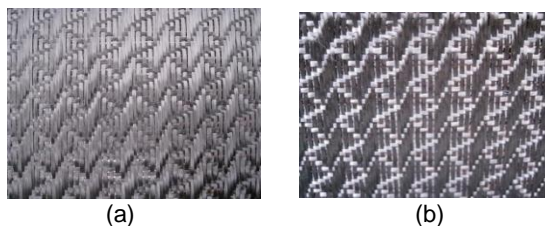


Figure 4 Change of the appearance under the different viewing angle.

The difference between pairs photos results in the unique light reflection of carbon fibers.

In Figure 5, the light reflection of the aligned carbon fibers is shown at $\theta_i / \theta_v / \theta_\omega = (45^\circ/0^\circ, 0^\circ, 45^\circ, 90^\circ)$. Difference of light reflection is very obvious.

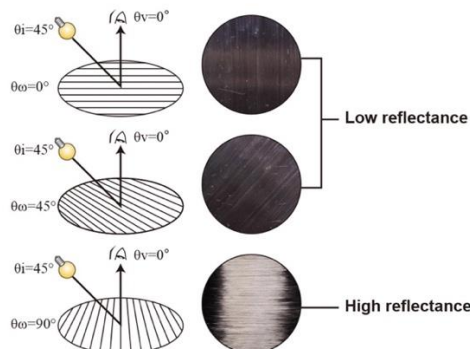


Figure 5 Reflection of carbon fibers at $\theta_i / \theta_v / \theta_\omega = (45^\circ/0^\circ, 0^\circ, 45^\circ, 90^\circ)$.

We asked students in design school to judge the stereoscopic feeling for seven samples woven from same yarn density but different design pattern. Participants ranked the samples according to the intensity of stereoscopic feeling. Normalized ranking method was used for the analysis. Participants looked the samples from different directions and also turned the samples. When two samples such as CF1(Plain weave) and CF6(arranged Shamon) as listed in Table 1 are compared, the significant difference was observed. Sample CF6 made stronger stereoscopic impression than CF1. One unit size of CF6 is much larger than that of CF1. Stereoscopic impression increased with the increase of one unit area. The interlace yarns and their angle also influenced on the light reflection pattern from the fabric surface.

Relationship between the subjective values of "stereoscopic" and warp weave factor(WF) showed positive correlation. The shadow appeared in the fabric contributed the "stereoscopic" perception. The unique profile of L^* values are observed at θ_ω measured with a goniospectrophotometric color measurement system. The change in lightness from shiny to dark was also related to the visual "stereoscopic" perception.

Table 1 Structure of Carbon fiber fabric

Symbol	CF1	CF6
structure		
Thickness(mm)	0.49	1.11
Warp weave factor	1	2.9

5 REFERENCES

- [1] Endo M., Kitaguchi S., Morita Hi., et al.: Characterization of Fabrics using the Light Reflectance and the Surface Geometry Measurements, *Journal of Textile Engineering* 2013, 59, pp. 75-81.
- [2] Davaajav N., Sukigara S., : Surface Characterization of Cashmere Fabrics Using Optical and Transient Thermal Properties, *Journal of Fashion Technology & Textile Engineering*, 2017, 6, Issue 1.1000165.
- [3] Awazitani T., Sukigara S., : Characterization of optical properties of traditional Japanese fabrics, *Textile Research Journal*, 2016,86, pp13-23.

INVESTIGATING THERMAL COMFORT PROPERTIES IN MOHAIR FABRICS

Adine Gericke¹, Jiri Militky², Mohanapriya Venkataraman², Divan Coetzee¹

¹ Department of Chemistry and Polymer Science, University of Stellenbosch, South Africa
email: agericke@sun.ac.za

² Department of Material Engineering, Faculty of Textile Engineering, Technical University of Liberec, Czech Republic, email: mohana.prasad@gmail.com

Abstract: This work forms part of a study on the thermal and moisture management properties of textile materials containing mohair fibers. A range of fabrics (comprising mohair yarns in different forms and structures) was developed and the thermal as well as moisture management properties evaluated. The extensive sample range allowed us to compare the properties of mohair with that of other fibers like wool, acrylic, cotton, polyester and regenerated cellulose in comparable fabric structures. The effect of variations in the yarn and fabric structures was also evaluated. This paper will focus on thermal comfort properties, including thermal conductivity and resistance as well as convective heat transfer.

Keywords: mohair, thermal comfort, thermal resistance, convective heat transfer

1 INTRODUCTION

Mohair, produced from the Angora goat, is regarded as one of the most luxurious and best quality natural fibers. Its unique combination of characteristics, such as luster, color reflection, resilience, fineness, exceptional wavy crimp structure, etc. leads to performance properties that made it popular in a wide range of applications in knitwear, suiting, blankets, upholstery, carpets, curtaining, etc. Mohair blends have also become popular in socks for leisure- as well as sports- and medical applications. In moving from traditional apparel and household items towards novel applications such as the above, where the achievement and maintenance of thermo-physiological comfort, even in extreme conditions, are of high importance, questions have been raised whether mohair fibers, on its own and in blends, would be suitable. Despite the popularity of the products, no published studies could be found on the thermo-physiological comfort properties of fabrics made of mohair.

The human body maintains thermal comfort by exchanging heat with the environment. The complex mechanism of dry heat transfer through textiles may involve conduction through the fibrous phase, radiation through fabric interstices and convection of air within the structure. At low wind speeds convection within a fabric is negligible and the heat flow through the fabric is dependent on a combination of conduction and radiation. Thermal resistance is the main parameter determining thermal comfort in clothing systems. Thermal resistance is inversely proportional to thermal conductivity and in a fabric structure it is mainly affected by parameters such as fabric thickness, areal density, cover factor, porosity and other specific fiber properties. These factors are closely related to the amount of air entrapped inside the fabric. The heat loss through conduction is thus closely related to the thickness of the fabric structure and the thermal conductivity of its fibers.

Heat transfer through fabrics in environmental conditions where there is wind flow or the object is moving involves

convection. This means that the thermal resistance of a textile may measure quite differently when tested under non-identical conditions or testing standards. Convective heat flow is of particular importance when the fabric structure is porous with high air permeability.

2 RESULTS AND CONCLUSIONS

Two sets of samples were tested on the Alambeta instrument to compare thermal resistance. In the first sample set, where a range of fabrics with varying weft yarn content was compared, it was found that the samples containing mohair or wool had a higher thermal resistance. Despite the weaving parameters and yarn sizes being kept constant, similar differences were found in the sample thickness values, with the mohair and wool fabrics measuring higher than the rest. The Spearman test indicated a high positive correlation between fabric thickness and thermal resistance ($r=0.86$, $p<0.01$), most probably as a result of the low conductivity of the air incorporated into yarns and among fibers.

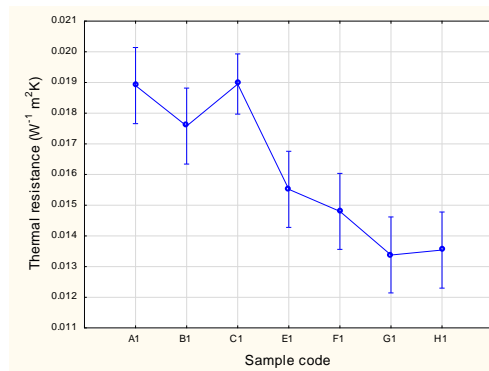


Figure 1 Thermal resistance of samples in first sample set

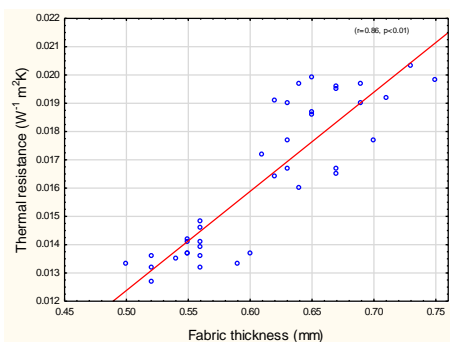


Figure 2 Thermal resistance as a function of fabric thickness (mm) of woven samples

In the second sample set, two fabrics with structurally comparable boucle yarns in the weft, varying only with regard to weft yarn fiber content, were compared. The first yarn was made up of mainly wool and mohair, but in the second 39% viscose rayon was added. It was found that the thermal resistance of the first was higher, but the correlation between fabric thickness and thermal resistance dominating as in the first set. The effect of individual fiber properties should however not be disregarded. The increase in thickness in the mohair fabrics can be ascribed to the physical properties of the fibers that the yarns are made of, which leads to a more bulky structure, incorporating more air and resultantly leading to a higher thermal resistance.

In the second part of the study the effect of yarn and fabric structural properties on convective heat flow through a fabric structure was investigated. A newly developed instrument, called the TP2, was used to measure convection through a range of fabrics with a dominantly mohair fiber composition. Samples varied in thickness and air permeability. Results showed a very high negative correlation between sample thickness and convective heat flow (I) ($r=0.94$, $p<0.01$) as well as between air permeability and convective heat flow ($r=0.6$, $p<0.01$). This confirms the previous findings with regard to the effect of the physical properties of mohair fibers on yarn and fabric properties.

This paper forms part of an ongoing study on the quantitative evaluation of the thermo-physiological performance properties of fabrics made of mohair fibers. Combinations of traditionally used mohair yarn structures in different fabric structures and combining mohair and wool with viscose rayon or bamboo viscose fibers and yarns are used to provide insight in how these variables can be applied to manipulate the properties of an end product.

Acknowledgement: The author would like to thank the Department of Material Engineering, Faculty of Textile Engineering, Technical University of for guidance and access to laboratory equipment in the execution of this project.

3 REFERENCES

1. Hunter L. Mohair: A review of its properties, processing and applications. Port Elizabeth: CSIR Division of Textile Technology; 1993.
2. Hunter L. Mohair, cashmere and other animal fibres. In: Handbook of Natural Fibres. Cambridge: Woodhead Publishing Ltd; 2012. p. 196–290
3. Hes L, Dolezal I. New Method Thermal and Equipment for Measuring Properties of Textiles. Sen'i Kikai Gakkaishi (Journal Text Mach Soc Japan), [1989;42(8):71–5. Available from: https://www.jstage.jst.go.jp/article/transjtmsj1972/42/8/42_8_T124/_pdf
4. Kaplan S, Karaman C. Thermal comfort performances of cellulosic socks evaluated by a foot manikin system and moisture management tester. International Journal of Clothing Science and Technology. 2019;
5. Militky, Jiri, Kremenakova D. a Simple Methods for Prediction of Textile Fabrics Thermal. In: HEFAT2007 5th International Conference on Heat Transfer, Fluid Mechanics and Thermodynamics. Sun City, Johannesburg; 2007.
6. Özgen B, Altaş S. The investigation of thermal comfort, moisture management and handle properties of knitted fabrics made of various fibres. Tekst ve Konfeksiyon. 2014;24(3):266–71.
7. Uttam D, Engineering T, Zail G, Campus S. Objective Measurement of Heat Transport through Clothing. Int J Eng Res Dev. 2012;2(12):43–7.
8. Zhu G, Kremenakova D, Wang Y, Militky J, Mazari FB. An analysis of effective thermal conductivity of heterogeneous materials. Autex Res J. 2014;14(1):14–21.

Development of Hand Evaluation System for Bed Linen

Meenakshi Ahirwar, Mesay Dubale and B K Behera

Department of Textile Technology, Indian Institute of Technology Delhi

meenakshi76361@gmail.com

Abstract: Technological development has introduced many new and modified non-conventional textile products in the field of automotive textiles, home textiles, sportswear and apparel textiles etc. In all these cases, the first assessment made is that of fabric hand as it is well known that “Fabric sells by hand and heft”. Fabric hand is the fundamental aspect, which determines the success or failure of many new products. Exploring the properties of the materials we sleep in is a healthy exercise to undertake. Bed linen is the materials laid above the mattress of a bed for hygiene, warmth, protection of the mattress, and decorative effect. The assessment of fabric hand can be accomplished by subjective, experimental and computational methods. And a comparison study is done for the authentication of the computational method. Also the Bed Linen Performance Index is calculated.

Keywords: Non-conventional fibres, Bed Linen, Step wise block regression, Total Hand Value

1 INTRODUCTION

The major requirement of a sheeting cloth is to be comfortable, nice touch and durable to wear and easy care. The subjective evaluation of fabric hand restricts the scientific understanding of the fabric properties. Hence, an objective hand evaluation system for bed linen has been devised in this research work. The factors contributing to the better handle of the bed linen are investigated. The different fibre type bed linen samples are tested on Kawabata Evaluation System. And the objective evaluation involves the use of KN equations already developed for certain products. And the computational method involves the selection of the key low stress mechanical properties for the development of the hand equation by using forward step wise block regression method. And the above obtained low stress mechanical properties are used to calculate primary hand values which further gives an index the “total hand value” of the bed linen. The total hand value determined is authenticated with the subjective hand evaluation by the experts, users and fabric manufacturers and also with the experimental hand value obtained by using DM-02 futon covering equation.

2 MATERIALS AND METHODS

2.1. Materials

A wide range of bed linen fabric samples with the different fibre mix are produced using 100% cotton and other non-conventional fibres like excel, modal, viscose and their blends with cotton.

2.2. Methods

2.2.1. Development of Hand equation of bed sheet

A new equation is developed for the hand evaluation of bed sheet fabrics using algorithm. Firstly, subjective evaluation for primary and total hand value is done by the judges. Then the testing of the samples is done on KES instrument. Then step wise block regression method is

used to find the coefficient of the primary and total hand value equations.

Equation for calculating PHV:

$$Y = C_0 + \sum_{i=1}^n C_i (X_i - \bar{X}_{mi}) / \sigma_i; \dots\dots\dots (1)$$

Y= primary hand value;

X_i= ith characteristic value or its logarithm;

X_{mi}, σ_i = mean value and the standard deviation of the ith characteristic value,

C₀, C_i parameter (constant coefficient),

N= Total number of mechanical properties.

With the help of different values of properties tested, different hand equations in the above format have been obtained as Y₁, Y₂, Y₃, Y_k.

The translation equation from PHV to THV developed for fabrics:

$$THV = C_{00} + \sum_{i=1}^k Z_i; \dots\dots\dots (2)$$

$$Z_i = C_{i1}(Y_i - M_{i1}) / \sigma_{i1} + C_{i2}(Y_i^2 - M_{i2}) / \sigma_{i2};$$

Here, Y_i = primary hand values, M_{i1}, M_{i2} = mean values of Y_i and Y_i², σ_{i1}, σ_{i2} = standard deviation of Y_i and Y_i², respectively. C₀₀, C_{i1}, C_{i2} = constant parameters and k = number of primary hands.

2.2.2. Subjective Evaluation of fabric

To determine the primary hand expressions of bed sheet fabric, a survey of 15 judges has been carried out. This survey was divided into two steps. In the first step of the survey, the experts were asked to give a rating and percentage to the primary hand attributes for a good bed sheet fabric.

In the second step of the survey, samples were given to them one by one and they ranked the samples according to the intensity of feeling in primary hand expression and total hand expression.

Table 1 Total Hand Value rating

THV	0	1	2	3	4	5
FEELING GRADE	Not useful	Poor	Fair	Average	Good	Excellent

2.2.3. Approach To Calculate The THV by Computational Method

Using the multi-variable regression method, subjective primary hand value is regressed with the mechanical properties of each of the blocks and the regression equations for each block are obtained as follows:

$$\text{Block: } Y_c = C_0 + C_1[A] + C_2[B] + C_3[C] + \dots (1);$$

Where, values given in square brackets indicate the normalized value or a logarithm value of the characteristic value of the corresponding block properties. The correlation between the above-mentioned three sets of Y_c values and the subjective primary hand value Y is checked. The procedure is followed for all the subjective primary hand values and the obtained values and coefficients are used in equation (1) and (2) to calculate the PHV and THV.

2.2.4 Experimental evaluation of fabrics

KES excel sheet contains many KES hand equations depending on the end uses and for this samples the futon covering equation is selected and according to this formula sixteen low-stress mechanical properties along with two other properties (Air Resistance and Water resistance) are measured. Total eighteen properties are included for calculating Total hand value according to this equation DM-02 [1].

2.2.5 Development of bed linen performance index (BLPI)

The seven important properties determined for the bed linen performance index are fabric hand, air permeability, moisture management, thermal resistance, abrasion resistance, fabric drapeability and crease recovery. A standard is developed to evaluate the performance of bed linen fabric using an objective measurement of fabric quality parameters. After evaluating the above properties the data is normalized to develop the index [2].

$$\text{Max Normalization} = \frac{x - \min x}{\max x - \min x} * (\text{new max} - \text{new min}) + \text{new}$$

Where x = original value
 Min x = minimum original value
 Max x = maximum original value
 New max = maximum of normalized dataset
 New min = minimum of the normalized dataset

3 RESULTS AND DISCUSSION

3.1 Comparison of Subjective, Experimental and Computational Total Hand Value

The Total Hand Value of the modal-cotton blend fabric shows highest THV as compared to other samples whereas 100% polyester fabric shows very poor hand value.

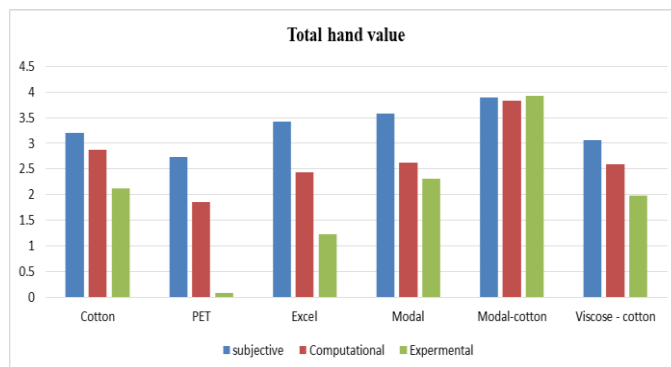


Figure 1 Comparison of Subjective, Experimental and Computational THV

3.2 Comparison of Subjective and Objective Bed Linen Performance Index

A Modal-cotton blend fabric shows highest bed linen performance than the other fabrics. These fabrics are highest in THV, Abrasion resistance, Crease recovery, and drape coefficient. 100% of Excel fibre has the very lowest performance index.

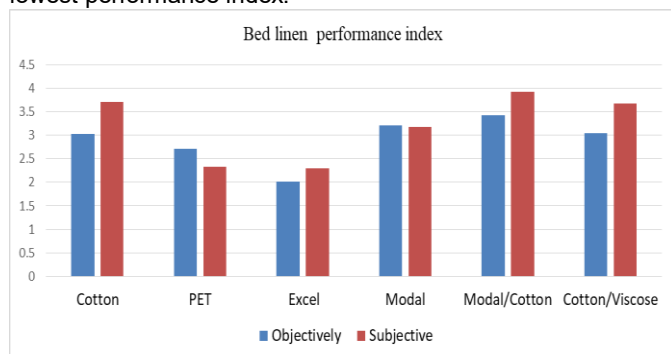


Figure 2 Comparison of subjective and objective BLPI

4. CONCLUSION

According to the computational equation, subjective hand value and experimental hand value, the modal/cotton blend fabric shows better hand value than the others. But 100% polyester fabric shows lower hand value than the other fabrics. The correlation coefficient between the subjective and computational is 0.835 and the correlation coefficient between subjective and experimental is 0.855. This indicates that the computational total hand value is estimated well. For the Bed Linen Performance Index the correlation between subjective and objective evaluations is very high ($R=0.82$). This indicates that the bed linen performance index could be estimated as well.

5 REFERENCES

- [1] Mitsuo Matsudaira and Masahiko Kubo; *Objective Evaluation of Hand for Futon Cloth*; journal of the Textile Machinery Society of Japan, Transactions, Vol.44, No.11T, 201- 7210(1991), Vol.46, No.1T, 18- 726(1993), Vol.46, No.97, 207- T214(1993).
- [2] Saranya C, Manikandan G. A Study on Normalization Techniques for Privacy Preserving Data Mining. 2013;5(3):2701-4

THE OBJECTIVE EVALUATION OF TOTAL HAND OF TOWEL FABRICS AND ITS CONFIRMATION BY SENSORY TEST

Jeoun Gyonran¹, Takako Inoue² and Morihiro Yoneda¹

¹ Nara Women's University, Kitaouyanishimachi Nara, e-mail: gkdzd429@ybb.ne.jp

² Sugiyama Jogakuen University, Hoshigaokamotomachi Chikusaku Nagoya, e-mail: inoue@sugiyama-u.ac.jp

Abstract: We previously established a method of objective evaluation of primary hand of towel fabrics made in Japan (Imabari and Sensyu). In this study, we try to evaluate the Total Hand Value (THV) of the same towel fabrics based on mechanical properties and primary hand. The results are confirmed by sensory test using experts and consumers.

Keywords: total hand value, hand value, sensory test, mechanical properties, objective evaluation

1 INTRODUCTION

The texture of a fabric is one of the important factors in judging the performance and quality of the fabric. Hand Values (HV) are calculated based on the mechanical properties of a fabric, and the methods developed and generally used for objectively evaluating Total Hand Value (THV) have so far been for men's suiting[1], ladies garments fabrics[2], dress-shirt fabrics[2], knitted fabrics used for underwear and outerwear[3], knitted fabrics used for underwear[4] [5], and futon cloth[6]-[8]. However, there are no examples of systematic research into methods for evaluating the texture of towel fabrics. For this reason, in this research, the objective evaluation methods developed thus far for the fabrics above are applied to towel fabrics, in order to not only clarify the performance of a "well-behaved" towel fabric, but also to create basic data on the performance design of towel fabrics.

2 EXPERIMENT

2.1 Measurement of Mechanical Properties[9]

In order to grasp the mechanical properties of towel fabrics, numerous types of face towels were selected randomly from commercially available Imabari and Sens-yu Face Towel products, and then 112 of these, chosen to reflect the widest quality range possible, were used as the study samples. These samples were used as the sample group for creating an objective evaluation formula. In addition, 20 other samples were collected as certification -test samples, in such a way that the distributions of mechanical characteristics would be similar.

The mechanical properties of the fabrics were measured under standard conditions using the KES-FB system. For surface- characteristic measurements, a 30×5 (mm, width × depth) contactor developed by Kawabata et al. was used. Surface roughness was measured under the standard measurement conditions for surface roughness.

2.2 Subjective Evaluation of Towel Fabrics Texture by Touch

The judges were 7 experts, 23 male consumers (21 to 57 years old), and 23 female consumers (21 to 51 years old). The seven in the expert group have worked from 6 to 44 years in the fields of weaving, dyeing, processing and testing of towels. Subjective evaluation of the towel fabrics was performed in five stages using a total of 132 20 × 20 (cm) fabric samples. First, the samples were divided into

"good", "average", "below average" and "not usable" categories. Next, the best ones among those in the "good" group and the poorest ones in the "below average" group were selected, and scores of 5, 4, 3, 2, 1 and 0 were given to them based on the quality of their hand feeling. This is called Total Hand Value (THV). Based on the subjective evaluation by hand evaluation, stepwise regression analysis of hand values was conducted to derive a formula for predicting THV. Furthermore, the relationship between mechanical properties and subjective evaluation was also examined.

3 RESULTS AND DISCUSSION

3.1 Subjective Evaluation of THV by Hand Evaluation

For every sample, the average value of all the judge's evaluations was obtained in each group, the correlation with each judge's evaluation value within each group was checked, and on the basis of this the judges with relatively good judgment were determined (N = 132, p <0.01, R > 0.332). Finally, five out of seven in the expert group, 21 out of 23 in the male consumer group, and all 23 in the female consumer group—the group that displayed the greatest degree of correlation—were chosen as "good". As shown in Table 1, the correlation coefficient R in the group and the correlation coefficient R between the groups were high, with correlation coefficients of 0.835 to 0.945 between groups.

Table 1 Mean correlation coefficient within groups (between a group mean and individuals within that group) and between groups (between the group means)

		R
Within Groups	Expert	0.682
	Male Consumer	0.664
	Female Consumer	0.776
Between Groups	Expert / Male Consumer	0.835
	Expert / Female Consumer	0.850
	Male Consumer / Female Consumer	0.945

In particular, there was a very great degree of correlation between the male and female consumer groups. In creating a formula for predicting THV of the towel fabric, the average

evaluation values of the expert group, male consumer group, and female consumer group were used.

3.2 Characteristics of Towel Fabric with Good Hand

In order to newly create a data chart for towel fabrics, a data chart of mechanical properties was created using the average value and the standard deviation value of 112 types of towel fabrics. The Hand Values are the six Hand Values "KOSHI", "NUMERI", "FUKURAMI", "HARI", "SHARI" and "SOFUTOSA"; to these were added mechanical characteristic values to create new data charts. As a result of plotting the characteristic values of the towel fabrics with good hand evaluation on the mechanical data chart created as a new data chart for towel fabrics, using the averages of the subjective evaluation values determined by all of the 49 judges selected, the mechanical properties and hand values of high THV samples were found to have a comparatively narrow distribution range.

Comparing those with high hand values and those with low hand values, in the case of the former, shearing properties had lower values and were softer, both the fluctuation in mean deviation of coefficient of friction MMD and mean deviation of surface roughness SMD were smaller, and surfaces were smoother. In addition, it was found that the values for "NUMERI" and "FUKURAMI" were greater, and those having appropriate thickness and weight were evaluated by the judges as towel fabrics having good hand evaluation.

3.3 Subjective Evaluation of THV by Hand Evaluation

The six Hand Values "KOSHI", "NUMERI", "FUKURAMI", "HARI", "SHARI" and "SOFUTOSA" are treated as variables for objective evaluation of towel fabrics. Stepwise-block-regression analysis was performed to predict the THV, with each HV as one block. The stepwise-block-regression equation used for the regression is as follows.

$$THV = C_0 + \sum_{i=1}^6 Z_i \quad (1)$$

$$Z_i = C_{i1} \left(\frac{Y_i - M_{i1}}{\sigma_{i1}} \right) + C_{i2} \left(\frac{Y_i^2 - M_{i2}}{\sigma_{i2}} \right) \quad (2)$$

Where, Z_i : Hand Value ($i = 1$ to 6),
 C_0, C_{i1}, C_{i2} : constant parameters,
 Y_i : variable, i -th characteristic value,
 M_{i1} : constant, average value of Y_i ,
 σ_{i1} : standard deviation of Y_i ,
 M_{i2} : constant, average value of Y_i^2 ,
 σ_{i2} : standard deviation of Y_i^2 .

The correlation coefficient R between the experimental value and the calculated value showed high regression accuracy, as shown in Fig.1. The values of mechanical properties of the certification-test samples were substituted into the objective evaluation equation, THV was calculated, and the correlation with the subjective evaluation value by hand evaluation was observed. It was confirmed that the characteristics of the Towel fabric can be discriminated using the characteristic values determined in the objective evaluation of THV.

It is felt that the series of research projects including that reported on herein can be a guide to controlling mechanical properties well in order to design towel fabrics with better texture.

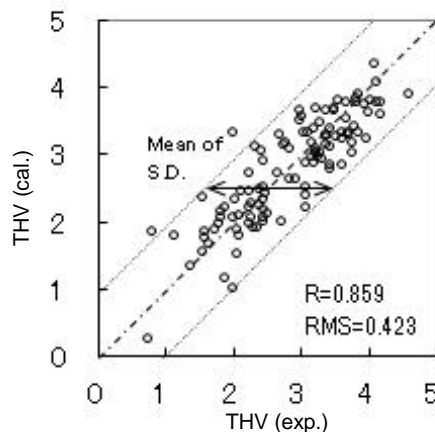


Figure 1 Correlation between THV evaluated for towel fabrics and THV calculated for the same

ACKNOWLEDGEMENT: We would like to express our gratitude to the late Emeritus Professor Masako Niwa, Nara Women's University, for guidance in conducting this research.

4 REFERENCES

- [1] S. Kawabata: The Standardization and Analysis of Hand Evaluation, second edition, *The Textile Machinery Society*, 1980
- [2] S. Kawabata and M. Niwa: *J. Text. Machinery Soc. Japan*, 1984, 37, T113-121
- [3] S. Kawabata and M. Niwa: *Proceedings of 3rd Japan-Australia Symposium, Text. Mach. Soc. of Japan*, 1985, 825-835
- [4] H. Sakaguchi, M. Niwa and S. Kawabata: *J. Text. Machinery Soc. Japan*, 1986, 39, T33-42
- [5] H. Sakaguchi, M. Niwa and S. Kawabata: *J. Text. Machinery Soc. Japan*, 1986, 39, T43-50
- [6] M. Matsudaira and M. Kubo: *J. Text. Machinery Soc. Japan*, 1991, 44, T201-210
- [7] M. Matsudaira and M. Kubo: *J. Text. Machinery Soc. Japan*, 1993, 46, T18-26
- [8] M. Matsudaira, F. Kiuchi and M. Kubo: *J. Text. Machinery Soc. Japan*, 1993, 46, T207-214
- [9] Jeoun Gyonran, Masako Niwa, Takako Inoue, and Morihiro Yoneda: *Proceeding of the 44th Textile Research Symposium IIT Delhi, Poster all papers.pdf*, 2016, pp. 37-40

Objective Hand Evaluation of Car Interior Materials

Takafumi Hata and Mari Inoue

Graduate School of Human Development and Environment, Kobe University,
3-11, Tsurukabuto, Nada-ku, Kobe, 657-8501, Japan, e-mail: 186d432d@stu.kobe-u.ac.jp

Abstract: The method of evaluating the hand of interior cover materials objectively was studied using KES (Kawabata Evaluation System). Samples of elastomer which were used as materials of car interior were evaluated by hand, and the compressional and surface properties of these samples were measured. Objective hand values were calculated by using equations KN101-W [1], and correlated with the subjective hand values. New equations for the hand evaluation were developed by regression analysis. It was found that it is possible to evaluate the hand of car interior materials objectively by using the physical properties. The effectiveness of the objective evaluating equations was confirmed.

Keywords: objective hand evaluation, car interior materials, Kawabata Evaluation System

1 INTRODUCTION

Touch feeling is considered as one of the additional values of car interior materials. It is necessary to reveal the interaction between tactile sensation and physical properties for designing products inducing better touch feeling. In our previous work, we developed equations evaluating the tactile sensation of car interior materials, however these equations had some prediction error. In this study, with more various samples, the objective evaluation of the hand of car interior materials was investigated using KES and the new equations for the evaluation were developed.

2 EXPERIMENTAL

2.1 Samples

Seventy-three samples of elastomer composed of different structures (three kinds of layers, eight kinds of base materials and six kinds of surface shapes) were prepared. Samples were divided into two groups in terms of the layer structures: one is the foamed sheet layered samples (seventeen samples, thickness: 3.622 ± 0.966 mm), the other is the single layered samples (fifty-nine samples, thickness: 2.221 ± 0.092 mm).

For developing the new equations, single layered samples were divided into two groups: Thirty-six samples (group A, thickness: 2.228 ± 0.088 mm) were used to derive the new regression equation and the rest, twenty-three samples (group B, thickness: 2.211 ± 0.096 mm), were used to survey the prediction ability of the new regression equations.

2.2 Subjective hand evaluation

Subjective evaluation by hand was carried out by forty-four judges. All samples were scored -3 to 3 for each tactile sensations, that is, *Yawaraka* (softness), *Zarazara* (roughness), *Shittori* (moistness), *Sarasara* (dry and smooth). This score is called the subjective hand values in this paper.

2.3 Measurement of the physical properties

Compressional properties (LC, WC, RC) were measured using a handy compression tester, KES-G5 (Kato Tech Co.). Surface frictional properties (MIU, MMD) were measured by a surface tester, KES-SE (Kato Tech Co.).

Surface roughness R_a was measured by 3D measurement microscope, VR-3050 (KEYENCE Co.). Testing conditions of compression property and surface frictional property were showed in Table 1. Objective hand values (*KOSHI*, *NUMERI*, *FUKURAMI*) were calculated with equations (KN101-W) which Kawabata developed [1].

Table 1 Measurement conditions of physical properties

Property	Measurement conditions
Compression	spherical contactor
	maximum pressure $P_{\max} = 5\text{ kPa}$
	speed : 0.003 mm/s
Surface friction	frictional contactor : 10×10 mm
	load for friction : 0.5N
	speed : 1 mm/s

2.4 Development of new equations

Multiple regression analysis, which used four subjective evaluation items as objective variables, physical properties as explanation variables, was carried out, and equations which evaluate hand value objectively were developed. For the analysis, subjective hand values were standardized. Equation (1) was used as a regression equation.

$$HV_i = C_{0i} + \sum_{j=1}^6 C_{ij} (X_j - M_j) / \sigma_j \quad (1)$$

Where, HV_i is hand value ($i = 1 \sim 4$), C_{0i} and C_{ij} are constants ($i = 1 \sim 4$), ($j = 1 \sim 6$), X_j is physical properties ($j = 1 \sim 6$), M_j is the mean value of X_j ($j = 1 \sim 6$), σ_j is the standard deviation of X_j ($j = 1 \sim 6$).

3 RESULTS AND DISCUSSION

3.1 Objective Hand Values

Table 2 shows correlation coefficients between subjective hand values and objective hand values calculated by KN-101-W [1]. *Yawaraka* (softness) was correlated with *KOSHI* and *FUKURAMI*. It shows that softness of these elastomer materials can be evaluated by equations for

fabric hand. High correlation ($R = 0.96$) was obtained between subjective hand values of *Yawaraka* (softness) and WC, which is the main contribution factor of *KOSHI* and *FUKURAMI*. On the other hand, *NUMERI* was not highly correlated with any subjective hand values. It was considered that *NUMERI* is not suitable for evaluating surface texture of these materials.

Table 2 Correlation coefficients between subjective hand values and objective hand values calculated by KN101-W

	<i>KOSHI</i>	<i>NUMERI</i>	<i>FUKURAMI</i>
<i>Yawaraka</i>	-0.84	-0.02	0.72
<i>Zarazara</i>	-0.37	-0.34	0.11
<i>Shittori</i>	-0.13	0.07	0.34
<i>Sarasara</i>	0.31	0.26	-0.21

3.2 Development of new equations for Hand

For evaluating sensations of surface texture (*Zarazara*, *Shittori*, *Sarasara*), we developed new equations by multiple regression analysis. Equations were developed for each two layered groups, due to the large difference of physical characteristic values, between two groups.

In the single layered group, *Ra* contributed to *Zarazara*, and WC contributed to the others. In previous work, as a characteristic for fabrics, the correlation between “*Shittori*” and WC has confirmed [2]. It was considered that the evaluation of *Shittori* for these elastomer materials were similar to these for fabrics.

In the foamed sheet layered group, characteristic values contributing to hand values were different from those in single layered materials. MIU contributed to *Shittori* and *Sarasara*. It has obtained the correlation between MIU and *Shittori* for fabrics [2]. Furthermore, it was suggested that *Shittori* and *Sarasara* can be distinguished by the coefficient of friction on samples, in the research for surface materials of steering [3]. These facts showed that *Shittori* and *Sarasara* can be evaluated by MIU.

However, as mentioned above, the physical properties contributing to hand values were different between two groups. As shown in Figure 1 and 2, the characteristic values that had linear relationship with *Shittori* were WC for single layered group, and MIU for foamed layered group. It is considered that this influenced the results of the regression analysis.

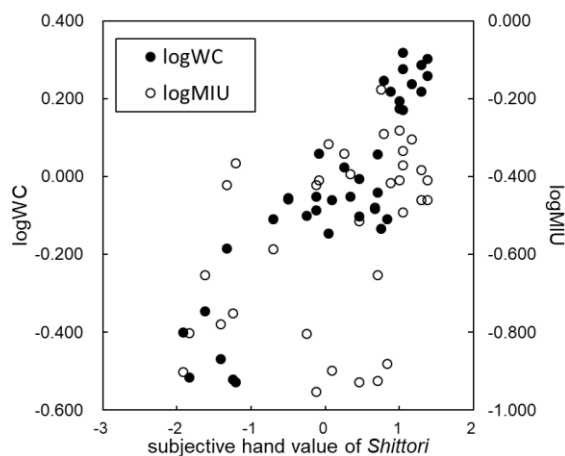


Figure 1 Relationship between WC, MIU and *Shittori* (single layered group)

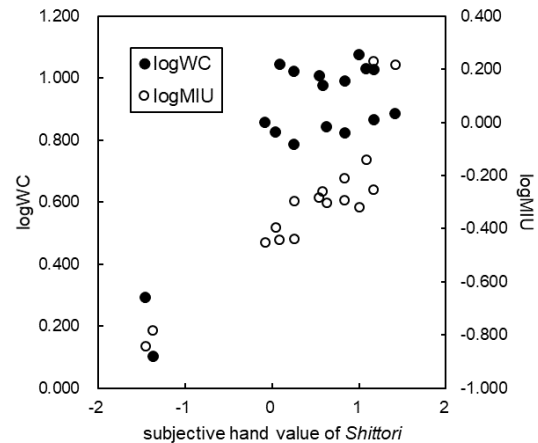


Figure 2 Relationship between WC, MIU and *Shittori* (foamed sheet layered group)

The effectiveness of equations was confirmed, as correlation coefficients between subjective hand value and the regression results and that between subjective hand values and the calculation results were higher than 0.6, for each hand values, shown in Table 3.

Table 3 Correlation coefficients, R , and regression error, RMS between regressed and experimental values, and those between calculated and experimental values

	regression results		calculation results	
	R	RMS	R	RMS
single layered group				
<i>Yawaraka</i>	0.92	0.38	0.71	0.88
<i>Zarazara</i>	0.91	0.41	0.91	0.42
<i>Shittori</i>	0.90	0.44	0.67	1.03
<i>Sarasara</i>	0.79	0.60	0.72	0.82
foamed sheet layered group				
<i>Yawaraka</i>	0.98	0.19	-	-
<i>Zarazara</i>	0.78	0.62	-	-
<i>Shittori</i>	0.93	0.37	-	-
<i>Sarasara</i>	0.82	0.48	-	-

4 CONCLUSION

In this study, objective hand evaluation of car interior materials was researched. Objective hand values were calculated by using equations KN101-W [1], and correlated with the subjective hand values. New equations for the hand evaluation were developed by regression analysis. It was found that it is possible to evaluate the hand of car interior materials objectively by using the physical properties. The effectiveness of the objective evaluating equations was confirmed.

5 REFERENCES

- [1] S. Kawabata, “*The Standardization and Analysis of Hand Evaluation (2ed.)*”, The HESC and The Text. Mach. Soc. of Japan (1980)
- [2] Y. Tanaka and S. Sukigara, “*Evaluation of “Shittori” Characteristic for Fabrics*”, Journal of Textile Engineering (2008), Vol.54, No.3, 75-81
- [3] Y. Nonaka, et al., “*The relationship between the touch feeling and physical characteristics for the interior material of vehicle*”, IEICE Technical Report HCS2015-31, HIP2015-31(2015-05) (in Japanese)

THERMAL COMFORT OF QUILTED BLANKETS

Lubos Hes¹, Monika Boguslawska - Baczek²

¹Technical University of Liberec, Faculty of Textile Engineering, Liberec, Czech Republic, lubos.hes@gmail.com

²University of Katowice School of Technology, Faculty of Architecture, Civil Engineering and Applied Art, Department of Design, Katowice, Poland, mbaczek01@gmail.com

Abstract: In Europe, continental quilts often serve as sleeping blankets. They consist of surface fabrics containing fibrous layers. In the study, the effect of the stitching geometry of surface fabrics on thermal resistance of eight differently stitched quilts is experimentally analysed. It was found, that with the increasing seam length, the mean thermal resistance decreases, as well as the mean thermal absorptivity (toward the skin of the sleeping person) and the mean evaporation resistance.

Keywords: quilted blankets, thermal properties, water vapour permeability, seam

1 INTRODUCTION

In recent decades, big attention has been paid to thermal comfort of textiles used for sleeping [1]. In Europe, as sleeping blankets often serve continental quilts. They consist of thermally insulating fibrous layer sandwiched between surface fabrics, stitched together by quilting seams. These stitches bring compactness of a quilt and relatively stable distribution (location) of the fibres on the quilt, but reduction of the fibrous layer thickness in seams and close the seams may cause changes of thermophysiological and thermal contact properties of quilts felt by a skin of a sleeping person.

In the study, 8 quilted blankets differing in the length of seams within the reference area were subject to testing of their thermophysiological and thermal contact properties by means of the ALAMBETA and PERMETEST non-destructive testing instruments [2]. All these blankets were plain weaves of the same or very similar square mass, same PES microfibre filling and cover fabrics consisting of 100% PES, 100% cotton and PES / cotton blends. The geometry of the analysed seams is displayed on the next Fig. 1



Figure 1 The appearance of a quilt blanket and a reference circular area (diameter 50 mm), determining the total seam

2 EXPERIMENTAL

2.1 Seam geometry

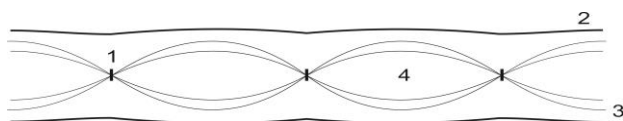


Figure 2: How seams reduce the effective thermal insulation

2.2 Experimental results

Table 1 Seam length and cover fabrics composition [3]

Sample	Cross seam length inside the 5 cm circle	Square seam length inside the 5 cm circle	Arithmetical mean	Surface fabrics
1.	27,4 cm	35,2 cm	31,3 cm	35 % cot 65 % PES
2.	21,1 cm	37,8 cm	29,5 cm	35 % cot 65 % PES
3.	27,8 cm	35,2 cm	31,5 cm	100 % PES
4.	32,5 cm	32,8 cm	32,7 cm	100 % PES
5.	35,3 cm	35,5 cm	35,4 cm	100 % PES
6.	33,2 cm	34,8 cm	34,0 cm	100 % PES
7.	37,6 cm	35,5 cm	36,6 cm	100 % cot
8.	27,4 cm	38,3 cm	32,9 cm	100 % cot



Figure 3 New ALAMBETA, a fast non-destructive tester of thermal insulation and thermal contact properties of fabrics [2]

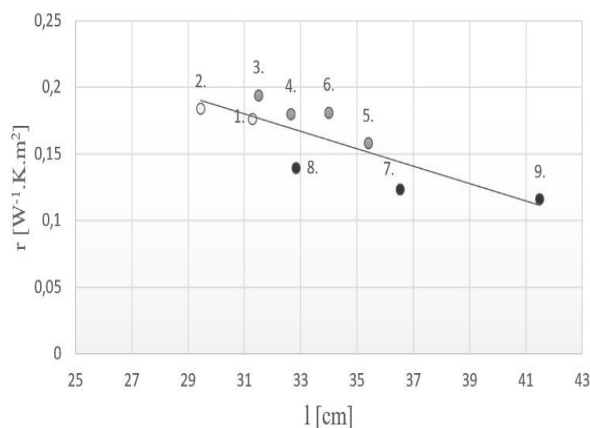


Figure 4 The effect of the total seam length of the tested samples 1-8 on thermal resistance of the quilt. Mark ● is 100% cotton, ○ PES / cotton blends. $R = -0,8142$

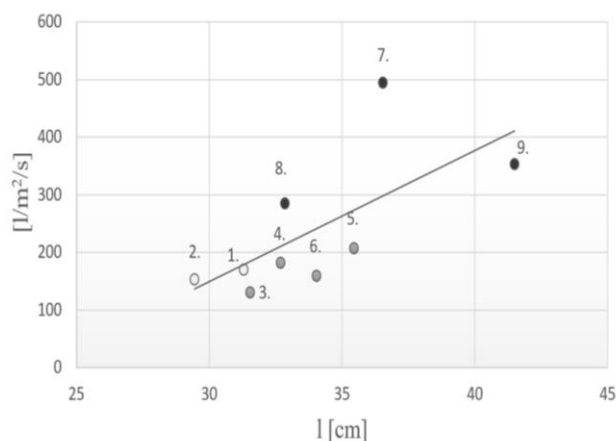


Figure 5 The effect of the total seam length of the tested samples 1-8 on air permeability of the quilt. Mark ● is 100% cotton, ○ PES / cotton blends. $R = -0,8142$

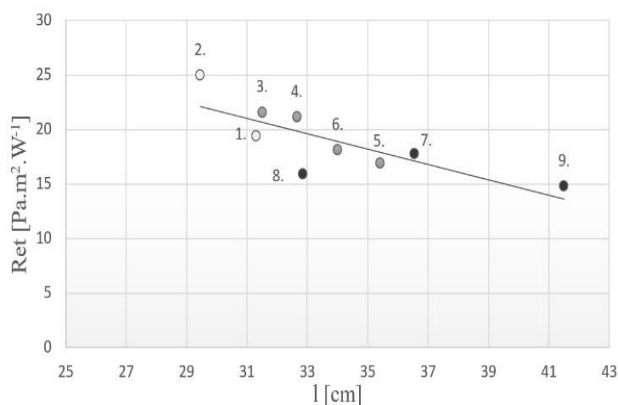


Figure 6 The effect of the total seam length of the tested samples 1-8 in on the evaporation resistance of the quilt. Mark ● is 100% cotton, ○ PES / cotton blends. $R = -0,787$

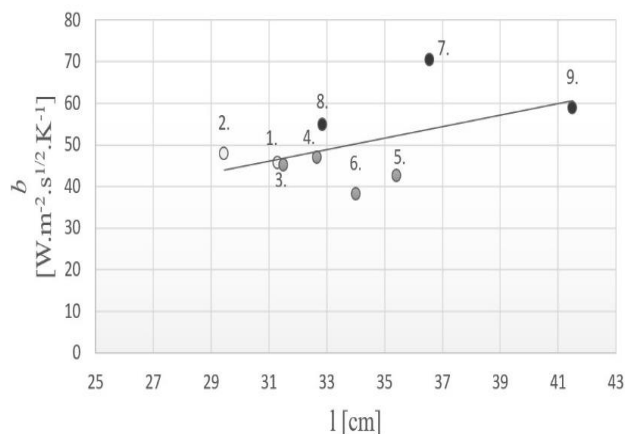


Figure 7 The effect of the total seam length of the tested samples 1-8 on thermal absorptivity of the quilt. Mark ● is 100% cotton, ○ PES / cotton blends. $R = 0,5023$

3 RESULTS EVALUATION AND CONCLUSIONS

It was found, that with the increasing seam length, the mean thermal resistance decreases, as well as the mean thermal absorptivity (toward the skin of a sleeping person) and the mean evaporation resistance. The observed better thermal contact feeling and higher water vapour permeability are the positive results of the increased length of the quilt seams, but the decrease of thermal insulation, most important property of blankets is the negative factor. Therefore, the length of the seams should be optimized.

References

- [1] Hes L., Bogusławska-Baczek M., Geraldès M.J. Thermal comfort of bed sheets under real conditions of use. In: *Journal of Natural Fibres*, 2014, vol. 11, issue 4, pp. 312–321.
- [2] Hes L., Araujo M and Djulay V. Effect of mutual bonding of textile layers on thermal insulation and thermal contact properties of fabric assemblies. *Textile Res J*, 1996; 66(4): 245-250.
- [3] Tomovova L. The effect of stitching on thermophysiological properties of quilted blankets. *BSc Thesis*, Technical University of Liberec, Faculty of Textiles, 2018.

Hand evaluation of towel and washing durability

Mari Inoue

Graduate School of Human Development and Environment, Kobe University,
3-11, Tsurukabuto, Nada-ku, Kobe, 657-8501, Japan, e-mail: inouema@kobe-u.ac.jp

Abstract: As a performance of the towel, good hand is regarded as high quality. Towels used every day as household goods are washed, and change in texture is inevitable. In this study, the towel before and after washing was used as a sample, and the subjective evaluation and physical properties were measured. As a result, it was possible to capture the change in the feel of the towel due to the number of times of washing, and to clarify the difference in durability depending on the washing method. The towel that used the softener did not decrease or tended to have a subjective rating even if the number of times of washing increased, and the towel that did not use the softener became lower in rating as the number of times of washing increased.

Keywords: hand evaluation, Towel, washing durability

1 INTRODUCTION

Towels are used in daily life and are washed repeatedly. It is desirable that the functionality and feeling in use do not deteriorate even after washing. Cleaning is known to increase flexural and shear stiffness, reduce elasticity and increase roughness [1, 2]. The purpose of this research is to capture the change in the feel of the towel due to the number of times of washing, and to clarify the difference in durability depending on the washing method.

2 EXPERIMENTAL

2.1 Samples

One type of towel was used as a sample. In order to observe the difference between the general course and the low flow course using the washing machine, the number of times of washing, and the washing due to the presence or absence of the softener, the subjective evaluation were performed and the physical property were measured.

2.2 Subjective evaluation

Subjective evaluation by touch was performed with 11 students as subjects. The evaluation items are 5 items: "fluffy-flat", "soft-hard", "elastic-not", "smooth-rough", "good-bad as a towel". The evaluation method used a seven-step SD method from -3 to +3. After that, the items of "plump", "soft", "elastic", "smooth" and "good touch as a towel" are regarded as the positive side, and the larger the value, the higher the evaluation.

2.3 Physical properties

Physical properties related to texture of fabric using KES (Kato Tech Co., Ltd.) [3], tensile properties *EMT*, *LT*, *WT*, *RT*, bending properties *B*, *2HB*, shear properties *G*, *2HG*, *2HG5*, surface properties *MIU*, *MMD*, *SMD*, The thickness *T* and the weight *W* were measured. Maximum tension of the tensile property is 250N/m, maximum curvature *K* of the bending property is $\pm 1.25 \text{ cm}^{-1}$, deformation speed is $0.5 \text{ cm}^{-1}/\text{s}$, contact load of surface friction property is 0.25N, contact load of surface roughness property is 0.05N.

3 RESULTS AND DISCUSSION

3.1 Subjective evaluation

In all evaluation items, a high positive correlation of 0.6 to 0.9 was confirmed between the items. Figure 1 shows a change in the evaluation of the feel of the skin by washing. The rating drops as you wash. This shows the same tendency for all subjective items. Evaluation at the time of washing and drying is higher than the evaluation only for washing. In addition, the evaluation value of the low flow rate course is higher than that of the general course. When a softener is used, the change in evaluation value is small in all subjective items even if the number of washings is increased.

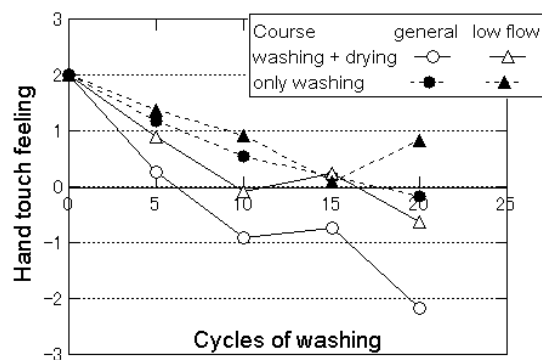


Figure 1 Change of touch feeling to the cycles of washings

3.2 Physical properties

Figure 2 shows the change in physical properties depending on the number of times of washing. As the number of cleanings increases, flexural properties, shear properties, and surface properties increase. Figure 3 is a chart showing changes in physical properties of whether to dry with a drier after washing or to dry naturally. Drying in the dryer after laundering increases bending, shear, and surface properties and reduces compressive

properties over laundering alone. That is, after washing, it is more durable to dry with a drier. In the case of a general washing course, bending, shearing, and surface properties increase in the case of only washing, but in the case of a low flow course, changes in physical property values are small. Figure 4 shows the change after washing due to the presence or absence of the softener. The use of softeners increased the surface properties.

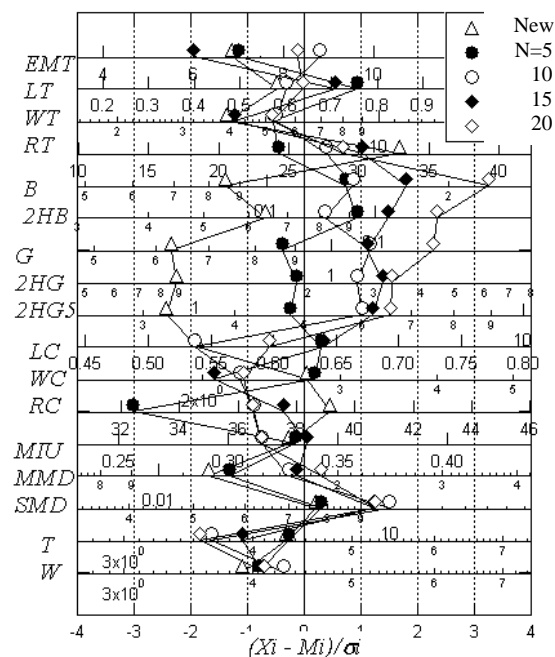


Figure 2 Change of physical properties to the cycles of washings

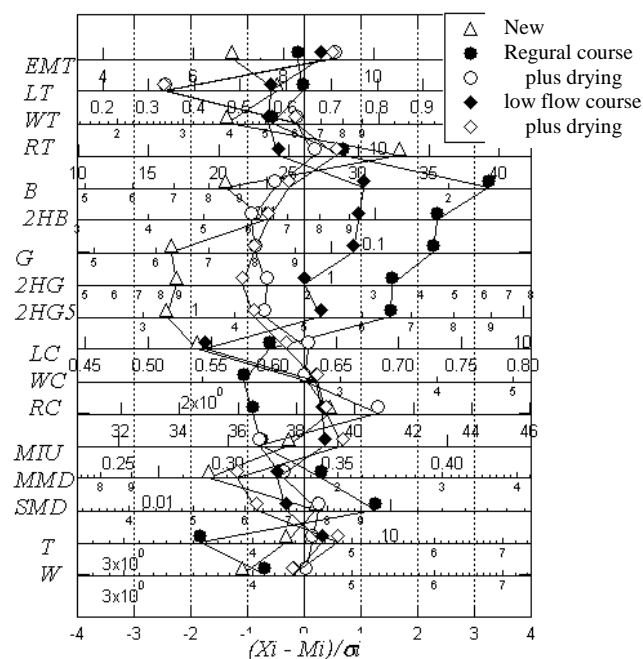


Figure 3 Change due to drying or not

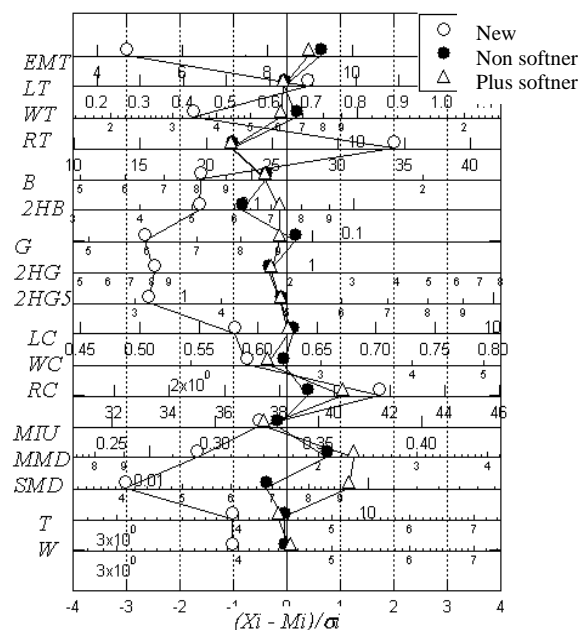


Figure 4 Change of physical property by washing method (presence or absence of softener)

3.3 The relationship between subjective evaluation value and physical properties

Comparing the change in subjective evaluation with washing and the change in physical properties, when washed and dried on the low flow course, the deterioration due to washing was small and the subjective evaluation of the towel was high.

4 CONCLUSION

In this study, the towel before and after washing was used as a sample, and the subjective evaluation and physical characteristics were measured.

As a result, it was possible to capture the change in the feel of the towel due to the number of times of washing, and to clarify the difference in durability depending on the washing method.

5 REFERENCES

- [1] T. Nishimatsu, et al.: Relation between Hand of Bath Towel and Physical Properties, Journal of Textile Engineering, Vol.60, No.6, pp.91-98 (2014)
- [2] H. Ushioda, et al.: Effects of softener-treated towels on human skin sensation, Journal of Home Economics of Japan, Vol.47, No.6, pp.579-588 (1996)
- [3] S.Kawabata, "The Standardization and Analysis of Hand Evaluation (2ed.)", The HESC and The Text. Mach. Soc. of Japan (1980)

INVESTIGATION OF THE INFLUENCE OF COMPRESSION ON THE IN PLANE PERMEABILITY OF FABRIC PREFORMS IN VIMP

Jinhua Jiang¹, Yi Geng², Qinghua Yu¹, Chenglong Zhang¹ and Nanliang Chen²

¹ Engineering Research Center of Technical Textiles, Ministry of Education, Donghua University, Shanghai 201620, China: jiangjinhua@dhu.edu.cn

² College of Textiles, Donghua University, Shanghai 201620, China

Abstract: In liquid composite molding (LCM) processes, permeability is the measurement for the ease of resin flow in porous media, closely related to the molding cycle and product quality of composites. The determination of accurate permeability values can not only improve the production efficiency but also effectively reduce the production of dry spot and stomata. Different preforms have different thickness and porosity under compression, and permeability will change under compression. Otherwise, some problems occur during the permeability tests by vacuum infusion molding process (VIMP). The ease of deformation of fabrics makes it difficult to seal the fiber preform tightly. Therefore, it is necessary to understand the influence of compression on the permeability of different layer preforms. To study the influence of addition of a cover and compression on the permeability of fiber reinforced material, in-plane permeability of glass fiber reinforcement was tested by VIMP. The results indicated that inserting cover mold changes the permeability of glass fiber preform. Different covers with different properties lead to different results. For different fabric layers, the effect of a cover on permeability of fiber reinforced material varies but could not show obvious regularity. Under the uncompressed condition, the permeability change of the preforms is related to fabric layers. With the increase of the number of layers, the permeability of the preform is decreased, which provides some theoretical guidance for composite manufacturing and optimization of technological parameters.

Keywords: permeability, vacuum infusion molding process, compression, fabric

1 INTRODUCTION

Vacuum infusion molding process (VIMP), developed from resin transfer molding (RTM), is a highly efficient composites molding technology, which has lots of advantages, such as environmental protection, ease to operate, low cost, flexible design, and is widely used in many fields including automobile manufacturing, construction and aerospace [1-3]. In this liquid composite molding (LCM) process, the reactive resin is pumped into the mold cavity to saturate fiber preform and expel the air inside after the fiber preform is closed by vacuum bag and sealed with sealing tape. Once the mold is completely filled, the resin injection is disconnected to allow the resin to cure [4-5]. In liquid composite molding (LCM) processes, permeability is the measurement for the ease of resin flow in porous media, closely related to the molding cycle and product quality of composites [6]. The determination of accurate permeability values can not only improve the production efficiency but also effectively reduce the production of dry spot and stomata. Therefore, to explore the relationship between the permeability and internal structure of fabric will play a great role in promoting the development of industry.

2 EXPERIMENTAL

2.1 Material

In this investigation, flow experiments were conducted with glass fiber reinforcements. The fabric structure is plain weave, warp yarn density and weft yarn density of which are both 5 yarns per centimeter. The surface density of fabric is 300g/m². The size of both PMMA

sheet and PVC sheet used in experiments is 400mm*120mm*2mm. The test fluid is silicone oil, and its viscosity is stable at 350mPa·s at room temperature.

2.2 Flow experiment method

The experimental device is a self-designed glass plate mold, and permeability test experiment is shown in Fig 1. The resin is injected linearly from the left side of fiber preform and vacuumed at the right side of that. Assuming that the resin is incompressible fluid and that the preform is porous medium, the flow of resin in preform obeys the law of Darcy.

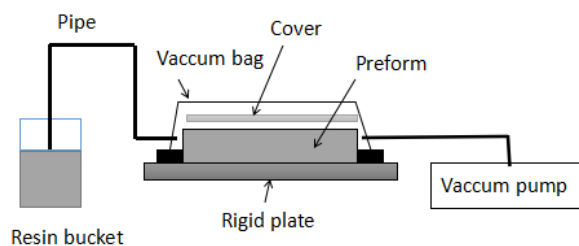


Figure 1 The schematic principle of VIMP

If only one dimensional flow is considered, the unidirectional flow equation of resin can be derived by Darcy's law:

$$u = -\frac{K}{\mu} \nabla P \quad (1)$$

With square of flow front position as ordinate and time as abscissa, the slope of fitting line can be calculated by linear fitting method. Then we can get:

$$K = \frac{k\mu\varphi}{2\Delta P} \quad (2)$$

3 RESULTS AND DISCUSSION

3.1 The influence of addition of a cover mold on permeability

Define

Fig. 3 is the relation curve between the resin flow front and time. Resin flows as far as 28.4cm, 29.0cm and 26.3cm respectively after 30 minutes' injection. Thus, it can be seen that different properties of thin sheets have different effects. Compared with the case without a cover mold, permeability increased by 7.5% with a PMMA sheet, but the permeability decreased by about 11.4% when inserting a PVC sheet.

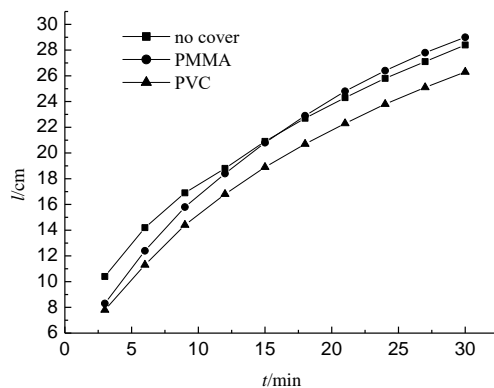


Figure 2 Relationship curves between resin flow front distance and filling time in VIMP

3.2 The influence of number of layers on permeability

Fig.3 is the permeability test result of preform with different fabric layers covered with different sheets.

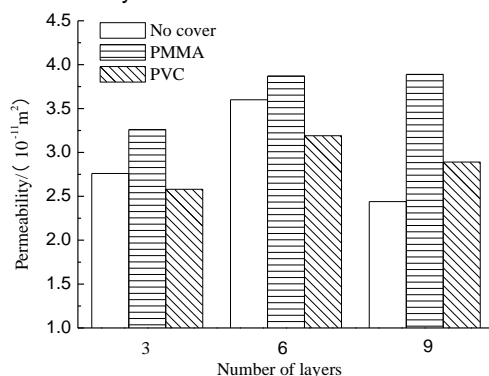


Figure 3 The permeability of preform of different layers with different cover plates

Preform of different fabric layers shows some differences in permeability. On the whole, with the increase of fabric layers, permeability of the preform first rises and then decreases. After inserting a PMMA hard sheet, permeability of preform increases, no matter how many layers the preform is. When the number of fabric layers is 9, addition of a PMMA sheet makes permeability increased about 60%. When the number of plies is 3 or 6, insertion of the PVC sheet reduces in-plane permeability of preform. The insertion of a PVC sheet is beneficial to resin flow only when the number of layers is 9. Therefore, the number of plies is an important factor affecting permeability of fiber reinforced materials.

4 CONCLUSION

The fiber reinforced material is considered as porous medium, so the application of Darcy's law is validated. Factors like the number of plies and cover mold were investigated. Results show: Adding a cover mold does not affect the fiber volume fraction of fiber reinforcement but changes their permeability. Different covers lead to different results. The existence of PMMA increases permeability of preform, because PMMA is too rigid to deform under vacuum state, which creates more space for resin saturation. Adding PVC cover mold hinders the flow of resin to some extent; in general, with the increase of fabric layers, permeability of preform firstly increased and then decreased; when the number of plies is 9, the permeability of fiber reinforced material can be remarkably improved by inserting a PMMA sheet.

ACKNOWLEDGEMENT: This work was financially supported by National Natural Science Foundation of China (NSFC 11472077), National Key R&D Pro-gram of China(2016YFB0303300), the Fundamental Research Funds for the Central Universities (2232019G-02).

5 REFERENCES

- [1] Jiang J, Su Y, Zhou L et al. Effect of Nesting on the Permeability of Multilayer Unidirectional Fabrics. *Applied Composite Materials*, 2016, pp. 1-18.
- [2] Li M, Wang S, Gu Y, et al. Dynamic capillary impact on longitudinal micro-flow in vacuum assisted impregnation and the unsaturated permeability of inner fiber tows. *Composites Science & Technology*, 2010, 70(11), pp. 1628-1636.
- [3] Yang jinshui, Xiao Jiayu, Zeng Jingcheng, et al. Study on resin flow in vacuum infusion molding process. *Aerospace Materials and Technology*, 2007, 37(5), pp. 22-26.
- [4] Cui Xin, Liu Jun, Xiao Jiayu, et al. Research progress of vacuum infusion molding process[J]. *Materials Review*, 2013, 27(17), pp. 14-18.
- [5] Chen D, Arakawa K, Uchino M. Effects of the addition of a cover mold on resin flow and the quality of the finished product in vacuum - assisted resin transfer molding. *Polymer Composites*, 2016, 37(5), pp. 1435-1442.
- [6] Gao Yantao, Li Wei, Luo Yongkang. Study on infiltration law and process optimization of multilayer glass fiber fabric in VARTM process. *Fiber Reinforced Plastics /Composites*, 2009(6), pp. 54-57.

Comfort Assessment of Bottom Mattress for Bedding Apparatus

Hiroyuki Kanai¹, Takuma Kobayashi¹, Hiroki Maru¹ and Shuhei Hanashiro²

¹ Shinshu university, Tokida 3-15-1, Ueda, Nagano, Japan, e-mail: kanai@shinshu-u.ac.jp

² MARUHACHI-PRODUCT, Shinyokohama 3-8-12, Kouhokuku, Yokohama, Kanagawa, Japan

Abstract: Japanese traditional style of bedding apparatus is called FUTON, which is consist of a pair of a bottom mattress, a quilt and a pillow. This kind of bedding apparatus is traditionally set directly on a straw-made cushioning mat which is called TATAMI-MAT, and is used. However, the recent bedding apparatus have variegated using novel materials and technologies according to the divergence of life style in Japan, such as increase of wooden floor for housing. In this study, first of all, we investigated the end-user's requirement of bedding apparatus through the usability test with commercial 5 different bottom mattress. Then, measuring the mechanical property, such as the compression property on samples of bedding apparatus was conducted. And explored the essential character of the compression property which delivering to the end-user's satisfaction.

Keywords: Bottom mattress for bedding, Comfort assessment, Copression property, Motion adaptability

1 INTRODUCTION

Japanese traditional style of bedding apparatus is called *FUTON*, which is consist of a pair of a bottom mattress, a quilt and a pillow. This kind of bedding apparatus is traditionally set directly on a straw-made cushioning mat which is called *TATAMI-MAT*, and is used. However, the recent bedding apparatus have variegated using novel materials and technologies according to the divergence of life style in Japan, such as increase of wooden floor for housing. In this study, first of all, we investigated the end-user's requirement of bedding apparatus through the usability test with commercial 5 different bottom mattress. Then, measuring the mechanical property, such as the compression property on samples of bedding apparatus was conducted. And explored the essential character of the compression property which delivering to the end-user's satisfaction.

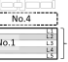
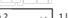



2 SAMPLES

The specification on 5 commercial *FUTON* samples was shown in Table1. The Bag shaped quilting was filled with assembly which is formed by multiple layer structures (i.e., No.1, 5) or single layer structures (i.e., No.2, 3, 4). Each layer structure is variously formed such as not only web of nonwoven but also urethan form. Note that, the No.1 was evaluated in an over-lay with No.4, because the maker recommends usage in overlay with No.1 and No.4 for superior function on a dispersing contact pressure. In addition, alone No.4 was also evaluated, in purpose of obtaining the reference data.

3 SENSORY EVALUATION

Sensory evaluation was conducted for understanding features of each *FUTON* sample in 3 different condition which supposed scene of practical use. In other word, (exp.i) assessing on lie down comfort under static dorsal posture for 20 s, (exp.ii) assessing motion adaptability

Table.1 Materials and layer structure of samples

Sample	Quilting			Material used in layer			Layer structural image
	Face	Materials	Mix. ratio (%)	Layers	Materials	Mix. ratio (%)	
No.1	Outside	Cotton	50	L.1	Wool	100	Over-layer  5 layers
		Polyester	50	L.2	Wool	100	
	Inside	Cotton	100	L.3	Polyester	70	
				L.4	Acrylate system fabric	30	
				L.5	Polyester	100	
No.2	Reversible	Cotton	100	L.1	Polyurethane foam	100	 1 layers
No.3	Outside	Polyester	100	L.1	Polyester	100	 1 layers
	Inside	Polyester	100				
No.4	Outside	Lam fur	100	L.1	Polyester	100	 1 layers
	Inside	Polyester	100				
No.5	Reversible	Polyester	100	L.1	polyester		 4 layers
				L.2	Wool	50	
				L.3	Polyester	50	
				L.4	Wool	50	
				L.5	Polyester	50	
				L.6	Polyethylen	100	

under turn over motion, and (exp.iii) assessing on easiness of posture keeping under static dorsal posture for 180 s

3.1 Methodology

(exp.i) a compressive sensation, an impression for usage, a preference for usage were evaluated with 14 adjectives, and (exp.ii) an easiness of the movement (i.e., turning over), deforming and following of *FUTON* to body movement were evaluated with 6 adjectives by paired comparison method, respectively. In addition, (exp.iii) an easiness of keeping posture was evaluated with 4 adjectives by semantic differential method.

7 graded scale system (± 3 pt : very, ± 2 pt : moderately, ± 1 pt : slightly, 0pt : neither) was used. 17 male and 16 female Japanese (20's : 15, 30's : 10, 40's : 2, 50's : 6 persons, respectively) were recruited as evaluators representing end-users of *FUTON* product. Experiment was conducted in a specific atmosphere ($23 \pm 2^\circ\text{C}$, $50 \pm 4\%\text{R.H.}$).

3.2 Applied rating scores to factor analysis

The factor analysis was applied to the mean preference scores and the mean rating scores obtained from exp.i-iii,

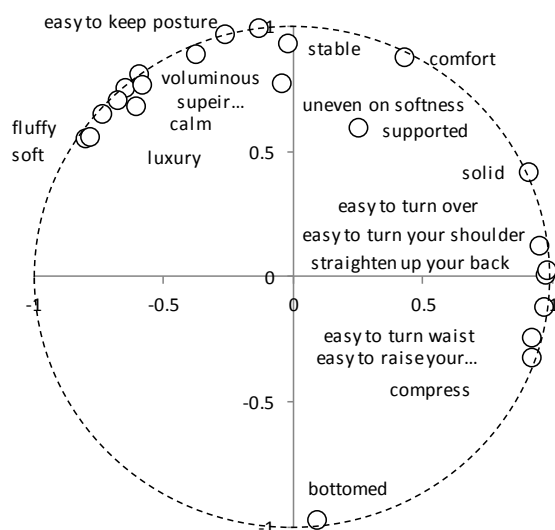


Figure 1 Factor loading

and varimax-rotation was processed. From the result of factor loadings shown in Fig.1, 2 common factors (CF), i.e., 1st CF (x-axis) : 'Easiness of the movement' and 2nd CF (y-axis) : 'Easiness of keeping posture' were interpreted.

4 COMPRESSION PROPERTY

In previous study, the static compression testing or dynamic compression test have been conducted to understand compression property for products of *FUTON*. The static compression test is the method for measuring the thickness with acting a constant weight on a sample. On the other hand, the dynamic compression test is the method for measuring a change of load as repellent force against continuous change of displacement. In this research, the original compression test combined with static and dynamic compression test was proposed.

4.1 Tester and Measurement

The compression tester shown in Fig. 2 was consisted of a contractor, a load-cell sensor, a lab-jack which make the unit displacing vertically.

Proposed method is change displacement from initial position to act load on *FUTON* via contractor and keep certain displacement so as to be acting target load on *FUTON*. Then, this procedure was repeated with change the target load increasing 10 N till 300 N which is the maximum target load. Mean value was calculated from 5

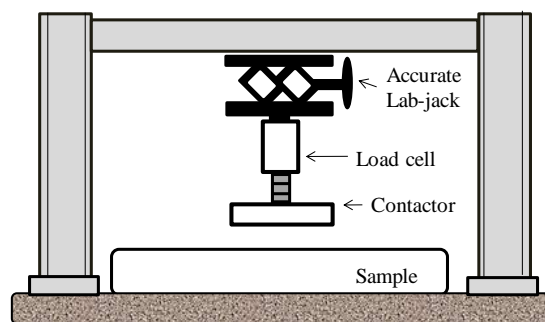


Figure 2 Tester for compression property

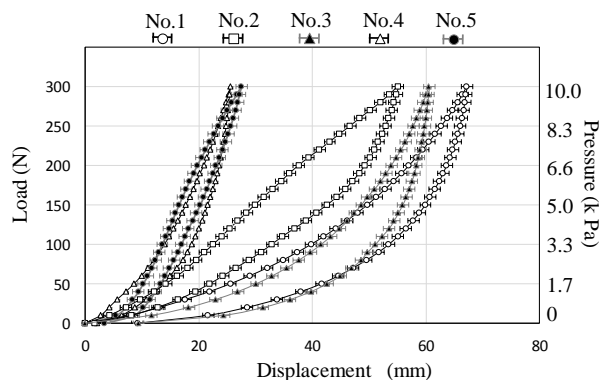


Figure 3 S-S curve obtained from compression test

datasets obtained from measuring at the location of buttocks on *FUTON*.

4.2 Characterization

The Stress-Strain curve obtained the compression test was shown in Fig.3. 12 characters were defined originally and values shown in Tab. 2 were calculated.

5 CORRELATION ANALYSIS

Correlation analysis between factor score of 2 CF obtained from factor analysis and 12 characters obtained from compression test was attempted. From the result, the 2nd CF, i.e., "Easiness of keeping posture" was highly correlated ($r = -0.96$, S.L.<1%) with Young's modulus in high pressure level (E_H), and that was correlated ($r = 0.93$, S.L.<5%) with the compression energy (WC). However, the 1st CF, i.e., "Easiness of the movement" was not correlated highly with any 12 characters.

Table. 2 Characterization on compression property

Sample	T_0 [mm]	ΔT_{20} [mm]	ΔT_{100} [mm]	$C\%$ [%]	Wc [mm·N]	Lc [a.u.]	Rc [%]	Sc_{30} [k Pa]	E_L [k Pa]	E_M [k Pa]	E_H [k Pa]	E_{MH} [k Pa]
No.1	123.7	28.9	67.3	54	660.6	0.65	57.1	2.890	0.056	0.145	0.245	0.397
No.2	85.5	16.2	55.1	64	754.7	0.91	66.2	3.987	0.102	0.222	0.204	0.200
No.3	91.3	32.9	60.6	66	481.9	0.53	56.2	1.353	0.043	0.192	0.361	0.608
No.4	43.0	9.9	25.6	60	276.4	0.72	64.1	2.934	0.174	0.385	0.544	0.793
No.5	68.8	11.0	27.5	40	329.4	0.80	73.5	7.101	0.119	0.551	0.473	0.388

PRESSURE COMFORT CHARACTERISTICS OF SPORTS SOCKS MADE OF MODIFIED SYNTHETIC MATERIALS WITH DIFFERENT WEAVES

Sibel KAPLAN, Betül AKGUNOGLU

Suleyman Demirel University, Textile Engineering Dept., Isparta, Turkey. e-mail: sibelkaplan@sdu.edu.tr

Abstract In this study, pressure applied by sports socks on lower leg part was investigated by pressure measurements and dynamic elastic recovery calculations by Reimann Sums Method giving idea about response of the garment to instant body movements from stress-strain hysteresis graphs (obtained for 30%, 40% and 50% extensions). Socks fabrics having different weaves (single jersey, tucked and terry) were produced from polyester, its modified form Thermocool® (Ne 26) and polypropylene, its modified form Polycolon® (Ne 34). Moreover, standard physical and mechanical tests such as weight, thickness, bursting strength were also carried out on 12 fabric samples (4 materials and 3 weaves). According to the results, polyester and Polycolon® created higher body pressure and dynamic recovery of polyester is better than the other materials.

Keywords sports socks, dynamic elastic recovery, pressure comfort, modified synthetic fiber.

1 INTRODUCTION

Sports socks are an important component of sports clothing that are used especially by professional sports people. As feet comfort is decisive on overall comfort of the body for thermal and pressure aspects; transfer properties, skin-fabric friction and pressure applied on foot and leg are commonly measured parameters. Skin-fabric friction and pressure characteristics are important also for sports performance besides comfort and an optimization is necessary for enabling thermal and pressure comfort on foot by changing material and weave of the fabrics on different parts of sports socks. Nowadays, there are special socks for every conceivable sport activity. Socks should rather be designed specific to the shoe, varieties of foot stresses, environmental and demands of the sport [1-2]. Compression support is provided in sports socks to help increasing the movement performance and in compression stockings and pantyhose for patients suffering some diseases such as varicose vein [3]. Elastic fabrics and their garments have instant response and return back to their original size and shape due to the physical movements of the body. These garments improve the sportsmen's performance by offering least resistance during garment stretch and they enhance the power by quick recovery due to elastane in the fabric. A simple and ordinary body movement expands the skin by about 10–50%. Therefore, the strenuous movements of active sports will require the least resistance from garment and instant recovery [4]

2 MATERIALS AND METHODS

2.1 Materials

Socks fabrics having different weaves (single jersey, tucked and terry) were produced from staple polyester, its modified form Thermocool® (Ne 26) and polypropylene, its modified form Polycolon® (Ne 34).

2.2 Methods

Samples were produced on a Lonati Socks Knitting Machine having 200 needles and 18E gauge in single jersey, tucked and terry weaves to simulate different regional parts on a standard sports socks. Single jersey

fabrics were knitted without elastane to see the material effects but 20/40 dtex/13f (spandex/polyamide) gipid yarn was used for tucked and terry fabrics. Dynamic elastic recovery (DER) characteristics of sports socks were investigating by calculations on stress-strain graphs of the single jersey fabrics which were obtained according to ASTM D 4964-96. Fabrics were stretched for 30%, 40% and 50% extensions and DER values were calculated by Riemann Sums Method for 50% extension by Equation 1 according to a preceding study [4]

$$DER (\%) = \frac{\text{Area under the unloading curve}}{\text{Area under the loading curve}} * 100 \quad (1)$$

Force values belonging to the determined extensions which give idea about the pressure applied by the fabric to the body were also recorded. Moreover, pressure applied by the single jersey fabrics were measured by a flexible pressure sensor system (Tekscan, USA). Fabrics were placed on a cylinder having a diameter of 10,2 cm which corresponds an extension of 60% and the pressure between fabric and cylinder was recorded at the center marked location of the circumferential line [5]. Standard physical and mechanical tests such as weight (TS 251), thickness (ASTM D1777-96), bursting strength (ISO 13938-2) were also carried out on 12 fabric samples (4 materials and 3 weaves). SPSS 21.0 Statistics Software (SPSS Inc. USA) was used for Analysis of variance (ANOVA) test for 95% confidence level.

3 RESULTS AND DISCUSSIONS

Physical and mechanical test results of the socks fabrics are compiled in Table 1. Statistical analysis results were summarized with letter codes, different letters showing significant differences on Table 1. According to bursting strength results, maximum values were obtained for polyester single jersey fabric. Polyester and Polycolon have superior tenacity values in case of material, a result in harmony with yarn strength values. Considering weave type, single jersey fabrics have the maximum bursting

strength values, tucked and terry fabrics have statistically identical values. Breaking elongation values were the maximum for polyester and Polycolon® and tucked weave created maximum elongation values.

Table 1. Physical and mechanical properties of socks fabrics

Fabric Code	Weave Structure	Raw Material	Weight (g/m ²) [S.S]	Thickness (mm) [S.S.]	Bursting Strength (kPa) [S.S]
PES	Single Jersey	%100 Polyester	255.20 ^d [2.34]	0.65 ^a [0.02]	240.43 ^a [11.01]
PES	Tucked	%78/15/7 Polyester/Polyamide/Ly	116.47 ^f [5.48]	1.62 ^e [0.04]	96.76 ^{ef} [1.92]
PES	Terry	%78/15/7 Polyester/Polyamide/Ly	544.62 ^a [26.80]	2.79 ^c [0.05]	101.63 ^{de} [0.35]
MPE S	Single Jersey	%100 Thermocool®	149.60 ^e [9.22]	0.67 ^a [0.03]	103.36 ^{de} [2.38]
MPE S	Tucked	%78/15/7 Thermocool®/Polyamide/Ly	264.87 ^d [3.00]	1.48 ^f [0.02]	90.63 ^{ef} [4.09]
MPE S	Terry	%78/15/7 Thermocool®/Polyamide/Ly	553.35 ^a [25.52]	2.92 ^b [0.05]	85.06 ^f [2.04]
PP	Single Jersey	%100 Polypropylene	93.70 ^g [1.92]	0.74 ^a [0.02]	133.5 ^c [3.55]
PP	Tucked	%74/17/9 Polypropylene/Polyamide/Ly	254.98 ^d [5.01]	1.54 ^f [0.02]	87.7 ^{ef} [2.58]
PP	Terry	%74/17/9 Polypropylene/Polyamide/Ly	520.98 ^b [4.46]	3.23 ^a [0.10]	105.9 ^{de} [4.63]
MPP	Single Jersey	%100 Polycolon	94.98 ^g [1.38]	0.73 ^a [0.01]	228.1 ^b [16.44]
MPP	Tucked	%74/17/9 Polycolon	263.40 ^d [3.21]	1.74 ^d [0.05]	114.96 ^c [2.04]
MPP	Terry	%74/17/9 Polycolon	475.33 ^c [12.04]	2.92 ^b [0.07]	100.03 ^{def} [5.08]

PES: Polyester, MPES: Thermocool®, PP: Polypropylene
MPP: Polycolon®

According to the DER results of wale direction (Figure 1), while standard polyester fabric had significantly the lowest DER values, modified polyester Thermocool® had significantly the maximum values showing its capability of

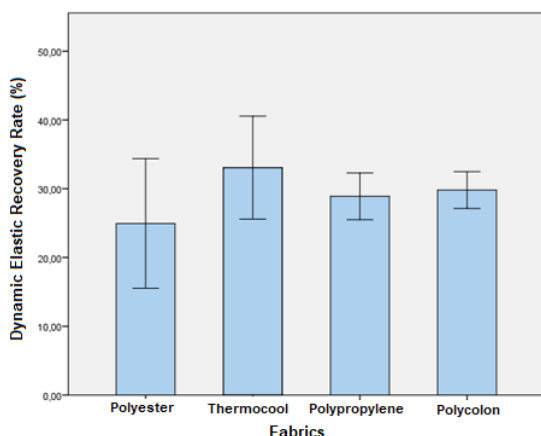


Figure 1. DER values of single jersey socks fabrics (wale direction)

instant response to body movements and return to their original size and shape. Course direction results are thought to have more influence on end use performance of the socks and according to them, polyester fabric had statistically the maximum DER values. Polypropylene fabrics had statistically identical and lower values for both directions. Maximum force results obtained for different elongations show that, Thermocool® and Polycolon® had maximum values for 30% elongation and polyester had maximum values for 40% and 50% elongations on wale direction. Course direction results are higher for Polycolon® (for 30% and 40%) and polyester (50%), meaning higher pressure applied on body. It can be concluded that, polyester and Polycolon® create higher pressure on body but dynamic recovery of polyester is superior to other materials. Summing up, interaction between socks and leg, affective also on necessary pressure on leg muscles for some sports, are related to elastic behavior of the fabric material.

CONCLUSIONS

Pressure comfort performances of synthetic materials, mainly designed for thermal comfort also differ according to frictional and mechanical properties that polyester and Polycolon® can be suggested for socks or garment regions needing extra pressure. Polyester is superior also for movement response being like a second skin.

ACKNOWLEDGEMENT

We thank to Suleyman Demirel University for supporting our study with the project having ID 4840-YL1-16.

REFERENCES

- 1) Baussan, E., Bueno, M. A., Rossi, R. M. and Derler, S., 2010, Experiments and modelling of skin-knitted fabric friction", *Wear*, Vol: 268(9),pp:1103-1110.
- 2) Richie, D.H. Socks: Hosiery - Essential equipment for the Athlete. [cited 2009/03/11]; Available from: <http://buildyourownnewsletters.com/content/socks-hosiery%E2%80%94essential-equipment-athlete>.
- 3) Dan, R., Fan, X. R., Xu, L. B., & Zhang, M. (2013). Numerical simulation of the relationship between pressure and material properties of the top part of socks. *Journal of the Textile Institute*, 104(8), 844-851.
- 4) Senthilkumar, M., Anbumani, N., 2011. Dynamics of Elastic Knitted Fabrics for Sports Wear. *Journal of Industrial Textiles*, 41(1), 13-24.
- 5) Sang, J.S, Lee, M.S. and Park, M.J., (2015). Structural effect of polyester SCY knitted fabric on fabric size, stretch properties and clothing pressure, *Fashion and Textiles*, 2:22.

CLOTHING COMFORT EVALUATION OF UNDERWEAR THROUGH COMPARISON BETWEEN POLYPROPYLENE YARN AND POLYESTER YARN

Yuki Karasawa¹, Mayumi Uemae¹, Hiroaki Yoshida¹ and Masayoshi Kamijo¹

¹ Shinshu University, 3-15-1 Tokida, Ueda-city, Nagano 386-8567, Japan: kamijo@shinshu-u.ac.jp

Abstract: The effectiveness of polypropylene (PP) as a yarn material of underwear was evaluated by comparison with polyester (PET), according to the psychophysiological responses of participants at the time of wearing. Underwear samples were made from two yarns; that is, PET/PP (PP spun yarn was used for the material on the skin side) and PET/PET (PET spun yarn was used for the material on the skin side). The outsides of both types of sample were PET spun yarn. Psychophysiological responses were measured when participants wore a sample during rest and exercise. It was found that the average skin surface temperature of PET/PP was consistently higher than that of PET/PET. Although the temperature decreased owing to perspiration after exercise for both samples, the decrease was less for PET/PP. It is thought that PET/PP dries quickly, lessening the decrease in skin temperature due to moisture from perspiration. Psychological evaluations revealed that participants felt less humidity after exercise when wearing PET/PP. The results suggest the possibility of developing underwear that provides warmth and dries quickly after exercise, using PP on the skin side of the fabric.

Keywords: polypropylene, clothing comfort, psychophysiological measurement, underwear

1 INTRODUCTION

Underwear is important clothing in that it is in direct contact with human skin. The requirements of underwear in terms of clothing comfort include lightness, good heat retention, good water absorption, and an ability to dry quickly.¹ Polypropylene (PP) has low thermal conductivity and good hydrophobicity² and is thus a potential material for use in high-performance underwear that is warm and quick drying. PP is the lightest among practical fibers (with specific gravity of 0.91)² and there is therefore the possibility of making lightweight clothing from PP yarn. The use of PP yarn may allow the production of highly functional underwear with excellent heat retention and a quick-drying property, but underwear made from PP yarn has not been widely used. At present, polyester (PET) fiber is widely used in the underwear market as a chemical fiber having good water absorption and a quick-drying property. The present study therefore measured the material characteristics of fabrics knitted from PP spun yarn and PET spun yarn, and recorded the psychophysiological responses of participants at the time of wearing underwear made from these materials. The sensations of clothing comfort reported by participants were then compared for the two types of underwear. The purpose of the study was to investigate the difference in characteristics of fabrics made from PP and PET chemical fibers, and to evaluate the clothing comfort of underwear made from PP spun yarn.

2 EXPERIMENT

2.1 Samples

Table 1 presents the knitting structures of underwear samples and the total mixing ratios of materials. Two types of sample, named PET/PP and PET/PET, were made. The knitted structure of a sample was a two-layer honeycomb structure on the skin side and a plain stitch on the outside. The material on the outside was PET spun yarn for each type of sample, while the material on the skin side was either PP or PET.

Table 2 gives measurements of material properties of samples and the statistically significant difference between samples according to Welch's t-test. Measurement items are tensile, shearing, bending, compression, surface, and heat transfer characteristics and air permeability obtained using a KES (Kawabata evaluation system) and water absorption and quick-drying characteristics obtained using the BOKEN method (BQE A 028). For all measurement items, the experimental environment was 20 °C and the relative humidity was 65%. Each test was conducted five times and measurements were averaged.

Measurements of material properties show that PET/PP had statistically better wicking and drying characteristics, and lower thermal conductivity owing to the low thermal conductivity of PP. The PET/PET sample material was thick but had low air flow resistance and thus good air permeability.

Table 1. Knitting structure and mixing ratio of each underwear sample

Symbol	Knitting structure		Total blend rate	Note
	Outside (Plain stitch)	Skin side (honeycomb)		
PET/PP	Polyester	Polypropylene	PET44%/PP56%	Diameter of knitting: 34" Number of needle: 2640 Gauge number: 24G
PET/PET		Polyester	PET100%	

Table 2. Material properties of each underwear sample and the results of Welch's t-test

Property	Item	PET/PP	PET/PET	t-test	Method
Heat transport property	Thermal conductance [W/(m ² ·K)]	0.0604	0.0664	□ □	KES-F7 Thermo-Lab
Water transport property	Wicking & Quick drying [%]	26.5	19.5	□	BOKEN BQE A028
Air permeability	Air flow resistance [kPa·s/m]	0.0407	0.0351	□ □	KES-F8
	Thickness [mm]	1.09	1.38	□ □	KES-FB3
	Weight [g/m ²]	157.2	164.8	□ □	Electronic balance

□ p<0.05, □ □ p<0.01

2.2 METHOD

Psychophysiological responses were obtained when participants wore underwear samples. Participants changed their upper garments for cotton underwear and wore long sweat pants, so that initial conditions were the same. They then entered a room kept at a constant temperature of 20°C and constant relative humidity of 65% and rested for 15 minutes as preliminary conditions. Participants then put on the underwear sample. Temperature and humidity sensors (Hygrocron, KN Laboratories, Inc.) were then attached to four points on the body (i.e., the left chest, abdomen, upper back, and lower back). Electrocardiogram (ECG) electrodes were attached to the upper sternum and apical part of the participant employing chest bipolar induction. A thermistor (TDS 2002A, BIOPAC Systems, Inc.) was attached under a naris to measure respiration. The experiment was then carried out for 60 minutes for each participant. The participant first rested for 20 minutes and then exercised on an exercise bike for 10 minutes at an intensity of 55% to 65% their maximum heart rate (in beats per minute) calculated as the difference between the value 220 and their age in years. After exercising, the participant rested again for 30 minutes.

Psychophysiological responses at the time of wearing the underwear were measured to evaluate the clothing comfort of the underwear. Physiological responses were ECG data, respiration recordings for 2 minutes every 10 minutes except immediately after exercise, and continuous recordings of the average skin temperature and average humidity in the clothing worn for 60 minutes. We used the semantic differential (SD) method for psychological responses and collected data five times every 10 minutes except during exercise. There were ten evaluation terms, such as Hot–Cool and Damp–Dry. The evaluation scale had seven steps (–3; extremely, –2; very, –1; slightly, 0; neither, +1; slightly, +2; very, +3; extremely). The participants were 10 male university students. Each participant wore one sample per day at the same time of day in consideration of the circadian rhythm of humans.

3 RESULTS AND DISCUSSION

Figure 1 shows the mean value of the skin surface temperature. This value was calculated from the average values of the nine participants for the four measurement points (i.e., the left chest, abdomen, upper back, and lower back) on the body. It is seen that the average temperature for PET/PP was consistently higher than that for PET/PET. This suggests that PET/PP has higher heat retention. In addition, the temperature decreased owing to a sweat chill after exercise, but the decrease was lower for PET/PP than for PET/PET. This suggests that perspiration was processed quickly by PET/PP, owing to the strong wicking and quick drying of the material.

As a result of SD method, a paired t-test of evaluation terms was performed for samples in each time zone (i.e., 0, 10, 30, 40, and 50 min) (Table 3). Immediately after exercise (at 30 min), PET/PP had significantly higher values than PET/PET ($p < 0.1$) for the terms Damp–Dry and Poorly ventilated–Well ventilated, which express the sensation of sweatiness due to heat and humidity. This result shows that PET/PP reduced the feeling of stuffiness generated by moisture after exercise. This is expected from the wicking and quick-drying characteristic of the two types of sample. It is thought that the PP sample easily absorbs perspiration after exercise, thus reducing the feeling of stuffiness.

To measure changes in autonomic nerve activity while participants wore the underwear, the CVRR, which is a coefficient of variation of the time between R waves (RR interval) obtained in an ECG, was calculated. We can understand the activation of the parasympathetic nerve system. The value of PET/PP tended to be higher at the end of the experiment (from 58 to 60 min). It is thought that the clothing stress after exercise was less when wearing PET/PP owing to the better water transport. Discomfort due to perspiration within the clothing was less for PET/PP.

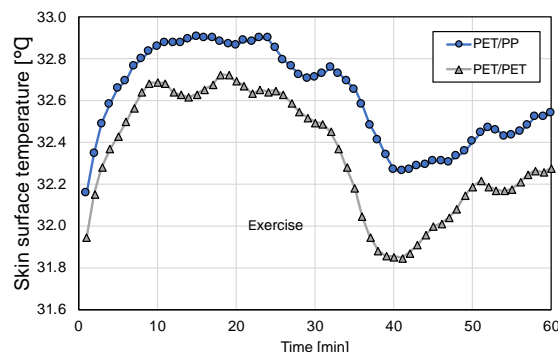


Figure 1. Average temperature of the skin surface temperature

Table 3. Results of paired t-tests performed on evaluation terms for samples in each time zone.

Evaluation terms of pair	Significant difference (**p<0.05, +p<0.1)				
	0min	10min	30min	40min	50min
Hot - Refreshing		+	+		
Cold - Warm					
Damp - Dry				+	
Poorly-ventilated - Well-ventilated				+	
Poor texture - Good texture	*				
Rough - Smooth					
Hard - Soft					
Heavy - Light				*	*
Thick - Thin					*
Uncomfortable - Comfortable					

4 CONCLUSION

The clothing comfort of PP, as compared with that of PET, was evaluated to verify the usefulness of PP as a underwear material. Measurements of material properties and psychophysiological responses when participants wore underwear samples revealed that PET/PP underwear outperforms PET/PET underwear in terms of thermal retention and quick drying, resulting in a weaker sweat chill and weaker feeling of stuffiness due to perspiration. The results suggest the possibility of designing highly functional underwear for winter using PP.

ACKNOWLEDGEMENT: We thank Glenn Pennycook, MSc, from Edanz Group (www.edanzediting.com/ac) for editing a draft of this manuscript.

5 REFERENCES

- [1] M. Iwaki, Y. Mesuda, N. Morikawa and M. Takatera, Journal of the Japan Research Association for Textile End-Uses, Vol.53, pp.209-214, 2012.
- [2] H. Yamamoto, The Properties of Polypropylene Multifilament Textile, J. Fiber Sci. Technol., 61(12), pp. 319-321, 2005.

COMFORT BEHAVIOR OF UNCONVENTIONAL NATURAL FIBRE BASED UNION FABRICS

Kavita¹, Lalit jajpura¹ and B. K. Behera²

¹ Department of Fashion Technology, BPS Mahila Vishwavidyalaya, Haryana 127021, e-mail: kavitalakhlan@gmail.com

² Department of Textile Technology, Indian Institute of Technology Delhi, New Delhi 110016, bijoy.behera@yahoo.com

Abstract: In recent years, consumers now become much more conscious about their choices than ever before. So in the view of sustainability, an attempt has been made to explore the possibilities of producing high quality apparel fabric from selected unconventional natural fibres such as Banana, Hemp, Linen and Ramie. A comparative study was made on the comfort behavior of these fibres fabrics and their respective union fabrics with cotton.

Keywords: Comfort, banana, hemp, linen, ramie, union fabric

1 INTRODUCTION

With advancements in time, people have placed a high emphasis on environment friendly materials and processes. This trend results in an encouragement of development and use of fibers from renewable sources as a substitute for conventional fibres like petroleum-based synthetic fibers and even cotton. As an alternate 'unconventional natural fibres' come in to the picture mainly because of two reasons; Firstly they don't have environmental issues as synthetic fibres have; Secondly, better utilization of land. Either they are obtained as by-product (Banana, Pina, Sugarcane etc) or grew on sub-secondary land with almost no use of pesticides and chemicals (Hemp, Ramie, Flax, Sisal, Kenaf etc). For clothing and apparels, one of the most important aspects is comfort. Comfort has totally replaced the durability and to some extent the aesthetics as far as the selection of garments/fabrics is concerned. Clothing comfort can be classified the three common parameters such as psychological comfort, tactile comfort and thermal comfort. Here, in this research, efforts are being made to explore the possibilities of producing high quality apparel fabric from unconventional natural fibres. For this, a comparative study was made on the comfort properties of Banana, Hemp, Linen and Ramie fibre fabrics and their respective union fabrics with cotton.

2 MATERIAL AND METHODS

2.1 Fibres used

For this research, the four unconventional fibres namely Banana, Hemp, Linen and Ramie are used. Cotton is used as reference fibre for comparison. Yarn samples of 30 Ne were developed from all five above fibres under industrial production conditions and used for fabric development under identical conditions.

2.2 Sample development

The nine grey fabric samples were prepared in a weaving mill under controlled manufacturing conditions using construction parameters as given in Table 1. The construction parameters were taken to maintain fabric areal density at 145 ± 10 gsm (gm per sq meter) taking into account the manufacturing constraints in the mill.

The chemical pretreatment of all the fabrics was carried out in industry maintaining standard parameters used in commercial production of cotton fabric. The sequence of chemical processes is as follows:

Desizing → Scouring → Bleaching → Neutralization → Stentering → Calendering → Folding

2.3 Evaluation of Thermal Insulation

The thermal insulation was evaluated on Thermolabo thermal tester. The Kawabata evaluation system (KES FB7-II) was used to measure the resistance to heat flow or thermal insulation value (TIV).

2.4 Evaluation Of Moisture Management

The liquid moisture transport properties in multi-dimensions called moisture management properties of the fabrics are evaluated on M290 MMT (Moisture Management Tester) manufactured by SDL Atlas Inc. (Rock Hill, SC) in accordance with AATCC Test Method 195-2009 (Liquid Moisture Management Properties of Textile Fabrics). Moisture management properties like absorption rate, one way transport capacity (or OWTC), spreading speed and overall moisture management capacity (OMMC) were reported and analyzed in this study.

2.5 Evaluation of Low stress Mechanical Properties and Hand

The Kawabata Evaluation System (KES) was used to measure fabric mechanical properties at low stress. KES system consists of four different modules for different testing e.g. KES-FB1 for tensile and shear tests, KES-FB2 for bending tests, KES-FB3 for compression properties testing and KES-FB4 for testing surface properties. Total 16 parameters describing fabric mechanical properties were obtained from the instrumental measurements. The 'primary hand values' pertaining to specific comfort aspects of the fabric and then 'total hand value (THV)' were calculated by the software using Kawabata equation.

Table 1 Fabric sample code and properties

Sample		Fabric property				
		GSM	TIV (%)	OWTC	THV-Winter	THV-Summer
C	100% Cotton	143	3.27	394.26	2.313	2.646
B	100% Banana	145	2.03	471.52	2.281	3.013
CB	Cotton-Banana Union Fabric	147	4.80	559.94	1.658	2.952
H	100% Hemp	136	1.61	995.37	2.284	2.82
CH	Cotton-Hemp Union Fabric	139	4.61	676.00	2.439	2.651
L	100% Linen	141	1.67	561.66	0.536	4.238
CL	Cotton-Linen Union Fabric	151	3.97	1085.88	1.711	2.789
R	100% Ramie	138	1.61	758.45	1.537	3.311
CR	Cotton-Ramie Union Fabric	144	4.91	889.24	1.711	2.789

3 RESULTS AND DISCUSSION

3.1 Fabric Thermal Insulation Property

For comfort feeling, body heat should be transmitted away from the body to the outer side of the clothing. The results of comparative analysis are enlisted in table 1. From the result outcomes we can see that fabric samples containing cotton indicate thermal insulation values on higher side as compared to pure fabrics of unconventional fibres. The reasons may be attributed to the structure of cotton fibre. Cotton fibre contains hollow lumen and twists causing more air entrapping in yarn. Whereas, the fibres of hemp, linen and ramie are smooth, straight and contain almost no lumen.

3.2 Fabric Moisture Management Properties

The findings compiled in Table 1 reveal that all the pure fabrics of unconventional fibres and their respective union fabrics have increased values of Accumulative one-way transport index (OWTC) as compared to the reference cotton sample. Generally fabrics which possess high OWTC values indicate that the liquid (sweat) can be quickly transferred from the surface next to the skin to the opposite surface and spread quickly on the fabric bottom surface with a large wetted area where it evaporates into the environment. This behavior can be attributed to the hygroscopic nature of the fibres used. Also the fibre properties like diameter, rigidity and cross-section play a major role in deciding. Hemp fabrics show a relatively higher OMTC values and bottom spreading speed. The bottom water radius is also higher than top in fabrics containing hemp. The fabrics containing linen falls in the next position after hemp in such type of overall moisture management.

3.3 Low stress Mechanical Properties

The THV of the fabric samples is estimated with the help of the primary hand values using the Kawabata-Niwa equations by KES system and the results are shown in table 1. The results depict that almost all the fabric samples exhibit higher THV for summer applications as compared to winter. The values of summer THV of all pure

unconventional fibre fabrics and their respective union fabrics are either comparable or better than 100% cotton. This trend strongly advocates the possibility of unconventional fibre fabrics to be used as an apparel fabric for summers.

4 CONCLUSION

- Through point of view of thermal comfort, unconventional fibre fabrics and their union fabrics with cotton perform better than 100% cotton and show higher heat transmission. These fabrics are more suitable for summer clothing provided other parameters are made suitable to meet the requirements.
- The hemp fabrics pure as well as union show better moisture management. The trend is then followed by linen.
- The fabrics from unconventional fibre give higher total hand value (THV) than cotton fabrics of similar construction and areal density, considering the fabrics are to be suitably used for men's summer shirting. Thus these fabrics can be used in apparels as they are skin friendly, comfortable and will not cause any unpleasant touch.

5 REFERENCES

- [1] Behera B K: Comfort and handle behavior of linen-blended fabrics. *AUTEX Research Journal*, Vol. 7, No 1, March 2007, pp:33-47.
- [2] Behera B K & Mishra R.: Comfort properties of non-conventional light weight worsted suiting fabrics, *Indian Journal of Fibre & Textile Research*, Vol. 32, March 2007, pp:72-79
- [3] Fan J & Hunter L, *Engineering Apparel Fabrics and Garments*. 2009.
- [4] Ozdemir H.: Thermal comfort properties of clothing fabrics woven with polyester/cotton blend yarns, *AUTEX Research Journal*, Vol. 17, No 2, June 2017, pp: 135-141.

MEASUREMENT OF TEMPERATURE DISTRIBUTION ON LOWER LEG WEARING DIFFERENT SIZES OF TROUSERS

KyoungOk Kim¹, Chen Lyu², Chunhong Zhu³, Hiroaki Ishizawa⁴ and Masayuki Takatera^{5*}

^{1,4,5} Shinshu University, Division of Kansei and Fashion Engineering, Institute for Fiber Engineering (IFES), Interdisciplinary Cluster for Cutting Edge Research (ICCER), Tokida 3-15-1, Ueda, Nagano, Japan, *takatera@shinshu-u.ac.jp

² Shinshu University, Graduate school of Science and Technology, Faculty of Textile Science and Technology, Tokida 3-15-1, Ueda, Nagano, Japan

^{1,3,4,5} Shinshu University, Faculty of Textile Science and Technology, Tokida 3-15-1, Ueda, Nagano, Japan

Abstract: The temperature distribution on lower leg wearing trousers in different postures were measured under different environmental temperature conditions. We made a polyester double weave fabric by interweaving copper and constantan wires of 0.1mm in diameters constituting thermocouple temperature sensors. We made a measuring garment using the fabric with 32 measuring points for shin (16 points) and calf (16 points) to measure temperature distribution. We put the measuring garment on a thermal manikin and measured temperature distribution of the measuring garments on sitting and standing postures. Then, we put one of three pairs of trousers (cotton 100%, S, M, L sizes) over the measuring garment and measured the temperatures distribution of the measuring garments. The environmental temperature was 15°C, 20°C and 25°C and the relative humidity was 65%. There is no forced convection. The electric power of the thermal mannequin was set to 58 W/m² (1 Met). The temperature difference between the wearing and unwearing a pair of trousers were similar regardless of the size of the trousers and the ambient temperature. However, the temperature difference was different depending on the measurement points. Comparing temperature differences by postures, the temperature differences of standing were larger than ones of sitting. As increasing air gap between body and trousers, the temperature differences became larger. However, when the air gap was larger than some limit, the temperature differences were smaller due to convection. When the air gap is zero, the temperature differences were small due to the conduction. The proposed method will be effective to obtain the detailed thermal information between body and clothing considering local insulation and conduction, and to design thermal comfort clothing.

Keywords: temperature distribution, thermocouple temperature sensors, trouser, thermal comfort

1 INTRODUCTION

By wearing clothing, the temperature between the human body and clothing is changed. Thus, it is important to measure the temperature to investigate the effect of clothing on thermal comfort. In our previous studies, we have developed a smart textile which incorporated thermocouple temperature sensors [1] and investigated the temperature distribution on an upper body surface of a thermal manikin by wearing the different size of T-shirts [2]. We also investigated the temperature distribution on a lower leg wearing trousers under different environmental temperature conditions on sitting posture [3]. In this study, we measured the temperature distribution on a lower leg wearing different sizes of trousers in different postures under different environmental temperature conditions.

2 EXPERIMENTS

We made a polyester double weave fabric by interweaving copper and constantan wires of 0.1mm in diameters constituting thermocouple temperature sensors. We made a measuring garment using the fabric with 32 measuring points for shin (16 points) and calf (16 points) to measure temperature distribution as shown in Figure 1. We put the measuring garment on a thermal manikin (THM, Kyoto Electronics Manufacturing Co., Ltd. Japan) and measured temperature distribution of the measuring garments on sitting and standing postures. Then, we put one of three

pairs of trousers (cotton 100%, S, M, L sizes) over the measuring garment and measured the temperatures distribution of the measuring garments. The environmental temperature (ET) was 15°C and 25°C and the relative humidity was 65%. There is no forced convection. The electric power of the thermal manikin was set to 58 W/m² (1 Met).

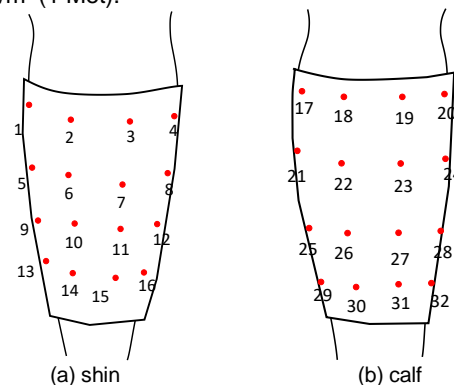


Figure 1 Measuring garment and measurement points [3]

3 RESULTS AND DISCUSSION

The temperature difference between the wearing and unwearing a pair of trousers were similar regardless of the

size of the trousers and the ambient temperature. However, the temperature difference was different depending on the measurement points.

The temperature difference between the wearing and unwearing a pair of trousers (S size) in sitting and standing postures are shown in Figures 2-5. Comparing temperature differences by postures, the differences in standing were larger than ones of sitting on average.

Tables 1 and 2 show the relationship between the air gap and the temperature differences in sitting and standing. As increasing air gap between body and trousers, the temperature differences became larger. However, when the air gap was larger than some limit, the temperature differences were smaller due to convection. When the air gap is zero, the temperature differences were small due to the conduction.

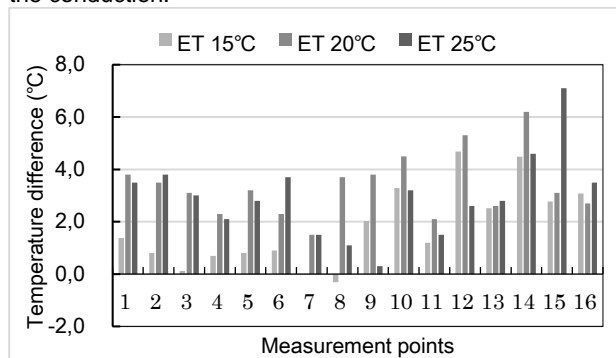


Figure 2 Temperature differences between measuring temperatures with and without trousers under different environment temperature in sitting posture (S size, shin) [3]

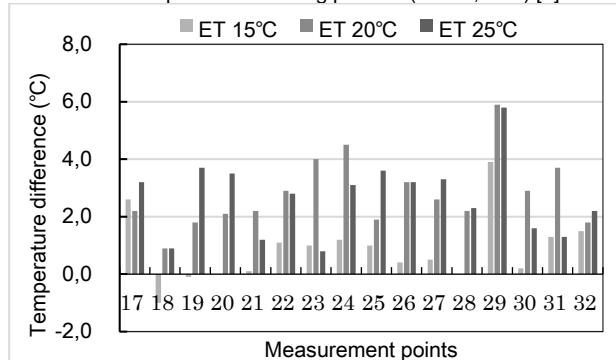


Figure 3 Temperature differences between measuring temperatures with and without trousers under different environment temperature in sitting posture (S size, calf) [3]

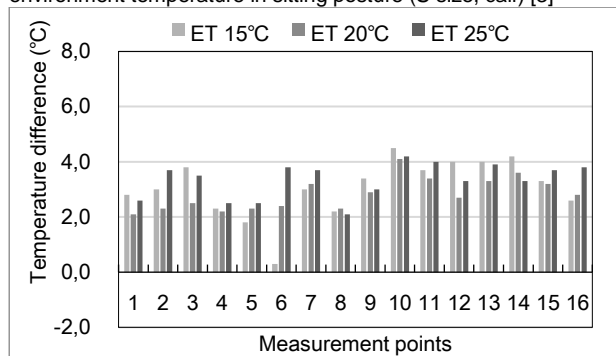


Figure 4 Temperature differences between measuring temperatures with and without trousers under different environment temperature in standing posture (S size, shin)

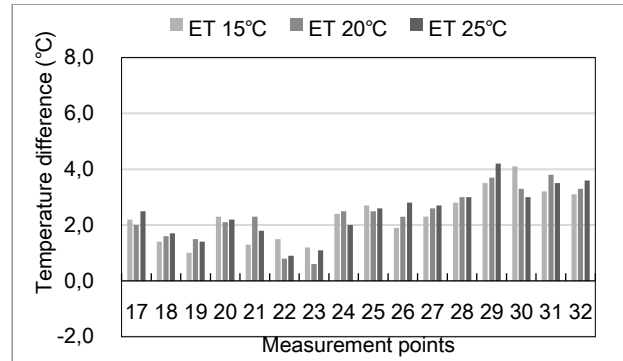


Figure 5 Temperature differences between measuring temperatures with and without trousers under different environment temperature in standing posture (S size, calf)

Table 1 Relationship between the air gap and the temperature differences in sitting and standing (S size)

Place (measurement points)	Air gap (%)	Temperature difference in sitting (°C)	Temperature difference in standing (°C)
A(1-4, 17-20)	0.9	2.0	2.3
B(5-8, 21-24)	0	1.9	2.0
C(9-12, 25-28)	0	2.5	3.1
D(13-16, 29-32)	10.1	3.3	3.5

Table 2 Relationship between the air gap and the temperature differences in sitting and standing (L size)

Place (measurement points)	Air gap (%)	Temperature difference in sitting (°C)	Temperature difference in standing (°C)
A(1-4, 17-20)	3.6	1.0	2.5
B(5-8, 21-24)	0.6	0.7	1.9
C(9-12, 25-28)	0.3	1.1	2.1
D(13-16, 29-32)	15.4	2.1	2.8

4 CONCLUSION

We successfully measured the temperature distribution on a lower leg wearing trousers in different postures under different environmental temperature conditions. By changing posture, the temperature distribution was different due to the different air gap between body and trousers. The proposed method will be effective to obtain the detailed thermal information between body and clothing considering local insulation and conduction, to design thermal comfort clothing.

5 REFERENCES

- [1] Zhu CH and Takatera M, Weaving and performance study on wearable textile thermocouple fabric. International Congress on Innovative Textiles 2011 (ICONTEX 2011), Istanbul, Turkey, 2011, pp. 493-498.
- [2] Takatera M, Uchiyama E, Zhu CH, Kim KO and Ishizawa H, Effect of air gap on apparent temperature of body wearing various sizes of T-shirt, in Proc. AUTEX 2017, 2017, Corfu (Kerkyra), Greece, pp. 29-31
- [3] Takatera M, Uchiyama E, Zhu CH, Kim KO and Ishizawa H, Measurement of temperature distribution on lower leg wearing trousers, in Proc. AUTEX 2018, 18th AUTEX World Textile Conference, Istanbul, Turkey, 2018

TEXTILE LAYERS ENABLING BACK REFLECTION OF HUMAN BODY THERMAL RADIATION

Křemenáková Dana¹, Militký Jiří¹, Novosad Andriana¹ Venkataraman Mohanapryia¹ and Večerník Josef²

¹ Dept of Material Engineering, TU Liberec, 46117 Liberec, Czechia: dana.kremenakova@tul.cz

² Večerník s.r.o Alšovice,

Abstract: The human body produces heat due to basal metabolism and specific physical activities. Up to 30% of this heat is emitted by radiation across the skin at wavelengths belonging to FIR region with maximum around 9.4 microns. Backscatter of this radiation from textile layer to human skin is supported by ceramic particles activated carbon particles, oxides and metals. Main aim of this contribution is description of preparation of special copper coated nonwoven polyester fibrous layers based on composite nonwovens MILIFE. The reflectance of the electromagnetic wave of these layers was tested by using of the integration ball principle. The mean total reflectance and corresponding 95% confidence intervals from five experimental spectra were calculated. The thermal insulation of copper coated MILIFE was characterized by infrared thermography measurement. The air and water vapor permeability were tested as well. It was found that the reflectance of copper coated MILIFE is increased by increasing of planar mass due to deposition of larger amount of copper.

Keywords: fabric spectral reflection, human skin thermal radiation, copper deposition, composite nonwoven

1 INTRODUCTION

The human body constantly produces heat as a result of basal metabolism, specific bodily activities, and ambient temperature humidity conditions. Depending on the ambient conditions, more than 30% of this heat is emitted by radiation across the skin at wavelengths from 4 to 14 μm with maximum 9.4 μm (far infrared region further FIR).

It has been verified that this FIR thermal energy has a number of positive effects on the human body as well. FIR reflection is supported by ceramic particles (mica, tourmaline, and basalt), activated carbon particles, oxides (Al_2O_3 , SiO_2 , ZnO , MgO , ZrO_2 , TiO_2 , CuO , Cu_2O) and metals (Fe, Ag, Cu, Zn, Ni) or metals particles. There are also selected systems containing bonded metal cations, carbon porous particles (such from bamboo stems) and natural materials (tourmaline, clam shells) that have a positive effect on FIR back reflection [5-7].

Main aim of this contribution is description of procedure for creation of FIR reflective textile layer as part of multi-layer textile structures having enhanced thermal protection (see. fig. 1).

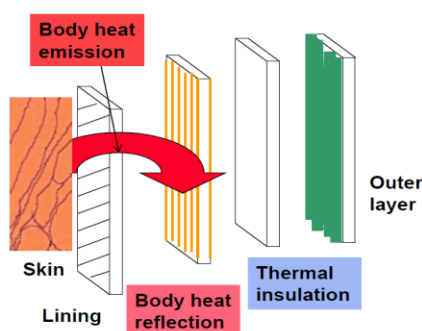


Figure 1 Multi layered thermal protective system

2 RADIATION AND REFLECTION OF SKIN

The ratio of the radiating power to the absorbing power is the same for all bodies at the same temperature (Kirchhoff law), and therefore a body which absorbs perfectly must radiate perfectly as well. Human skin is classified as nearly ideal black body i.e. ideal radiator (difference from ideal black body is about 1 %) [1]. In accordance with Wien law is wavelength λ_m [m] corresponding to maximal radiating power related to reciprocal value of skin temperature T_s [K] ($\lambda_m = 2,898 \cdot 10^{-3} / T_s$). At "normal" skin temperature (34 °C) is the maximum wavelength equal to $\lambda_m = 9,4 \mu\text{m}$. The human body has no appreciable radiation of wavelengths shorter than 4 μm [1]. The maximum skin radiation energy for emission of skin radiating to surroundings at 22° C is about $11.5 \cdot 10^{-6} \text{ W/cm}^2$ [1]. There is a low reflecting and transmitting power of the skin for radiation in the region in which the skin radiates. At 2 μm is skin reflection about 7 % only and it is monotonously decreasing above this wavelength. Above 6.5 -7.5 μm is skin reflection equal to zero [2]. Infra-red transmission through skin, even of the most penetrating rays, is of small proportion, about 95 % of these being absorbed within 2 mm of the surface and 99 % within 3 mm of the surface [3].

3 EXPERIMENTAL PART

Composite nonwovens composed of cross-over layers of monofilaments have very low thickness, excellent shape stability and mechanical properties compared to traditional nonwoven fabrics. An example of these unique materials is the MILIFE® product of JX Nippon ANCI Corporation, composed of a machine-directional (MD-oriented) and cross-directional (CD-oriented) layer of polyester fibers.

Both layers are thermally pointed together. MILIFE is a promising material for surface metallization because it is composed of a dense network of monofilaments joined by fixed points. PET material can be easily activated by hydrolysis (preferably) or by plasma pretreatment

3.1 Preparation of active layers

For preparation of active layer having enhanced FIR reflection the MILIFE with planar mass 10 g/m² (abbreviation MI 10) and planar mass 30 g/m² (abbreviation MI 30) were selected. The basic characteristics of these materials are given in tab. 1.

Table 1. Selected properties of original and activated layers

Property	Unit	MI 10	MIC 10	MI 30	MIC 30
Planar mass	[g/m ²]	11.43	10.52	30.58	32.23
Thickness	[mm]	0.08	0.07	0.13	0.14
Force at break	[N/5 cm]	12.1-27.2*	20.9-28.6*	79.8-96.3*	72.83-88.5*
Deformation at break	[%]	8.8-12.0*	10.7-12.8*	9.7-19.1*	10.7-17.9*
Air permeability	[mm/s]	502.4	350.7	581.7	706.9
Water vapor permeability	[%]	90.3	99.0	79.7	57.11
Thermal insulation I	[-]	0.09-0.11*	0.29-0.39*	0.14-0.24*	0.50-0.64*
Reflectance at 10 μm	[%]	6-7*	20-29*	8-9*	48-52*

* limits of 95 % confidence interval

MILIFE layers were firstly activated for higher surface tension (more than 50 mN m) by plasmatic pretreatment. Surface deposition was realized in two steps. Firstly the deposition of Nickel by electro-less plating was realized. In the second step the deposition of copper from cuprous salts by autocatalytic activation in strong alkali bath at ambient temperature was used. Selected properties of final active layers with surface deposition of metals (abbreviation MIC 10 and MIC 30) are given in tab. 1. Samples MIC contains 3 gm⁻² of copper/nickel with portion of nickel approx. 8 % only.

3.2 Measurement of Spectral Reflectance

The reflectance of the electromagnetic wave of textiles was tested using the integration ball principle on the Mid-IR IntegratIRTM (PIKE TechnologiesTM). The principle is to measure the specimen for the reflection of the infrared ray with a range of 2 to 20 μm. The beam strikes the specimen at an angle of 8° and interacts with its surface. The reflected radiation component is further diffusively reflected from the surface of the integration ball, and its values for individual wavelengths are recorded on a nitrogen-cooled measurement sensor.

3.3 Infrared Thermography

Infrared thermography measurement was conducted by using thermal camera to find the thermal insulation values *I* (see eqn (1)). A vertical hot plate maintained at constant temperature around 40 °C was used as heat source, the specimen was flatly attached onto the hot plate with the help of a frame tool, after 2 min thermal images were taken by thermal camera at a distance of 40 cm from the hot plate. The room temperature was kept at 25 ± 2 °C. A thermal image reveals the amount of radiation emitted by the heat plate through the fabric.

$$I = (B - F) / (B - R) \quad (1)$$

where B - instrument temperature (i.e. 40 °C), F- fabric temperature, R- room temperature. Thermal insulation values are given in tab. 1.

4 RESULTS AND DISCUSSION

The mean values and limits of 95 % confidence interval of spectral reflectance of layers MI and MIC are given in fig. 2.

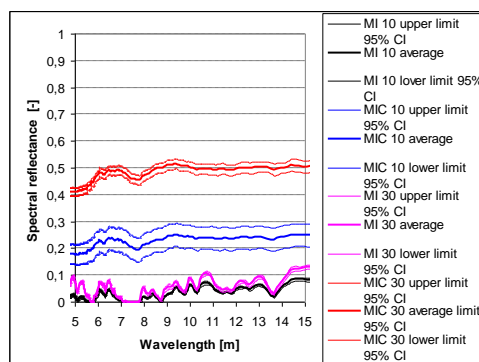


Figure 2 Spectral reflectance of layers MI (original) and MIC (copper coated)

In the work [6-7] the nano-porous metallized POE layer (MP), PET film coated by metallic film (MM) and prints of sparse metallic dots onto the inside of garments (Omni-Heat OH) were compared. Reflectance at 10 μm were MP: 95 %, MM: 26 %, and OH: 17 % [7]. It is therefore visible that the MILIFE based layers have the similar reflectance (excluding MP) but outperforms in air permeability and water vapor permeability i.e. comfort related properties.

Acknowledgement: This work was supported by project SPETEX CZ.01.1.02/0.0/0.0/16_079/0008314 of the Ministry of Industry and Trade and by project of the Ministry of Education, Youth and Sports of the Czech Republic and the European Structural and Investment Funds – Hybrid Materials for Hierarchical Structures (HyHi, Reg. No. CZ.02.1.01/0.0/0.0/16_019/0000843).

REFERENCES

- [1] Hardy J. D.: The radiation of heat from the human body III. , *J. Clin. Invest.* 13, 615-620, (1934)
- [2] Hardy J. D.: The radiation of heat from the human body IV. , *J. Clin. Invest.* 13, 817-831, (1934)
- [3] Hardy J. D.: The radiation of heat from the human body IV. , *J. Clin. Invest.* 14, 1-9, (1935)
- [4] Herman I.P.: *Physics of the Human Body*, Springer International Publishing Switzerland 2016
- [5] Pakdel E. et al.: Advanced functional fibrous materials for enhanced thermoregulating performance, *ACS Applied Materials & Interfaces*, Mar 2019, DOI: 10.1021/acsami.8b19067
- [6] Cai L. et al.: Warming up human body by nanoporous metallized polyethylene textile, *Nature communications*, 8, 496 (2017) DOI: 10.1038/s41467-017-00614-4
- [7] Cai L. et al.: Warming up human body by nanoporous metallized polyethylene textile, *Electronic Supplementary Material*

THERMAL INSULATION PROPERTIES OF THE SEERSUCKER WOVEN FABRICS OF DIFFERENT STRUCTURE

Malgorzata Matusiak

Lodz University of Technology, Faculty of Material Technologies and Textile Design, Institute of Architecture of Textiles,
90-924 Lodz, 116 Zeromskiego str., e-mail: malgorzata.matusiak@p.lodz.pl

Abstract: The seersucker woven fabrics are characterized by an occurring the puckered and flat strips in warp direction. The width of the puckered strips and the distance between the successive puckered strips can be different. The repeat of the seersucker effect influences the properties of the seersucker woven fabrics. The aim of presented work was to investigate the influence of the seersucker repeat and a kind of the weft yarn on thermal insulation properties of the fabrics. 9 variants of the seersucker woven fabrics made of cotton were the objects of the investigations. The fabrics differ between each other with the aspect of the width of the puckered strips and the distance between the puckered strips. Additionally, 3 kinds of weft yarns have been applied as a weft. Measurement of the thermal insulation properties of the fabrics was done by means of the Alambeta device. On the basis of the results it was possible to assess the influence of the main structural factors on the values of the thermal properties such as: thermal conductivity, thermal absorptivity, thermal diffusivity and thermal resistance. In order to assess the statistical significance of stated relationships between the structural parameters and the thermal insulation properties the statistical analysis was performed by means of the ANOVA. Obtained results confirmed that there is possible to shape the thermal insulation properties of the seersucker woven fabrics in a conscious and knowledge-based way.

Keywords: seersucker woven fabrics, structure, thermal comfort, thermal resistance, thermal conductivity

1 INTRODUCTION

The seersucker woven fabrics are characterized by an occurring the puckered and flat strips in the warp direction. Such kind of structure is formed directly on the loom having two warp beams [1, 2]. The width of the puckered strips and the distance between the successive puckered strips can be different. Additionally, in both areas of the seersucker woven fabrics: flat and puckered different weaves can be applied. All this factors: weave, the repeat of the seersucker effect and also a kind of yarn in warps and weft influence the properties of the seersucker woven fabrics. Some researcher consider that due to their structure the seersucker woven fabrics are characterize by very good comfort related properties [1, 3].

The aim of presented work was to investigate the influence of the seersucker repeat and a kind of the weft yarn on the thermal insulation properties of the seersucker woven fabrics.

2 EXPERIMENTAL

2.1 Material

9 variant of the seersucker woven fabrics were the objects of the investigation. The fabrics were manufactured from cotton yarns. In the experimental fabrics 3 kinds of repeat of the seersucker pattern and 3 kinds of the weft yarns were applied. Both warps: basic and puckering were made from the same yarn: 20 tex x 2 cotton. The following variants of pattern of the seersucker effect were applied:

- variant 1 (MM1) – width of puckered and flat strips appropriately: 5 mm and 8 mm,
- variant 2 (MM2) – width of puckered and flat strips appropriately: 9 mm and 18 mm,
- variant 3 (MM3) – width of puckered and flat strips appropriately: 11 mm and 41 mm.

As a weft the following yarns were used: 20 tex x 2, 25 tex x 2 and 30 tex x 2.

2.2 Methods

Measurement of the thermal insulation properties of the fabrics was done by means of the Alambeta device (fig.1). In order to assess the statistical significance of stated relationships between the structural parameters and the thermal insulation properties of the seersucker woven fabrics the statistical analysis was performed by means of the multi-factor ANOVA.



Figure1 The Alambeta device applied in measurement [4]

3 RESULTS AND DISCUSSION

Results of measurement of thermal insulation properties of the investigated seersucker woven fabrics are presented in fig. 2 - 6. It is clearly seen that both the pattern of the seersucker effect and a kind of weft yarn significantly influence the properties of the fabrics.

Results from the Alambeta were analyzed statistically using multi-factor ANOVA. It was stated that the pattern of the seersucker effect influence the thermal insulation properties of the seersucker woven fabrics and the

influence is statistically significant at the probability level $p=0.05$.

A kind of weft yarn also influences the thermal insulation properties of the fabrics. However the influence of a kind of yarn is statistically significant only on the thermal resistance of the seersucker woven fabrics. In the case of the thermal resistance the statistically significant interaction was stated between the main factors: the repeat of the seersucker effect and a kind of weft yarn.

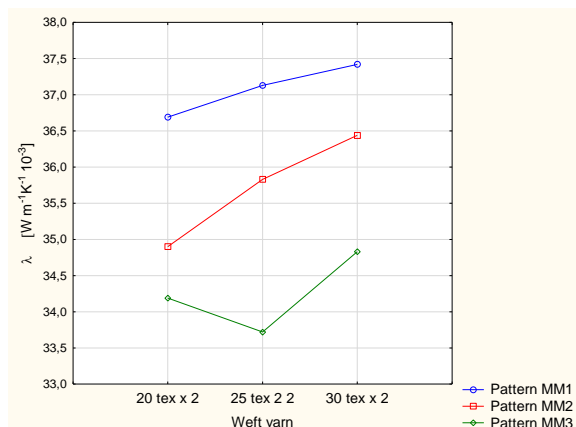


Figure 2. Thermal conductivity of the investigated seersucker woven fabrics

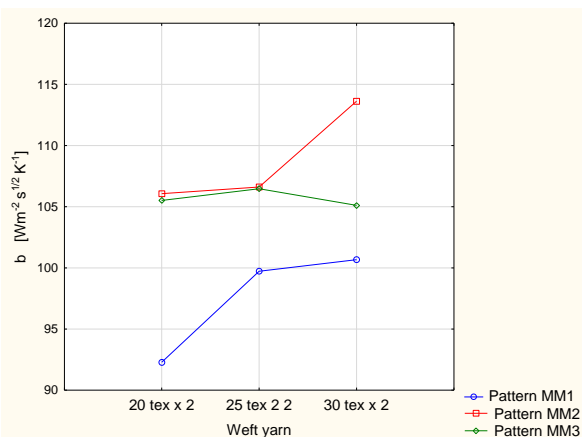


Figure 3. Thermal absorptivity of the investigated seersucker woven fabrics

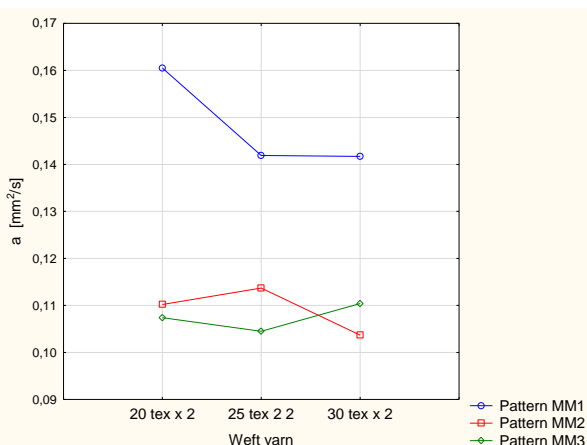


Figure 4. Thermal diffusivity of the investigated seersucker woven fabrics

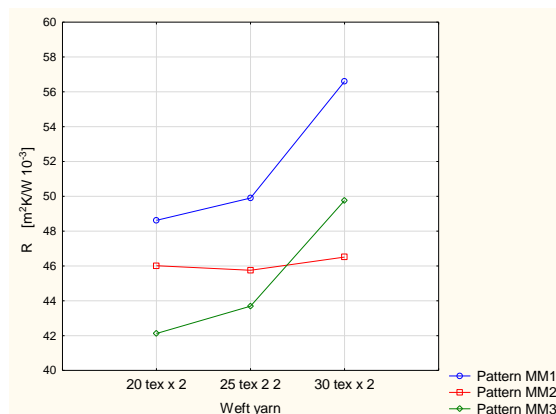


Figure 5. Thermal resistance of the investigated seersucker woven fabrics

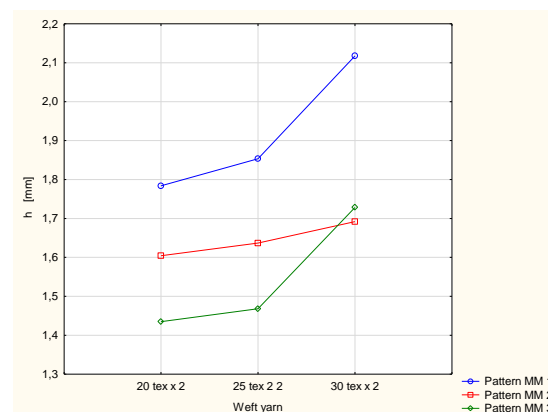


Figure 6. Thickness of the investigated seersucker woven fabrics According to the Alambeta

4 CONCLUSIONS

Performed investigations confirmed that the repeat of the seersucker effect is very important from the point of view of the thermal insulation properties of the seersucker woven fabrics. The influence of the kind of weft yarn is statistically significant only in the case of the thermal resistance of fabrics.

ACKNOWLEDGEMENT: This work is financed by National Science Centre, Poland in the frame of the project titled „Geometrical mechanical and biophysical parameterization of the three-dimensional woven structures”, project No. 2016/23/B/ST8/02041.

5 REFERENCES

- [1] Gandhi K.: *Woven Textiles Principles, Technologies and Applications*, 1st ed., Woodhead Publishing, New Delhi, 2012.
- [2] Matusiak M., Zieliński J., Kwiatkowska M.: Measurement of tensile properties of seersucker woven fabrics of different structure. *Fibres & Textiles in Eastern Europe* 2019; 27, 2(134): 58-67.
- [3] Matusiak M., Fraczkak Ł.: Comfort-related properties of seersucker fabrics in dry and wet state, *International Journal of Clothing Science and Technology* 2017; 29, 3: 366-379.
- [4] *Alambeta Catalogue*, Sensora (Czech Republic) 2017

ENGINEERING STRETCH FABRIC FOR IMPROVED MECHANICAL COMFORT

Sunny Pannu¹ and B. K. Behera²

¹Department of U.I.E.T, Maharshi Dayanand University, Rohtak, Haryana 124001

²Department of Textile Technology, Indian Institute of Technology Delhi

Abstract: The role of fabric dimensional parameters such as end density, pick density, elastic yarn component, width, shrinkage, recovery, growth percentage, and physical properties like crease recovery angle, wrinkle, drape and finally low stress mechanical properties are analysed for stretch denim. The stretch denim was prepared with and without heat setting process with a prime motivation to understand and eliminate the heat setting process if possible. The sole object is to achieve an ideal practical and feasible route to prepare cost effective 'stretch fabric' with adequate comfort and handle values. In this research, the role of weave design and fabric construction parameters, shrinkage behavior, spandex percentage, weaving speed, and finally the heat setting treatment on mechanical comfort of the fabric were studied with a view to optimize these variables to engineer a high quality fabric.

Keywords: stretch fabric, mechanical comfort, heat setting, growth percent, shrinkage behaviour

1 INTRODUCTION

The comfort level of fabric plays a decisive role in its acceptance for mass consumption. This is mostly determined by the mechanical properties of the fabric at low stress level. The evolution of spandex is among new tools to enhance mechanical properties of the fabric. The virtue of 'stretch' adds to the comfort level but at the same time its behavior towards the processes, both mechanical and chemical, becomes decisive factor to limit its exploitation in enhancing comfort properties of fabric. The object is thus to analyse the role of important processes like heat setting and finishing on the properties and performance of 'stretch fabric'. It focuses on optimization of various process variables to evolve cost effective and time saving process and at the same time to obtain required hand value of fabric as per the end use.

2 MATERIALS AND METHODS

2.1 Materials

In this study, woven fabric samples were prepared in a weaving mill under controlled manufacturing conditions. The warp yarns taken are 100% cotton spun on Open End spinning system. The weft yarns are the cotton wrapped spandex-core spun yarns. To study the effect of heat setting and finishing, the fabric sample is divided into three groups, each following a different processing route as shown and coded below.

WH	Grey fabric Without Heat set
HP	Grey fabric Heat set then Pretreated
PH	Grey fabric Pretreated then Heat set

The fabric samples were tested for important physical and mechanical properties viz., fabric count, fabric width and fabric shrinkage and functional properties of fabric tensile and tear strength, fabric

crease recovery, fabric wrinkle recovery and drape. All the fabric samples were evaluated for their low stress mechanical properties and Total hand value.

3 RESULTS AND DISCUSSION

The without heat set, heat set then pretreated and pretreated then heat set samples were tested for EPI, PPI, GSM, Width, Shrinkage, Growth, Recovery, Elongation and Total Hand value.

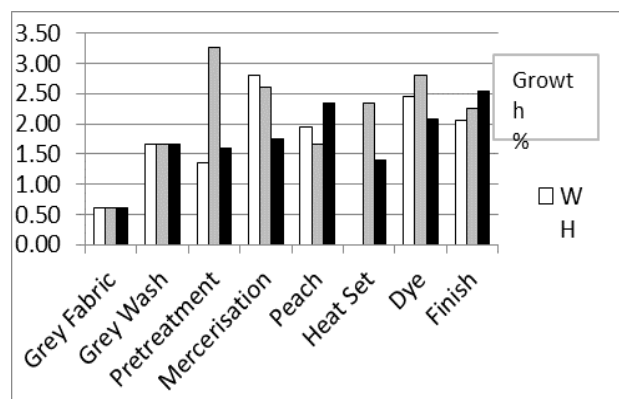


Figure 1 Effect of different processes on Growth

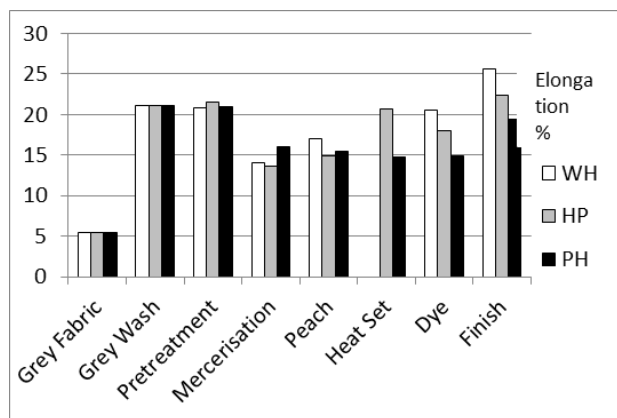


Figure 2 Effect of different processes on Elongation

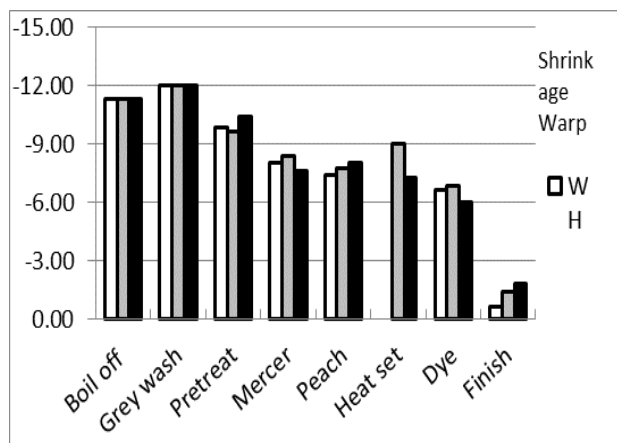


Figure 3 Effect of different processes on Warp Shrinkage

The results reveal that there is no significant difference in end density between the three samples due to the three different processing approaches. Though, the grey washing results in an increase in end density in general, there is an overall increase in EPI due to different finishes applied on the fabric. Further investigation shows a falling trend in PPI due to finishes applied on fabric. Among the three methods the *Heat set then Pretreat* shows comparatively more decrease in PPI. However, PPI of *without heat set* samples show a very significant increase after finishing. There is an increasing trend of fabric areal density due to different finishing routes. The *without heat set* sample shows comparatively higher increase in areal density followed by *heat set then pre treated* and *pretreated then heat set* sample respectively.

4 CONCLUSION

There is improvement in crease recovery angle in all the three samples after finishing treatment. However, *without heat set* sample shows the most significant increase in crease recovery angle. The three object samples were found unsuitable for summer suiting and fit well for winter application as found in their Total Hand Value result.

4 REFERENCES

1. Choudhary AK, Sheena B. Influences of elastane content, aesthetic finishes and fabric weight on mechanical and comfort properties of denim fabrics. *J Textile Eng Fashion Technol.* 2018; 4(1):36–42

2. Gorjanc, D.S.; Bizjak, M. Impact of Pre-Finishing Process on Comfort Characteristics of Stretchable Cotton Fabric. *J. Eng. Fibers Fabr.* **2015**, *10*, 57–68
3. Kumar MS, Anbumani N, Hayavadana J. Elastane fabric - A tool for stretch applications in sports. *Indian J Fibre & Textile Research.* 2011, 36(3):300–307.
4. El-Ghezal S, Babay A, Dhouib S, Cheikhrouhou M. Study of the impact of elastane's ratio and finishing process on the mechanical properties of stretch denim. *J Text Inst* 2009; 100, NO. 3:245–53.

TRAJECTORY SIMILARITY OF THE THUMB AND INDEX FINGER DURING NATURAL FABRIC ASSESSMENT BY A NON-EXPERT

Raphael Santos¹, Yuta Yamaguchi¹ and Sachiko Sukigara²

¹Kyoto Institute of technology, Matsugasaki, Sakyo-ku, Kyoto city, Kyoto, Japan, raphajp@yahoo.com.br

²Kyoto Institute of technology, Matsugasaki, Sakyo-ku, Kyoto city, Kyoto, Japan, sukigara@kit.ac.jp

Abstract: In this study we analyzed the similarity of finger trajectories based on patterns of speed of non-experts during the evaluation of two sets of fabric samples, similar and dissimilar. We hypothesize that the trajectory of the fingers during the evaluation of similar fabrics is similar and dissimilar for dissimilar fabrics. To test this hypothesis, we applied a method of similarity assessment suggested by Dodge[1][2]. The results indicated the patterns of speed are slightly associated with the complexity of the task the subject is faced with.

Keywords: fabric assessment, finger movement similarity, trajectory segmentation, motion capture, sensory test

1 INTRODUCTION

Textile tests such as the Kawabata evaluation system and sensory tests are the basic tools available to understand the mechanical properties of textiles and surveying the customer preference. Sensory tests require a good amount of thought into the design, is time consuming and relies on the availability of human resources. We believe the process of sensory testing could be improved by collecting objective data from the subject during the textile evaluation. This data could possibly be used to improve the reliability of the sensory test and to better understand the preferences of the consumer.

In this study we investigated the similarity of the trajectories of the thumb and index fingers of different subjects during the evaluation of two sets of fabric samples (Similar and dissimilar). More specifically, we measured the patterns of speed at which the thumb and index fingers of non-expert subjects moved during the unconstrained evaluation of fabric samples. We employed a modified edit distance, which is a metric to measure the similarity between string sequences suggested by Dodge[1][2]. We used this metric due to the random nature of the finger trajectory during the evaluation, even when assessing the same sample multiple times. In other words, there is no benefit in investigating the spatial properties of the trajectory.

In this experiment intuitively we assume the hypothesis that the speed patterns of the fingers during the evaluation of similar fabrics should be similar and in contrast the patterns should be dissimilar in the case of dissimilar fabrics.

2 EXPERIMENTAL

The evaluation of the samples was carried out under two conditions, respectively experiment A and Experiment B. In experiment A, five specimens of the same sample were presented to the subject. In experiment B, five specimens, each of 5 different samples were presented to the subjects. In addition, during each experiment the subjects were also required to score each of the samples in terms of roughness between 0 and 100.

2.1 Samples

Five different samples were used in the experiment. The samples were all black color and intentionally selected to have very different physical properties. We expected the subjects to easily discern the samples during the experiment. The sample size was 20x10 cm.

Table 1 Sample specification

Sample	Structure	Thickness (mm)	Weight (g/m ²)	MIU (warp/weft)		MMD (warp/weft)		SMD (μm) (warp/weft)	
A	wedge_slab	1.02	214	0.27	0.31	0.01	0.03	6.95	14.18
B	31twill	2.03	406	0.56	0.34	0.02	0.01	9.07	3.41
C	satin	0.22	9	0.31	0.19	0.01	0.01	0.25	0.24
D	21twill	0.80	243	0.16	0.17	0.02	0.01	4.37	9.91
E	plain	0.30	155	0.18	0.20	0.01	0.01	3.68	3.95

2.2 Subjects

Twelve subjects (5 males, 7 females, 20-30 years old) participated in the experiment. Due to the unconstrained nature of the experiment, 5 subjects were excluded because they used fingers without markers to evaluate the sample or in the case of severe marker occlusion. The effective number of subjects were 8 (4 males, 4 females).

2.3 Experiment room

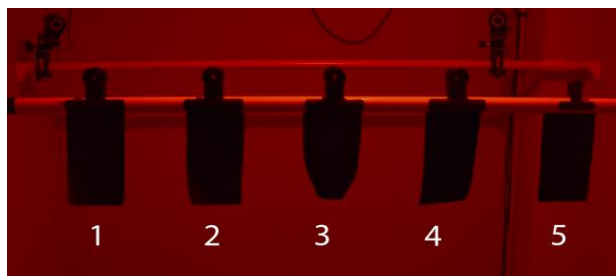


Figure 1. Sample arrangement in experimental room

In a room about 5 square meters, 6 motion capture cameras were laid out to record the trajectory of markets located at the index finger, thumb and arm of each subject's dominant-hand side. The sample arrangement, Fig. 1, seeks to emulate the conditions a customer would encounter in a retail shop. The room was illuminated by a dim 1.5-watt red LED bulb set at about 55 cm above the samples. This was purposely made so the surface reflections and textures of the samples could not be easily distinguished. The illuminance at the sample height was about 1 Lux.

2.4 Data collection

First, the subject participated in experiment A (same sample, 5 specimens), after the experiment A was completed, the subject waited outside of the room while new samples were arranged, the subject then went back into the room and proceeded with experiment B (one specimen of each of the 5 samples). For the duration of all experiments motion capture data was collected at 120 fps. The duration of the experiment and the order of evaluation for each sample were completely at the subject's will.

2.5 Analysis

We compared the similarity of the trajectories of the thumb, and index finger in experiment A and experiment B using the method suggested by Dodge[1][2]. This method operates as follows: first, a motion parameter profile (in our experiment, speed) is computed from the trajectory data; Second, local features of the profile are extracted according to variations of amplitude and frequency. Later, the motion parameter profiles are segmented into a sequence of class labels, where the class is defined by certain range of variations of amplitude and frequency. Finally, these motion parameter classes are compared in pairs using a modified version of the edit distance, the Normalized Weighted Edit Distance (NWED). For further information refer to the Dodge[1][2].

3 RESULTS AND DISCUSSION

We compared the similarity of trajectories for both experiments independently. For 5 subjects out of 8, the similarity of finger trajectories between samples in experiment A and experiment B were analogous, with experiment B showing slightly more similarity. The result for one subject in this group of can be seen in Fig. 2. Two subjects showed certain amount of dissimilarity in experiment A and relatively increased similarity in experiment B. Lastly, one subject showed relatively dissimilar patterns of speed in both experiments.

The results of the roughness score showed that samples B and C were easily discernible by the subjects, while other samples had some degree of variability. In Fig. 3, the normalized results for experiment B are shown. We believe the reason for the variability is for a degree due to individuality, however, we noted considerable discrepancy in the absolute score of the same sample in both experiments. We may conclude that, the order which the samples were presented also accounts for the variability.

The outcome of the similarity analysis opposed our initial hypothesis where we thought similar samples would spark

similar trajectories. We believe that experiment A was much more demanding on the subject's evaluation efforts which in turn forced a more thorough investigation and consequently slightly more complex trajectory patterns. In experiment B, on the other hand, the samples could be more easily distinguished, so less effort was necessary.

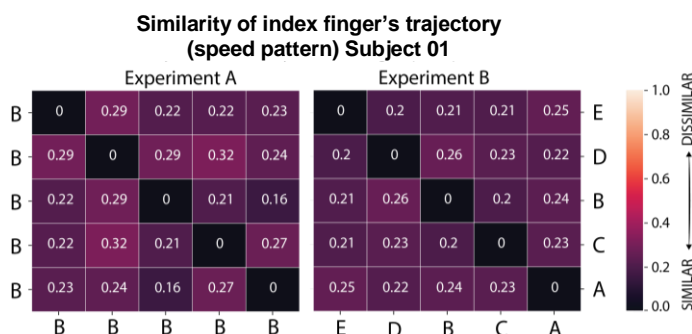


Figure 2. Similarity analysis of subject 1, for experiments A and B. Values close 0 means stronger similarity. Values close to 1 mean dissimilar trajectory. In experiment B the similarity values are slightly smaller then in experiment A.

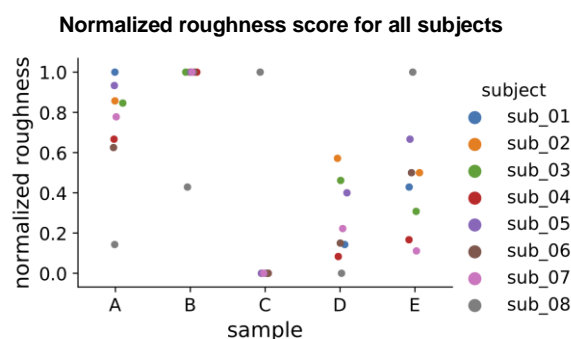


Figure 3. Samples B and C were easily discerned by all subjects, while other samples were scored with some degree of variability.

4 CONCLUSION

In this study, we measured the patterns of speed at which the thumb and index fingers of non-expert subjects moved during the unconstrained evaluation of fabric samples. Based on the similarity of these patterns we may hypothesize that patterns of speed are slightly associated with the complexity of the task the subject is faced with.

5 REFERENCES

- [1] Dodge, S., Weibel, R., & Forootan, E. (2009). Revealing the physics of movement: Comparing the similarity of movement characteristics of different types of moving objects. *Computers, Environment and Urban Systems*, 33(6), 419-434.
- [2] Dodge, S., Laube, P., & Weibel, R. (2012). Movement similarity assessment using symbolic representation of trajectories. *International Journal of Geographical Information Science*, 26(9), 1563-1588 materials.

DEPENDENCE OF TEXTILE STRUCTURE ON HEAT TRANSMISSION

Lexi Tu^{1,2}, Haoxuan Shi³, Xinrong Luo⁴, Hua Shen^{1,2*}

¹ College of Textiles, Donghua University, Renmin North Road, Shanghai, 201620, China, e-mail: shenhua@dhu.edu.cn

² Key Laboratory of Textile Science & Technology of Ministry of Education, College of Textiles, Donghua University, Shanghai, 201620, China, e-mail: shenhua@dhu.edu.cn

³ Nantong Cellulose Fibers Company Limited, Nantong, Jiangsu, 226008, China, e-mail: shihaoxuan@126.com

⁴ China Testa Textile Testing Services, Zhenyuan Road, Shaoxing, 312071, China, e-mail: 378312057@qq.com

Abstract: A finite element model, which developed according to the structure of textile, was employed to investigate the heat transmission. The relationship between weaving density, thickness, thermal conductivity, porosity and heat transmission was then analyzed by comparing the simulating result with different initial and boundary conditions.

Keywords: finite element model, heat transmission, simulation

1 INTRODUCTION

It is widely recognized that clothing is essentially important for regulating the heat exchange between the human body and the environment [1]. The thermal comfort, which is related to the heat transferring behavior in the clothing, is regarded to be an important factor when designing clothing [2-4]. However, because a fabric is commonly formed by individual yarns interlacing with each other at a certain weave angle and contains many contact areas in the interwoven structure, the heat transmission mechanism through a textile is not yet well understood. In addition, the air in the fibrous porous structure makes the heat transmission much more complicated.

2 PROCEDURE

2.1 Samples

Three fabrics with apparently different structure, thickness, fiber composition and material constants were used as experimental samples in this study. As can be seen in Table 1, sample #1 shows markedly higher thermal conductivity in both longitudinal and transverse directions of the yarn than the other samples, as it is made of unique polyethylene fiber. Sample #2 and #3 are separately made of cotton fiber and wool fiber, with relatively lower thermal conductivity. The thermal conductivity in the longitudinal direction was obtained from the literature [5,6], while the other material constants were measured experimentally.

Table 1 Characterizations of samples

	Thickness (m) $\times 10^{-4}$	Fiber composition (%)	Mass density (kg/m ³)	Specific heat kJ/(kg·K)	Thermal conductivity W/(m·K)	
					λ_L	λ_T
#1	3.17	Polyethylene Fiber 100	970.0	2.00	4.00	0.143
#2	1.72	Cotton 100	1500.0	1.21	2.88	0.059
#3	2.80	Wool 100	1280.0	1.36	0.48	0.053

λ_L : Thermal conductivity in longitudinal direction

λ_T : Thermal conductivity in transverse direction

2.2 Experimental measurement of thermal resistance

The ThermolabII Tester KES-F7 (Kato Tech Co., Ltd., Japan) was employed to examine the heat transmission process of samples. During the measurement, the sample was firstly placed evenly on the cooling base which was constantly maintained at 20°C. Then the BT-BOX was gently placed on the fabric to form a 10°C temperature difference between the top and bottom surface of experimental fabric. The obtained heat flux was adopted to calculate the thermal resistance of experimental fabric by the following equation:

$$R = A \times (T_1 - T_2) / q \quad (1)$$

Where R is the thermal resistance of the measured samples, A is the area of test plate, T₁ and T₂ (°C) are the temperatures of BT-BOX and cooling base, respectively, q is the heat flux recorded by the sensor in test plate. Each test was repeated for three times to gain the average result with variation.

2.3 Modeling and finite element analysis

A finite element model (FEM), which allow separate heat transmission along the longitudinal and transverse direction of yarns as well as through the contacting interface between multilayer samples, was developed in the nonlinear analysis FEM code (Marc Mental) to investigate the heat transmission through a fabric during the measurement of thermal resistance. The construction of the FEM model was based on a quarter of the ThermolabII Tester KES-F7 due to its symmetry.

3 RESULT AND DISCUSSION

3.1 Model validation

Comparing the results obtained from simulation and experiment, it was observed that only a slight difference for all the samples with various structure, thickness, fiber composition and material constants was observed, suggesting reliability of the proposed model for investigating the heat transmitting mechanism in a real fabric.

3.2 Relationship between thickness and thermal resistance

With the enhancement of thickness, the thermal resistance of a fabric calculated in the FEM model was found to linearly increase. However, the thermal resistance recorded by the ThermolabII Tester KES-F7 appears to increase slightly slower than the simulating values with increasing thickness. This was supposed to be caused by the heat leakage at the edge of BT-BOX in the experiment.

3.3 Relationship between thermal conductivity and heat leakage

The temperature distribution in the model suggested that heat leaked in a more accelerated way when the testing fabric possessed better thermal conductivity, resulting in higher leaking percentage was calculated. Because the heat transmission and temperature distribution in a fabric was strongly associated with the thermal conductivity of yarn.

4 CONCLUSION

A finite element model was developed based on the structure of textile, and then it was employed to investigate the heat transferring mechanism. The heat

transmission with relation of weaving density, thickness, thermal conductivity, porosity and heat transmission was analyzed with different initial and boundary condition were applied on the developed model.

5 REFERENCES

- [1] Havenith G. Interaction of clothing and thermoregulation. *Curr Probl Dermatol* 2003, 1: 221-230.
- [2] Li Y. The science of clothing comfort. *Text Prog* 2001, 31: 1-135.
- [3] Spencer-Smith J L. The physical basis of clothing comfort, part 2: heat transfer through dry clothing assemblies. *Cloth Res J* 1977; 5(1): 3-17.
- [4] Sevilgen G, Kilic M. Numerical analysis of air flow, heat transfer, moisture transport and thermal comfort in a room heated by two-panel radiators. *Enger Buildings* 2011, 43(1): 137-146.
- [5] Hearle J W S and Morton W E. Physical properties of textile fibres. *Amsterdam: Elsevier* 2008, pp.174–175.
- [6] Hearle J W S, Grosberg P and Backer S. *Structural mechanics of fibers, yarns, and fabrics*. New York: Wiley-Interscience, 1969, pp.332–335.

THE INVESTIGATION ON THERMAL PROPERTIES OF CONDUCTIVE KNITTED FABRICS UNDER DIFFERENT VOLTAGES

Liu Su ¹, Sun Kexia ² and Long Hairu ³

¹Engineering Research Center of Technical Textile, Ministry of Education, College of Textiles, Donghua University, Room 4016, Block 3, No.2999 North Ren Min Road, Songjiang district, Shanghai, China, e-mail: liusu@dhu.edu.cn

²Engineering Research Center of Technical Textile, Ministry of Education, College of Textiles, Donghua University, Room 4016, Block 3, No.2999 North Ren Min Road, Songjiang district, Shanghai, China, e-mail: 2529742654@qq.com

³Engineering Research Center of Technical Textile, Ministry of Education, College of Textiles, Donghua University, Room 4016, Block 3, No.2999 North Ren Min Road, Songjiang district, Shanghai, China, e-mail: hrlong@dhu.edu.cn

Abstract: This paper presents a study of resistance values and temperatures of conductive knitted fabric under different voltages with time. Six knitted fabrics with different structures were manufactured using Computerized flat knitting machine by uniform sizes, 1cmX1cm and 2cmX2cm. Samples were all made from wool and two different silver-coated yarns: one is for electrode area; wool yarn and the other one are used to manufacture the heating area. The resistance values of samples subjected to different lateral tension under different voltages are measured by a KEITHLEY sourcemeter. And Samples with size 2X2cm were selected for resistance and temperature testing simultaneously. Experimental results showed that the resistance decreases as the tensile force increases. In tension-free state, the resistance values increase in a short time and decrease faster in the first 1000 seconds, then slows down. The temperature values gradually increase in the first 1000 seconds and tend to stabilize after a certain period. Based on these results, the best knitting structure will be selected.

Keywords: knitted heating fabric, thermal properties, knitted structures

1 INTRODUCTION

Multifunctional smart textiles become the trend of new generation textiles [1]. Conductive textiles are nowadays used in a broad variety of applications in the area of smart textiles, such as sensors [2], heaters [3], capacitors, etc...[4,5]. As for conductive fabric, there are several available technologies: Weaving or knitting metal wires or conductive threads into the textile; deposition/coating of conductive polymers; printing conductive inks[10]. Some researchers began to study the factors affecting the electrical properties of conductive fabrics. In this paper, resistance and temperature changes of conductive knitted fabrics with different structures at different voltages will be studied. Two experiments were conducted to investigate the resistance values of each sample under different voltages and the resistance and temperature values of part of the samples under different voltages.

2 EXPERIMENT APPROACH

2.1 Materials

Due to the excellent thermal insulation properties of the wool, silver-coated yarns (A and B) and wool were used to knit the conductive fabric in the experiment. The yarn A is for electrode area, while wool and yarn B (20D, 40D, 100D, 140D) are separately used to manufacture the heating area. The electrode part and the electrical part are connected by intarsia technology.

2.2 Method

All the samples with six different structures were manufactured on LONGXING computerized flat knitting machine 12G. Every structure is made for two sizes in the heating area, 1X1cm and 2X2cm. The diagram of each structure was illustrated in Fig.1. After knitting, samples are placed flat on the table under no tension without washing treatment.

machine 12G. Every structure is made for two sizes in the heating area, 1X1cm and 2X2cm. The diagram of each structure was illustrated in Fig.1. After knitting, samples are placed flat on the table under no tension without washing treatment.

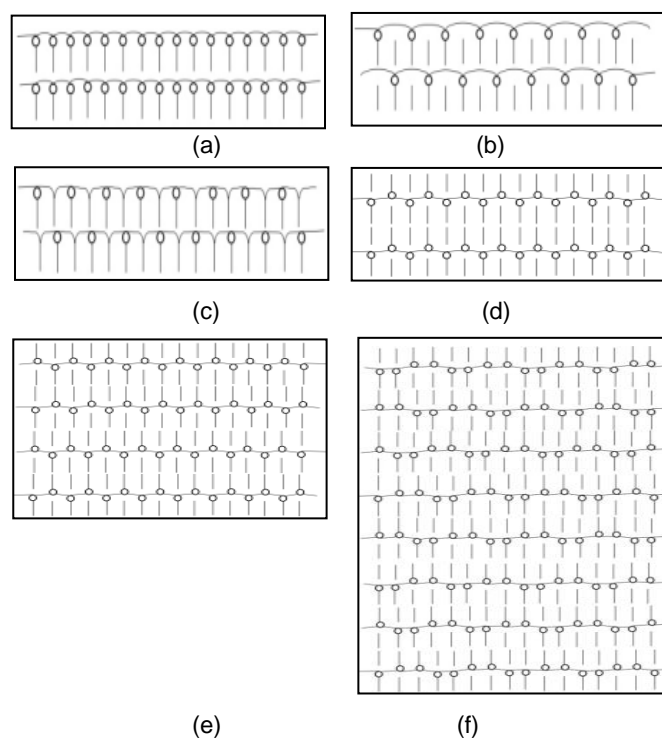


Fig. 1 the diagram of each structure((a)knit;(b)knit and float;(c):knit and tuck;(d)1X1 rib;(e)interlock;(f)derivative rib)

Experiment 1 the resistance values of each sample under different voltages with different fineness yarns subjected to different tension

A sourcemeter is connected to the sample through the electrode in a four-wire test. To observe the changes in resistance values, different voltages were set on the computer. At each voltage, the resistance value of each sample with different fineness yarns was read on the computer when subjected to different tension.

Experiment 2 the resistance and temperature values of each sample under different voltages

Samples with size 2X2cm were selected for resistance and temperature testing simultaneously. Different voltages were supplied to heat samples with size 2X2cm for 3600s. The resistance values were recorded on the computer every second. In the first 5 minutes, the temperature values at 1, 2, 3, and 5 minutes were recorded, and then the temperature value was recorded every 5 minutes in the experiment. Each sample was left for 24h or longer after the test to ensure that the sample could recover to its original condition preparation for next testing.

3 CONCLUSION

Tab.1 Resistance change of 70D sample under different tension

	0N	1N	2N	5N	10N
1V	2.311	2.254	2.251	2.251	2.251
2V	2.316	2.253	2.252	2.247	2.219
3V	2.328	2.252	2.251	2.24	2.221

As can be seen from Tab.1, when the 70D sample is subjected to tensile force, the resistance decreases as the tensile force increases. Through the resistance test of samples with different fineness and same structure, the resistance decreases as the fineness increases.

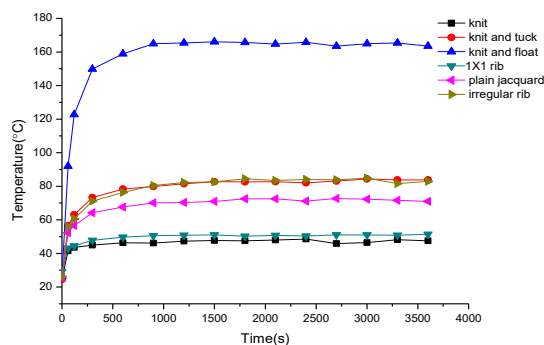


Fig.2 Sample temperature change with time

When conductive fabrics are supplied with power, the resistance values increase in a short time and then gradually decrease. It decreases faster in the first 1000 seconds of the experiment, then slows down. The temperature values gradually increase in the first 1000 seconds and tend to stabilize after a certain period as shown in Fig.2. Among all the structures, two needle beds fabric is more suitable for wearable textiles due to its electrothermal stability.

Furthermore, the investigation on thermal properties of conductive knitting fabrics under different voltages is analyzed and this discovery can be further used for heating fabric in wearable textiles related fields.

4 REFERENCES

- [1] Dias T., Hurley W., Monaragala R., et al.: development of electrically active textiles. *Advances in Science and Technology* 2008, 60:74-84.
- [2] Gilbert D M., Mert Ö., Anne S., et al.: designing of conductive yarn knitted thermal comfortable shirt using battery operated heating system. *TEKSTİL ve KONFEKSİYON* 2014, 24.
- [3] Ehrmann A., Blachowicz T.: *Conductive Yarns, Fabrics, and Coatings*. Springer International Publishing 2017.
- [4] Hao D., Xu B., Cai Z.: Polypyrrole coated knitted fabric for robust wearable sensor and heater. *Journal of Materials Science: Materials in Electronics* 2018.
- [5] Chin-Mei L., Pei-Chen H., Ching-Hui L., et al.: property evaluation of functional thermal-regulating/wicking conductive knitted fabrics. *EDP Sciences: MATEC Web of Conferences* 110, 07021 (2017).

VISUAL PERCEPTION AND EVALUATION OF WOMEN'S SHIRT FABRICS BASED ON FAST FASHION E-COMMERCE PLATFORM

Run Qiu, Na Li, Run Wen*

College of Textiles, Donghua University, Renmin North Road, Shanghai, 201620, China, e-mail: rain@dhu.edu.cn

Abstract: It is particularly important for fast fashion brands to manage their own stores well through visual marketing on the platform. The topic will take fast fashion women's shirts and shirts as an example, through subjective questionnaire survey and objective eye tracking experiment, to explore consumers' preferences and psychological preferences for four factors of shirt appearance: style, fabric, color and pattern.

Keywords: fast fashion, shirt fabric, e-commerce platform, visual perception, eye tracking experiment

1 INTRODUCTION

With the improvement of living standard and product design level, consumers pay more and more attention to perceptual consumption in visual aesthetics. Fast fashion brands have rapidly risen in China's clothing market by virtue of their advantages of low price, fashion and fast updating, catering to the personalized needs of consumers today. At the same time, with the improvement of science and technology and the development of the Internet, contemporary young groups have favored e-commerce platform. It is particularly important for fast fashion brands to manage their own stores well through visual marketing on the platform. This topic will take fast fashion women's shirts and shirts as an example, through subjective questionnaire survey and objective eye tracking experiment, to explore consumers' preferences and psychological preferences.

2 EXPERIMENTAL

2.1 Selection of Appearance Factors

Selection of Appearance Factors and Level of Fast Fashion Women's Shirts On the basis of consulting literature, collecting popular information and visiting the staff of fast fashion brand offline stores, the level selection questionnaire of fast fashion women's shirts is designed. The preferences of consumers are investigated from four aspects: style, fabric, color and pattern, and the factors and levels of eye movement experiment are finally determined.

2.2 Design eye movement experiment

Eye-tracking experiment of fast fashion women's shirt's visual preference takes 16 groups of sample pictures as experimental samples. Eye tracking data of 100 people are selected from valid experimental data. Descriptive analysis is made on four eye tracking data indicators: fixation time, number of fixation points, number of return views and first entry time. The number of two indicators for further data analysis such as one-way ANOVA and hot zone map analysis.

2.3 Data analysis combined with questionnaires

Eye movement experiment questionnaire includes investigation and analysis of the purchase preference score of fast fashion women's shirts, the semantic style score of six kinds of fast fashion common shirt fabrics,

and the consumer psychology and behavior when they buy clothes on e-commerce platform.

3 RESULTS AND DISCUSSION

3.1 Hotspot map

Hotspot maps show the focus of the subjects' attention in the whole sample picture to compare the visual attractiveness of each visual object to the subjects. Concerned areas can form "hot areas" of different shapes and areas according to the distribution and concentration of gaze points. In Fig. 1, the color of the hot spot can directly reflect the participants' attention to a certain area. The order of fixation time from short to long is green, yellow and red. The redder the color, the higher the participants' attention to this area. The following picture is a hot spot map, which superimposes the eye movement images of ten subjects. From the hot spots of each shirt, it can be seen that the neck and chest of the shirt are the focus of the subjects.

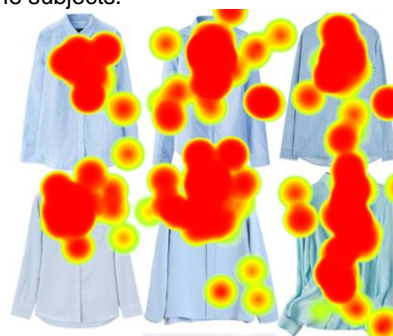


Fig. 1 Hotspot map

3.2 Trajectory diagram

The trajectory diagram shows the position and sequence of the fixation points on each experimental sample. Fig. 2, the center of the gaze points indicates the order of the gaze points with numbers. The serial number increases in turn from the beginning, and the eye movement starting point marked "1" is the image. The smaller the number in the circle, the more attention the participants paid to the area. The two adjacent fixation points are connected by a straight line, which represents the path and process of a saccade. The following is a trajectory map that superimposes the eye movement images of ten subjects.

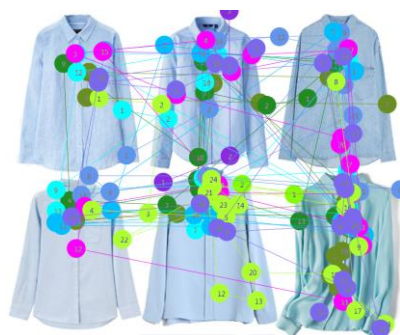


Fig. 2 Trajectory diagram

3.3 Textile Semantic Style Perception

The subjects' visual perception of cotton fabrics' style tended to be "smooth" and "delicate", while the other styles were relatively neutral; the visual perception of linen fabrics tended to be "blocked", "rough", "cool", "leisure" and "dull"; the visual perception of cotton and linen fabrics tended to be "blocked" and "dull"; and the visual perception of denim fabrics tended to be "rested". The visual perception of chiffon fabrics tends to be "artificial", "soft" and "cool". The visual perception of silk fabrics tends to be "smooth", "soft", "delicate", "cool", "high-grade" and "shiny". According to the statistical results, the cognitive Atlas of six kinds of women's shirt fabrics are drawn. From figure 3, figure 4, figure 5, figure 6, Figure 7 and figure 8, it can be seen that the style of silk is the most prominent, while the style of cotton and Jean Fabrics is relatively less obvious.

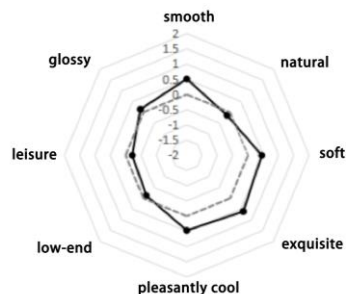


Fig. 3 Cognitive Map of Cotton Fabric

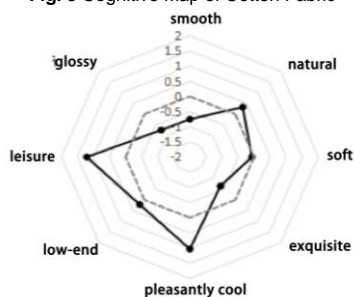


Fig. 4 Cognitive Map of Linen Fabric

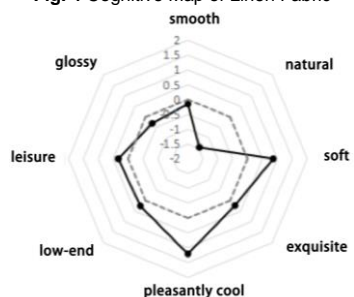


Fig. 5 Cognitive Map of Cotton and Linen Fabric

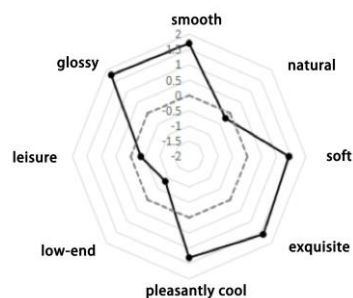


Fig. 6 Cognitive Map of Denim Fabric

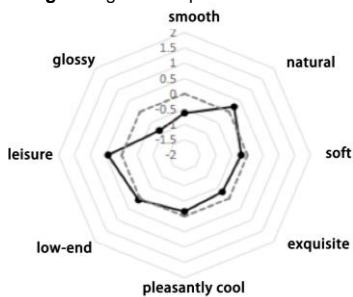


Fig. 7 Cognitive Map of Chiffon Fabric

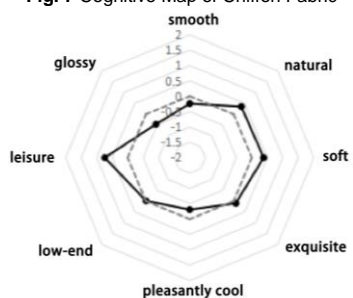


Fig. 8 Cognitive Map of Silk Fabric

4 CONCLUSION

①The basic style and the style with neck and waist design at the same time can attract more attention of the subjects.

②Silk and chiffon get the most attention, cotton and hemp as shirt display attracts the attention of the subjects, while hemp as fabric display attract the attention of the subjects. The whirlpool method is the best way to show the fabric.

③Soft color can attract the attention of the subjects more quickly, and the attention time is the longest.

④Partially patterned shirts and pure-color shirts have a relatively long time of attention and a large number of people look back.

5 REFERENCES

- [1] Mahapatra S, Patle B K, Jha A K, et al. Fuzzy logic control of a WMR[C] // 2012 International Conference on Computing, The Communication and Applications. Dindigul: The IEEE, 2012:1-5.
- [2] Duchowski A T. Eye tracking Methodology Theory and Practice[M]. London Springer, 2003.
- [3] SHAO Dan, YANG Yixiong, SUN Miaodi. Research on consumer perception clues of clothing online shopping based on eye movement experiment[J]. *Silk*, 2013, 50(20):28-34.

Evaluation of Tactile Feels of Towel after Washing

Hiroko YOKURA¹, Yuriko KIBAYASHI² and Sachiko SUKIGARA²

¹ Shiga University, Shiga, Japan, yokura@edu.shiga-u.ac.jp

² Kyoto Institute of Technology, Kyoto, Japan, sukigara@kit.ac.jp

Abstract: The tactile evaluation of cotton towels was carried out for 16 samples which varied in the washing number of times. The tactile feels of towels were assessed by 27 female students and 25 male students (20-24 years old). The surface and compression properties of fabrics were measured with the KES system. When the washing number of times increased, the evaluation of softness and smoothness of the towels greatly decreased. These perceptual changes were related to the surface properties and compression linearity (LC). The frictional force F_f during the movement of friction contactor on piles is found as the useful indicators to investigate the tactile change of towel fabrics after washing.

Keywords: washed towel, tactile feels, compression property, surface property

1. INTRODUCTION

Towels are used directly on the skin. One of the important factors related to the quality of towels is tactile feelings. According to previous studies for towels [1, 2], the surface and compression properties are correlated to the degree of softness and smoothness. The smoothness of towel can be changed according to the number of washing cycles. The question is that this tactile change makes consumer to generate the out of use decision and what is the reason behind. First, we present the changes the surface and compression properties of towels after various washing times. The objective of this study is to find how the changes in tactile feels of washed towels are link with their compression and surface properties.

2. EXPERIMENTAL

2.1 Samples

We collected five commercially produced towels (Table 1). The towels A, B, C were woven by the same process with different yarn counts and density, obtained from the company in Imabari, Japan. These towels were washed with a home washing machine (National VR-N1100) under the standard condition. We made 16 towels which varied in the washing number of times.

Table 1 Samples

No.	Yarn Counts (tex)			Pile Ratio	Grand yarn Density		Thickness (mm)	Weight (g/m ²)
	Warp	Weft	Pile		Warp (ends/cm)	Weft (pick/cm)		
A	14.8/2	36.9	19.7	5.5	11.9	21.7	4.94	313
B		29.6				17.7	4.72	315
C							4.80	272
D	29.6	19.7	29.6	5.5	11.9	13.8	4.97	310
E	29.6	29.6	29.6	3.9	10.6	13.0	2.96	216

2.2 Subjective Hand Evaluations

The tactile feels of towels were assessed by 27 female students and 25 male students (20-24 years old). They evaluated towels by touching them by hand. They were asked only to judge the tactile feel based on the sensations from contact with the materials. They evaluated the degree of "soft-hard", "smooth-rough",

"want to use-not want to use" and "prefer-not prefer" in random order, using a scale from -2 to 2 according to the semantic differential method. The mean scores of the subjective values were used to represent the hand values of each towel sample.

We selected nine towels for the normalized ranking method to obtain ranking scale of smoothness and softness. The participants were 23 female students (19-23 years old).

2.3 Surface and Compression Properties

The compression properties of towels were measured with the KES-F3 compression tester under the standard conditions. The surface properties were measured with KES-SE surface tester. A weight of 0.5N was applied on the frictional sensor (10mm x 10mm) to measure the frictional properties. On the roughness sensor, a weight of 0.05N was applied.

We measured frictional force F_f during the movement of friction contactor on piles. A weight of 0.05N is applied on the frictional sensor (1 piano wire of 0.5 mm diameter) with a sweep velocity of 1mm/s.

3. RESULTS AND DISCUSSIONS

The tactile feel of washed towel was related to their surface properties and compression linearity (LC). Figure 1 shows the relationship between the subjective hand evaluation of smoothness and LC of towels.

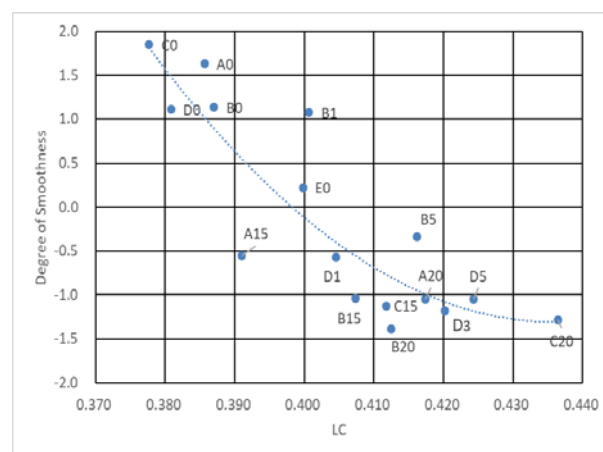


Figure 1 Subjective evaluation of smoothness versus LC. The number shows the washing number of cycles.

Figure 2 shows the relationship between the subjective hand evaluation of softness and LC of towels. Figure 3 shows the relationship between the subjective hand evaluation of want to use and LC of towels. Towels with a small value of the LC were estimated to provide smooth and soft hand, and the students prefer and “want to use” these towels. Compared with the evaluation of male and female students in Fig.3, the female students were more sensitive to the change in tactile feelings of fabrics. From these figures, we may conclude that washed towels with the LC value of larger than 0.41 are likely to have rough and hard hand. Significant relationship was not obtained between the changes of tactile feels and compression energy (WC) for washed towels.

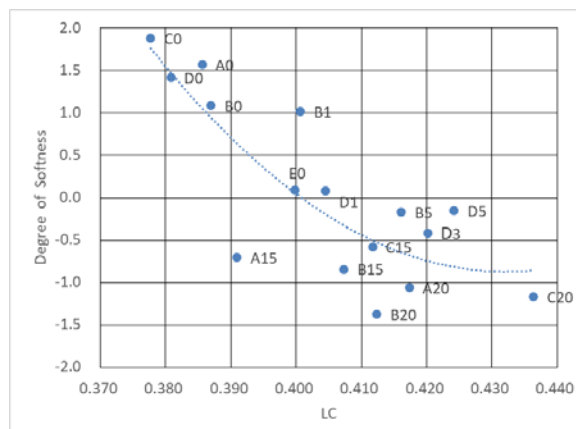


Figure 2 Subjective evaluation of softness versus LC. The number shows the washing number of cycles.

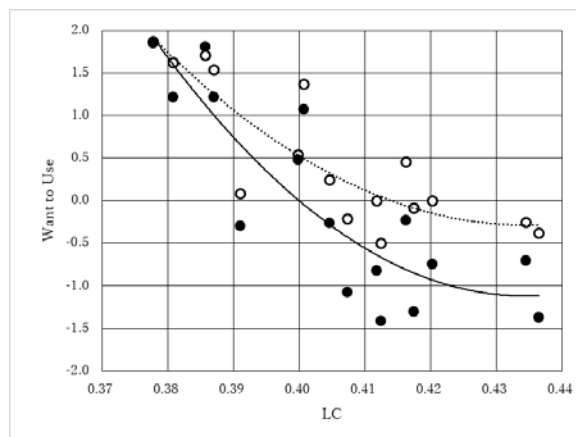


Figure 3 Subjective evaluation of want to use versus LC. ○: male students, ●: female students

For the surface properties, towel with a smaller value of the geometrical roughness (SMD) was found significantly related to the soft and smooth hand. Figure 4 shows the relationship between the subjective hand evaluation of smoothness and SMD of towels. Towels with a small value of SMD were estimated to provide smooth hand. Figure 5 shows the surface of the towel C before and after washing. Pile intertwines with each other by washing, therefore, the feelings were not smooth and soft.

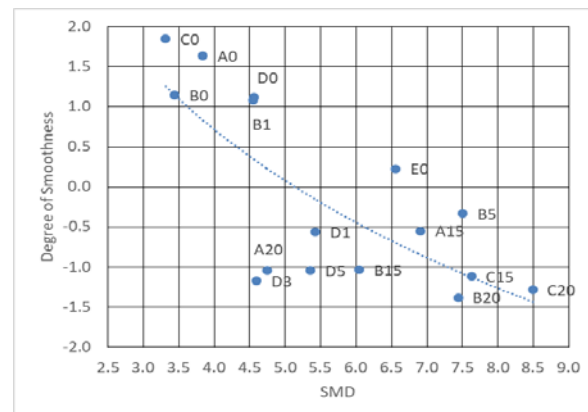


Figure 4 Subjective evaluation of smoothness versus SMD. The number shows the washing number of times.



Figure 5 Surface of the towel C before and after washing.

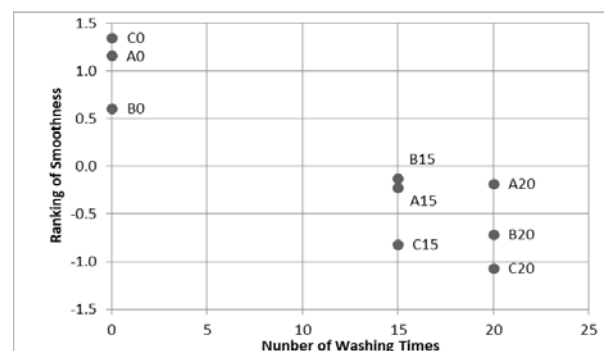


Figure 6 Ranking of smoothness versus number of wash cycles.

The evaluations of smoothness and softness of the towel fabric greatly decreased after wash. Figure 6 shows the relationship between the subjective ranking of smoothness and the number of wash cycles. Before wash, the towel C0 which made from smaller values of weft yarn density and yarn count could produce smooth and soft handle. After the wash number of times increased, the evaluation of smoothness of the towel fabric C20 greatly decreased. The towel fabric A20 with larger values of weft yarn density and yarn count showed significantly smoother hand than that of C20.

In addition, the frictional force F_f during the movement of friction contactor on piles was also related to the good hand. The F_f value was the useful indicator to estimate the tactile change of pile surface for washed towels.

ACKNOWLEDGEMENT: We wish to express our thanks to Ms. Yuna Takami of Shiga University for her technical assistance.

4. REFERENCES

- [1] J. P. Singh and S. Verma, *Woven Terry Fabrics*, WPT184, Textile Institute (2017)
- [2] H. Yokura, et al., *Proc. TRS42*, (2014)

MEASUREMENT OF EFFECTIVE THERMAL CONDUCTIVITY OF FIBER ASSEMBLY AND 3D HEAT CONDUCTION ANALYSIS

Morihiro Yoneda¹ and Chie Nakajima¹

¹ Nara Women's University, Kitaouya-nishimachi Nara Japan, e-mail: gkdzd429@ybb.ne.jp

Abstract: In order to evaluate thermal insulation properties of fiber assembly, we have developed a method to measure effective thermal conductivity of fiber assembly using KES-F7 Thermo Labo II apparatus. As a result, the effective thermal conductivity is divided into three parts, i.e. component of heat conduction in fiber, component of radiative heat transfer and component of gas conduction in air. In this study, the measurement system is investigated based on three-dimensional heat conduction analysis to improve the measurement system.

Keywords: Effective Thermal Conductivity, Fiber Assembly, 3D Heat Conduction

1. Introduction

In order to evaluate thermal insulation properties of fiber assembly in low fiber volume fraction, we have developed a method to measure effective thermal conductivity of sample using guarded hot plate (GHP) method [1]. In this study, analysis of three-dimensional heat conduction is conducted using Finite Element Method (FEM) to know the details of heat flux in the measurement system. Improvement of the measurement method is investigated based on the results of calculation.

2. Measurement of Thermal Conductivity

2.1 Measurement Method

Effective thermal conductivity is measured based on Guarded Hot Plate (GHP) method using Thermo Labo II apparatus (Kato Tech Ltd.) [2]. Schematic diagram of measurement part (section) is shown in Fig. 1. Fiber assembly with sample frame is placed between heat source plate (BT-Box, 30 °C) and heat sink (20 °C) and measurement of heat flow, q is carried out. Effective thermal conductivity λ (W/mK) is calculated from the following equation.

$$\lambda = Qd / A \Delta T \quad (1)$$

where, Q : Electric power to keep steady state (W), d : Sample thickness (m), A : Area of heat source plate (m²), and ΔT : Temperature difference between heat source plate and heat sink (K).

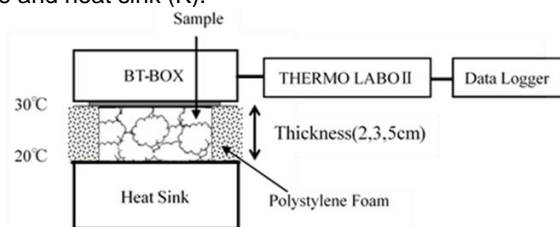


Fig.1 Measurement system

2.2 Sample

Four kinds of fiber materials used in this experiment such as Cupra fiber (CU), Polyester fiber with round section (RPE), Polyester fiber with heteromorphic section (WPE) and Polytrimethylene terephthalate fiber (PTT).

In this experiment, the effect of fiber volume fraction and sample thickness on effective thermal conductivity is investigated. Fiber volume fraction, ϕ is changed by five

stages (0.001, 0.005, 0.010, 0.025, 0.030) and sample thickness, d is changed by three stages (2, 3, 5 cm).

2.3 Results of Measurement

An example of the measurement is shown in Fig.2 (sample: CU, $d=3\text{cm}$). It is conjectured that the mechanism of heat transfer within fiber assembly consists of three components, i.e. heat conduction in fiber, radiative heat transfer in pore between fibers and gas conduction (air). Here, it is supposed that heat flows through parallel model made of three components. Measured value of effective thermal conductivity, λ (W/mK), is expressed by the following equation as function of fiber volume fraction, ϕ [3].

$$\lambda = A\phi + B/\phi + C \quad (2)$$

where A (Wm²/Kkg), B (Wkg/m⁴K) are constant coefficients and C (W/mK) is constant. The first term at right side denotes conductive heat transfer in fiber, the second term denotes radiative heat transfer and the third term denotes conductive heat transfer through gas. Results of the effective thermal conductivity of fiber assembly are analyzed by non-linear regression method based on eq. (2), and the values of A , B and C are estimated.

Calculated curves of each component using estimated values of A , B and C are shown in Fig.2. As shown in Fig.2, component of heat conduction in fiber $A\phi$, component of radiative heat transfer, B/ϕ and component of gas conduction, C can be separated experimentally.

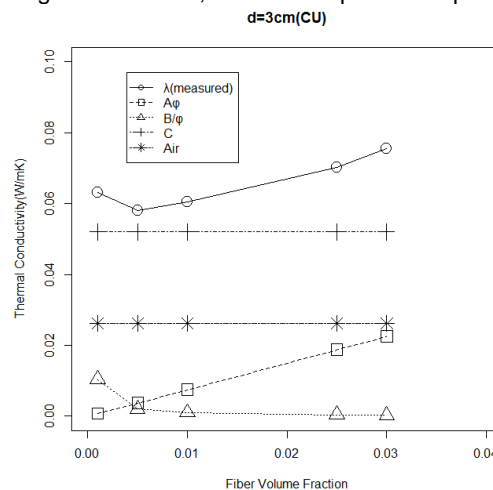


Fig.2 Effective thermal conductivity(CU, $d=3\text{cm}$)

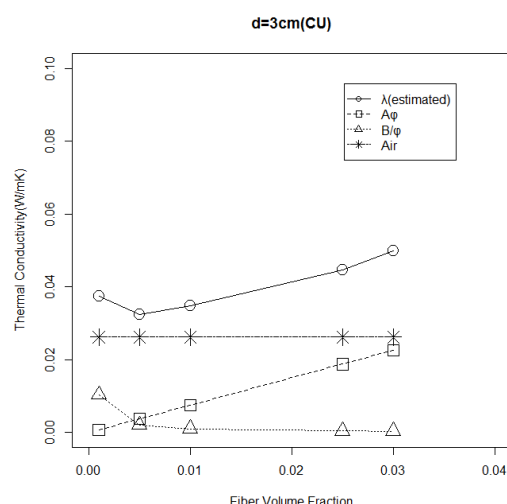


Fig.3 Results after calibration

As shown in Fig.1, the measurement system consists of fiber sample and sample frame made of polystyrene (PS) foam. Therefore, it is supposed that heat leakage from the side wall of the frame may be included in gas conduction, C . Here, let us suppose that following equation holds.

$$C = C' + \lambda_{\text{air}} \quad (3)$$

where C' is constant independent of fiber volume fraction, ϕ , and λ_{air} : thermal conductivity of air. As we have got an experimental result that C' and thickness, d have good correlation, following equation is obtained to calibrate heat leakage from side wall.

$$C' \approx 0.9325 d \quad (4)$$

Based on discussion above, total heat leakage total heat leakage C' can be eliminated from C value. Here, C value is replaced by λ_{air} ($=C - C'$). The results are shown in Fig.3. As shown in Fig.3, λ_{air} plays the most important part in effective thermal conductivity, and component of heat conduction in air, $A\phi$, follows. Component of radiative heat transfer, B/ϕ , is negligible small.

3. Heat Conduction Analysis by FEM

3.1 Modeling

Heat conduction analysis using Finite Element Method (FEM) is carried out to know three-dimensional temperature distribution of the measurement system. Sample frame is made of polystyrene foam filled with fiber assembly. Taking symmetry into account, modelling is carried out for a quarter of sample system. Mesh segmentation using tetrahedron element is shown in Fig.4.

The value of thermal conductivity assigned is 0.03 (W/mK) for fiber assembly and 0.035 (W/mK) for sample frame, respectively.

Procedure of calculation is as follows. (1) mesh segmentation, (2) assignment of boundary condition and material properties, (3) calculation of nodal point temperature, and (4) visualization of temperature distribution.

Boundary conditions used for the calculation are as follows (U: temperature).

(1) Upper side: $U=10$, (2) Lower side: $U=0$, (3) Section: $dU/dx=0$ ($q=0$), (4) Side wall of frame: unknown.

To carry out calculation, the boundary condition of the side wall of the frame must be assigned. In this study, it is assumed that outer surface of the frame is controlled by air or water flow with constant velocity and temperature. Here, heat transfer boundary condition is assigned to outer surface as follows.

$$q = H(T - T_s) \quad (5)$$

where, H : heat transfer coefficient (W/m²K), T : representative temperature of the flow(K), T_s : surface temperature of the frame(K).

3.2 Results of Calculation

An example of temperature distribution is shown in Fig.5, where $d=3\text{cm}$, $H=30$ and $T=0$.

On the outer surface of the frame (left side), temperature falls at the edge because of acceleration of heat transfer. On the section of sample (right side), we can look over temperature distribution from sample to frame. Parallel isotherm is observed at the section of fiber assembly. This fact suggests that eq.(1) is applicable to the calculation of thermal conductivity. In contrast, temperature gradient is observed at the section of frame. The existence of temperature gradient indicates that heat may flow from fiber assembly to outer surface. Heat leakage from the side wall can be predicted using this temperature gradient.

References

- [1] Yoneda M, Nakajima C: Journal of Textile Engineering, 2016; 62: 105-116
- [2] Kawabata S: Journal of Textile Machinery Society of Japan, 1984; 37: 130-138
- [3] Ohmura T, Tsuboi M, Onodera M, Tomimura T: Proceedings of the Institute for Functional Material Science (Kyusyu University), 2002; 16: 13-17

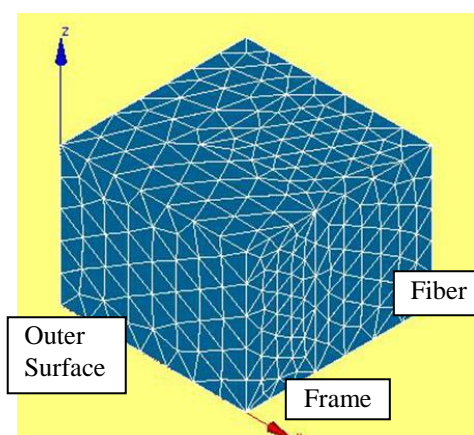


Fig.4 Mesh segmentation by tetrahedron

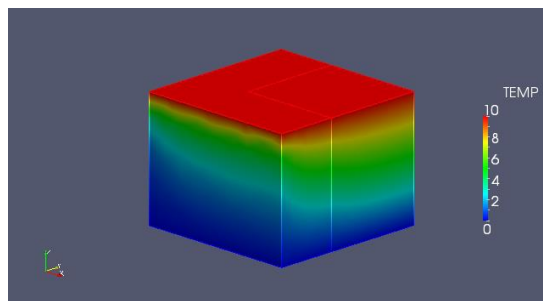


Fig.5 3D temperature distribution ($d=3\text{cm}$, $H=30$)

8. Apparel Science and Production Technology

REVIEW OF MEN'S DRESS SHIRT PATTERN DEVELOPMENT FOR THE LAST 100 YEARS

Frederick Tungshing Fung¹, Lubos Hes² and Vladimir Bajzik³

^{1,2,3} Technical University of Liberec, Faculty of Textile Engineering, Department of Evaluation, Studentska 1402/2 46117 Liberec, Czech Republic.

e-mail:¹ tassfashion@gmail.com, ² lubos.hes@gmail.com, ³ vladimir.bajzik@tul.cz

Abstract: From the nineteenth century until now, men's dress shirt pattern has been evolving and changing for the comfort and style that people need. No matter the fit of the dress shirt pattern is loose or tight, the style is fancy or practical; the pattern is always traced back from the original try and error draping techniques. This article is a look back on how the shirt pattern has been developed in the last hundred years and a discussion in conclusion to see the future development of shirt pattern will be.

Keywords: clothing pattern, dress shirt, fit, pattern development, , wearing comfort

1 INTRODUCTION

The very first shirt was found in Egypt around c. 3000 B.C. revealing the shirt was made up by three simple pattern pieces: lower front piece, lower back piece and upper front continued to upper back jointed at the shoulder and connected to the sleeve [1]. The whole piece of the front-back-shoulder-sleeve was pleated to create room for moving and to accommodate the shoulder, the chest and the arm these 3 major body shapes (Fig.1). Since then, even the pattern shapes of shirt have been developed and been changed, however; the basic shapes of the shirt pattern are remain very similar [2-3] that the major pattern pieces in a men's shirt are always with the front, the back and the sleeve. Development of men's shirt in those days were mainly by experience, practice, try and error. Draping and simple calculated drafting were/are the common practice [4-5]. This article is a review of the dress shirt pattern for the last hundred years analyzing the changing and evolvement of the pattern then looking forwards to the future development of it.



Figure 1. The oldest shirt found in Egypt revealing connected shoulder and arm piece by pleating

2 BASIC DRESS SHIRT PATTERN

The fundamental shirt pattern set is developed from three basic shirt blocks which are front, back and sleeve (Fig. 2). A complete set of shirt pattern is made up of 7 pieces which are Front, Back, Back Yoke, Sleeve, Cuff, Collar and Collar stand (Fig. 3A-G). This set of pattern can also fit to women's figure when added in darts which take up the extra fabric under the bust and in the back, then being sewn together to fit better on female's torso (Fig. 4). Other details like buttonhole plackets, cuff plackets, pocket and facing are developed for functionality, wearing comfort and style.

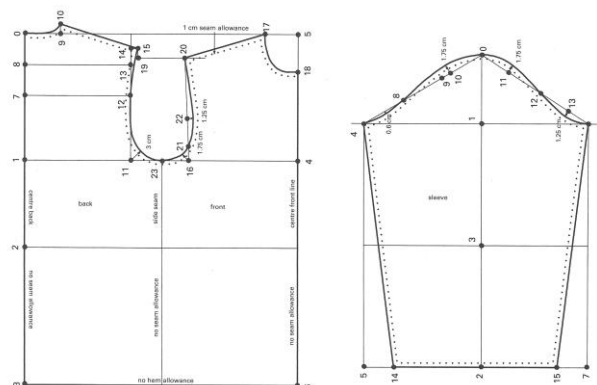


Figure 2. Basic bodice blocks: front, back and sleeve from which the complete shirt pattern set and other upper body garment patterns are developed

3 BREIF HISTORY OF SHIRT

In seventeenth century, shirt was worn in Europe as an undergarment to protect the expensive waistcoat wearing on top from sweat and soil [6]. Early in the eighteenth century, Beau Brummel [7] an iconic figure in Regency England brought shirt into spotlight and turned

it into an essential garment for men. During the nineteenth century, shirt was considering as a luxurious attire due to heavy labour to keep it clean and white. Until later in the mid-nineteenth century when the laundry techniques were improved, shirt market were expanding with affordable prices then shirt was truly gaining its popularity.

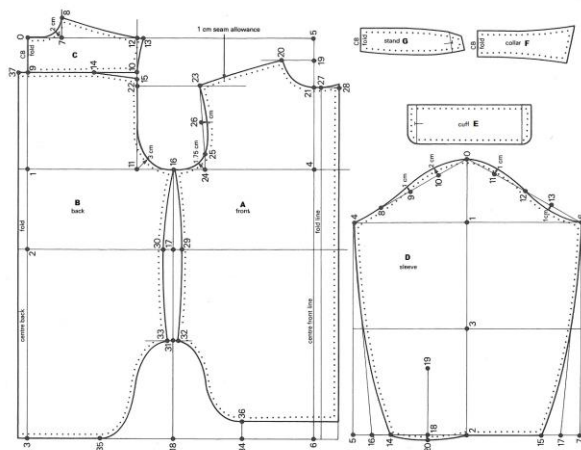


Figure 3 A-G. A complete set of shirt pattern A-front; B-back; C-back yoke; D-sleeve; E-cuff; F-collar; G-collar stand

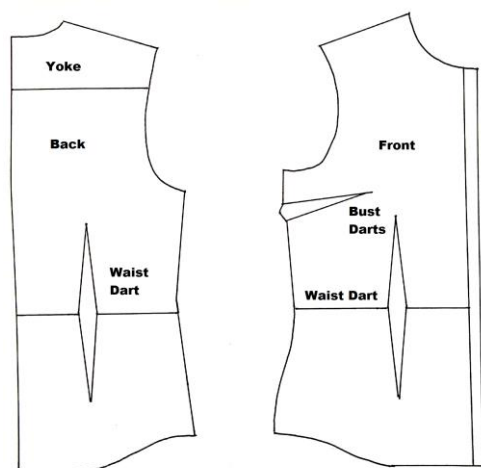


Figure 4. Women's front, back and yoke pattern pieces are similar to men's except the bust and waist darts are added in to better fit the female body

For the last hundred years, shirt style and fit are constantly changing; from broad shoulder and wider chest circumference to allow more mobility but bulky, and to the slim fit which is narrower from the shoulder down to chest and waist and limiting movement yet provides the wearer a slender look. Moreover, the stylish cuffs, ever changing sleeve length, dozens of collar and collar stand combination plus decorative buttonhole plackets; shirt has been evolved into a big market in the garment industry [8].

4 DISCUSSION AND CONCLUSION

Shirt is an important piece of garment for both men and women. Since shirt slowly gaining its popularity in the nineteenth century until today, the market demand of shirt is still growing globally [9]. Especially nowadays, new technologies are involved and materials are

invented; more and more innovative textiles and smart garments are developing. However, the clothing pattern is still rely on the fundamental basic bodice and sleeve blocks which are originally derived from draping techniques hundreds of years ago. With these hi-tech fabric slowly filling in the garment business, would the traditional basic blocks be compatible to the new materials; or should there be a new set of clothing pattern developed. Even clothing pattern is produced with the CAD system, it is still based on the basic blocks. Does it make sense?

New pattern set should be researched and be invented. New pattern blocks should focus on thermal insulation to keep wearer warm, sweating efficiency and cooling effect by researching on clothing air gaps and pattern sizes and shapes relationship. Of course, body movements and wearing comfort cannot be neglected. New materials and new pattern set create the new world in the future.

5 REFERENCES

- [1] Gant. *History Of The Shirt-Shirt Guide*-<http://www.gant.com/shirtguide/shirt-history>
- [2] Dean Brough. *Neo – Dandy*. Queensland University of Technology Creative Industries, 2008
- [3] Cunnington, Cecil Willett, and Phillis Cunnington. *The History of Underclothes*. Courier Corporation, 1992.
- [4] W.H. Hulme. *The Theory of Garment Pattern Making*. The National Trade Press Limited, 1945.
- [5] Aldrich, Winifred. *Metric Pattern Cutting for Menswear*. John Wiley & Sons, 2011.
- [6] "Shirt." In *Wikipedia*, June 24, 2018. <https://en.wikipedia.org/w/index.php?title=Shirt&oldid=847293342>.
- [7] "Beau Brummell." In *Wikipedia*, May 12, 2019. https://en.wikipedia.org/w/index.php?title=Beau_Brummell&oldid=896792895.
- [8] "100 Years of Fashion: Men ★ Glam.Com - YouTube." Accessed May 16, 2019. <https://www.youtube.com/watch?v=DaSkMWVIFU&list=WL&index=23&t=0s>.
- [9] Lu, Author Sheng. "Statistics: Global Apparel Market 2016-2020." *FASH455 Global Apparel & Textile Trade and Sourcing* (blog), October 16, 2016. <https://shenglufashion.com/2016/10/16/statistics-global-apparel-market-2016-2018/>.

6 CREDIT OF FIGURES

Figure 1. "See the World's Oldest Dress."

National Geographic News, February 18, 2016.

<https://news.nationalgeographic.com/2016/02/160218-oldest-dress-egypt-tarkhan-archaeology/>.

Figure 2-3. Aldrich, Winifred. *Metric Pattern Cutting for Menswear*. John Wiley & Sons, 2011.

Figure 4. Owned figure.

CIRCULATING PRE-OWNED FASHION ---- O2O TRADE OF SECONDHAND TEXTILES IN CHINA

Qing Li¹, Jin Peng²

^{1,2} Southwest University, Chongqing, China, e-mail: qingli@swu.edu.cn

Abstract: Use the O2O business model to build an online-to-offline platform to circulate our pre-owned fashion. The secondhand clothing will be divided into three categories according to their conditions: for sell at a discounted price, for sell at a very low price or as a donation, for disruptive recycling. A brand name will be created (or shared) to earn trust and build reputation in society, and to ensure safety and hygiene of the clothing. Online services include supply and demand information for resell and/or donation of the pre-owned clothing. Offline services will be chain retail shops. The prolonged life of our textiles can promote quality fashion products with a green process, and help to reduce the use of our scarce natural resources.

Keywords: fashion, O2O, second hand textile, recycle, environment sustainability

1 INTRODUCTION

It is estimated that an average of 30% clothes in every household are not in use, and almost 50% unwanted clothing is comprised of 70-90% new or brand new. They are quite often discarded from a spur-of-the-moment purchase or by young people whose dress sense changes frequently, or by parents whose children have out-grown them. It is a shame to see these clothes go to the disruptive recycling stage, consuming energy for the reproduction. Instead, they could easily be reused. An increasing global demand will be clean energy and natural resource. We can save the workload in the industry from an excessive production and make our environment a cleaner and greener place, if we can prolong the life of our products by circulating and reusing them. It is a long term sustainable development, and everybody on the Earth is part of it.

2 BACKGROUND

Textile industry relies heavily on natural resources and has a big impact on the environment. For example, synthetic fibres are made from coal, petroleum or natural gas; cotton/wool growing needs plenty of fresh water; textile wet processing such as dyeing causes problems such as waste-water discharge. It is estimated that humans are using 30% more resources than the Earth can replenish each year. The problem is getting worse as populations and consumption keep growing.

The world is producing millions of tons of secondhand clothing each year. In China alone, the annual production of so called "waste" textiles is 20 million tons, among them, only 15% get a comprehensive utilization.

Unlike in western countries, there are no secondhand retail shops in China at present. The technical way of textile recycle is to use mechanical or chemical treatment to disrupt the fibre or fabric and make them reusable. The disruptive textile recycling technology has developed rapidly in recent years. While it has facilitated the saving of

tons of textiles from dumps and landfills, it can be labor and energy intensive.

Almost 50% unwanted clothing is comprised of 70-90% new or brand new. They are quite often discarded from a spur-of-the-moment purchase or by young people whose dress sense changes frequently, or by parents whose children have out-grown them. These clothes could easily be reused. Prolonging the life of textiles can help saving our planet by reducing excessive and unnecessary production and reducing the use of our scarce natural resources.

China is the the world's most populous country with the largest textile production. The secondhand textile recycling rate is however, relatively low in comparison with other countries (Figure 1). The successful model of circulating pre-owned fashion can set an example for other developing countries.

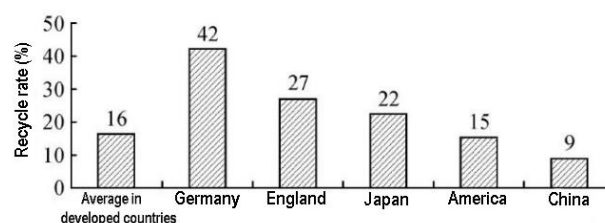


Figure 1 Secondhand textiles recycle in some countries[1]

3 O2O MODEL

3.1 What is O2O

O2O refers to Online-to-Offline or Offline-to-Online, which uses the internet to expand the scope of traditional shops by offering people maximum information of what they can access. Meanwhile, the offline retail services give people

the opportunity to see and try on the actual clothing to ensure satisfaction which online retail services are unable to achieve. "Seeing is believing" can remove hygiene concern of the pre-owned clothes from people, which is one of the reasons that secondhand retail shops have difficulties being accepted in China. Online and offline complement each other and develop together (Figure 2).

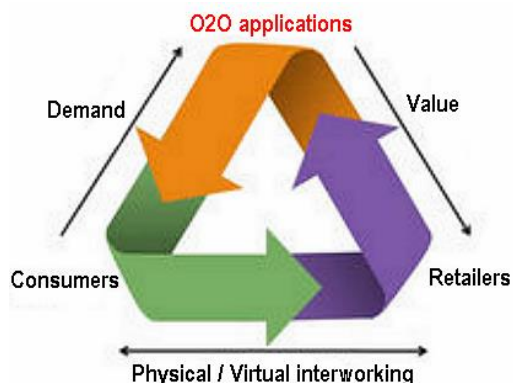


Figure 2 O2O model[2]

3.2 3 categories for pre-owned clothes

The collected pre-owned clothes can be grouped into three categories for different purposes: those of 70% new to brand new goes to resell, 40-70% new goes to the needed for very cheap price or as a free donation, and the rest goes to the disruptive recycling. There will be no waste in the chain and consumers at all levels can find their positions. O2O system is a win-win model for both customers and environment. It provides people with a platform to circulate and to make the best of what is not being used, saving tons of textiles from dumps and landfills.

3.3 The users

Almost everybody can be the user of the platform. The users varies from people living affluently in the cities who want to give away their clothes to the needed but do not know how to do it, to the people living in remote country with limited access to the outside world and/or cannot afford new clothing; from parents whose children grow quickly and do not want to spend too much on their clothing, to people who like to follow fashion but have a limited budget etc. The O2O system can give everyone the opportunity and platform to find what they want.

4 COMPETITIONS

4.1 Current fashion market

Internet has changed the way people live significantly in the past decade. Nowadays in China, people can have almost anything and everything delivered to their doorsteps by touching the computer screen at home. Internet has undoubtedly become a major source of information on the various products available. There has been constant complaint however, that the clothes purchased online do not always meet consumers satisfaction as it can be difficult to make a judgement based on what's shown on the screen. The lack of direct person-to-goods experience of the online shopping can result in an increasing number of brand new "waste" fashion in the household.

While one competition comes from the current fashion market where new clothing is inexpensive and within easy reach from the internet, fitting in overseas markets (such as Africa) is an alternative for textile reusing. In addition to the shipping cost however, saving them from the landfills is a concern. Plus there is domestic needs in China. O2O may start in China and eventually become international. It not only helps to expand the life of our products, but also helps to develop an environmental conscious mindset in our society.

4.2 Culture challenges

The biggest challenge comes from the mindset of the people. Unlike in other countries, people in China are less willing to accept the concept of secondhand clothing. In addition to hygiene/health concerns, wearing secondhand clothes seems to be tantamount to publicly declare that they are losers, plus cheap new clothes are within easy reach. While the way people perceive can be changed to some extent through education and development of an environmental conscious mindset, changes in deep root of the culture will take time. Chinese government has come out with a number of policies and regulations towards environment protection in recent years. Much of them however, are at technical levels. Education and encouragement on the changes in people's mindset seems to have received little attention. It will be good to see support from the government on this people-oriented issue. After all, it is people's behavior that is changing the world.

5 IMPACT TO FASHION INDUSTRY

5.1 Environmental conscious mindset

An environmental conscious mindset can be put into the start-stop chain in the fashion industry. These include mindset of the fashion designers, the manufacturers, and the customers. Improvement on environmental conscious mindset will be reflected by how successful the secondhand retail service is, how popular the designed website is, and various viewpoints from the fashion designers, the manufacturers, and the customers.

5.1 Quality improvement

Circulating pre-owned fashion will urge the industry to improve the quality of fashion products. Opening up of secondhand retail market will see a slight decreasing demand for new clothing. The fashion industry will realize that only quality clothing with green-process can be adored and owned by customers for a long time. The rule of "survival of the fittest" is expected to apply to the fashion industry with the implementation of the idea. Those with less quality and environment oriented will be eliminated.

ACKNOWLEDGEMENT: China Southwest University Grant Scheme (project ID: SWU116040) is acknowledged by the authors.

6 REFERENCES

- [1] Zhang F., Yang S., Du P., waste textile recycling review. *Modern Textile Technology*, 2015, 23, pp. 56-62.
- [2] Chen Y., Guo D, China's O2O business model based on multi-case analysis. *Macroeconomic Studies*, 2015, 4, pp. 14-22.

9. Environment and Sustainability

MULTICOMPONENT FIBER RECYCLING – ANALYSIS OF HETEROGENOUS HYDROLYTIC KINETICS

Arun Aneja¹, Karel Kupka², Jiri Militky³

¹ East Carolina University, Department of Engineering, Greenville, NC 27858, USA, email: anejaap@gmail.com

² TriloByte Statistical Software, Ltd., St. Hradiste 300, CZ 53352 Pardubice, Czech Republic

³ Faculty of Textile Engineering, Technical University of Liberec, Czech Republic

Abstract: Consumer awareness of the importance of environmental stewardship has led to increased demand for products manufactured with minimal impact on the world's well-being. The demand for textiles that have a "green" pedigree has grown even in the face of economic hardships endured recently by many consumers. The environmental benefits gained from using recycled raw materials rather than virgin materials to make products include conservation of natural resources, reduced energy consumption, carbon dioxide (CO₂) and other emission reduction, and waste not entering landfills. Some of these products may command higher prices than their traditional counterparts, partly because the practice of recycling has not been fully adopted by consumers, so supply of recycled materials is limited — for example, today, only about one-quarter of the plastic bottles consumed in the United States are recycled, but that percentage is increasing year by year. However, these products also tend to be made using cleaner, more efficient processes. Thus one may say that the higher cost is mitigated by the longer-term benefits gained by living in a cleaner, healthier world with abundant natural resources. Apparel and textiles account for approximately 10 % of the total global carbon footprint. Annually, more than 60 million tons of textiles is disposed of in landfills or burnt at global level. Currently, textiles are at the bottom of all industries in terms of recycling with no acceptable strategy for a sustainable future. The present paper seeks to develop recycling technology for heterogeneous kinetics of multicomponent textile waste. This should lead to closed loop strategy towards a circular economy. The waste transformation to basic materials can be reused for textile or plastic production. Two special reaction kinetic models were developed: (i) Surface reaction rate controlling, and (ii) Penetrant in solid phase rate controlling. Justification with mono and multicomponent neutral and acid hydrolysis was shown. To develop design considerations of the recycling reaction behavior a DOE was developed using the critical process parameters. The aim was primarily at separation of cotton/polyester or wool/polyester blends by acid hydrolysis reaction and high-pressure neutral hydrolysis of PET to recover the basic monomeric constituents. Carboxyl end group concentration was used to follow the extent of reaction. The activation energies of acid hydrolysis reaction with cotton were estimated to be 72.8 kJ/mol and 41.5 kJ/mol for multicomponent blend. The basic kinetic and thermodynamic data developed was used in the design of a pilot-plant of the process.

Keywords: modelling, sustainability, recycling, multicomponent textile waste

1 INTRODUCTION

Consumer awareness of the importance of environmental stewardship has led to increased demand for products manufactured with minimal impact on the world's well-being. The demand for textiles that have a "green" pedigree has grown even in the face of economic hardships endured recently by many consumers.

The environmental benefits gained from using recycled raw materials rather than virgin materials to make these products include conservation of natural resources as well as reduced energy consumption, carbon dioxide (CO₂) and other emissions, and waste going to landfills. Some of these products may command higher prices than their traditional counterparts, partly because the practice of recycling has not been fully adopted by consumers, so supply of recycled materials is limited — for example, today, only about one-quarter of the plastic bottles consumed in the United States are recycled, but that percentage is increasing year by year. However, these products also tend to be made using cleaner, more efficient processes. So one may say that the higher cost

is mitigated by the longer-term benefits gained by living in a cleaner, healthier world with abundant natural resources.

Poly(ethylene terephthalate), PET is a commodity polymer used as a high-molecular weight polymer (intrinsic viscosity, 0.82 dL/g) in bottles for packaging fluids such as mineral water and soft drinks and also used as a moderate molecular weight polymer (IV 0.6 dL/g) in textile fibers with highest global consumption. Recycling of the polymer is desired to reduce the environmental impact of plastics but suffers from the following factors. During the life cycle of PET polymer, the material characteristics change due to thermal and environmental influences. For example, the IV of the PET bottle reduces from 0.82 dL/g to less than 0.76 dL/g. In addition, diffusion of filled product into the PET bottle polymer also causes contamination and degradation of the polymer. The present paper deals with heterogeneous reaction kinetics of neutral hydrolysis of PET and acid hydrolysis of cotton and PET/cotton blend.

2 EXPERIMENTAL

Experiments were conducted using two pure components: 100 % cotton yarn and wool fibers and two 50:50 blends of the these pure components with polyester. Polyester yarn was used for the hydrolysis reactions. A mixture of 50 wt % polyester and 50 wt % wool was prepared by weighing 0,5 g of polyester fibers and 0,5 g of wool fibers. Polyester/cotton blend fabric (50:50) was used for the separation of polyester and cotton. Acid hydrolysis of pure and blend fibers was performed in batch glass reactor equipped with magnetic stirrer.

All samples were cut into segments approximately 1 cm long, dried for 12 h at 105 °C and stored in desiccators until used. Acid hydrolysis was performed using two different mineral acids, HCl and H₃PO₄ at two different concentrations. The reactions were optimized for 1 g of sample and 20 mL of acid. The solid:liquid ratio was maintained at 1:20 in all batch operations. The temperature ranged from 55 °C to 120 °C and different agitation speeds were used. Kinetic data was established for the hydrolysis of pure components, followed by the study of blends.

The first step of the process was removal of natural fibers (cotton and wool) from blends, by acid hydrolysis. A Box-Behnken experimental design was employed to determine the optimal conditions for natural fibers removal and to maximize information obtained.

The second step was neutral hydrolysis of polyester fabric at 250 °C and 35-38 bars carried out in a high-pressure reactor, shown in the Figure 1. The process was evaluated at two different weight (PET/water) ratios (1:8 and 1:10), consistent with minimal water utilization. The products of the reaction were purified by dissolving in sodium hydroxide solution, followed by precipitation in hydrochloric acid, rinsed with water and finally analyzed on a Perkin Elmer FT-IR Spectrum GX spectrometer.

3 RESULTS & DISCUSSION

Polyester Neutral Hydrolysis

The experiment was performed in subcritical water at T=523 K. Estimated parameters of (7) are: $D=1.5 \cdot 10^{-4}$, $C=1.04$ with end-of-reaction time $t_E=195$ min. [3]. The parameters of the nonlinear model (7) were estimated by least squares nonlinear regression.

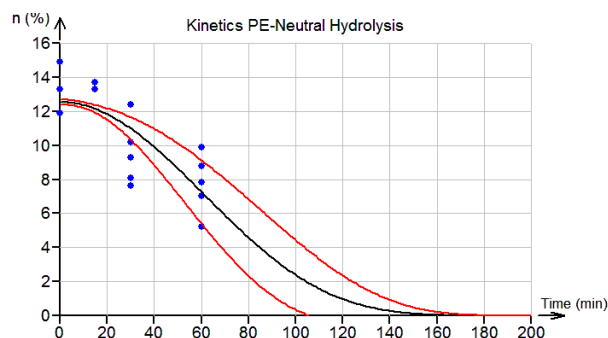


Figure 1. Kinetics of PET Neutral Hydrolysis

Case 2: Cotton Acid Hydrolysis

The acid hydrolysis of cotton was conducted at 75, 95 and 120 °C. The kinetic curve predicted by model (Equation 7) at 120 °C and the activation energy plot are shown in Figure 5 & Figure 6. The activation energy of acid hydrolysis reaction of pure cotton was found to be 72.8 kJ/mol [4]. Computed parameters of the kinetic model (7) are given in Table 1.

Table 1. Estimated kinetics parameters for cotton acid hydrolysis

T [K]	D	C	Scale parameter Q_S	End-of- reaction time t_E [sec]
393	9.97 E-008	0.994	100.03	7730
368	1.49 E-008	0.992	100.39	19960
348	6.40 E-009	0.996	99.74	30570

Case 3: PET/Cotton 50:50 Blend Acid Hydrolysis

The acid hydrolysis of PET/cotton blend was conducted at 55 and 70 °C. The kinetic curve predicted by model (Equation 7) at 70 °C and the activation energy plot are shown in Figure 7 & Figure 8. The activation energy of acid hydrolysis reaction of PET-cotton blend was found to be 41.5 kJ/mol [5]. Computed parameters of the kinetic model obtained from Equation are provided.

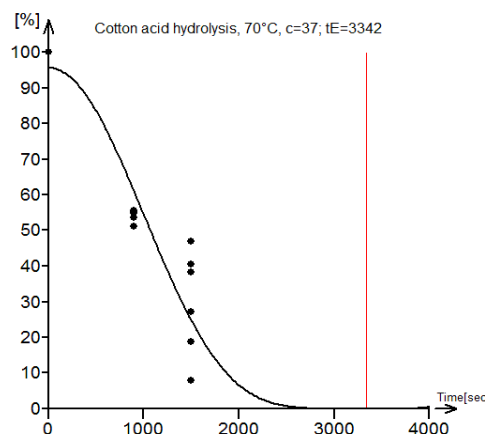


Figure 2. Model versus experimental data of PET/Cotton acid hydrolysis at 70 °C. End-of-reaction time t_E is marked by the vertical line.

4 REFERENCES

- [1] Recycling textiles, <http://ec.europa.eu/research/growth/gcc/projects/recycling-textiles.html> Accessed: 2013-01-08
- [2] Y. Wang, J. Wan, Y. Ma, M. Huang. Hydrolysis kinetics characteristic of recycled fiber in subcritical water. *Bioresource Technology*, Volume 105, February 2012, Pages 152-159

RESEARCH OF ARCHAEOLOGICAL TEXTILES IN THE CZECH REPUBLIC

Helena Březinová¹, Milena Bravermanová²

¹Institute of Archaeology of the CAS, Letenská 4, Praha 1, Czech Republic, brezinova@arup.cas.cz

²Institute of Archaeology of the CAS, Letenská 4, Praha 1, Czech Republic, milena.bravermanova@seznam.cz

Abstract: Archaeological textile finds represent a unique and, thanks to their organic nature, a rare source for learning about an important component of material culture, that was part of the daily life of people in the past. Thorough research, analyses, processing and the evaluation of preserved textiles provides an overview of the development of used materials and their working, as well as of the method, level and organisation of textile production and all related crafts.

Keywords: archaeological textile, textile technology, Czech Republic, textile production

Textile production represented an important component of the economy, and textile material, as well as all products made from it, formed a significant part of the material culture of all periods of historic development. When examining the historical development of textile production, finds of textile remains and tools and equipment that were used in the lengthy process of making textiles – from acquiring the raw materials to the final product – provide a good source of information.

Archaeological textile finds represent a unique and, thanks to their organic nature, a rare source for learning about an important component of material culture, that was part of the daily life of people in the past. Thorough research, analyses, processing and the evaluation of preserved textiles provides an overview of the development of used materials and their working, as well as of the method, level and organisation of textile production and all related crafts.



Figure 1 Band with added gold and silk weft thread woven on a tablet loom, 14th century, Prague Castle © authors

detailed documentation, which provide technical information on the method of processing and production of textile products. Optical microscope and SEM, are used to track and evaluate the following parameters: textile type; the number and dimensions of fragments; current colour; utilised textile materials; fibre morphology; weave; thread count on a 10 mm area of fabric; surface finish by fulling; the direction of thread twisting; thread thickness; another description recording decorative elements, faults, fixed edges, stitches, etc. Along with an evaluation of the find circumstances and an analysis of analogies and historical contexts, the textile technology study is the basis for interpreting the original function and method of use of the individual textile fragments.



Figure 2 Fragment of silk fabric, 14th century, Prague, © authors

The professional processing of archaeological textile fragments is based on a study of textile technology and

The detailed processing of preserved prehistoric and medieval textiles provides valuable information on the

growing of cultural crops containing textile fibres, on the level of technical advancement of equipment and tools, the level and organisation of textile production, variability of textile techniques, the diversity of products, distribution, trade and the share of domestic production and imported goods.

Archaeological textiles have been in the Czech Republic intensively and systematically treated since the 1990s [1]. The territory of our country does not offer too suitable conditions for preserving archaeological organic material, therefore, fabric remnants are scarce, but appearing finds. Small textile scraps from medieval town waste layers and objects, remnants of fabric structure in corrosive products of metal objects coming from grave finds of the younger prehistoric age and early middle ages can be encountered

most frequently of all. Relatively well preserved fabrics also appear together with human remains in tombs and crypts of the medieval as well as modern age.

ACKNOWLEDGEMENT: *Supported by the grant project the Czech Science Foundation 19-00166S*

REFERENCES

- [1] Bravermanová M., Březinová H.: Archaeological Textile Research in the Czech Republic. In: Bravermanová, M. – Březinová, H. – Malcolm-Davies, J. (Eds.) 2017: Archaeological Textiles – Links Between Past and Present. NESAT XIII. Liberec – Praha, 11-17.

DEVELOPMENT OF THERMALLY INSULATED CONSTRUCTION STRUCTURE BY SUSTAINABLE NATURAL FIBERS

Hafsa Jamshaid^{1,2}, Ali Raza¹, Sikander Abbas Basra¹, Rajesh Mishra²,

¹ *Protective Textile Research Group, Faculty of Textile Engineering, National Textile University, Pakistan.*

² *Faculty of Textile Engineering, Department of Material Engineering, Technical University of Liberec, Liberec, Czech Republic.*

Abstract: Now-a-days, growing use of bio composites has substantial prospective for constructive environmental outcomes. There is an interest in the development of new materials from renewable resources. The aim of present work is using sustainable natural fibers i.e. sugar cane, sisal, coconut and jute fiber beside basalt fiber to reinforce concrete and to investigate thermal insulation aspects of textile reinforced concrete (TRC) for its usability in the built environment. Thermal conductivity, scanning electron microscope (SEM) and thermo-gravimetric analysis (TGA) tests were performed on plain/simple concrete and fibre reinforced concrete (RC) samples. Thermo-gravimetric analysis shows that Sugarcane, Basalt and Jute fibres reinforced concrete samples have better thermal stability as compared with plain/simple concrete sample up to 50°C that is appropriate for hot atmosphere however Sisal and Coconut RC samples have relatively lower thermal stability. Consequently, applying these fibres based concrete materials in construction may result in lower energy cost and will have positive effect on the atmosphere.

Keywords: Natural fiber, Textile Reinforced Concrete, TGA, Thermal conductivity

1 INTRODUCTION

The energy consumption is the main issues of the 21st century. The cooling and heating systems in structures are constraints in the way of sustainability. The fuel resources are reducing day by day. Extreme rise in fuel demand causes air pollution and variation in climate [1], [2]. Building design and architecture can reduce energy consumption. By suitable designing and thermal insulation can play a vital role in the reduction of energy consumption especially in buildings that is located where climate conditions are harsh [3], [4].

There are several advantages of home and building insulations. Insulation increase the comfort in homes and building, keep healthful environment inside structure, decrease the consumption of energy and have a good impact on environment. Addition of suitable insulation to a present home keep the temperature in control, make the living environment of home enjoyable, particularly in locations where weather extremes. By Insulation with appropriate material, the structure converts into energy efficient structure. Insulator material keeps the structure cool in the summer season and in winter season warm. This technique decrease the no. of appliances that are used for cooling, heating purposes and is required to keep the structure comfortable for living. By doing this, home electricity bills reduces that is beneficial for economy. Several types of insulator materials are used for building insulation like fiber glass, mineral wool, polystyrene etc. Many organic and inorganic materials have been used for thermal insulation but they all are not sustainable and natural. Therefore the present research work purpose is to reinforce sustainable natural fibers in concrete and analysis regarding their thermal insulation properties to find their suitability.

2 MATERIALS AND METHODS

2.1 Materials:

- Sand, Aggregates (crushed stone), water and Cement.
- Natural Fibers e.g. Sisal, Sugarcane, Coconut, Jute and Basalt.



Figure1: Natural Fibers

2.2 Testing :

Thermal conductivity, Scanning Electronic Microscope and thermo-gravimetric analysis (TGA) tests were performed of plain concrete and fibre reinforced concrete (RC) samples.

3 RESULTS AND DISCUSSIONS

The thermal conductivity of the material depends on the nature of the material, the cross section area (A) and temperature gradient. Improvement in thermal insulation was observed by increasing the fibers percentages. Increasing fiber contents in concrete mixture, voids are formed that are also good insulator against heat that is shown in the SEM images. Thermo-gravimetric analysis shows that Sugarcane, Basalt and Jute fibres RC samples have better thermal stability as compared with plain concrete sample up to 50°C.

4 CONCLUSIONS

Thermal conductivity obtained results show that by increasing the natural sustainable fibres (Coconut, Jute, Sugar cane, Basalt, Sisal) percentages in concrete the value of thermal conductivity decreased.

SEM images of fibres reinforced concrete were taken to show the bonding of fibres with concrete mixture.

Thermo-gravimetric analysis shows that Sugarcane, Basalt and Jute fibres RC samples have better thermal stability as compared with plain concrete sample up to

50°C that is appropriate for Pakistan atmosphere however Sisal and Coconut RC samples have relatively less thermal stability.

Consequently, applying these fibres RC materials in construction may result low energy cost and will have positive effect on the atmosphere.

5 REFERENCES

- [1] Yannas S.,: Toward more sustainable cities, *Sol. Energy*, vol. 70, no. 3, pp. 281–294, 2001.
- [2] Agoudjil B., Benchabane A., Boudenne A., Ibos L., and Fois M., :Renewable materials to reduce building heat loss: Characterization of date palm wood," *Energy Build.*, vol. 43, no. 2–3, pp. 491–497, 2011.
- [3] Papadopoulos A.M.,:State of the art in thermal insulation materials and aims for future developments, *Energy Build.*, vol. 37, no. 1, pp. 77–86, 2005.
- [4] Cabeza L.F, Castell A., Medrano,M, I. G.Martorell, Pérez, and IFernández I, :Experimental study on the performance of insulation materials in Mediterranean construction, *Energy Build.*, vol. 42, no. 5, pp. 630–636, 2010.

ECOLOGICAL TREATMENT OF WOOL USING NATURAL POLYPHENOL SUBSTANCES

Hana Křížová¹ and Jakub Wiener²

¹Technical University of Liberec, Institute for Nanomaterials, Advanced Technologies and Innovation, Department of the Preparation and Analysis of Nanostructures, Bendlova 1409/7, Liberec, Czech Republic, e-mail: hana.krizova@tul.cz

²Technical University of Liberec, Faculty of Textile Engineering, Department of Material Engineering, Studentská 2, Liberec, Czech Republic, e-mail: jakub.wiener@tul.cz

Abstract: The aim of this work is to give an overview of the possibilities of sheep wool treatment using natural extracts based on polyphenols. In this work, few applications of plant polyphenols on sheep wool are presented, e.g. mordanting, dyeing, elimination of odor or antibacterial treatment. These methods of green chemistry represent environmentally friendly methods of wool treatment, which are a sustainable alternative to chemical processes.

Keywords: wool, tannin, polyphenols, odor, antibacterial, treatment

1 INTRODUCTION

Even today, when synthetic fiber fabrics flood the global markets, wool is still a highly desirable textile material. Clothing comfort, durability, great thermal insulation, soil resistance, flame resistance, warmth even in wet conditions, biodegradability, and many other features are the main advantages of this natural material. However, industrial wool processing is often environmentally problematic because it leads to mass use of coarse chemistry, from washing over the pretreatment, dyeing and subsequent finishing processes. Green chemistry offers ecological alternatives of wool processing for clothing and technical applications, in almost all technological steps.

2 NATURAL POLYPHENOLS

Natural polyphenols are commonly present in plants and trees. They have a lot of interesting properties due to their structure with many hydroxyls on aromatic rings (Figure 1). They form complexes with various substances - mainly proteins and amino acids: the leather tanning process is also based on protein coagulation.

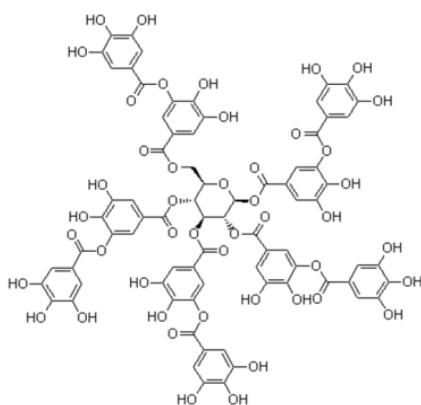


Figure 1 Tannic acid - hydrolysable tannin often used in laboratory tests as a standard polyphenol compound

Reactions of wool with plant polyphenols are based on reactions leading to formation of complexes, formation of numerous hydrogen bridges, and antioxidant reactions (chemical reduction) [1]. These “skills” of polyphenols in contact with proteins lead, for example, to the destruction of bacteria or reduction of bacterial growth [2], stronger binding of dyes to the surface of the fibers [3], changes in conformation of the proteins, even their denaturation [4], crosslinking [5], and deactivation or decomposition of other low-molecular substances and volatiles created on the surface of fibers [6].

3 USE OF POLYPHENOLS FOR WOOL TREATMENT

3.1 Tannins as mordants of wool before dyeing

Tannins have been used as mordants in conjunction with metal salts (eg. CuSO_4 , SnCl_2 , SnCl_4 , FeSO_4 , $\text{KAl}(\text{SO}_4)_2$, etc.) for hundreds of years. Phenolic groups of tannins can form effective bonds with different types of fibers and help the fixation of dyes. Tannin-based mordants have found use in cotton dyeing that has very low affinity for most natural dyes. However, a similar procedure is also applicable to wool fibers. The classical method is two-phase: firstly, the fibers are pretreated with tannin, secondly, the metal salts are applied, and the dyeing follows. This process is based on the idea that the tannin penetrates the fiber and the subsequent application of metal salts (Fe, Cr, Cu, Al, Pb or Sn ions) results in “in situ” complexes (tannates). This fixes the tannin on the dyed material and consequently the natural dye is bound to the fiber more firmly and with higher affinity.

The use of metal salts is a serious ecological drawback of this dyeing system, therefore ecologically more acceptable substitutes, such as enzymes, are also sought. The use of enzymes has some specifics, since enzymes work mostly under moderate temperature and pH conditions. Enzymes require a specific substrate and

are sensitive to the presence of metal ions that reduce enzyme activity as so-called catalytic poisons. Enzymes are obtained, for example, as products of bacteria or mold and their disadvantage is the high purchase price. An advantage of enzymes is their biodegradability and thus environmental friendliness. As tannins bind very well with the proteins, the single-phase treatment of the fabrics before treatment with the complex of tannin, amylase, protease and lipase, is highly effective. The dye is removed from solution onto the fiber with subsequent improved wet fastnesses. [7]

3.2 Dyeing of wool using polyphenolic dyes

Plant polyphenols are several thousand substances including a large group of flavonoids. They have two substituted benzene rings: A and B, with the pyran ring C fused to ring A. This pyran ring contains trivalent oxygen which allows the formation of oxonium salts by its positive charge. Many flavonoids are important as plant dyes, especially yellow flavones and flavonols (from Latin *flavus* = yellow) and their name is the basis of the name of the whole group. The chalcones and aurones are also yellow, the flavanones are colorless or yellowish, and the specific group are red, pink, purple, blue, orange, but also yellow anthocyanins. They occur, for example, in plant flowers, leaves and fruits. Although anthocyanins have unstable shades and low lightfastness, they have always been used for textile dyeing. Plinius already mentioned blueberries used in Gaul for dyeing of slave garments to purple [8]. The anthocyanins are most suitable for dyeing of animal fibers, such as wool [9] [10] and silk. Without the addition of inorganic mordants, the anthocyanins stain the fabrics in red-brown tones. With alum, especially on the wool, they give shades of yellow-brown [11] and the reaction with ferrous ions changes the shade to gray to black.

In Scotland, the freeze-dried fruits of *Ligustrum vulgare* were previously used to color the wool pre-sunk with aluminum, iron, and soda to achieve a deep blue color. And in the Shetland Islands in 1840, they routinely dye sheep's wool using blueberries similar to black shrubs (*Empetrum nigrum*) on a violet-blue hue. [12]

3.3 Elimination of wool odor

The main cause of the unpleasant wool odor are bacteria on the surface of wool fibers. They decompose fat, keratin and other organic substances to form volatile substances that are the source of odor. The study [13] has shown that the heat treatment of raw wool by the tannin solution significantly reduced the intensity of wool odor. At the same time, the treated wool acquired some antimicrobial resistance. Significant improvement in olfactory perception of wet tannin-treated wool have been demonstrated through sensory analysis of the panel of evaluators and using the gas chromatography.

3.4 Antibacterial treatment of wool surface

The mechanism of antimicrobial activity of some polyphenolic substances is not yet fully understood. Their biological activity has been shown to be dependent on the molar content and spatial configuration of the o-phenolic hydroxyl group [14], and the interaction with proteins, and hence the enzymatic system of bacteria, may play a further role. Binding with bacterial proteins (MRSA) [15] or

toxins can reduce the effect of bacteria. An important role can be also played by chelation of trace elements, as this would limit the bacterial metabolism.

4 CONCLUSION

Plant polyphenols of various compositions can be easily extracted from cheap and widely available vegetable sources, such as agricultural and forestry wastes. This makes the proposed processes of wool treatments affordable, environmentally friendly, and sustainable as they don't require the use of expensive chemicals or energy-intensive technologies.

ACKNOWLEDGEMENT: You can write acknowledgement here.

5 REFERENCES

- [1] Andrade Jr, R. G., et al.: The antioxidant effect of tannic acid on the in vitro copper-mediated formation of free radicals. *Arch Biochem Biophys* 2005, 437(1), pp. 1-9.
- [2] Scalbert, A.: Antimicrobial properties of tannins. *Phytochemistry* 1991, 30(12), pp. 3875-3883.
- [3] Burkinshaw, S. M., Kumar, N.: A tannic acid/ferrous sulfate aftertreatment for dyed nylon 6, 6. *Dyes Pigm* 2008, 79(1), pp. 48-53.
- [4] Hagerman, A. E., Butler, L. G.: Protein precipitation method for the quantitative determination of tannins. *J Agric Food Chem* 1978, 26(4), pp. 809-812.
- [5] Heijmen, F. H., et al. : Cross-linking of dermal sheep collagen with tannic acid. *Biomaterials* 1997, 18(10), pp. 749-754.
- [6] Lisovac, A. M., Shooter, D.: Volatiles from sheep wool and the modification of wool odour. *Small Rumin Res* 2003, 49(2), pp. 115-124.
- [7] Vankar, P. S., et al.: Enzymatic natural dyeing of cotton and silk fabrics without metal mordants. *J Clean Prod* 2007, 15, pp.1441-1450.
- [8] König, J. R.: Zur Geschichte der Pigmente: Plinius und seine „Naturalis Historia“. *Fette, Seifen, Anstrichmittel* 1960, 62, pp. 629-637.
- [9] Bechtold, T., et al.: Anthocyanin dyes extracted from grape pomace for the purpose of textile dyeing. *J Sci Food Agric* 2007, 87, pp. 2589-2595.
- [10] Karaboyaci, M., Uğur, S. S.: Ecological wool dyeing with pulps of lavender, broom, and red wine. *J Text I* 2014, 105(8), pp. 821-827
- [11] Schweppe, H.: Handbuch der Naturfarbstoffe. Ecomed Landsberg, 1993.
- [12] Grierson, S.: Vegetable Dyes of Scotland. *J Soc Dyers Colours* 1984, 100, pp. 209-211.
- [13] Křížová, H., Wiener, J.: Tannin treatment of sheep wool. *Vlákna a Textil* 2019, in press.
- [14] Schofield, P. et al.: Analysis of condensed tannins: a review. *Anim. Feed Sci Tech* 2001. 91, 21-40.
- [15] Akiyama, H. et al.: Antibacterial action of several tannins against *Staphylococcus aureus*. *J Antimicrob Chemother* 2001, 48, pp. 487-491.

A SMART AND SUSTAINABLE SPINNING FOR COLORFUL TEXTILES

Rui-Hua Yang

School of Textiles and Clothing, Jiangnan University,
1800 Lihu Avenue, Wuxi, Jiangsu Province, 214122, P.R. China
e-mail: yangrh@jiangnan.edu.cn

Abstract: By dynamically controlling the feeding amount and feeding ratio of the three feeding rollers with Program Logical Control system under the requirements of yarn spinning parameters, it is possible to effectively produce colorful textiles by configuring the final yarn density and the blending ratio of three components to produce multi-segment gradient yarns, segment-color yarn, and segment-color slub yarn named as multi-segment blending yarns. The smart and sustainable spinning method was proposed. Different kinds of colorful fancy yarns including gradient yarns, segment color yarns and slub yarns were produced. The fiber blending effects were demonstrated by slices of yarn cross-section, and the surface morphology of yarns were figured out by the photo of yarns. Integrally Knitting seamless sweater and different type of pattern were designed and knitted by multi-segment blending yarns. The free change of colors along the length direction of a single yarn provides an effective method for integrated rapid design and production of sweaters through mutual design of the overall pattern and the structure of the colorful fabric.

Keywords: three-channel rotor spinning, gradient yarn, segment yarn, pattern design, colorful textile

1 INTRODUCTION

Colors and patterns are an important criterion of sweaters. For the modern sweaters, it has been a trend to combine patterns with the overall shape of the sweater, and then apply the pattern as a whole to the contour of the sweater [1-2]. The overall pattern of colorful fabric is generally achieved by interweaving of different colorful yarns. However, the pattern design is complicated, and the knitting process is rather difficult. With the mutual design of the overall pattern of the sweater and the fabric structure, as demonstrated by Fig.1, the integrated design and production of sweaters can be realized quickly with multi-segment blending colorful yarns such as rotor spinning gradient yarns and segment color yarns.

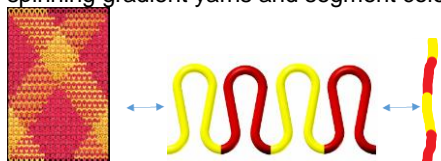


Figure 1 Mutual design of the fabric and yarn

Rotor spinning is the second-largest spinning method that is second only to ring spinning in terms of market share. It has the advantages of high production efficiency and short process flow. In recent years, the speed of the rotor has been increased, and the large package of the bobbin has been used for spinning. Significant progress has been made in the expansion of suitable spinning counts, and has attracted widespread attention from the industry and scholars. Three-channel rotor spinning machine can produce rotor spun yarns with multiple segments and different colors by three prime colorful fibers. Blending pre-colored fibers to obtain a wide variety of colors is an important coloration method in the textile industry. Generally, the blends of a limited number of pre-colored fibers (or primaries) can obtain any desired color within the color gamut by formulating recipes. Three-channel rotor spinning is a novel method of blending pre-colored fibers which is smart and flexible. It is different from current color yarn spinning process. During current color yarn spinning process, mixing and spinning is usually completed in

different processes: mixing first, and then spinning yarn. Such spinning processes are complex.

This article briefly introduces the production method and product features of multi-segment three-channel rotor spinning blended yarn, and its use in the mutual design of sweater and yarns.

2 SPINNING MECHANISM

2.1 Spinning machine

The schematic diagram of the three-channel rotor spinning process is shown in Fig.2 and Fig.3. As observed, the three fiber strips (components and colors can be the same or different) are fed to the opening roller through their corresponding feeding rollers. Then the continuous and tight fiber strips are divided into sparse streams by splitting to achieve separation and orientation of the fibers. Under the acceleration airflow in the fiber transport channel, the streams are further separated into a single fiber to enter the rotor.

Such single fibers are collected in the groove at the bottom of the rotor with the centrifugal force of the high-speed rotor. Accordingly, through stripping, opening, cleaning, carding, and transfer of the carding roller, fiber bundles are separated into single fibers. Afterwards, multiple rovings are asynchronously fed into the rotor spinning unit. Multi layers of condensed fibers are combined as a bundle and twisted to form a yarn. Subsequently, the yarns are wound onto a tube by winding roller. With such a spinning process, the objective of flexibility, high efficiency, and high yield are realized.

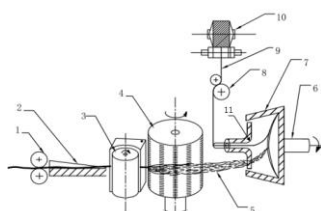


Figure 2 Three channel digital rotor spinning feed mechanism (a-1, combined feed rollers; 2, collector; 3, main roller; 4, carding roller; 5, fiber transport channel; 6, bearing; 7, rotor; 8, guide roller; 9- yarn; 10, bobbin; 11, ceramic false twister)

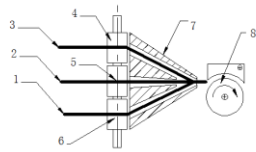


Figure 3 Three channel digital rotor spinning feed mechanism (1, 2, 3, rovings; 4, 5, 6, combined feed rollers; 7, collector; 8 main roller.)

3 COLORFULL TEXTILES PRODUCED BY THE NOVEL SPINNING

3.1 Knitting colorfull fabrics

Knitted fabrics were produced with multi-colorful yarns produced by the above mentioned spinning method, as shown in Figure 4-6. The multi-segment rotor spinning yarns and their fabrics are rich in color, strong in gradation, and dynamic, reflecting strong individuality and avant-garde features. 3-D mixed colors obtained by colorful fibers show a gentler feature compared to traditional powder mixed colors. The distinct colors of segmented fabrics demonstrate an excellent effect of segment color. Besides, the color of slub yarn has clear bamboo textures with prominent bamboo color and three-dimensional texture effects.



Figure 4 Gradient colorfull fabrics



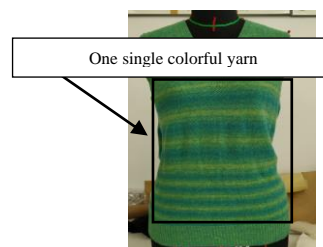
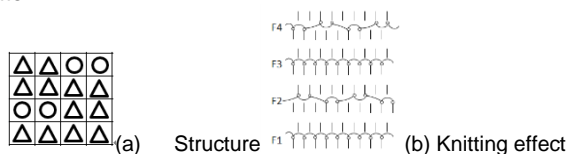
Figure 5 Segment colorfull fabrics



Figure 6 Colorfull fabrics knitted by colorfull slub yarn

3.2 Multi-section sweater with gradient color

Integrally Knitted seamless sweaters are produced with multi-section color blended yarn with 46 segments as listed in Fig.7. The length of the colorful yarn is combined with knitted fabric structure to form a perfect natural pattern.



(c) seamless sweater

Figure 7 Colorful sweater of multi-section color-blended yarn

3.3 Pattern examples knitted by multi-section color-blended yarn

The fabric of parallelogram and arrow-shaped pattern were produced with multi-colorful yarns produced by the above mentioned spinning method, shown by Fig.8-9. The desired pattern is formed by properly combining the segmental length of the corresponding color of the yarn with the fabric structure and the length of the coil together.



Figure 8 Parallelogram pattern

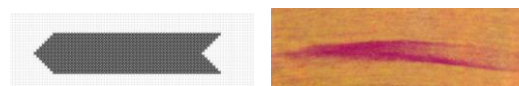


Figure 9 Arrow-shaped pattern

4 CONCLUSION

A smart and sustainable spinning for colorful textiles was proposed in this research. The mono-fiber strips of the three primary colors (Red, Yellow and Blue) are fed separately and the yarns of any color are spun by the blending of the three primary colors during the yarn spinning process. The method has high flexibility and adaptability and is an effective method for producing color yarns to reduce environmental pollution.

ACKNOWLEDGEMENT

This work was supported by Natural Science Foundation of Jiangsu Province of China No. BK20181350.

5 REFERENCES

- [1] Ohta K., Sakaue K., Tamura H.. Pattern recognition of fabric surfaces. Journal of Textile Machine Sociology Japanese, 1986, 32, pp. 7-10.
- [2] Zheng D., Wang L.. Multi-scale density detection for yarn-dyed fabrics with deformed repeat patterns. Textile Research Journal, 2017, 87(20), pp. 2524-2540.

Industrial Hemp as a Sustainable Textile Fibre to produce High quality Apparel Fabric

Dhirendra Sharma¹, Priyal Sawla¹, Meenakshi Ahirwar² and B K Behera²

¹MLV Textile and Engineering College, Bhilwara dhirendra.mlvti@gmail.com

²Department of Textile Technology, Indian Institute of Technology Delhi meenakshi76361@gmail.com

Abstract: Hemp is the natural bast fibre with better moisture absorbency, strength and durability. Hemp also has certain special properties like non-allergic, non-irritant, antistatic and antibacterial. Hemp cultivation has several advantages compared to cotton that is hemp requires less water, fertilizers and pesticides. In this research, yarn and fabric samples are prepared from 100% cotton, 70:30 cotton/hemp and 50:50 cotton/hemp blends, both on ring and compact spinning systems. Fabrics are prepared for both top and bottom wear. Tensile strength of yarns is determined. Fabrics produced were characterized on Kawabata system to evaluate their low stress mechanical properties and the Total Hand Value for both top and bottom applications. Other aesthetic properties like drape, pilling is also determined and compared with 100% cotton fabric.

Keywords: Industrial Hemp, Sustainable fibre, Low stress mechanical properties, Total Hand Value

1 INTRODUCTION

Hemp is the oldest natural fibre with good strength and durability. Hemp acts as a natural weed suppressor [1]. If hemp is grown on the same ground for the second time it will weaken all perennial grasses or may kill them. It is UV resistant, antimicrobial, and requires less water and pesticides than the cotton plant [2]. Hemp has tremendous potential for production of high quality apparel grade fabrics. Fabric handle is dependent on complex interactions among tensile, bending, shear and compressive deformation at low stress. It is a very complex compilation of all fabric properties which can be assessed by human touch. Handle properties includes stiffness, softness, smoothness, bulkiness and crispiness of the fabric. However, the concept of fabric handle measurement has completely transformed with the invention of Kawabata Evaluation System [3] which measures the low stress mechanical properties (tensile, shear, bending and compression) of fabrics and predicts the fabric total hand value.

2 MATERIALS AND METHODS

2.1 Materials

The fabric samples with the different fibre mix are produced using 100% cotton, cotton-hemp blend for both bottom and top wear.

2.2 Methods

All the yarn samples are prepared on yarn sample line in an industrial mill. Sizing of yarn samples were done on CCI tech sample sizing machine. The plain woven grey fabric samples were produced on CCI Tech sample weaving machine. After this the fabrics are desized, scoured, bleached and converted to RFD fabrics.

2.2.1 Testing of Fabric Samples

2.2.1.1 Evaluation of fabric aesthetic properties

Aesthetic properties determined are drape, pilling and crease recovery angle using the Cusick Drape Tester, Martindale abrasion and pilling tester, Crease Recovery Tester respectively.

2.2.1.2 Evaluation of low stress mechanical properties

Low stress mechanical properties of fabrics are measured using Kawabata Evaluation System (KES). Tensile and shear, bending, compression and surface properties are evaluated using KES-FB1, KES-FB2, KES-FB3 and KES-FB4 respectively [3]. The sample size taken is 20*20cm. Ten readings in warp and weft direction are taken for each sample. Sixteen low stress mechanical properties are evaluated to calculate the primary and total hand value.

Equation for calculating PHV:

$$Y = C_0 + \sum_{i=1}^N C_i (X_i - \bar{X}_{mi}) / \delta_i$$

Y = primary hand value;

X_i = ith characteristic value or its logarithm;

X_{mi}, σ_i = mean value and the standard deviation of the ith characteristic value,

C₀, C_i parameter (constant coefficient),

N = Total number of mechanical properties.

With the help of different values of properties tested, different hand equations in the above format have been obtained as Y₁, Y₂, Y₃,, Y_k.

The translation equation from PHV to THV developed for fabrics:

$$THV = C_{00} + \sum_{i=1}^k Z_i$$

$$Z_i = C_{i1} (Y_i - M_{i1}) / \delta_{i1} + C_{i2} (Y_{i2} - M_{i2}) / \delta_{i2}$$

Here, Y_i = primary hand values, M_{i1}, M_{i2} = mean values of Y_i and Y_{i2}, σ_{i1}, σ_{i2} = standard deviation of Y_i and Y_{i2}, respectively. C₀₀, C_{i1}, C_{i2} = constant parameters and k = number of primary hands.

2.2.1.3 Evaluation of other fabric properties

Tensile and tear strength test for fabrics is carried out using ASTM D 5034 and ASTM D 434 respectively.

3 RESULTS AND DISCUSSION

3.1 Fabric aesthetic properties

3.1.1 Pilling

100% cotton both compact and ring fabrics shows slight surface fuzzing and partially formed pills in both 16Ne and 30Ne count. In case of 70:30 cotton-hemp fabrics, the moderate surface fuzzing or moderate pilling is observed. In 50:50 cotton-hemp fabrics, distinct surface pilling is observed along-with pills of varying size and density covering a large proportion of the specimen surface.

3.1.2 Crease Recovery Angle

100% cotton fabric shows low crease recovery angle than 70:30 and 50:50 cotton-hemp fabric. This means that as the angle are increasing, more recovery of fabric take place. This is because the elastic recovery of fibres is better in hemp fibres so the stored elastic energy is sufficient to overcome the friction that resists the movement to yarn and fibres.

3.2 Low stress mechanical properties for suiting fabric

In order to evaluate the handle behavior of cotton and cotton-hemp blended fabrics, low stress mechanical properties such as tensile, bending, shear, compression and surface properties are measured on Kawabata system [4]. These parameters are entered into the Kawabata hand equation to calculate the primary hand value and the total hand value (THV) in table 1.

Table 1 Fabric hand values

Fabric (16Ne)		PRIMARY HAND VALUES				Total Hand Value THV
		KOSHI	SHARI	FUKU	HARI	
Ring fabric	100% cotton	6.987	4.916	4.523	6.733	3.179
	C: H (70:30)	7.556	5.570	4.127	7.319	3.208
	C:H (50:50)	7.824	5.921	4.043	7.394	3.290
Compact fabric	100% cotton	7.218	4.620	4.798	6.936	3.062
	C: H (70:30)	7.490	5.459	4.640	7.562	3.203
	C:H (50:50)	8.053	6.455	4.295	8.032	3.324

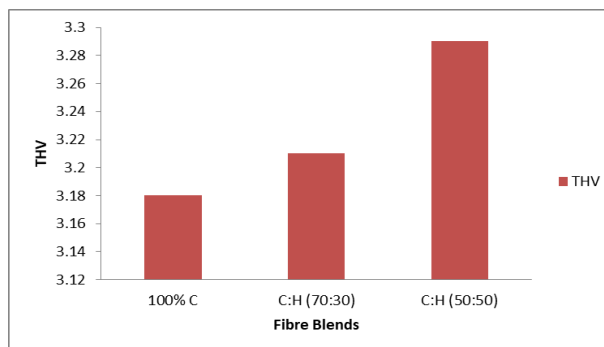


Figure 4.2 Comparison of THV for different blends

4 CONCLUSION

The pilling effect is more in 50:50 cotton/hemp blend due to the short fibres as the number of binding are less in this yarn. The 100% cotton has less pilling as the short fibres are less. Drape properties are better in 100% cotton than other fibre mix. Cotton-hemp blended fabrics give comparatively higher toughness. 50:50 cotton-hemp fabrics offer the highest tensile resilience, bending rigidity and bending hysteresis. 50:50 cotton-hemp fabrics give the highest shear rigidity and shear hysteresis along with higher surface friction and roughness value; followed by 70:30 cotton-hemp fabric and 100% cotton fabric. Compressional resilience for cotton-hemp blended fabrics is found to be lower than that of cotton fabric. 100% cotton fabrics have higher Fukurami value, indicating that these fabrics are softer, smoother and compressible. Cotton-hemp blended fabric produces highest Koshi value as the hemp fibres are coarser and stiffer. Shari value is more in 50:50 cotton-hemp followed by 70:30 cotton-hemp and 100% cotton for both compact and ring fabric. Hari values are higher in 50:50 cotton-hemp due to the high friction coefficient of hemp fibres. 50:50 cotton-hemp fabrics give higher total hand value (THV) than cotton fabrics of similar construction and areal density, considering the fabrics are to be used for summer suiting wear.

6 REFERENCES

- [1] Kaiser, C., Cassady, C. and Ernst, M., 2014. Industrial Hemp Production. Center for Crop Diversification Crop Profile, p.6.
- [2] Sacilik, K., Öztürk, R. and Keskin, R., 2003. Some physical properties of hemp seed. Biosystems engineering, 86(2), pp.191-198.
- [3] Behera, B.K. and Hari, P.K., 1994. Fabric quality evaluation by objective measurement.
- [4] Behera, B.K., 2007. Comfort and handle behaviour of linen-blended fabrics. AUTEX Research

10. Biomedicals

Planar polymeric nanofibrous patches for sealing the gastrointestinal anastomoses

Zuzana Oulehlová¹, Markéta Klíčová¹, Jana Horáková¹, Andrea Klápšťová¹, Václav Liška², Jáchym Rosendorf², Richard Pálek² and Lenka Červenková²

¹ Department of Nonwovens and Nanofibrous Materials, Faculty of Textile Engineering, Technical University of Liberec, Studentska 1402/2, 460 01 Liberec, Czechia, zuzana.oulehlova@tul.cz

² Charles Univerzity, Faculty of Medicine in Pilsen, Biomedical Center, alej Svobody 1655/76, 323 00 Plzeň

Abstract: Post-operative complications remain serious problem in gastrointestinal surgery. One of the most frequent and most dreaded issues is anastomotic leakage (AL). The uncontrolled leak of the colonic content into the abdominal cavity significantly increases the mortality (6 – 22%). Hence various barrier kinds of protection were tried both experimentally and clinically. However, the large randomised clinical trials showed no improvement after applying the commercially available products for prevention of the AL. In our study we focused on fabrication of the nanofibrous patches, that could serve as a barrier kind for the AL avoidance. The planar polymeric nanofibrous mats were produced by using Nanospider™, since the device allows large scale production of nanofibers via electrospinning. Various types of biocompatible and biodegradable polymers were used such as poly-ε-caprolacton (PCL) and poly(L-Lactide-co-ε-Caprolactone) (PLCL). The nanofibrous materials were tested in vivo; as an animal model was chosen a Prestice black-pied pig. The safety of the nanofibrous material was proven. All laboratory findings were to be found in the range of physiological values without any morphological changes. No mortality and no sepsis were observed and all the anastomoses were well healed. In this paper, the novel form of the material is introduced. The material consists of electrospun and electrosprayed PCL solution and should serve for preventing AL and also the peritoneal adhesion.

Keywords: component, formatting, style, styling, insert (keywords)

1 INTRODUCTION

Anastomotic leakage (AL) remains one of the most common post-operative complication in gastrointestinal surgery.¹ The uncontrolled leak of the colonic content into abdomen frequently leads to peritonitis, abscess formation or sepsis.² The fast detection is crucial, however it is demanding to identify the presence of AL early. The other post-operative complication is called peritoneal adhesion (PAs), which are the bonds created between different abdominal organs after performing the surgical anastomosis. PAs can cause abdominal discomfort or passage blockage and thus decrease the life quality of a patient. On the market there are various products, which should serve for preventing the AL or PAs. Unfortunately, the huge randomized studies have shown no beneficial potential of these products in preventing such complications.

We developed a novel method for preventing the AL. By using the electrospun nanofibrous layers made of poly-ε-caprolacton (PCL) and poly(L-Lactide-co-ε-Caprolactone) (PLCL) we were able to successfully cover the surgical gastrointestinal anastomosis, resulting in well healed tissue. On the other hand, the amount of adhesions was more likely increased. In this paper the novel form of the sealing material is introduced. This material has two sides with different properties and combines the electrospun PCL nanofibrous layer and on the other side the electrosprayed droplets of PCL, which should simulate the lotus leaf effect and act as an extremely hydrophobic material. Thus one side of the material (electrosprayed droplets) is non-adhesive while the other side (PCL nanofibers) creates adhesive layer. The adhesive layer will be then attached to the surgical anastomosis, while

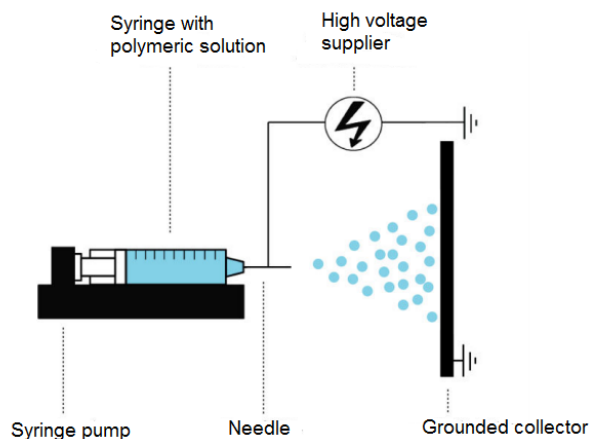
the other side will be in contact with other abdominal tissue and prevent PAs.

2 METHODS

Materials. Firstly, the needle electrospraying of the low concentration solutions of PCL (Sigma Aldrich) were prepared to prove the creation of the droplets under the electrostatic field. For this purpose three solutions of PCL were prepared in concentrations 10% w/w., 5% w/w, 3% w/w. As a dissolving system the mixture of chloroform (Penta) : ethanol (Penta) : acetic acid (Penta) in a 8/1/1 v/v ratio was used. The solutions were stirred with a magnetic stirrer for 24 hours and immediately electrosprayed via needle electrospinning. The apparatus can be seen on the Picture 1.

Equally, the solutions for the Nanospider™ (NS 1WS500U, Elmarco) fabrication were prepared. Firstly, the nanofibrous layer of PCL (16% wt., dissolving system chloroform (Penta) : ethanol (Penta) : acetic acid (Penta) in a 8/1/1 v/v ratio) was created. Secondly, the 3% wt. PCL solution (dissolving system chloroform (Penta) : ethanol (Penta) : acetic acid (Penta) in a 8/1/1 v/v ratio) was electrosprayed. Thus the composite layer combining fibers and droplets was fabricated.

Characterization techniques. The morphology of the material was observed by using SEM (scanning electron microscope) VEGA3 SBU – EasyProbe microscope, Tescan (Czech Republic). The wettability measurement was performed by using See System 6.2 (Advex Instruments, Czech Republic). The adhesion of cells was made by primarily *in vitro* tests with 3T3 mice fibroblasts.

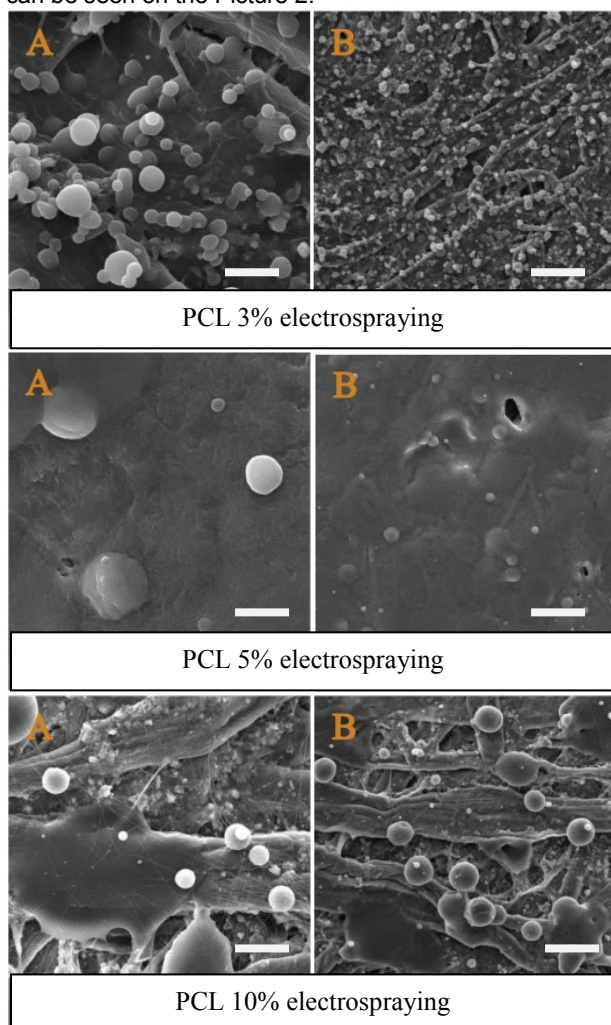


Picture 1: Needle electrospinning apparatus.

3 RESULTS

3.1 Needle-electrospinning

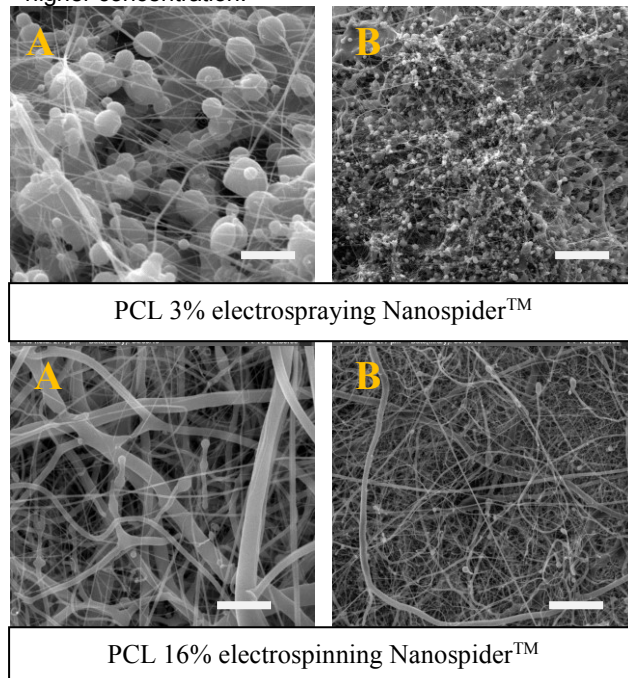
SEM observations of needle electrospinning technique can be seen on the Picture 2.



Picture 2: SEM pictures of needle-electrospinning of PCL solutions. Scale 10 μm (A) and 50 μm (B).

3.2 NanospiderTM (needleless) electrospinning/electrospraying

Based on previous needle-electrospinning results, for the NanospiderTM electrospinning was chosen the 3% w/w PCL solution. The conditions for needleless electrospinning were successfully found. Picture 3 depicts the electrospayed droplets and also the nanofibrous layer of PCL, created from solution with higher concentration.



Picture 3: Needleless electrospinning of 3% wt. PCL solution and needleless electrospinning of 16% wt. PCL solution. Scale 10 μm (A) and 50 μm (B).

4 CONCLUSION

The conditions for needleless electrospinning of PCL solutions were successfully found. The novel material for sealing the gastrointestinal anastomoses was introduced.

Acknowledgement

Authors would like to thank Student Grant Competition (SGS) 2019 at the Technical University of Liberec.

5 REFERENCES

1. Murrell, Z. A. & Stamos, M. J. Reoperation for Anastomotic Failure. *Clin. Colon Rectal Surg.* **19**, 213–216 (2006).
2. Sparreboom, C. L., Wu, Z.-Q., Ji, J.-F. & Lange, J. F. Integrated approach to colorectal anastomotic leakage: Communication, infection and healing disturbances. *World J. Gastroenterol.* **22**, 7226–7235 (2016).

INTERNATIONAL COOPERATION OF FACULTY OF TEXTILE ENGINEERING FROM LIBEREC WITH JAPAN PARTNERS

Pavla Těšínová

Technical University of Liberec, Faculty of Textile Engineering, Czech Republic, e-mail: pavla.tesinova@tul.cz

Abstract: This abstract describes cooperation basis of Faculty of Textile Engineering of Technical University of Liberec with partners from Japan who are mainly Kyoto Institute of Technology, ShinShu University (Campus Ueda) and The Textile Machinery Society of Japan. Personal contacts cooperation was followed early by student's internship basis. Mobilities are supported by local financial sources and projects for example Erasmus+ Credit mobility KA107.

Keywords: international cooperation, Erasmus+, internships

1 INTRODUCTION

Faculty of Textile Engineering of Technical University of Liberec (FT) was established in the year 1960 as the second faculty of former University and provides as the only one in Czech Republic academic education through whole textile subject. There is possible to study textile materials and technologies, clothing technologies, textile marketing and design. FT offers higher education in the bachelor, master, resp. follow-up master and doctoral study programs. All study programs are accredited in Czech and English language and in full-time and part-time forms. The faculty participates in greatness on cooperation with industry and solves a lot of projects supported by various grants [1].

2 ERASMUS+

Erasmus+ is the EU Programme in the fields of education, training, youth and sport in act by REGULATION (EU) No 1288/2013 OF THE EUROPEAN PARLIAMENT AND OF THE COUNCIL of 11 December 2013 establishing 'Erasmus+'. The Union programme for education, training, youth and sport chosen as a key to promote common European values, foster social integration, enhance intercultural understanding and a sense of belonging to a community, and to prevent violent radicalisation [4]. The mobility project comprises the following activities [4,5]:

- Student mobility for studies to/from Partner Countries;
- Student mobility for traineeship to/from Partner Countries;
- Staff mobility for teaching to/from Partner Countries;
- Staff mobility for training to/from Partner Countries

3 COOPERATION WITH INTERNATIONAL ORGANISATIONS

3.1 General cooperation

FT has got currently 28x Memorandum of Understanding and 68x Erasmus+ Inter-Institutional Agreement including so called Credit mobility KA107 for mobility within out of EU countries [2]. Beside national participation at Association of Textile, Clothing and Leather Industry (ATOK), The Cluster of Technical Textiles (CLUTEX) and Czech Technology Platform for Textiles (CTPT) showing activity with Czech industry FT is a member or associate at Association of Universities for Textiles (Autex),

European Federation of National Engineering Associations (FEANI) and European Technology Platform for Textiles & Clothing (EURATEX) to support and form international textile and related community [3].

3.2 FT cooperation with Japan

FT is proud to be a partner in cooperation with Kyoto Institute of Technology (KIT), ShinShu University (Ueda) and The Textile Machinery Society of Japan. University cooperation is covered under the umbrella of MOU and Erasmus+ Inter-Institutional Agreements. All FT, KIT and ShinShu are members of Autex association what gives opportunity to form together university level of textile and related education and fit it for industry needs in each region specifications and shear good practice examples for strengthening this important high-level education, R&D&I and transfer of knowledge.

Academic staff of FT participated regularly at the Textile Research Symposium organized mainly by The Textile Machinery Society of Japan. The first participation can be found from 1996.

KIT cooperates with FT from the 90's of 20th century at least. During 30 years of cooperation was actively kept mainly by Prof. Kawabata, Prof. Sato, Prof. Ysunaga and Prof. Sukigara on the side of KIT and Prof. Militký, Prof. Vik and Prof. Kús from FT. Both research was and continue mainly in the colorimetry and clothing comfort not only by KES Kawabata measuring system. The first MOU was signed in 1999, renewed in 2006 on faculty levels and on university level in 2015. This gives opportunity to strengthen existing bonds and continue broadening of cooperation with Kyoto Design Lab and students study stays.

Formalised cooperation with ShinShu University was covered by university MOU signed in 2011 when faculty level agreements and individual contacts run before that time. Both universities are interested in nanotechnology and use of nanoparticles and its application in textile engineering field. Clothing evaluation and thermo-physiological comfort is a key cooperation in application of wearable sensors also in technical apparel. For example Prof. Ohkawa, Prof. Kanai, Prof. Kajiwawa and Prof. Hamada were the main partners to build functional cooperation with teams of Prof. Militký and Prof. Kús.

Shinshu University agreed to progress mobility of students within Erasmus+ Credit mobility KA107 and application in 2017 was successful allows to exchange both staff and students. This year 2019 was applied too and we are eagerly waiting for results at the end of June when KIT joined our application.

3.3 Delegation of FT in Japan

The dean of FT visited Japan in November 2019 to strengthen cooperation and show official interest to promote mobility of academic staff and students.



Figure 1 Meeting of delegation FT with the dean of Faculty of Textile Science and Technology ShinShu University Prof. Makoto Shimosaka and his team, November 2018

The dean, her team and representative of Faculty of Art and Architecture TUL were warmly welcomed at both universities and visited institutes. They discussed on the possible cooperational topics including systems how to realise it in near future.



Figure 2 Meeting of delegation FT and FUA with the colleagues Prof. Sachiko Sukigara, Prof. Tetsuya Sato, Prof. Hidekazu Yasunaga at KIT, November 2018

4 MOBILITY OF STUDENTS

As academic cooperation was possible to build space for students exchanges we can show numbers of mobility from the 2015 year and minimum one month long as registered in TUL online Study Agenda in Table 1. More students from KIT visited FT but included in short research periods thus not registered as an internship scholarship holders.

Students were related research topics about colorimetry, clothing comfort, wearable electronic and material engineering with overlapping to project management when building project work and time management. The shortest stay in a month ratio but the longest internship

lasted whole one year and another one is prepared to start nowadays.

Students follow study and research work according to the regulations of host country study system with recognition and acceptance after the stay at home university. Preferred are ECTS credits which can be transferred from the local grades and accepted for the home study course. It allows students to pass courses without necessity of prolongation of their study at home. Another possibility is research related to the students final work topic. It gives progressive results combining laboratory equipment of all involved institutions which includes not only pure measurement but also view to the different research and project management because of the national specifications.

Table 1 Mobility numbers from 2015 to 2019 for one month and longer stays

Type of mobility	University in Japan	
	Kyoto Institute of Technology	ShinShu University
Incoming	3	5 +3 later in 2019
Outgoing	3	7

5 CONCLUSION

FT and their partner universities, KIT and ShinShu University are experienced in cooperation not only within research but can manage quality exchange of students based on the advantage of prior successful and continuous academic cooperation. It was already realised mobility in call 2017 of Erasmus+ and we are looking forward to future with new Erasmus+ or other projects for mobility and research too.

Supported were not only participants above mentioned but also all people in contact with them. Regional and international importance are high hand in hand with internationalisation at home for students and staff involved.

ACKNOWLEDGEMENT: The mobility is financially supported by the Erasmus+ KA107 č.2017-1-CZ01-KA107-034883.

6 REFERENCES

- [1] Welcome on web of Faculty of Textile Engineering TU Liberec: Ft.Tul.cz. Welcome on web of Faculty of Textile Engineering TU Liberec [online]. Liberec: FT TUL, year not defined [cit. 2019-04-08]. Available at: <http://www.ft.tul.cz/en/>
- [2] Annual Report 2018: Activity Report of Faculty of Textile Engineering. 1 In edition process. Liberec: FT TUL, 2019.
- [3] Cooperation: Ft.Tul.cz. International Activities. [online]. Liberec: FT TUL, year not defined [cit. 2019-04-08]. Available at: <http://www.ft.tul.cz/en/research/cooperation/international-activities>
- [4] Erasmus+ Programme Guide Version 3 (2018): 10/08/2018 European Commission.
Erasmus+. International Credit Mobility. Frequently Asked Questions for Higher Education Institutions (HEIs). (2015) European Commission

ANALYSIS FOR STRUCTURAL DISTRIBUTION OF MELTBLOWN NONWOVEN FABRIC TO THICKNESS DIRECTION USING X-RAY CT

KyoungHou KIM^{1,2}, Kohei OYA¹, Kouta MOCHIZUKI¹, Toshifumi IKAGA¹, Yutaka OHKOSHI^{1,2}

¹ Faculty of Textile Science and Technology, Shinshu University, 3-15-1 Tokida, Ueda, Nagano 386-8567, Japan, e-mail: Khkim@shinshu-u.ac.jp

² Division of Frontier Fibers, Institute for Fiber Engineering, Shinshu University, 3-15-1 Tokida Ueda, Nagano prefecture, 386-8567, Japan

Abstract: In order to investigate the influence of the internal structure distribution of MB nonwoven fabric on physical properties, MB nonwoven fabrics were prepared under different spinning conditions and the structural distribution along the thickness direction was evaluated with X-ray Computer Tomography. PET resin (IV: 0.65 dl / g, Tm: 255 °C) was spun through two kinds of nozzles with different nozzle diameters, that is, 0.35 and 0.70 mm. For the obtained fabrics, a tomographic image of 1024 × 1024 pixel in machine direction (MD) × cross direction (CD) was taken using micro X-ray CT (Skyscan 1272, Bruker Co.) with a resolution of 1 μm/voxel. From binarized tomographic images and object ratio of the tomographic images, the fiber volume fraction at each thickness position was determined. As a result, the fiber volume fraction increased gradually as the distance from the conveyor surface increases, while decreased as the determine position approached the nozzle. It is explained by the fact that, at a position close to the conveyor surface, the fiber layer is strongly compressed by suction force, but the suction force decreased with being close to the nozzle. Moreover, the fiber volume fraction of the nozzle diameter 0.35 mm is lower than that of 0.70 mm. It is considered that the fibers are deposited on the collector before it is solidified sufficiently and are fused together in the nozzle diameter 0.70 mm.

Keywords: meltblown nonwoven fabric, X-ray CT, spinning condition, fiber volume fraction

1 INTRODUCTION

Melt-blowing is a process used to produce nonwoven fabrics consisting of microfibers. In melt-blowing, a melt extruded from a die is blown and thinned by high-velocity hot air and then solidified by cooling in ambient air while exhibiting a vibration in the transverse direction (whipping). The resultant fibers are collected on a wire screen with the aid of air suction, and bonded together by a combination of entanglement and thermal adhesion[1].

The structure of melt-blown nonwoven fabrics is largely decided by the fiber lay-down pattern, which is influenced by the manufacturing conditions. Because the fiber motion in the whole die-to-collector region can describe the lay-down pattern, much research has been performed to understand the fiber motion during melt-blowing. The whipping in a single-orifice melt-blowing device was measured online using high-speed strobe photography[2], and they reported that a longer distance from the die and a higher air flow rate increased the whipping amplitude and decreased its frequency.

X-ray micro computed tomography (XCT or μCT), which is nondestructive and does not require sample pretreatment, has also been used to analyze the microstructure of fibrous materials, including yarns, knitted and nonwoven fabrics[3]. Furthermore, some of the research have focused on the structural profile along the thickness direction. We analyzed the profile of fiber volume fraction and orientation of needle-punched nonwoven fabric using XCT by separating individual fibers[4]. These studies indicate that XCT is a powerful technique to analyze the structural profile of fabrics along the thickness direction. We also investigated the microstructure of melt-blown nonwoven fabrics using XCT. In particular, the profiles of fiber volume fraction and in-plane fiber orientation along

the thickness direction are evaluated. The effects of die-to-collector distance (DCD), air suction (AS), and blowing air flow rate (AFR) on the microstructure of the fabrics are studied.

However, the difference in the degree of the fiber attenuation and the solidification, which greatly affects the orientation and the density of the fibers, is due to the diameter of the nozzle, but no researches in this point have been found. Therefore, in this study, the effect of the nozzle diameter on the mechanical properties and the internal structure of the nonwoven fabric was investigated through XCT method. The mechanical properties of the produced nonwoven fabric also were measured and the relationship between the structure and mechanical properties was investigated.

2 EXPERIMENTALS

2.1 Melt-blowing

Polyethylene terephthalate (BELLPET TK3, Bell Polyester Products, Inc. Yamaguchi, Japan) pellets were used for melt-blowing. The intrinsic viscosity and melting point of the pellets were 0.65 dl/g and 255 °C, respectively. The pellets were dried under vacuum at 120 °C for 12 h prior to use.

A pilot-scale melt-blowing apparatus (MB-0300, Nippon Nozzle Co., Ltd., Kobe, Japan) was used in this study. The nozzle had a width of 400 mm and angle (α) of 60°, and the setback distance (ds) was set at 0 mm. The nozzle diameters were 0.35mm (hereinafter referred to as φ 0.35), 0.70mm (φ 0.70). Two series of melt-blown samples were obtained by changing DCD and nozzle diameter. Six

samples were prepared by changing with three DCDs in each nozzle diameter, without changing AFR and AS, as detailed shown in Table 1.

Table 1. Melt-blowing conditions for each series of experiment.

Sample (Dia-DCD)	Nozzle Diameter r (mm)	Number of orifices	AFR (m ³ /h)	AS (rpm)	DCD (mm)
ϕ 0.35-20	0.35	432	200	3500	20
ϕ 0.35-50					50
ϕ 0.35-70					70
ϕ 0.70-20	0.70	302			20
ϕ 0.70-50					50
ϕ 0.70-100					100

2.2 X-ray micro computed tomography

The samples were observed by XCT (Skyscan 1272, Bruker, MA, USA), using a device with a maximum resolution of 350 nm/voxel. Six specimens with dimensions of 10 × 10 mm were used for each sample. The specimen was mounted perpendicular to the stage by using adhesive tack. X-rays generated at 30 kV and 200 μ A were irradiated onto each specimen without a filter. A total of 1922 transmission images with 2452 × 1640 pixels (1 μ m/pixel) was obtained by rotating each specimen by 0.1°/image.

Grayscale tomographic images with 256 gradation were reconstructed by the software NRecon (Bruker). Here, the brightnesses of 0 and 255 were set as the maximum of blank air and the maximum of the specimen, respectively. The tomographic images were then binarized using the software CTAn (Bruker) by thresholding at 1. Corresponding 3D and projection images were constructed using the software CTvol (Bruker) and CTAn, respectively.

From the binarized tomographic images that are parallel to the fabric surface, fiber diameter, the fiber volume fraction of each tomographic image, and basis weight were measured. We determined fiber diameter by manually measuring the diameters of 200 fibers selected randomly.

3 RESULTS AND DISCUSSION

Fig. 1 shows the average fiber volume fraction along the thickness direction of the nonwoven fabric calculated from the tomographic image of six samples. In the images, the volume fraction less than 1% was defined as the bottom side. All the samples were prepared with the same weight, and thus the decrease of the fiber volume fraction could be considered as the increase of the nonwoven fabric thickness.

Except for DCD20, the fabrics obtained from ϕ 0.35 show lower fiber volume fraction, indicating larger fabric thickness, than ϕ 0.70. It could be because the thinner fibers from ϕ 0.35 was retarded the accumulating time on the conveyor by whipping of fibers than thicker fibers from ϕ 0.70.

For the DCD20, the thicker fibers from ϕ 0.70 makes a large number of fusion points and a large fusion area, and

thus the fabric thickness decreased comparing to that of ϕ 0.35.

The distribution of the fiber volume fraction along the thickness direction show a feature consist of a central portion of high volume fraction and two surface portions of low volume fraction, without being concentrated in any thickness position. All the samples of ϕ 0.70 in every DCD has mainly higher fiber volume fraction than the sample of ϕ 0.35 in the center. It could be seen that the decrease of the fiber volume fraction in the center is due to the increase in the fabric thickness as described above. Accordingly, it indicates that the increase of the nonwoven fabric thickness has an influence to both the low density zone in two end sides and the high density zone in the center.

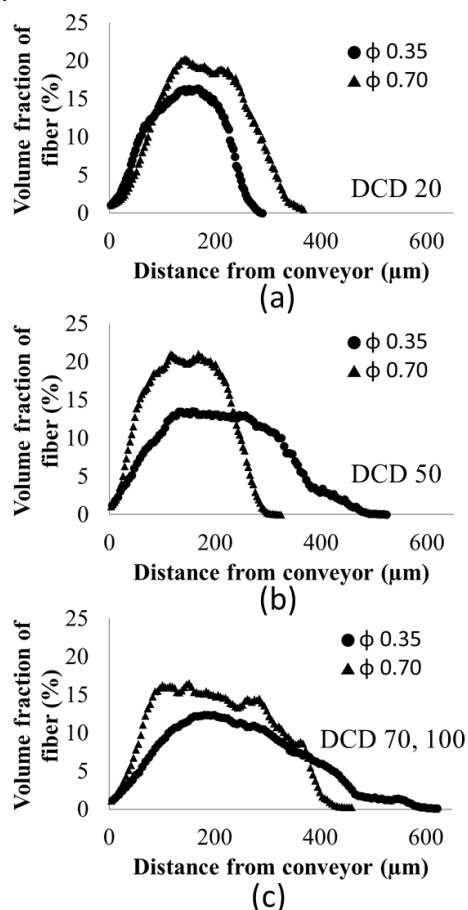


Fig. 1. Profiles of the fiber volume fraction plotted along the distance from bottom surface for six specimens.

4 REFERENCES

- [1] Russell SJ. *Handbook of nonwovens*. 1st ed. Cambridge: Woodhead Publishing Ltd, 2006, pp.172 and p.409.
- [2] Rao RS and Shambaugh RL. Vibration and stability in the melt blowing process. *Ind Eng Chem Res* 1993; 32, pp. 3100–3111.
- [3] Jeon SY, Yu WR, Kim MS, et al. Predicting the tensile strength of needle-punched nonwoven mats using X-ray computed tomography and a statistical model. *Fibers Polym* 2014; 15: pp.1202–1210.
- [4] Ishikawa T, Ishii Y, Nakasone K, et al. Structure analysis of needle-punched nonwoven fabrics by X-ray computed tomography. *Text Res J*; 2019, 89 pp. 20–31.

Title	47th TEXTILE RESEARCH SYMPOSIUM – Book of abstracts
Editor	Ing. Miroslava Pechočiaková, Ph.D.
Publisher	Technical University in Liberec Studentská 1402/2, Liberec 1, 46117, Czech Republic
Approved by	Rector's Office of Technical University of Liberec Ref. no, RE 20/19 30 th May 2019
Date of issue	June 2019
Edition	First
Number of Copies	135
Printed by	Vysokoškolský podnik s.r.o., Studentská 1402/2, Liberec 1, 46117, Czech Republic
Publication Number	55-020-19

ISBN 978-80-7494-473-4